**Development and Characterization of Non-heme Iron Biocatalysts for Complex Molecule Synthesis**

by

Tyler Joseph Doyon

A dissertation submitted in partial fulfillment
of the requirements for the degree of
Doctor of Philosophy
(Chemical Biology)
in the University of Michigan
2020

Doctoral Committee:

Assistant Professor Alison R. H. Narayan, Chair
Professor Nicolai Lehnert
Professor Anna K. Mapp
Professor David H. Sherman

Tyler J. Doyon

tydoyon@umich.edu

ORCID iD:  0000-0002-6885-7487

## Dedication

*This dissertation is dedicated to my family, without whom none of this would be possible.*

## Acknowledgements

This incredible journey would not have been possible without the unwavering support of my family, friends and colleagues whom I have relied on during these past few years. I would first like to thank my advisor Prof. Alison Narayan for her support and guidance. From the very beginning, she encouraged me to pursue science with vigor and excitement and gave me room to explore new areas and ideas that captured my attention. Alison has provided me with boundless opportunities to develop new skills and works incredibly hard to ensure the safety, security and success of all of her students, which has been particularly reassuring during these challenging pandemic times. I deeply thank Alison for the opportunities she has given me and for her guidance through this incredible journey. In my time at the University of Michigan, I have been fortunate to be mentored by numerous incredible scientists, including my first rotation with Prof. David Sherman. David has continued to mentor me in his role as a committee member and I thank him for his guidance over all these years. I wish to thank my other committee members, Prof. Anna Mapp and Prof. Nicolai Lehnert for their continued guidance and support as I progressed through my degree. I would also like to acknowledge and thank my incredible collaborators at the University of Michigan, Prof. Markos Koutmos, Dr. Leena Mallik, Dr. Troy Wymore and Prof. Paul Zimmerman. We have achieved such exciting and valuable work together and I deeply appreciate their contributions and mentorship over these years.

My friends, and especially my coworkers in the Narayan lab, have been incredible these past five years. It has been an honor and a privilege to work with this esteemed group of extremely

talented scientists, whom I have come to regard as family. The day-to-day marathon of graduate school would have been impossible without your friendship, guidance and your senses of humor. Together, we built a group that will continue to contribute work of incredible value to the field of biocatalysis and organic chemistry. We have shared in our successes and in hard times, and the bond that we have forged between us we will carry through the rest of our lives. I wish you all the very best in your future endeavors and I look forward to seeing you again.

I would also like to specifically acknowledge several labmates who have directly contributed to the work described in this dissertation. Dr. Summer Baker Dockrey, Jonathan Perkins, Di Yang, Evan Romero, and Kevin Skinner have all been instrumental in the development and completion of these projects. Thank you all for your hard work and dedication to this work. I also wish to thank Dr. Wendy Feng for her tireless work keeping our mass spectrometry and NMR equipment operational for all of these years.

Last, and most of all, I wish to acknowledge my family. Words simply cannot express how deeply grateful I am to them for supporting my goals and dreams. I would not have made it through this journey without them. Together, we have experienced some incredibly challenging times these past few years. And yet, through it all, we managed to maintain our strength and our senses of humor. I have leaned on all of you and you have given me the strength and inspiration to carry on. You encouraged me and helped me keep the faith through this challenging and rewarding experience. I will be forever grateful to all of you for your unconditional love and support. I could not have done it without you.

## Table of Contents

## List of Tables

## List of Figures

## List of Abbreviations

ADH – alcohol dehydrogenase

ATA – aminotransferase

α-KG – α-ketoglutarate

AIBN – 2,2'-azobis(2-methylpropionitrile)

AMDase – arylmalonate decarboxylase

BLAST – basic local alignment search tool

CAN – ceric ammonium nitrate

ChCl – choline chloride

DDQ – 2,3-dichloro-5,6-dicyanobenzoquinone

DES – deep eutectic solvent

DKR – dynamic kinetic resolution

DMF – dimethylformamide

DMSO – dimethylsulfoxide

ER – 'ene' reductase

$FADH_2$ – flavin adenine dinucleotide

FMN – flavin mononucleotide

HPLC – high performance liquid chromatography

IEDDA – inverse electron demand Diels-Alder

IRED – imine reductase

KRED – keto-reductase

LC – liquid chromatography

LFRP – living free-radical polymerization

MS – mass spectrometry/mass spectrometer

Na Asc – sodium ascorbate

NADP+/NADPH – nicotinamide adenine dinucleotide phosphate

NBS – *N*-bromosuccinimide

NCS – norclaurine synthase

NCBI – National Center for Biotechnology Information

NHI – non-heme iron

Ni-NTA – nickel nitriloacetic acid

NMR – nuclear magnetic resonance

*o*-QM – *ortho*-quinone methide

PAD – phenolic acid decarboxylase

PBS – phosphate buffered saline

PSase – Pictet-Spenglerase

PCR – polymerase chain reaction

PDB – Protein Data Bank

rt – room temperature

SDM – site-directed mutagenesis

SDS-PAGE – sodium dodecylsulfate polyacrylamide gel electrophoresis

TEMPO – (2,2,6,6-tetramethylpiperidin-1-yl)oxidnyl

THIQ – tetrahydroisoquinoline

TPPTS – 3,3’,3’’-phosphanetrityltris(benzenesulfonic acid) trisodium salt

UPLC – ultra performance liquid chromatography

4-OT – 4-oxycrotonate tautomerase

## Abstract

Nature has evolved myriad biocatalytic tools for selective synthesis. The three-dimensional architecture of an enzyme active site enables the direct construction of new bonds with exquisite site-, chemo-, and stereo-selectivity. Seeking to take advantage of these characteristics, researchers have leveraged biocatalysts for the rapid synthesis of natural products and complex molecules, developing sustainable methods to address long-standing challenges in synthetic chemistry. In recent years, this approach has been expanded to combine chemo- and biocatalytic methods in a single vessel, enabling transformations of increasing complexity to occur in a streamlined process. This thesis describes the development of novel, one-pot chemoenzymatic methods for the synthesis of complex molecules and natural products. Specifically, this work leveraged non-heme iron (NHI) alpha-ketoglutarate-dependent enzymes to access reactive *ortho*-quinone methide (*o*-QM) and radical intermediates for the construction of chroman and tropolone natural products. These studies provide a platform for the development of NHI enzymes as scalable and selective catalysts for the synthesis of complex molecules.

The described research involved the development NHI enzymes CitB and ClaD to perform selective benzylic C–H hydroxylation of *ortho*-phenolic compounds. This biocatalytic method offered numerous advantages over small molecule oxidants, which often exhibit poor site- and chemo-selectivity for benzylic hydroxylation reactions. In comparison, CitB and ClaD provided strict control over the site of oxidation, avoiding the need for blocking or protecting groups to

achieve selective catalysis. The substrate scope of this transformation was evaluated for these biocatalysts and a scalable reaction platform was developed for this transformation, demonstrating the ability of NHI enzymes to serve as sustainable and selective catalysts for benzylic C–H hydroxylation. The products of this selective oxidation were fully characterized and were shown to serve as reactive precursors for the formation of *o*-QMs in a one-pot process. Compared to traditional synthetic approaches to one-pot *o*-QM generation, a biocatalytic route offers the advantage of selective oxidation, leading to controlled generation of the reactive *o*-QM intermediate. These intermediates were elaborated in one-pot, modular chemoenzymatic fashion through 1,4-addition and [4+2] cycloaddition reactions demonstrating the synthetic utility of this approach for synthesizing complex scaffolds. Overall, this biocatalytic reaction platform offered an improved selectivity profile over traditional oxidative approaches to *o*-QM synthesis, enabling facile one-pot benzylic oxidation and functionalization in a scalable reaction format.

A second focus of this work involved the chemoenzymatic synthesis of 7-membered aromatic compounds known as tropolones. Efficient synthetic access to this structurally-diverse class of metabolites represents a significant challenge to the development of novel tropolone pharmaceuticals. To address this hurdle, NHI enzymes XenC and TropC were leveraged for their native ring expansion function to develop an efficient one-pot, two-enzyme reaction for the synthesis of substituted tropolones. Reactions with XenC were leveraged in the efficient chemoenzymatic synthesis of a variety of non-natural tropolones including the deoxygenated form of tropolone natural product epolone B. The reactivity of a putative Diels-Alderase was also explored in this reaction, providing a potentially selective route to the synthesis of bioactive tropolone natural products. Furthermore, this work explored the mechanism of the native ring

expansion reaction performed by NHI enzyme TropC and provided evidence of a radical-based reaction through structural characterization of the enzyme, as well as mutagenesis and computational analysis. These observations led to a revised proposal for fungal tropolone biosynthesis and provided critical insight into an understudied NHI-catalyzed transformation.

# Chapter 1: One-pot Chemoenzymatic Reaction Sequences for Complex Molecule Synthesis



## 1.1 Introduction

Groundbreaking discoveries in protein engineering and the development of non-native enzymatic reactions, coupled with an ever-expanding database of natural protein sequences, have positioned biocatalysis to be increasingly impactful in synthetic chemistry.[1-3] In particular, chemoenzymatic cascades and one-pot reaction sequences are powerful tools for the efficient synthesis of chemical building blocks, natural products, and pharmaceutical agents.[1-3] These reaction sequences are often inspired by Nature's methods for generating natural products, wherein multiple transformations are performed in a single vessel (for example, a cell) to quickly generate molecular complexity. Biocatalysis can provide an array of advantages over traditional synthetic methods, offering improved site-, stereo-, and chemoselectivity, in addition to mild reaction conditions.[1-6] Chemoenzymatic, one-pot reaction sequences combine the benefits of biocatalytic methods with the potential to perform multiple transformations in a single reaction vessel with high specificity.[1-3] In contrast to many traditional synthetic transformations, chemoenzymatic reactions are typically performed at ambient temperatures and under mild, aqueous conditions.[4-5]

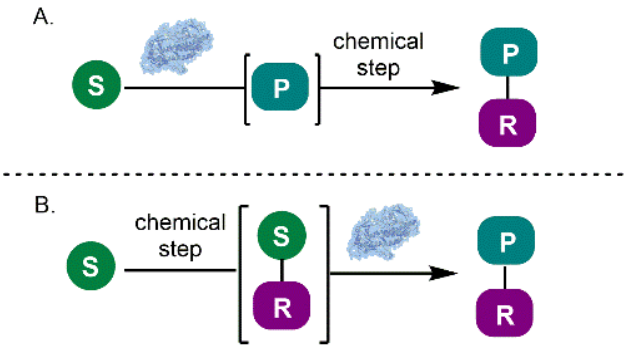


**Figure 1.1. One-pot chemoenzymatic transformations.**
A. Biocatalyst-generated products are modified through a chemical reaction. B. Chemically-modified substrates undergo a second biocatalytic transformation. S = enzyme substrate, P = enzymatic product, R = chemical modification.

Using enzymes, transformations that traditionally require incompatible reaction conditions can often be performed in a single vessel without issue. Efforts combining traditional chemical methods and biocatalytic reactions are currently underexploited. However, such hybrid strategies have the potential to expand the repertoire of transformations to access previously inaccessible chemical space that cannot be achieved with biocatalysis or chemocatalysis alone.

Chemoenzymatic processes have been applied to the synthesis of an array of high-value molecules, including bioactive natural products, drugs and pharmaceutical intermediates, such as cholesterol-lowering Lipitor® (atorvastatin), and the diabetes control drug Januvia® (sitagliptin).[4-6] A variety of enzyme classes have been used in cascade or sequential one-pot processes including oxygenases, halogenases, oxidases, reductases, decarboxylases and lipases among others.[4-5] These reactions are designed to operate in a complementary fashion, where a chemical step generates a substrate for a subsequent enzymatic reaction, or a chemical step is used to modify the product of an enzymatic process (Figure 1.1). In order to optimize reaction conditions, chemoenzymatic one-pot reactions have featured a diverse array of approaches.[7-8] Reaction processes can occur in a cascade, or tandem format in which all reagents and catalysts are added to a single mixture and both the chemical and biocatalytic transformations are allowed to proceed simultaneously.[7-8] In contrast, some chemoenzymatic one-pot processes feature a modular or stepwise approach in

which one reaction is allowed to proceed to completion prior to the addition of reagents or initiators for a second transformation. Such strategies are often used to circumvent compatibility challenges between chemo- and biocatalytic reactions.[7-8] An additional category of chemoenzymatic transformation includes cooperative systems in which conversion of a starting material to a reactive intermediate is a reversible process (Figure 1.2).[8] This process generates a substrate for an irreversible downstream reaction that, in turn, improves flux through the cascade to deliver products. Examples of each type of reaction platform are featured throughout this chapter.

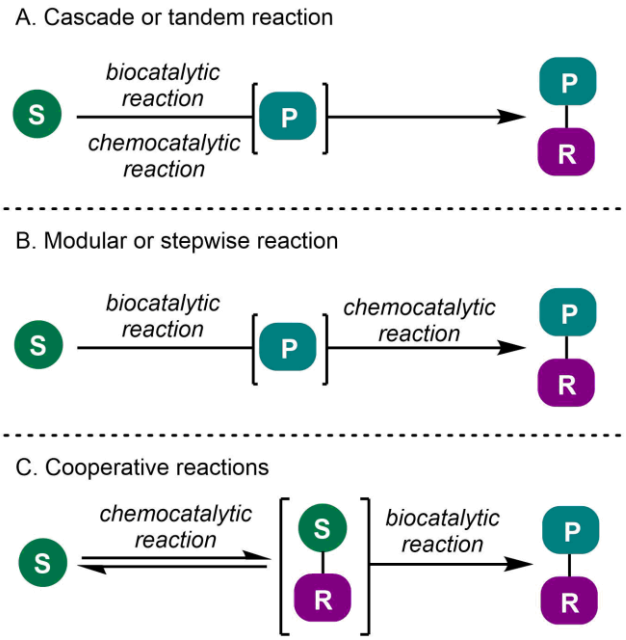


**Figure 1.2. Types of one-pot chemoenzymatic transformations.** A. Cascade or tandem reaction in which both reactions are performed simultaneously. B. Modular or stepwise approach in which chemical and biocatalytic steps are separated temporally but occur in the same vessel. C. Cooperative system in which a reversible reaction generates substrate for an irreversible downstream reaction. S = enzyme substrate, P = enzymatic product, R = chemical modification.

Challenges in the construction of compatible chemoenzymatic one-pot reaction platforms have involved the creative development of novel processes to overcome these limitations. For example, chemocatalytic reactions can be difficult to adapt to the aqueous reaction conditions required for many biocatalytic reactions.[7-8] Chemical catalysts may be sensitive to water-induced catalyst poisoning or generate unwanted side products through alternative reaction pathways. On the other hand, biocatalysts may perform poorly under non-aqueous environments or under the increased temperatures required for several chemocatalytic reactions.[7-8] Furthermore, biocatalysts may undergo denaturation in the presence

of some chemical reagents. To overcome these challenges, several novel chemoenzymatic reaction platforms have been developed, including reactions using cosolvents, biphasic systems, supramolecular reaction scaffolds, encapsulated enzyme techniques and the use of deep eutectic solvents.[7-8] These reaction systems have been leveraged for a plethora of chemoenzymatic systems, enabling the coupling of previously incompatible chemical and biocatalytic processes and broadening the scope of possible transformations that can be performed using a chemoenzymatic process. Transformations utilizing chemoenzymatic strategies are highlighted within this chapter, demonstrating the ways in which these advancements have resulted in a complete renaissance in the organic synthesis of complex molecule.[7-8]

## 1.2 Chemoenzymatic one-pot sequences

*Aldol reactions paired with enzymatic processes*

Aldol reactions are a key transformation in the synthesis of new C−C bonds. These reactions often occur at room temperature and can be catalyzed asymmetrically using sustainable organocatalysts. As a result, these transformations are particularly amenable to integration with biocatalytic processes. In one example, Gröger and coworkers designed chemoenzymatic sequences for the one-pot stereo-divergent synthesis of enantioenriched 1,3-diols and demonstrated the concept of enzyme-catalyzed modification of a chemically-generated product.[9] After an initial organo-catalyzed asymmetric aldol reaction (**1.1** to **1.3**, Figure 1.3A), the resulting ketone (**1.2**) was reduced stereo-specifically by a nicotinamide adenine dinucleotide phosphate hydride (NADPH)-dependent alcohol dehydrogenase (ADH). By selecting an appropriate aldol catalyst and ADH, the configuration of each stereocenter could be controlled. This allowed access to all four possible stereoisomers for the resulting 1,3-diol in good yields and with high levels of

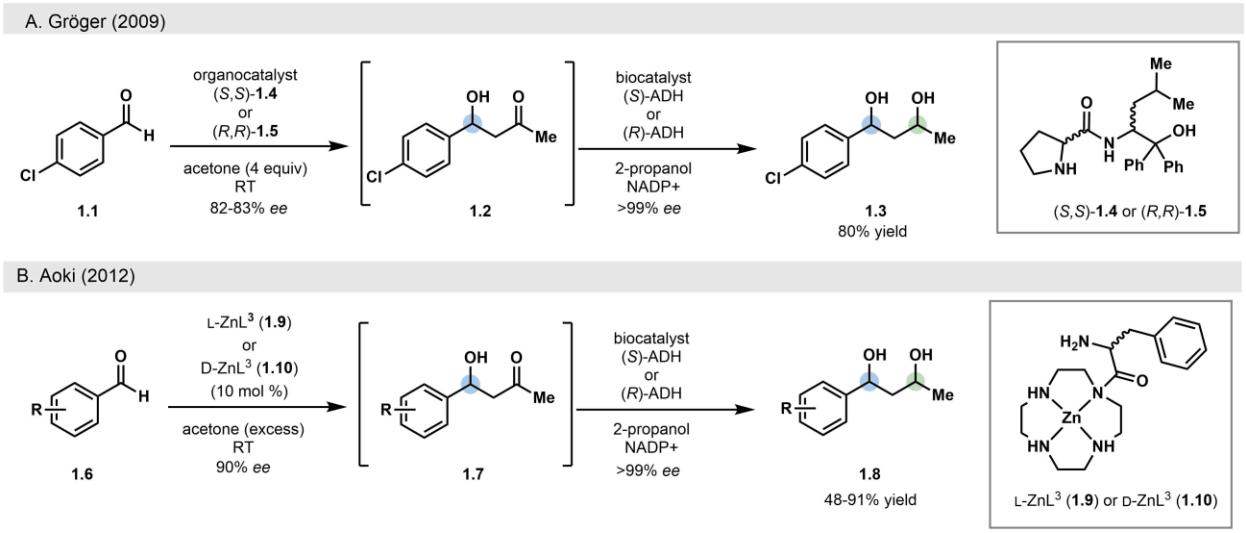


**Figure 1.3. Stereodivergent chemoenzymatic one-pot synthesis of 1,3-diols.**
A. Organo-catalyzed asymmetric aldol reaction paired with stereoselective reduction using KREDs. B. Zn-catalyzed asymmetric aldol reaction paired with stereoselective reduction using KREDs.

enantio- and diastereoselectivity. In comparison, traditional synthetic approaches to selectively access each of the possible stereoisomers require numerous steps and are typically accomplished by modular asymmetric synthesis of each stereocenter using transition metal-catalyzed processes.[10-11] Aoki and coworkers developed a similar one-pot stereodivergent synthesis of enantioenriched 1,3-diols through a Zn-catalyzed enantioselective aldol reaction, followed by an analogous enantioselective reduction with complementary NADPH-dependent ADHs (**1.6-1.8**, Figure 1.3B).[12] These conditions offered improved enantioselectivity in the aldol step, translating to improved diastereomeric ratios of products following the enzyme-catalyzed reduction. Such examples also highlight the utility of cascade biocatalysis for performing enantioselective reductions, providing selective access to any of the desired possible stereoisomers in a one-pot process.

*Chemoenzymatic cyclization cascades*

Chemoenzymatic one-pot reactions offer significant advantages for the selective oxidation of molecules, particularly for those with redox-sensitive functional groups. The ability to perform selective oxidations without protecting group manipulations allows for one-pot cascade sequences that would be challenging using traditional synthetic methods alone. The opportunities afforded by selective biocatalytic functionalization has inspired new routes to synthetically challenging target molecules. For example, the Turner group has pioneered a number of chemoenzymatic processes for the selective synthesis of nitrogen-containing heterocycles. They have established a variety of approaches, including the chemoenzymatic kinetic resolution of cyclic amines and cascades for cyclization to form an imine, followed by selective reduction using imine reductases (Figure 1.4A).[13-16] These methods enabled facile access to enantioenriched amine scaffolds that

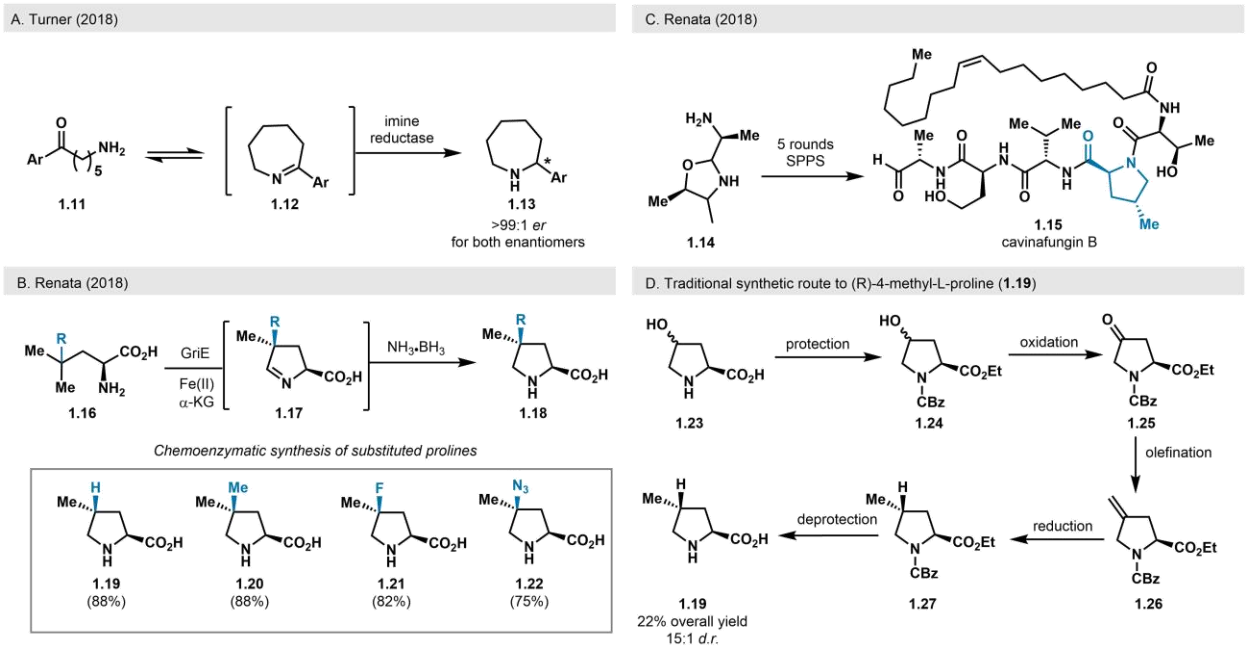


**Figure 1.4. Chemoenzymatic one-pot syntheses of cyclic amines.**
A. Imine condensation paired with asymmetric imine reduction. B. NHI dioxygenase-catalyzed oxidation and cyclization paired with chemical imine reduction. C. Application of **1.19** to the synthesis of cavinafungin B. D. Comparison of chemoenzymatic approach to traditional synthesis of 4-substituted proline derivatives.

are key components of natural products and pharmaceuticals, demonstrating that such syntheses can be performed in a direct and highly selective manner.[13-16]

Utilizing an amine cyclization technique, Renata and coworkers recently developed a one-pot chemoenzymatic method that proceeded through an intermediate imine to generate L-proline derivatives (**1.16-1.22**), a motif common to a number of acyldepsipeptide antibiotics (Figure 1.4B).[17] Their approach leverages the ability of GriE, an α-ketoglutarate-dependent non-heme iron dioxygenase, to perform two successive C–H oxidations on the terminal methyl group of L-leucine, to generate an aldehyde intermediate.[17] *In situ* intramolecular condensation to form imine intermediate **1.17** is followed by borazane reduction to afford L-proline derivatives **1.19-1.22** in good yields. Renata and coworkers subsequently applied the chemoenzymatic synthesis of proline derivative **1.19** for the first total synthesis of the antiviral lipopeptide natural product cavinafungin B (**1.15**).[18] This method demonstrates the efficiency of performing complementary chemoenzymatic transformations in one-pot without the need for isolation of reaction intermediates.[17] In comparison, an established synthetic route to access 4-methylproline (**1.19**) involves multiple steps, including protection of L-4-hydroxyproline (Figure 1.4D, **1.23-1.24**), oxidation to the corresponding ketone (**1.24-1.25**), olefination with Petasis reagent (**1.25-1.26**), hydrogenation with Crabtree's catalyst (**1.26-1.27**) and, finally, global deprotection to yield **1.19** with moderate diastereomeric ratios.[19] Thus, the chemoenzymatic approach employing GriE represents a more efficient, sustainable and selective route for the synthesis of proline derivatives.

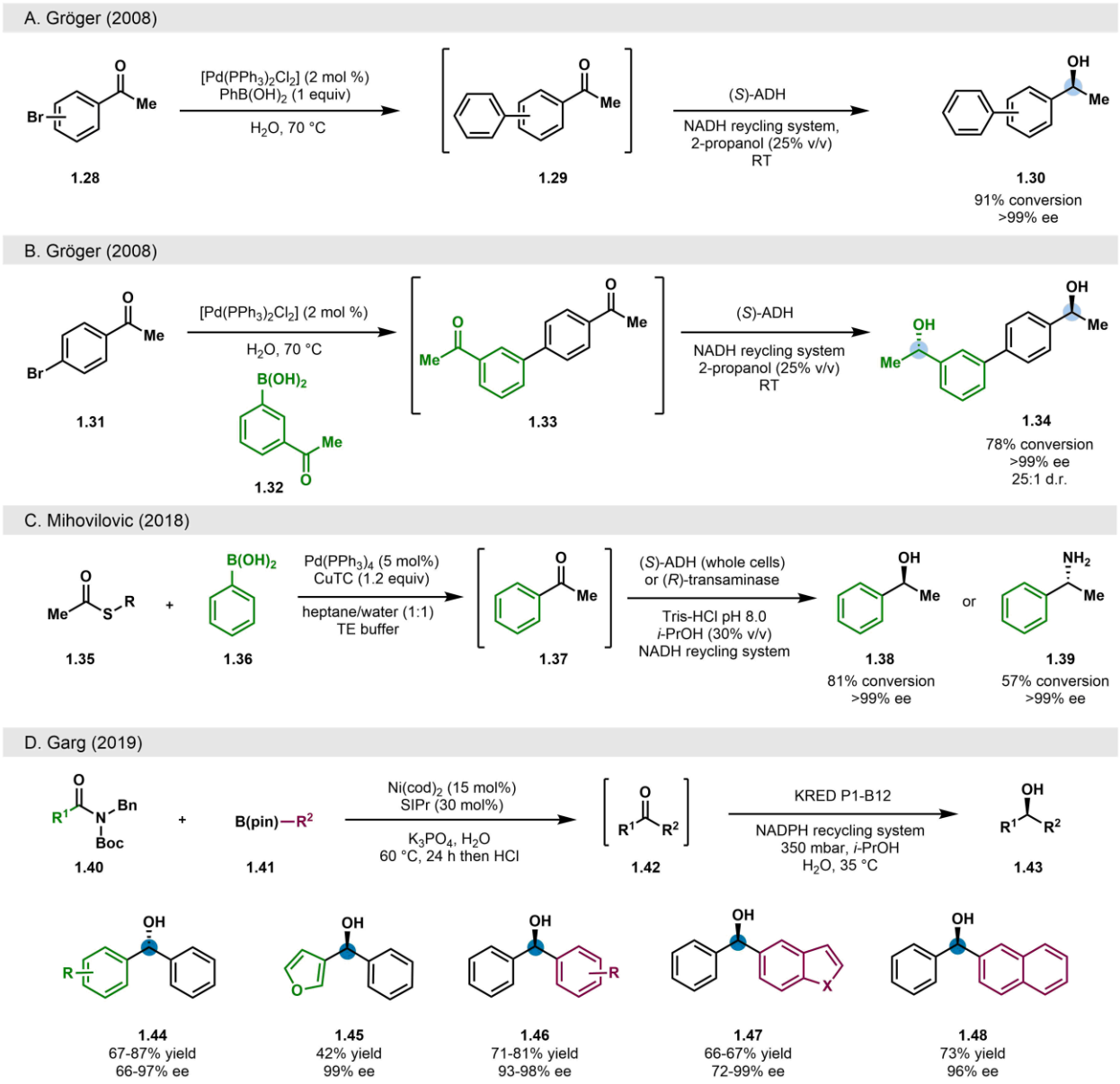


**Figure 1.5. Chemoenzymatic one-pot cross-couplings paired with enzymatic reductions.** A. Suzuki-Miyaura cross-coupling reaction paired with asymmetric KRED-catalyzed reductions. B. Suzuki-Miyaura cross-coupling reaction paired with asymmetric KRED-catalyzed reductions. C. Liebeskind-Srogl cross-coupling paired with asymmetric biocatalytic reductive amination and KRED-catalyzed reduction. D. Ni-catalyzed cross-coupling paired with KRED-catalyzed reductions.

*Chemoenzymatic cross-coupling transformations*

Significant effort has been devoted to the development of high utility chemoenzymatic sequences. For example, the combination of transition metal-catalyzed and biocatalytic reactions in a single vessel allows chemists to perform transformations that are generally not possible using biocatalysts alone. In some cases, cross-coupling reactions can be used to generate substrates *in situ* for a biocatalyst, or they can be leveraged for further diversification of an enzyme product.[7, 20-23] Innovative work by Gröger and coworkers demonstrated that palladium-catalyzed cross-couplings could be paired in a modular fashion with the asymmetric reduction of aryl ketones for the generation of enantioenriched biaryl benzylic alcohols (**1.30** and **1.34**, Figure 1.5A and 1.5B).[20] Either of the desired enantiomers could be accessed using complementary ADHs, giving products with the targeted configuration with nearly perfect selectivity and in good yields.[20] This was the first demonstration of a cross-coupling reaction used in a one-pot fashion with a biocatalytic reaction, expanding the scope of transformations that are possible through chemoenzymatic processes and inspiring future innovation in combining transition-metal catalysis and biocatalysis.

Since these initial studies by the Gröger group, other cross-coupling reactions have been developed that leverage highly selective enzyme-mediated reductions to synthesize more complex targets.[24] For example, the Mihovilovic group has innovated in this area, expanding the cross-coupling portion of this modular reaction to include the Liebeskind-Srogl (L-S) reaction, which couples boronic esters and thioesters in a palladium-catalyzed process (Figure 1.5C, **1.35-1.39**).[24] They combined this transformation with downstream reductive reactions, including *in-situ* KRED- and transaminase-catalyzed diversification of the resulting ketone. As with the reactions developed by the Gröger group, these one-pot cascade processes were highly successful, boasting moderate to good yields and high levels of enantioselectivities.[24] Similarly, the Garg group applied this modular reaction design to the nickel-catalyzed coupling of amides with boronic esters, followed

by enantioselective reduction using an engineered ketoreductase to deliver enantioenriched, biaryl alcohols in moderate to good yields (see Figure 1.5D, **1.44-1.48**).[25]

Cross-coupling reactions have also been applied in the modification of enzyme-generated products. In particular, Suzuki-Miyaura and Heck reactions have been used to diversify the products of engineered flavin-dependent halogenases (Figure 1.6A). The Micklefield group has leveraged this type of approach for the site-selective one-pot synthesis of biaryls and aryl-indoles (see **1.49-1.53**).[26] Using a molecular weight cutoff device to effectively compartmentalize their chosen halogenase, they coupled site-selective bromination with palladium-catalyzed cross-coupling reactions in an aqueous medium, allowing for the generation of cross-coupled species in moderate to good yields.[26] They reported that compartmentalization of their enzyme led to improved yields in the cross-coupling reactions and improved flux through this cascade reaction.[26] As an alternative to the compartmentalized one-pot chemoenzymatic approach, the Lewis group

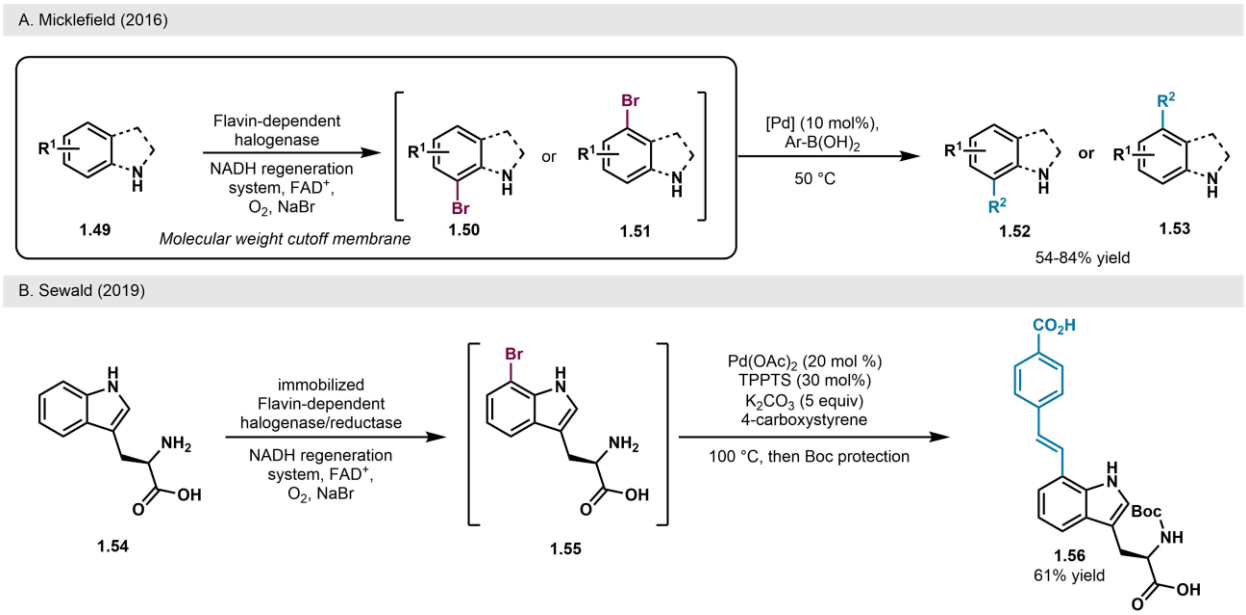


**Figure 1.6. One-pot enzymatic halogenation paired with cross-coupling reactions.**
A. Compartmentalized enzymatic halogenation paired with Suzuki-Miyaura cross-couplings. B. Biocatalytic halogenation using immobilized enzyme paired with Heck coupling.

has also reported a halogenase/cross-coupling sequence in which the crude extract of a biocatalytic halogenation reaction was used directly in palladium-catalyzed cross-coupling transformations.[27]

Sewald and coworkers took a modular approach to the Heck coupling of styrene with unprotected tryptophan, performing a stepwise, enzyme-catalyzed bromination by using a combination of an immobilized flavin-dependent halogenase and a reductase, followed by palladium-catalyzed Heck coupling at elevated temperatures (Figure 1.6B, **1.54-1.56**).[28] This reaction resulted in the streamlined synthesis of modified tryptophans in moderate yield without the need for protection or deprotection procedures.[28] Overall, these procedures provide a site-selective and highly efficient method for the diversification of aryl species in a one-pot process. Such processes also demonstrate that challenges in compatibility between enzymatic and transition-metal catalyzed processes could be overcome through the creative application of biochemical tools, such as inexpensive and reusable molecular weight cutoff devices.[26]

*Ruthenium-catalyzed metathesis paired with enzyme processes*

One limitation in the development of one-pot chemoenzymatic processes is the frequent incompatibility of conditions for the chemocatalytic and biocatalytic reactions.[8, 21-23] For example, some biocatalysts are highly sensitive to organic solvents, while many chemical catalysts cannot operate in aqueous or aerobic conditions. These contradictory requirements can make some desirable chemoenzymatic transformations logistically difficult or impossible.[8] However, recent innovations have enabled the combination of otherwise incompatible transformations.[8] In one example, Hartwig and Zhao developed a tandem chemoenzymatic reaction for the conversion of simple alkenes to substituted, enantioenriched epoxides through an initial olefin metathesis with Hoveyda-Grubbs second-generation catalyst, followed by epoxidation with $P450_{BM3}$ variants (see

Figure 1.7A and 1.7B).[21-22] In this case, the seemingly incompatible processes could be accomplished in a common reaction vessel by using a biphasic system of isooctane and aqueous buffer.[21-22] This solution was effective, generating enantioenriched epoxides in yields that were often greater than those achieved for each standalone reaction.[21-22] This increase in yield is likely the result of a change in equilibrium for the metathesis reaction caused by the consumption of the metathesis product in the subsequent biocatalytic reaction, an example of a cooperative chemoenzymatic cascade process.[22] Similarly, Turner and Castagnolo developed a system for the

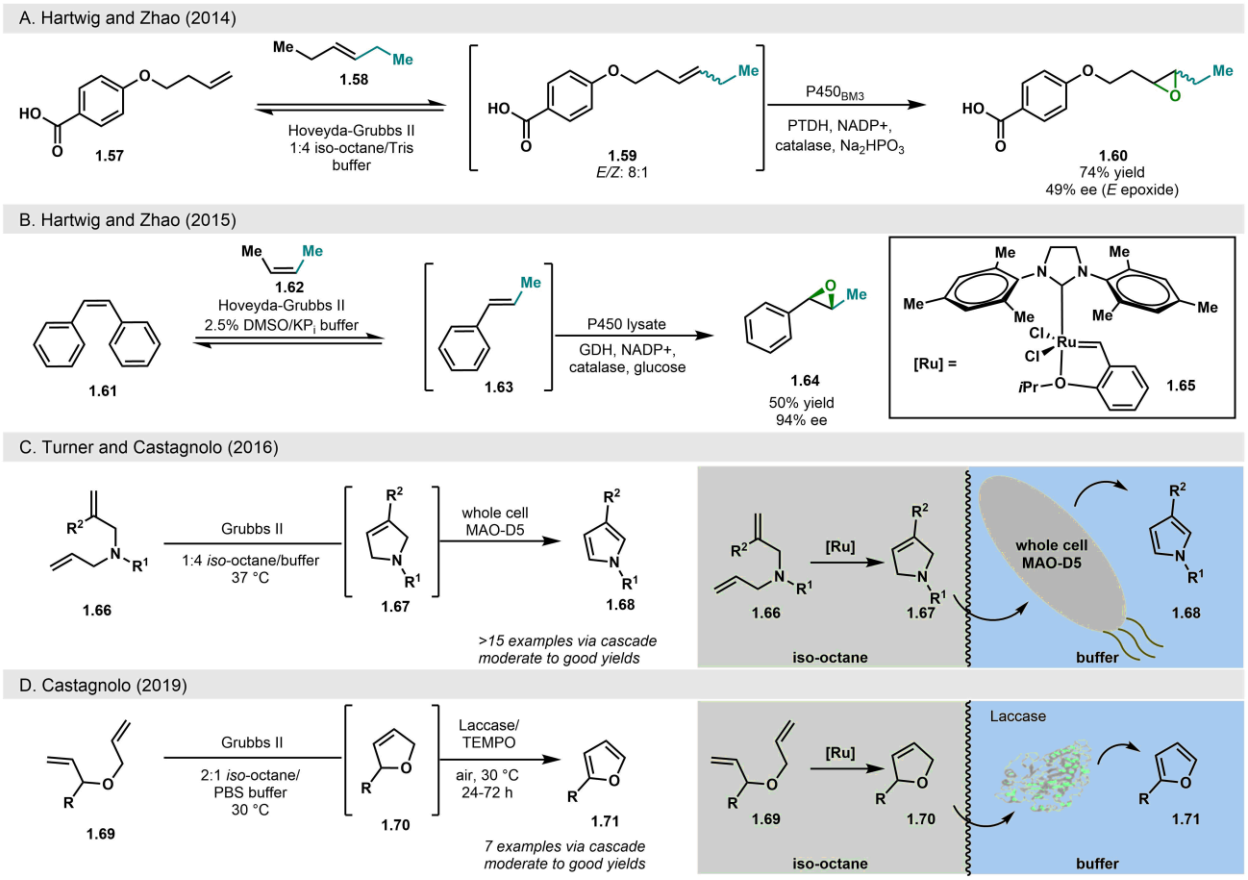


**Figure 1.7. Ruthenium-catalyzed metathesis reactions paired with biocatalytic processes.** A. Biphasic Hoveyda-Grubbs II-catalyzed metathesis combined with enzymatic epoxidation. B. Hoveyda-Grubbs II- catalyzed metathesis combined with enzymatic epoxidation. C. Grubbs II-catalyzed cyclization paired with enzymatic oxidation to form pyrroles. D. Grubbs II-catalyzed cyclization paired with enzymatic oxidation to form furans.

chemoenzymatic synthesis of substituted pyrroles (Figure 1.7C).[23] This reaction sequence featured an olefin metathesis mediated by the second generation Grubbs catalyst, followed by monoamine oxidase-D5 (MAO-D5)-catalyzed oxidation to generate pyrrole products (see **1.66-1.68**). This method used whole cells containing the biocatalyst as an alternative to purified protein or crude cell lysate, providing a simple and scalable platform for the oxidation of the cyclic amine to the final pyrrole product.[23] Traditional methods for this oxidation require stoichiometric oxidants, such as hypervalent iodide,[29] or transition-metal catalysts with TEMPO.[30] In comparison, the biocatalytic process presented here is selective for the oxidation of amines and uses molecular oxygen as the stoichiometric oxidant. Thus, this biphasic chemoenzymatic system provides several advantages over traditional approaches to pyrrole synthesis.[23] Following the development of this system, the Castagnolo group was able to apply this same chemoenzymatic reaction process to the synthesis of substituted furans, using a commercially-available laccase and TEMPO in a biphasic medium to oxidize the 2,5-dihydrofuran up to the aromatic furan (see **1.69-1.71**).[31] Catalytic TEMPO was required to initiate electron-transfer to the laccase system, as molecular oxygen alone was not enough to catalyze the laccase-mediated oxidation.[31]

*Copper-catalyzed chemoenzymatic transformations*

Copper-catalyzed processes have been widely utilized for biorthogonal transformations in chemical biology. For example, the copper-catalyzed [3+2] addition between alkynes and azides–known as "click" chemistry–has enabled small molecule-based tagging of biological molecules, including proteins, nucleic acids and other targets in aqueous media and under biologically-relevant conditions.[32-33] As a result of this compatibility with aqueous conditions, the combination of copper- and enzyme-catalyzed transformations in one-pot systems has also found success.[34-37]

For example, Omori and coworkers developed a cascade reaction that combined a stereoselective enzyme-catalyzed reduction of azide-containing ketone **1.72** with a copper-catalyzed click reaction with various alkyne partners (Figure 1.8A, **1.72-1.74**).[34] The ketoreductase activity demonstrated in this cascade was developed using a known reaction between ketones and reductase-producing endophytic bacteria that reside in the root of carrots (*D. carota*).[34] The transformation provided an

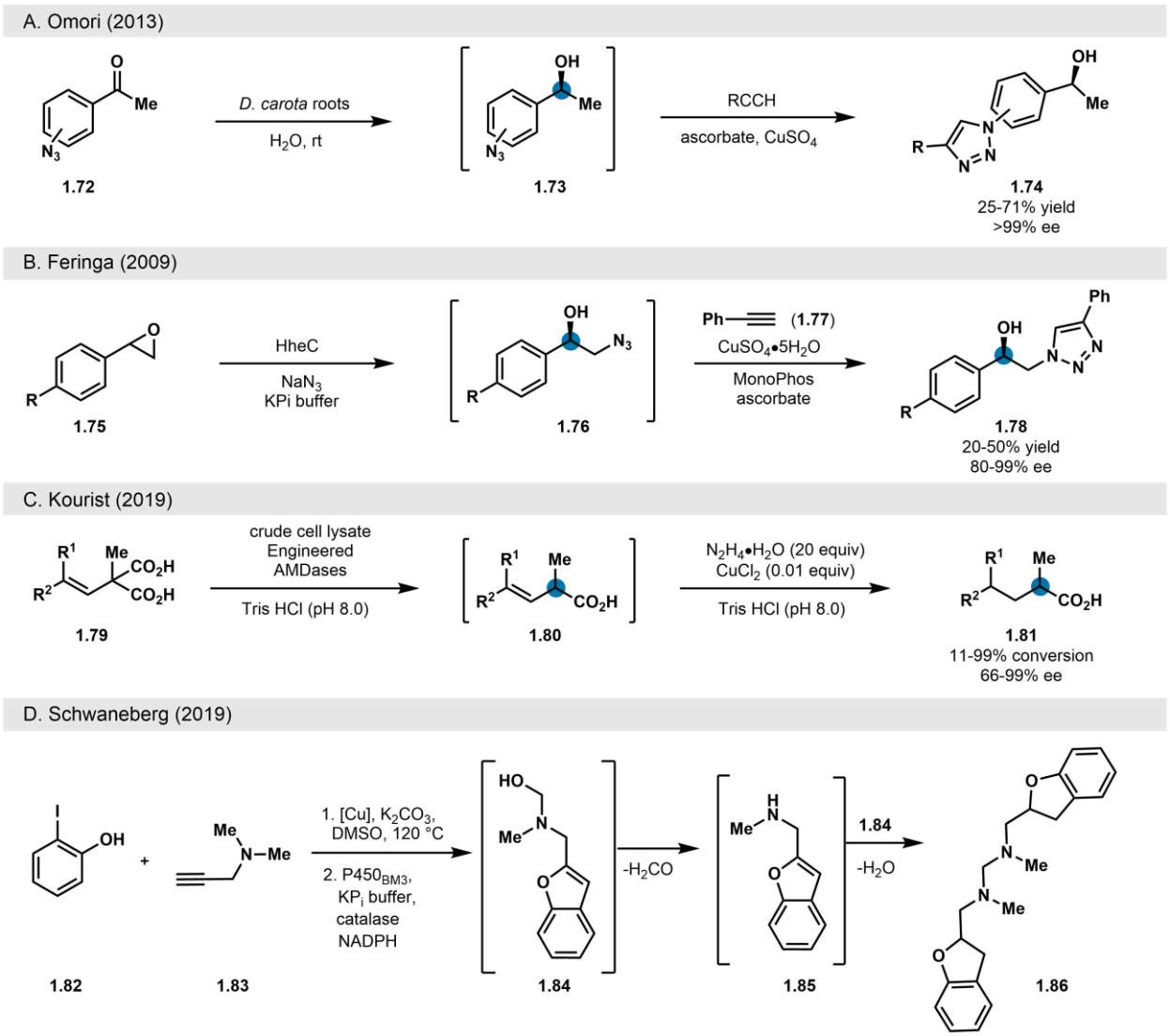


**Figure 1.8. Copper-catalyzed reactions paired with biocatalytic processes.**
A. Enzymatic reduction of ketones by endophytic bacteria in carrot roots paired with "click" reactions. B. Enzymatic asymmetric epoxide opening paired with "click" reactions. C. Biocatalyst-mediated decarboxylation, followed by Cu-catalyzed reduction. D. Cu-catalyzed cross-coupling reaction paired with chemoenzymatic dimerization cascade.

inexpensive, scalable and renewable source of reductase that proved compatible with downstream copper-catalyzed "click" reactions. This one-pot transformation delivered enantioenriched benzylic alcohols functionalized with diverse triazoles in moderate to good yields and excellent enantioselectivities.[34] Another one-pot chemoenzymatic reaction using "click" chemistry was coupled with the kinetic resolution of racemic epoxides.[35] Feringa and coworkers showed that halohydrin dehalogenase HceC from *Agrobacterium radiobacter* could stereoselectively deliver nucleophilic azide to epoxides in a non-native reaction, resulting in the formation of enantioenriched benzylic alcohols possessing azide functionalization (see Figure 1.8B, **1.75-1.78**).[35] Copper-catalyzed "click" reactions were simultaneously used to further diversify this scaffold to generate chiral α-hydroxy-triazoles (such as **1.78**) with moderate to good yields and enantioselectivities.[35] These transformations take advantage of the compatibility of "click" chemistry with biological molecules, leveraging these reactions for the rapid synthesis of diverse scaffolds from simple precursors.

Chemoenzymatic processes that utilize copper-catalyzed reactions are not limited to "click" chemistry. Biocompatible transformations involving copper-mediated reductions and cross-couplings have also been recently reported. For example, Kourist and coworkers coupled a one-pot enzyme-catalyzed decarboxylation with a copper-catalyzed alkene reduction to produce enantioenriched 2-methylalkanoic acids (Figure 1.8C, **1.79-1.81**).[36] Engineered arylmalonate decarboxylases (AMDases) catalyzed the initial decarboxylation reaction resulting in the formation of an enantioenriched β,γ-unsaturated carboxylic acid (**1.80**).[36] Previous directed evolution campaigns provided the authors with available AMDase variants that could catalyze the formation of the (*R*)- or (*S*)-enantiomer of the enzyme product.[36] Subsequent copper-catalyzed

diimide reduction of the β,γ-unsaturated carboxylic acid **1.80** resulted in the formation of the fully saturated product with fair to excellent yields and enantioselectivities.[36]

Copper-mediated cross-coupling reactions have also been used in conjunction with enzymatic processes.[37] Schwaneberg and coworkers recently developed a chemoenzymatic synthesis of bis-benzofuran **1.86** using a copper-catalyzed Sonogashira reaction, coupled with a P450-mediated oxidation/formaldehyde elimination reaction to generate a dimerized product.[37] This cascade takes advantage of the ability of $P450_{BM3}$ to perform a site-selective C–H oxidation reaction on methyl groups attached to heteroatoms, effectively demethylating the substrate through the loss of formaldehyde.[37] The hydroxymethyl-amine intermediate **1.84** serves as an electrophile for nucleophilic dimerization with loss of formaldehyde to form the product bis-benzofuran **1.86** in a one-pot process. Schwaneberg and coworkers developed a water-compatible Sonigashira reaction through comparative screening of ligands, with copper scorpionate serving as the ideal system for this transformation and providing the cyclized benzofuran product in quantitative yield.[37] When combined in a one-pot process with $P450_{BM3}$, the dimerized furan was synthesized in good yield over two steps.[37] These reactions illustrate that copper-dependent processes can be combined in a direct manner with biocatalysts to streamline synthetic routes and to perform complex, selective transformations in a single vessel, broadly expanding the scope of accessible chemoenzymatic processes.

*Chemoenzymatic transformations using supramolecular complex chemistry*

Synthetic chemists have long sought ways to mimic the selectivity profiles of enzyme catalysts. In an enzyme, the three-dimensional architecture often dictates the reactivity of a substrate by making a specific portion of the substrate accessible to reactive species. Taking

inspiration from Nature, chemists have sought to control the site- and stereoselectivity of a reaction by mimicking the constraints of an enzyme active site. One way of achieving such selectivity is through the use of supramolecular scaffolds containing reactive transition-metal complexes.[38] This species, known as a host-guest complex, provides a defined three-dimensional cavity in which the substrate can react with a metal catalyst, influencing both the reaction rate and stereochemical outcome of a particular transformation through cavity-substrate interactions.[38] These complexes also serve to sequester reactive transition-metal species, preventing catalyst degradation and side reactions from occurring.[38-39] Furthermore, supramolecular complexes often assist with solubilization of metal complexes containing hydrophobic ligands, generating a water-soluble catalyst mixture.[38-39] These characteristics make supramolecular complexes particularly amenable to one-pot chemoenzymatic reactions, as metal sequestration prevents biocatalyst destruction and allows for reduced biocatalyst loading.[38-39]

Toste and coworkers developed a gallium-based supramolecular scaffold that contained a Au(I)-phosphine complex capable of performing hydroalkoxylation of allenes (Figure 1.9A).[39] This reaction was paired in a one-pot cascade with enantioselective hydrolysis of allene **1.87** to generate the enantioenriched free alcohol **1.88**.[39] Gold-catalyzed cyclization of **1.88** *in situ* generated substituted tetrahydrofuran **1.89** in moderate diastereoselectivity. Toste and coworkers demonstrated that the use of an un-sequestered Au(I)-complex in the presence of a lipase was deleterious to enzyme activity.[39] Au(I)-complexes are particularly reactive with thiol-containing molecules, such as cysteine residues in enzymes, resulting in enzyme degradation. Thus, a gold-catalyzed process would not have been feasible without the use of a host-guest complex, enabling the combination of previously incompatible chemical and biocatalytic processes.[39]

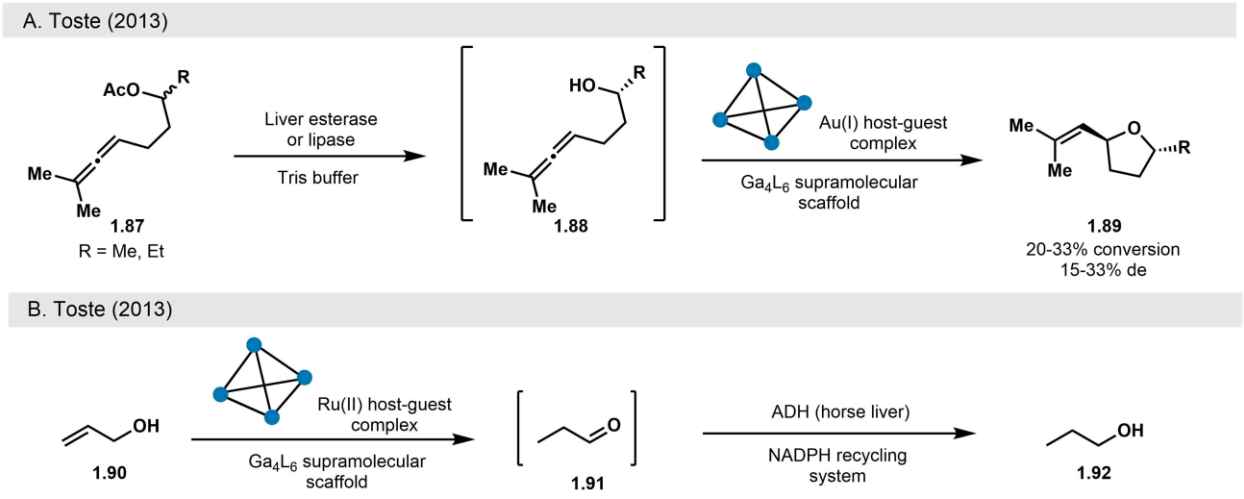


**Figure 1.9. One-pot supramolecular complex chemistry paired with enzymatic reactions.** A. Biocatalytic kinetic resolution of γ-acylated allenes paired with Au-catalyzed hydroalkoxylation. B. Ru-catalyzed isomerization of α,β-unsaturated alcohols paired with biocatalytic aldehyde reduction.

Toste and coworkers also demonstrated that a ruthenium-catalyzed process could be developed using a host-guest complex (Figure 1.9B).[39] This cascade reaction commenced with an initial Ru(II)-catalyzed isomerization of allylic alcohol **1.90**, followed by reduction of the resulting isopropanal (**1.91**) using an alcohol dehydrogenase (ADH) to produce isopropanol (**1.92**).[39] Sequestration of the ruthenium complex again prevented side reactivity with the biocatalyst in this one-pot cascade, delivering isopropanol in a 61% yield.[39] This method provides a means by which enzymatic and transition-metal processes can perform concurrent catalysis with reduced biocatalyst degradation, resulting in more sustainable reaction conditions and direct synthesis of desired products.[39]

*Photocatalytic one-pot chemoenzymatic reactions*

In recent years, photocatalytic systems have enabled highly efficient transformations, particularly when used to mediate transition-metal catalyzed redox processes for catalyst

regeneration.[40-41] While numerous small molecule catalytic processes have been combined with biocatalysts in a one-pot process, photochemical reactions have been generally underexplored in chemoenzymatic cascade reactions. However, the mild conditions employed for numerous photochemical methods make these reactions highly amenable for combination with biocatalytic processes.[40-41] In addition, photocatalytic processes are typically more sustainable than traditional small-molecule catalysis, requiring relatively low catalyst loading and avoiding stoichiometric use of chemical reductants for catalyst turnover.[40-41] Organic photocatalysts have also been used in place of transition-metal complexes and many, such as flavin mononucleotide (FMN), are derived from bio-renewable sources, improving the sustainability profile of the reaction.[40]

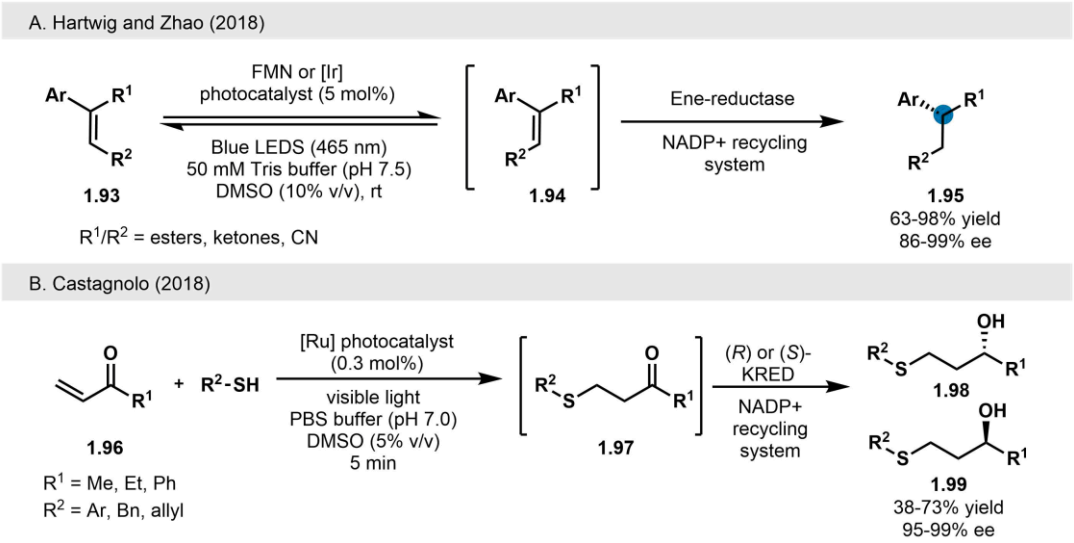


**Figure 1.10. Photocatalytic reactions paired with enzymatic reactions.**
A. Photocatalytic alkene isomerization paired with asymmetric biocatalytic alkene-reduction. B. Photocatalyzed Michael addition paired with KRED-catalyzed ketone reduction.

Hartwig, Zhao and coworkers developed a cooperative photo-chemoenzymatic method for the stereoconvergent reduction of alkene mixtures using ene-reductases (ERs) (Figure 1.10A).[40] Numerous ERs have been characterized and shown to catalyze the reduction of only the *E*-isomer

of alkenes.[42] Hartwig and Zhao designed a cooperative chemoenzymatic cascade reaction in which photocatalytic isomerization of alkenes would generate substrates for biocatalytic reduction by ERs (**1.93-1.95**).[40] The photoisomerization reaction could be carried out with FMN or using an iridium photocatalyst in the presence of blue LED lights. This reaction design "funnels" mixtures of isomeric alkenes in a reversible photoisomerization reaction toward formation of *E*-isomer substrates that could be accepted as substrates by ERs for non-reversible reduction, leading to the stereoconvergent synthesis of enantioenriched benzylic alkyls in moderate to excellent yields and high enantioselectivities.[40]

In another example, Castagnolo and coworkers designed a one-pot chemoenzymatic route featuring a photocatalytic thio-Michael reaction paired with KREDs to access enantioenriched 1,3-mercaptoalkanols (Figure 1.10B).[41] A ruthenium photocatalyst was utilized under visible light conditions to couple various thiols and α,β-unsaturated ketones to form 1,3-mercaptoketones (see **1.97**) as substrates for *R*- or *S*-selective KREDs.[41] This cascade resulted in the direct generation of volatile sulfur compounds (VSCs), such as **1.98**, that are commonly used in food flavoring.[41] Enantiomers of VSCs can be distinguished through olfactory senses, as one enantiomer often has a pleasant smell or taste, while the other is unpleasant.[41] As a result of olfactory distinction, precise enantioselective control over the synthesis of VSCs is critical for producing the desired effects. This chemoenzymatic approach provides a sustainable and highly selective platform for VSC synthesis with a variety of thiol and ketone functionalities, leading to improved control over olfactory characteristics.

*Chemoenzymatic synthesis and modification of aldehydes and ketones*

Aldehydes and ketones have long been utilized as an important synthetic handle in the synthesis of complex molecules. In order to take advantage of the synthetic utility of this group, several one-pot chemoenzymatic methods have drawn on the generation and functionalization of an aldehyde as a key step in the reaction sequence.[43-45] In these examples, the aldehyde or ketone serves as an intermediate in further diversification of the molecule of interest through a one-pot cascade. For example, Gröger and coworkers developed a chemoenzymatic cascade that commences with a Wacker oxidation of styrenes, followed by enantioselective reduction using an alcohol dehydrogenase (ADH) to deliver the corresponding benzylic alcohol in moderate yields and excellent enantioselectivity (Figure 1.11A, see **1.100-1.102**).[43] This synthesis allows for direct, one-pot access to chiral benzylic alcohols from commercially-available styrenes.

Faber and coworkers also developed a modular chemoenzymatic reaction to generate benzylic alcohols (Figure 1.11B).[44] Galactose oxidase from *Fusarium* NRRL 2903, together with horseradish peroxidase and the reductant 2,2′-Azino-bis(3-ethylbenzothiazoline-6-sulfonic acid) diammonium salt (ABTS) to degrade hydrogen peroxide, catalyzes chemoselective oxidation of primary benzylic alcohols to the corresponding benzaldehyde (**1.104**).[44] Following enzymatic generation of the aldehyde *in situ*, an indium-catalyzed allylation was performed to generate racemic substituted benzylic alcohols (**1.105**).[44] These methods provide a direct synthesis of benzylic alcohols from commercial starting materials in a one-pot fashion, illustrating the advantages of chemoenzymatic methods in catalyzing chemo- and stereoselective chemical transformations.

In addition to serving as synthetic handles for aldol reactions, aldehydes can also be modified through the condensation of hydroxylamine to form an aldoxime.[45] These compounds serve as useful synthetic intermediates and can be transformed into amides through a Beckmann

rearrangement, reduced directly to form amines, or dehydrated to form nitriles.[45] Molinari and coworkers developed a chemoenzymatic one-pot procedure for the synthesis of aldoximes using whole-cell biotransformations with acetic acid bacteria (Figure 1.11C).[45] A strain of *Gluconobacter oxydans* was used to perform oxidation of 2-phenylethanol (**1.106**) to 2-

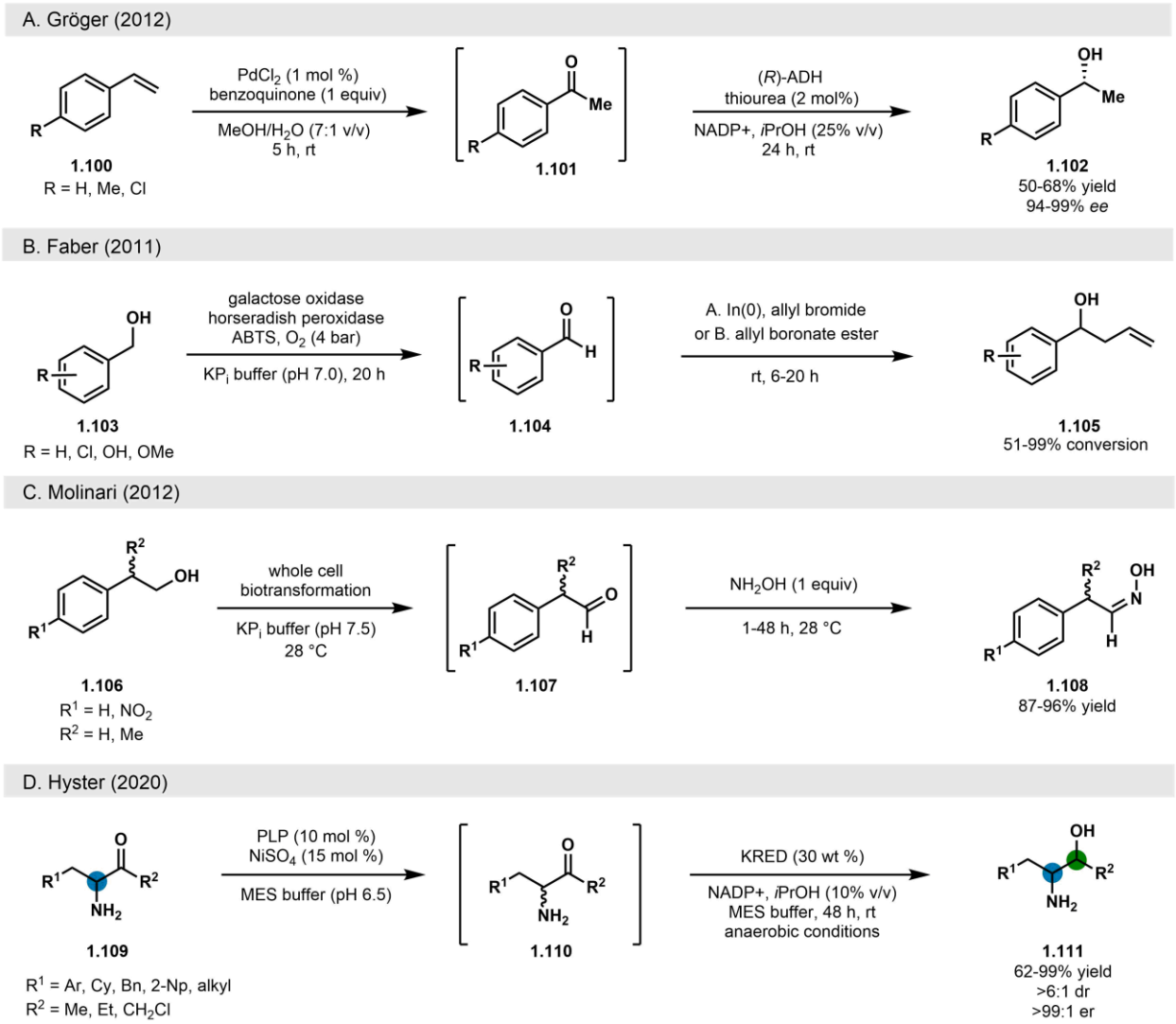


**Figure 1.11. Chemoenzymatic one-pot synthesis and modification of aldehydes and ketones.** A. Pd-catalyzed Wacker oxidation paired with asymmetric biocatalytic reduction. B. Biocatalytic oxidation of benzylic alcohols paired with chemical allylation. C. Biocatalytic oxidation of alcohols paired with amine condensation to generate aldoximes. D. Pyridoxal phosphate-catalyzed racemization of α-aminoketones paired with KRED-catalyzed reduction.

phenylacetaldehyde (**1.107**). The aldehyde species generated *in situ* then underwent a condensation reaction with hydroxylamine to directly produce oxime **1.108**.[45] This process was optimized for biocatalyst loading, reaction temperature, and hydroxylamine loading to generate aldoximes, such as **1.108**, in good yield.[45] This one-pot procedure demonstrates the ability of chemoenzymatic processes to directly generate synthetic handles for the streamlined synthesis of complex molecules. Furthermore, acetic acid bacteria are widely used in industrial fermentation processes, providing a highly scalable biotransformation for the direct synthesis of aldoximes.

Stereoenriched 2-aminoalcohols are a common motif in a wide variety of pharmaceuticals and their derivatives.[46] The development of small molecule-based methods which provide access to all of the possible stereoisomers is challenging, owing to the requirement for extensive catalyst development for each desired transformation. Hyster and colleagues recently developed a one-pot chemoenzymatic approach to address these challenges, featuring pyridoxal phosphate (PLP)-catalyzed racemization of the α-amino stereocenter, followed by stereoselective reduction by KREDs to deliver all four possible stereocenters in an enzyme-dependent fashion (Figure 1.11D).[46] The use of PLP in this reaction sequence reduces the pKa of the α-amino proton by many orders of magnitude, allowing deprotonation to proceed at near-physiological pH and enabling concomitant use of KREDs in a one-pot kinetic resolution process (see **1.109**-**1.110**). In addition, numerous screened KREDs exhibited both enantio- and diastereoselectivity in the reduction process, leading to the selective synthesis of all possible α-aminoalcohols (see **1.110**-**1.111**).[46]

*Chemoenzymatic processes using lipases*

Lipases are critical metabolic enzymes for the hydrolysis of lipids to form free fatty acids, enabling the metabolism of these molecules in various organisms.[47] Lipases have also served as

highly efficient biocatalysts for scalable industrial processes.[47] In particular, these enzymes can be leveraged as enantioselective hydrolytic biocatalysts, delivering a particular stereoisomer selectively by allowing the simple kinetic resolution or dynamic kinetic resolution (DKR) of a racemic mixture.[48]

Bisogono and coworkers developed a novel chemoenzymatic multicomponent reaction (MCR) for the synthesis of β-thioketones (Figure 1.12A).[49] A β-haloketone (**1.112**) was combined with a thioketone salt (**1.114**) and an alkyl halide (**1.113**) under basic conditions to directly form the acylated vinylogous thiol **1.115**.[49] Following the addition of Tris buffer, the commercially-available lipase B from *Candida antarctica* (CAL-B) was used to hydrolyze the acyl group to

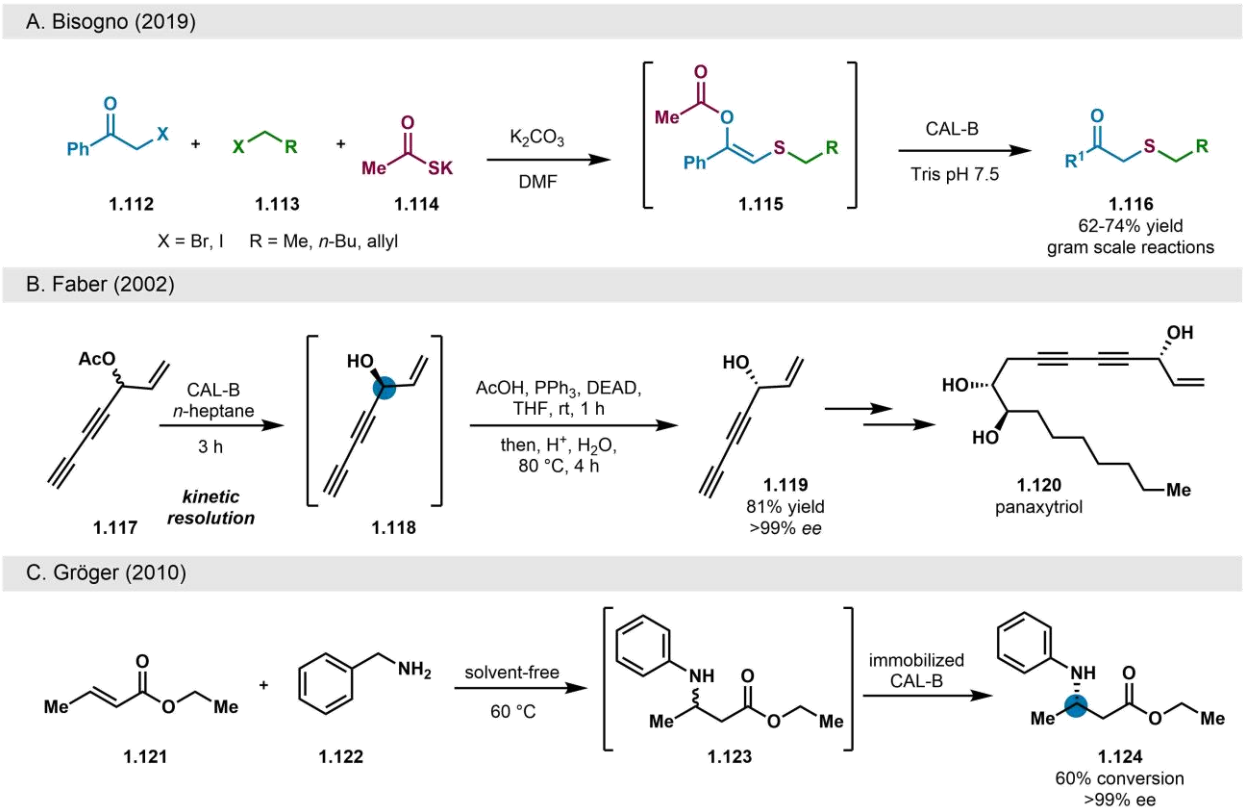


**Figure 1.12. Lipase-catalyzed chemoenzymatic transformations.**
A. Multicomponent reaction (MCR) paired with lipase-catalyzed diacylation. B. Lipase-catalyzed kinetic resolution of α-hydroxyalkynes paired with *in situ* Mitsonobu reaction in the synthesis of panaxytriol. C. Michael addition paired with lipase-catalyzed kinetic resolution of β-aminoesters.

generate β-thioketones, such as **1.116**, in good yields.[49] This one-pot process represents a rare use of MCR within the context of a chemoenzymatic platform and demonstrates the ability of CAL-B to work within complex reaction mixtures. In addition, this reaction can be performed on a gram scale to generate large quantities of β-thioketone products.[49]

Faber and coworkers also leveraged CAL-B for the selective synthesis of complex molecules (Figure 1.12B).[50] In particular, they aimed to develop a chemoenzymatic synthesis of the acetylenic natural product panaxytriol (**1.120**), which has been employed in traditional Japanese medicine for a variety of maladies and has documented anti-cancer activities.[50] They sought to stereoselectively construct allylic alcohol fragment **1.119** through CAL-B-catalyzed de-acylation of racemic acylated material (**1.117**).[50] Kinetic resolution using CAL-B resulted in a selective synthesis of **1.118** with the *R*-conformer generated by the enzyme in the native reaction. However, the natural product configuration is *S* at this stereocenter, requiring a stereoinversion step achieved by performing an *in situ* Mitsonobu reaction on alcohol **1.118**.[50] This final step generated the required stereochemistry for the allylic alcohol fragment which was carried forward in the total synthesis of panaxytriol (**1.120**).[50]

β-amino acids are critical synthetic building blocks in the construction of pharmaceuticals and natural products.[51] Therefore, methods to build these molecules stereoselectively, sustainably and on an industrial scale are vital to the efficient synthesis of drug molecules containing these moieties. Gröger and coworkers sought to develop a one-pot chemoenzymatic route for the synthesis of β-amino acids, taking advantage of the stereo-specific nature of the lipase CAL-B to achieve the selective synthesis of a single enantiomer (Figure 1.12C).[52] Their cascade commenced with Michael addition of benzylamine (**1.122**) to an α,β-unsaturated ester (**1.121**), generating the racemic β-amino acid product **1.123**.[52] Immobilized CAL-B was then employed for selective

aminolysis of the *R*-enantiomer of the β-amino acid, leaving the *S*-enantiomer untouched as the product (**1.124**).[52] This kinetic resolution step could be repeated to achieve good conversion of the *S*-enantiomer with excellent enantioselectivity. The immobilized enzyme could also be efficiently recycled up to four times, demonstrating the sustainability of this system for the synthesis of chiral building blocks.[52]

*Chemoenzymatic modification of nitrogen-containing compounds*

Nitrogen-containing compounds are key components of pharmaceuticals and natural products.[53] Novel methods for modification of these compounds are critical for the development of efficient synthetic routes. Toward this end, chemoenzymatic processes possess distinct advantages for the direct synthesis of nitrogen-containing complex molecules and building blocks. For example, Poelarends and coworkers demonstrated that γ-aminobutyric acids (GABAs) could be synthesized directly and selectively using a chemoenzymatic one-pot route.[53] GABAs are a common motif in pharmaceutically-active compounds used in pain management and are therefore highly attractive targets for the development of efficient and sustainable syntheses. 4-oxocrotonate tautomerase (4-OT) was previously shown to perform Michael addition of enolates to nitroalkenes with moderate enantioselectivity.[53] In their efforts to improve this known transformation, Poelarands and coworkers undertook a protein evolution campaign, developing a 4-OT capable of catalyzing highly enantioselective Michael addition of acetaldehyde (**1.125**) to nitroalkenes (**1.126**), generating nitro-aldehyde compounds (**1.127**) with exquisite selectivity (Figure 1.13A).[53] The evolved "Michaelase" was then paired in a cascade process with an alcohol dehydrogenase, which catalyzed chemoselective oxidation of the aldehyde to produce γ-nitrobutyric acids

(**1.128**).[53] Following this two-enzyme cascade, a water-compatible nitro reduction was performed using $NiCl_2$ and $NaBH_4$, yielding the target GABA compound (**1.128**).[53] A variety of pharmaceutically-active GABAs were produced using this method in moderate to good yields and with excellent enantioselectivities.[53] This method represents a significant advancement in the efficient and sustainable synthesis of GABAs, laying the groundwork for chemoenzymatic industrial applications.

The enantioselective synthesis of organic building blocks is essential for improving the efficient construction of pharmaceuticals and natural products. Such efficiency can be improved by the development of novel methods to build these organic moieties in a direct and highly

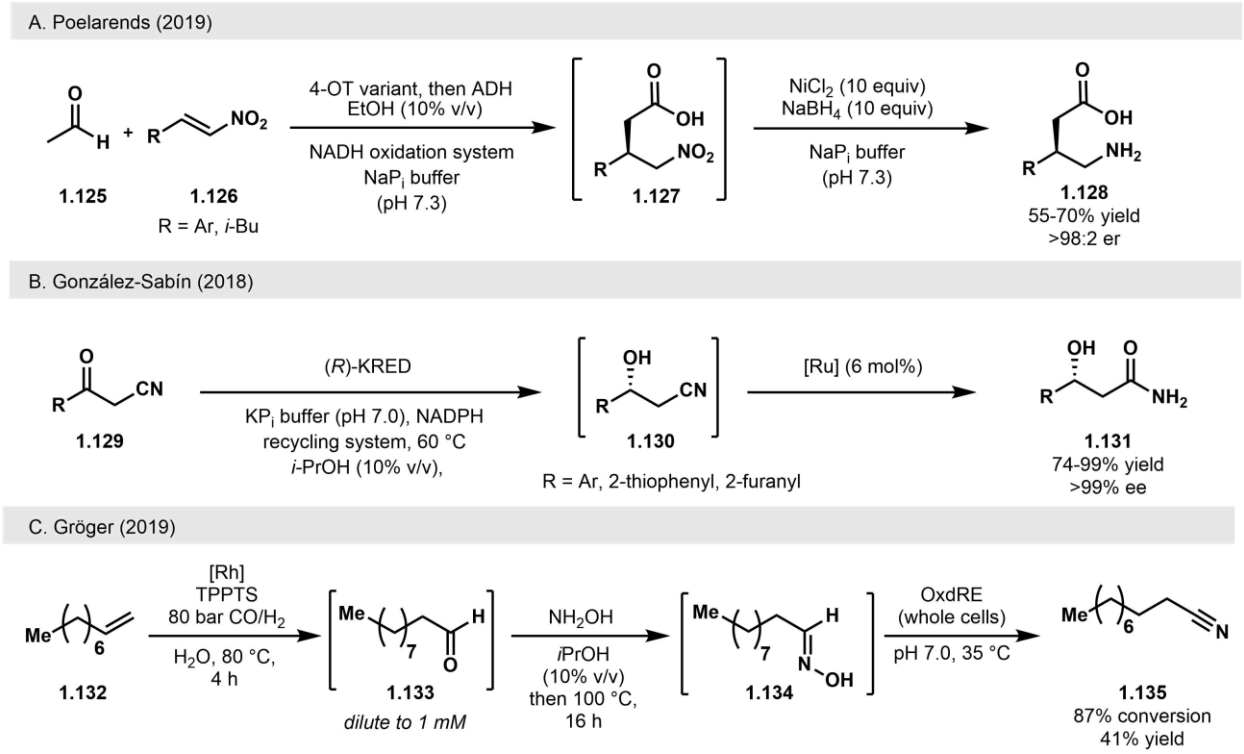


**Figure 1.13. Chemoenzymatic modification of nitrogen-containing compounds.**
A. Addition of acetaldehyde to nitroalkenes catalyzed by engineered "Michaelase" paired with *in situ* oxidation catalyzed by alcohol dehydrogenase. *In situ* nitro reduction using nickel and sodium borohydride completes the synthesis of GABAs. B. KRED-catalyzed asymmetric reduction paired with Ru-catalyzed nitrile oxidation. C. Rh-catalyzed hydroformylation paired with amine condensation and aldoxime dehydratase elimination to form alkylnitriles.

selective fashion.[54] Gonzalez-Sabin and coworkers sought to construct optically-active β-hydroxyamides (such as **1.131**) through enantioselective biocatalytic reduction of α-cyanoketones, utilizing a KRED to generate the desired *R*-enantiomer of alcohol **1.130** (Figure 1.13B).[54] In cascade with the biocatalytic reaction, they leveraged a water-stable ruthenium catalyst to perform a concomitant hydration and transfer hydrogenation, directly producing the desired β-hydroxyamide **1.131** with good yields and excellent enantioselectivities.[54] The use of a ruthenium catalyst in cascade with a biocatalyst represents a rare transformation amongst one-pot chemoenzymatic processes.[54] Their efforts demonstrated that a phase-separated or compartmentalized catalyst was not necessary for these types of systems, leaving open the possibility for new reaction development in this area.

The advantages of chemoenzymatic one-pot reactions are not limited to the synthesis of complex molecules and pharmaceuticals. The merits of these transformations can also be applied to the production of bulk chemicals.[55] For example, long-chain alkyl nitriles have become essential commodity chemicals used as solvents, and in the synthesis of quaternary amine surfactants.[56] As a result, the development of new methods for synthesizing these compounds is critical for improving the sustainability and safety profiles of these transformations. Gröger and coworkers sought to take on this challenge and develop a chemoenzymatic route for the synthesis of long-chain nitriles, particularly *n*-nonanenitrile (Figure 1.13C, **1.135**).[55] Their synthetic route commenced with rhodium-catalyzed hydroformylation of octene (**1.132**) under aqueous conditions to produce nonanal (**1.133**).[55] Following this reaction, the product solution was diluted to 1.0 mM for downstream enzymatic reactions. Hydroxylamine was then added to the solution, resulting in condensation with aldehyde **1.133**, generating the aldoxime species **1.134**.[55] An aldoxime dehydratase suitable for catalyzing elimination of **1.134** was identified through screening of a set

of five homologous enzymes. The chosen biocatalyst, OxdRE, was then added in a whole-cell format to the reaction mixture, producing *n*-nonanenitrile (**1.135**) in high conversion and good yield over three steps in a single vessel.[55] This new method avoids safety challenges in using dangerous inorganic cyanides on an industrial scale, thus offering an improved alternative to traditional synthesis of alkyl nitriles.[55]

*Chemoenzymatic methods using Deep Eutectic Solvents (DESs)*

One of the most significant challenges in combining chemo- and biocatalytic processes is the incompatibilities between the reaction conditions required for the chemical and biocatalytic steps.[7, 21] For example, destructive cross-reactivity between transition-metal catalysts and a biocatalyst can result in denaturation of the enzyme.[7, 21] In the same vein, transition-metal catalysts often do not perform well in the aqueous environments required for biocatalysts and may require a phase-separated system to avoid catalyst poisoning by water.[7, 21] This challenge can limit the overall scope of chemo- and biocatalytic transformations that can be combined in a one-pot process. Therefore, the development of novel systems that can overcome these limitations enables highly efficient one-pot chemoenzymatic transformations with improved catalytic parameters. In recent years, systems utilizing deep eutectic solvents (DESs) have been explored for chemoenzymatic reactions featuring water-sensitive transition-metal catalyzed transformations.[57]

DESs are solvent-salt mixtures that typically feature a hydrogen bond accepting quaternary ammonium salt, such as choline chloride (ChCl), and a hydrogen bond donor, such glycerol or saccharides.[57] These solvent systems have been utilized for transition-metal catalyzed reactions in recent years, improving the solubility of organometallic catalysts under aqueous conditions, eliminating the need for organic cosolvents and resulting in a more sustainable reaction profile.[57]

DESs also improve the efficiency of aqueous transition-metal catalysis by reducing water-related catalyst destruction, further improving the sustainability of these reactions. These reaction profile improvements are well-suited to chemoenzymatic processes, eliminating the need for biphasic reaction systems or organic cosolvents in combining chemical and biocatalytic steps in a one-pot system.[57]

Taking advantage of the improved characteristics of a DES-based system, Gröger and coworkers developed a one-pot chemoenzymatic reaction platform featuring a DES system containing ChCl and glycerol with a phosphate buffer (Figure 1.14A).[58-59] Under DES reaction conditions, they performed a Suzuki-Miyaura cross-coupling reaction to generate a biphenyl

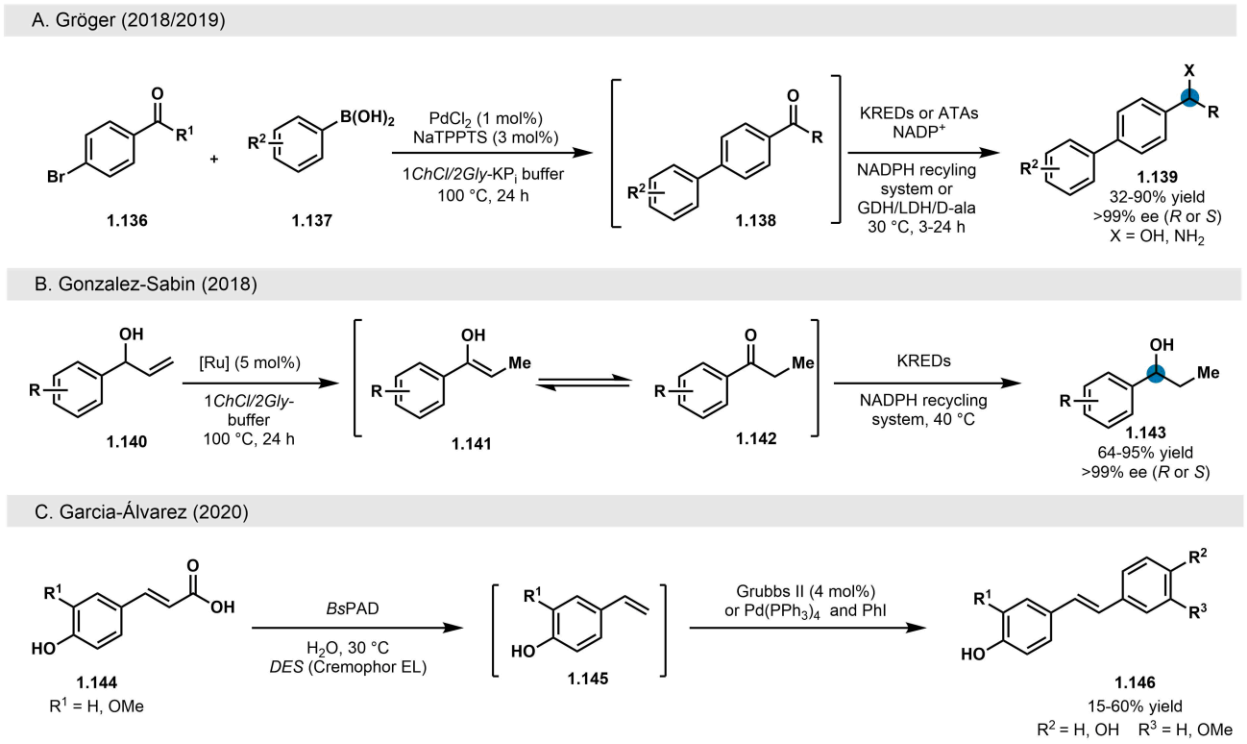


**Figure 1.14. Chemoenzymatic one-pot reactions performed in deep eutectic solvents (DESs).** A. Suzuki-Miyaura cross coupling paired with KRED-catalyzed reduction or transaminase-catalyzed reductive amination. B. Ru-catalyzed alkene isomerization paired with KRED-catalyzed asymmetric reduction. C. Enzyme-catalyzed decarboxylation paired with Ru-catalyzed olefin metathesis or Heck cross-coupling.

ketone (such as **1.138**), coupled in a modular fashion with KREDs or transaminases to deliver enantioenriched benzylic amines or alcohols in moderate to good yields (see **1.139**).[58-59] The enantioselectivities achieved in these reactions were tuned by screening a library of reductive enzymes to give the desired enantiomer, providing a one-pot system for accessing all possible enantiomers of the resulting benzylic functionalized species.[58-59]

Gonzalez-Sabin and coworkers also developed a system utilizing a DES system to perform a ruthenium-catalyzed alkene isomerization of an allylic alcohol to generate a benzylic ketone (Figure 1.14B, see **1.140**-**1.143**).[60] Reduction using KREDs resulted in the formation of enantioenriched benzylic alcohol (such as **1.143**) in moderate to good yields and excellent enantioselectivities.[60] Notably, this reaction was performed in a cascade format and did not require a biphasic reaction mixture to prevent water-related destruction of the ruthenium catalyst. This catalyst behavior demonstrates the potential for DESs to allow previously incompatible chemical and biocatalytic processes in a single vessel and under mild, sustainable conditions.[60] Garcia-Alverez and coworkers built upon this work to develop a chemoenzymatic cascade reaction featuring an enzyme-catalyzed decarboxylation of α,β-unsaturated acids (such as **1.144**) to produce styrenes (Figure 1.14C, **1.145**).[61] An immobilized phenolic acid decarboxylase from *B. subtilis* (*Bs*PAD) was used to efficiently generate styrenes in the DES environment.[61] The biocatalyst-generated styrenes were then subjected to olefin metathesis using Grubbs 2$^{nd}$ generation catalyst to deliver substrate dimers, or a Heck cross-coupling to generate unsymmetrical aromatic olefins (see **1.146**).[61] These transformations were achieved in a one-pot process, demonstrating the versatility of DES environments in permitting diverse chemoenzymatic processes without the requirement of volatile organic cosolvents or biphasic reaction mixtures.[61] Efforts to develop novel systems for one-pot chemoenzymatic transformations have great potential to broaden the scope of

feasible chemical and biological transformations that can be combined in a single vessel. Such discoveries facilitate the removal of the barriers that prevent widespread adoption of chemoenzymatic processes in synthetic routes, leading to more efficient and sustainable syntheses.

*Chemoenzymatic polymer synthesis*

As the demand for synthetic materials continues to increase, the efficient and economical synthesis of polymers continues to be of great importance.[62-63] The search for more sustainable and environmentally-friendly polymerization methods has made enzymatic catalysis an attractive option. In particular, chemoenzymatic cascades for polymerization possess numerous desirable characteristics for sustainable synthesis, including: 1) robust and selective biocatalytic reactions; 2) the ability to recycle and immobilize biocatalysts; 3) elimination of metal-based catalysts from the reaction process and 4) reduced chemical waste.[62-63] Cascade reactions of this nature have used lipases as catalysts for ring-opening polymerization as well as to modify polymer building blocks

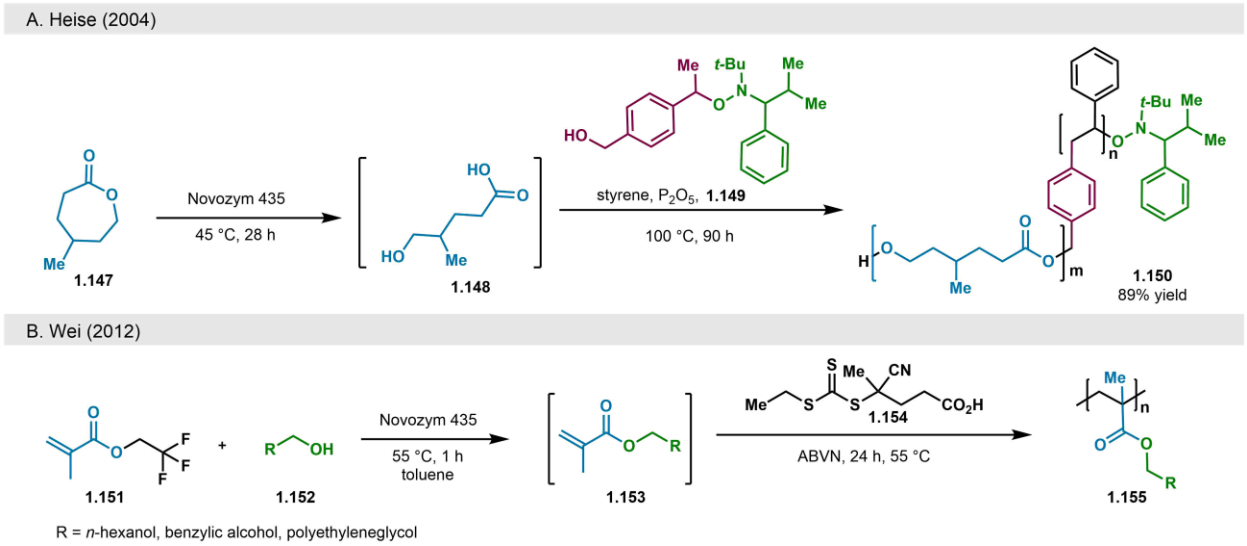


**Figure 1.15. Chemoenzymatic one-pot polymerization reactions.**
A. Lipase-catalyzed ring-opening of ε-caprolactone and *in situ* polymerization with styrene using a dual-headed radical initiator in living free radical polymerization (LFRP). B. Lipase-catalyzed monomer diversification and atom transfer radical polymerization (ATRP) with methacrylates.

before polymerization. As mentioned previously, lipases are a class of enzymes that primarily hydrolyze esters to yield free alcohols. Many of these biocatalysts have been well-studied, engineered, and commercialized as highly robust catalysts that are tolerant to both heat and organic solvents.[47] In addition, some lipases can be immobilized, rendering a recyclable biocatalyst for use in industrial processes. As a result, lipases represent a highly targeted class of enzymes for industrial biocatalysis, including polymer synthesis.

Heise and coworkers took advantage of the sustainable aspects of lipase-catalyzed reactions by developing the first one-pot chemoenzymatic polymerization cascade (Figure 1.15A).[63] Using the commercial lipase Novozym 435, they achieved hydrolysis of 4-methyl-ε-caprolactone (**1.147**) to generate free acid **1.148**.[63] Nitroxide **1.149** was then used as a dual-headed radical initiator in living free-radical polymerization (LFRP) to induce polymerization of styrene and form the non-ester portion of the polymer.[63] Simultaneously, esterification and polymerization of the benzylic alcohol portion of the nitroxide initiator **1.149** resulted in the formation of a polymeric chain of aliphatic esters from the lipase-generated free acid **1.150**. While this cascade was performed in one pot, precise control could be exerted over the polymerization process by changing the reaction temperature.[63] Homolysis of nitroxide **1.149** does not occur until temperatures exceed 90 °C, preventing cross-reactivity challenges of rapid LFRP in the presence of the biocatalyst. In addition, control of polymer composition can be achieved by adjustment of the reaction temperature as the reaction stoichiometry changes during the operation.[63] This optimization delivered a highly sustainable polymerization reaction combining chemo- and biocatalysis in a single vessel and improved on previous efforts using sequential enzymatic and chemical reactions.[64]

Lipases, such as Novozym 435, have also been used to modify the monomeric subunits of polymers in cascade reactions. Wei and coworkers leveraged the hydrolytic abilities of Novozym 435 to perform transesterification of trifluoroethyl ester **1.151** in the presence of various alcohols to generate new methacrylate monomers (Figure 1.15B, **1.153**).[62, 65] As new monomers were formed during the enzymatic reaction, radical initiator (2-bromoisobutyrate) was added to induce polymerization between the newly formed methacrylate monomers (**1.153**) and trifluoroethylmethacrylate (**1.151**). This polymer composition generated by this atom transfer radical polymerization process could thus be controlled by monitoring the progress of the enzymatic reaction and inducing polymerization when monomer composition was ideal.[65] Careful kinetic analyses of both the enzymatic and chemical processes led to idealized conditions for the desired final polymer composition. A variety of alcohols were screened in this process, including aliphatic alcohols, benzylic alcohols, and glycols, yielding several functional polymers with distinct properties.[65] Thus, this one-pot chemoenzymatic process provided a highly tunable and sustainable method for the direct synthesis of complex polymers.

*Chemoenzymatic synthesis of tetrahydroisoquinolines*

Tetrahydroisoquinoline (THIQ) is a common core in a variety of biologically-active natural products and pharmaceuticals with antitumor and antiparasitic activities.[66] The development of one-pot chemoenzymatic methods for building diverse THIQ cores has been explored extensively by numerous groups in order to rapidly generate libraries of these compounds.[66] The biosynthesis of norcoclaurine, a plant natural product that has been used in ancient Chinese medicine, provided inspiration for the development of novel chemoenzymatic routes to access these compounds.[67] In particular, the final biosynthetic step involves a stereoselective Pictet-Spengler reaction catalyzed

by the Pictet-Spenglerase (PSase) known as norcoclaurine synthase (NCS).[67-68] In contrast, small molecule-based synthetic approaches require the use of chiral transition-metal catalysts to selectively produce the natural product scaffold.[68] Macone and coworkers leveraged NCS for one-pot synthesis of (*S*)-norcoclaurine from the renewable feedstock L-tyrosine (Figure 1.16A, **1.156**-**1.158**).[68] This approach allows for *in situ* generation of aldehyde **1.157**, which tends to polymerize in aqueous solutions and thus, must be generated and used quickly.[68] Aldehyde **1.157** was produced directly by oxidative decarboxylation of L-tyrosine (**1.156**), using sodium hypochlorite as a stoichiometric oxidant.[68] NCS was shown to be active in the presence of hypochlorite ion, allowing this reaction to be run in a cascade format and generating the natural product in high yield and enantioselectivity. This cascade prevented polymerization of aldehyde **1.157** and oxidation of dopamine that previously plagued attempts to generate (*S*)-norcoclaurine (**1.158**) biocatalytically on a synthetically-tractable scale.[68] Mullowney and coworkers were inspired by this sodium hypochlorite approach in their design of a similar chemoenzymatic route to generate norcoclaurine analogs.[69] Using various tyrosine amino acid analogs, they used hypochlorite-mediated oxidative

decarboxylation to generate aldehydes (Figure 1.16B, see **1.159-1.160**) *in situ*. NCS then catalyzed formation of various norcoclaurine derivatives (see **1.161**) in a highly selective fashion with moderate to good yields through their cascade.[69]

Rother and coworkers developed an alternative chemoenzymatic strategy to access the THIQ core through a cascade reaction (Figure 1.16C).[70] A carboligase from *E. coli* was first used to perform a stereoselective addition of pyruvate to benzaldehyde **1.162**, generating the α-hydroxyketone **1.163** in a highly selective manner.[70] A second stereoselective reductive amination was performed using a transaminase from *C. violaceum*, producing the α-amino-benzylic alcohol **1.164**. A Pictet-Spengler reaction was then performed *in situ* using potassium phosphate as a base

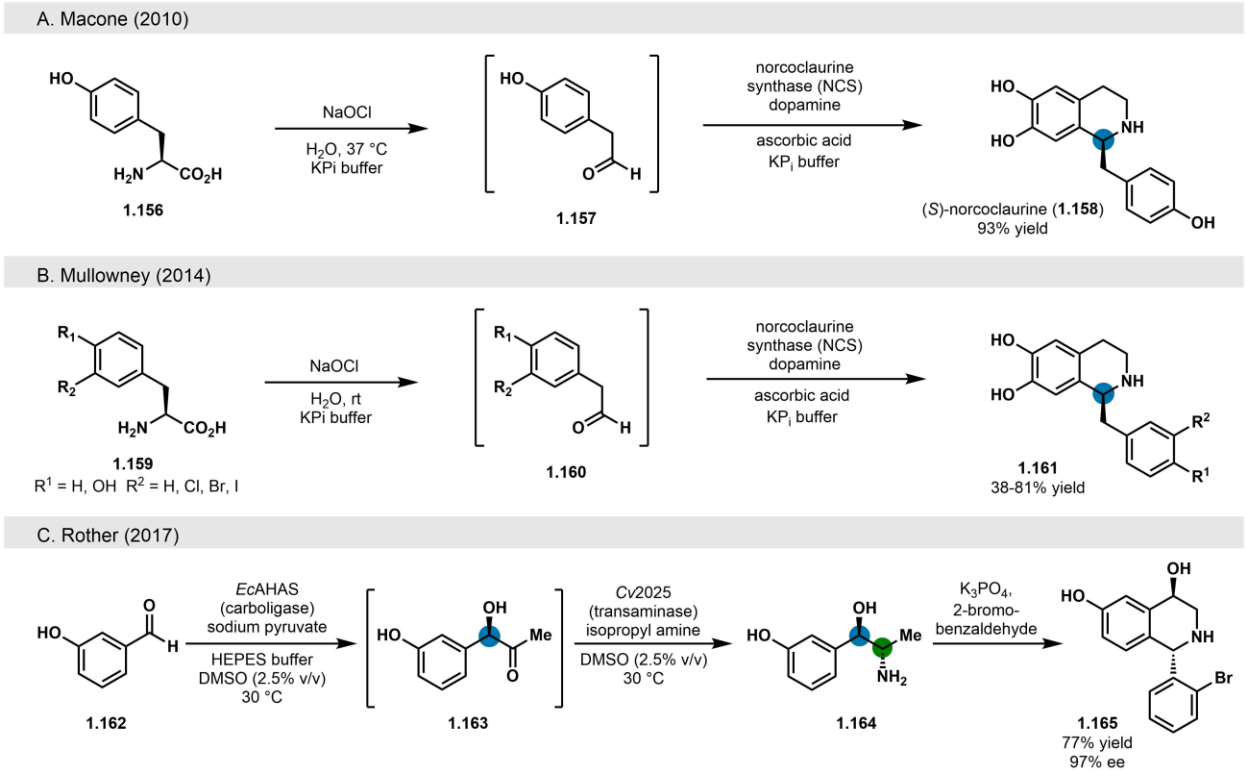


**Figure 1.16. Chemoenzymatic one-pot synthesis of tetrahydroisoquinolines (THIQs).** A. Hypochlorite-mediated oxidative decarboxylation of L-tyrosine paired with asymmetric Pictet-Spenglerase reaction catalyzed by NCS. B. Hypochlorite-mediated oxidative decarboxylation of L-tyrosine analogs paired with asymmetric Pictet-Spenglerase reaction catalyzed by NCS. C. Biocatalytic carboligation and asymmetric reductive amination paired with Pictet-Spenglerase reaction.

and 2-bromobenzaldehyde as the corresponding aldehyde reaction partner. This yielded the THIQ **1.165** in good yield and excellent diastereoselectivity. This approach provides the advantage of pre-arranged, enzyme-derived stereocontrol of the Pictet-Spengler reaction, allowing for the selective generation of THIQ **1.166** in an opposite configuration to that delivered by the native NCS reaction.[70]

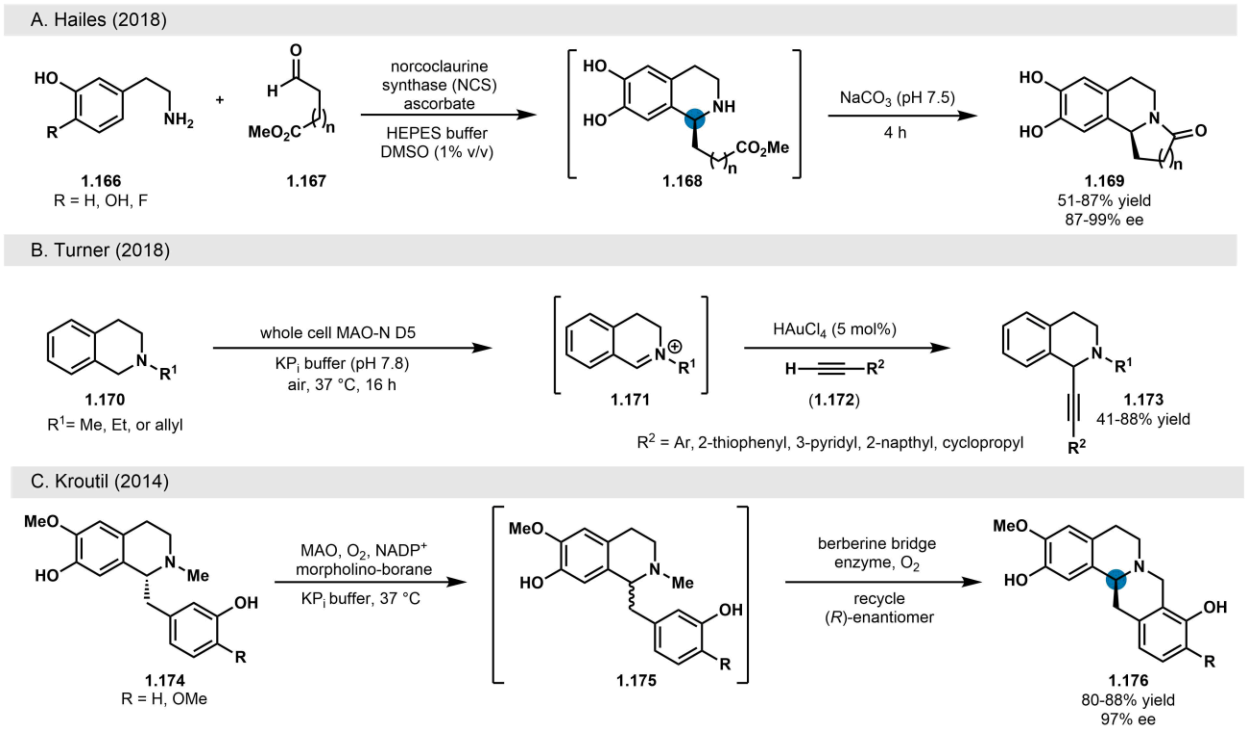


**Figure 1.17. Chemoenzymatic one-pot synthesis of tetrahydroisoquinoline derivatives.** A. NCS-catalyzed asymmetric Pictet-Spengler reaction paired with chemical cyclization to form tricyclic THIQs. B. MAO-catalyzed amine oxidation paired with Au-catalyzed alkyne addition. C. MAO-catalyzed amine oxidation and chemical racemization paired with berberine bridge enzyme oxidative cyclization to form tetraacyclic THIQ scaffolds.

Hailes and coworkers further developed the NCS reaction in a chemoenzymatic cascade to build tricyclic THIQs.[71] Their reaction featured NCS-catalyzed Pictet-Spenger reactions using aldehyde reaction partners containing alkyl chains with terminal methyl esters (Figure 1.17A, **1.166-1.169**).[71] The resulting THIQ products were generated stereoselectively, producing products with pendant alkyl esters located alpha to the amine (**1.168**). Following the enzymatic formation

of THIQs, sodium carbonate was added to induce cyclization and form amide linkages with the free amine of the THIQ (see **1.168**-**1.169**).[71] This reaction resulted in the formation of tricyclic THIQs in moderate to good yields and with good enantioselectivity.

The generation of diverse THIQs through chemoenzymatic cascade is not limited to methods that produce the core scaffold.[72] Turner and coworkers developed a method for α-functionalization of the THIQ core with alkynes that featured site-selective MAO-catalyzed oxidation of the α-position to form an imine (Figure 1.17B, see **1.170**-**1.171**).[72] This was followed by gold-catalyzed nucleophilic addition of alkynes to the MAO-generated imine, resulting in the formation of α-functionalized THIQs. This one-pot process allowed for diversification of THIQs with a variety of alkynes under mild reaction conditions and with precise site-selectivity provided by the enzymatic oxidation. In addition, this method was the first to feature a free gold complex in a concurrent system with a biocatalyst and did not require a modular approach to the reaction.[72]

Processes that improve the stereoselectivity profiles in THIQ synthesis are critical for developing THIQs for pharmaceutical purposes. To this end, enzymatic processes that build THIQs, such as the Pictet-Spenglerase NCS, often only construct a single enantiomer of THIQ, providing precise stereoselectivity in the synthesis of these complex molecules.[67] Kroutil and coworkers leveraged the enantioselectivity of berberine bridge enzyme to construct tetracyclic alkaloids, such as **1.176** (Figure 1.17C).[73] Their chemoenzymatic cascade featured a racemization reaction in which one enantiomer of THIQ **1.174** was oxidized using an MAO, followed by racemic reduction with water-compatible morpholino-borane to generate *rac*-**1.175**.[73] A single enantiomer of compound **1.175** was accepted by berberine bridge enzyme and cyclized to form the enantiopure alkaloid (*S*)-**1.176.** As this process was performed in cascade, the enantiomer (*R*)-**1.175** was continually recycled through oxidation with MAO and reduction with borane, resulting

in the synthesis of (*S*)-alkaloid **1.176** in good yield and excellent enantioselectivities through dynamic kinetic resolution.[73]

*Chemoenzymatic synthesis of reactive intermediates*

Synthetic approaches to natural products often take inspiration from biosynthetic pathways, attempting to mimic the elegance of Nature's ability to rapidly generate complexity from simple building blocks.[74] Toward this goal, biosynthetic intermediates are often targeted as

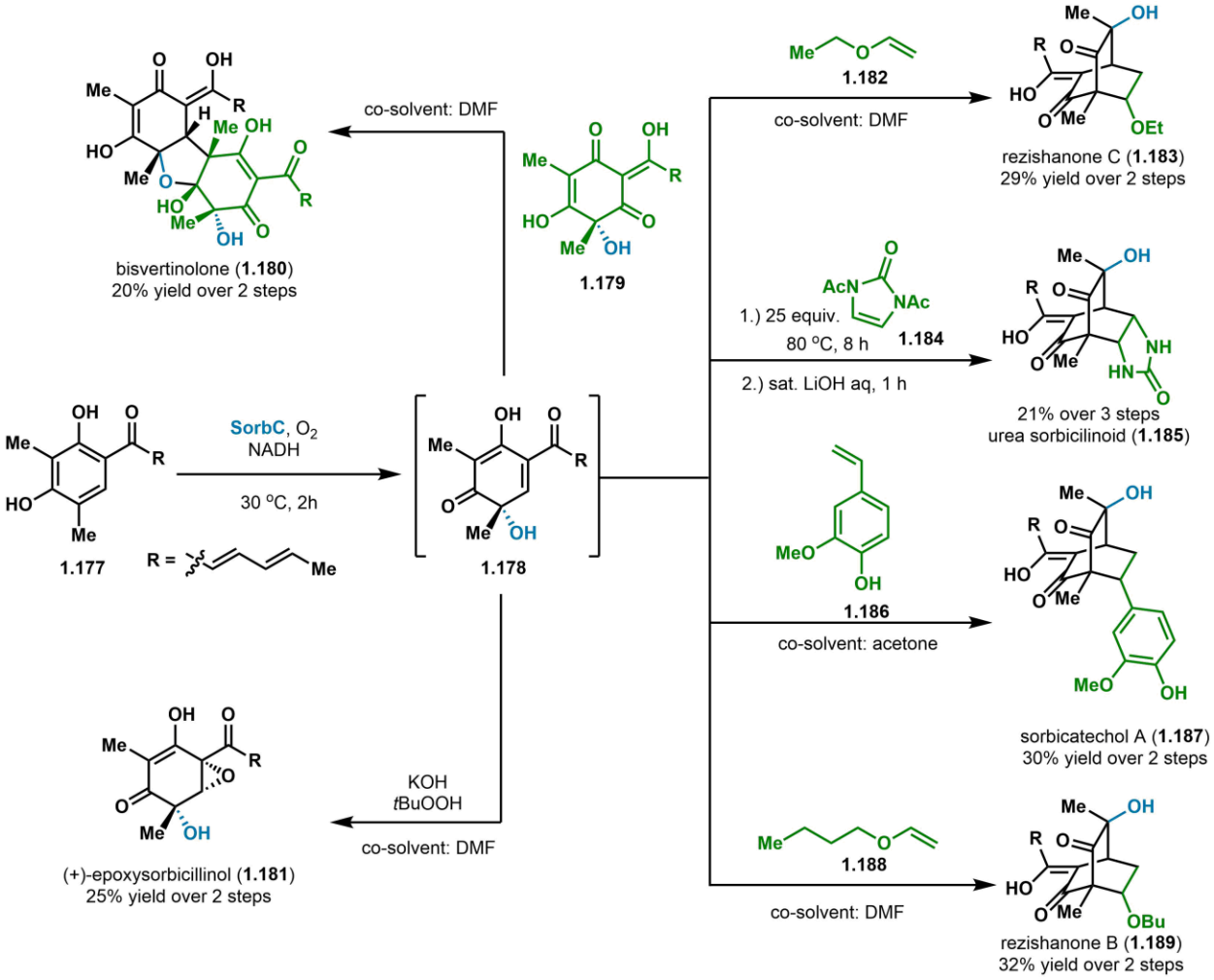


**Figure 1.18. Chemoenzymatic one-pot synthesis and derivatization of *o*-quinols.** SorbC-catalyzed asymmetric oxidative dearomatization of ketones and subsequent derivatization through Diels-Alder, Michael addition/ketalization and asymmetric epoxidation.

intermediates in the total synthesis of natural products.[74] However, accessing biosynthetic intermediates using traditional methods can prove challenging, particularly for highly reactive molecules.

Highly reactive biosynthetic intermediates often represent a branching point for diversification to a variety of natural products. Thus, access to these molecules can set the stage for a divergent approach toward a suite of natural products. One such intermediate, **1.178**, is involved in the biosynthesis of sorbicillinoid natural products, a structurally diverse class of secondary metabolites from fungi which possess numerous biological activities (Figure 1.18).[29] Cox and coworkers identified the enzyme responsible for the generation of this intermediate in the fungus *Penicillium chrysogenum*.[75] This enzyme, SorbC, is a flavin-dependent monooxygenase that natively performs an enantioselective oxidative dearomatization on sorbicillin (**1.177**) or dihydrosorbicillin to generate reactive diene products sorbicillinol (**1.178**) or dihyrosorbicillinol, respectively.[75] These biosynthetic intermediates can be further elaborated through subsequent transformations, including Diels-Alder cycloadditions and Michael addition reactions, to generate bisvertinolone (**1.180**), rezishanone B (**1.189**) and C (**1.183**), (+)-epoxysorbicillinol (**1.181**), and urea sorbicillinoid (**1.185**) among others.[31] Developing a synthetic route that incorporates oxidative dearomatization has great potential for the divergent synthesis of this class of molecules and synthetic analogs.[76-78] However, oxidative dearomatization is a challenging transformation to achieve chemically with site- and stereoselectivity, making it difficult to produce a single desired isomer and reducing the utility of this strategy for selective synthesis of complex molecules.[30-32] Furthermore, the intermediates generated by oxidative dearomatization are highly reactive, rendering their isolation and characterization difficult. To overcome these challenges, our group[79] and others[80-81] have developed chemoenzymatic one-pot approaches toward sorbicillinoid natural

products. In particular, SorbC-catalyzed oxidative dearomatization generates reactive diene **1.178,** which can be further elaborated to sorbicillinoid natural products in a cascade or sequential fashion (Figure 1.18). We performed extensive characterization of the substrate scope of SorbC, demonstrating the structural requirements for productive binding and catalysis and also developed a one-pot chemoenzymatic route to urea sorbicillinoid (**1.185**) through the biocatalytic generation of **1.178**, followed by cycloaddition with biacylated urea **1.184** and deprotection to yield **1.185**.[79] Gulder and coworkers have also demonstrated the power of this chemoenzymatic approach to access numerous sorbicillinoid natural products.[80-81] For example, bisvertinolone (**1.180**) was synthesized by [4+2] cycloaddition with the SorbC-generated dienophile **1.178**, using DMF as a cosolvent. Diels-Alder reactions with vinyl ethers **1.182** and **1.188**, as well as styrene **1.186**, led to the synthesis of rezishanone C (**1.183**), rezishanone B (**1.189**) and sorbicatechol A (**1.187**), respectively.[81] In addition, Gulder and coworkers performed the first enantioselective synthesis of (+)-epoxysorbicillinol (**1.181**) through the epoxidation of intermediate **1.178** *in situ* using Weitz-Scheffer conditions.[81] They note that pre-complexation of the potassium *tert*-butoxide species allows for the addition of the nucleophilic peroxide to the same face as the SorbC-installed hydroxyl group, thus promoting the selective epoxidation of **1.178**.[81] These chemoenzymatic approaches offer significant advantages over existing synthetic routes, including improved enantioselectivity, reduced step count and improved yields.[80-81] Efforts such as these are critical for improving access to these compounds to enable biological studies and the determination of structure-activity relationships.[25-27]

As the field of biocatalysis continues to expand and play a greater role in synthetic chemistry, it is reasonable to expect that the development of innovative one-pot chemoenzymatic processes will likewise see continued growth. In particular, the combination of biocatalytic and

transition metal-catalyzed transformations is representative of this new frontier in biocatalysis. Efforts in this area will likely continue to increase in order to exploit the breadth of transition-metal catalyzed reactions that have been established, broadening the chemical space that can be accessed through chemoenzymatic approaches. Furthermore, the ever-growing repository of annotated natural product biosynthetic pathways will similarly lead to the increasingly strategic use of biosynthetic enzymes to directly generate intermediates toward the synthesis of natural products.[6, 74] A chemoenzymatic approach to the synthesis of complex molecules can provide selectivity, efficiency, and sustainability and, thus, stands to exert a significant influence on the field of complex molecule synthesis.[6] The methods highlighted here demonstrate the power of pairing the selectivity of biocatalytic reactions with subsequent transformations to improve the efficiency and sustainability of a synthesis. As the volume of genome sequences available continues to grow, and new enzymes and transformations are discovered, it is reasonable to expect that the influence of biocatalysis will continue to expand. Chemoenzymatic strategies will play a central role in this expansion, improving the synthetic utility of these transformations and bridging the gap between the traditional synthetic and biocatalysis communities.

### 1.3 Thesis Overview

The following chapters present the development of one-pot chemoenzymatic reaction sequences for the synthesis of natural products, natural product analogs, and other complex molecules. In particular, we used α-ketoglutarate-dependent (α-KG) non-heme iron (NHI) enzymes to catalyze challenging reactions with precise control over chemo- and site-selectivity. These transformations were utilized in reaction sequences featuring chemical steps and directly

deliver products with increased chemical diversity, such as tropolone and chroman natural products.[82] General contributions to the work presented in this thesis are as follows: substrate synthesis was performed in collaboration with Dr. Summer Baker Dockrey, Jonathan Perkins and Evan Romero. X-ray crystal structures presented for TropC were solved by Dr. Leena Mallik and Prof. Markos Koutmos (University of Michigan). Computational calculations were performed in collaboration with Kevin Skinner and Prof. Paul Zimmerman (University of Michigan).

## 1.4 Non-heme iron α-ketoglutarate dependent dioxygenases

*Non-heme iron α-ketoglutarate-dependent dioxygenases*

Non-heme iron (NHI) α-ketoglutarate-dependent (α-KG) dioxygenases are a diverse class of enzymes, responsible for a plethora of oxidative transformations in the context of secondary metabolism.[83-84] These biocatalysts couple the activation of molecular oxygen to the

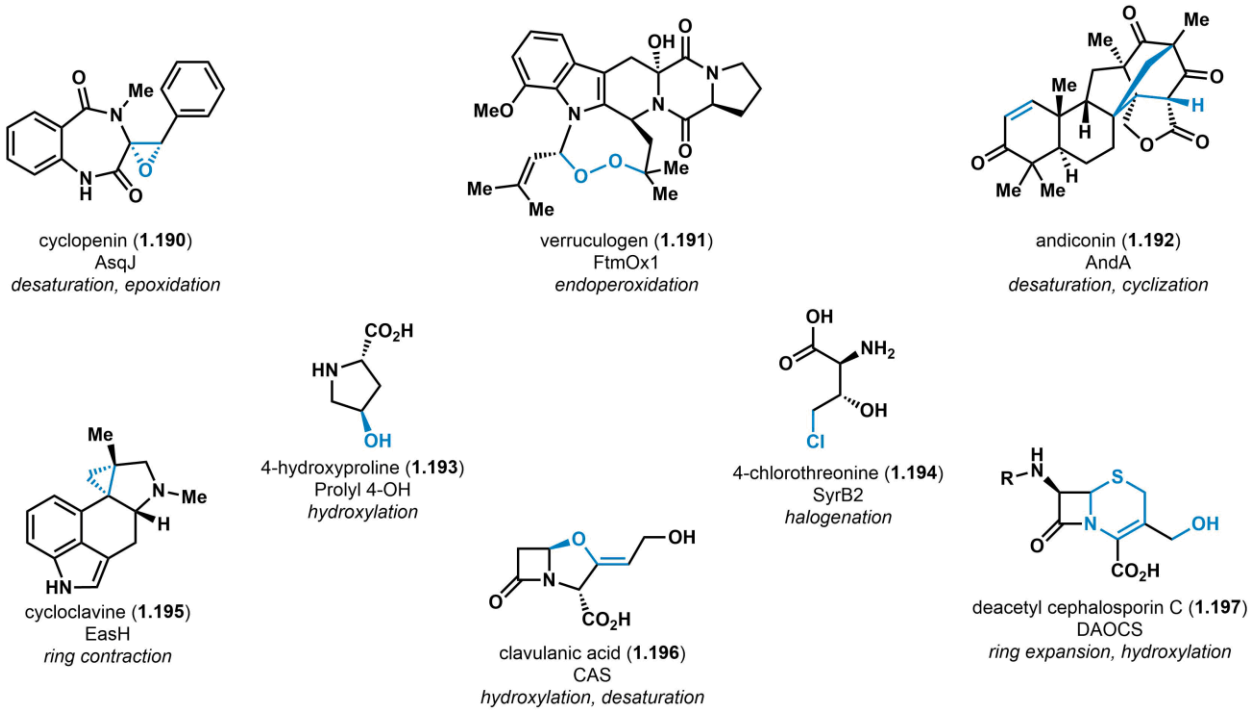


**Figure 1.19. Representative transformations catalyzed by NHI α-KG-dependent dioxygenases.**

decarboxylation of α-oxoacids, generating an iron(IV)-oxo species capable of performing hydrogen-atom abstraction.[84-85] Following the formation of an iron(IV)-oxo species, a vast number of transformations can be achieved, including: hydroxylation, epoxidation, epimerization, desaturation, endoperoxidation, halogenation, demethylation, cyclization, ring contraction and ring expansion (Figure 1.19). This breadth of natural chemical diversity illustrates the inherent potential of NHI enzymes to be developed into synthetically-useful biocatalysts, which can enable highly chemo-, site- and stereoselective transformations. The selectivity of many NHI-catalyzed reactions is unmatched by traditional small molecule catalysis, making these enzymes powerful tools for developing novel reactions as well as direct and efficient synthetic routes to target molecules. However, despite their broad potential as valuable biocatalysts, NHI enzymes have generally been underutilized in chemoenzymatic one-pot processes, with limited examples of their use.[86] Recent efforts to utilize NHI enzymes in synthetic routes have demonstrated that highly scalable platforms can be developed for these enzymes.[17, 82, 86] In addition, Kourist and coworkers recently demonstrated that α-KG can be generated *in situ* through enzymatic oxidation of inexpensive and renewable L-glutamate by L-glutamate oxidase.[87] This reaction was coupled with the action of an α-KG-dependent NHI enzyme on a near-process scale, producing product on the multi-gram scale and illustrating the scalability and sustainability offered for the use of α-KG-dependent enzymes.[87] Our work further demonstrates the scalability and synthetic utility of NHI enzymes in building complex molecules and natural products through the development of novel chemoenzymatic reaction sequences.[82]

*Mechanism of oxygen activation in α-KG-dependent NHI enzymes*

Non-heme iron-dependent enzymes that activate molecular oxygen for oxidative chemistry often do so through diverse reaction mechanisms. For NHI enzymes which do not require a co-substrate, such as catechol dioxygenases, cysteine dioxygenases or isopenicillin N synthase, oxygen is activated through direct binding of the substrate to the non-heme iron center, leading to the formation of an iron-oxygen complex which catalyzes the respective reaction.[85] In comparison, α-KG-dependent NHI enzymes leverage the oxidative decarboxylation of co-substrate α-oxoacids to generate an iron(IV)-oxo active species.[83, 85, 88] This reaction commences with 2-point coordination of α-KG, followed by substrate binding, weakening coordination of the axial water ligand, and allowing molecular oxygen to coordinate in the open axial site.[83, 85, 88] One-electron reduction of oxygen from the enzyme–iron(II) complex (**1.199**) is proposed to generate a reactive, 6-coordinate iron(III)-superoxo species (**1.200**).[83, 88-90] The terminal oxygen radical of species **1.200** is then proposed to react with the α-oxo double bond of α-KG to generate an iron(IV)-peroxyhemiketal species (**1.201**) capable of undergoing two-electron oxidative decarboxylation to form the active iron(IV)-oxo species (**1.202**).[83, 85, 88-90] The resulting iron(IV)-oxo species is highly oxidizing and capable of H atom abstraction with the substrate (shown as R–H), directly producing a substrate radical and iron(III)-hydroxyl species **1.203**.[91-94] In a canonical hydroxylation reaction, the resulting substrate radical and the iron(III)-hydroxyl species react in a one-electron process known as rebound hydroxylation (**1.203**-**1.198**).[92] The formation of a substrate radical also represents a branching point for catalysis of alternative reactions including radical rearrangement,

desaturation, epoxidation, endoperoxidation, and halogenation. Many of these non-hydroxylation reactions have been studied in detail and mechanisms have been proposed for radical termination by the iron(III)-hydroxyl species to restart the catalytic cycle.[92]

Many years of intensive spectroscopic and structural studies have led to the establishment of the canonical mechanism of oxygen activation in α-KG-dependent NHI enzymes (Figure 1.20). Early advances in this area involved detailed mechanistic studies of taurine dioxygenase (TauD) from *E. coli* that natively catalyzes the oxidative cleavage of taurine to form aminoacetaldehyde and inorganic sulfite.[91] Several steps of the TauD reaction have been characterized through extensive spectroscopic analysis which has been used to identify key intermediates in the catalytic cycle including (1) the high-spin TauD–Fe(II)–α-KG complex, (2) the high-spin TauD–Fe–α-KG–

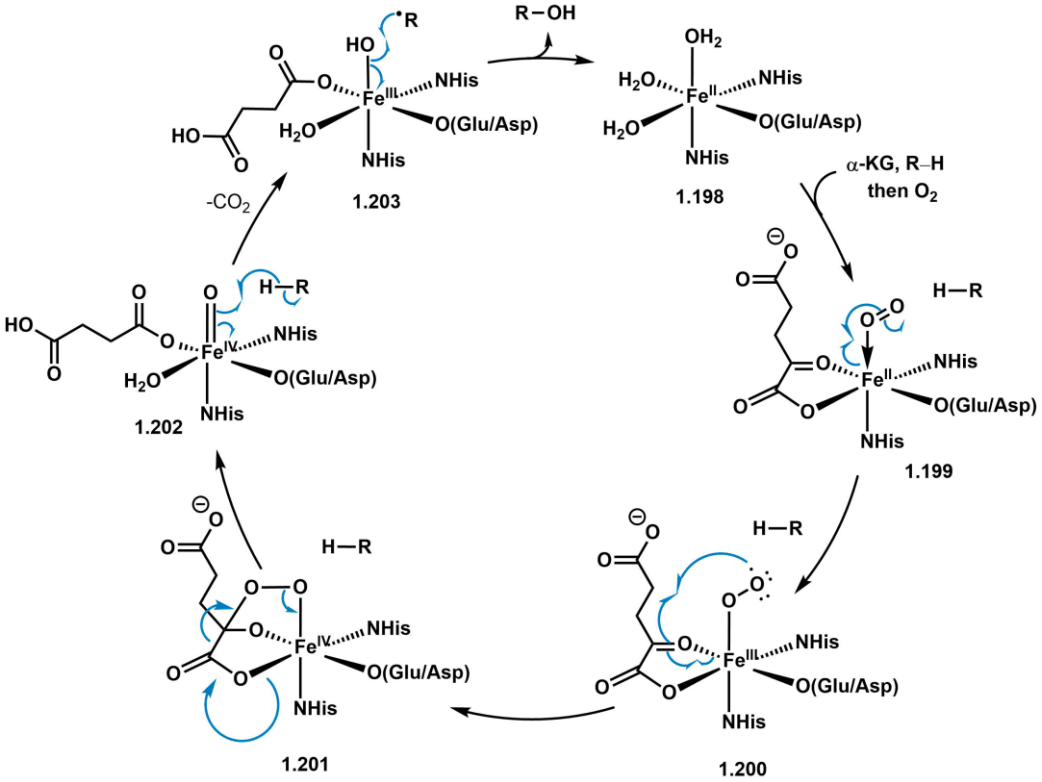


**Figure 1.20. Mechanism of molecular oxygen activation in α-KG-dependent NHI enzymes.**

substrate complex, (**1.199**), and (3) the Fe(IV)-oxo active species (**1.202**).[91-98] Similar intermediate complexes have also been observed in other α-KG-dependent NHI enzymes, including prolyl-4-hydroxylase and deacetoxy-cephalosporin C synthase (DAOCS).[99-100]

Detailed analyses have revealed that substrate binding and oxygen activation by decarboxylation of α-KG (**1.199-1.202**) occur in a concerted process in these model systems.[88, 100] These observations establish substrate binding as a "gatekeeper" interaction in preventing unwanted access to the highly-reactive Fe(IV)-oxo species. In this model, coupling substrate binding to the activation of oxygen prevents enzymatic self-immolation by the undesired generation of reactive oxidant capable of oxidizing enzymatic residues directly or through the release of harmful reactive oxygen species such as hydrogen peroxide into the cellular environment.[100] Only molecules that can achieve productive binding geometries can, therefore, be oxidized, avoiding oxidation of non-substrate molecules and allowing precise spatiotemporal control over the chemo- and site-selectivity of the reaction.[88, 100]

*Structural features of α-KG-dependent NHI enzymes*

Decades of structural studies of the α-KG-dependent subclass of NHI enzymes have revealed highly conserved structural motifs.[101-102] The major defining fold for this enzyme class is a double-stranded β-helix (DSBH) structure, defined as the "jelly-roll fold" (also the cupin fold) for its pastry-like resemblance.[101, 103-104] The jelly roll motif consists of a β-sandwich structure with eight anti-parallel β-sheets that contain the iron complex and defines the architecture of the active

site (Figure 1.21).[105] The jelly roll fold is "distorted" in that one end of the β-sandwich is held together tightly, and the other end is more open, creating space for substrate entry.[102, 104]

Additional architectural features that assist in substrate recognition are also quite common in α-KG-dependent NHI enzymes, including α-helices or loops, which generate key substrate contacts in the active site.[103, 106] Substrate recognition elements can assist in the preorganization of the enzyme, generating the active enzyme-substrate-cosubstrate complex that can engage in oxygen activation and productive catalysis.[103, 106] C-terminal regions of NHI enzymes have been shown to be quite mobile and capable of participating in conformational changes.[101, 103] There is also evidence that α-KG binding is a key component of this process, leading to active site preorganization and engaging primary substrate recognition elements for subsequent substrate binding.[101] In structures of NHI enzymes, α-KG (or the non-cleavable mimic *N*-oxalylglycine) typically coordinates the NHI center in a bidentate fashion with the C1-carboxylate bound equatorially to the metal complex.[101, 105] The non-coordinating carboxylate group of α-KG interacts with a polar, cationic residue (typically arginine) that assists in maintaining a proper geometry for oxidative decarboxylation of the cofactor and the subsequent release of carbon dioxide during catalysis.[101, 103-104] The size of the co-substrate also often dictates the order of events in catalysis, as α-KG cannot typically enter the active site to bind while the substrate is bound.[100-101] These characteristics of active site preorganization lend to a

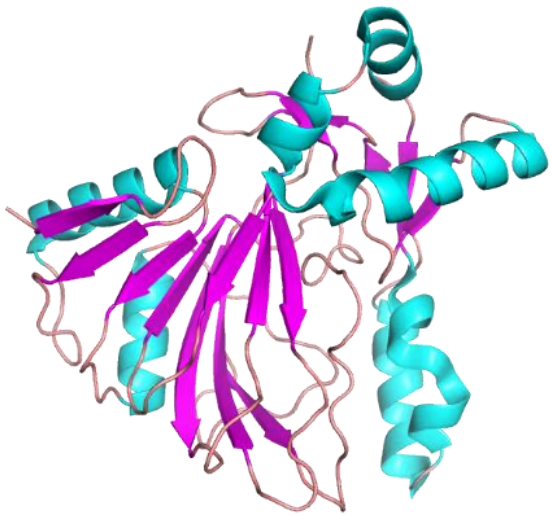

**Figure 1.21. Ribbon representation of model NHI enzyme TauD.**
Crystal structure of TauD (PDB: 1GY9) illustrating the canonical β-sandwich structure (purple) conserved in NHI enzymes.

generalized model of ordered binding in NHI enzymes in which α-KG must bind first, leading to active site preorganization, followed by substrate binding and catalysis as described in the previous section.[100]

Although substrate recognition elements vary widely amongst α-KG-dependent NHI enzymes, the NHI metal complex itself is typically conserved.[101-102] With certain exceptions (such as NHI halogenases), these biocatalysts bind iron through a facial triad made up of two histidine residues and one carboxylate residue that can be either aspartic acid or glutamic acid.[101-102] The 2-His-1-carboxylate scaffold is easily identified within the DSBH fold through sequence alignment, possessing a highly conserved HXD/E---H motif in which X can be any residue.[102] The resulting facial triad is often located near the "open" end of the β-sandwich motif, allowing co-substrate and substrate access to the catalytic center (for example, see Figure 1.22).[101, 105] In the case of NHI halogenases, the carboxylate residue in the HXD/E---H motif is often replaced with alanine or glycine, opening up a separate site for halide ($Cl^-$ or $Br^-$) coordination and subsequent C–H halogenation activity.[101, 104, 107]

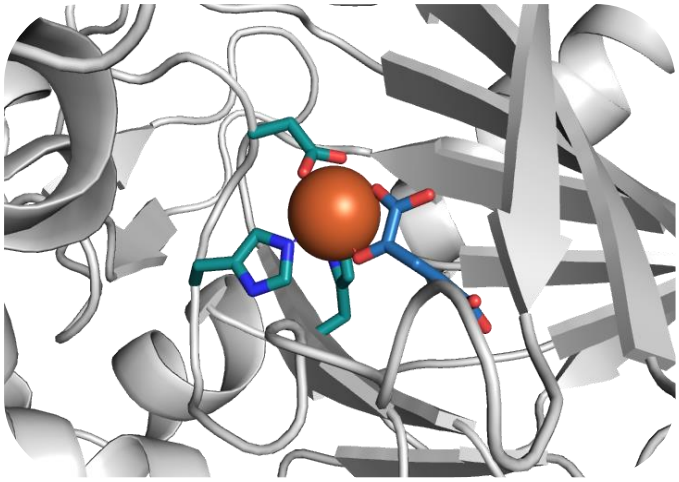

**Figure 1.22. NHI active site in TauD.**
Crystal structure of TauD (PDB: 1GY9) illustrating the NHI center. The iron ion (brown) is coordinated by the 2-His-1-carboxylate facial tried (teal) and α-KG (blue).

## 1.5 References


(1) García-Junceda, E.; Lavandera, I.; Rother, D.; Schrittwieser, J. H., (Chemo)enzymatic cascades—Nature's Synthetic Strategy Transferred to the Laboratory. *J. Mol. Catal. B: Enzym.* **2015**, *114*, 1-6.

(2) Ricca, E.; Brucher, B.; Schrittwieser, J. H., Multi-Enzymatic Cascade Reactions: Overview and Perspectives. *Adv. Synth. Catal.* **2011**, *353* (13), 2239-2262.

(3) Sperl, J. M.; Sieber, V., Multienzyme Cascade Reactions—Status and Recent Advances. *ACS Catalysis* **2018**, *8* (3), 2385-2396.

(4) Sun, H.; Zhang, H.; Ang, E. L.; Zhao, H., Biocatalysis for the synthesis of pharmaceuticals and pharmaceutical intermediates. *Bioorg. Med. Chem.* **2018**, *26* (7), 1275-1284.

(5) Patel, R. N., Chemo-enzymatic synthesis of pharmaceutical intermediates. *Expert Opin. Drug Disc.* **2008**, *3* (2), 187-245.

(6) Li, F.; Zhang, X.; Renata, H., Enzymatic C–H functionalizations for natural product synthesis. *Curr. Opin. Chem. Biol.* **2019**, *49*, 25-32.

(7) Huang, X.; Cao, M.; Zhao, H., Integrating biocatalysis with chemocatalysis for selective transformations. *Curr. Opin. Chem. Biol.* **2020**, *55*, 161-170.

(8) Denard, C. A.; Hartwig, J. F.; Zhao, H., Multistep One-Pot Reactions Combining Biocatalysts and Chemical Catalysts for Asymmetric Synthesis. *ACS Catal.* **2013**, *3* (12), 2856-2864.

(9) Baer, K.; Krausser, M.; Burda, E.; Hummel, W.; Berkessel, A.; Groger, H., Sequential and modular synthesis of chiral 1,3-diols with two stereogenic centers: access to all four stereoisomers by combination of organo- and biocatalysis. *Angew. Chem. Int. Ed. Engl.* **2009**, *48* (49), 9355-8.

(10) Binder, J. T.; Kirsch, S. F., Iterative approach to polyketide-type structures: stereoselective synthesis of 1,3-polyols utilizing the catalytic asymmetric Overman esterification. *Chem. Commun. (Camb.)* **2007**, (40), 4164-6.

(11) Kumar, P.; Tripathi, D.; Sharma, B. M.; Dwivedi, N., Transition metal catalysis-a unique road map in the stereoselective synthesis of 1,3-polyols. *Org. Biomol. Chem.* **2017**, *15* (4), 733-761.

(12) Sonoike, S.; Itakura, T.; Kitamura, M.; Aoki, S., One-pot chemoenzymatic synthesis of chiral 1,3-diols using an enantioselective aldol reaction with chiral $Zn^{2+}$ complex catalysts and enzymatic reduction using oxidoreductases with cofactor regeneration. *Chem. Asian. J.* **2012**, *7* (1), 64-74.

(13) Carr, R.; Alexeeva, M.; Dawson, M. J.; Gotor-Fernández, V.; Humphrey, C. E.; Turner, N. J., Directed Evolution of an Amine Oxidase for the Preparative Deracemisation of Cyclic Secondary Amines. *ChemBioChem* **2005**, *6* (4), 637-639.

(14) Dunsmore, C. J.; Carr, R.; Fleming, T.; Turner, N. J., A Chemo-Enzymatic Route to Enantiomerically Pure Cyclic Tertiary Amines. *J. Am. Chem. Soc.* **2006**, *128* (7), 2224-2225.

(15) Ghislieri, D.; Houghton, D.; Green, A. P.; Willies, S. C.; Turner, N. J., Monoamine Oxidase (MAO-N) Catalyzed Deracemization of Tetrahydro-β-carbolines: Substrate Dependent Switch in Enantioselectivity. *ACS Catal.* **2013,** *3* (12), 2869-2872.

(16) Zawodny, W.; Marshall, J. R.; Finnigan, J. D.; Turner, N. J.; Clayden, J.; Montgomery, S. L., Chemoenzymatic synthesis of substituted azepanes by sequential biocatalytic reduction and organolithium-mediated rearrangement. *J. Am. Chem. Soc.* **2018**, 140, 51, 17872-17877.

(17) Zwick, C. R., 3rd; Renata, H., Remote C-H Hydroxylation by an alpha-Ketoglutarate-Dependent Dioxygenase Enables Efficient Chemoenzymatic Synthesis of Manzacidin C and Proline Analogs. *J. Am. Chem. Soc.* **2018**, *140* (3), 1165-1169.

(18) Zwick, C. R.; Renata, H., A one-pot chemoenzymatic synthesis of (2*S*, 4*R*)-4-methylproline enables the first total synthesis of antiviral lipopeptide cavinafungin B. *Tetrahedron* **2018**, *74* (45), 6469-6473.

(19) Murphy, A. C.; Mitova, M. I.; Blunt, J. W.; Munro, M. H. G., Concise, Stereoselective Route to the Four Diastereoisomers of 4-Methylproline. *J. Nat. Prod.* **2008**, *71* (5), 806-809.

(20) Burda, E.; Hummel, W.; Groger, H., Modular chemoenzymatic one-pot syntheses in aqueous media: combination of a palladium-catalyzed cross-coupling with an asymmetric biotransformation. *Angew. Chem. Int. Ed. Engl.* **2008**, *47* (49), 9551-9554.

(21) Denard, C. A.; Huang, H.; Bartlett, M. J.; Lu, L.; Tan, Y.; Zhao, H.; Hartwig, J. F., Cooperative tandem catalysis by an organometallic complex and a metalloenzyme. *Angew. Chem. Int. Ed. Engl.* **2014**, *53* (2), 465-469.

(22) Denard, C. A.; Bartlett, M. J.; Wang, Y.; Lu, L.; Hartwig, J. F.; Zhao, H., Development of a One-Pot Tandem Reaction Combining Ruthenium-Catalyzed Alkene Metathesis and Enantioselective Enzymatic Oxidation To Produce Aryl Epoxides. *ACS Catal.* **2015**, *5* (6), 3817-3822.

(23) Scalacci, N.; Black, G. W.; Mattedi, G.; Brown, N. L.; Turner, N. J.; Castagnolo, D., Unveiling the Biocatalytic Aromatizing Activity of Monoamine Oxidases MAO-N and 6-HDNO: Development of Chemoenzymatic Cascades for the Synthesis of Pyrroles. *ACS Catal.* **2017**, *7* (2), 1295-1300.

(24) Schaaf, P.; Bayer, T.; Koley, M.; Schnürch, M.; Bornscheuer, U. T.; Rudroff, F.; Mihovilovic, M. D., Biocompatible metal-assisted C–C cross-coupling combined with biocatalytic chiral reductions in a concurrent tandem cascade. *Chem. Commun.* **2018**, *54* (92), 12978-12981.

(25) Dander, J. E.; Giroud, M.; Racine, S.; Darzi, E. R.; Alvizo, O.; Entwistle, D.; Garg, N. K., Chemoenzymatic conversion of amides to enantioenriched alcohols in aqueous medium. *Commun. Chem.* **2019**, *2* (1), 82.

(26) Latham, J.; Henry, J.-M.; Sharif, H. H.; Menon, B. R. K.; Shepherd, S. A.; Greaney, M. F.; Micklefield, J., Integrated catalysis opens new arylation pathways via regiodivergent enzymatic C–H activation. *Nat. Commun.* **2016**, *7* (1), 11873.

(27) Durak, L. J.; Payne, J. T.; Lewis, J. C., Late-Stage Diversification of Biologically Active Molecules via Chemoenzymatic C−H Functionalization. *ACS Catal.* **2016**, *6* (3), 1451-1454.

(28) Gruß, H.; Belu, C.; Bernhard, L. M.; Merschel, A.; Sewald, N., Fluorogenic Diversification of Unprotected Bromotryptophan by Aqueous Mizoroki–Heck Cross-Coupling. *Chem. Eur. J.* **2019**, *25* (23), 5880-5883.

(29) Nicolaou, K. C.; Mathison, C. J.; Montagnon, T., New reactions of IBX: oxidation of nitrogen- and sulfur-containing substrates to afford useful synthetic intermediates. *Angew. Chem. Int. Ed. Engl.* **2003**, *42* (34), 4077-4082.

(30) Zhang, E.; Tian, H.; Xu, S.; Yu, X.; Xu, Q., Iron-Catalyzed Direct Synthesis of Imines from Amines or Alcohols and Amines via Aerobic Oxidative Reactions under Air. *Org. Lett.* **2013**, *15* (11), 2704-2707.

(31) Risi, C.; Zhao, F.; Castagnolo, D., Chemo-Enzymatic Metathesis/Aromatization Cascades for the Synthesis of Furans: Disclosing the Aromatizing Activity of Laccase/TEMPO in Oxygen-Containing Heterocycles. *ACS Catal.* **2019**, *9* (8), 7264-7269.

(32) Thirumurugan, P.; Matosiuk, D.; Jozwiak, K., Click Chemistry for Drug Development and Diverse Chemical–Biology Applications. *Chem. Rev.* **2013**, *113* (7), 4905-4979.

(33) Moses, J. E.; Moorhouse, A. D., The growing applications of click chemistry. *Chem. Soc. Rev.* **2007**, *36* (8), 1249-1262.

(34) de Souza de Oliveira, C.; de Andrade, K. T.; Omori, A. T., One-pot chemoenzymatic synthesis of chiral disubstituted 1,2,3-triazoles in aqueous media. *J. Mol. Catal. B: Enzym.* **2013**, *91*, 93-97.

(35) Campbell-Verduyn, L. S.; Szymański, W.; Postema, C. P.; Dierckx, R. A.; Elsinga, P. H.; Janssen, D. B.; Feringa, B. L., One pot 'click' reactions: tandem enantioselective biocatalytic epoxide ring opening and [3+2] azide alkyne cycloaddition. *Chem. Commun.* **2010**, *46* (6), 898-900.

(36) Enoki, J.; Mügge, C.; Tischler, D.; Miyamoto, K.; Kourist, R., Chemoenzymatic Cascade Synthesis of Optically Pure Alkanoic Acids by Using Engineered Arylmalonate Decarboxylase Variants. *Chem. Eur. J.* **2019**, *25*, 5071-5076.

(37) Mertens, M. A. S.; Thomas, F.; Nöth, M.; Moegling, J.; El-Awaad, I.; Sauer, D. F.; Dhoke, G. V.; Xu, W.; Pich, A.; Herres-Pawlis, S.; Schwaneberg, U., One-Pot Two-Step

Chemoenzymatic Cascade for the Synthesis of a Bis-benzofuran Derivative. *Eur. J. Org. Chem.* **2019**, *37*, 6341-6346.

(38) Brown, C. J.; Toste, F. D.; Bergman, R. G.; Raymond, K. N., Supramolecular Catalysis in Metal–Ligand Cluster Hosts. *Chem. Rev.* **2015**, *115* (9), 3012-3035.

(39) Wang, Z. J.; Clary, K. N.; Bergman, R. G.; Raymond, K. N.; Toste, F. D., A supramolecular approach to combining enzymatic and transition metal catalysis. *Nat. Chem.* **2013**, *5* (2), 100-103.

(40) Litman, Z. C.; Wang, Y.; Zhao, H.; Hartwig, J. F., Cooperative asymmetric reactions combining photocatalysis and enzymatic catalysis. *Nature* **2018**, *560* (7718), 355-359.

(41) Lauder, K.; Toscani, A.; Qi, Y.; Lim, J.; Charnock, S. J.; Korah, K.; Castagnolo, D., Photobiocatalytic One-Pot Cascades for the Enantioselective Synthesis of 1,3-Mercaptoalkanol Volatile Sulfur Compounds. *Angew. Chemie. Int. Ed. Engl.* **2018**, *57* (20), 5803-5807.

(42) Toogood, H. S.; Scrutton, N. S., Discovery, Characterization, Engineering, and Applications of Ene-Reductases for Industrial Biocatalysis. *ACS Catal.* **2018**, *8* (4), 3532-3549.

(43) Schnapperelle, I.; Hummel, W.; Gröger, H., Formal Asymmetric Hydration of Non-Activated Alkenes in Aqueous Medium through a "Chemoenzymatic Catalytic System". *Chem. Eur. J.* **2012**, *18* (4), 1073-1076.

(44) Fuchs, M.; Schober, M.; Pfeffer, J.; Kroutil, W.; Birner-Gruenberger, R.; Faber, K., Homoallylic Alcohols via a Chemo-Enzymatic One-Pot Oxidation–Allylation Cascade. *Adv. Synth. Catal.* **2011**, *353* (13), 2354-2358.

(45) Zambelli, P.; Pinto, A.; Romano, D.; Crotti, E.; Conti, P.; Tamborini, L.; Villa, R.; Molinari, F., One-pot chemoenzymatic synthesis of aldoximes from primary alcohols in water. *Green Chem.* **2012**, *14* (8), 2158-2161.

(46) Cao, J.; Hyster, T. K., Pyridoxal-Catalyzed Racemization of α-Aminoketones Enables the Stereodivergent Synthesis of 1,2-Amino Alcohols Using Ketoreductases. *ACS Catal.* **2020,** *10* (11), 6171-6175.

(47) Reetz, M. T., Lipases as practical biocatalysts. *Curr. Opin. Chem. Biol.* **2002**, *6* (2), 145-150.

(48) Ghanem, A.; Aboul-Enein, H. Y., Application of lipases in kinetic resolution of racemates. *Chirality* **2005**, *17* (1), 1-15.

(49) Heredia, A. A.; López-Vidal, M. G.; Kurina-Sanz, M.; Bisogno, F. R.; Peñéñory, A. B., Thiol-free chemoenzymatic synthesis of β-ketosulfides. *Beilstein J. Org. Chem.* **2019**, *15*, 378-387.

(50) Mayer, S. F.; Steinreiber, A.; Orru, R. V. A.; Faber, K., Chemoenzymatic Asymmetric Total Syntheses of Antitumor Agents (3*R*,9*R*,10*R*)- and (3*S*,9*R*,10*R*)-Panaxytriol and (*R*)-

and (*S*)-Falcarinol from Panax ginseng Using an Enantioconvergent Enzyme-Triggered Cascade Reaction. *J. Org. Chem.* **2002**, *67* (26), 9115-9121.

(51) β-Amino Acids in Natural Products. In *Enantioselective Synthesis of β-Amino Acids*, pp 19-91.

(52) Weiß, M.; Brinkmann, T.; Gröger, H., Towards a greener synthesis of (*S*)-3-aminobutanoic acid: process development and environmental assessment. *Green Chem.* **2010**, *12* (9), 1580-1588.

(53) Biewenga, L.; Saravanan, T.; Kunzendorf, A.; van der Meer, J.-Y.; Pijning, T.; Tepper, P. G.; van Merkerk, R.; Charnock, S. J.; Thunnissen, A.-M. W. H.; Poelarends, G. J., Enantioselective Synthesis of Pharmaceutically Active γ-Aminobutyric Acids Using a Tailor-Made Artificial Michaelase in One-Pot Cascade Reactions. *ACS Catal.* **2019**, *9* (2), 1503-1513.

(54) Liardo, E.; González-Fernández, R.; Ríos-Lombardía, N.; Morís, F.; García-Álvarez, J.; Cadierno, V.; Crochet, P.; Rebolledo, F.; González-Sabín, J., Strengthening the Combination between Enzymes and Metals in Aqueous Medium: Concurrent Ruthenium-Catalyzed Nitrile Hydration - Asymmetric Ketone Bioreduction. *ChemCatChem* **2018**, *10* (20), 4676-4682.

(55) Plass, C.; Hinzmann, A.; Terhorst, M.; Brauer, W.; Oike, K.; Yavuzer, H.; Asano, Y.; Vorholt, A. J.; Betke, T.; Gröger, H., Approaching Bulk Chemical Nitriles from Alkenes: A Hydrogen Cyanide-Free Approach through a Combination of Hydroformylation and Biocatalysis. *ACS Catal.* **2019**, *9* (6), 5198-5203.

(56) Reck, R. A., Industrial uses of palm, palm kernel and coconut oils: Nitrogen derivatives. *J. Am. Oil Chem. Soc.* **1985**, *62* (2), 355-365.

(57) Smith, E. L.; Abbott, A. P.; Ryder, K. S., Deep Eutectic Solvents (DESs) and Their Applications. *Chem. Rev.* **2014**, *114* (21), 11060-11082.

(58) Paris, J.; Telzerow, A.; Ríos-Lombardía, N.; Steiner, K.; Schwab, H.; Morís, F.; Gröger, H.; González-Sabín, J., Enantioselective One-Pot Synthesis of Biaryl-Substituted Amines by Combining Palladium and Enzyme Catalysis in Deep Eutectic Solvents. *ACS Sustain. Chem. Eng.* **2019**, *7* (5), 5486-5493.

(59) Paris, J.; Ríos-Lombardía, N.; Morís, F.; Gröger, H.; González-Sabín, J., Novel Insights into the Combination of Metal- and Biocatalysis: Cascade One-Pot Synthesis of Enantiomerically Pure Biaryl Alcohols in Deep Eutectic Solvents. *ChemCatChem* **2018**, *10* (19), 4417-4423.

(60) Cicco, L.; Ríos-Lombardía, N.; Rodríguez-Álvarez, M. J.; Morís, F.; Perna, F. M.; Capriati, V.; García-Álvarez, J.; González-Sabín, J., Programming cascade reactions interfacing biocatalysis with transition-metal catalysis in Deep Eutectic Solvents as biorenewable reaction media. *Green Chem.* **2018**, *20* (15), 3468-3475.

(61) Ríos-Lombardía, N.; Rodríguez-Álvarez, M. J.; Morís, F.; Kourist, R.; Comino, N.; López-Gallego, F.; González-Sabín, J.; García-Álvarez, J., DESign of Sustainable One-Pot Chemoenzymatic Organic Transformations in Deep Eutectic Solvents for the Synthesis of 1,2-Disubstituted Aromatic Olefins. *Front. Chem.* **2020**, *8* (139), 1-11.

(62) Wang, S.; Fu, C.; Zhang, Y.; Tao, L.; Li, S.; Wei, Y., One-Pot Cascade Synthetic Strategy: A Smart Combination of Chemoenzymatic Transesterification and Raft Polymerization. *ACS Macro Lett.* **2012**, *1* (10), 1224-1227.

(63) van As, B. A. C.; Thomassen, P.; Kalra, B.; Gross, R. A.; Meijer, E. W.; Palmans, A. R. A.; Heise, A., One-Pot Chemoenzymatic Cascade Polymerization under Kinetic Resolution Conditions. *Macromolecules* **2004**, *37* (24), 8973-8977.

(64) Hawker, C. J.; Hedrick, J. L.; Malmström, E. E.; Trollsås, M.; Mecerreyes, D.; Moineau, G.; Dubois, P.; Jérôme, R., Dual Living Free Radical and Ring Opening Polymerizations from a Double-Headed Initiator. *Macromolecules* **1998**, *31* (2), 213-219.

(65) Fu, C.; Tao, L.; Zhang, Y.; Li, S.; Wei, Y., Combining chemoenzymatic monomer transformation with ATRP: a facile "one-pot" approach to functional polymers. *Chem. Commun.* **2012**, *48* (72), 9062-9064.

(66) Hagel, J. M.; Facchini, P. J., Benzylisoquinoline Alkaloid Metabolism: A Century of Discovery and a Brave New World. *Plant Cell Physiol.* **2013**, *54* (5), 647-672.

(67) Samanani, N.; Liscombe, D. K.; Facchini, P. J., Molecular cloning and characterization of norcoclaurine synthase, an enzyme catalyzing the first committed step in benzylisoquinoline alkaloid biosynthesis. *Plant J.* **2004**, *40* (2), 302-313.

(68) Bonamore, A.; Rovardi, I.; Gasparrini, F.; Baiocco, P.; Barba, M.; Molinaro, C.; Botta, B.; Boffi, A.; Macone, A., An enzymatic, stereoselective synthesis of (*S*)-norcoclaurine. *Green Chem.* **2010**, *12* (9), 1623-1627.

(69) Maresh, J. J.; Crowe, S. O.; Ralko, A. A.; Aparece, M. D.; Murphy, C. M.; Krzeszowiec, M.; Mullowney, M. W., Facile one-pot synthesis of tetrahydroisoquinolines from amino acids via hypochlorite-mediated decarboxylation and Pictet–Spengler condensation. *Tetrahedron Lett.* **2014**, *55* (36), 5047-5051.

(70) Erdmann, V.; Lichman, B. R.; Zhao, J.; Simon, R. C.; Kroutil, W.; Ward, J. M.; Hailes, H. C.; Rother, D., Enzymatic and Chemoenzymatic Three-Step Cascades for the Synthesis of Stereochemically Complementary Trisubstituted Tetrahydroisoquinolines. *Angew. Chem. Int. Ed. Engl.* **2017**, *56* (41), 12503-12507.

(71) Zhao, J.; Lichman, B. R.; Ward, J. M.; Hailes, H. C., One-pot chemoenzymatic synthesis of trolline and tetrahydroisoquinoline analogues. *Chem. Commun.* **2018**, *54* (11), 1323-1326.

(72) Odachowski, M.; Greaney, M. F.; Turner, N. J., Concurrent Biocatalytic Oxidation and C–C Bond Formation via Gold Catalysis: One-Pot Alkynylation of N-Alkyl Tetrahydroisoquinolines. *ACS Catal.* **2018**, *8* (11), 10032-10035.

(73) Schrittwieser, J. H.; Groenendaal, B.; Resch, V.; Ghislieri, D.; Wallner, S.; Fischereder, E.-M.; Fuchs, E.; Grischek, B.; Sattler, J. H.; Macheroux, P.; Turner, N. J.; Kroutil, W., Deracemization By Simultaneous Bio-oxidative Kinetic Resolution and Stereoinversion. *Angew. Chem. Int. Ed.* **2014**, *53* (14), 3731-3734.

(74) Bulger, P. G.; Bagal, S. K.; Marquez, R., Recent advances in biomimetic natural product synthesis. *Nat. Prod. Rep.* **2008**, *25* (2), 254-297.

(75) Fahad, A. A.; Abood, A.; Fisch, K. M.; Osipow, A.; Davison, J.; Avramovic, M.; Butts, C. P.; Piel, J.; Simpson, T. J.; Cox, R. J., Oxidative dearomatisation: the key step of sorbicillinoid biosynthesis. *Chem. Sci.* **2014**, *5* (2), 523-527.

(76) Bosset, C.; Coffinier, R.; Peixoto, P. A.; El Assal, M.; Miqueu, K.; Sotiropoulos, J.-M.; Pouységu, L.; Quideau, S., Asymmetric Hydroxylative Phenol Dearomatization Promoted by Chiral Binaphthylic and Biphenylic Iodanes. *Angew. Chem. Int. Ed.* **2014**, *53* (37), 9860-9864.

(77) Volp, K. A.; Harned, A. M., Chiral aryl iodide catalysts for the enantioselective synthesis of *para*-quinols. *Chem. Commun.* **2013**, *49* (29), 3001-3003.

(78) Zhu, J.; Grigoriadis, N. P.; Lee, J. P.; Porco, J. A., Synthesis of the Azaphilones Using Copper-Mediated Enantioselective Oxidative Dearomatization. *J. Am. Chem. Soc.* **2005**, *127* (26), 9342-9343.

(79) Baker Dockrey, S. A.; Lukowski, A. L.; Becker, M. R.; Narayan, A. R. H., Biocatalytic site- and enantioselective oxidative dearomatization of phenols. *Nat. Chem.* **2017**, *10*, 119.

(80) Sib, A.; Gulder, T. A. M., Stereoselective Total Synthesis of Bisorbicillinoid Natural Products by Enzymatic Oxidative Dearomatization/Dimerization. *Angew. Chem. Int. Ed.* **2017**, *56* (42), 12888-12891.

(81) Sib, A.; Gulder, T. A. M., Chemo-enzymatic Total Synthesis of Oxosorbicillinol, Sorrentanone, Rezishanones B and C, Sorbicatechol A, Bisvertinolone, and (+)-Epoxysorbicillinol. *Angew. Chem. Int. Ed.* **2018**, *57* (44), 14650-14653.

(82) Doyon, T. J.; Perkins, J. C.; Baker Dockrey, S. A.; Romero, E. O.; Skinner, K. C.; Zimmerman, P. M.; Narayan, A. R. H., Chemoenzymatic o-Quinone Methide Formation. *J. Am. Chem. Soc.* **2019,** *141* (51), 20269-20277.

(83) Martinez, S.; Hausinger, R. P., Catalytic Mechanisms of Fe(II)- and 2-Oxoglutarate-Dependent Oxygenases. *J. Biol. Chem.* **2015**, *290* (34), 20702-20711.

(84) Islam, M. S.; Leissing, T. M.; Chowdhury, R.; Hopkinson, R. J.; Schofield, C. J., 2-Oxoglutarate-Dependent Oxygenases. *Annu. Rev. Biochem.* **2018**, *87* (1), 585-620.

(85) Bugg, T. D. H.; Ramaswamy, S., Non-heme iron-dependent dioxygenases: unravelling catalytic mechanisms for complex enzymatic oxidations. *Curr. Opin. Chem. Biol.* **2008**, *12* (2), 134-140.

(86) Zwick, C. R.; Renata, H., Harnessing the biocatalytic potential of iron- and α-ketoglutarate-dependent dioxygenases in natural product total synthesis. *Natural Product Reports* **2020**, advance article.

(87) Busch, F.; Brummund, J.; Calderini, E.; Schürmann, M.; Kourist, R., Cofactor Generation Cascade for α-Ketoglutarate and Fe(II)-Dependent Dioxygenases. *ACS Sustain. Chem. Eng.* **2020**, *8* (23), 8604-8612.

(88) Borowski, T.; Bassan, A.; Siegbahn, P. E. M., Mechanism of Dioxygen Activation in 2-Oxoglutarate-Dependent Enzymes: A Hybrid DFT Study. *Chem. Eur. J.* **2004**, *10* (4), 1031-1041.

(89) Krebs, C.; Galonić Fujimori, D.; Walsh, C. T.; Bollinger, J. M., Non-Heme Fe(IV)–Oxo Intermediates. *Acc. Chem. Res.* **2007**, *40* (7), 484-492.

(90) Solomon, E. I.; Decker, A.; Lehnert, N., Non-heme iron enzymes: Contrasts to heme catalysis. *Proc. Natl. Acad. Sci.* **2003**, *100* (7), 3589-3594.

(91) Bollinger Jr., J. M.; Price, J. C.; Hoffart, L. M.; Barr, E. W.; Krebs, C., Mechanism of Taurine: α-Ketoglutarate Dioxygenase (TauD) from Escherichia coli. *Eur. J. Inorg. Chem.* **2005**, *2005* (21), 4245-4254.

(92) Grzyska, P. K.; Appelman, E. H.; Hausinger, R. P.; Proshlyakov, D. A., Insight into the mechanism of an iron dioxygenase by resolution of steps following the Fe(IV)═O species. *Proc. Natl. Acad. Sci.* **2010**, *107* (9), 3982-3987.

(93) Price, J. C.; Barr, E. W.; Tirupati, B.; Bollinger, J. M.; Krebs, C., The First Direct Characterization of a High-Valent Iron Intermediate in the Reaction of an α-Ketoglutarate-Dependent Dioxygenase: A High-Spin Fe(IV) Complex in Taurine/α-Ketoglutarate Dioxygenase (TauD) from Escherichia coli. *Biochemistry* **2003**, *42* (24), 7497-7508.

(94) Price, J. C.; Barr, E. W.; Glass, T. E.; Krebs, C.; Bollinger, J. M., Evidence for Hydrogen Abstraction from C1 of Taurine by the High-Spin Fe(IV) Intermediate Detected during Oxygen Activation by Taurine:α-Ketoglutarate Dioxygenase (TauD). *J. Am. Chem. Soc.* **2003**, *125* (43), 13008-13009.

(95) Ryle, M. J.; Padmakumar, R.; Hausinger, R. P., Stopped-Flow Kinetic Analysis of Escherichia coli Taurine/α-Ketoglutarate Dioxygenase: Interactions with α-Ketoglutarate, Taurine, and Oxygen. *Biochemistry* **1999**, *38* (46), 15278-15286.

(96) Riggs-Gelasco, P. J.; Price, J. C.; Guyer, R. B.; Brehm, J. H.; Barr, E. W.; Bollinger, J. M.; Krebs, C., EXAFS Spectroscopic Evidence for an Fe═O Unit in the Fe(IV) Intermediate Observed during Oxygen Activation by Taurine:α-Ketoglutarate Dioxygenase. *J. Am. Chem. Soc.* **2004**, *126* (26), 8108-8109.

(97) Proshlyakov, D. A.; Henshaw, T. F.; Monterosso, G. R.; Ryle, M. J.; Hausinger, R. P., Direct Detection of Oxygen Intermediates in the Non-Heme Fe Enzyme Taurine/α-Ketoglutarate Dioxygenase. *J. Am. Chem. Soc.* **2004**, *126* (4), 1022-1023.

(98) Neidig, M. L.; Brown, C. D.; Light, K. M.; Fujimori, D. G.; Nolan, E. M.; Price, J. C.; Barr, E. W.; Bollinger, J. M.; Krebs, C.; Walsh, C. T.; Solomon, E. I., CD and MCD of CytC3 and Taurine Dioxygenase: Role of the Facial Triad in α-KG-Dependent Oxygenases. *J. Am. Chem. Soc.* **2007**, *129* (46), 14224-14231.

(99) Hoffart, L. M.; Barr, E. W.; Guyer, R. B.; Bollinger, J. M.; Krebs, C., Direct spectroscopic detection of a C–H-cleaving high-spin Fe(IV) complex in a prolyl-4-hydroxylase. *Proc. Natl. Acad. Sci.* **2006,** *103* (40), 14738-14743.

(100) Goudarzi, S.; Iyer, S. R.; Babicz, J. T.; Yan, J. J.; Peters, G. H. J.; Christensen, H. E. M.; Hedman, B.; Hodgson, K. O.; Solomon, E. I., Evaluation of a concerted vs. sequential oxygen activation mechanism in α-ketoglutarate–dependent nonheme ferrous enzymes. *Proc. Natl. Acad. Sci.* **2020**, *117* (10), 5152-5159.

(101) Aik, W. S.; Chowdhury, R.; Clifton, I. J.; Hopkinson, R. J.; Leissing, T.; McDonough, M. A.; Nowak, R.; Schofield, C. J.; Walport, L. J., CHAPTER 2 Introduction to Structural Studies on 2-Oxoglutarate-Dependent Oxygenases and Related Enzymes. In *2-Oxoglutarate-Dependent Oxygenases*, The Royal Society of Chemistry: 2015; pp 59-94.

(102) Hegg, E. L.; Jr, L. Q., The 2-His-1-Carboxylate Facial Triad — An Emerging Structural Motif in Mononuclear Non-Heme Iron(II) Enzymes. *Eur. J. Biochem.* **1997**, *250* (3), 625-629.

(103) Aik, W.; McDonough, M. A.; Thalhammer, A.; Chowdhury, R.; Schofield, C. J., Role of the jelly-roll fold in substrate binding by 2-oxoglutarate oxygenases. *Curr. Opin. Struct. Biol.* **2012**, *22* (6), 691-700.

(104) Clifton, I. J.; McDonough, M. A.; Ehrismann, D.; Kershaw, N. J.; Granatino, N.; Schofield, C. J., Structural studies on 2-oxoglutarate oxygenases and related double-stranded beta-helix fold proteins. *J. Inorg. Biochem.* **2006**, *100* (4), 644-669.

(105) Elkins, J. M.; Ryle, M. J.; Clifton, I. J.; Dunning Hotopp, J. C.; Lloyd, J. S.; Burzlaff, N. I.; Baldwin, J. E.; Hausinger, R. P.; Roach, P. L., X-ray Crystal Structure of Escherichia coli Taurine/α-Ketoglutarate Dioxygenase Complexed to Ferrous Iron and Substrates. *Biochemistry* **2002**, *41* (16), 5185-5192.

(106) Iyer, L. M.; Abhiman, S.; de Souza, R. F.; Aravind, L., Origin and evolution of peptide-modifying dioxygenases and identification of the wybutosine hydroxylase/hydroperoxidase. *Nucl. Acids. Res.* **2010**, *38* (16), 5261-5279.

(107) Blasiak, L. C.; Drennan, C. L., Structural Perspective on Enzymatic Halogenation. *Acc. Chem. Res.* **2009**, *42* (1), 147-155.

## Chapter 2: Chemoenzymatic Ortho-quinone Methide Formation and Elaboration



### 2.1 Introduction

Nature has developed strategies for generation of highly reactive intermediates in the synthesis of complex secondary metabolites.[1-2] For example, cyclases control the reactivity of cationic or anionic intermediates in the selective biosynthesis of complex natural products.[1, 3] This observed reactivity is controlled by the active site of the biocatalysts, directing the reaction outcome through controlled generation and orientation of the reactive intermediate.[1, 3] Synthetic approaches that mimic biosynthetic pathways often encounter challenges in reproducing the elegance of these evolved methods, at times requiring blocking groups to achieve selectivity, or are inherently incompatible with a breadth of functional groups.[4-7] *Ortho*-quinone methides (*o*-QMs, **2.4**) have been implicated in the biosynthesis of several families of natural products, as these versatile intermediates can readily participate in inverse electron-demand Diels-Alder (IEDDA) or 1,4-addition reactions.[4-6] For example, the penilactone (see **2.1**),[8] peniphenone (see **2.5**),[8] and communol (**2.2**)[9] families of natural products are proposed to arise from benzylic oxidation of clavatol (**2.17**), *o*-QM formation and derivatization to produce a variety of structurally-related

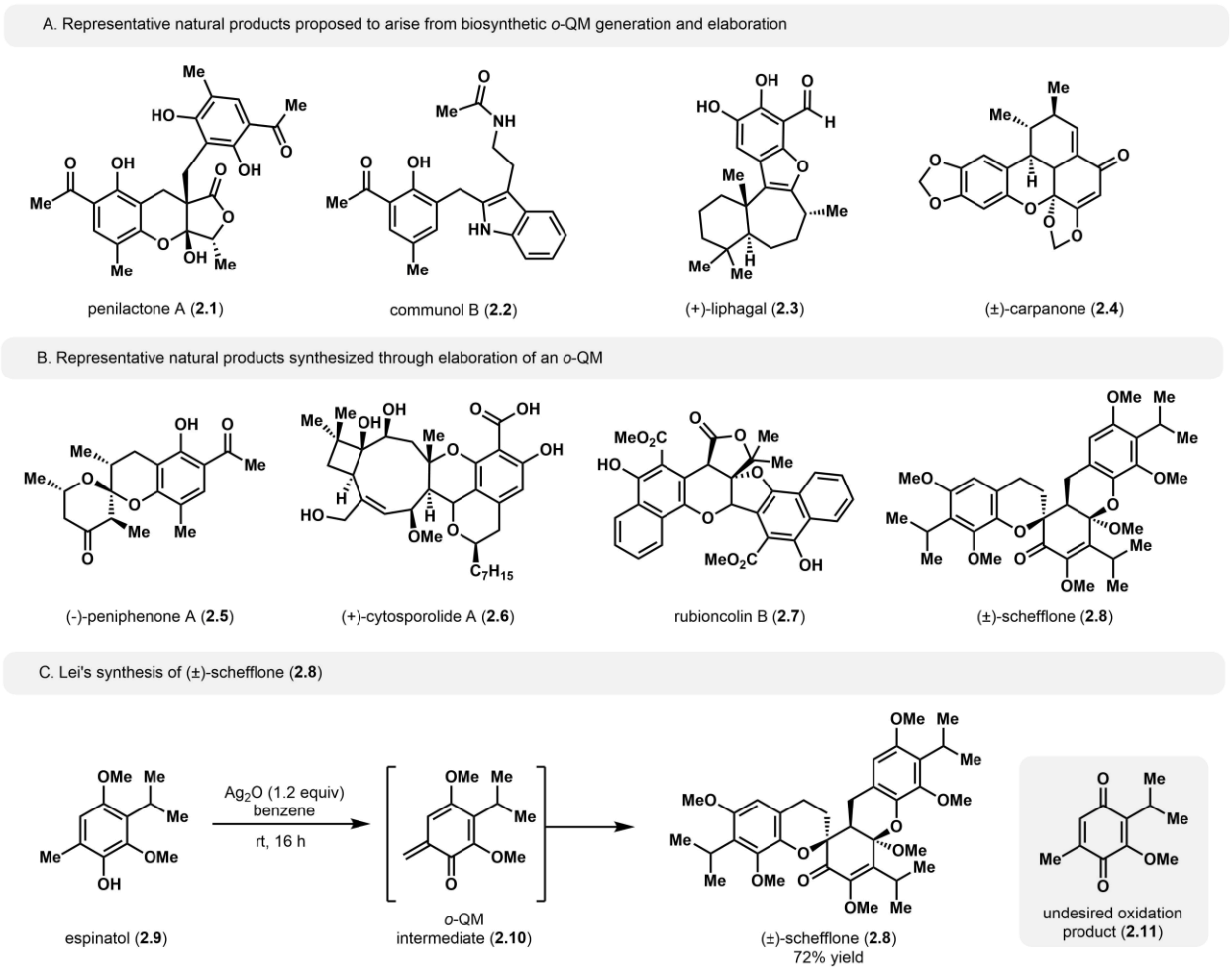


**Figure 2.1. *Ortho*-quinone methide-derived natural products**
A. Representative natural products proposed to arise from biosynthetic *o*-QM generation and elaboration. B. Representative natural products synthesized through elaboration of an *o*-QM. C. Lei's synthesis of (±)-schefflone (**2.8**).

fungal metabolites (Figure 2.1A).[10] Other complex natural products, such as (±)-liphagal (**2.3**)[11-12] and (±)-carpanone (**2.4**)[13-14] are proposed to be generated through modification of *o*-QMs, demonstrating the structurally-diverse array of natural products which can be constructed from this common intermediate (Figure 2.1A). In addition, *o*-QMs have been leveraged for the efficient synthesis of complex natural products and bioactive compounds, such as (−)-peniphenone A (**2.5**),[15] (+)-cytosporolide A (**2.6**),[16] rubioncolin B (**2.7**),[17] and (±)-schefflone (**2.8**),[18] among numerous others.[4-7] These examples demonstrate the synthetic utility of *o*-QMs, which enable

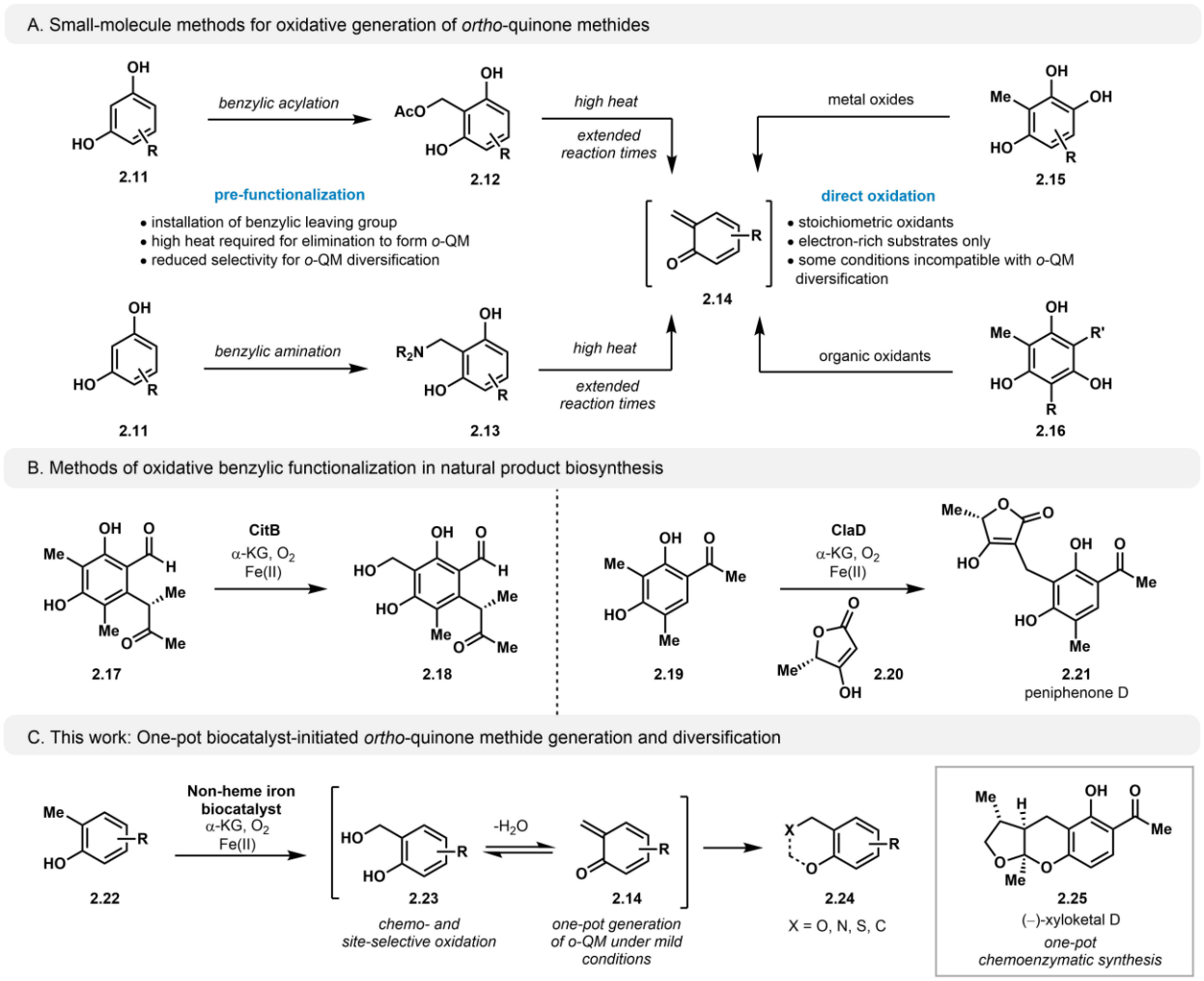


**Figure 2.2. *Ortho*-quinone methide generation and benzylic functionalization**
A. Oxidative methods for generation of *ortho*-quinone methides (*o*-QMs). B. Biocatalytic oxidative benzylic functionalization. C. This work: One-pot biocatalyst-initiated *o*-QM generation and diversification.

direct access to complex, bioactive products through IEDDA or 1,4-addition reactions. Therefore, the development of novel, efficient, and sustainable methods for accessing *o*-QM intermediates provides powerful opportunities for streamlined construction of natural products and their derivatives.[19]

*Oxidative access to ortho-quinone methides*

Synthetic strategies have been developed to access *o*-QMs through the oxidative functionalization of phenolic substrates to generate *o*-QM precursors (Figure 2.2A, **2.11**-**2.12**).[4-7] These methods typically involve the installation and activation of a benzylic leaving group, followed by prolonged heating to generate the corresponding *o*-QM.[15, 20-21] Direct oxidation methods using transition metals or organic oxidants have enabled access to *o*-QMs in a one-pot system without the need for pre-functionalization of the substrate (Figure 2.2A, **2.15**-**2.16**).[4-7, 22-28] However, this approach is generally restricted to electron-rich compounds and often exhibits a lack of control over the chemo- or site-selectivity of oxidation.[4-7, 22-28] For example, in Lei's one-pot synthesis of (±)-schefflone (**2.8**), the natural product is produced through $Ag_2O$-mediated oxidation of an electron-rich *o*-QM precursor (espinatol, **2.9**) and subsequent trimerization of the resulting *o*-QM intermediate **2.10**.[18] In order to achieve the desired transformation, numerous small molecule oxidants and reaction conditions were screened.[18] Most conditions led to undesired oxidation of the aromatic ring of espinatol (**2.9**), forming *p*-quinol product **2.11** as the major product.[18] Only one set of oxidative reaction conditions selectively produced the desired product (**2.8**), highlighting chemo-selectivity challenges which can prevent oxidative *o*-QM synthesis.[18] Extensive screening of small molecule oxidants is often a requirement in the development of direct, oxidative routes to *o*-QMs, presenting a major roadblock to the efficient syntheses of these intermediates.[4, 18] Furthermore, one-pot generation and functionalization of *o*-QMs requires a delicate balance between reactivity of the oxidant and compatibility with reagents for *o*-QM diversification.[4, 27] Often, oxidizing reagents which are required for *o*-QM generation can interfere with downstream functionalization of *o*-QMs or prove incompatible with sensitive moieties present within the substrate.[4] For example, an oxidative approach largely precludes the use of

redox-sensitive nucleophiles, such as thiols and amines, in 1,4-addition reactions with the *o*-QM, thus preventing downstream *o*-QM functionalization. We envisioned that a biocatalytic platform for *o*-QM formation and interception could address these challenges of chemo- and site-selectivity and enable one-pot generation and derivatization of an *o*-QM.

Inspired by the efficiency of Nature's approach, we sought to exploit an enzymatic strategy for *o*-QM creation.[8] Biosynthetically, *o*-QMs are proposed to arise from *ortho*-cresol precursors (see **2.17**, **2.19**, Figure 2.2B) through hydroxylation at the benzylic position, followed by loss of water to afford an *o*-QM under mild intracellular conditions.[8] These intermediates can be intercepted by bioavailable dienophiles or nucleophiles to build the core scaffold of various natural products, including peniphenone D (**2.21**).[8] We envisioned a biocatalytic approach to oxidative *o*-QM generation would afford a selective and sustainable method for increasing the structural complexity of simple arene precursors (Figure 2.2C). This approach would combine the selectivity advantages of biocatalytic pre-functionalization with the ability to generate and diversify *o*-QMs in a single vessel under mild conditions. We also anticipated that the reactive nature of *o*-hydroxybenzylic alcohols would reduce required reaction times and temperatures, leading to efficient functionalization of the resulting *o*-QM.

*Biocatalytic benzylic C–H oxidation*

Nature has evolved numerous tools for the oxidation of benzylic C–H bonds. Several reports have highlighted the utility of biotransformations in accomplishing this challenging reaction.[29-34] These methods rely on native monooxygenases present in microbes to accomplish benzylic oxidation on a range of substrates.[29-34] Several cytochromes P450 have also been identified as promising *in vitro* catalysts for benzylic C–H oxygenation.[35-43] Whereas these

biocatalytic methods do not offer complete control over the final oxidation state of the product, they successfully reduce the overall environmental impact of the transformation by using earth-abundant iron as the catalytic metal, molecular oxygen as the stoichiometric oxidant, and water as the bulk solvent.[35-43]

Motivated by the advantages of an enzymatic approach to benzylic hydroxylation, we sought to demonstrate the chemo- and site-selectivity of biocatalytic C–H functionalization and opportunities for cascade reactions under biocatalytic reaction conditions. We anticipated that an α-ketoglutarate-dependent (α-KG) non-heme iron oxygenase could be employed for the selective oxidation of primary benzylic C–H bonds. This well-studied enzyme family has demonstrated scalability[44] and tunability through protein engineering to alter substrate scope.[45] By coupling the activation of molecular oxygen to the decarboxylation of inexpensive α-oxoacid co-substrates, these enzymes generate an iron(IV)-oxo species capable of hydrogen-atom abstraction.[46-47] α-KG-dependent non- heme iron oxygenases catalyze a wide variety of selective transformations following this conserved mechanism, including hydroxylation, halogenation, epoxidation, desaturation, epimerization, endo-peroxidation, ring-contraction, and ring-expansion.[46-48] Unlike many P450s, α-KG-dependent non-heme iron oxygenases do not require an exogenous reductase to complete their catalytic cycle.[46-47] We anticipated that the simple reaction requirements of this enzyme class would provide distinct advantages in developing a widely applicable platform.

Our search for biocatalysts capable of selective benzylic C–H hydroxylation led us to two homologous fungal NHI oxygenases (sharing 54% sequence identity): CitB, from *Monascus ruber*, and ClaD, native to *Penicillium crustosum*.[49] Cox and coworkers demonstrated through *in vivo* experiments that CitB performs a benzylic hydroxylation in the biosynthesis of the mycotoxin citrinin (**2.17**-**2.18**, Figure 2.2B).[49] ClaD was shown by Li and coworkers to perform a similar

transformation in the biosynthesis of peniphenones and penilactones (Figure 2.2B, **2.19**-**2.21**).[8] We envisioned employing CitB and ClaD as general catalysts for benzylic hydroxylation of *ortho*-cresol substrates. We anticipated that, following benzylic C–H bond oxidation, an *o*-QM intermediate (see **2.22**-**2.24** Figure 2.2C) could be accessed and intercepted with a variety of nucleophiles or dienophiles to form benzylic C–O, C–N, C–S, and C–C bonds in a biomimetic fashion.[8] Here, we demonstrate this approach with two biocatalysts, but we anticipate this chemoenzymatic platform could be executed with a plethora of wild-type enzymes to access more diverse substrates and complementary selectivity.

## 2.2 Analytical-scale biocatalytic benzylic C–H hydroxylation

*Proof-of-principle transformation and comparative study with chemical oxidations*

Toward developing a chemoenzymatic method for benzylic C–H functionalization, we tested the feasibility of biocatalytic C–H hydroxylation, coupled with *o*-QM formation and derivatization with a model substrate (see **2.26**, Figure 2.3) that captures the conserved methyl resorcinol core of CitB and ClaD's native substrates. This model compound maintained the redox-sensitive aldehyde moiety and hydroxyl groups present in the citrinin biosynthetic intermediate (**2.27**). Model compound **2.26** was completely consumed in 3 h upon exposure to 0.4 mol % CitB in the presence of α-KG, an iron(II) source and sodium ascorbate in 50 mM TES buffer at pH 7.5 (Figure 2.3). From this reaction, a single benzylic alcohol product (**2.27**) was isolated in 82% yield without any evidence of oxidation of either the aldehyde or the resorcinol core. This result demonstrated that CitB could function on a non-native substrate with the robustness needed for preparative-scale synthesis with precise chemo- and site-selectivity. As a comparative measure,

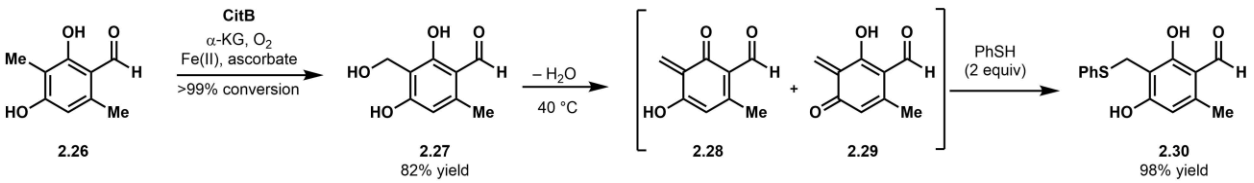


**Figure 2.3. Initial experiments to assess feasibility of NHI biocatalyst-initiated *o*-QM formation and functionalization.**

we subjected substrate **2.26** to several chemical oxidation conditions and did not observe conversion to the desired benzylic alcohol **2.27** (see Table 2.S1). For example, attempts to oxidize **2.26** with DDQ[50] resulted in over-oxidation to the bis-aldehyde and no reaction was observed upon exposure of **2.26** to $MnO_2$[51] or $Ag_2O$.[52] Efforts to perform benzylic hydroxylation with $K_2S_2O_8$[53] or cerium ammonium nitrate[54] led to decomposition of the substrate. Radical bromination conditions with AIBN/NBS resulted in aromatic bromination and did not generate the desired benzylic halide for subsequent hydrolysis to the benzyl alcohol.[55] These results capture the challenge in accomplishing this seemingly simple benzylic hydroxylation in the presence of redox-sensitive aldehyde and phenolic groups. Next, the reactivity of benzylic alcohol **2.27** was investigated under aqueous conditions. Gratifyingly, upon gentle heating in the presence of thiophenol, alcohol **2.27** was quantitatively transformed into thioether **2.300** through an anticipated *o*-QM intermediate (**2.28**-**2.29**). These experiments provided evidence for *o*-QM formation under remarkably mild conditions compared to previous reports for the generation of *o*-QMs from *ortho*-hydroxy benzylic alcohols.[5, 56-57]

*Analytical-scale substrate screen and analysis*

Evidence that CitB is sufficiently robust to perform preparative-scale reactions and provide access to *o*-QMs under mild conditions spurred further investigation of this chemoenzymatic

strategy, including studies with the homologous NHI enzyme, ClaD. To investigate the substrate scope of CitB and ClaD, a panel of substrates was synthesized possessing a conserved *ortho*-cresol core (Figure 2.4).[58] This panel was designed to define the electronic and steric parameters of substrates that undergo a productive reaction with the NHI biocatalysts. Compounds **2.19**, **2.26**, and **2.31**-**2.50** were subjected to analytical-scale reactions with CitB and ClaD, using standard conditions for α-KG-dependent non-heme iron oxygenases.[48] These analytical-scale reactions were performed *in vitro* with purified enzyme (Figure 2.S5), as well as in whole cell or crude cell lysate format (Figure 2.4). For CitB, a whole cell reaction platform led to efficient benzylic C–H hydroxylation. Whereas, filtered crude cell lysate produced the best results for ClaD. Both of these reaction platforms provide an operationally-simple method (see Section 2.6, Part III) for preparing and using NHI biocatalysts in a manner that is amenable to preparative-scale reactions, avoiding arduous protein purification steps.[59-61]

Analytical-scale reactions revealed that CitB and ClaD each selectively hydroxylate compounds with a variety of steric and electronic properties (Figure 2.4). Introducing bulky, electron-withdrawing or electron-donating groups at either the C5 or C6 position was tolerated in reactions with CitB. However, ClaD demonstrated limitations in its ability to accept larger groups, such as phenyl substituents at C5 and C6 (see **2.44** and **2.40**). The complementarity in substrate scope between CitB and ClaD is also observed in the substitution at C4. For CitB, the formyl group at C4 can be substituted with alternative electron-withdrawing substituents such as a nitro group (**2.33**) or imine (**2.32**). However, substrates with greater steric bulk at C4, such as ketone substrates, were generally not hydroxylated by CitB. ClaD demonstrated complimentary activity in its ability to react with ester (**2.36**) and a variety of ketones (see **2.34**, **2.35**, **2.37**). The importance of this C4 substituent is also highlighted by the lack of reaction observed with 2,5-

dimethylresorcinol (**2.31**). Based on preliminary analysis of models of these biocatalysts, we anticipate that a hydrogen bond acceptor is critical at the C4 position to achieve a catalytically active conformation of the substrate-enzyme complex. Current efforts are focused on obtaining homologues or enzyme variants that do not require substrates bearing a hydrogen bond acceptor, such as an aldehyde, for a productive reaction to occur.

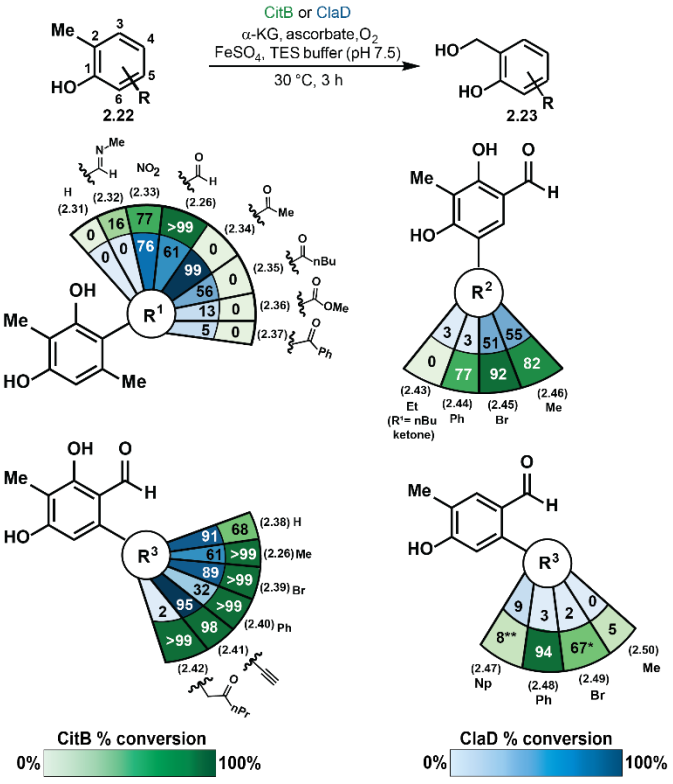


**Figure 2.4. Substrate scope for CitB and ClaD-catalyzed benzylic C–H hydroxylation.** Reaction conditions: 2.5 mM substrate, 45 mg/mL CitB wet cell pellet or 10% v/v ClaD crude cell lysate, 50 mM TES pH 7.5, 5 mM α-ketoglutaric acid (α-KG), 8 mM sodium ascorbate (NaAsc), 0.1 mM ferrous sulfate ($FeSO_4$), 30 °C, 100 rpm shaking, 3 h. [*] with 15% acetonitrile as cosolvent. [**] with 15% tetrahydrofuran as cosolvent. Conversion to product was quantified by UPLC-DAD analysis.

To probe the substrate scope of our biocatalysts beyond resorcinol substrates, phenolic compounds **2.50** and **2.S6** (see Figure 2.S5) were subjected to NHI hydroxylation conditions. Phenol **2.50** was converted to the corresponding benzylic alcohol; however, the position of the hydroxyl group proved to be important for catalysis as phenol **2.S6** was not oxidized by either CitB or ClaD. These results motivated us to synthesize an additional panel of phenolic substrates to further assess the scope of NHI biocatalytic hydroxylation (**2.47**-**2.49**). In the case of CitB, increasing the steric bulk at the C5 position increased the conversion of substrates to hydroxylated products except for 2-naphthyl substrate **2.47**, which

demonstrated decreased conversion, possibly reflecting the steric limitations of the CitB active site. ClaD showed minimal ability to hydroxylate phenolic substrates **2.47**-**2.50**.

Detailed analysis of reactions of CitB and ClaD with a diverse library of substrates demonstrated that these related enzymes exhibited complementary reactivity toward *o*-cresol substrates. Furthermore, these two enzymes represent a minute fraction of the annotated NHI sequences.[35-36] We anticipate that the substrate scope of this NHI platform for *o*-QM generation can be further expanded by screening NHI enzyme libraries for activity against target substrates. Enzymes demonstrating even low levels of activity with test compounds would serve as excellent starting points for routine protein engineering to achieve improved product yields.

### 2.3 Preparative-scale biocatalytic benzylic C−H hydroxylation and computational analysis

As a next step in the evaluation of the synthetic utility of biocatalytic benzylic hydroxylation, we performed reactions on preparative-scale using whole cell (CitB) and crude cell lysate (ClaD) conditions (Figure 2.5). This method enabled routine performance of reactions on >500 mg scale without the requirement for protein purification. Isolation and characterization of C5-substituted benzylic alcohol products **2.27** and **2.54**-**56** was achieved with yields that corresponded to starting material consumption. For example, benzylic alcohol **2.27** was isolated in 82% yield. However, poor isolated yields were obtained for substrates with C6-substituents, despite nearly complete consumption of starting material (see **2.57**-**2.61**). Further analysis of the crude product mixture from these reactions revealed a second product, in which a molecule of ascorbic acid had been incorporated, presumably through interception of an intermediate *o*-QM (see Figure 2.S63).

The observed reactivity of C6-substituted alcohols was explored computationally in collaboration with Kevin Skinner and Prof. Paul Zimmerman. This reactivity can be explained by

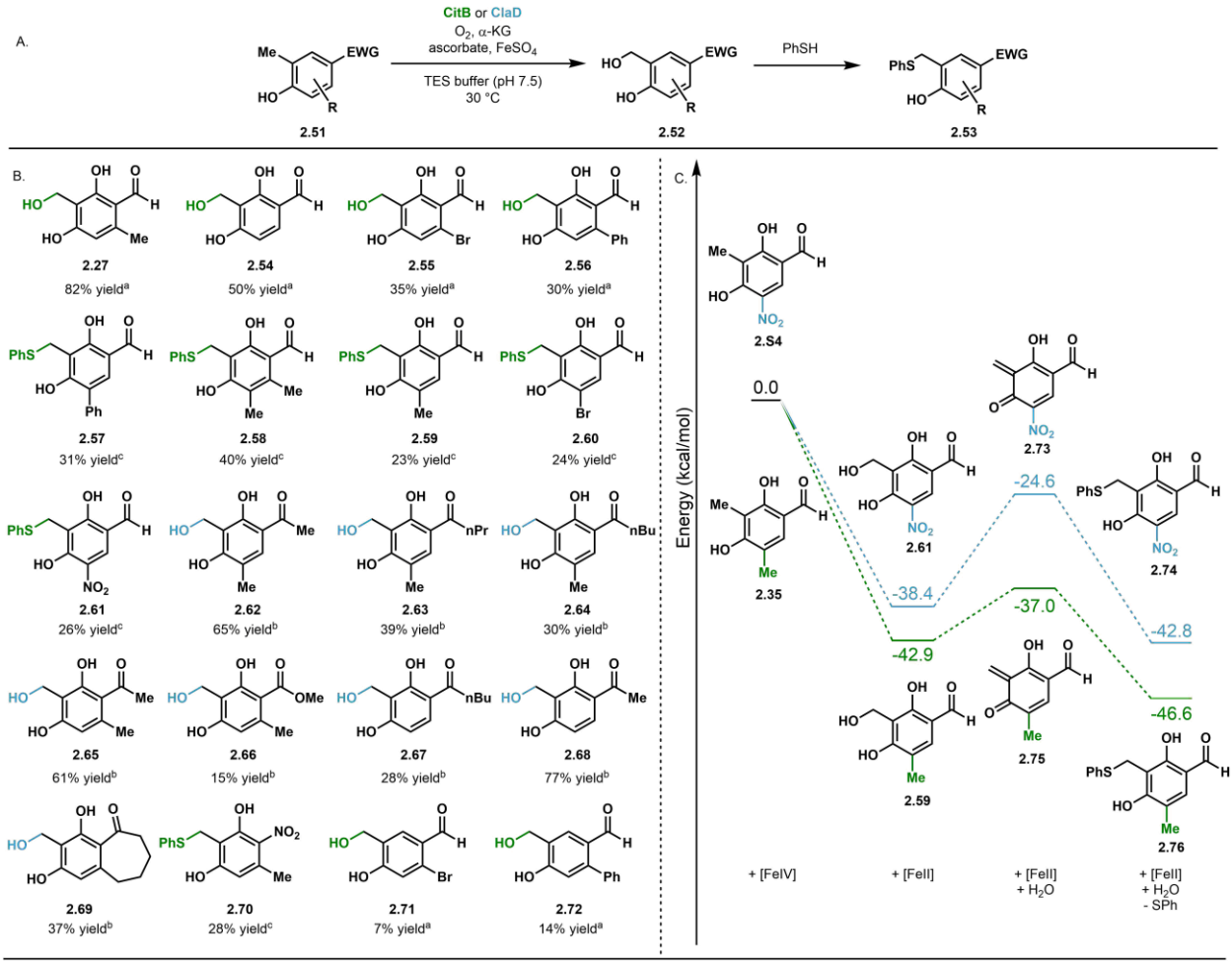


**Figure 2.5. Preparative-scale biocatalytic benzylic C–H hydroxylation and computational analysis.**

A. General scheme for CitB and ClaD-catalyzed benzylic hydroxylation and in situ functionalization with thiophenol. B. Preparative scale reaction isolated yields for CitB-catalyzed hydroxylation and functionalization. Reaction conditions: 2.5 mM substrate, [a]45 mg/mL CitB wet cell pellet or [b]10% v/v ClaD clarified cell lysate, 50 mM TES pH 7.5, 5 mM α-ketoglutaric acid (α-KG), 8 mM sodium ascorbate (NaAsc), 0.1 mM ferrous sulfate ($FeSO_4$), 30 °C, 100 rpm shaking, 3 h. [c] PhSH was added directly to reaction mixture after conversion to benzylic alcohol and incubated at 40 °C, 3 h, 100 rpm shaking. C. Thermodynamic analysis of C6-methyl (green) and C6-nitro (blue) substrates. Structures represent the starting material, benzylic alcohol product, *o*-QM, and thiophenol adducts (left to right). The energies are mass balanced with a truncated 2-His-1-Asp non-heme iron system (see Figure 2.S86). Geometry optimizations and frequency calculations were performed at B3LYP 6-311++G** and 6-31G** for iron. Computational analysis performed by Kevin Skinner.

thermodynamics of the reaction sequence of **2.51** to **2.53** (Figure 2.5A), which includes hypothetical substrates to explore the electronic effects at both the C5 and C6 positions (see Section 2.6 Part XIV for detailed analysis). We identified a relationship between inductive effects and Gibbs free energy. The thermodynamic trends indicated that benzylic alcohols with electron-withdrawing substituents at the C6-position were less thermodynamically stable, making these substrates more reactive and prone to generation of an *o*-QM. This computational data supported our experimental observations. Therefore, we hypothesized that higher yields could be achieved if the reactive benzylic alcohol products were first trapped *in situ* as more stable benzylic thioethers. The corresponding thermodynamic analysis of thiophenol adducts **2.74** and **2.76** revealed that, regardless of substitution, the benzylic thioethers are lower in energy than their respective benzylic alcohol precursors (Figure 2.5C, Figures 2.S88 and 2.S89). To test this hypothesis, we developed an *in situ* functionalization protocol, demonstrating that increasing the reaction temperature to 40 °C and adding two equivalents of thiophenol led to the isolation of the desired benzylic thioethers **2.57**-**2.61** and **2.70** as the sole product in each reaction.

### 2.4 One-pot chemoenzymatic *o*-QM formation and elaboration

Motivated by this initial success in generating and diversifying *o*-QMs under mild conditions, we assessed the range of products accessible through this cascade. First, a panel of nucleophiles was evaluated in 1,4-addition reactions (Figure 2.6, **2.80-2.84)**. Both linear and branched alcohols were competent nucleophiles, affording the desired products (**2.80**-**2.82**) in good yields. A secondary amine nucleophile was also productive (**2.84**); however, reactions with primary amines resulted in an undesired condensation reaction with the pendant aldehyde. Thiol

nucleophiles reacted smoothly to provide the desired conjugate addition products (**2.30** and **2.83**) in excellent yields. The comparatively high yield of thioether adducts relative to alkyl ether adducts is likely due to the increased nucleophilicity of sulfur compared to the alcohol precursor as well as the increased stability of the sulfur adducts.

The feasibility of benzylic C–C bond formation was probed through inverse electron-demand Diels-Alder (IEDDA) reactions. The reactivity of biocatalyst-generated benzylic alcohol **2.27** with various dienophiles was evaluated through a one-pot reaction sequence. Following generation of **2.27** by CitB, the reaction mixture was heated to 45 °C in the presence of ethyl vinyl ether. Gratifyingly, chroman products **2.85** and **2.86** were produced in 64% and 27% yield, respectively. Reactions with electron-rich dienophiles (**2.87**-**2.90**) proceeded smoothly to deliver mixtures of two isomeric products derived from the two possible *o*-QM intermediates (**2.28** and **2.29**). Reactions employing electron-rich dienophiles typically afforded 4:1 mixtures of isomeric products, favoring the product derived from reaction with the C1 *o*-QM (**2.28**). Reactions with styrenes **2.91**-**2.94** were also carried out. Due to the electron-deficient character of these dienophiles, these reactions required a higher temperature, 65 °C, to undergo a productive reaction.[4] The major products of these IEDDA reactions resulted from reaction with *o*-QM **2.29**. This operationally-simple, one-pot protocol accomplishes the direct conversion of benzylic C–H bonds to C–O, C–N, C–S and C–C bonds, allowing for direct access to diverse chemical scaffolds and demonstrating the synthetic utility of these biocatalysts.

Upon the observation that *o*-QM generation occurs at reduced temperatures, we hypothesized that these reactions likely proceed through low barrier processes. This was assessed and confirmed computationally using benzylic alcohol **2.27**. We generated models for both C1 and C3 *o*-QMs and modelled the subsequent IEDDA reactions (Figure 2.S82). In this model, *o*-QM

generation was found to proceed through a concerted, low barrier transition state, while reactions with ethyl vinyl ether and styrene were found to proceed through concerted, asynchronous transition states that are typically proposed for IEDDA mechanisms (Figures 2.S83 and 2.S84).

To highlight the advantages of this biocatalytic route to *o*-QMs, we sought applications that require chemoselectivity and mild reaction conditions. Specifically, we tested this chemistry in the selective modification of biomolecules, an application that demands both of these attributes.[62-64] We envisioned the selective modification of cysteine residues in peptides and proteins could be possible under physiological conditions. Two complementary peptides were synthesized: one peptide that contained a cysteine residue (**2.97**) and another in which the cysteine was replaced with a lysine residue (**2.S15**). Substrate **2.26** was subjected to *in vitro* CitB-catalyzed hydroxylation conditions in the presence of either peptide **2.97** or **2.S15**. After an 18 h incubation the cysteine-containing peptide was converted only to singly-modified peptide **2.98** (61% conversion). Under the same conditions, the peptide containing a lysine in place of cysteine (**2.S15**) was not modified. These cascade reactions demonstrate the utility of this biocatalytic method for *in situ* functionalization of peptides. We anticipate this method could be applied to the selective labelling of peptides with reactive molecules generated *in situ*. Further, the compatibility of this method with aldehyde and alkyne substrates provides an additional handle for introducing chromophores or fluorophores using biorthogonal chemistry.[65-67]

Finally, to highlight the advantages of our mild one-pot protocol we targeted the chroman natural product, (–)-xyloketal D (**2.25**), a fungal metabolite from *Xylaria* sp. first isolated from the South China Sea.[68] Synthetic strategies have been developed for the synthesis of (–)-xyloketal D including a Diels-Alder cycloaddition by Wilson,[20] a sequential Michael-addition ketalization sequence by Flörke[69] and, more recently, a gold-catalyzed cycloisomerization reported by Sarkar

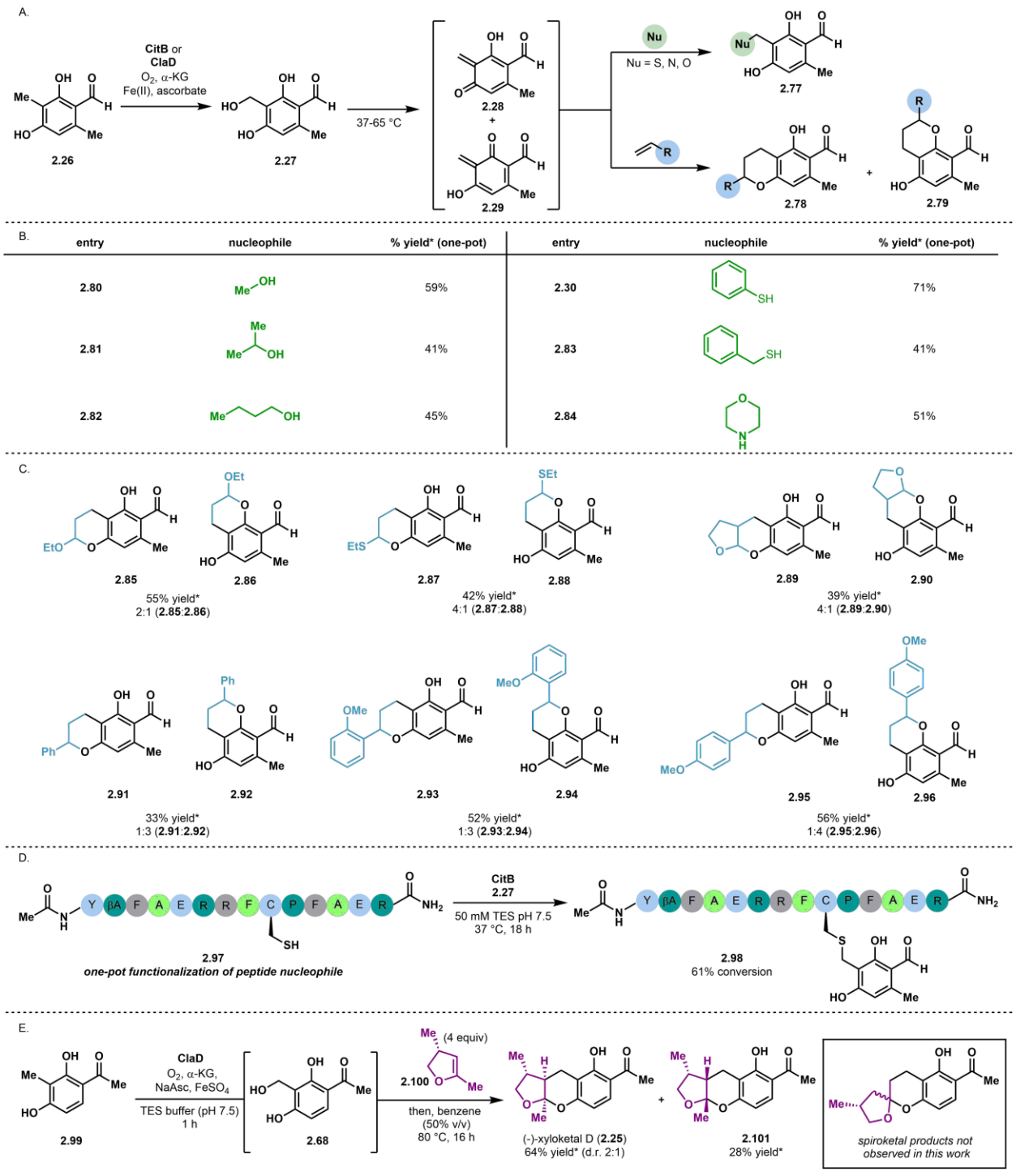


**Figure 2.6**. **One-pot NHI biocatalyst-initiated *o*-QM generation and diversification.**
A. Synthetic scheme for one-pot NHI biocatalyst-initiated *o*-QM generation and diversification. B. Yields of one-pot Michael addition reactions. C. Yields of one-pot IEDDA reactions. D. One-pot functionalization of cysteine-containing peptide. E. One-pot chemoenzymatic synthesis of (–)-xyloketal D (**2.25**). *HPLC yield

and Panda in 2013.[70] Wilson and co-workers employed an *o*-QM as a key intermediate, with thermal conditions for *o*-QM generation leading to a 37% combined yield of 4 products, including (**–**)-xyloketal D (**2.25**) and the associated ketal diastereomer (**2.101**), as well as two diastereomeric spiroketals, in a 2:1 ratio of ketal to spiroketal isomers. In this case, the formation of spiroketal products is a result of undesired isomerization of the dienophile under the thermal reaction conditions.[20] Our chemoenzymatic strategy avoids this issue by providing a more reactive *o*-QM precursor (see Figure 2.S93) circumventing any dienophile isomerization challenges. After synthesis of chiral dienophile **2.100,** according to Wilson's established procedure, we subjected methyl ketone **2.99** to our conditions for biocatalytic benzylic C–H hydroxylation with ClaD crude lysate, obtaining complete conversion to benzylic alcohol **2.68**. Following the enzymatic C–H benzylic hydroxylation step, benzene was added directly to the biocatalytic reaction mixture, along with dienophile **2.100**. The reaction tube was sealed and heated to 80 °C for 16 h. This process generated (–)-xyloketal D (**2.25**, 64% yield) in a 2:1 ratio with its diastereomer (**2.101**, 28% yield) and no detectable formation of unwanted spiroketal products. Thus, our approach enabled a one-pot chemoenzymatic synthesis of (–)-xyloketal D (**2.25**), with improved yields and under mild conditions.[20] We anticipate this one-pot chemoenzymatic strategy will facilitate the streamlined synthesis of a variety of natural products.

## 2.5 Conclusions

We have demonstrated the utility of a biocatalytic platform for chemo- and site-selective C–H functionalization of *ortho*-cresol substrates. Leveraging this biocatalytic hydroxylation, *o*-QMs can be accessed readily and intercepted in one-pot to form C–C, C–N, C–S, and C–O bonds.

The chemoselective, mild nature of this sequence allows for interception of *o*-QMs with small-molecule and peptide nucleophiles as well as electron-rich dienophiles, exemplified in the total synthesis of (–)-xyloketal D. This platform offers a strategy for accessing *o*-QMs that is complementary to existing methods, offering new options to practicing organic chemists. We anticipate that biocatalyst-initiated *o*-QM generation can be broadly applied to other biocatalysts capable of benzylic C–H hydroxylation and will enable transformations complementary to small molecule catalysts and reagents.

## 2.6 Experimental

### I. Substrate and peptide synthesis

**General Information:** All reagents were used as received unless otherwise noted. Reactions were carried out under a nitrogen atmosphere using standard Schlenk techniques unless otherwise noted. Solvents were degassed and dried over alumina columns on an MBraun solvent system (Innovative Technology, Inc., Model PS-00-3). Reactions were monitored by thin layer chromatography using Millipore 60 F254 pre-coated silica TLC plates (0.25 mm) which were visualized using UV, *p*-anisaldehyde, CAM, DNP, or bromocresol green stains. Flash column chromatography was performed using Machery-Nagel 60 μm (230-400 mesh) silica gel. All compounds purified by column chromatography were sufficiently pure for use in further experiments unless otherwise indicated. $^{1}$H and $^{13}$C NMR spectra were obtained in $CDCl_3$ at rt (25 °C), unless otherwise noted, on Varian 400 MHz or Varian 600 MHz spectrometers. Chemical shifts of $^{1}$H and $^{13}$C NMR spectra were recorded in parts per million (ppm) on the δ scale. High resolution electrospray mass spectra were obtained on an Agilent 1290 Series Infinity II HPLC with a 6230 Series Time-of-Flight mass spectrometer or an Agilent 1290 Series Infinity HPLC with a 6545 Series Quadrupole-Time-of-

Flight mass spectrometer. UPLC-PDA spectrometric traces were obtained on a Waters Aquity H-class instrument. IR spectra were recorded on a Perkin-Elmer Spectrum BX FT-IR spectrometer.

Compounds **2.8**, **2.26**, **2.23**, **2.26**-**2.28**, **2.30**-**2.36**, and **2.39** were prepared and characterized by our lab previously.[58] Details of this characterization can be found in the Supplementary Information of the provided reference. Compound **2.29** (methyl atratate) was purchased from Sigma Aldrich and used without further purification.

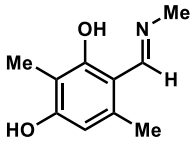


**2,5-dimethyl-4-((methylimino)methyl)benzene-1,3-diol (2.32)**

A flame-dried vial equipped with a stir bar was charged with 2,4-dihydroxy-3,6-dimethylbenzaldehyde (100 mg, 0.604 mmol, 1.00 equiv), methylamine hydrochloride (80 mg, 1.2 mmol, 2.0 equiv), and MeOH (1.2 mL, 0.50 M). The reaction was heated at 65 °C with stirring for 18 h during which time a pink solid precipitated out of the reaction. After cooling to room temperature, EtOAc (5 mL) was added to the reaction mixture. The reaction mixture was filtered to collect the pink solid. The pink solid was dissolved in water (5 mL) and added to a separatory funnel followed by the addition of saturated $NaHCO_3$ (10 mL). This mixture was extracted with EtOAc (3 x 15 mL). The combined organic layers were washed with brine, dried over $Na_2SO_4$, and concentrated under reduced pressure to afford 107 mg (99% yield) of the title compound as a pink solid. The material was used without further purification. **$^1$H NMR** (599 MHz, $CDCl_3$) δ 8.37 (s, 1H), 6.09 (s, 1H), 3.39 (s, 3H), 2.32 (s, 3H), 2.09 (s, 3H); **$^{13}$C NMR** (151 MHz, $CDCl_3$) δ 168.1,

162.5, 158.1, 137.3, 110.1, 109.3, 108.0, 42.8, 18.7, 7.4; **HRMS (ESI)** *m/z*: $[M-H]^-$ calculated for $C_{10}H_{12}NO_2^-$ 178.0874, found 178.0877; **IR** (thin film): 2925, 2652, 1733, 1643, 1606, 1502, 1457, 1392, 1351, 1256, 1148, 1111, 1029, 1005 $cm^{-1}$.

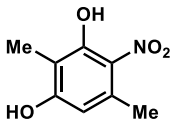


**2,5-dimethyl-4-nitrobenzene-1,3-diol (2.33)**

A flame-dried round-bottom flask equipped with a stir bar was charged with 2,5-dimethylbenzene-1,3-diol (100 mg, 0.724 mmol, 1.00 equiv) and $Cu(NO_3)_2 \cdot 2.5H_2O$ (101 mg, 0.434 mmol, 0.600 equiv). The flask was cooled to 0 °C and $Ac_2O$ (1 mL, 0.7 M) was added to the reaction. The reaction was stirred for 3 h before water (5 mL) was added to the reaction and the mixture extracted with EtOAc (3 x 10 mL). The combined organic layers were washed with brine, dried over $Na_2SO_4$, and concentrated under reduced pressure. Purification on silica gel (gradient elution 1% to 75% EtOAc in hexanes) afforded 64 mg (35% yield) of the title compound as a yellow solid. All spectroscopic data for the compound was in accordance with literature values.[71] **$^1$H NMR** (599 MHz, $CD_3OD$) δ 6.32 (s, 1H), 2.49 (s, 3H), 2.06 (s, 3H); **HRMS (ESI)** *m/z*: $[M-H]^-$ calculated for $C_8H_8NO_4^-$ 182.0459, found 182.0460.

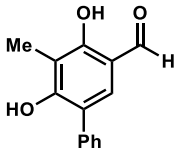


**4,6-dimethoxy-5-methyl-[1,1'-biphenyl]-3-carbaldehyde (2.48)**

A flame-dried round-bottom flask equipped with a magnetic stir bar was charged with 5-bromo-2,4-dimethoxy-3-methylbenzaldehyde (200 mg, 0.772 mmol, 1.00 equiv), $K_2CO_3$ (267 mg, 1.93

mmol, 2.50 equiv) and 1,4-dioxane (4 mL, 0.25 M). Phenylboronic acid (188 mg, 1.54 mmol, 2.00 equiv) and $Pd(PPh_3)_4$ (89 mg, 0.077 mmol, 0.10 equiv) were added to the flask. The reaction mixture was stirred and heated at 80 °C for 24 h before being cooled to rt and quenched by addition of 5 mL of saturated $NaHCO_3$. The reaction mixture was extracted with EtOAc (3 x 20 mL). The combined organic layers were washed with brine, dried over $Na_2SO_4$, and concentrated under reduced pressure. The crude solid was transferred to a flame-dried round-bottom flask equipped with a magnetic stir bar and dichloromethane (3 mL, 0.25 M) was added. The flask was cooled to -78 °C before $BBr_3$ (183 μL, 1.92 mmol, 2.50 equiv) was added to the reaction dropwise by syringe over 5 min. The reaction was removed from the cooling bath, allowed to warm to room temperature, and stirred for 18 h. Next, the reaction was cooled to 0 °C and quenched by slow addition of ice water (5 mL) by syringe followed by stirring for 10 min. The reaction mixture was extracted with EtOAc (3 x 10 mL). The combined organic layers were washed with brine, dried over $Na_2SO_4$, and concentrated under reduced pressure. Purification on silica gel (gradient elution 5% to 40% EtOAc in hexanes) afforded 148 mg (84% yield) of the title compound as a white solid. **$^1$H NMR** (599 MHz, $CD_3OD$) δ 9.70 (s, 1H), 7.45 (d, *J* = 7.3 Hz, 2H), 7.41 (t, *J* = 7.6 Hz, 2H), 7.35 (s, 1H), 7.33 (t, *J* = 7.4 Hz, 1H), 2.14 (s, 3H); **$^{13}$C NMR** (151 MHz, $CD_3OD$) δ 196.7, 162.1, 161.4, 138.9, 134.9, 130.5, 129.5, 128.2, 124.2, 116.0, 112.8, 7.9; **HRMS (ESI)** *m/z*: $[M-H]^-$ calculated for $C_{14}H_{11}O_3^-$ 227.0714, found 227.7011; **IR** (thin film): 2926, 1625, 1425, 1377, 1305, 1188, 1073, 746, 703, 573 $cm^{-1}$.

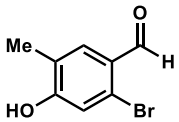


**2-bromo-4-hydroxy-5-methylbenzaldehyde (2.49)**

A flame-dried round-bottom flask equipped with a magnetic stir bar was charged with 5-bromo-2-methylphenol (2.00 g, 10.7 mmol, 1.00 equiv) and dichloromethane (107 mL, 0.1 M). The reaction was cooled to 0 °C and $TiCl_4$ (1.41 mL, 12.8 mmol, 1.20 equiv) was added dropwise. The reaction was stirred at 0 °C for 30 min before dichloromethyl methyl ether (1.06 mL, 11.8 mmol, 1.10 equiv) was added dropwise. The reaction mixture was allowed to warm to room temperature over 18 h with stirring. The reaction mixture was transferred to a separatory funnel and quenched by addition of saturated $NaHCO_3$ (150 mL). The mixture was extracted with dichloromethane (3 x 100 mL). The combined organic layers were washed with brine, dried over $Na_2SO_4$, and concentrated under reduced pressure. Purification on silica gel (gradient elution 5% to 40% EtOAc in hexanes) afforded 528 mg (23% yield) of the title compound as a white solid. **$^1$H NMR** (599 MHz, $CD_3OD$) δ 10.08 (s, 1H), 7.66 (s, 1H), 7.03 (s, 1H), 2.17 (s, 3H); **$^{13}$C NMR** (151 MHz, $CD_3OD$) δ 191.9, 163.6, 132.9, 126.9, 126.8, 126.7, 119.8, 15.7; **HRMS (ESI)** *m/z*: $[M-H]^-$ calculated for $C_8H_6O_2Br^-$ 212.9557, found 212.9576; **IR** (thin film): 3083, 1650, 1580, 1494, 1263, 1139, 981, 901, 850, 641, 447 $cm^{-1}$.

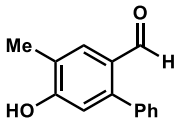


**4-hydroxy-5-methyl-2-phenylbenzaldehyde (2.48)**

A flame-dried round-bottom flask equipped with a magnetic stir bar was charged with 2-bromo-4-hydroxy-5-methylbenzaldehyde (25 mg, 0.12 mmol, 1.0 equiv), $K_2CO_3$ (48 mg, 0.35 mmol, 3.0 equiv), and 1,4-dioxane (1.0 mL, 0.12 M). Phenylboronic acid (28 mg, 0.23 mmol, 2.0 equiv) and $Pd(PPh_3)_4$ (27 mg, 0.023 mmol, 0.20 equiv) were added to the flask. The reaction mixture was stirred and heated at 80 °C for 24 h before being cooled to room temperature and quenched by addition of 3 mL of saturated $NaHCO_3$. The reaction mixture was extracted with EtOAc (3 x 10

mL). The combined organic layers were washed with brine, dried over $Na_2SO_4$, and concentrated under reduced pressure. Purification on silica gel (gradient elution 5% to 40% EtOAc in hexanes) afforded 15 mg (48% yield) of the title compound as a yellow solid. **$^1$H NMR** (599 MHz, $CD_3OD$) δ 9.66 (s, 1H), 7.76 (s, 1H), 7.50-7.38 (m, 3H), 7.38-7.31 (m, 2H), 6.75 (s, 1H), 2.26 (s, 3H); **$^{13}$C NMR** (151 MHz, $CD_3OD$) δ 192.5, 162.5, 148.4, 139.4, 131.4, 131.0, 129.4, 129.0, 127.0, 126.3, 116.9, 15.8; **HRMS (ESI)** *m/z*: $[M-H]^-$ calculated for $C_{14}H_{11}O_2^-$ 211.0765, found 211.0766. **IR** (thin film): 2923, 2329, 1742, 1650, 1578, 1487, 1276, 1138, 979, 872, 768, 703, 649 $cm^{-1}$.

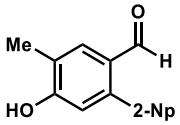


**4-hydroxy-5-methyl-2-(naphthalen-2-yl)benzaldehyde (2.47)**

A flame-dried round-bottom flask equipped with a magnetic stir bar was charged with 2-bromo-4-hydroxy-5-methylbenzaldehyde (25 mg, 0.12 mmol, 1.0 equiv), $K_2CO_3$ (48 mg, 0.35 mmol, 3.0 equiv), and 1,4-dioxane (1.0 mL, 0.12 M). Naphthalene-2-boronic acid (42 mg, 0.23 mmol, 2.0 equiv) and $Pd(PPh_3)_4$ (27 mg, 0.023 mmol, 0.20 equiv) were added to the flask. The reaction mixture was stirred and heated at 80 °C for 24 h before being cooled to room temperature and quenched by addition of 3 mL of saturated $NaHCO_3$. The reaction mixture was extracted with EtOAc (3 x 10 mL). The combined organic layers were washed with brine, dried over $Na_2SO_4$, and concentrated under reduced pressure. Purification on silica gel (gradient elution 5% to 40% EtOAc in hexanes) afforded 14.6 mg (48% yield) of the title compound as a white solid. **$^1$H NMR**

(599 MHz, $CD_3OD$) δ 9.72 (s, 1H), 7.96-7.87 (m, 3H), 7.81 (s, 1H), 7.80 (s, 1H), 7.56-7.51 (m, 2H), 7.49 (dd, *J* = 8.3, 1.5 Hz, 1H), 6.86 (s, 1H), 2.28 (s, 3H); **$^{13}$C NMR** (151 MHz, $CD_3OD$) δ 192.5, 162.5, 148.2, 136.8, 134.5, 134.2, 131.6, 130.0, 129.1, 128.9, 128.8, 128.7, 127.8, 127.6, 127.3, 126.4, 117.2, 15.9; **HRMS (ESI)** *m/z*: $[M-H]^-$ calculated for $C_{18}H_{13}O_2^-$ 261.0921, found 261.0917; **IR** (thin film): 2991, 2913, 1732, 1436, 1373, 1241, 1042, 952, 696 $cm^{-1}$.

**Peptide Synthesis**

Sequence of peptides used in this study:

A. Ac-Tyr-βAla-Phe-Ala-Glu-Arg-Arg-Phe-Cys-Pro-Phe-Ala-Glu-Arg-$NH_2$

B. Ac-Tyr-βAla-Phe-Ala-Glu-Arg-Arg-Phe-Lys-Pro-Phe-Ala-Glu-Arg-$NH_2$

**Peptide design and synthesis:** The peptides listed above were designed from a sequence reported to have a ligandable cysteine residue, based on screens with cysteine-reactive probes.[72] The peptides synthesized using standard FMOC solid-phase synthesis methods on a Liberty Blue Microwave Synthesizer (CEM). Rink Amide ProTide resin (CEM) was utilized for peptide synthesis, providing C-terminal amide protection upon cleavage of the peptide. Amino acid coupling reactions were performed by mixing diisopropylcarbodiimide (7 equiv relative to resin, ChemImpex), Oxyma Pure (5 equiv, CEM), and amino acid (5 equiv) in *N*,*N*-dimethylformamide, followed by irradiation to maintain a temperature of 90 °C for 4 min. FMOC protecting groups were removed by suspending the resin in 20% piperidine in *N*,*N*-dimethylformamide with 0.2 M Oxyma Pure and irradiating to maintain a temperature of 90 °C for 1 min. The resin was rinsed (4 times each cycle) with *N*,*N*-dimethylformamide between deprotection and coupling steps. The final peptide was FMOC deprotected and was incubated with acetic anhydride in the presence of

triethylamine for N-terminal acetylation. The resulting peptide was cleaved from the resin with 95% trifluoroacetic acid (Sigma Aldrich), 2.5% $ddH_2O$, and 2.5% triisopropylsilane (Sigma Aldrich). The resin was incubated in the resulting solution for 4 h at RT under continuous mixing conditions before filtration to remove resin. The resin was rinsed with three volumes dichloromethane and the resulting solution was concentrated to 1 mL total volume under a stream of nitrogen gas in a 15 mL Falcon tube. The peptide was precipitated by the addition of 10 mL of cold diethyl ether, followed by overnight incubation at -20 °C. The precipitate was collected by centrifugation and dried under a stream of nitrogen gas. After drying, the crude peptide mixture was dissolved in 1:1 MeCN/$ddH_2O$ containing 1% formic acid (2 mL total volume).

**Peptide purification:** The peptide was purified by reverse-phase HPLC using an Agilent 1260 Series LC-DAD with a 150 x 30 mm Luna Omega 5 μm PS $C_{18}$ column (Phenomenex) under the following conditions: mobile phase (solvent A: $ddH_2O$ + 0.1% trifluoroacetic acid; solvent B: acetonitrile) gradient elution over 40 min (10% to 50% solvent B). The purity of the peptides was assessed by analytical LC/MS on an Agilent 1290 Series Infinity II HPLC with a 6230 Series Time-of-Flight (TOF) mass spectrometer. Samples were analyzed on a Phenomenex Aeris 3.6 μm WIDEPORE C4 column (2.1 x 50 mm) under the following conditions: mobile phase (solvent A: $ddH_2O$ + 0.1% trifluoroacetic acid; solvent B: acetonitrile + 0.1% trifluoroacetic acid) gradient elution over 6 min (5% to 100% solvent B). The purified peptide fractions were combined and concentrated to dryness under a stream of nitrogen gas. The peptide was then resuspended in minimal DMSO (20 μL) and the concentration quantified by UV-vis spectrometry on a Nanodrop spectrophotometer based on the absorbance of the N-terminal tyrosine at 280 nm ($\varepsilon_{280}$ = 1280 $M^{-1}cm^{-1}$). The peptide stock was then diluted to 2.5 mM in DMSO and stored at -20 °C.

## III. Plasmid and protein information

**Plasmids:** The gene encoding *citB* (KT781075.1) was codon-optimized for overexpression in *E. coli* and synthesized by GeneArt (ThermoFisher). The synthesized sequence was cloned by GeneArt into a pET-151 vector containing the T7 expression system, ampicillin resistance, and N-terminal 6 x His-tag encoded upstream from the insert gene. No further modifications to this plasmid construct were necessary.

The gene encoding *claD* (QBK15042.1) was codon-optimized for overexpression in *E. coli* and synthesized by Twist Bioscience. The synthesized sequence was cloned by Twist Bioscience into a pET-28a vector containing the T7 expression system, kanamycin resistance, and N-terminal 6 x His tag encoded upstream from the insert gene. No further modifications to this plasmid construct were necessary.

**Codon-Optimized *citB* Sequence (including 6 x His Tag)**

ATGCATCATCACCATCACCATGGTAAGCCTATCCCTAACCCTCTCCTCGGTCTCGATTCTACGG
AAAACCTGTATTTTCAGGGAATTGATCCCTTCACCATGCCGATTAGCACCAAAAGCAGCTTTTA
TCTGCCTGCAGTTGATATTAGCCCGTATCTGCAGGATCCGAATAGTGATGCAGCACGTAAAGTT
ATTGATGATGTTCGTGCAGCATGTACCAGCACCGGTTTTTTTCAGCTGTTAGGTCATGGTATTA
GTCCGGCACTGCAGCAGAGCGTTTTTGCAGCAGCAGCAAAATTCTTTGCACTGCCGAGTGATGT
TAAAAGCCGTTGTCGTAATGTTGGTTTTCGTGGTTATGATCCGATGGCAAGCCAGAGCTATGAA
CTGGGTGTTCTGCCGGATCTGAAAGAAGGTTTTATTGCCGGTAAAGATATTCCGCTGGATGATC
CGCGTGTTGCAAGCCAGCGCTTTTTTATGGGTCAGAATGCATGGCCTCCGAGCGAACTGCTGCC
GGAAGCAAATTTTCGTCGTCCGATTGAAGAATATTATCAGGCAATGCTGAAACTGTGTTGGGTT
GTTCTGGATCTGGTTGCAGCAACCCTGCCGTATGGTCCGCATGTTTTTGATGAATTCAAAGAAA
ATGATCCGGCATGTCCGCTGCGTCTGCTGCATTATCCGCCTGCACCGGCACCGGATGTTGCAAA

AGGTCGTCAGCTGGGTAGCAGCGCACATACCGATTTTGGTGCAATTACCCTGCTGTTACAGGAT
GATCATAGCGGTCTGGAAGTTCAGGATTGTGAAACCGGTGAATGGATTGGTGTTCCGCCTAATA
AAGATGCCTATGTTGTTAATCTGGGCGATATGATGAGCCGTATTACCCGTGGTCACTATAAAAG
CAGCATTCATCGTGTGATTAACCAGAATCTGACCGATCGTTATAGCGTGGTGTTTTTTTTCGAT
GGCAATCTGGATTATCGTCTGCGTCCTCTGGATCGTGTTGGTCAGAATTGGGATGAAGAAGATA
CCCTGACCGTTGAAGAACATATGCTGGAACGTACCACCACCACCTATAATCTGAAAGTGAAATA
A

**CitB Protein Sequence (including 6 x His Tag)**

MHHHHHHGKPIPNPLLGLDSTENLYFQGIDPFTMPISTKSSFYLPAVDISPYLQDPNSDAARKV
IDDVRAACTSTGFFQLLGHGISPALQQSVFAAAAKFFALPSDVKSRCRNVGFRGYDPMASQSYE
LGVLPDLKEGFIAGKDIPLDDPRVASQRFFMGQNAWPPSELLPEANFRRPIEEYYQAMLKLCWV
VLDLVAATLPYGPHVFDEFKENDPACPLRLLHYPPAPAPDVAKGRQLGSSAHTDFGAITLLLQD
DHSGLEVQDCETGEWIGVPPNKDAYVVNLGDMMSRITRGHYKSSIHRVINQNLTDRYSVVFFFD
GNLDYRLRPLDRVGQNWDEEDTLTVEEHMLERTTTTYNLKVK

**Codon-Optimized *claD* Sequence (including 6 x His Tag)**

ATGGGCAGCAGCCATCATCATCATCACAGCAGCGGCCTGGTGCCGCGCGGCAGCCATATGA
TGCCGGTGCTGTCGAATCCGAGCTTTTATCTGCCACTGGTGGATATCACCCCGTTCCTGGAGAA
CCCGCATGGCGCAGCGGCGCAGGATGTCATCGAAAGCGTGCGTACCGCCTGCAAAAGCACCGGT
TTTTTTCAGATCAAAGGTCATCAGGTGCCGCTGCGTTTGCAAAAATCGGTGTTCGAAGCCAGCG
CGCGTTTCTTTGCGCTGCCTCTCAAAAACAAACTCGAACTCGACAGCCGCAAAACCGTTGGCTT
CCGCGGTTACGATGTCATGGAAACGCAAAGCTACGAACTGGAATTTGGCGCGGTGCAGGAAGCG

GATGCGTTGCGCGATATCAAAGAAGGCTTTTTTATTGCCACCGACCTGCCGCCGGATCATCCGC

ATGTCGCCAACGGTCGTTTTTTGCAGGGCCCGAACGTCTGGCCGAAACCAGAACAGCTGGCGCC

GGAAGATTTCCAGAGCGTACTGGAAGAATATTACACCGAAATGCAGCGTCTGTCTCATGTGGTG

TTGTCGCTGCTGGCAGCAACGCTGCCGTATGGTCCGCACGTTTTCGACGAGCTGGAAACCTGCG

ATCCGATGTCGTTGCTGCGCCTGCTGCATTATCCGCGCGGCTTGGAAAAACAGGATGGCAAAAA

ACTGCAACTGGGTGCCGGGGAACATACCGATTTTGGTACCTTTACCCTGTTACTGCAGGACGAG

CATCCTGGCCTGGAAGTGCAAGACAGTGTCACCGGCGAATGGCACGGCGTGCCACCGCAGGAGG

ATGTTTATATCGTCAACGTTGCCGATATTCTGTCCACCATGACCGAGGGCGATTACAAGTCTTC

TGTGCATCGCGTGTGGAACATCAAGAGCAACGATCGCTACAGCGTCGTGTTTTTCTACGACGGC

AACCTGGATTACAAAGTCAAACCGTTACGCAGCAGCGGTCAGGACGAAAACGAAGAAATCGATG

CACCGACCATCGAAGAGCACGTCCGTTCGCGTCTCACTGCCAGTTATGCCATTTAA

**ClaD Protein Sequence (including 6 x His Tag)**

MGSSHHHHHHSSGLVPRGSHMMPVLSNPSFYLPLVDITPFLENPHGAAAQDVIESVRTACKSTG

FFQIKGHQVPLRLQKSVFEASARFFALPLKNKLELDSRKTVGFRGYDVMETQSYELEFGAVQEA

DALRDIKEGFFIATDLPPDHPHVANGRFLQGPNVWPKPEQLAPEDFQSVLEEYYTEMQRLSHVV

LSLLAATLPYGPHVFDELETCDPMSLLRLLHYPRGLEKQDGKKLQLGAGEHTDFGTFTLLLQDE

HPGLEVQDSVTGEWHGVPPQEDVYIVNVADILSTMTEGDYKSSVHRVWNIKSNDRYSVVFFYDG

NLDYKVKPLRSSGQDENEEIDAPTIEEHVRSRLTASYAI

**Protein overexpression and purification:** The plasmid containing *citB* or *claD* was transformed using a standard heat-shock protocol for chemically competent *E. coli* into BL21(DE3) cells. Overexpression of *citB* and *claD* was achieved using 4% glycerol (v/v) Terrific Broth (TB) in 2.8

L flasks. 500 mL portions of autoclaved media were inoculated with 5 mL of overnight culture prepared from a single colony in Luria Broth (LB) and 100 μg/mL ampicillin or 50 μg/mL kanamycin (Gold Biotechnology). Cultures were grown at 37 °C and 200 rpm until the optical density (at 600 nm) reached 0.8. The cultures were then cooled to 20 °C for 1 h and protein expression was induced with 0.2 mM isopropyl-β-D-1-thiogalactopyranoside (IPTG, Gold Biotechnology). Expression was continued at 20 °C overnight (approx. 18 h) at 200 rpm. The typical yield for one 500 mL culture cell pellet (wet cell pellet) was ~25 g.

**General purification procedure:** 50-60 g of cell pellet containing CitB or ClaD was resuspended in 250 mL of lysis buffer containing 50 mM Tris HCl (pH 7.4), 300 mM NaCl, 10 mM imidazole and 10% glycerol. The mixture was homogenized using a handheld dounce homogenizer. Approximately 1 mg/mL lysozyme (Gold Biotechnology) was added prior to 1 h incubation on a rocker held at 4 °C. Cells were lysed by sonication of the total cell lysate in 100 mL batches on ice. Each cycle of sonication was 10 s sonication, followed by a 20 s rest period, for a total of 6 min at 60% power. The total cell lysate was centrifuged at 45,000 x g for 30 min and the supernatant was removed. The cell lysate was incubated with 3 mL of Ni-NTA resin (Thermo) for 1 h at 4 °C with gentle rocking. The supernatant was filtered through a fritted 50 mL plastic column (Gold Biotechnologies) to isolate the Ni-NTA resin. The resin was washed with 100 mL of wash buffer containing 50 mM Tris HCl (pH 7.4), 300 mM NaCl, 25 mM imidazole and 10% glycerol. The protein was then eluted using 15 mL of an elution buffer containing 50 mM Tris HCl (pH 7.4), 300 mM NaCl, 250 mM imidazole and 10% glycerol. The eluted protein was concentrated to a volume of 2.5 mL using a 30 KDa molecular weight cutoff ultrafiltration device (Amicon). The concentrated protein was desalted using a PD-10 desalting column that was pre-equilibrated with

a storage buffer containing 50 mM Tris HCl (pH 7.4), 300 mM NaCl, and 10% glycerol. The protein was eluted from the column with 3.5 mL of storage buffer, before flash freezing in liquid nitrogen and storage at -80 °C. Protein concentration was determined by the A280 absorbance method using a Nanodrop spectrophotometer. The concentration was corrected using the estimated extinction coefficient from the ProtParam tool on the Expasy server (CitB: $\varepsilon = 1.128$; ClaD $\varepsilon = 0.890$). **Average yield:** 60 mg/L of CitB; 41 mg/L of ClaD.

**Preparation of clarified crude cell lysate (ClaD only):** 50-60 g of cell pellet containing ClaD was resuspended to a volume of 45 mg/mL in lysis buffer containing 50 mM Tris HCl (pH 7.4), 150 mM NaCl, and 10% glycerol. The mixture was homogenized using a handheld dounce homogenizer. Approximately 1 mg/mL lysozyme (Gold Biotechnology) was added prior to 1 h incubation on a rocker held at 4 °C. Cells were lysed by sonication of the total cell lysate in 100 mL batches on ice. Each cycle of sonication was 10 s sonication, followed by a 20 s rest period, for a total of 6 min at 60% power. The total cell lysate was centrifuged at 45,000 x g for 30 min and the supernatant was removed. The resulting supernatant was clarified by filtration through a 0.4 μm sterile filtration device. Aliquots of lysate were flash frozen in liquid nitrogen and stored at -80 °C until needed.

**Figure 2.S1. SDS-PAGE gel of purified CitB (40.61 kDa with 6x His tag)**

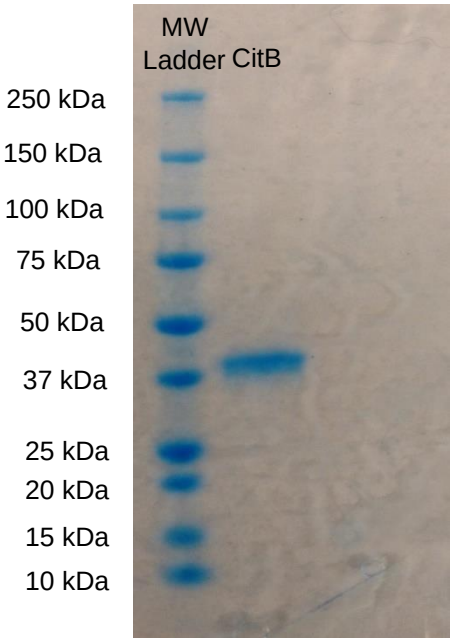


**Figure 2.S2. SDS-PAGE gel of purified ClaD (40.40 kDa with 6x His tag)**

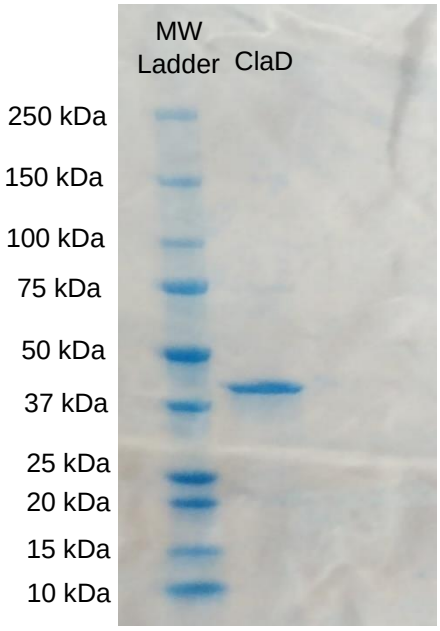

**III. Biocatalytic reactions and products**

**Stock solutions:** Stock solutions of each substrate (50 mM) were prepared by dissolving the substrate in DMSO (analytical grade). Stock solutions of α-ketoglutaric acid (125 mM), ferrous sulfate (10 mM) and sodium ascorbate (50 mM) were freshly prepared before each use, stored on ice, and used within 3 h. Aliquots of CitB (124 μM) and ClaD (80 μM) were stored at -80 °C until needed.

***In vitro* analytical-scale reactions (CitB and ClaD):** Each reaction contained 50 mM TES buffer pH 7.5 (2.5 μL of a 1 M solution), 2.5 mM substrate (2.5 μL, 50 mM), 10 μM CitB (4 μL, 124 μM) or ClaD (6.25 μL, 80 μM), 5 mM α-ketoglutaric acid (2 μL, 125 mM), 0.1 mM ferrous sulfate heptahydrate (0.5 μL, 10 mM), 8 mM sodium ascorbate (8 μL, 50 mM) and Milli-Q water to a final volume of 50 μL. Reactions were carried out at 30 °C for 3 h and quenched by the addition of 3 volumes of acetonitrile containing 3.5 mM pentamethyl benzene as an internal standard. Precipitated biomolecules were pelleted by centrifugation (17,000 x g, 20 min). The supernatant was analyzed by UPLC-DAD and conversion obtained by comparison to calibration curves of each substrate.

**Whole cell analytical-scale reactions (CitB):** Except where otherwise noted, each reaction contained 50 mM TES buffer pH 7.5 (25 μL of a 1M solution), 2.5 mM substrate (25 μL, 50 mM), 22.5 mg CitB wet cell pellet (45 mg/mL), 5 mM α-ketoglutaric acid (20 μL, 125 mM), 0.1 mM ferrous sulfate (5 μL, 10 mM), 8 mM sodium ascorbate (80 μL, 50 mM) and Milli-Q water to a final volume of 500 μL. Reactions were carried out at 30 °C for 3 h and quenched by the addition of 3 volumes of acetonitrile containing 3.5 mM pentamethylbenzene as an internal standard. The supernatant was analyzed by UPLC-DAD and conversion obtained by comparison of remaining starting material to calibration curves of each substrate.

**Crude cell lysate analytical-scale reactions (ClaD):** Each reaction contained 50 mM TES buffer pH 7.5 (2.5 μL of a 1 M solution), 2.5 mM substrate (2.5 μL, 50 mM), 10% v/v ClaD (5 μL) or 5 mM α-ketoglutaric acid (2 μL, 125 mM), 0.1 mM ferrous sulfate heptahydrate (0.5 μL, 10 mM), 8 mM sodium ascorbate (8 μL, 50 mM) and Milli-Q water to a final volume of 50 μL. Reactions were carried out at 30 °C for 1 h and quenched by the addition of 3 volumes of acetonitrile containing 3.5 mM pentamethyl benzene as an internal standard. Precipitated biomolecules were pelleted by centrifugation (17,000 x g, 20 min). The supernatant was analyzed by UPLC-DAD and conversion obtained by comparison to calibration curves of each substrate.

**Determination of percent conversion:** Percent conversion was determined by analysis of each reaction after 3 h. PDA spectrometric analysis was performed on a Waters Aquity H-Class instrument, using a Phenomenex Kinetex (1.7 μm C18, 2.1 x 150 mm) column under the following conditions: mobile phase (Solvent A: deionized water + 0.1% formic acid; Solvent B: acetonitrile + 0.1% formic acid) 5% to 100% solvent B over 2 min, 100% solvent B for 1 min; flow rate: 0.5 mL/min. Based on the calibration curves of the starting materials, the percent conversion of the substrate to hydroxylated product was calculated with $AUC_{substrate}$ (300 nm)/$AUC_{internal\ standard}$ (270 nm). *In vitro* reactions were performed and analyzed in triplicate, while whole cell reactions were performed and analyzed in duplicate with reported conversions as an average of those trials.

**General procedure for whole cell milligram-scale reactions:** Except where otherwise noted, preparative-scale enzymatic reactions were conducted on 20-40 mg of each substrate under the following conditions: 2.5 mM substrate, 50 mM TES buffer pH 7.5, 5 mM α-ketoglutaric acid, 0.1 mM ferrous sulfate, 8 mM sodium ascorbate, 45 mg/mL CitB wet cell pellet. Reactions were performed in Erlenmeyer flasks of appropriate volume to achieve proper oxygenation (at least 3

times reaction volume) and shaken at 100 rpm at 30 °C. Reaction progress was monitored at hourly intervals by analysis of a 50 μL aliquot by UPLC-DAD. The aliquot was processed in the manner described for *in vitro* analytical scale determination of reaction conversion. Upon satisfactory conversion of the substrate, the product(s) were isolated in the following manner. **Isolation procedure:** The reaction mixture was transferred to a 50 mL falcon tube and 2 volumes of acetone were added. The mixture was centrifuged at 4,500 x g for 10 min to separate the biomolecule components from the aqueous reaction mixture. The supernatant was removed and acetone removed under reduced pressure. The supernatant was acidified to pH 2.0 with 0.1 M HCl. The organic materials were extracted from the aqueous layer with ethyl acetate (3 x 50 mL). The organic fractions were pooled and concentrated under reduced pressure to yield a crude mixture. To ensure maximal product recovery, the pelleted wet cell components were extracted with hexanes and ethyl acetate. These fractions were concentrated under reduced pressure to yield a separate crude mixture. These mixtures were purified by either preparative HPLC or flash silica gel chromatography (Biotage).

**General procedure for crude cell lysate milligram-scale reactions:** Except where otherwise noted, preparative-scale enzymatic reactions were conducted on 20-100 mg of each substrate under the following conditions: 2.5 mM substrate, 50 mM TES buffer pH 7.5, 5 mM α-ketoglutaric acid, 0.1 mM ferrous sulfate, 8 mM sodium ascorbate, 10% v/v ClaD clarified crude lysate (prepared from 45 mg/mL wet whole cell suspension). Reactions were performed in Erlenmeyer flasks of appropriate volume to achieve proper oxygenation (at least 3 times reaction volume) and incubated at 30 °C. Reaction progress was monitored at hourly intervals by analysis of a 50 μL aliquot by UPLC-DAD. The aliquot was processed in the manner described for *in vitro* analytical scale

determination of reaction conversion. Upon satisfactory conversion of the substrate, the product(s) were isolated in the following manner. **Isolation procedure:** The reaction mixture was acidified to pH 2.0 with 0.1 M HCl. The organic materials were extracted from the aqueous layer with ethyl acetate (3 x 50 mL). The organic fractions were pooled and concentrated under reduced pressure to yield a crude mixture. These fractions were concentrated under reduced pressure to yield a separate crude mixture. These mixtures were purified by either preparative HPLC or flash silica gel chromatography (Biotage).

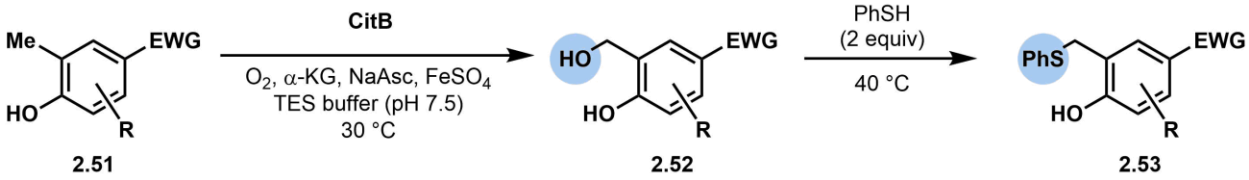


**Figure 2.S3. Whole-cell milligram-scale CitB reactions with *in situ* functionalization.**

**Modified procedure for whole-cell milligram-scale reactions with *in situ* functionalization:** Preparative-scale reactions with *in situ* functionalization using thiophenol were set up using a protocol identical to the general procedure for whole cell milligram-scale reactions, except that after 1 h, 2 equiv of thiophenol was added and the temperature increased to 40°C.

**Procedure for one-pot whole-cell chemoenzymatic cascade reactions (nucleophile addition):** Analytical scale whole-cell cascade reactions were performed in 15 mL Falcon tubes (in duplicate trials) in a manner analogous to analytical-scale CitB reactions, except that after 3 h, cell pellet was spun down at 4,000 x g for 5 min. 2 equiv of nucleophile were added directly to the supernatant. Each Falcon tubes was shaken at 400 rpm and 37 °C for 16 h. 50 μL of the reaction was removed and diluted 10x with acetonitrile containing 3.5 mM pentamethyl benzene as internal

standard. For reactions run neat in nucleophilic solvent, 50 µL of sample was concentrated to dryness under reduced pressure. The dried film was then diluted 10 x with acetonitrile and internal standard, plus 50 µL of dd$H_2O$ to dissolve associated reaction salts. Samples were analyzed by UPLC using the method for determination of conversion percentage described previously, except for morpholine adduct **77**, which was analyzed using a hydrophilic interaction column (HILIC) under the following conditions: mobile phase (Solvent A: deionized water + 0.1% formic acid; Solvent B: acetonitrile + 0.1% formic acid) 85% to 40% solvent B over 7 min, 85% solvent B for 6 min; flow rate: 0.45 mL/min. HILIC column = Waters Acquity 1.7 µm UPLC BEH Amide HILIC 2.1 x 100 mm. Samples were quenched by the addition of 3 equiv solution containing 1:1 deionized water and acetonitrile, with 3.5 mM L-tryptophan as internal standard.

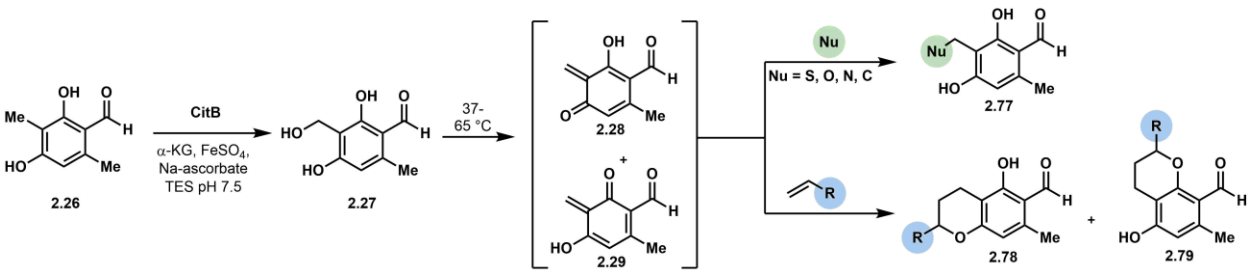


**Figure 2.S4. One-pot whole-cell chemoenzymatic cascade reactions.**

**Procedure for one-pot whole-cell chemoenzymatic cascade reactions (Diels-Alder reactions):** Analytical scale whole-cell cascade reactions were performed in 1 dram reaction vials (duplicate) in a manner analogous to analytical scale CitB reactions, except that the reactions were stirred at 100 rpm using a Teflon stir bar for 3 h at 30 °C. After 3 h, 10 equiv of dienophile was added to the vial which was sealed with an air-tight cap and heated to 60 °C (65 °C for styrene and 2,3-dihydrofuran) for 16 h. For reactions using styrenes as a dienophile, 50 µL of the reaction was removed and diluted 10x with acetonitrile containing 3.5 mM pentamethyl benzene as an internal

standard. For reactions with all other dienophiles, 50 μL of sample was reduced to dryness under reduced pressure. The dried film was then diluted 10 x with acetonitrile and internal standard, plus 50 μL of dd$H_2O$ to dissolve associated reaction salts. Samples were analyzed by UPLC using the method for determination of conversion percentage described above. Reactions were performed in triplicate, with reported conversions as an average of those trials.

**Purification by preparative HPLC:** For purification of milligram-scale reactions, the resulting crude mixture was taken up in a 60:40 mixture of milli-Q water:acetonitrile (2 mL). The product(s) were purified from this mixture by preparative HPLC using a Phenomenex Kinetex 5 μm C18, 150 x 21.2 mm column under the following conditions: mobile phase (Solvent A: deionized water + 0.1% formic acid; Solvent B: acetonitrile + 0.1% formic acid) 5% to 100% solvent B over 13 min, 100% solvent B for 4 min; flow rate: 11.5 mL/min.

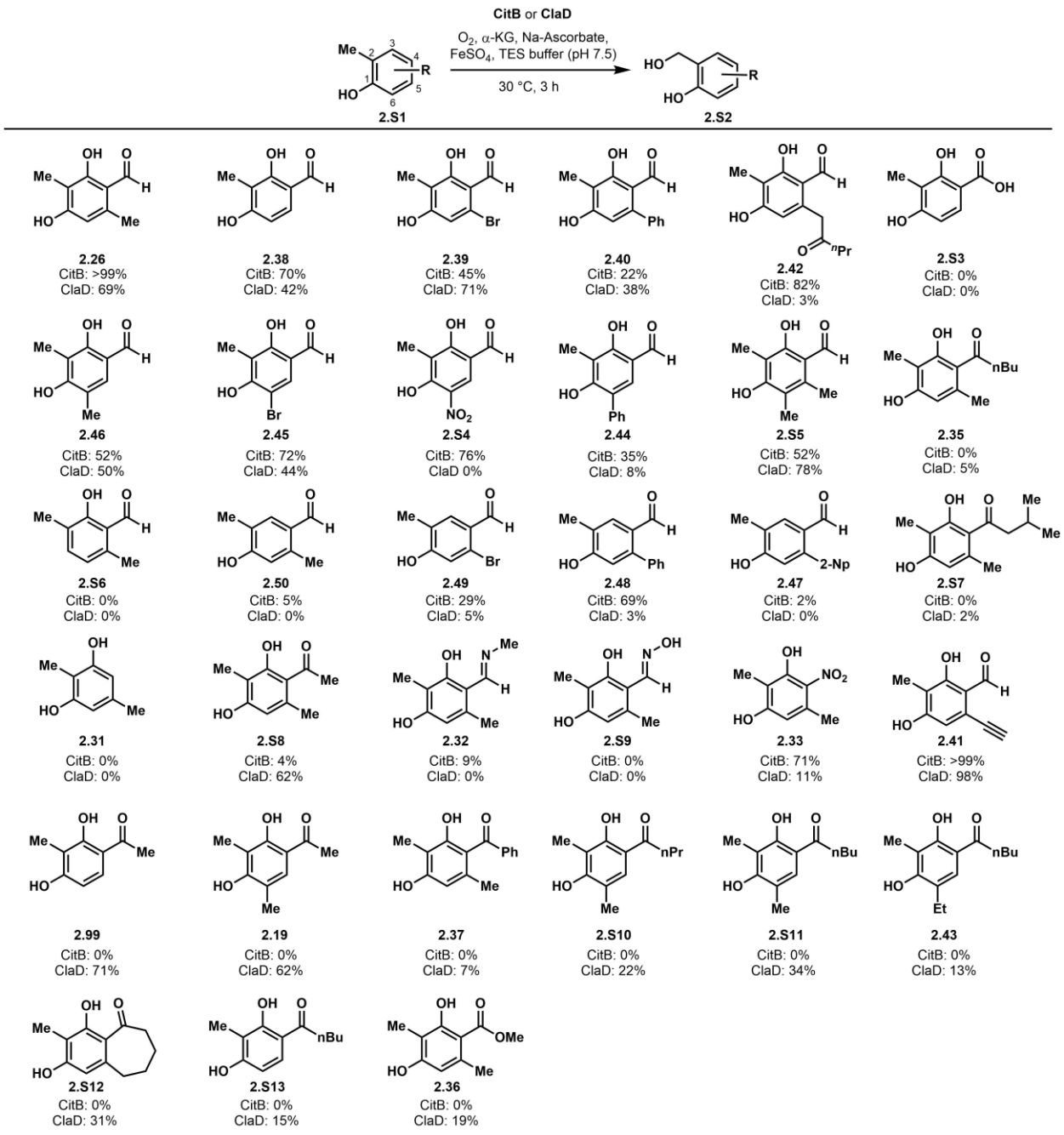


**Figure 2.S5. *In vitro* conversion of phenolic substrates in CitB- and ClaD-catalyzed benzylic hydroxylation.**

Reaction conditions: 2.5 mM substrate, 10 μM CitB or ClaD, 50 mM TES pH 7.5, 5 mM α-ketoglutaric acid (α-KG), 8 mM sodium ascorbate (Na Asc), 0.1 mM ferrous sulfate ($FeSO_4$), 30 °C, 3 h. Np = 2-naphthyl. Conversion to product was quantified by UPLC-DAD analysis using 3.5 mM pentamethylbenzene as internal standard.

**Products of biocatalytic benzylic C–H hydroxylation**

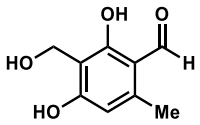


**2,4-dihydroxy-3-(hydroxymethyl)-6-methylbenzaldehyde (2.27)**

The title compound was synthesized according to the general procedure for milligram-scale whole cell enzymatic hydroxylation with CitB. The reaction was performed with 500 mg of starting material. Purification by flash chromatography afforded 460 mg (84% yield) of the title compound as a white solid. **$^{1}$H NMR** (400 MHz, MeOD) δ 10.07 (s, 1H), 6.26 (s, 1H), 4.68 (s, 2H), 2.50 (s, 3H); **$^{13}$C NMR** (150 MHz, MeOD) δ 194.5, 165.5, 165.4, 145.5, 113.7, 112.8, 111.2, 53.7, 18.2; **HR-ESI-MS**: m/z calcd for $C_9H_{11}O_4^+$ $[M+H-H_2O]^+$: 165.0546, found: 165.0544; **IR** (thin film): 3268, 2922, 1605, 1484, 1438, 1244, 1115, 966, 840, 565 $cm^{-1}$.

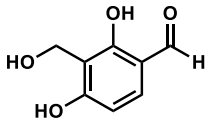


**2,4-dihydroxy-3-(hydroxymethyl)benzaldehyde (2.54)**

The title compound was synthesized according to the general procedure for milligram-scale whole cell enzymatic hydroxylation with CitB. The reaction was performed with 20 mg of starting material. Purification by preparative HPLC afforded 10.6 mg (50% yield) of the title compound as a white solid. **$^{1}$H NMR** (400 MHz, $CD_3OD$) δ 9.68 (s, 1H), 7.46 (d, *J* = 8.8, 1H), 6.50 (d, J = 8.8, 1H), 4.73 (s, 2H); **$^{13}$C NMR** (150 MHz, $CD_3OD$) δ 196.2, 165.7, 163.5, 136.4, 115.8, 114.6, 109.4, 53.7; **HR-ESI-**MS: m/z calcd for $C_8H_{11}O_4^+$ $[M+H-H_2O]^+$: 151.0390, found: 151.0393; **IR** (thin film): 3254, 2920, 2530, 2274, 1608, 1495, 1435, 1383, 1321, 1249, 1077 $cm^{-1}$.

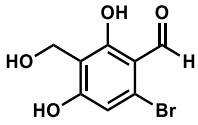


**6-bromo-2,4-hydroxy-3-(hydroxymethyl)benzaldehyde (2.55)**

The title compound was synthesized according to the general procedure for milligram-scale whole cell enzymatic hydroxylation with CitB. The reaction was performed with 20 mg of starting material. Purification by preparative HPLC afforded 7.4 mg (35% yield) of the title compound as a tan film. **$^{1}$H NMR** (400 MHz, $CD_3OD$) δ 10.07 (s, 1H), 6.73 (s, 1H), 4.68 (s, 2H); **$^{13}$C NMR** (150 MHz, $CD_3OD$) δ 195.3, 165.0, 164.7, 128.6, 113.0, 111.2, 110.8, 61.3; **HR-ESI-MS**: m/z calcd for $C_8H_9O_4Br^+$ $[M+H-H_2O]^+$: 228.9495, found: 228.9493; **IR** (thin film): 3129, 2831, 1617, 1460, 1425, 1248, 1109, 1019 $cm^{-1}$.

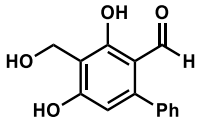


**3,5-dihydroxy-4-(hydroxymethyl)-[1,1'-biphenyl]-2-carbaldehyde (2.56)**

The title compound was synthesized according to the general procedure for milligram-scale whole cell enzymatic hydroxylation with CitB. The reaction was performed with 20 mg of starting material, using 30 mg/mL CitB wet cell pellet. Purification by preparative HPLC afforded 6.8 mg (30% yield) of the title compound as a white film. **$^{1}$H NMR** (400 MHz, $CD_3OD$) δ 9.53 (s, 1H), 7.43 (m, 3 H), 7.38 (m, 2H), 6.38 (s, 1H), 2.58 (s, 2H); **$^{13}$C NMR** (150 MHz, $CD_3OD$) δ 195.9, 165.1, 150.4, 139.0, 130.8, 130.7, 130.1, 129.4, 129.3, 129.0, 114.0, 113.0, 111.0, 53.7; **HR-ESI-MS**: m/z calcd for $C_{14}H_{13}O_4^+$ $[M+H-H_2O]^+$: 227.0703, found: 227.0705; **IR** (thin film): 3296, 2924, 1616, 1428, 1381, 1254, 1107, 1022, 855 $cm^{-1}$.

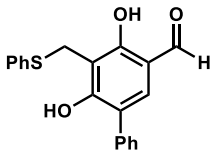


**2,4-dihydroxy-3-((phenylthiol)methyl)-5-phenylbenzaldehyde (2.57)**

The title compound was synthesized according to the modified procedure for milligram-scale whole cell enzymatic hydroxylation with CitB and *in situ* functionalization with thiophenol. The reaction was performed with 20 mg of starting material. Purification by flash chromatography afforded 9.2 mg (31% yield) of the title compound as a white solid. **$^{1}$H NMR** (400 MHz, $CD_3OD$) δ 9.67 (s, 1H), 7.78 (s, 1H), 7.37 (m, 10H), 4.28 (s, 2H); **$^{13}$C NMR** (150 MHz, $CD_3OD$) δ 196.2, 162.3, 138.4, 138.1, 136.4, 131.8, 129.7, 128.5, 127.4, 124.6, 115.7, 113.4, 27.9; **HR-ESI-MS**: m/z calcd for $C_{20}H_{17}O_3S^+$ $[M+H]^+$: 337.0893, found: 337.0903; **IR** (thin film): 3057, 2926, 2854, 1606, 1549, 1456, 1438, 1306, 1087 $cm^{-1}$.

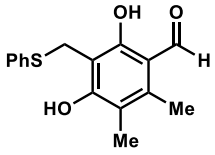


**2,4-hydroxy-3-(hydroxymethyl)-5,6-dimethylbenzaldehyde (2.58)**

The title compound was synthesized according to the general procedure for milligram-scale whole cell enzymatic hydroxylation with CitB. The reaction was performed with 20 mg of starting material, using 30 mg/mL CitB wet cell pellet. Purification by preparative HPLC afforded 12.8 mg (40% yield) of the title compound as a white solid. **$^{1}$H NMR** (400 MHz, $CD_3OD$) δ 10.15 (s, 1H), 7.37 (d, $J$ = 8.0, 2H), 7.23 (t, $J$ = 8.0, 2H), 7.15 (t, $J$ = 8.0, 1H) 4.23 (s, 2H), 2.46 (s, 3H), 2.11 (s, 3H); **$^{13}$C NMR** (150 MHz, $CD_3OD$) δ 195.3, 163.0, 163.0, 142.1, 138.4, 131.2, 129.6, 127.1, 117.3, 113.9, 109.9, 27.5, 14.0, 11.66; **HR-ESI-MS**: m/z calcd for $C_{16}H_{17}O_3S^+$ $[M+H]^+$: 289.0893,

found: 289.0882; **IR** (thin film): 3337, 2943, 2831, 1606, 1447, 1269, 1225, 1173, 1116, 1022 $cm^{-1}$.

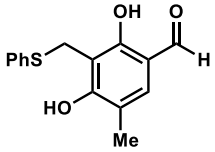


**2,4-dihydroxy-5-methyl-3-((phenylthio)methyl)benzaldehyde (2.59)**

The title compound was synthesized according to the general procedure for milligram-scale whole cell enzymatic hydroxylation with CitB and *in situ* functionalization with thiophenol. The reaction was performed with 40 mg of starting material. Purification by flash chromatography afforded 14.8 mg (23% yield) of the title compound as a white solid. **$^{1}$H NMR** (400 MHz, $CD_3OD$) δ 9.63 (s, 1H), 7.31 (s, 1H), 4.87 (s, 2H), 2.16 (s, 3H); **$^{13}$C NMR** (150 MHz, $CD_3OD$) δ 196.3, 164.5, 160.5, 135.7, 119.1, 115.1, 112.5, 56.8, 15.3; **HR-ESI-MS**: m/z calcd for $C_{15}H_{15}O_3S^+$ $[M+H]^+$: 275.0736, found: 275.0737; **IR** (thin film): 3335, 2925, 1619, 1479, 1438, 1387, 1332, 1273, 1175, 1121 $cm^{-1}$.

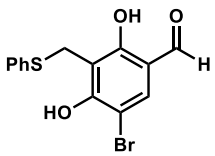


**5-bromo-2,4-dihydroxy-3-((phenylthiol)methyl)benzaldehyde (2.60)**

The title compound was synthesized according to the modified procedure for milligram-scale whole cell enzymatic hydroxylation with CitB and *in situ* functionalization with thiophenol. The reaction was performed with 20 mg of starting material. Purification by flash chromatography afforded 6.8 mg (24% yield) of the title compound as a white film. **$^{1}$H NMR** (400 MHz, $CD_3OD$) δ 9.64 (s, 1H), 7.75 (s, 1H), 7.39 (m, 2H), 7.23 (m, 3H), 4.23 (s, 2H); **$^{13}$C NMR** (150 MHz, $CD_3OD$) δ 195.4, 167.5, 137.6, 137.5, 131.6, 129.4, 127.2, 116.6, 114.8, 102.1, 27.9, 16.8; **HR-**

**ESI-MS**: m/z calcd for $C_{14}H_{12}O_3SBr^+$ $[M+H]^+$: 338.9685, found: 338.9710; **IR** (thin film): 3299, 3058, 2927, 2854, 1603, 1549, 1455, 1438, 1304, 1173, 1084 $cm^{-1}$.

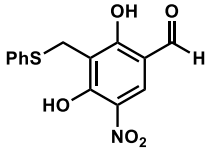


**2,4-dihydroxy-5-nitro-3-((phenylthiol)methyl)benzaldehyde (2.61)**

The title compound was synthesized according to the modified procedure for milligram-scale whole cell enzymatic hydroxylation with CitB and *in situ* functionalization with thiophenol. The reaction was performed with 20 mg of starting material. Purification by flash chromatography afforded 8.0 mg (26% yield) of the title compound as a yellow film. **$^1$H NMR** (599 MHz, $(CD_3)_2CO$) δ 10.04 (s, 1H), 8.75 (s, 1H), 7.49-7.26 (m, 5H), 4.29 (s, 2H); **$^{13}$C NMR** (150 MHz, $(CD_3)_2CO$) δ 196.0, 173.6, 132.6, 130.5, 129.6, 128.8, 128.4, 126.5, 125.5, 114.5, 107.8, 25.9; **HR-ESI-MS**: m/z calcd for $C_{14}H_{12}NO_5S^+$ $[M+H]^+$: 306.0431, found: 306.0426; **IR** (thin film): 2924, 2854, 1709, 1625, 1540, 1456, 1267, 1158, 1092 $cm^{-1}$.

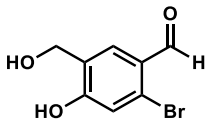


**2-bromo-4-hydroxy-5-(hydroxymethyl)benzaldehyde (2.71)**

The title compound was synthesized according to the general procedure for milligram-scale whole cell enzymatic hydroxylation with CitB. The reaction was performed with 40 mg of starting material. Purification by preparative HPLC afforded 2.7 mg (7% yield) of the title compound as a tan film. **$^1$H NMR** (400 MHz, $CD_3OD$) δ 10.14 (s, 1H), 7.94 (s, 1 H), 7.07 (s, 1H), 4.60 (s, 2H); **$^{13}$C NMR** (150 MHz, $CD_3OD$) δ 191.6, 162.4, 130.3, 130.2, 128.0, 126.8, 120.0, 59.5; **HR-ESI-**

**MS** m/z calcd for $C_8H_8BrO_3^+$ $[M+H]^+$: 230.9651, found: 230.9657; **IR** (thin film): 3258, 2925, 2855, 1621, 1433, 1381, 1256, 1106 $cm^{-1}$.

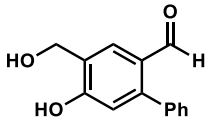


**4-hydroxy-5-(hydroxymethyl)-2-phenylbenzaldehyde (2.72)**

The title compound was synthesized according to the modified procedure for milligram-scale whole cell enzymatic hydroxylation with CitB and *in situ* functionalization with thiophenol. The reaction was performed with 40 mg of starting material. Purification by preparative HPLC afforded 6.0 mg (14% yield) of the title compound as a white film. **$^1$H NMR** (400 MHz, $CD_3OD$) δ 9.71 (s, 1H), 8.04 (s, 1H), 7.46-7.38 (m, 5H), 6.79 (s, 1H), 4.70 (s, 2H); **$^{13}$C NMR** (150 MHz, $(CD_3)_2CO$) δ 189.4, 138.0, 129.8, 128.3, 128.2, 128.0, 127.8, 127.1, 116.5, 59.8; **HR-ESI-MS**: m/z calcd for $C_{14}H_{13}O_3^+$ $[M+H]^+$: 229.0859, found: 229.0855; **IR** (thin film): 3266, 2925, 1659, 1602, 1484, 1282, 1015 $cm^{-1}$.

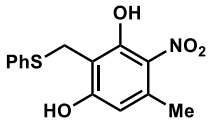


**5-methyl-4-nitro-2-((phenylthio)methyl)benzene-1,3-diol (2.70)**

The title compound was synthesized according to the modified procedure for milligram-scale whole cell enzymatic hydroxylation with CitB and *in situ* functionalization with thiophenol. The reaction was performed with 20 mg of starting material. Purification by preparative HPLC afforded 8.1 mg (28% yield) of the title compound as a yellow solid. **$^1$H NMR** (600 MHz, $(CD_3)_2CO$) δ 11.40 (s, 1H), 10.02 (s, 1H), 7.44 (d, $J$ = 7.4, 2H), 7.29 (t, $J$ = 7.4, 2H), 7.20 (t, $J$ = 7.4, 1H), 6.50 (s, 1H), 4.27 (s, 2H), 2.52 (s, 3H); **$^{13}$C NMR** (150 MHz, $(CD_3)_2CO$) δ 160.9, 156.0, 137.7, 137.4,

129.5, 129.1, 128.7, 125.9, 111.5, 110.9, 26.6, 22.0; **HR-ESI-MS**: m/z calcd for $C_{14}H_{13}O_3^+$ $[M+H]^+$: 292.0268, found: 292.0261; **IR** (thin film): 3356, 2931, 1603, 1549, 1455, 1415, 1306, 1173, 1006 $cm^{-1}$.

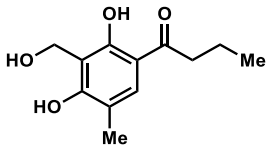


**1-(2,4-dihydroxy-3-(hydroxymethyl)-5-methylphenyl)butan-1-one (2.63)**

The title compound was synthesized according to the procedure for milligram-scale crude cell reactions with ClaD. The reaction was performed with 20 mg of starting material. Purification by flash chromatography afforded 8.5 mg (39% yield) of the title compound as a white solid. **$^1$H NMR** (600 MHz, $CD_3CN$) δ 13.15 (s, 1H), 7.60 (s, 1H), 4.92 (s, 2H), 2.91 (t, *J* = 7.4, 2H), 2.14 (s, 3H), 1.70 (sxt, *J* = 7.4, 2H), 0.99 (t, *J* = 7.4, 3H); **$^{13}$C NMR** (150 MHz, $CD_3CN$) δ 205.8, 162.2, 159.7, 131.1, 111.9, 110.9, 57.4, 39.5, 39.4, 18.0, 14.4, 13.1; **HR-ESI-MS**: m/z calcd for $C_{12}H_{15}O_3^+$ $[M+H-H_2O]^+$: 207.1016, found: 207.1024; **IR** (thin film): 3333, 2957, 2358, 1622, 1168, 997, 661 $cm^{-1}$.

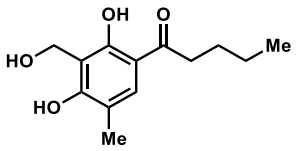


**1-(2,4-dihydroxy-3-(hydroxymethyl)-5-methylphenyl)pentan-1-one (2.64)**

The title compound was synthesized according to the procedure for milligram-scale crude cell reactions with ClaD. The reaction was performed with 20 mg of starting material. Purification by flash chromatography afforded 6.5 mg (30% yield) of the title compound as a white solid. **$^1$H NMR** (600 MHz, $CD_3CN$) δ 13.15 (s, 1H), 7.60 (s, 1H), 4.92 (s, 2H), 2.94 (t, *J* = 7.4, 2H), 2.14 (s, 3H) 1.66 (p, *J* = 7.4, 2H), 1.40 (sxt, *J* = 7.4, 2H), 0.95 (t, *J* = 7.4, 3H); **$^{13}$C NMR** (150 MHz,

$CD_3CN$) δ 206.0, 162.2, 159.7, 131.1, 116.7, 111.8, 110.5, 57.5, 37.3, 26.7, 22.1, 14.4, 13.2; **HR-ESI-MS**: m/z calcd for $C_{13}H_{17}O_3^+$ $[M+H-H_2O]^+$: 221.1172, found: 221.1178; **IR** (thin film): 3394, 2955, 2352, 2025, 1225, 961, 740 $cm^{-1}$.

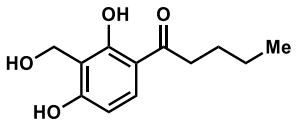


**1-(2,4-dihydroxy-3-(hydroxymethyl)phenyl)pentan-1-one (2.67)**

The title compound was synthesized according to the procedure for milligram-scale crude cell reactions with ClaD. The reaction was performed with 20 mg of starting material. Purification by flash chromatography afforded 6.1 mg (28% yield) of the title compound as a white solid. **$^1$H NMR** (600 MHz, $CD_3CN$) δ 7.71 (d, *J* = 8.9, 1H), 6.40 (d, *J* = 8.9, 1H), 4.72 (s, 2H), 2.91 (t, *J* = 7.5, 2H), 1.67 (m, 2H), 1.40 (m, 2H), 0.95 (t, *J* = 3H); **$^{13}$C NMR** (150 MHz, $CD_3CN$) δ 205.5, 163.2, 131.4, 113.4, 112.2, 106.9, 52.7, 48.1,. 37.0, 26.9, 22.0, 12.8; **HR-ESI-MS**: m/z calcd for $C_{12}H_{15}O_3^+$ $[M+H-H_2O]^+$: 207.1016, found: 207.1019; **IR** (thin film): 3301, 2512, 1654, 1441, 982 $cm^{-1}$.

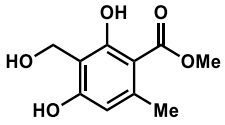


**Methyl-2,4-dihydroxy-3-(hydroxymethyl)-6-methylbenzoate (2.66)**

The title compound was synthesized according to the procedure for milligram-scale crude cell reactions with ClaD. The reaction was performed with 20 mg of starting material. Purification by flash chromatography afforded 4 mg (7% yield) of the title compound as a white solid. **$^1$H NMR** (600 MHz, $CD_3OD$) δ 6.25 (s, 1H), 4.71 (s, 2H), 3.91 (s, 3H), 2.46 (s, 3H); **$^{13}$C NMR** (150 MHz, $CD_3CN$) δ 172.3, 163.3, 160.9, 142.3, 111.2, 110.5, 53.2, 50.8, 22.9; **HR-ESI-MS**: m/z calcd for

$C_{12}H_{11}O_4^+$ $[M+H-H_2O]^+$: 195.0652, found: 195.0667; **IR** (thin film): 3388, 2954, 2364, 1719, 1647, 1439, 1317, 1276, 1198, 1165, 981 $cm^{-1}$.

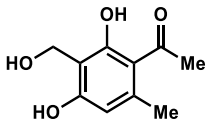


**1-(2,4-dihydroxy-3-(hydroxymethyl)-6-methylphenyl)ethan-1-one (2.65)**

The title compound was synthesized according to the procedure for milligram-scale crude cell reactions with ClaD. The reaction was performed with 20 mg of starting material. Purification by flash chromatography afforded 13.2 mg (61% yield) of the title compound as a white solid. **$^1$H NMR** (600 MHz, $CD_3CN$) δ 13.90 (s, 1H), 6.26 (s, 1H), 4.80 (s, 2H), 2.61 (s, 3H), 2.53 (s, 3H); **$^{13}$C NMR** (150 MHz, $CD_3CN$) δ 205.0, 163.4, 161.4, 141.8, 114.3, 111.7, 109.9, 56.6, 32.4, 23.9; **HR-ESI-MS**: m/z calcd for $C_{10}H_{11}O_3^+$ $[M+H-H_2O]^+$: 179.0703, found: 179.0703; **IR** (thin film): 3283, 2357, 1963, 1607, 1428, 1268, 1001 $cm^{-1}$.

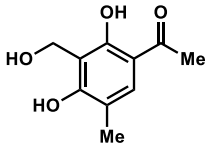


**1-(2,4-dihydroxy-3-(hydroxymethyl)-5-methylphenyl)ethan-1-one (2.62)**

The title compound was synthesized according to the procedure for milligram-scale crude cell reactions with ClaD. The reaction was performed with 20 mg of starting material. Purification by flash chromatography afforded 14.1 mg (65% yield) of the title compound as a white solid. **$^1$H NMR** (600 MHz, $CD_3CN$) δ 13.01 (s, 1H), 7.57 (s, 1H), 4.92 (s, 2H), 2.52 (s, 3H), 2.14 (s, 3H); **$^{13}$C NMR** (150 MHz, $CD_3CN$) δ 203.6, 162.3, 159.5, 131.8, 116.7, 112.3, 110.4, 57.4, 25.6, 14.4;

**HR-ESI-MS**: m/z calcd for $C_{10}H_{11}O_3^+$ $[M+H-H_2O]^+$: 179.0703, found: 179.0707; **IR** (thin film): 3270, 2356, 2013, 1713, 1486, 1371, 1333, 1269, 1190, 1083, 1004 $cm^{-1}$.

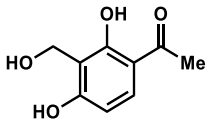


**1-(2,4-dihydroxy-3-(hydroxymethyl)phenyl)ethan-1-one (2.68)**

The title compound was synthesized according to the procedure for milligram-scale crude cell reactions with ClaD. The reaction was performed with 20 mg of starting material. Purification by flash chromatography afforded 76 mg (69% yield) of the title compound as a white solid. **$^1$H NMR** (600 MHz, $CD_3CN$) δ 13.17 (s, 1H), 7.68 (d, *J* = 8.8, 1H), 6.41 (d, *J* = 8.8, 1H), 4.82 (s, 1H), 2.53 (s, 1H); **$^{13}$C NMR** (150 MHz, $CD_3CN$) δ 203.7, 163.4, 161.8, 132.2, 112.9, 112.1, 107.9, 55.9, 25.6; **HR-ESI-MS**: m/z calcd for $C_9H_9O_3^+$ $[M+H-H_2O]^+$: 165.0546, found: 165.0557; **IR** (thin film): 3320, 2956, 2360, 2341, 1981, 1615, 987 $cm^{-1}$.

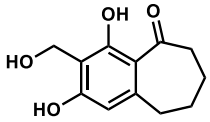


**2,4-dihydroxy-3-(hydroxymethyl)-6,7,8,9-tetrahydro-5H-benzo[7]annulen-5-one (2.69)**

The title compound was synthesized according to the procedure for milligram-scale crude cell reactions with ClaD. The reaction was performed with 10 mg of starting material. Purification by flash chromatography afforded 4.1 mg (37% yield) of the title compound as a white solid. **$^1$H NMR** (600 MHz, $CD_3CN$) δ 13.70 (s, 1H), 6.27 (s, 1H), 4.80 (s, 2H), 2.93-2.85 (m, 2H), 2.83-2.76 (m, 2H), 1.88-1.75 (m, 4H). **$^{13}$C NMR** (150 MHz, $CD_3CN$) δ 208.7, 163.1, 162.1, 147.2,

113.2, 109.8, 56.2, 40.9, 32.9, 27.1, 24.2, 20.4; **HR-ESI-MS**: m/z calcd for $C_{12}H_{13}O_3^+$ [M+H-$H_2O$]$^+$: 205.0859, found: 205.0856; **IR** (thin film): 3282, 2281, 1617, 1182 $cm^{-1}$.

## IV. Chemical oxidation reactions of substrate 2.26

**Table 2.S1. Chemical oxidation reactions of substrate 2.26.**

| **Reaction**[50-55] | **Result** |
|---|---|
| CitB | benzylic alcohol |
| $MnO_2$ | starting material |
| DDQ | quinone |
| $K_2S_2O_8$ | decomposition |
| CAN, AcOH | decomposition |
| AIBN, NBS | aromatic bromination |
| $Ag_2O$, MeOH | starting material |

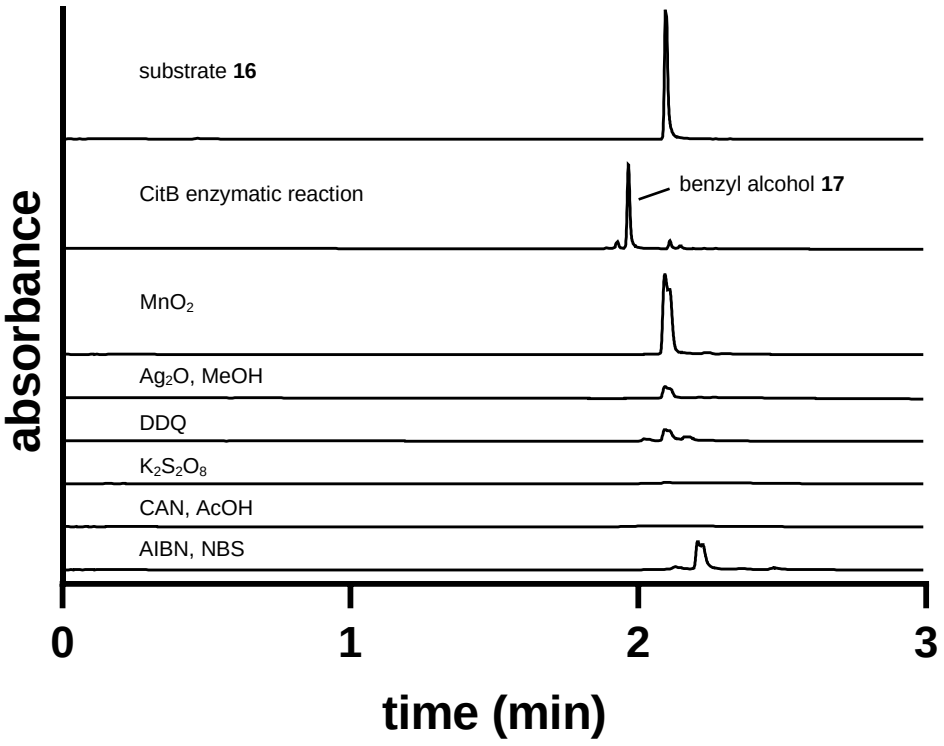


**Figure 2.S6. Chemical oxidation reactions of substrate 2.26.**
Each chemical oxidation reaction was performed according to the general procedure in the given references.

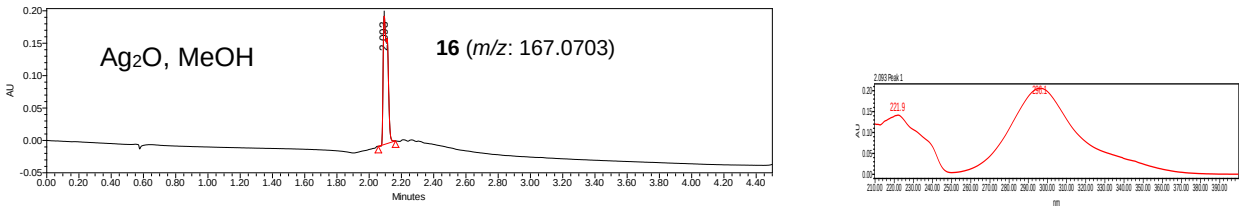


**Figure 2.S7. $Ag_2O$ oxidation reaction of substrate 2.26.**
PDA trace of reaction analyzed at 300 nm.

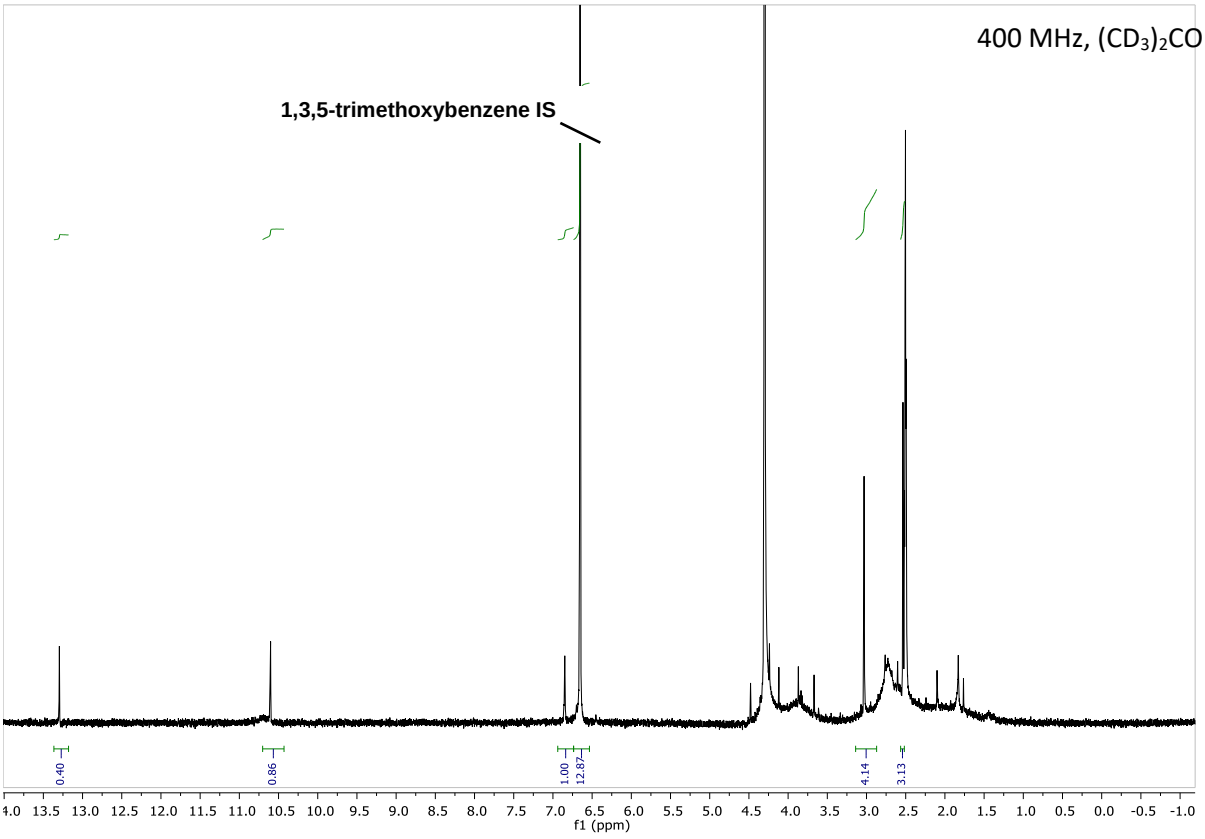


**Figure 2.S8. Crude NMR of $Ag_2O$ oxidation reaction of substrate 2.26.**
Spectrum recorded on 400 MHz NMR in DMSO with 50 mM 1,3,5-trimethoxybenzene as internal standard.

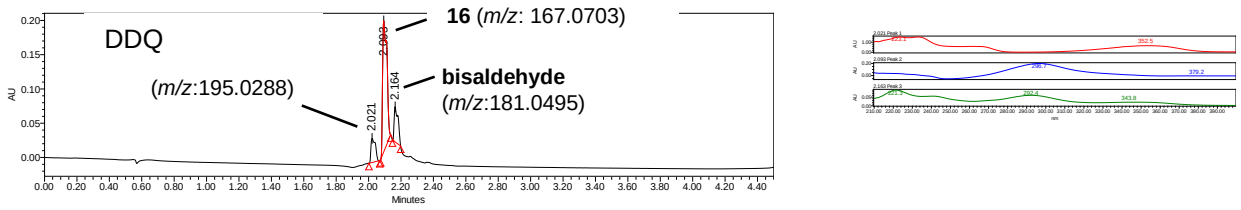


**Figure 2.S9. DDQ oxidation reaction of substrate 2.26.**
PDA trace of reaction analyzed at 300 nm.

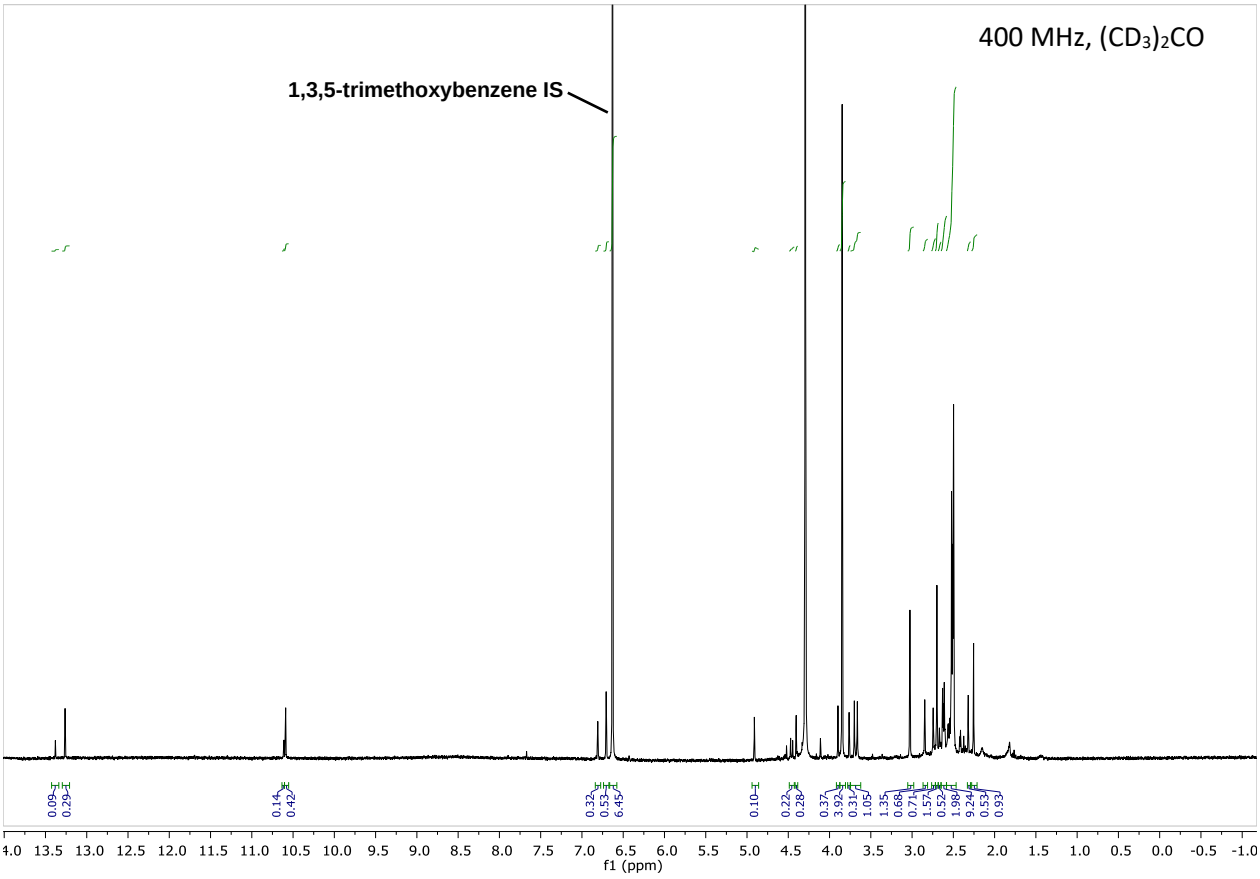


**Figure 2.S10. Crude NMR of DDQ oxidation reaction of substrate 2.26.**
Spectrum recorded on 400 MHz NMR in DMSO with 50 mM 1,3,5-trimethoxybenzene as internal standard.

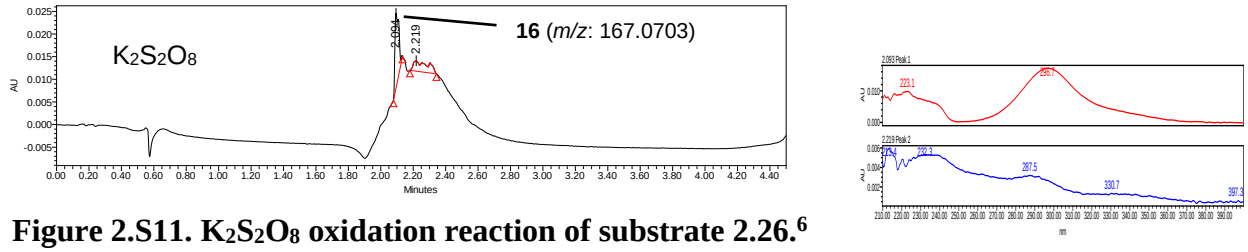


**Figure 2.S11. $K_2S_2O_8$ oxidation reaction of substrate 2.26.[6]**
PDA trace of reaction analyzed at 300 nm.

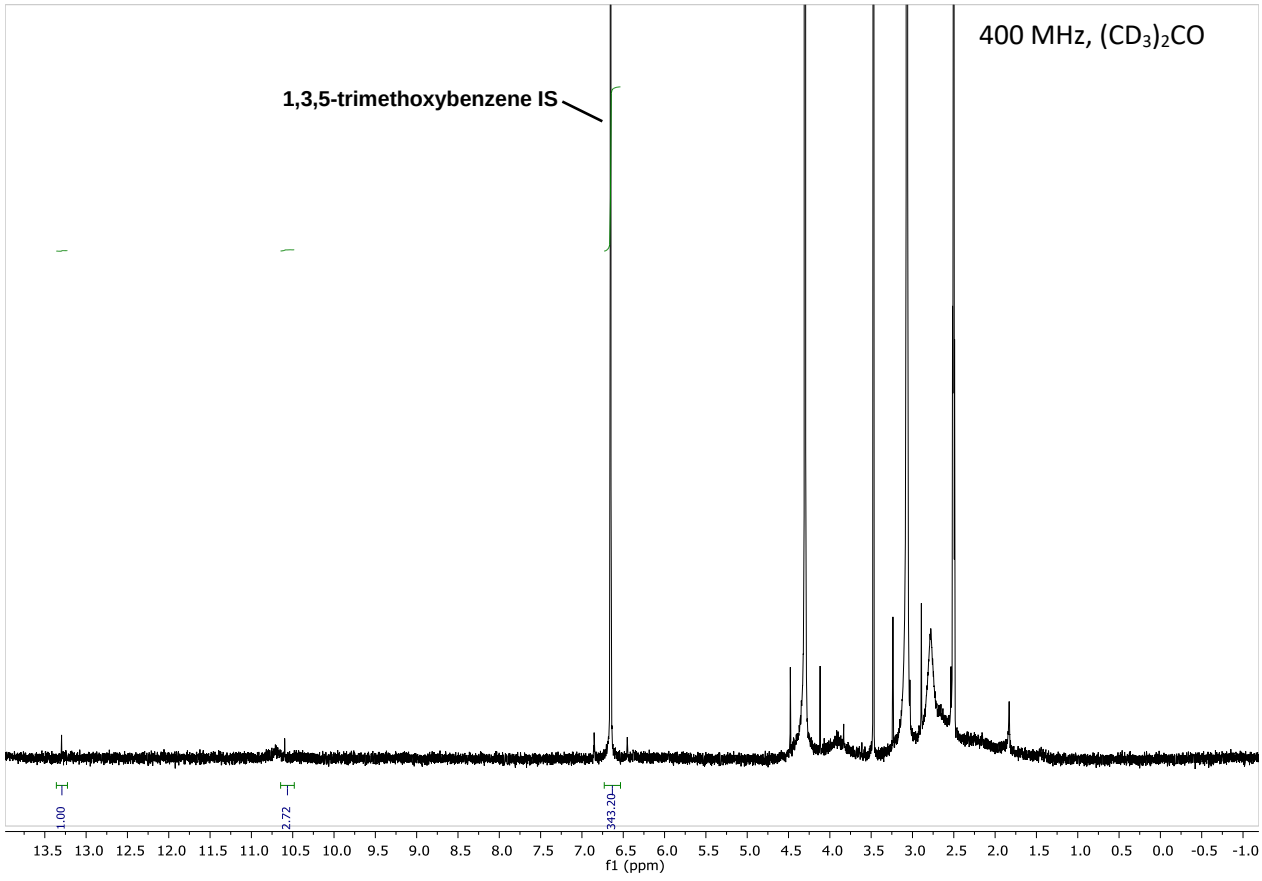


**Figure 2.S12. Crude NMR of $K_2S_2O_8$ oxidation reaction of substrate 2.26.[6]**
Spectrum recorded on 400 MHz NMR in DMSO with 50 mM 1,3,5-trimethoxybenzene as internal standard

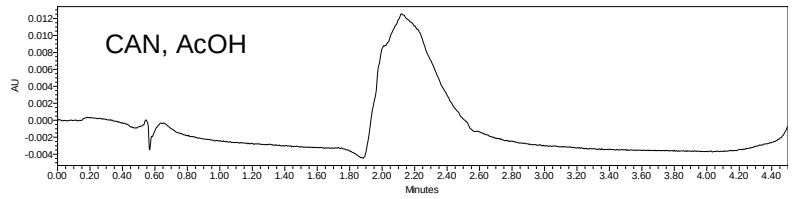


**Figure 2.S13. Ceric ammonium nitrate (CAN) oxidation reaction of substrate 2.26.**[7]
PDA trace of reaction analyzed at 300 nm.

400 MHz, $(CD_3)_2CO$

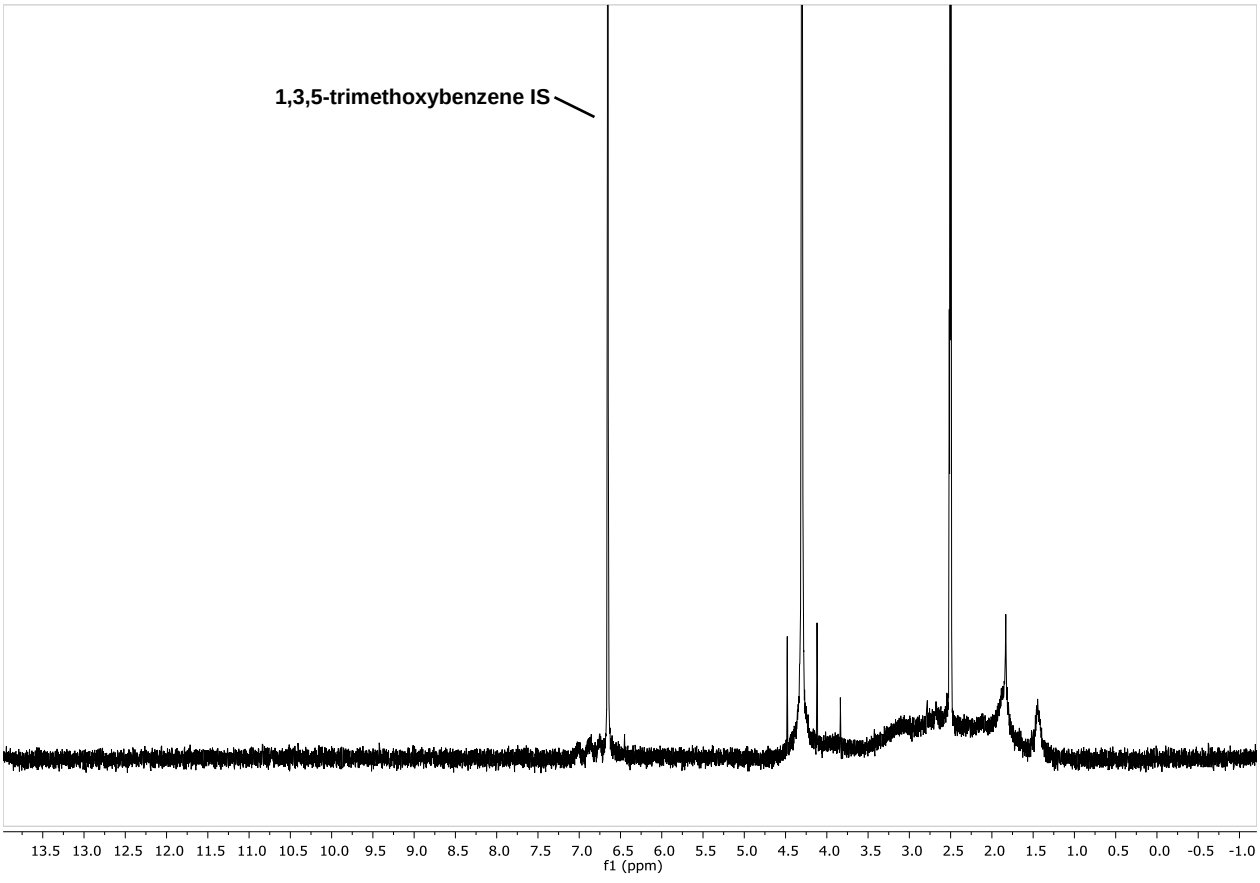


**Figure 2.S14. Crude NMR of CAN oxidation reaction of substrate 2.26.**
Spectrum recorded on 400 MHz NMR in DMSO with 50 mM 1,3,5-trimethoxybenzene as internal standard.

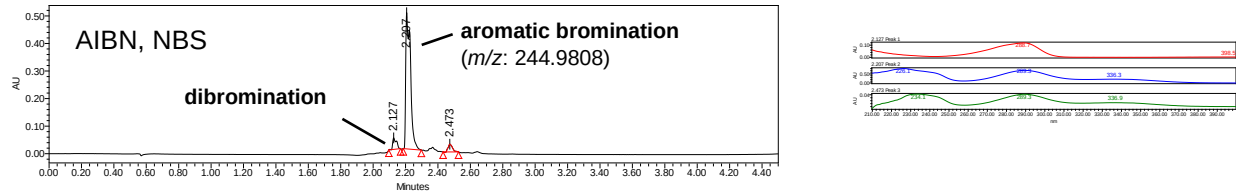


**Figure 2.S15. AIBN, NBS oxidation reaction of substrate 2.26.**[8]
PDA trace of reaction analyzed at 300 nm.

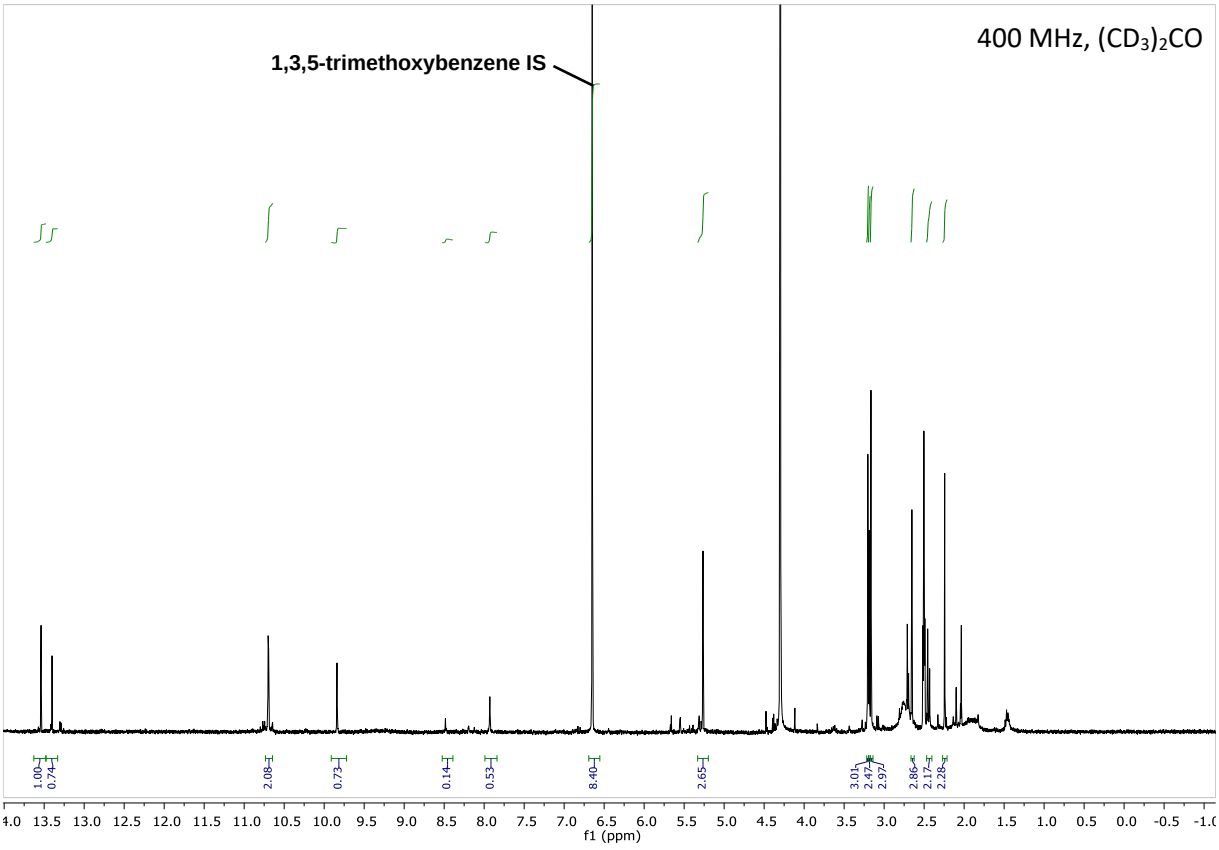


**Figure 2.S16. Crude NMR of AIBN, NBS oxidation reaction of substrate 2.26.**
Spectrum recorded on 400 MHz NMR in DMSO with 50 mM 1,3,5-trimethoxybenzene as internal standard.

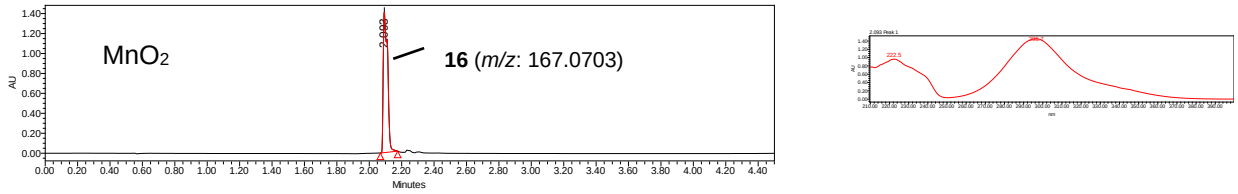


**Figure 2.S17. $MnO_2$ oxidation reaction of substrate 2.26.**[9]
PDA trace of reaction analyzed at 300 nm.

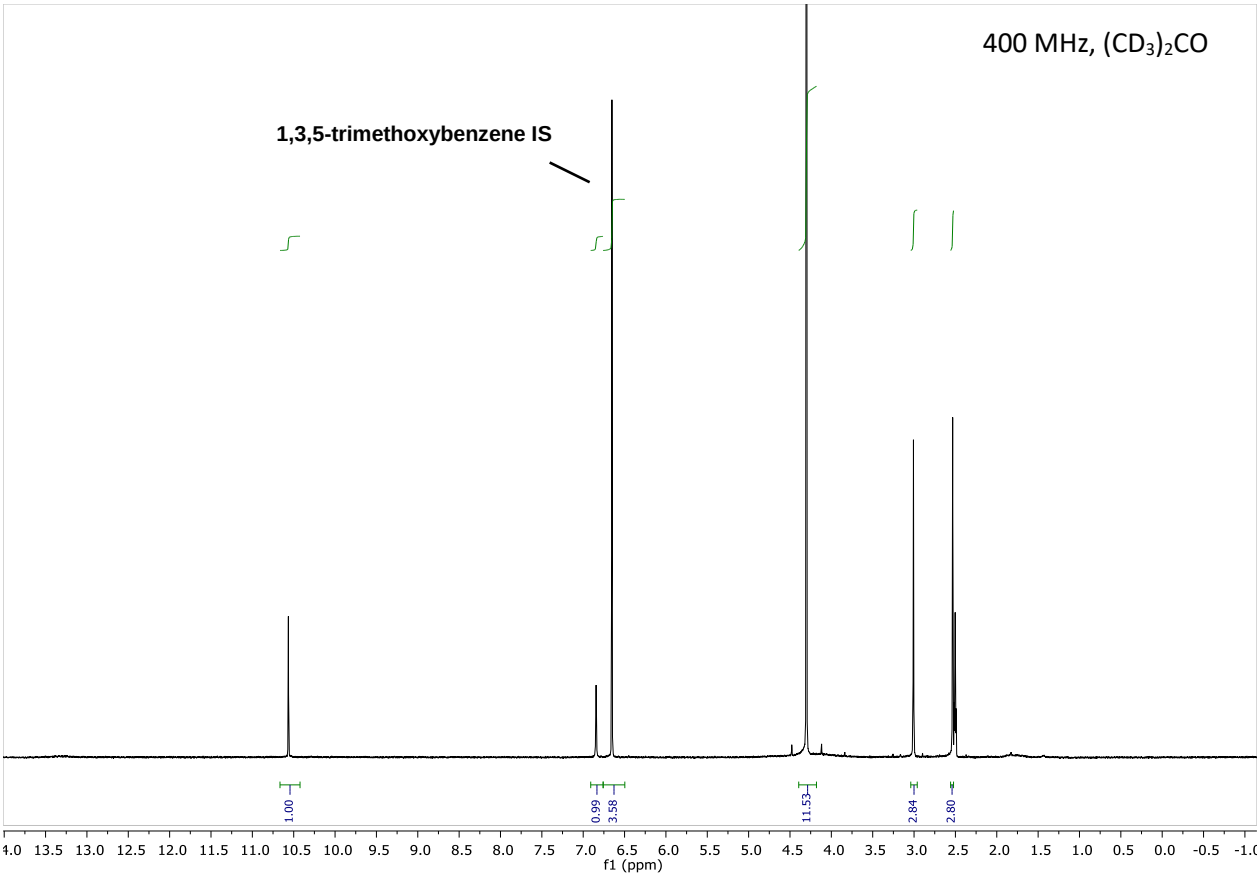


**Figure 2.S18. Crude NMR of $MnO_2$ oxidation reaction of substrate 2.26.**
Spectrum recorded on 400 MHz NMR in DMSO with 50 mM 1,3,5-trimethoxybenzene as internal standard.

**Part V. Benzylic functionalization of NHI enzyme-generated benzylic alcohols**

**Figure 2.S19. Benzylic functionalization of benzylic alcohol 2.27 with nucleophiles.**

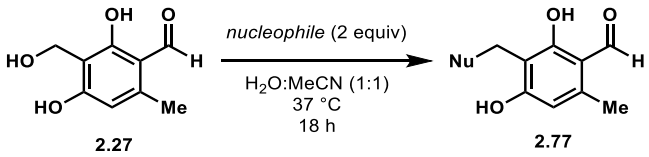


**General procedure for *ortho*-quinone methide conjugate addition reactions:** Benzylic alcohol **2.27** (20 mg, 0.11 mmol, 1.0 equiv) was added to an oven-dried 1 dram vial equipped with a stir bar and dissolved in 1 mL of 1:1 $H_2O$:MeCN. Nucleophile (2.0 equiv) was then added to the vial and the reaction heated at 37 °C for 18 h. The solvent and excess nucleophile were removed under reduced pressure. Purification on silica gel afforded the desired 1,4-addition product.

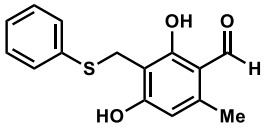


**2,4-dihydroxy-6-methyl-3-((phenylthio)methyl)benzaldehyde (2.30)**

The title compound was synthesized according to the general procedure for *ortho*-quinone methide conjugate addition reactions using thiophenol (22 μL, 0.22 mmol) as the nucleophile. Purification on silica gel (gradient elution 1% to 75% EtOAc in hexanes) afforded 30 mg (98% yield) of **2.20** as an off-white solid. **$^1$H NMR** (400 MHz, $CD_3OD$) δ 10.02 (s,1H), 7.39 (d, *J* = 7.3 Hz, 2H), 7.23 (t, *J* = 7.6 Hz, 2H), 7.15 (t, *J* = 7.3 Hz, 1H), 6.23 (s,1H), 4.13 (s, 2H), 2.47 (s, 3H); **$^{13}$C NMR** (101 MHz, $CD_3OD$) δ 194.5, 165.1, 164.9, 144.9, 138.9, 131.2, 129.6, 127.0, 113.7, 110.9, 110.5, 27.2, 18.2; **HRMS (ESI)** *m/z*: $[M+H]^+$ calculated for $C_{15}H_{13}O_3S^+$ 275.0736, found 275.0737; **IR** (thin film): 3076, 2242, 1584, 1480, 1430, 1330, 1256, 1025, 988, 844, 736, 687, 634, 560, 504 $cm^{-1}$.

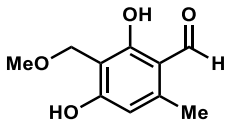


**2,4-dihydroxy-3-(methoxymethyl)-6-methylbenzaldehyde (2.80)**

The title compound was synthesized according to the general procedure for *ortho*-quinone methide conjugate addition reactions using methanol (1 mL) as both the solvent and nucleophile. Purification on silica gel (gradient elution 1% to 75% EtOAc in hexanes) afforded 16 mg (73% yield) of **2.73** as a colorless oil. **$^{1}$H NMR** (400 MHz, $CD_3OD$) δ 10.07 (s, 1H), 6.27 (s, 1H), 4.53 (s, 2H), 3.35 (s, 3H), 2.51 (s, 3H); **$^{13}$C NMR** (151 MHz, $CD_3OD$) δ 194.6, 166.2, 166.1, 146.3, 113.7, 111.2, 110.1, 63.1, 58.1, 18.3; **HRMS (ESI)** *m/z*: $[M+H]^+$ calculated for $C_{10}H_{11}O_4^+$ 197.0808, found 197.0802; **IR** (thin film): 2924, 1622, 1428, 1245, 1123 $cm^{-1}$.

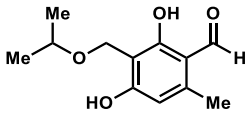


**2,4-dihydroxy-3-(isopropoxymethyl)-6-methylbenzaldehyde (2.81)**

The title compound was synthesized according to the general procedure for *ortho*-quinone methide conjugate addition reactions using isopropanol (1 mL) as both the solvent and nucleophile. Purification on silica gel (gradient elution 1% to 75% EtOAc in hexanes) afforded 15 mg (61% yield) of **2.74** as a colorless oil. **$^{1}$H NMR** (599 MHz, $CD_3OD$) δ 10.05 (s, 1H), 6.25 (s, 1H), 4.58 (s, 2H), 3.74 (hept, *J* = 6.1 Hz, 1H), 2.49 (s, 3H), 1.18 (d, *J* = 6.1 Hz, 6H); **$^{13}$C NMR** (151 MHz, $CD_3OD$) δ 194.6, 166.1, 166.0, 146.0, 113.7, 111.3, 110.6, 72.6, 59.4, 22.4, 18.3; **HRMS (ESI)** *m/z*: $[M+H]^+$ calculated for $C_{12}H_{15}O_4^+$ 225.1121, found 225.1106; **IR** (thin film): 3219, 2925, 1621, 1489, 1229, 1119 $cm^{-1}$.

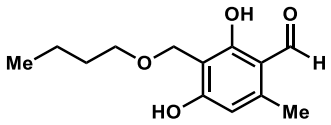


**2,4-dihydroxy-3-(*n*-butoxymethyl)-6-methylbenzaldehyde (2.82)**

The title compound was synthesized according to the general procedure for *ortho*-quinone methide conjugate addition reactions using isopropanol (1 mL) as both the solvent and nucleophile. Purification on silica gel (gradient elution 1% to 75% EtOAc in hexanes) afforded 12 mg (47% yield) of **2.75** as a colorless solid. **$^1$H NMR** (599 MHz, $CD_3OD$) δ 10.06 (s, 1H), 6.26 (s, 1H), 4.56 (s, 2H), 3.50 (t, *J* = 6.6 Hz, 2H), 2.49 (s, 3H), 1.55 (dt, *J* = 14.5, 6.7 Hz, 2H), 1.36 (h, *J* = 7.4 Hz, 2H), 0.90 (t, *J* = 7.4 Hz, 3H); **$^{13}$C NMR** (151 MHz, $CD_3OD$) δ 194.7, 166.1, 166.0, 146.1, 113.7, 111.2, 110.4, 71.1, 61.5, 32.7, 20.3, 18.3, 14.2; **HRMS (ESI)** *m/z*: $[M+H]^+$ calculated for $C_{13}H_{17}O_4^+$ 239.1278, found 239.1222; **IR** (thin film): 2913, 1618, 1435, 1302, 1016, 951, 697 $cm^{-1}$.

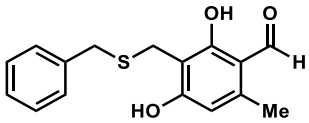


**3-((benzylthio)methyl)-2,4-dihydroxy-6-methylbenzaldehyde (2.83)**

The title compound was synthesized according to the general procedure for *ortho*-quinone methide conjugate addition reactions using benzylmercaptan (26 μL, 0.22 mmol) as the nucleophile. Purification on silica gel (gradient elution 1% to 75% EtOAc in hexanes) afforded 31 mg (97% yield) of **2.76** as an off-white solid. **$^1$H NMR** (599 MHz, $CD_3OD$) δ 10.03 (s, 1H), 7.32 (d, *J* = 7.1 Hz, 2H), 7.24 (t, *J* = 7.6 Hz, 2H), 7.17 (t, *J* = 7.3 Hz, 1H), 6.24 (s, 1H), 3.78 (s, 2H), 3.69 (s, 2H), 2.48 (s, 3H); **$^{13}$C NMR** (151 MHz, $CD_3OD$) δ 194.5, 165.0, 165.0, 144.5, 140.5, 129.9, 129.2,

127.6, 113.7, 112.3, 111.2, 37.7, 24.0, 18.1; **HRMS (ESI)** *m/z*: $[M+H]^+$ calculated for $C_{16}H_{15}O_3S^+$ 289.0893, found 289.0887; **IR** (thin film): 3083, 1606, 1429, 1288, 1255, 1102, 699 $cm^{-1}$.

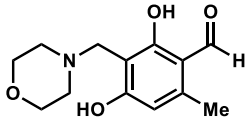


**2,4-dihydroxy-6-methyl-3-(morpholinomethyl)benzaldehyde (2.84)**

The title compound was synthesized according to the general procedure for *ortho*-quinone methide conjugate addition reactions using morpholine (19 μL, 0.22 mmol) as the nucleophile. Purification on silica gel (gradient elution 1% to 75% EtOAc in hexanes) afforded 18 mg (65% yield) of **77** as a white solid. **$^1$H NMR** (599 MHz, $CD_3OD$) δ 10.00 (s, 1H), 6.18 (s, 1H), 3.84 (s, 2H), 3.75 (m, 4H), 2.70 (m, 4H), 2.47 (s, 3H); $^{13}$C NMR (151 MHz, $CD_3OD$) δ 193.9, 169.4, 165.5, 145.5, 113.0, 112.8, 105.8, 67.3, 53.8, 53.2, 18.3; **HRMS (ESI)** *m/z*: $[M+H]^+$ calculated for $C_{13}H_{16}NO_4^+$ 252.1230, found 252.1279; **IR** (thin film): 2850, 1620, 1483, 1363, 1293, 1269, 1243, 1114, 997, 861, 626 $cm^{-1}$.

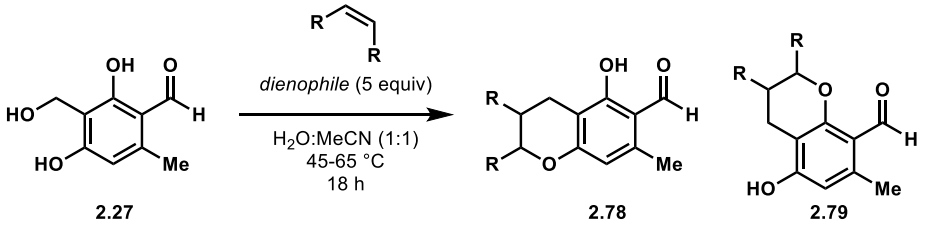


**Figure 2.S20. Inverse electron-demand Diels-Alder reactions with benzylic alcohol, 2.27.**

**General procedure for Diels-Alder reactions:** Benzylic alcohol **2.27** (20 mg, 0.110 mmol, 1.0 equiv) was added to an oven-dried 1 dram vial equipped with a stir bar and dissolved in 1 mL of 1:1 $H_2O$:MeCN. Dienophile (5 equiv) was then added to the vial and the reaction heated at 45-65 °C for 18 h. The solvent and excess dienophile were removed under reduced pressure. Purification on silica gel afforded the cycloadduct products.

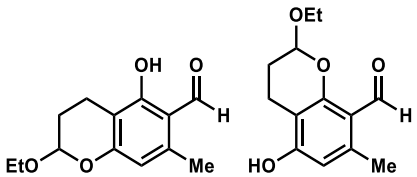


2.85 2.86

**2-ethoxy-5-hydroxy-7-methylchromane-6-carbaldehyde (2.85) and 2-ethoxy-5-hydroxy-7-methylchro-mane-8-carbaldehyde (2.86)**

The title compounds were synthesized according to the general procedure for *ortho*-quinone methide Diels-Alder reactions using ethyl vinyl ether (53 μL, 0.549 mmol) as the dienophile and heating at 45 °C. The reaction gave a 2:1 ratio of **2.85** and **2.86**, respectively (as judged by the $^{1}$H NMR spectrum of the unpurified reaction mixture). Purification on silica gel (gradient elution 1% to 75% EtOAc in hexanes) afforded 16 mg (61% yield) of **2.85** and 8 mg (30% yield) of **2.86** as colorless oils.

Data for **2.85**: **$^{1}$H NMR** (599 MHz, $CDCl_3$) δ 12.68 (s, 1H), 10.07 (s, 1H), 6.21 (s, 1H), 5.26 (s, 1H), 3.87 (dq, *J* = 14.3, 7.1 Hz, 1H), 3.65 (dq, *J* = 14.3, 7.1 Hz, 1H), 2.73 – 2.62 (m, 2H), 2.49 (s, 3H), 2.06 (dq, *J* = 13.3, 4.7 Hz, 1H), 1.94 – 1.84 (m, 1H), 1.20 (t, *J* = 7.1 Hz, 3H); **$^{13}$C NMR** (151 MHz, $CDCl_3$) δ 193.1, 163.2, 159.5, 141.0, 112.9, 111.4, 108.5, 97.8, 64.2, 25.7, 18.0, 15.1, 13.9; **HRMS (ESI)** *m/z*: $[M+H]^+$ calculated for $C_{13}H_{15}O_4^+$ 237.1121, found 237.1084; **IR** (thin film): 2928, 1622, 1579, 1483, 1325, 1281, 1242, 1217, 1132, 1099, 1046, 967, 934, 850 $cm^{-1}$.

Data for **2.86**: **$^{1}$H NMR** (599 MHz, $CD_3OD$) δ 10.38 (s, 1H), 6.27 (s, 1H), 5.38 (s, 1H), 3.88 (dt, *J* = 14.3, 7.2 Hz, 1H), 3.76 – 3.64 (m, 1H), 2.65 (dd, *J* = 10.1, 6.0 Hz, 2H), 2.47 (s, 3H), 2.08 – 2.02 (m, 1H), 1.99 – 1.93 (m, 1H), 1.21 (t, *J* = 7.1 Hz, 3H); **$^{13}$C NMR** (151 MHz, $CD_3OD$) δ 191.9, 162.2, 159.6, 142.7, 116.9, 111.7, 109.0, 98.8, 65.3, 26.6, 22.2, 15.6, 15.5; **HRMS (ESI)** *m/z*:

[M+H]$^+$ calculated for $C_{13}H_{15}O_4^+$ 237.1121, found 237.1073; **IR** (thin film): 2924, 1626, 1493, 1327, 1282, 1243, 1100, 1049, 935, 851 cm$^{-1}$.

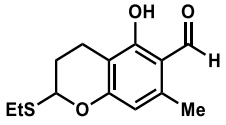


**2-(ethylthio)-5-hydroxy-7-meth-ylchromane-8-carbaldehyde (2.87)**

The title compounds were synthesized according to the general procedure for *ortho*-quinone methide Diels-Alder reactions using ethyl vinyl sulfide (56 μL, 0.549 mmol) as the dienophile and heating at 45 °C. The reaction gave a 4:1 ratio of **2.87** and **2.88**, respectively (as judged by the $^1$H NMR spectrum of the unpurified reaction mixture). Purification on silica gel (gradient elution 1% to 75% EtOAc in hexanes) afforded 19 mg (70% yield) of **2.87**. **$^1$H NMR** (599 MHz, $CD_3OD$) δ 10.10 (s, 1H), 6.23 (s, 1H), 5.64 (t, *J* = 4.0 Hz, 1H), 2.80 (dq, *J* = 13.0, 7.4 Hz, 1H), 2.75 – 2.66 (m, 2H), 2.63 (ddd, *J* = 16.8, 10.2, 6.2 Hz, 1H), 2.21 (dddd, *J* = 14.0, 10.2, 6.3, 3.8 Hz, 1H), 2.11 (ddt, *J* = 14.3, 6.2, 4.4 Hz, 1H); **$^{13}$C NMR** (151 MHz, $CD_3OD$) δ 195.1, 164.3, 161.1, 142.8, 114.2, 112.8, 109.1, 82.5, 27.4, 25.7, 18.0, 16.8, 15.6; **HRMS (ESI)** *m/z*: [M+H]$^+$ calculated for $C_{13}H_{15}O_3S^+$ 253.0893, found 253.0844; **IR** (thin film): 2926, 1624, 1578, 1481, 1419, 1372, 1321, 1279, 1239, 1116, 853 cm$^{-1}$.

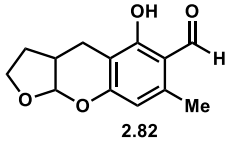

2.82

**5-hydroxy-7-methyl-2,3,3a,9a-tetrahydro-4H-furo[2,3-b]chromene-6-carbaldehyde (2.89) and 5-hydroxy-7-methyl-2,3,3a,9a-tetrahydro-4H-furo[2,3-b]chromene-8-carbaldehyde (2.90)**

The title compounds were synthesized according to the general procedure for *ortho*-quinone methide Diels-Alder reactions using 2,3-dihydrofuran (42 μL, 0.549 mmol) as the dienophile and heating at 45 °C. The reaction gave a 4:1 ratio of **2.89** and **2.90**, respectively (as judged by the $^{1}$H NMR spectrum of the unpurified reaction mixture). Purification on silica gel (gradient elution 1% to 75% EtOAc in hexanes) afforded 18 mg (70% yield) of **2.89** as a white solid. **$^{1}$H NMR** (599 MHz, $CDCl_3$) δ 12.73 (s, 1H), 10.06 (s, 1H), 6.23 (s, 1H), 5.59 (d, *J* = 3.9 Hz, 1H), 4.18 – 4.11 (m, 1H), 4.02 (q, *J* = 8.4 Hz, 1H), 2.94 (d, *J* = 17.3 Hz, 1H), 2.79 (dd, *J* = 17.3, 6.3 Hz, 1H), 2.75 – 2.65 (m, 1H), 2.49 (s, 3H), 2.08 (td, *J* = 11.6, 10.5, 5.4 Hz, 1H), 1.69 (p, *J* = 9.7 Hz, 1H); **$^{13}$C NMR** (151 MHz, $CDCl_3$) δ 193.0, 163.8, 160.1, 141.6, 113.0, 111.2, 104.6, 101.0, 68.5, 36.3, 27.5, 18.4, 18.0; **HRMS (ESI)** *m/z*: $[M+H]^+$ calculated for $C_{13}H_{13}O_4^+$ 235.0965, found 235.0976; **IR** (thin film): 2897, 1620, 1483, 1423, 1374, 1319, 1280, 1240, 1140, 1106, 1051, 931, 833, 547 cm$^{-1}$.

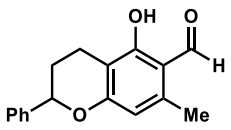

2.84

**5-hydroxy-7-methyl-2-phenylchromane-6-carbaldehyde (2.91)**

The title compound was synthesized according to the general procedure for *ortho*-quinone methide Diels-Alder reactions using styrene (63 μL, 0.549 mmol) as the dienophile and heating at 65 °C. The reaction gave a 1:3 ratio of **2.91** and **2.92**, respectively (as judged by the $^{1}$H NMR spectrum of the unpurified reaction mixture). Purification on silica gel (gradient elution 1% to 75% EtOAc in hexanes) afforded 6 mg (33% yield) of **2.91** as a colorless oil. **$^{1}$H NMR** (599 MHz, $CDCl_3$) δ 12.78 (s, 1H), 10.08 (s, 1H), 7.45 – 7.29 (m, 5H), 6.30 (s, 1H), 5.09 (dd, *J* = 10.2, 2.1 Hz, 1H), 2.82 (dt, *J* = 16.8, 4.3 Hz, 1H), 2.69 (ddd, *J* = 17.0, 11.0, 6.1 Hz, 1H), 2.51 (s, 3H), 2.27 (ddt, *J* = 13.4, 5.7, 2.8 Hz, 1H), 2.03 (ddt, *J* = 21.0, 10.7, 5.5 Hz, 1H); **$^{13}$C NMR** (151 MHz, $CDCl_3$) δ

193.0, 163.7, 162.3, 141.1, 140.6, 128.6, 128.1, 125.9, 112.7, 111.4, 107.9, 78.5, 28.8, 18.2, 18.0. **HRMS (ESI)** *m/z*: $[M+H]^+$ calculated for $C_{17}H_{15}O_3^+$ 269.1172, found 269.1186; **IR** (thin film): 3433, 2923, 1624, 1514, 1373, 1280, 1238, 1132, 1025, 819 $cm^{-1}$.

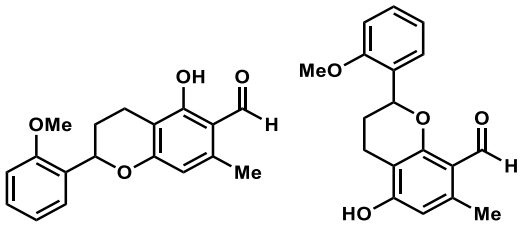


2.93 2.94

**5-hydroxy-2-(2-methoxyphenyl)-7-methylchromane-6-carbaldehyde (2.93) and 5-hydroxy-2-(2-meth-oxyphenyl)-7-methylchromane-8-carbaldehyde (2.94)**

The title compounds were synthesized according to the general procedure for *ortho*-quinone methide Diels-Alder reactions using 2-methoxystyrene (74 μL, 0.549 mmol) as the dienophile and heating at 65 °C. The reaction gave a 1:3 ratio of **2.93** and **2.94**, respectively (as judged by the $^1H$ NMR spectrum of the unpurified reaction mixture). Purification on silica gel (gradient elution 1% to 75% EtOAc in hexanes) afforded 16 mg (39% yield) of **2.93** and 6 mg (13% yield) of **2.94** as white solids.

Data for **2.93**: **$^1$H NMR** (599 MHz, $CDCl_3$) δ 12.78 (s, 1H), 10.08 (s, 1H), 7.40 (d, *J* = 7.4 Hz, 1H), 7.30 (t, *J* = 7.7 Hz, 1H), 7.00 (t, *J* = 7.4 Hz, 1H), 6.92 (d, *J* = 8.2 Hz, 1H), 6.30 (s, 1H), 5.47 (d, *J* = 9.5 Hz, 1H), 3.86 (s, 3H), 2.77 (d, *J* = 16.8 Hz, 1H), 2.70 (ddd, *J* = 16.8, 10.8, 6.0 Hz, 1H), 2.51 (s, 3H), 2.33 – 2.21 (m, 1H), 1.89 (dh, *J* = 15.5, 5.6 Hz, 1H); **$^{13}$C NMR** (151 MHz, $CDCl_3$) δ 192.9, 163.7, 162.8, 155.8, 140.9, 129.1, 128.8, 126.2, 120.7, 112.6, 111.4, 110.4, 108.2, 73.3, 55.4, 27.4, 18.3, 18.0; **HRMS (ESI)** *m/z*: $[M+H]^+$ calculated for $C_{18}H_{17}O_4^+$ 299.1278, found 299.1279; **IR** (thin film): 2923, 1642, 1576, 1492, 1436, 1340, 1303, 1240, 1016, 952, 824, 750 $cm^{-1}$.

Data for **2.94**: **$^{1}$H NMR** (599 MHz, $CD_3OD$) δ 10.37 (s, 1H), 7.42 (d, *J* = 7.5 Hz, 1H), 7.30 (t, *J* = 7.7 Hz, 1H), 7.02 (d, *J* = 8.2 Hz, 1H), 6.99 (t, *J* = 7.5 Hz, 1H), 6.25 (s, 1H), 5.41 (d, *J* = 9.8 Hz, 1H), 3.87 (s, 3H), 2.81 – 2.61 (m, 2H), 2.47 (s, 3H), 2.33 – 2.23 (m, 1H), 1.87 (dh, *J* = 16.5, 6.0 Hz, 1H); **$^{13}$C NMR** (151 MHz, $CD_3OD$) δ 192.0, 163.1, 162.9, 157.4, 142.8, 130.7, 129.9, 126.9, 121.7, 116.6, 111.6, 111.4, 108.7, 74.6, 55.9, 28.7, 22.3, 20.3; **HRMS (ESI)** *m/z*: $[M+H]^+$ calculated for $C_{18}H_{17}O_4^+$ 299.1278, found 299.1276; **IR** (thin film): 2927, 1625, 1494, 1373, 1281, 1238, 1136 $cm^{-1}$.

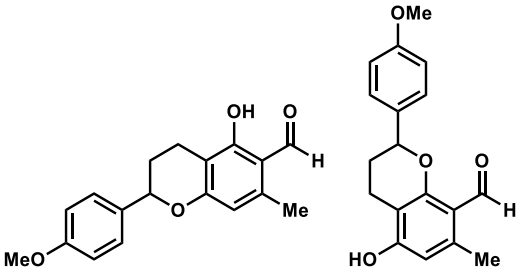


**5-hydroxy-2-(4-methoxyphenyl)-7-methylchromane-6-carbaldehyde (2.95) and 5-hydroxy-2-(4-meth-oxyphenyl)-7-methylchromane-8-carbaldehyde (2.96)**

The title compounds were synthesized according to the general procedure for *ortho*-quinone methide Diels-Alder reactions using 4-methoxystyrene (73 μL, 0.549 mmol) as the dienophile and heating at 65 °C. The reaction gave a 1:4 ratio of **2.95** and **2.96**, respectively (as judged by the $^{1}$H NMR spectrum of the unpurified reaction mixture). Purification on silica gel (gradient elution 1% to 75% EtOAc in hexanes) afforded 18 mg (44% yield) of **2.95** and 5 mg (12% yield) of **2.96** as white solids.

Data for **2.95**: **$^{1}$H NMR** (599 MHz, $CDCl_3$) δ 12.77 (s, 1H), 10.07 (s, 1H), 7.32 (d, *J* = 8.5 Hz, 2H), 6.93 (d, *J* = 8.6 Hz, 2H), 6.27 (s, 1H), 5.03 (dd, *J* = 10.5, 2.4 Hz, 1H), 3.82 (s, 3H), 2.84 (ddd, *J* = 16.9, 5.6, 3.1 Hz, 1H), 2.67 (ddd, *J* = 17.1, 11.3, 6.1 Hz, 1H), 2.49 (s, 3H), 2.23 (ddd, *J* = 11.1,

5.9, 2.9 Hz, 1H), 2.09 – 1.94 (m, 1H); **$^{13}$C NMR** (151 MHz, $CDCl_3$) δ 192.9, 163.7, 162.4, 159.5, 141.0, 132.7, 127.4, 114.0, 112.7, 111.4, 107.9, 78.3, 55.3, 28.6, 18.4, 18.0; **HRMS (ESI)** *m/z*: $[M+H]^+$ calculated for $C_{18}H_{17}O_4^+$ 299.1278, found 299.1268; **IR** (thin film): 2924, 1578, 1496, 1422, 1291, 1239, 1086, 757, 695 $cm^{-1}$.

Data for **2.96**: **$^1$H NMR** (599 MHz, $((CD_3)_2SO)$ δ 10.46 (s, 1H), 10.30 (s, 1H), 7.36 (d, *J* = 8.4 Hz, 2H), 6.94 (d, *J* = 8.5 Hz, 2H), 6.26 (s, 1H), 5.09 (d, *J* = 10.0 Hz, 1H), 3.74 (s, 3H), 2.68 – 2.54 (m, 2H), 2.38 (s, 3H), 2.17 (d, *J* = 13.4 Hz, 1H), 1.98 – 1.86 (m, 1H); **$^{13}$C NMR** (151 MHz, $((CD_3)_2SO)$ δ 189.0, 160.6, 160.6, 158.9, 140.1, 133.0, 127.3, 114.9, 113.9, 110.2, 107.1, 76.9, 55.1, 27.8, 21.6, 18.9; **HRMS (ESI)** *m/z*: $[M+H]^+$ calculated for $C_{18}H_{17}O_4^+$ 299.1278, found 299.1268; **IR** (thin film): 2925, 1619, 1570, 1427, 1293, 1247, 1120, 729 $cm^{-1}$.

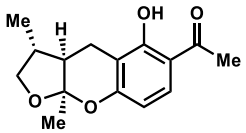

(**2.15**) (-)-xyloketal D

**(-)-xyloketal D (2.25)**

Enantiomerically pure xyloketal D was prepared through the inverse electron-demand Diels-Alder reaction of enzymatically prepared benzylic alcohol **2.68** and dienophile **2.100**. Benzylic alcohol **2.68** (35 mg, 0.192 mmol, 1.0 equiv) was added to an oven-dried 1 dram vial equipped with a stir bar and dissolved in MeCN (2 mL). Dienophile **2.100** (49 μL, 0.384 mmol, 2.0 equiv) was then added to the vial and the reaction heated at 75 °C for 18 hours until starting material was completely consumed as determined by UPLC-DAD analysis. The reaction was concentrated to remove solvent and excess dienophile. The reaction gave a 2:1 mixture of diastereomers (as judged by $^1$H NMR and UPLC-DAD analysis of the unpurified reaction). Purification on silica gel (gradient elution 1% to 5% EtOAc in hexanes) afforded 23 mg (46% yield) of (-)-xyloketal D.

Reaction analysis by UPLC-DAD with product standard curve showed full conversion of starting material after 18 hours and 66% yield of (-)-xyloketal D when the reaction was performed in benzene and heated at 80 °C. All spectroscopic data for the compound matched previously reported literature values.

Data for **2.25**: **$^{1}$H NMR** (599 MHz, $CDCl_3$) δ13.11 (s, 1H), 7.52 (d, *J* = 8.9 Hz, 1H), 6.36 (d, *J* = 8.9 Hz, 1H), 4.20 (t, *J* = 8.4 Hz, 1H), 3.56 (t, *J* = 8.6 Hz, 1H), 2.96 (d, *J* = 17.8 Hz, 1H), 2.72 (dd, *J* = 17.9, 6.5 Hz, 1H), 2.54 (s, 3H), 2.14 – 2.03 (m, 1H), 1.98 (dd, *J* = 11.3, 6.5 Hz, 1H), 1.53 (s, 3H), 1.08 (d, *J* = 6.5 Hz, 3H); **$^{13}$C NMR** (151 MHz, $CDCl_3$) δ 202.7, 162.9, 159.5, 130.0, 113.1, 108.8, 108.3, 106.1, 77.2, 77.0, 76.8, 74.3, 46.9, 35.1, 26.1, 22.7, 18.0, 15.8; **HRMS (ESI)** *m/z*: $[M+H]^+$ calculated for $C_{18}H_{17}O_4^+$ 299.1278, found 299.1268; **$[\alpha]^{23}_D$** = -73.50° (c. 0.100, $CHCl_3$).

## Part VI. Substrate and product calibration curves

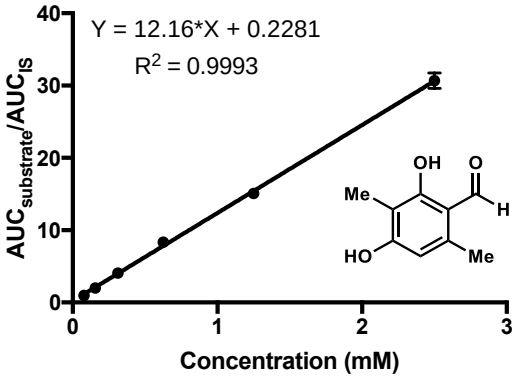


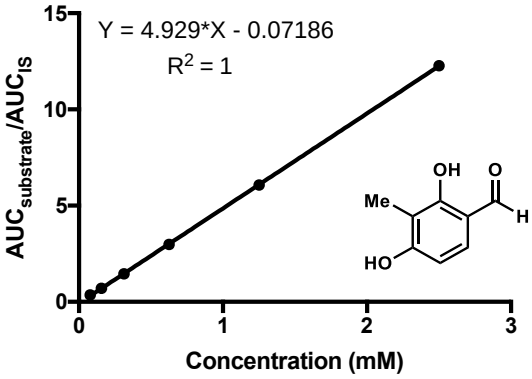


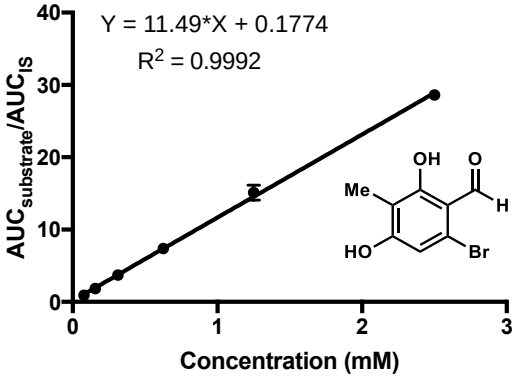


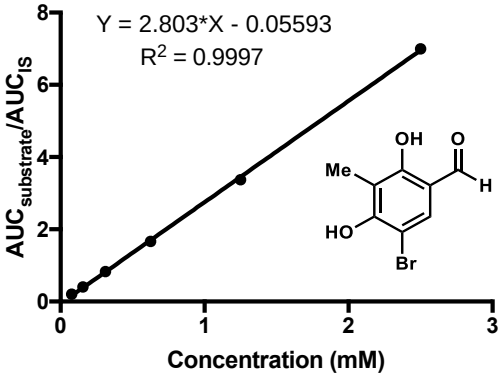


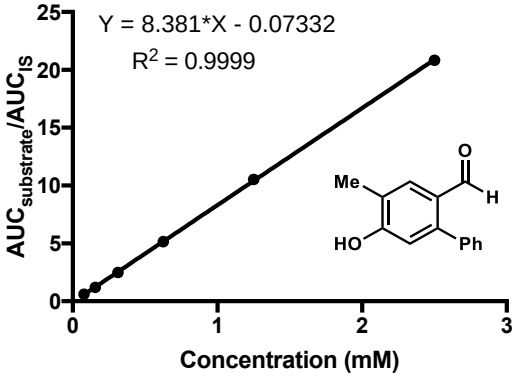


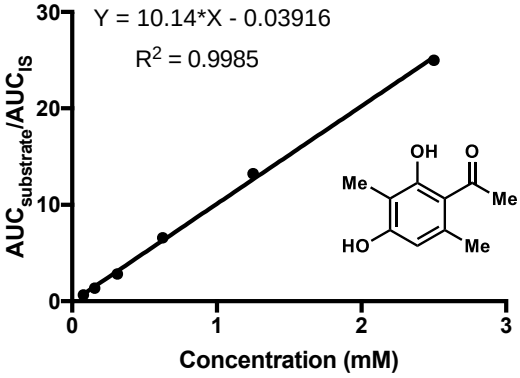

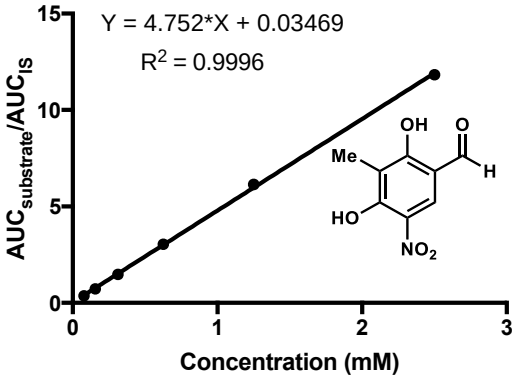
Y = 4.752*X + 0.03469
R2 = 0.9996
AUCsubstrate/AUCIS
Concentration (mM)
OH
O
Me
H
HO
NO2

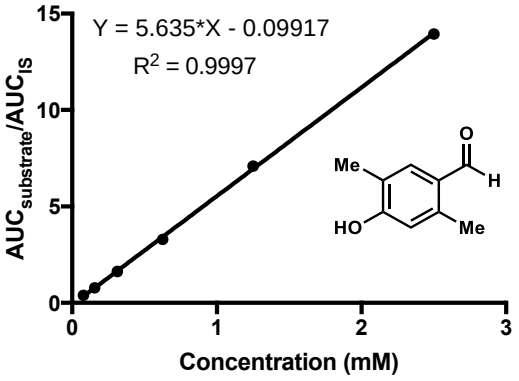
Y = 5.635*X - 0.09917
R2 = 0.9997
AUCsubstrate/AUCIS
Concentration (mM)
O
Me
H
HO
Me

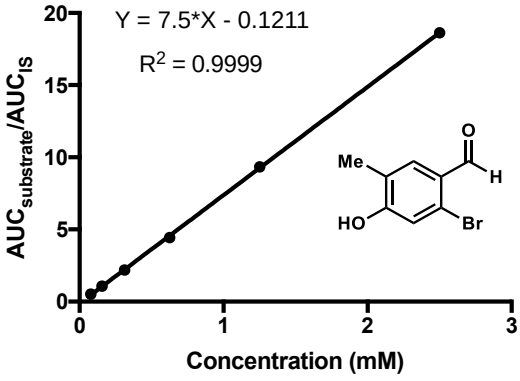
Y = 7.5*X - 0.1211
R2 = 0.9999
AUCsubstrate/AUCIS
Concentration (mM)
O
Me
H
HO
Br

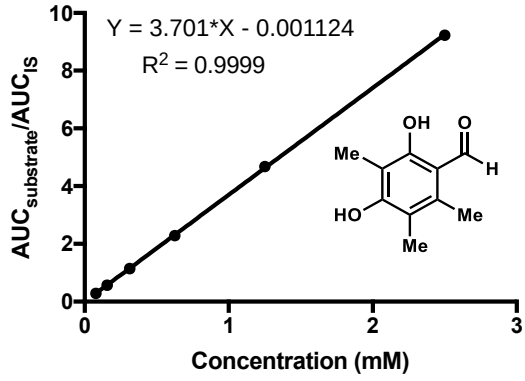
Y = 3.701*X - 0.001124
R2 = 0.9999
AUCsubstrate/AUCIS
Concentration (mM)
OH
O
Me
H
HO
Me
Me

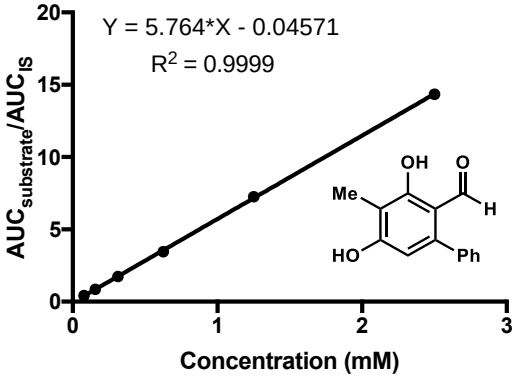
Y = 5.764*X - 0.04571
R2 = 0.9999
AUCsubstrate/AUCIS
Concentration (mM)
OH
O
Me
H
HO
Ph

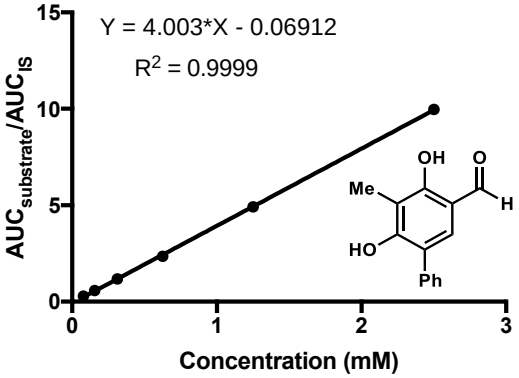
Y = 4.003*X - 0.06912
R2 = 0.9999
AUCsubstrate/AUCIS
Concentration (mM)
OH
O
Me
H
HO
Ph

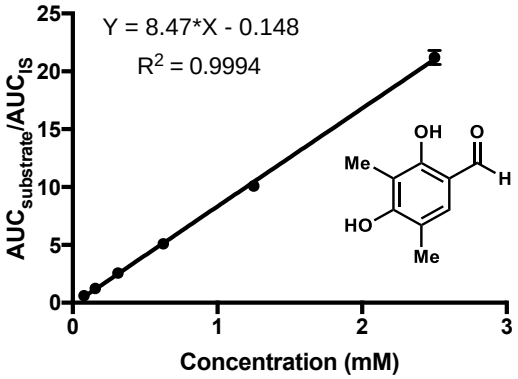
Y = 8.47*X - 0.148
R2 = 0.9994
AUCsubstrate/AUCIS
Concentration (mM)
OH
O
H
Me
HO
Me

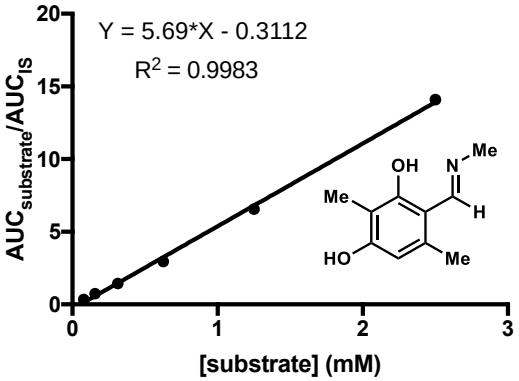
Y = 5.69*X - 0.3112
R2 = 0.9983
AUCsubstrate/AUCIS
[substrate] (mM)
OH
N
Me
H
Me
HO
Me

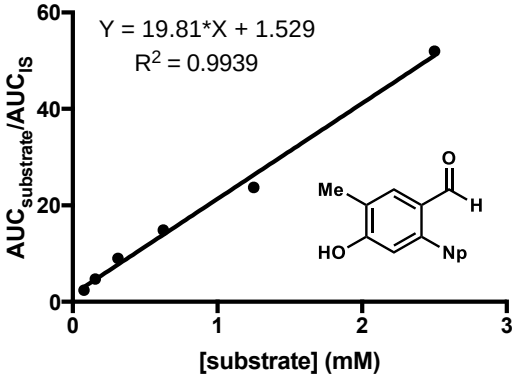
Y = 19.81*X + 1.529
R2 = 0.9939
AUCsubstrate/AUCIS
[substrate] (mM)
O
H
Me
HO
Np

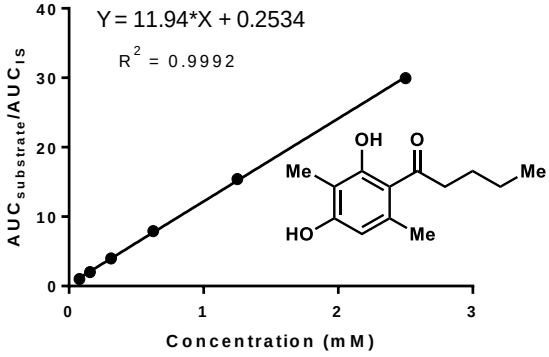
Y = 11.94*X + 0.2534
R2 = 0.9992
AUCsubstrate/AUCIS
Concentration (mM)
OH
O
Me
Me
HO
Me

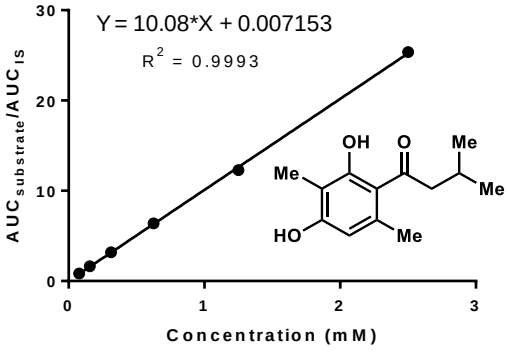
Y = 10.08*X + 0.007153
R2 = 0.9993
AUCsubstrate/AUCIS
Concentration (mM)
OH
O
Me
Me
Me
HO
Me

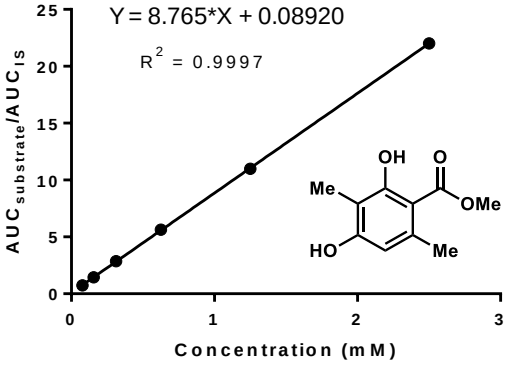
Y = 8.765*X + 0.08920
R2 = 0.9997
AUCsubstrate/AUCIS
Concentration (mM)
OH
O
Me
OMe
HO
Me

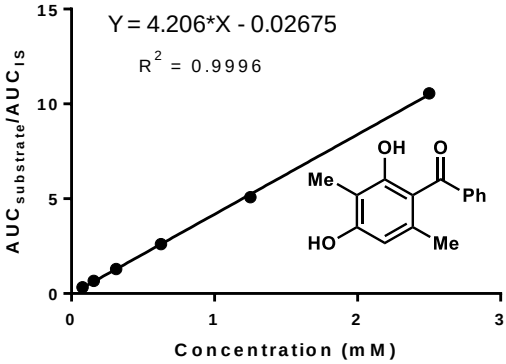
Y = 4.206*X - 0.02675
R2 = 0.9996
AUCsubstrate/AUCIS
Concentration (mM)
OH
O
Me
Ph
HO
Me

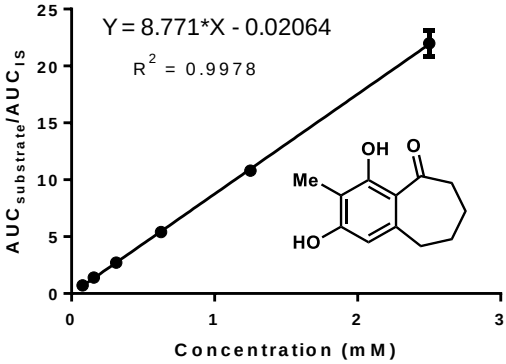
Y = 8.771*X - 0.02064
R2 = 0.9978
AUCsubstrate/AUCIS
Concentration (mM)
OH
O
Me
HO

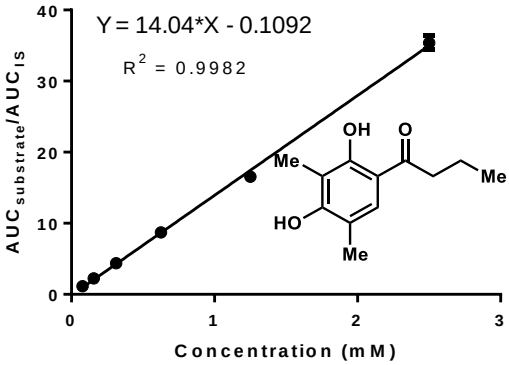
Y = 14.04*X - 0.1092
R2 = 0.9982
AUCsubstrate/AUCIS
Concentration (mM)
OH
O
Me
Me
HO
Me

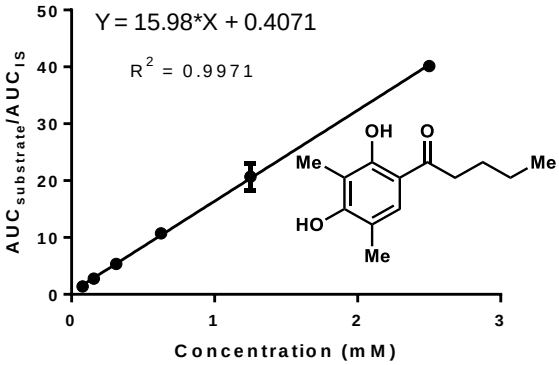
Y = 15.98*X + 0.4071
R2 = 0.9971
AUCsubstrate/AUCIS
Concentration (mM)
OH
O
Me
Me
HO
Me

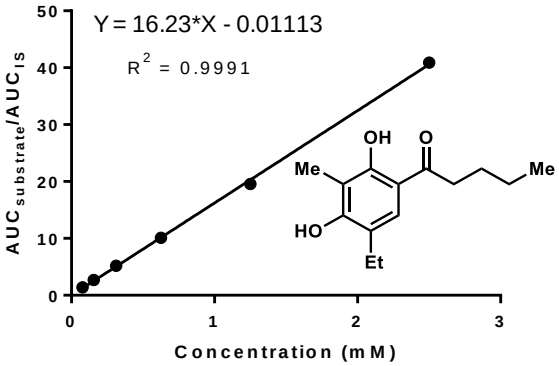
Y = 16.23*X - 0.01113
R2 = 0.9991
AUCsubstrate/AUCIS
Concentration (mM)
OH
O
Me
Me
HO
Et

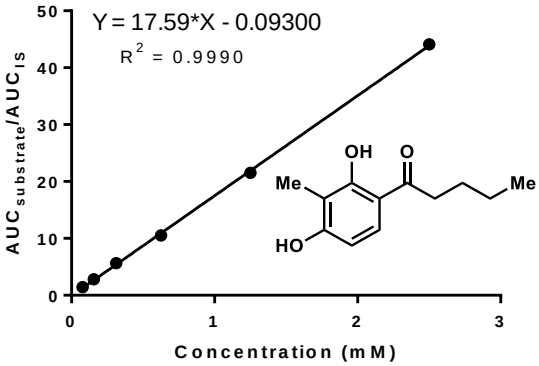
Y = 17.59*X - 0.09300
R2 = 0.9990
AUCsubstrate/AUCIS
Concentration (mM)
OH
O
Me
Me
HO

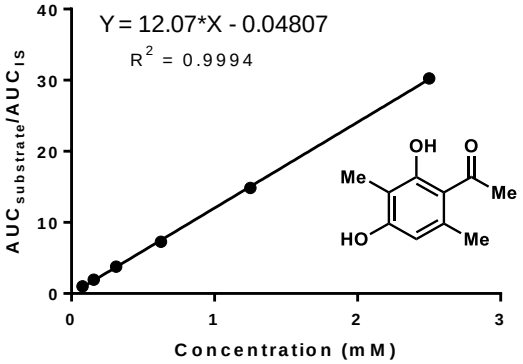
Y = 12.07*X - 0.04807
R2 = 0.9994
AUCsubstrate/AUCIS
Concentration (mM)
OH
O
Me
Me
HO
Me

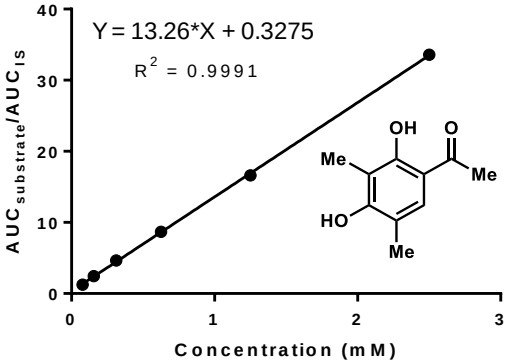
Y = 13.26*X + 0.3275
R2 = 0.9991
AUCsubstrate/AUCIS
Concentration (mM)
OH
O
Me
Me
HO
Me

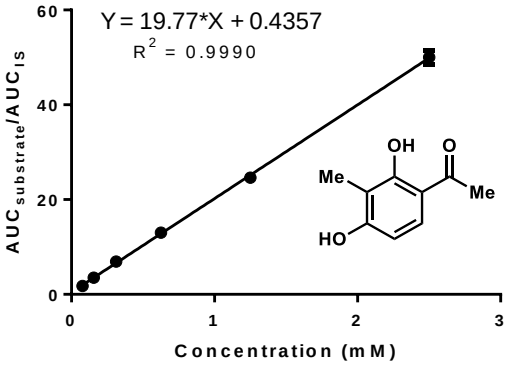
Y = 19.77*X + 0.4357
R2 = 0.9990
AUCsubstrate/AUCIS
Concentration (mM)
OH
O
Me
Me
HO

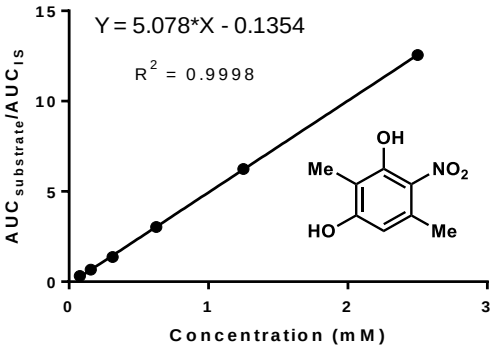
Y = 5.078*X - 0.1354
R2 = 0.9998
AUCsubstrate/AUCIS
Concentration (mM)
OH
Me
NO2
HO
Me

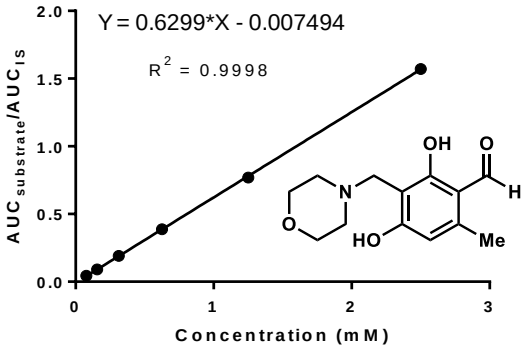
Y = 0.6299*X - 0.007494
R2 = 0.9998
AUCsubstrate/AUCIS
Concentration (mM)
OH
O
N
O
H
HO
Me

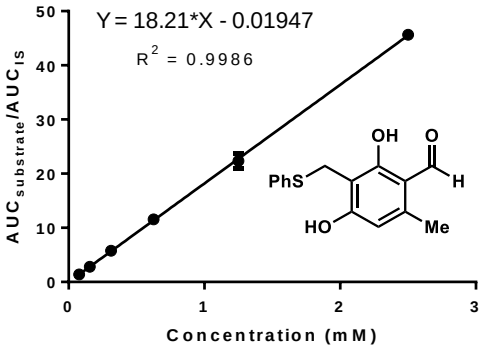
Y = 18.21*X - 0.01947
R2 = 0.9986
AUCsubstrate/AUCIS
Concentration (mM)
OH
O
PhS
H
HO
Me

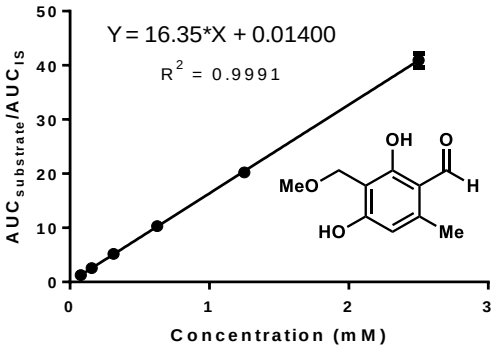
Y = 16.35*X + 0.01400
R2 = 0.9991
AUCsubstrate/AUCIS
Concentration (mM)
OH
O
MeO
H
HO
Me

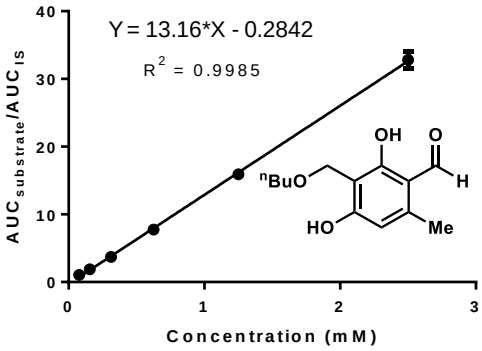
Y = 13.16*X - 0.2842
R2 = 0.9985
AUCsubstrate/AUCIS
Concentration (mM)
OH
O
nBuO
H
HO
Me

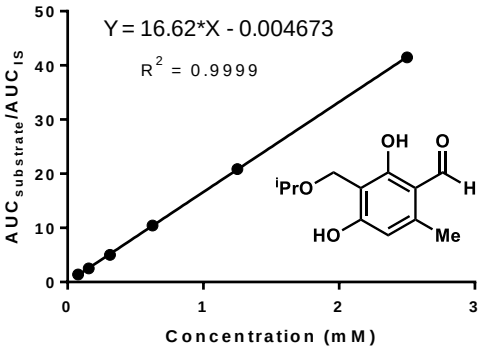
Y = 16.62*X - 0.004673
R2 = 0.9999
AUCsubstrate/AUCIS
Concentration (mM)
OH
O
iPrO
H
HO
Me

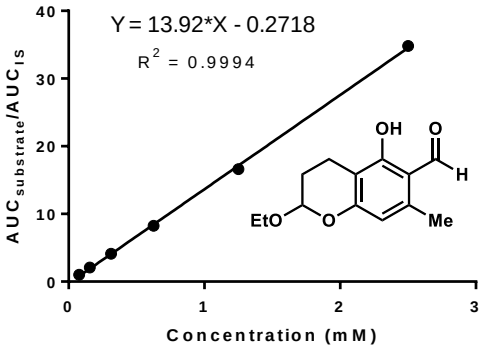
Y = 13.92*X - 0.2718
R2 = 0.9994
AUCsubstrate/AUCIS
Concentration (mM)
OH
O
H
EtO
O
Me

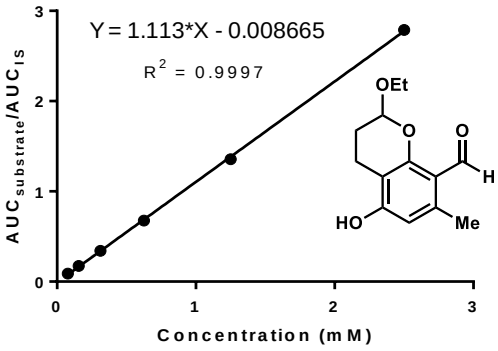
Y = 1.113*X - 0.008665
R2 = 0.9997
AUCsubstrate/AUCIS
Concentration (mM)
OEt
O
O
H
HO
Me

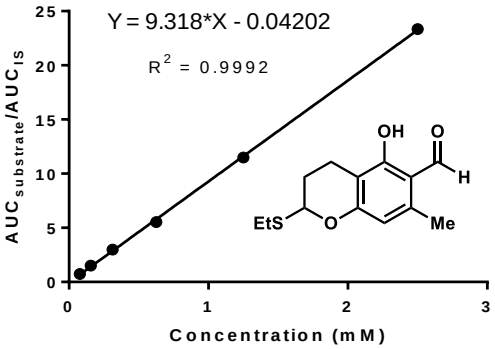
Y = 9.318*X - 0.04202
R2 = 0.9992
AUCsubstrate/AUCIS
Concentration (mM)
OH
O
H
EtS
O
Me

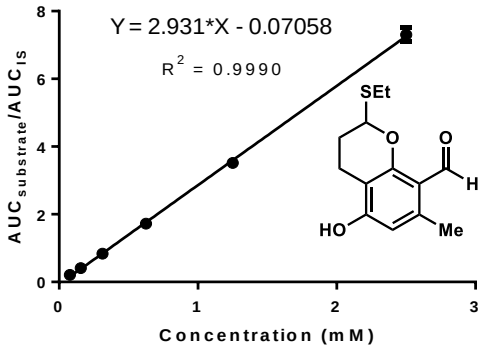
Y = 2.931*X - 0.07058
R2 = 0.9990
AUCsubstrate/AUCIS
Concentration (mM)
SEt
O
O
H
HO
Me

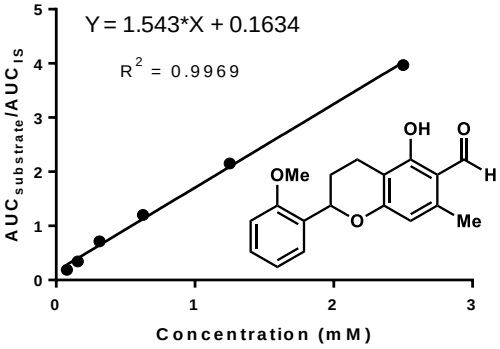
Y = 1.543*X + 0.1634
R2 = 0.9969
AUCsubstrate/AUCIS
Concentration (mM)
OH
O
H
OMe
O
Me

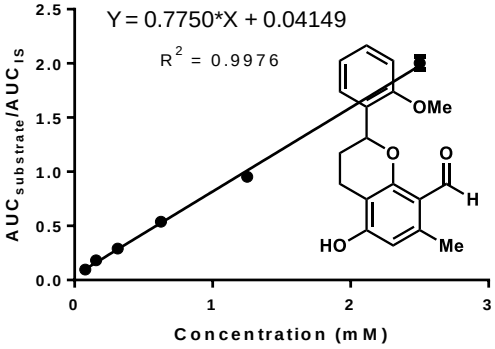
Y = 0.7750*X + 0.04149
R2 = 0.9976
AUCsubstrate/AUCIS
Concentration (mM)
OMe
O
O
H
HO
Me

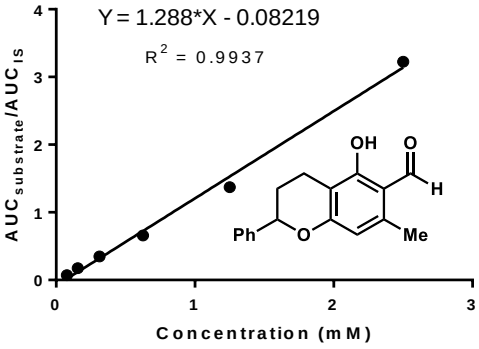
Y = 1.288*X - 0.08219
R2 = 0.9937
AUCsubstrate/AUCIS
Concentration (mM)
OH
O
H
Ph
O
Me

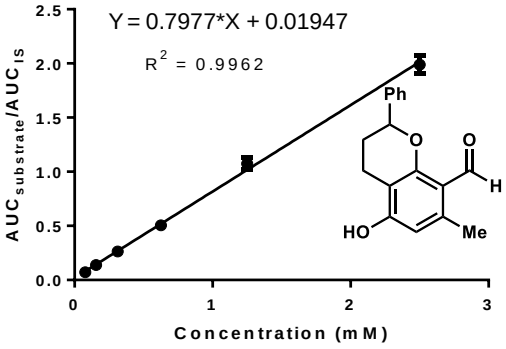
Y = 0.7977*X + 0.01947
R2 = 0.9962
AUCsubstrate/AUCIS
Concentration (mM)
Ph
O
O
H
HO
Me

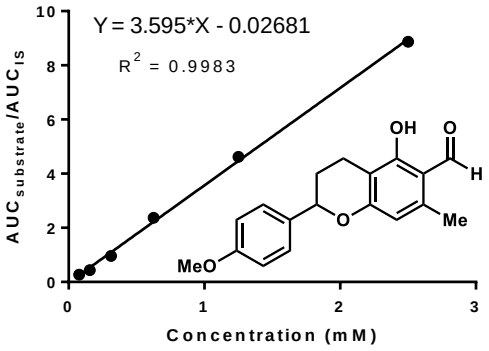
Y = 3.595*X - 0.02681
R2 = 0.9983
AUCsubstrate/AUCIS
Concentration (mM)
OH
O
H
Me
MeO

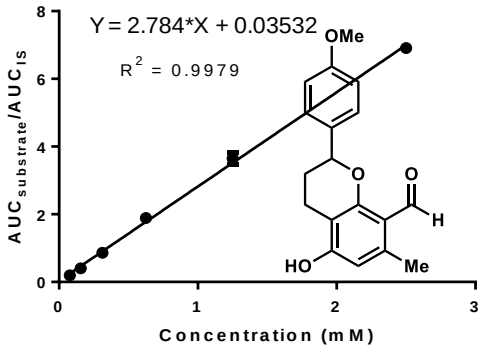
Y = 2.784*X + 0.03532
R2 = 0.9979
AUCsubstrate/AUCIS
Concentration (mM)
OMe
O
H
HO
Me

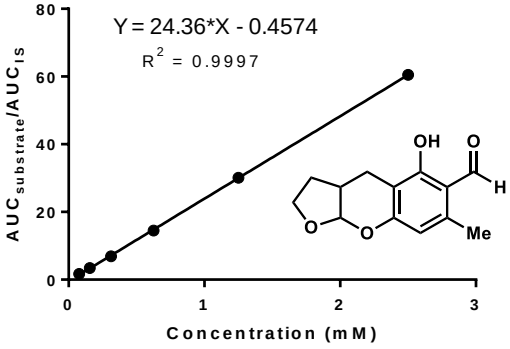
Y = 24.36*X - 0.4574
R2 = 0.9997
AUCsubstrate/AUCIS
Concentration (mM)
OH
O
H
Me

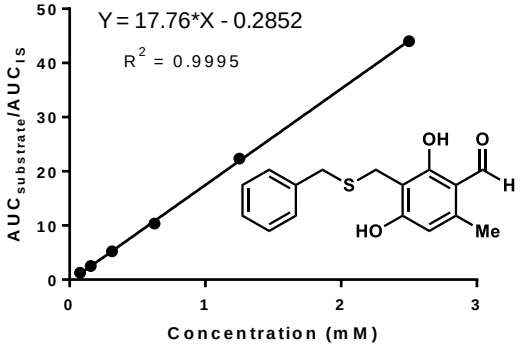
Y = 17.76*X - 0.2852
R2 = 0.9995
AUCsubstrate/AUCIS
Concentration (mM)
OH
O
H
S
HO
Me

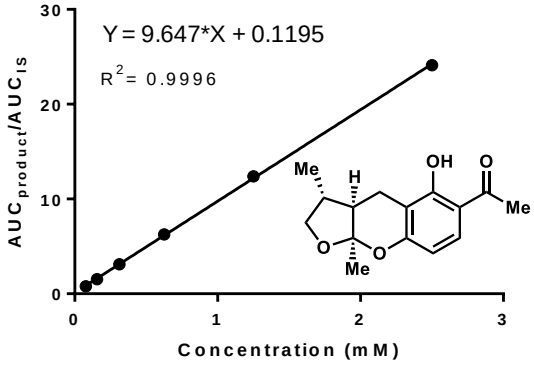
Y = 9.647*X + 0.1195
R2 = 0.9996
AUCproduct/AUCIS
Concentration (mM)
Me
H
OH
O
Me
Me

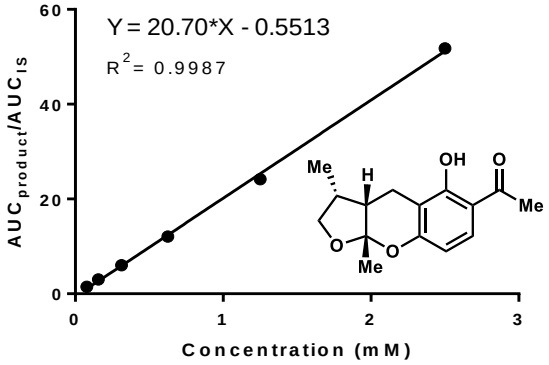
Y = 20.70*X - 0.5513
R2 = 0.9987
AUCproduct/AUCIS
Concentration (mM)
Me
H
OH
O
Me
Me

## Part VII. UPLC traces of CitB-catalyzed biocatalytic reactions

**Figure 2.S21. Benzylic hydroxylation of 2.26 by CitB.**
PDA traces of enzymatic reaction and control reaction.

### With CitB

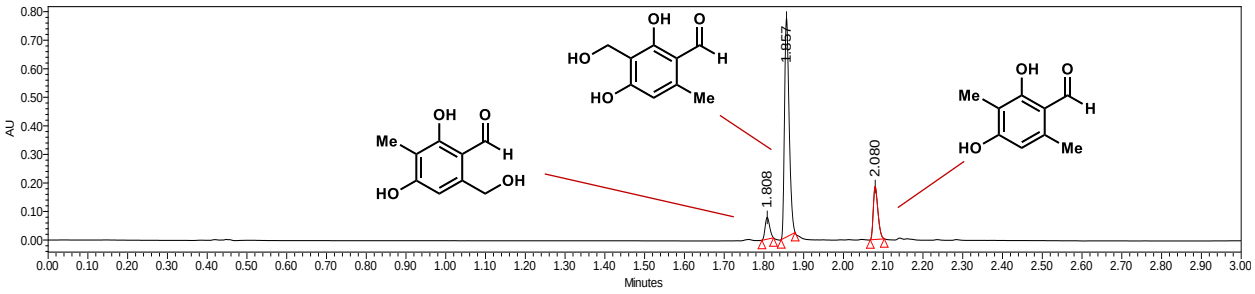


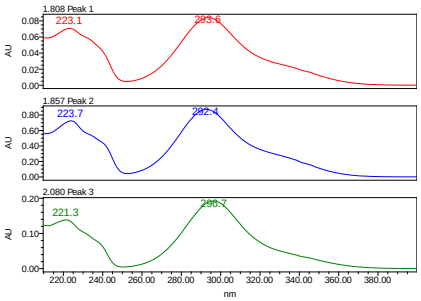


| | Retention Time | Area | % Area | Height |
|---|---|---|---|---|
| 1 | 1.808 | 60277 | 7.28 | 76765 |
| 2 | 1.857 | 617301 | 74.60 | 767275 |
| 3 | 2.080 | 149848 | 18.11 | 185817 |

### No enzyme control

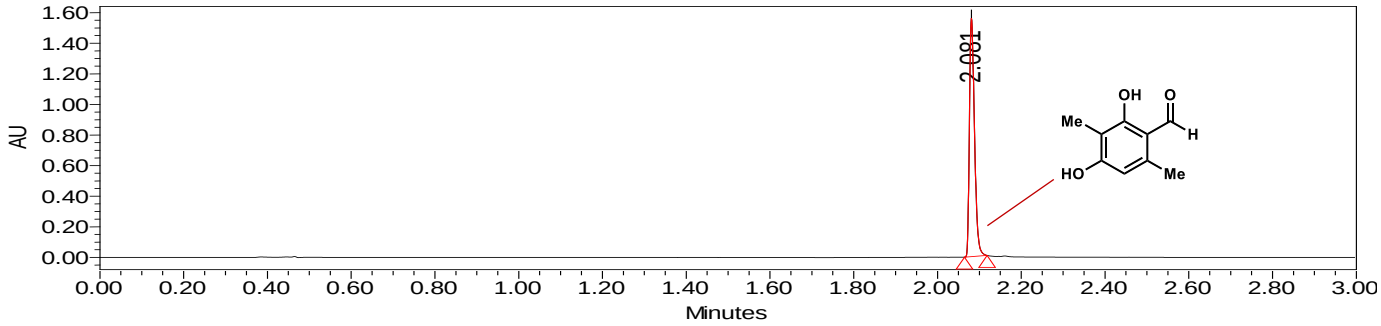


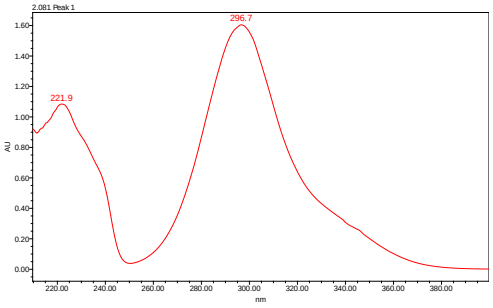


| | Retention Time | Area | % Area | Height |
|---|---|---|---|---|
| 1 | 2.081 | 1311812 | 100.00 | 1557555 |

**Figure 2.S22. Benzylic hydroxylation of 2.38 by CitB.**
PDA traces of enzymatic reaction and control reaction.

## With CitB

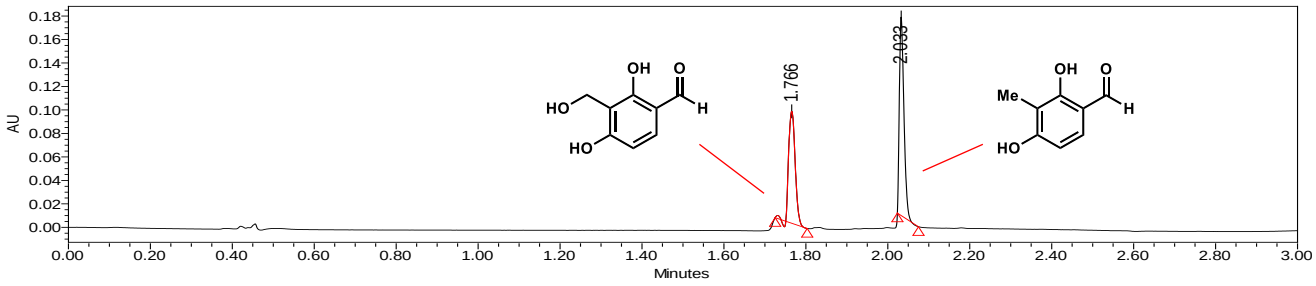


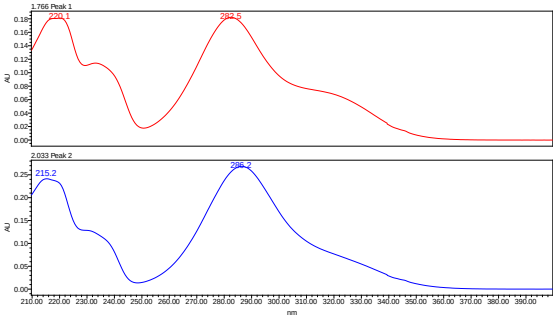


| | Retention Time | Area | % Area | Height |
|---|---|---|---|---|
| 1 | 1.766 | 106501 | 41.09 | 96087 |
| 2 | 2.033 | 152671 | 58.91 | 179576 |

## No Enzyme Control

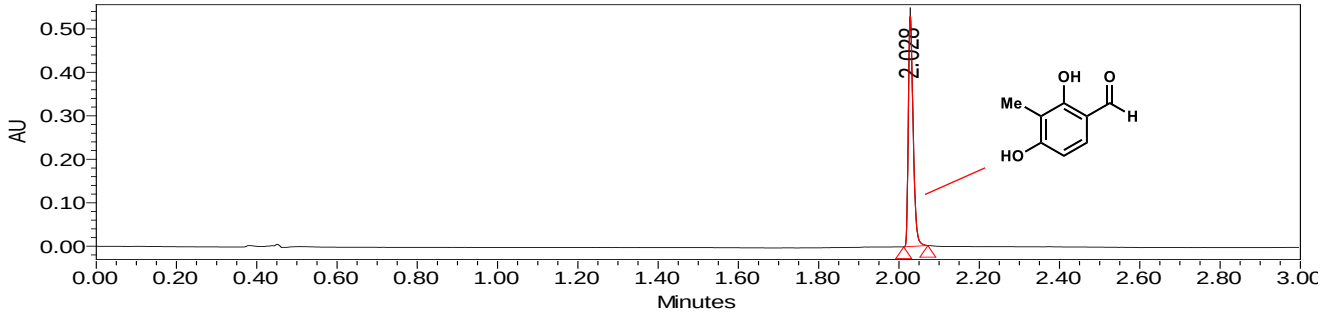


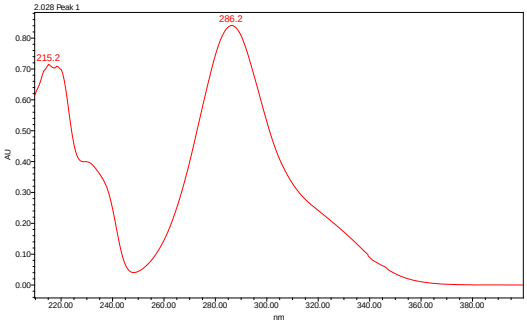


| | Retention Time | Area | % Area | Height |
|---|---|---|---|---|
| 1 | 2.028 | 440126 | 100.00 | 529701 |

**Figure 2.S23. Benzylic hydroxylation of 2.39 by CitB.**
PDA traces of enzymatic reaction and control reaction.

## With CitB

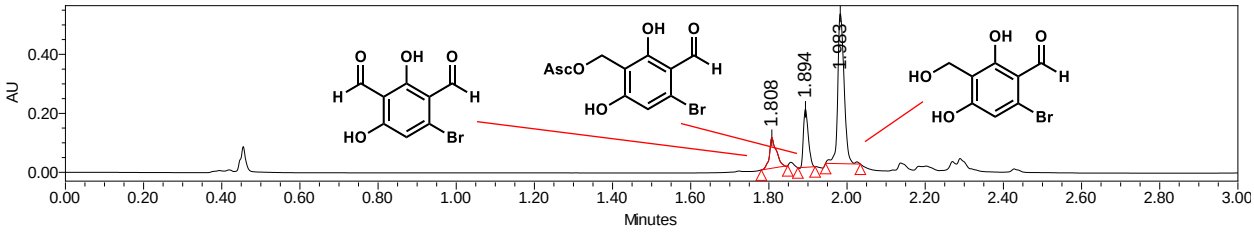


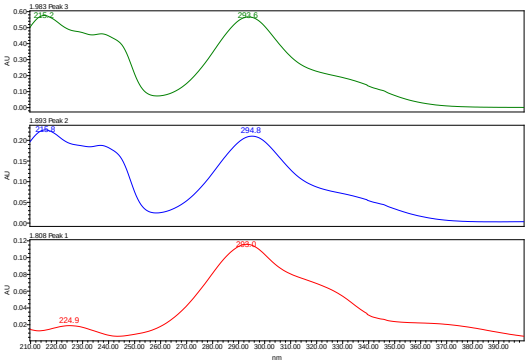


| | Retention Time | Area | % Area | Height |
|---|---|---|---|---|
| 1 | 1.808 | 128097 | 14.58 | 103791 |
| 2 | 1.894 | 171465 | 19.52 | 197059 |
| 3 | 1.983 | 579028 | 65.90 | 508932 |

## No Enzyme Control

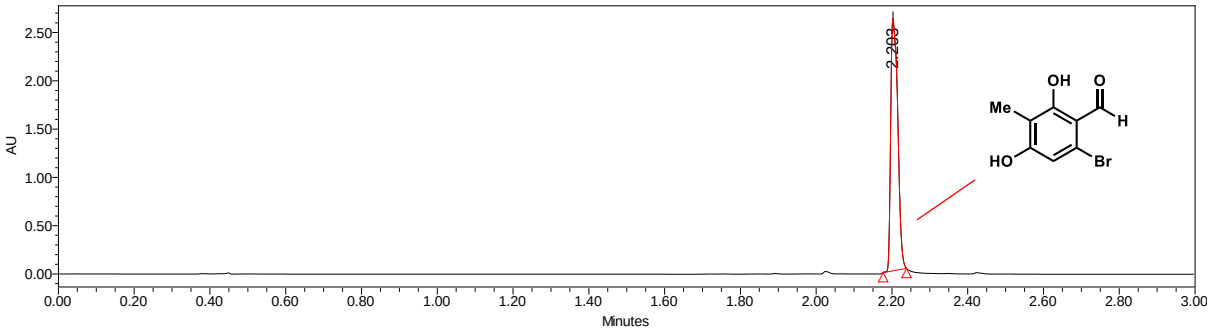


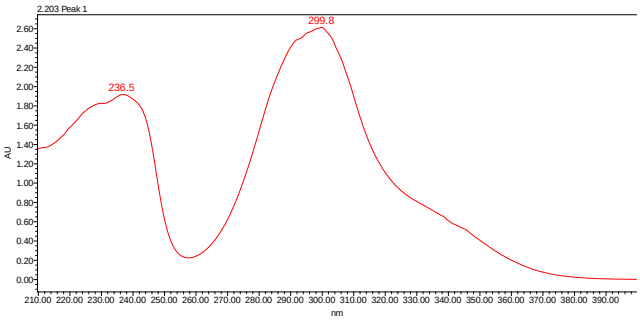


| | Retention Time | Area | % Area |
|---|---|---|---|
| 1 | 2.203 | 3364169 | 100.00 |

**Figure 2.S24. Benzylic hydroxylation of 2.40 by CitB.**
PDA traces of enzymatic reaction and control reaction.

## With CitB

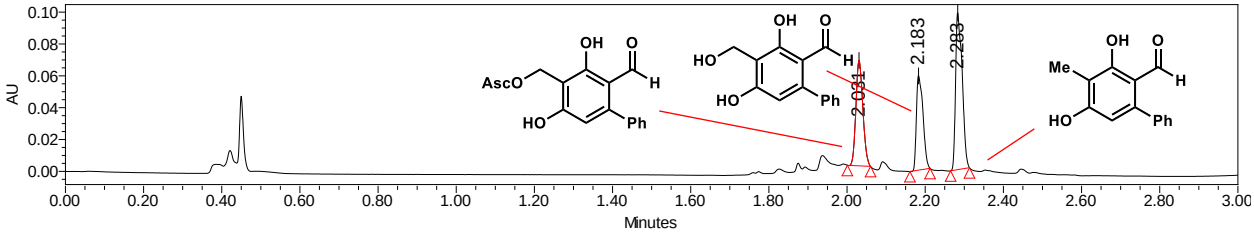


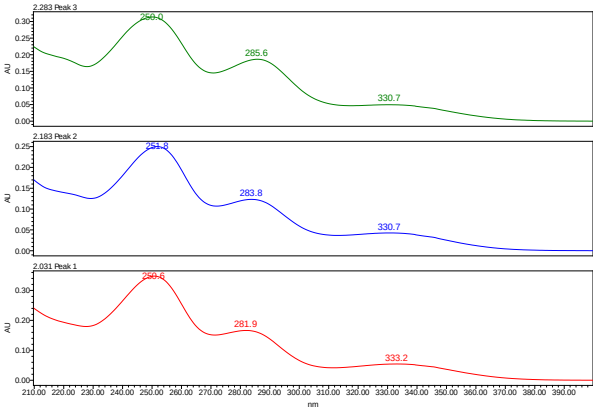


| | Retention Time | Area | % Area | Height |
|---|---|---|---|---|
| 1 | 2.031 | 81644 | 30.74 | 66110 |
| 2 | 2.183 | 69007 | 25.98 | 59416 |
| 3 | 2.283 | 114961 | 43.28 | 98454 |

## No Enzyme Control

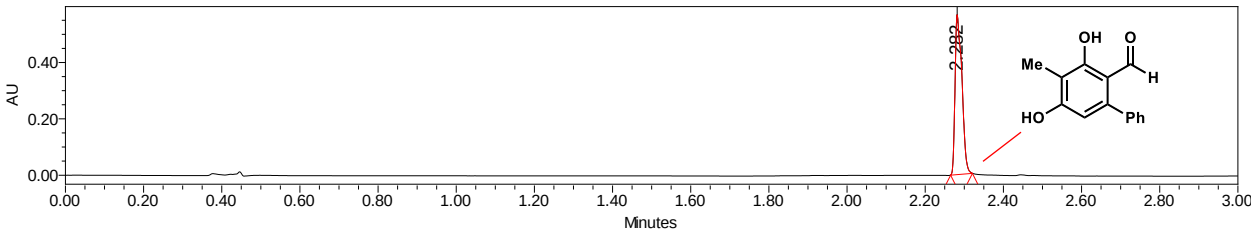


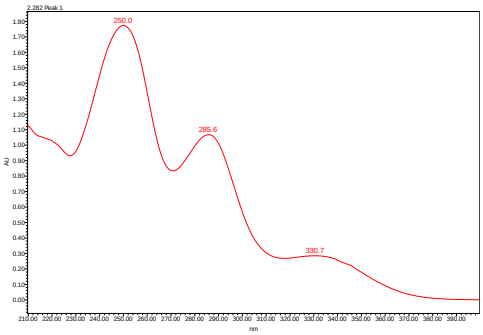


| | Retention Time | Area | % Area | Height |
|---|---|---|---|---|
| 1 | 2.282 | 688212 | 100.00 | 567732 |

**Figure 2.S25. Benzylic hydroxylation of 2.S5 by CitB.**
PDA traces of enzymatic reaction and control reaction.

## With CitB

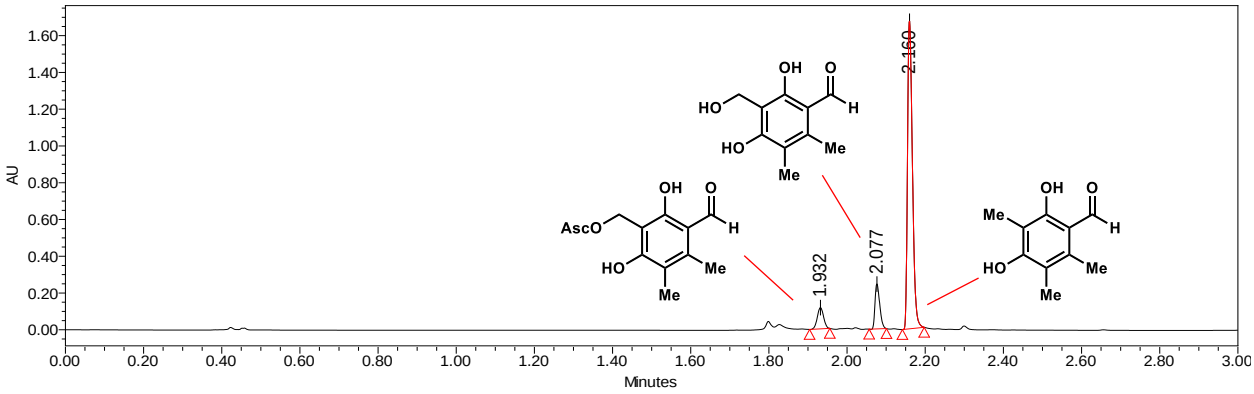


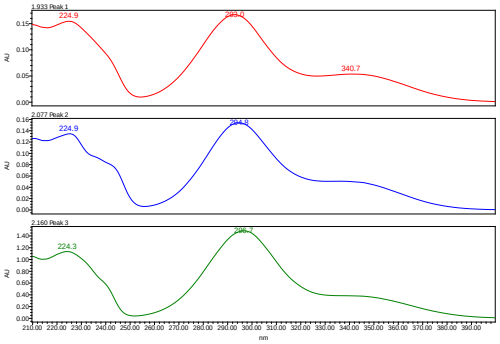

| | Retention Time | Area | % Area | Height |
|---|---|---|---|---|
| 1 | 1.933 | 162421 | 10.45 | 145194 |
| 2 | 2.077 | 117134 | 7.53 | 142594 |
| 3 | 2.160 | 1275214 | 82.02 | 1447841 |

## No Enzyme Control

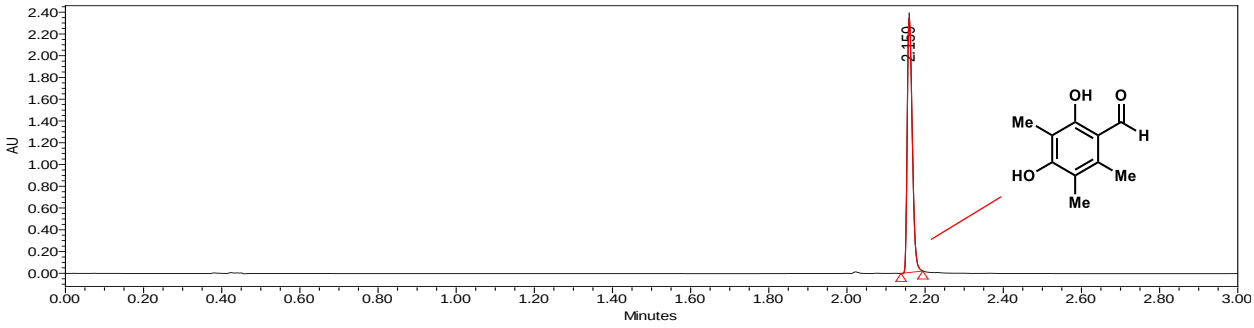


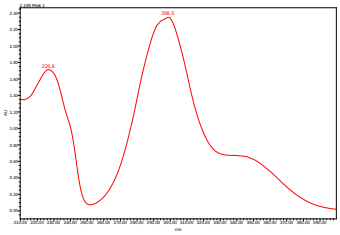

| | Retention Time | Area | % Area | Height |
|---|---|---|---|---|
| 1 | 2.159 | 2103425 | 100.00 | 2334654 |

**Figure 2.S26. Benzylic hydroxylation of 2.46 by CitB.**
PDA traces of enzymatic reaction and control reaction.

## With CitB

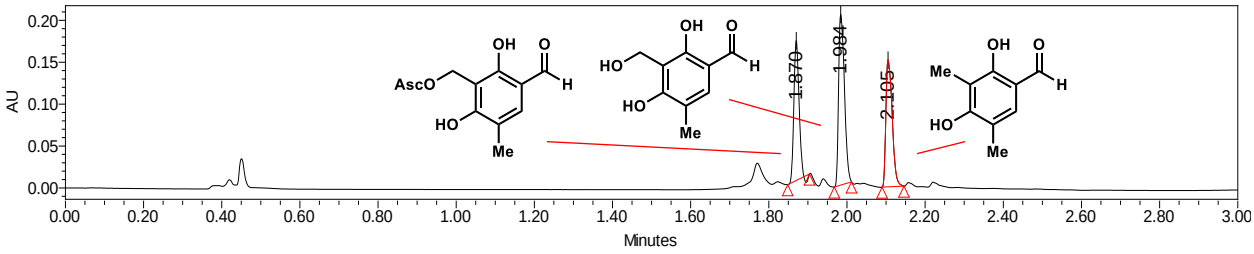


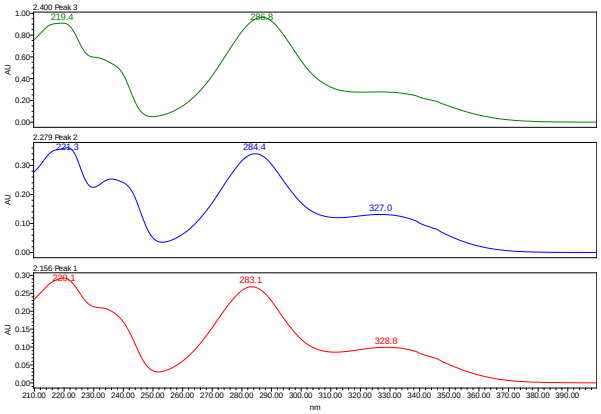


| | Retention Time | Area | % Area | Height |
|---|---|---|---|---|
| 1 | 2.156 | 88057 | 16.11 | 122058 |
| 2 | 2.279 | 104200 | 19.07 | 171834 |
| 3 | 2.400 | 354268 | 64.82 | 564898 |

## No Enzyme Control

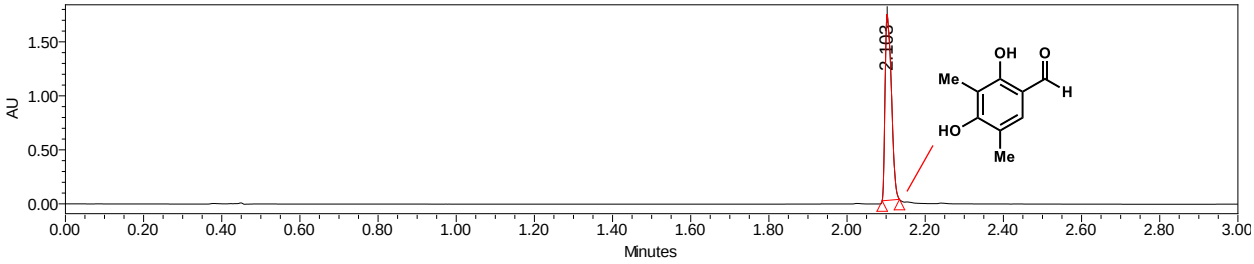


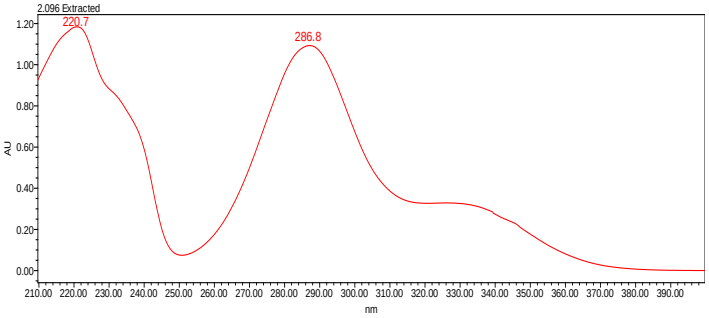


| | Retention Time | Area | % Area |
|---|---|---|---|
| 1 | 2.103 | 1934409 | 100.00 |

**Figure 2.S27. Benzylic hydroxylation of 2.45 by CitB.**
PDA traces of enzymatic reaction and control reaction.

## With CitB

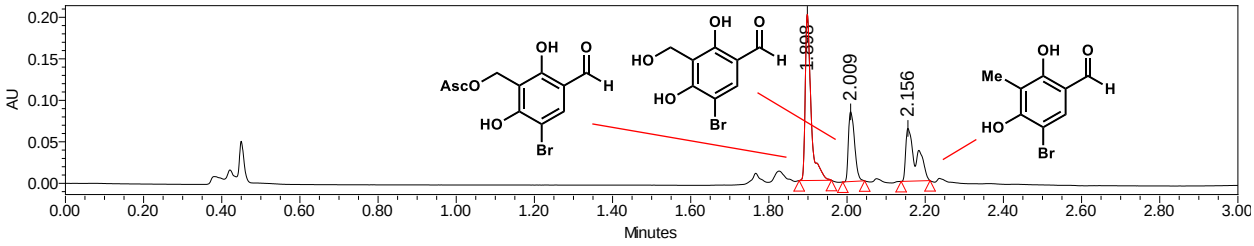


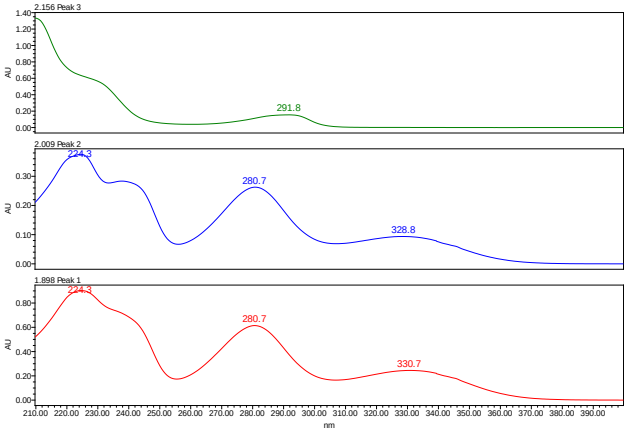


| | Retention Time | Area | % Area | Height |
|---|---|---|---|---|
| 1 | 1.898 | 206718 | 49.42 | 200189 |
| 2 | 2.009 | 92301 | 22.07 | 84095 |
| 3 | 2.156 | 119266 | 28.51 | 63782 |

## No Enzyme Control

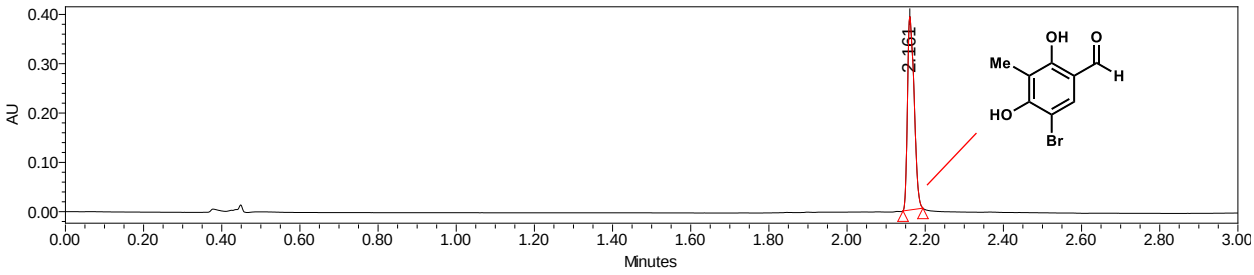


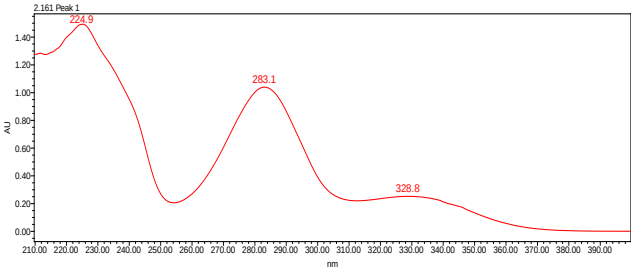


| | Retention Time | Area | % Area |
|---|---|---|---|
| 1 | 2.161 | 462518 | 100.00 |

**Figure 2.S28. Benzylic hydroxylation of 2.S4 by CitB.**
PDA traces of enzymatic reaction and control reaction.

## With CitB

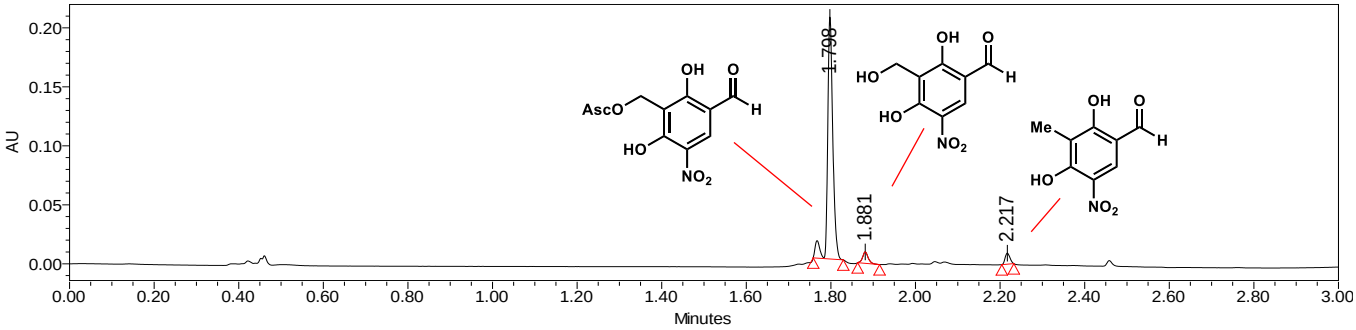


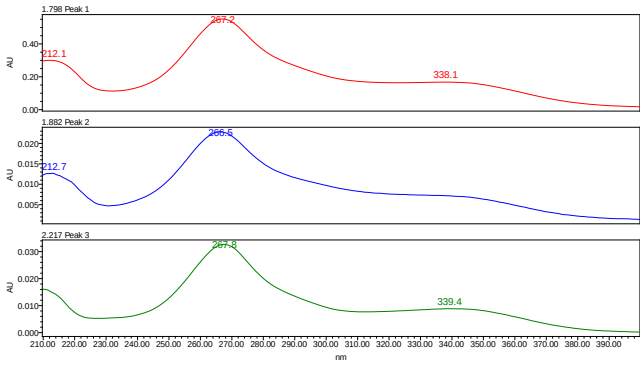


| | Retention Time | Area | % Area | Height |
|---|---|---|---|---|
| 1 | 1.798 | 178212 | 91.61 | 205348 |
| 2 | 1.881 | 8876 | 4.56 | 9736 |
| 3 | 2.217 | 7446 | 3.83 | 9399 |

## No Enzyme Control

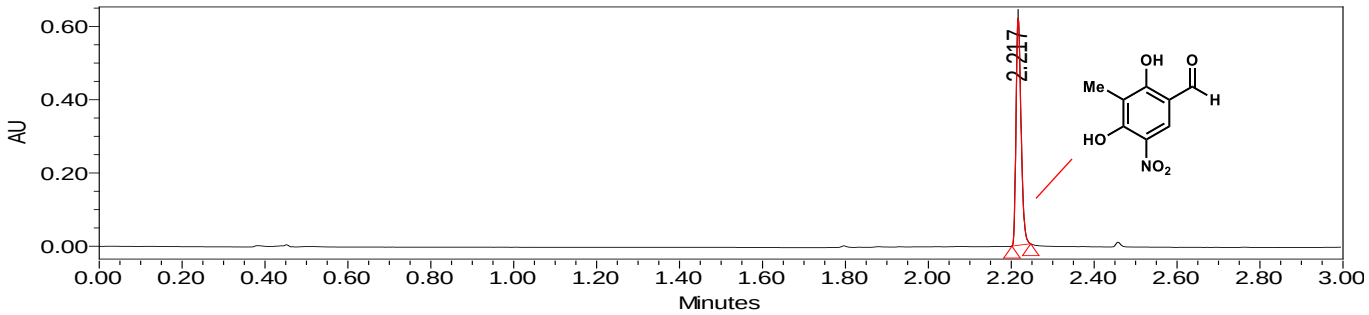


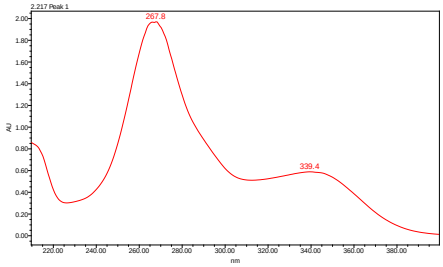


| | Retention Time | Area | % Area | Height |
|---|---|---|---|---|
| 1 | 2.217 | 523699 | 100.00 | 619137 |

**Figure 2.S29. Benzylic hydroxylation of 2.44 by CitB.**
PDA traces of enzymatic reaction and control reaction.

## With CitB

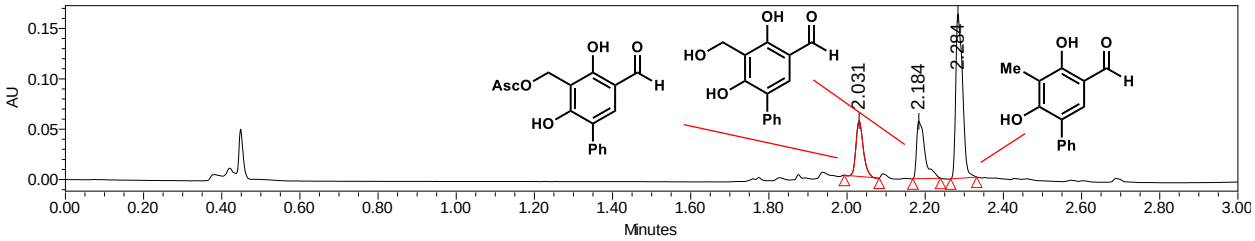


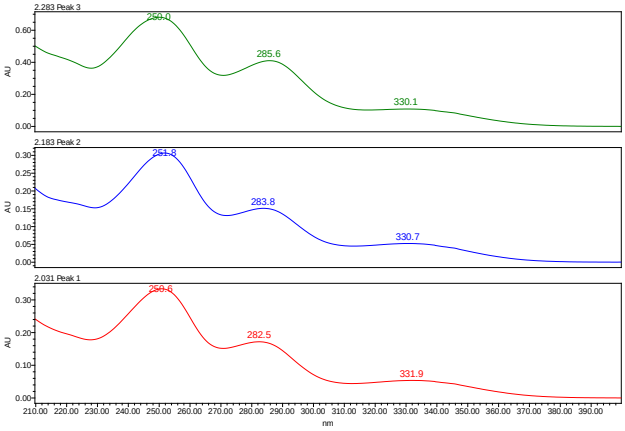


| | Retention Time | Area | % Area | Height |
|---|---|---|---|---|
| 1 | 2.031 | 72174 | 20.42 | 55343 |
| 2 | 2.184 | 84576 | 23.93 | 57187 |
| 3 | 2.284 | 196618 | 55.64 | 163569 |

## No Enzyme Control

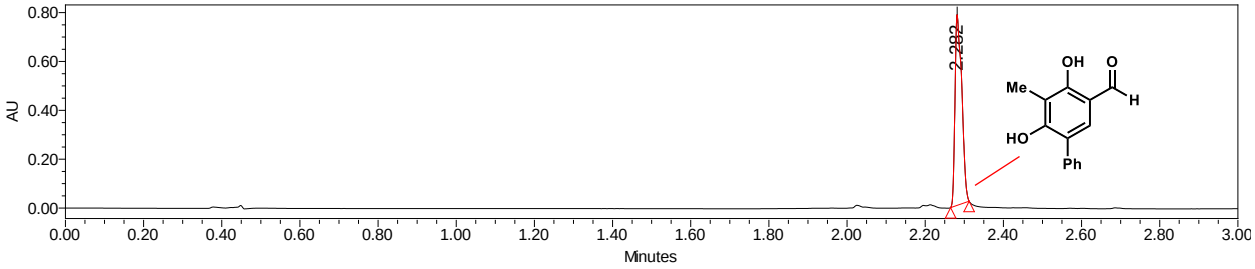


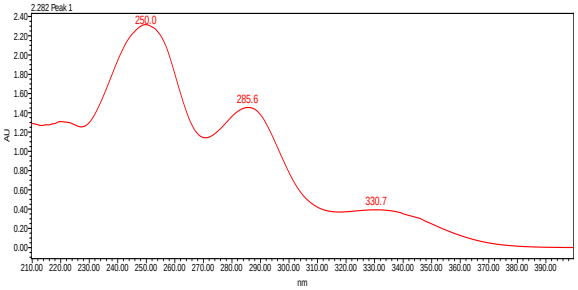


| | Retention Time | Area | % Area |
|---|---|---|---|
| 1 | 2.282 | 935160 | 100.00 |

**Figure 2.S30. Benzylic hydroxylation of 2.50 by CitB.**
PDA traces of enzymatic reaction and control reaction.

## With CitB

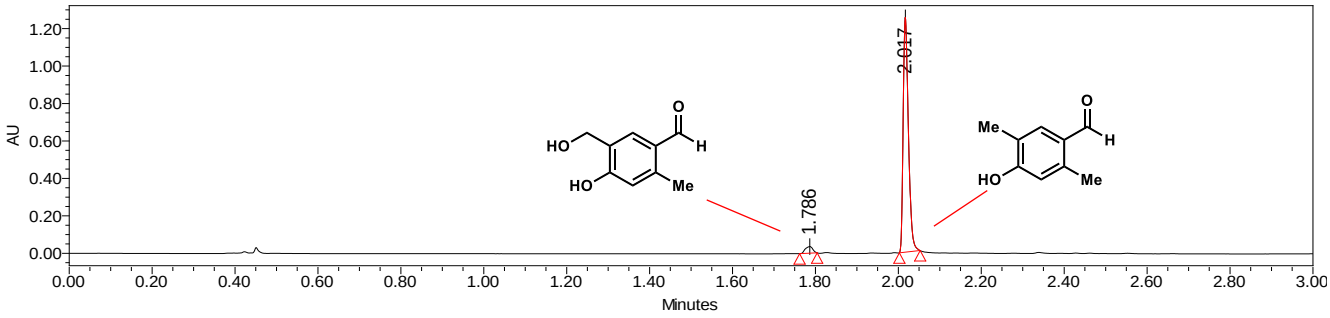


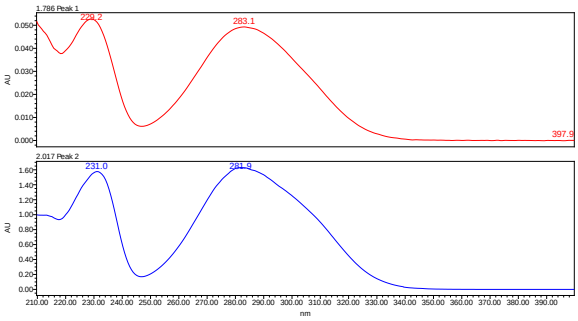


| | Retention Time | Area | % Area | Height |
|---|---|---|---|---|
| 1 | 1.786 | 48006 | 4.14 | 37151 |
| 2 | 2.017 | 1111944 | 95.86 | 1254418 |

## No Enzyme Control

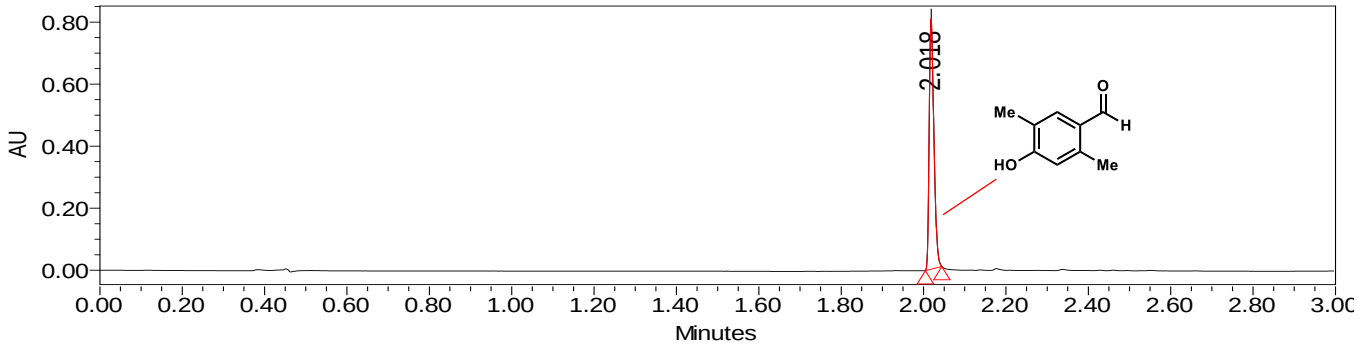


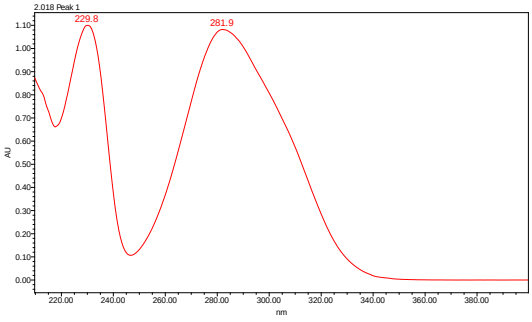


| | Retention Time | Area | % Area | Height |
|---|---|---|---|---|
| 1 | 2.018 | 641158 | 100.00 | 807200 |

**Figure 2.S31. Benzylic hydroxylation of 2.49 by CitB.**
PDA traces of enzymatic reaction and control reaction.

## With CitB

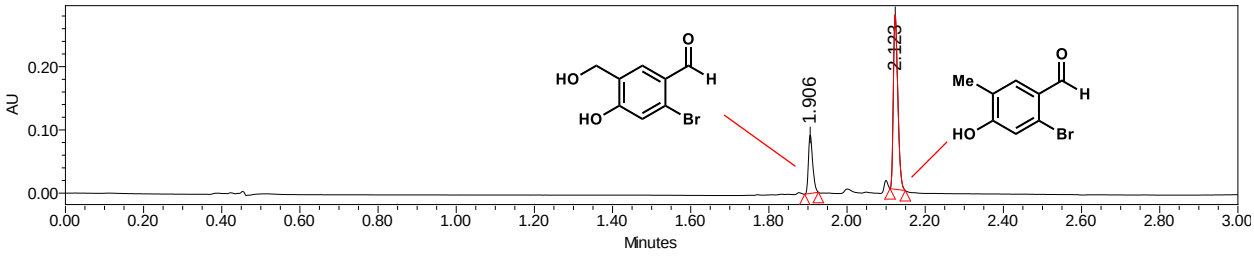


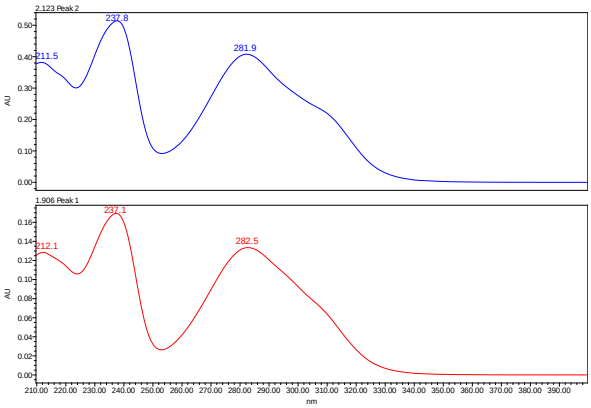


| | Retention Time | Area | % Area | Height |
|---|---|---|---|---|
| 1 | 1.906 | 70147 | 24.27 | 92506 |
| 2 | 2.123 | 218853 | 75.73 | 275931 |

## No Enzyme Control

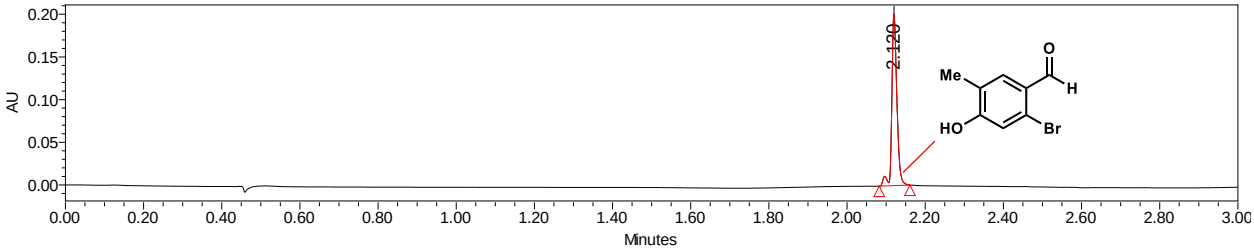


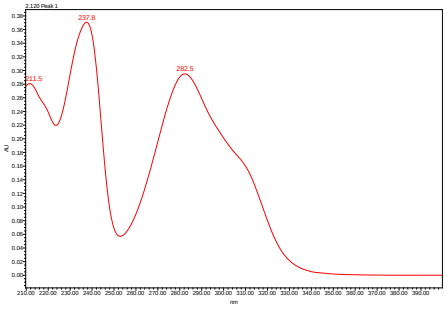


| | Retention Time | Area | % Area | Height |
|---|---|---|---|---|
| 1 | 2.120 | 181187 | 100.00 | 201068 |

**Figure 2.S32. Benzylic hydroxylation of 2.48 by CitB.**
PDA traces of enzymatic reaction and control reaction.

## With CitB

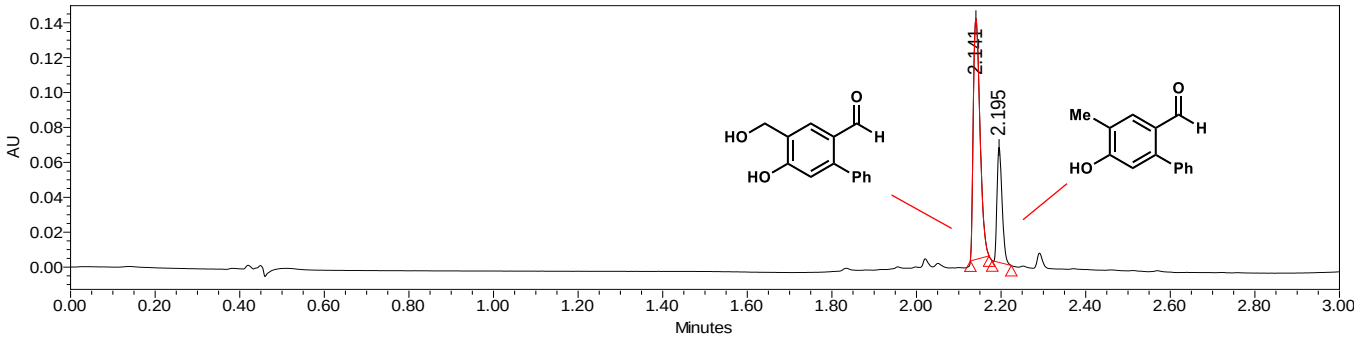


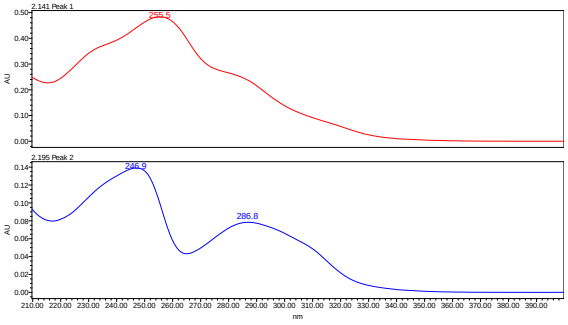


| | Retention Time | Area | % Area | Height |
|---|---|---|---|---|
| 1 | 2.141 | 155984 | 73.88 | 139978 |
| 2 | 2.195 | 55158 | 26.12 | 66133 |

## No enzyme control

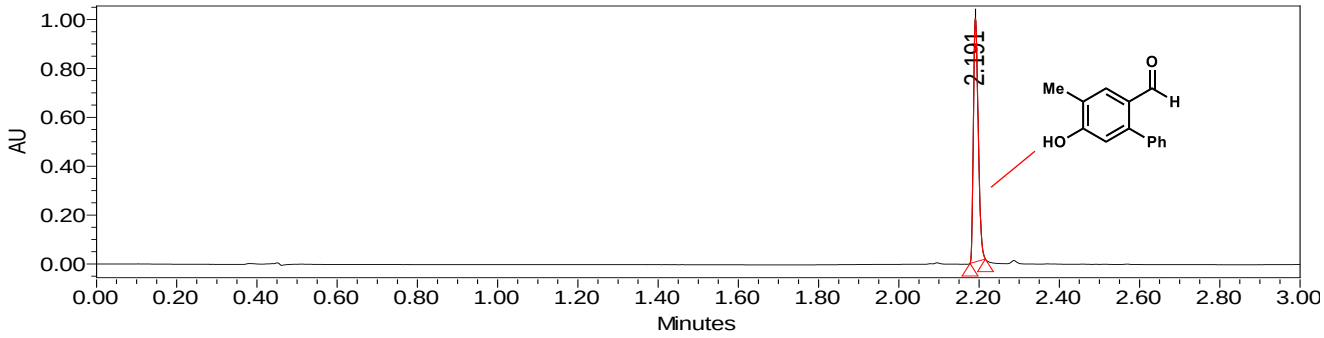


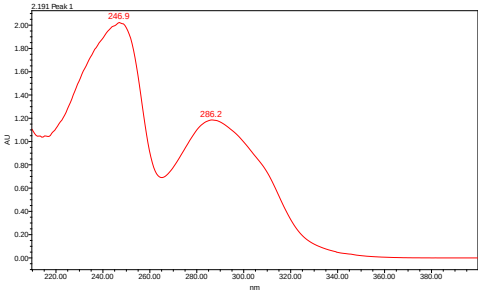


| | Retention Time | Area | % Area | Height |
|---|---|---|---|---|
| 1 | 2.191 | 836389 | 100.00 | 995849 |

**Figure 2.S33. Benzylic hydroxylation of 2.47 by CitB.**
PDA traces of enzymatic reaction and control reaction.

## With CitB

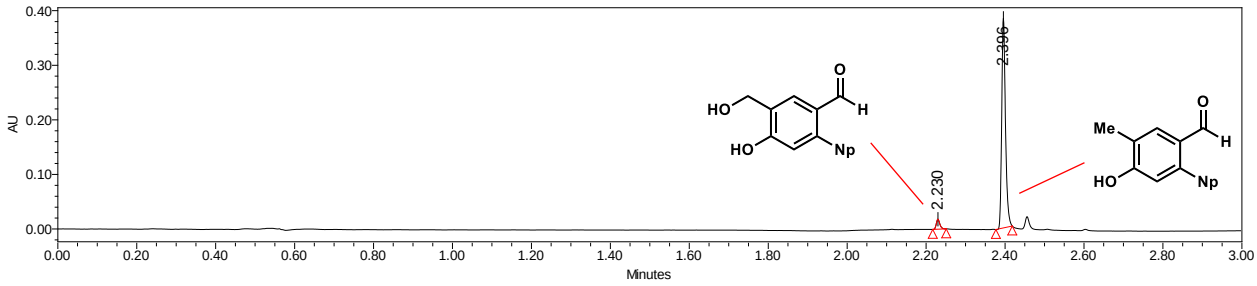


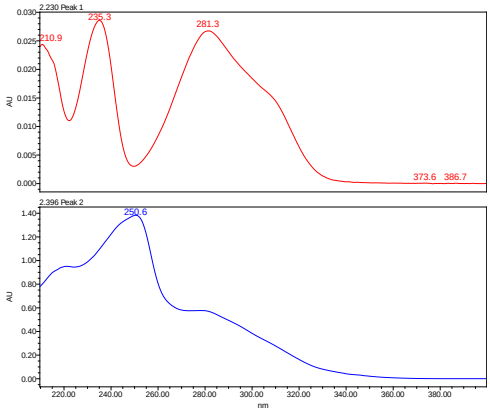


| | Retention Time | Area | % Area | Height |
|---|---|---|---|---|
| 1 | 2.230 | 11489 | 4.33 | 18425 |
| 2 | 2.396 | 253676 | 95.67 | 383695 |

## No Enzyme Control

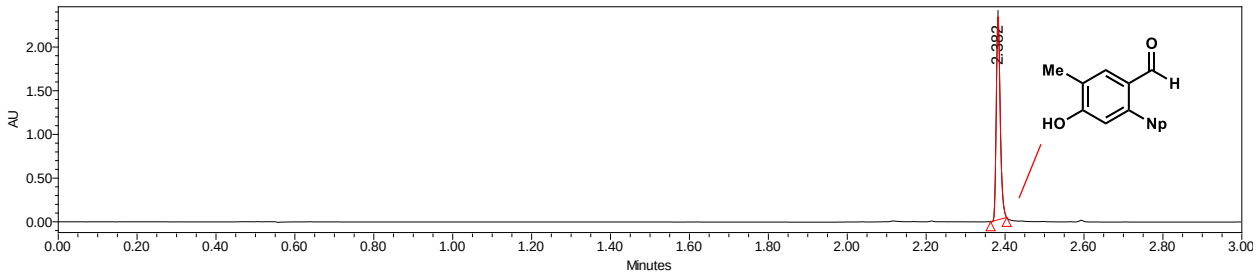


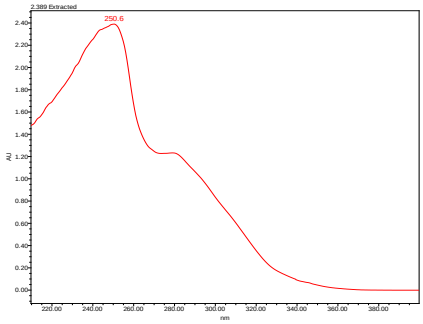


| | Retention Time | Area | % Area | Height |
|---|---|---|---|---|
| 1 | 2.382 | 1630305 | 100.00 | 2323928 |

**Figure 2.S34. Benzylic hydroxylation of 2.S8 by CitB.**
PDA traces of enzymatic reaction and control reaction.

## With CitB

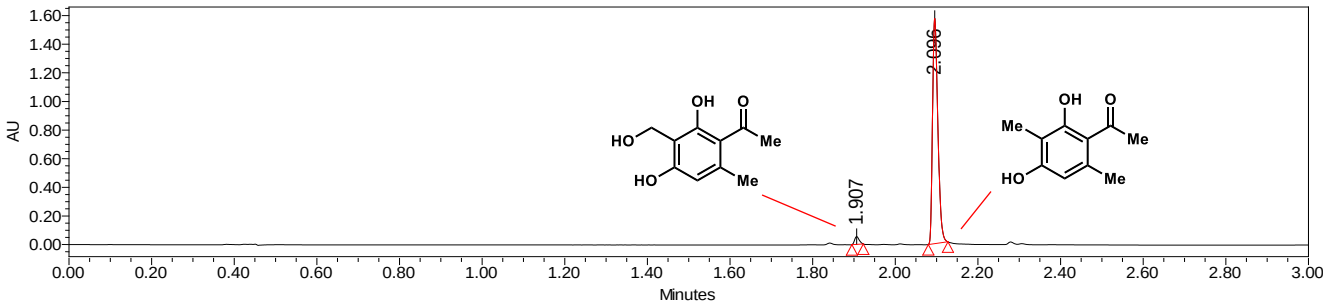


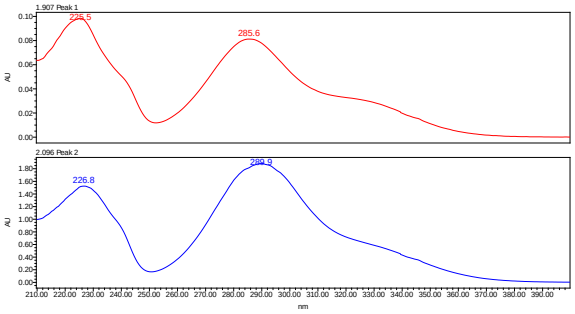


| | Retention Time | Area | % Area | Height |
|---|---|---|---|---|
| 1 | 1.907 | 41893 | 2.89 | 54401 |
| 2 | 2.096 | 1405932 | 97.11 | 1575505 |

## No Enzyme Control

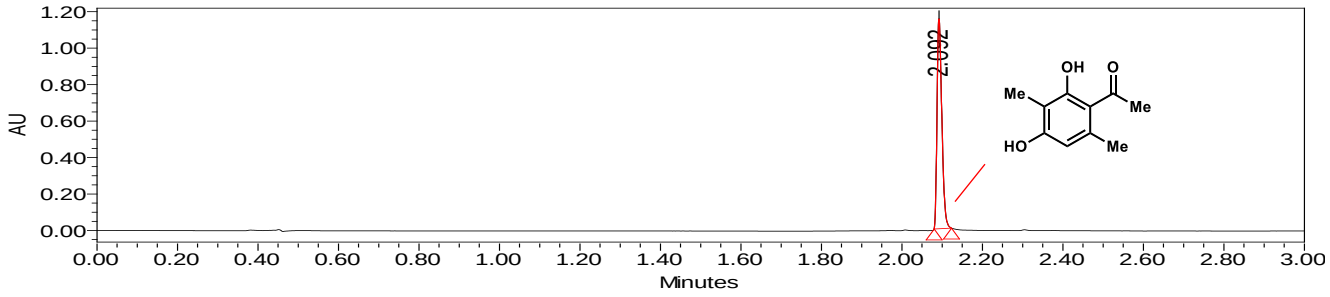


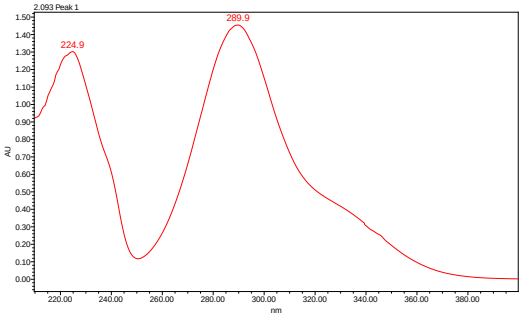


| | Retention Time | Area | % Area | Height |
|---|---|---|---|---|
| 1 | 2.092 | 956958 | 100.00 | 1153000 |
| | | | | |

**Figure 2.S35. Benzylic hydroxylation of 2.42 by CitB.**
PDA traces of enzymatic reaction and control reaction.

## With CitB

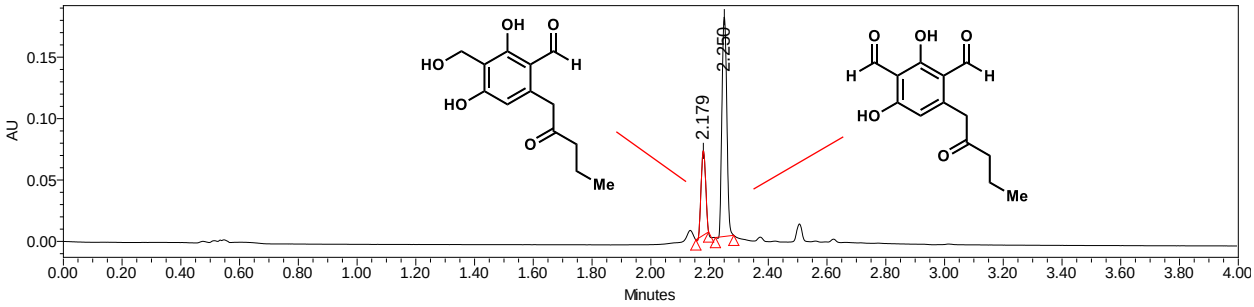


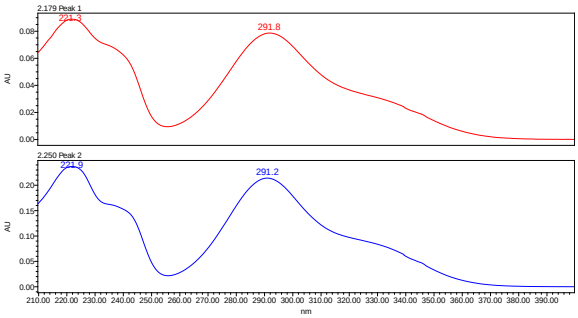


| | Retention Time | Area | % Area | Height |
|---|---|---|---|---|
| 1 | 2.179 | 74913 | 26.66 | 68811 |
| 2 | 2.250 | 206069 | 73.34 | 178596 |

## No Enzyme Control

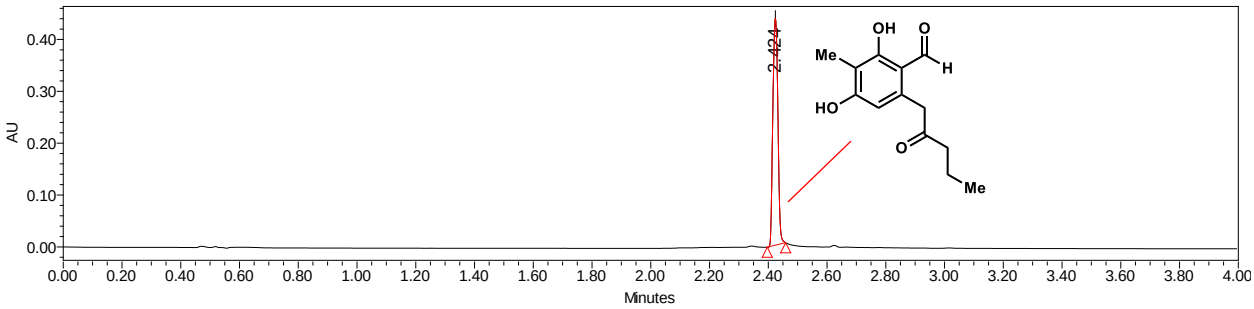


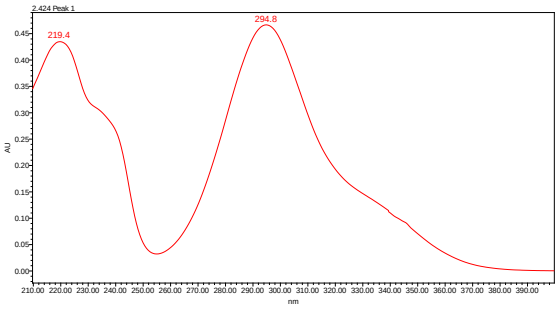


| | Retention Time | Area | % Area | Height |
|---|---|---|---|---|
| 1 | 2.424 | 519715 | 100.00 | 438090 |

**Figure 2.S36. Benzylic hydroxylation of 2.33 by CitB.**
PDA traces of enzymatic reaction and control reaction.

## With CitB

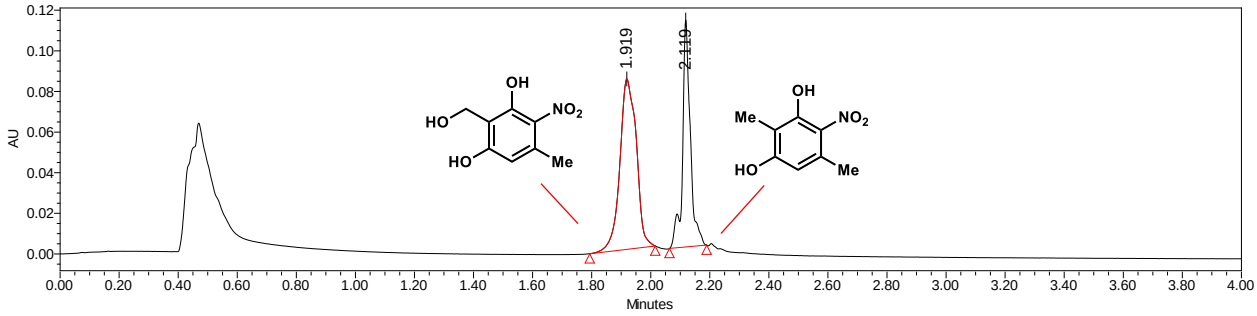


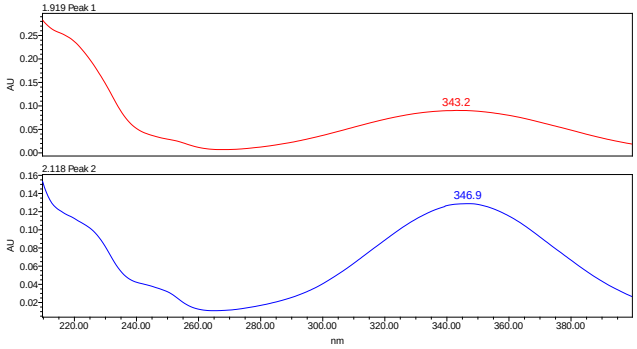


| | Retention Time | Area | % Area | Height |
|---|---|---|---|---|
| 1 | 1.919 | 325393 | 61.26 | 83942 |
| 2 | 2.119 | 205798 | 38.74 | 111809 |

## No Enzyme Control

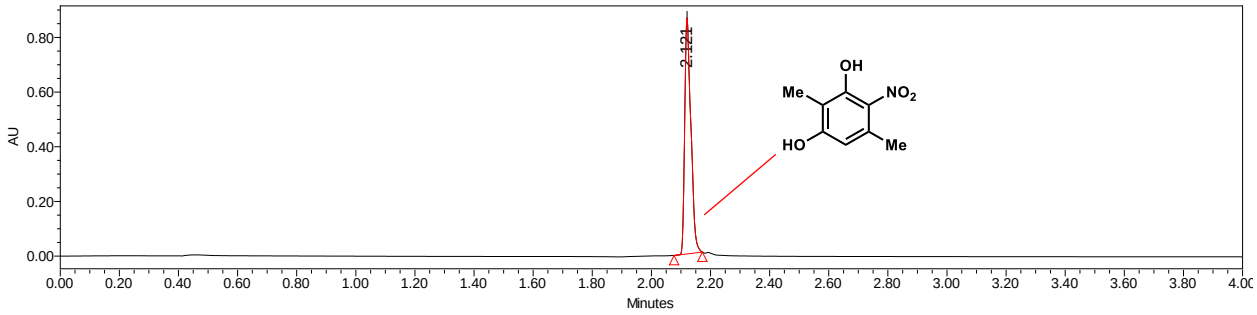


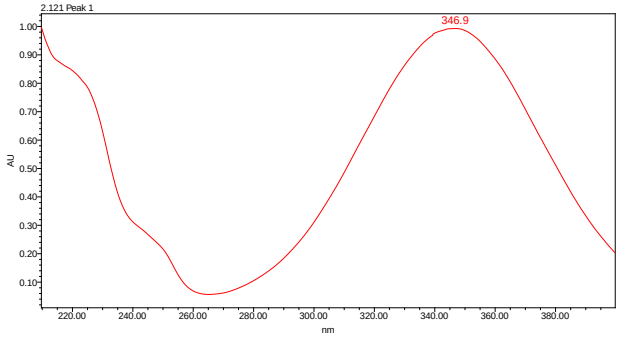


| | Retention Time | Area | % Area | Height |
|---|---|---|---|---|
| 1 | 2.121 | 1250924 | 100.00 | 863894 |

**Figure 2.S37. Benzylic hydroxylation of 2.32 by CitB.**
LC/MS traces of enzymatic reaction and control reaction.

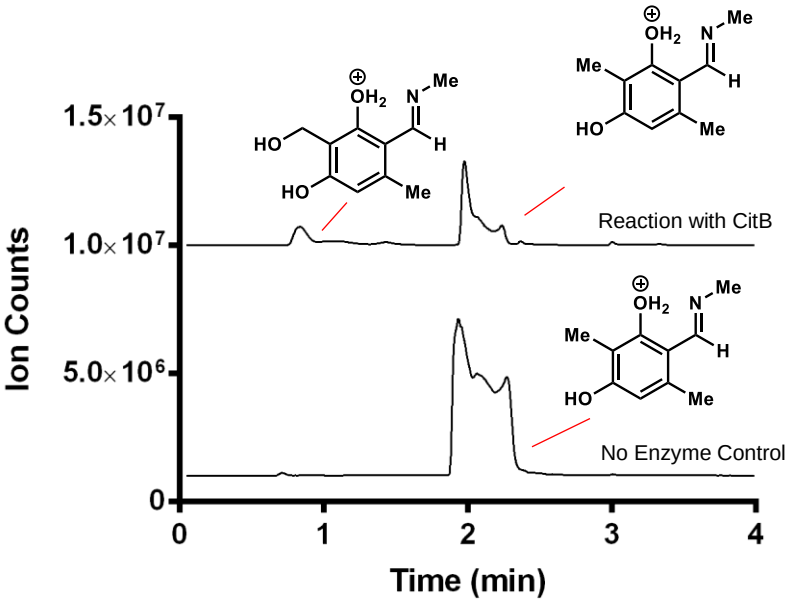

## Part VIII. UPLC traces of ClaD-catalyzed biocatalytic reactions

**Figure 2.S38. Benzylic hydroxylation of 2.26 by ClaD.**
PDA traces of enzymatic reaction and control reaction.

### With ClaD

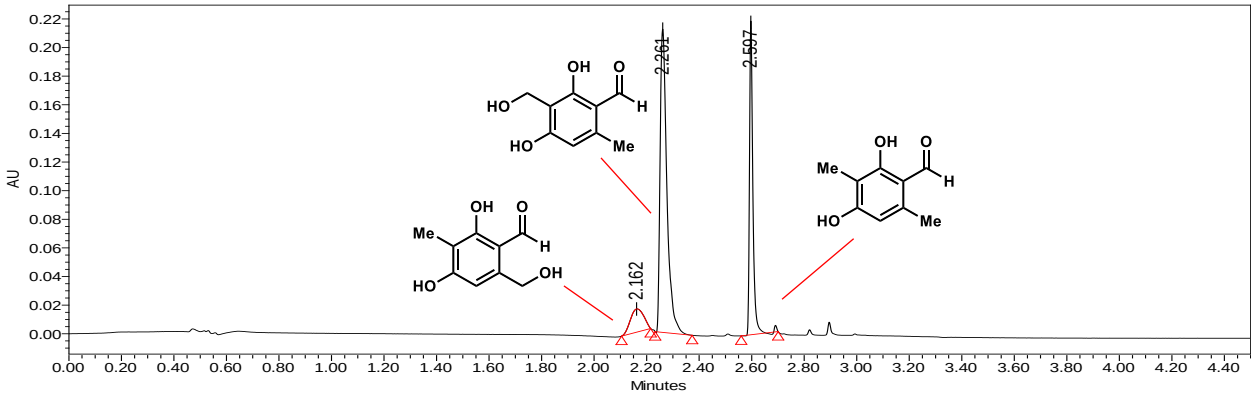


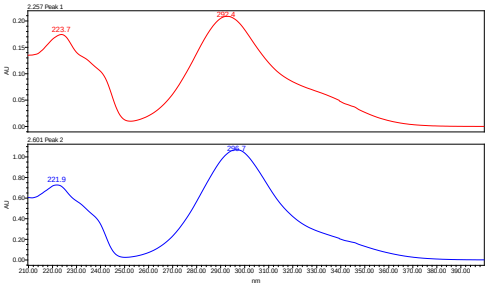


| | Retention Time | Area | % Area | Height |
|---|---|---|---|---|
| 1 | 2.257 | 372059 | 27.82 | 183479 |
| 2 | 2.601 | 965233 | 72.18 | 1038145 |

### No Enzyme Control

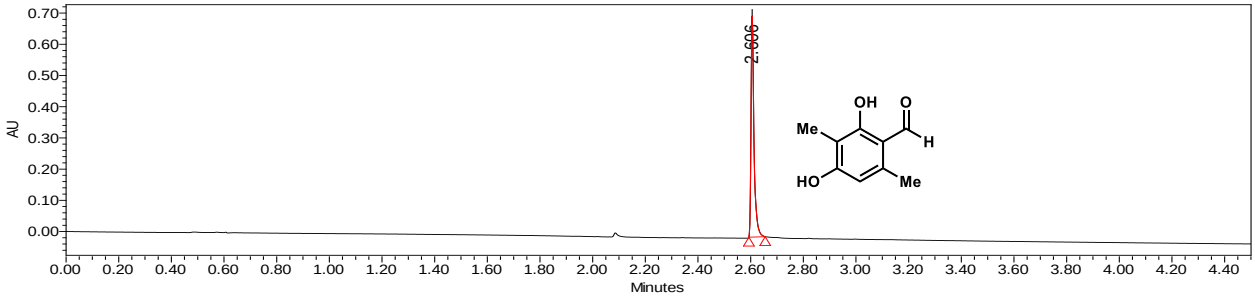


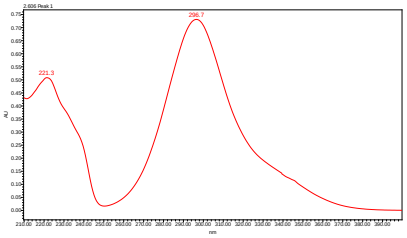


| | Retention Time | Area | % Area | Height |
|---|---|---|---|---|
| 1 | 2.606 | 552559 | 100.00 | 707838 |

**Figure 2.S39. Benzylic hydroxylation of 2.35 by ClaD.**
PDA traces of enzymatic reaction and control reaction.

## With ClaD

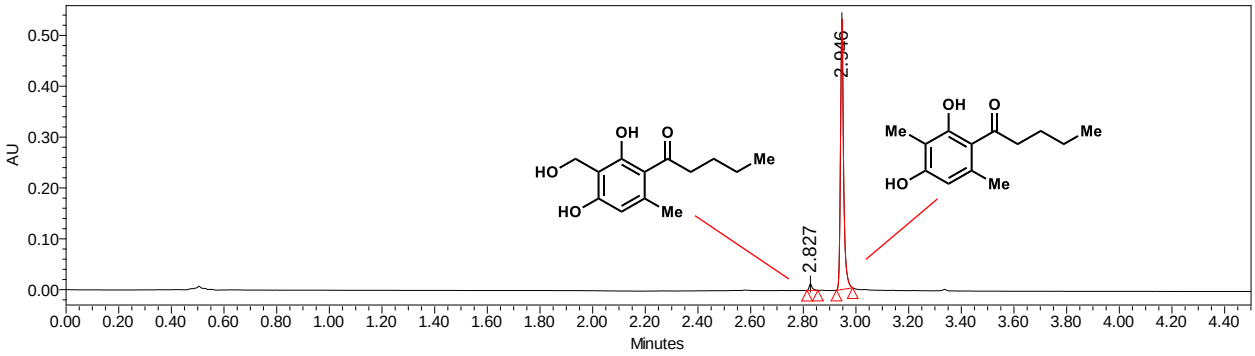


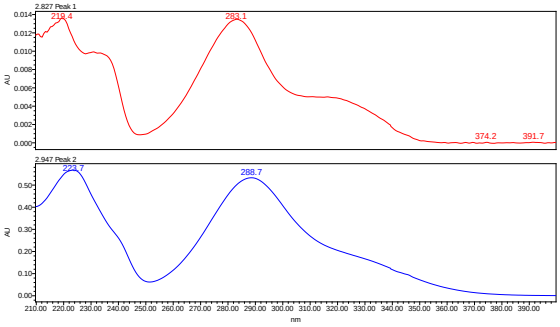


| | Retention Time | Area | % Area | Height |
|---|---|---|---|---|
| 1 | 2.827 | 10070 | 2.26 | 12630 |
| 2 | 2.946 | 435438 | 97.74 | 531349 |

## No Enzyme Control

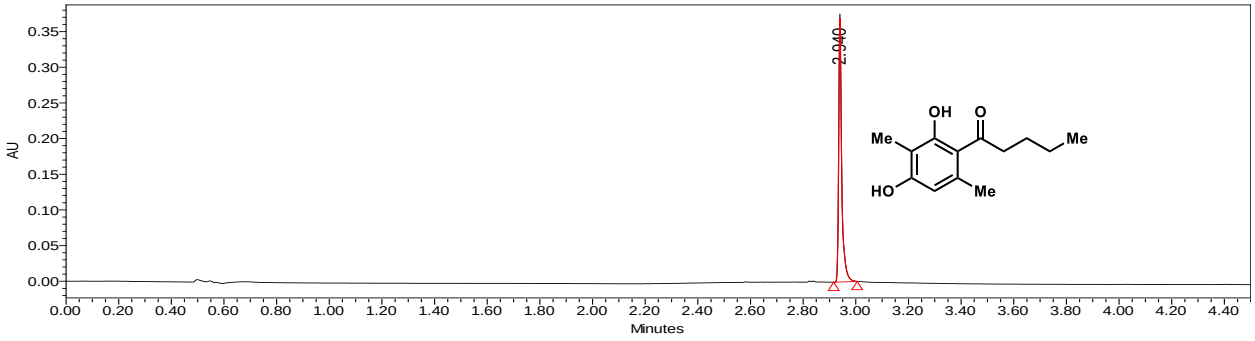


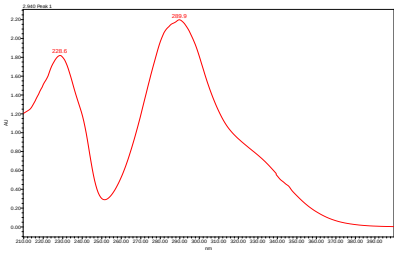


| | Retention Time | Area | % Area | Height |
|---|---|---|---|---|
| 1 | 2.940 | 298836 | 100.00 | 370517 |

**Figure 2.S40. Benzylic hydroxylation of 2.S7 by ClaD.**
PDA traces of enzymatic reaction and control reaction.

## With ClaD

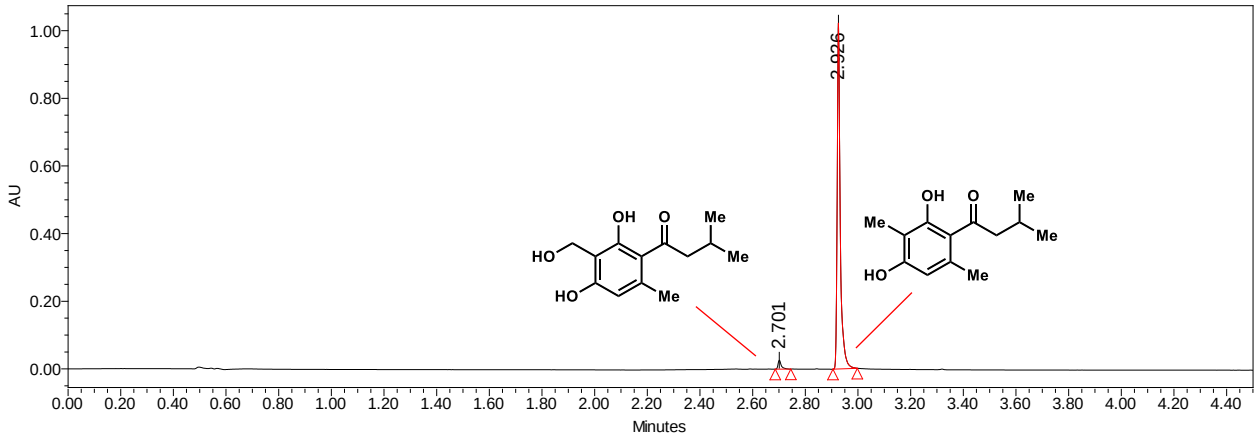


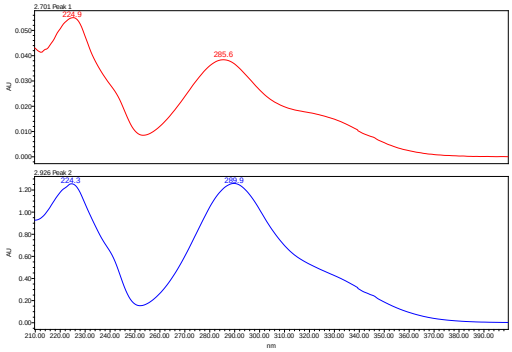


| | Retention Time | Area | % Area | Height |
|---|---|---|---|---|
| 1 | 2.701 | 22569 | 2.65 | 26526 |
| 2 | 2.926 | 828224 | 97.35 | 1022478 |

## No Enzyme Control

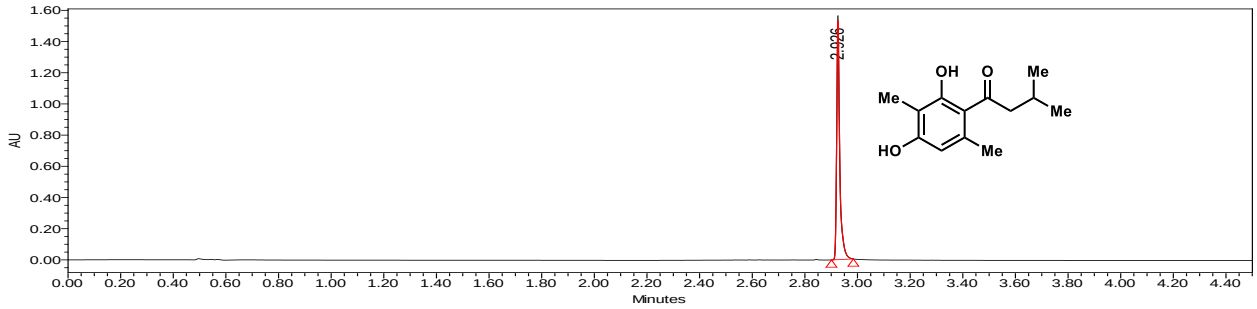


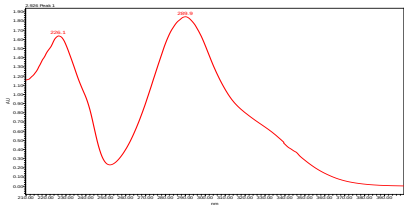

| | Retention Time | Area | % Area | Height |
|---|---|---|---|---|
| 1 | 2.926 | 1241096 | 100.00 | 1532691 |

**Figure 2.S41. Benzylic hydroxylation of 2.40 by ClaD.**
PDA traces of enzymatic reaction and control reaction.

## With ClaD

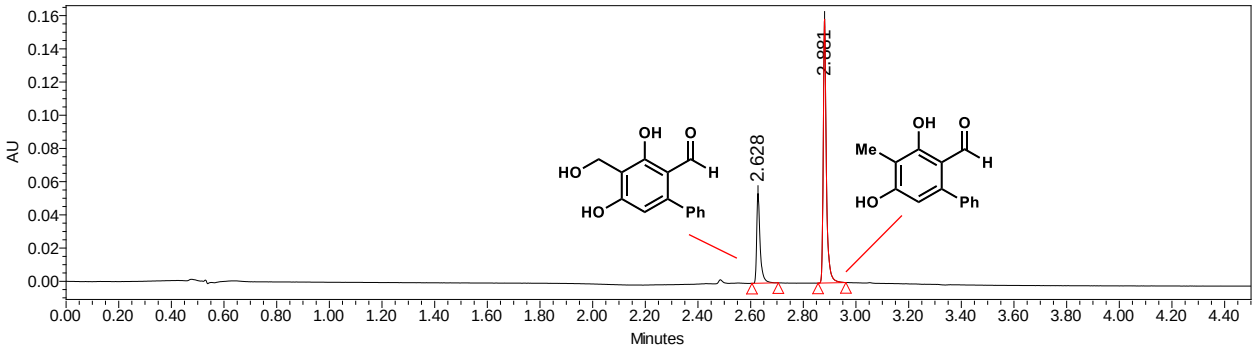


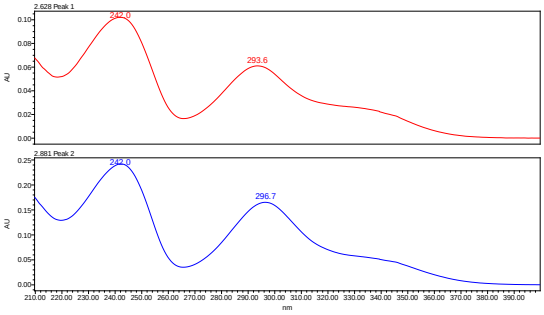


| | Retention Time | Area | % Area | Height |
|---|---|---|---|---|
| 1 | 2.628 | 49270 | 27.38 | 54215 |
| 2 | 2.881 | 130673 | 72.62 | 158993 |

## No Enzyme Control

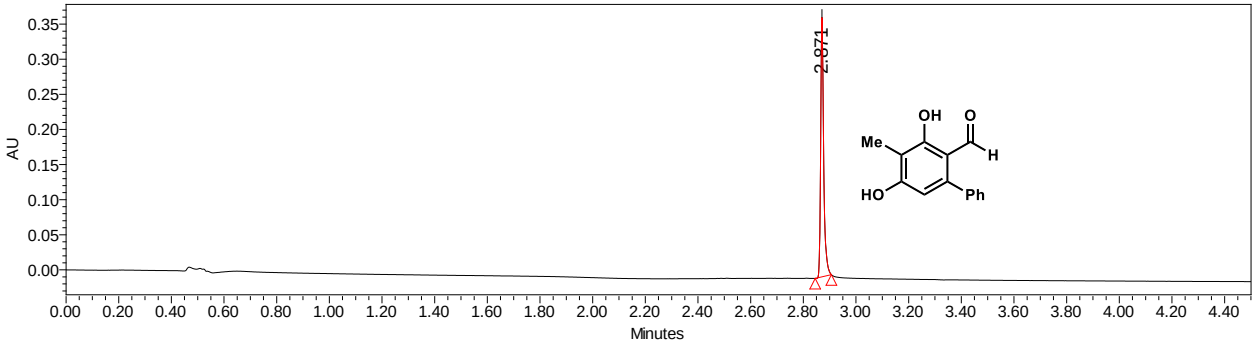


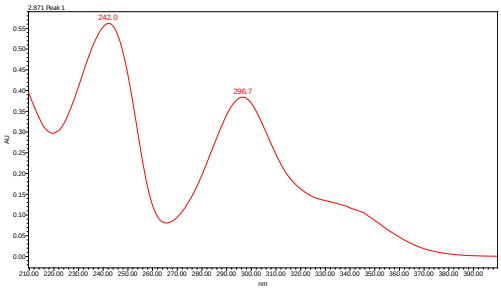


| | Retention Time | Area | % Area | Height |
|---|---|---|---|---|
| 1 | 2.871 | 292001 | 100.00 | 369040 |

**Figure 2.S42. Benzylic hydroxylation of 2.39 by ClaD.**
PDA traces of enzymatic reaction and control reaction.

## With ClaD

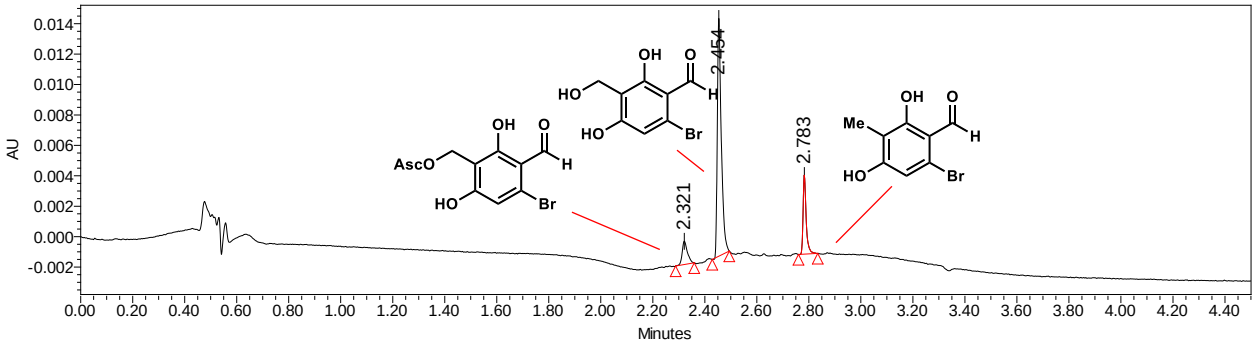


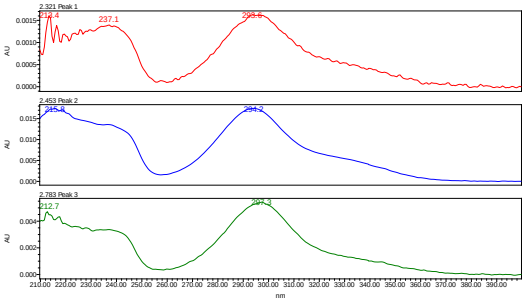

| | Retention Time | Area | % Area | Height |
|---|---|---|---|---|
| 1 | 2.321 | 2148 | 9.27 | 1533 |
| 2 | 2.454 | 16733 | 72.18 | 15666 |
| 3 | 2.783 | 4302 | 18.56 | 5206 |

## No Enzyme Control

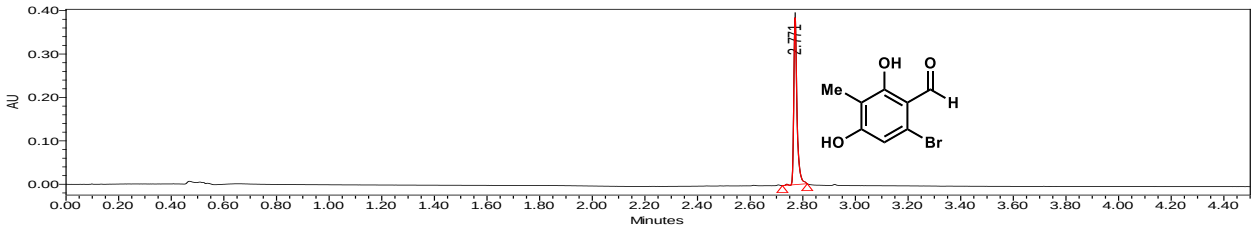


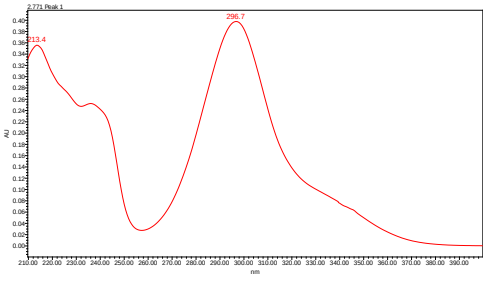

| | Retention Time | Area | % Area | Height |
|---|---|---|---|---|
| 1 | 2.771 | 324677 | 100.00 | 384271 |

**Figure 2.S43. Benzylic hydroxylation of 2.36 by ClaD.**
PDA traces of enzymatic reaction and control reaction.

## With ClaD

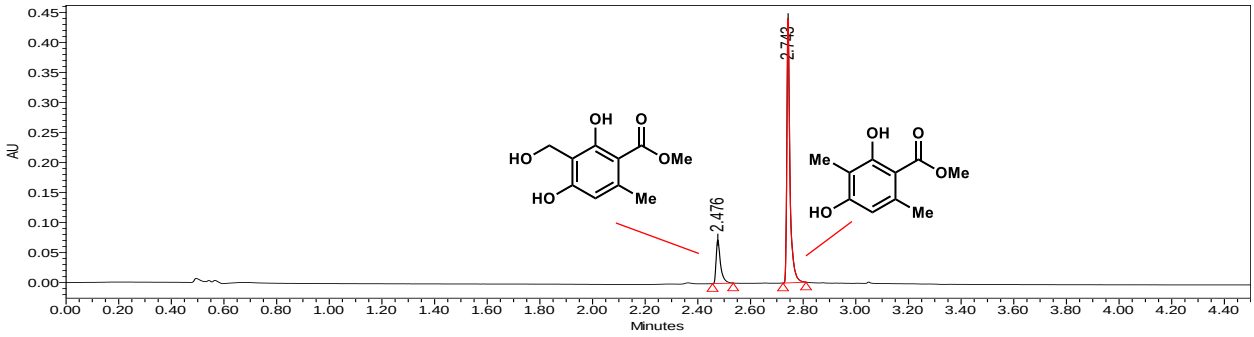


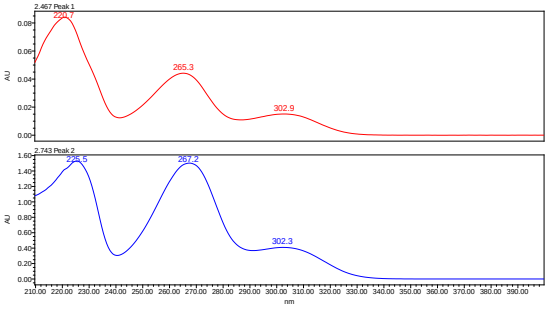


| | Retention Time | Area | % Area | Height |
|---|---|---|---|---|
| 1 | 2.476 | 84170 | 18.80 | 72961 |
| 2 | 2.743 | 363593 | 81.20 | 440078 |

## No Enzyme Control

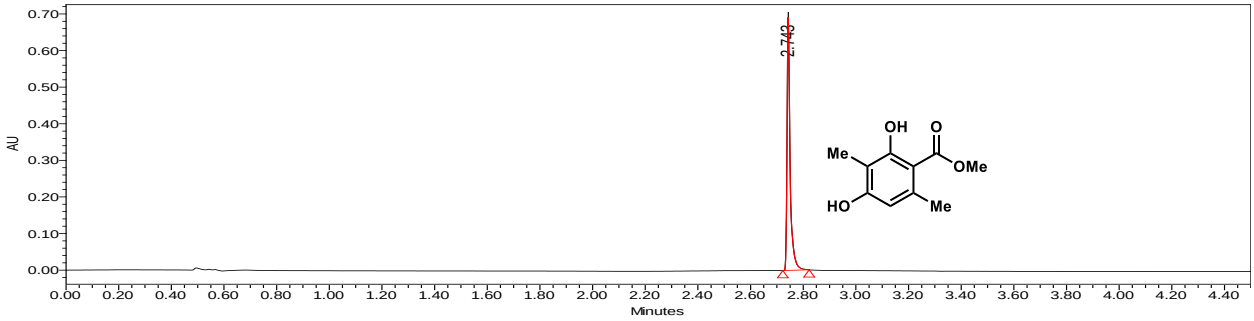


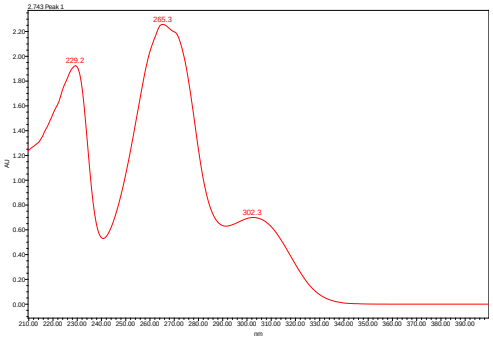


| | Retention Time | Area | % Area | Height |
|---|---|---|---|---|
| 1 | 2.743 | 568850 | 100.00 | 692384 |

**Figure 2.S44. Benzylic hydroxylation of 2.19 by ClaD.**
PDA traces of enzymatic reaction and control reaction.

## With ClaD

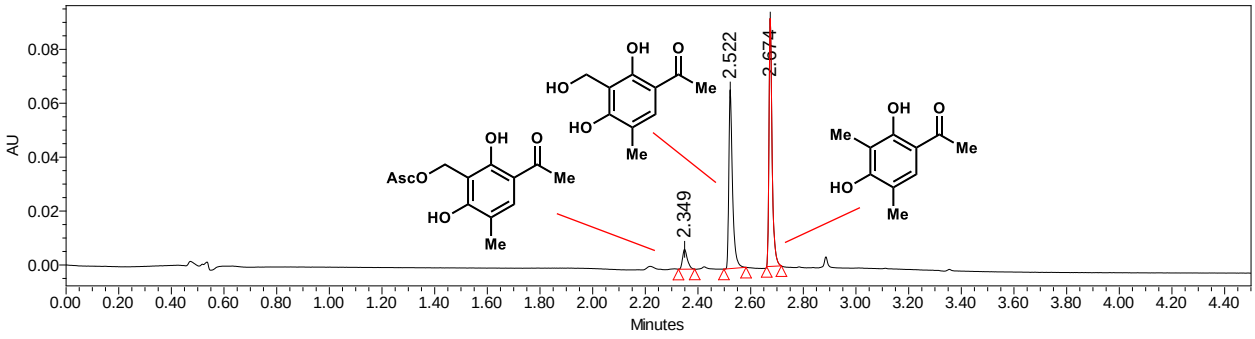


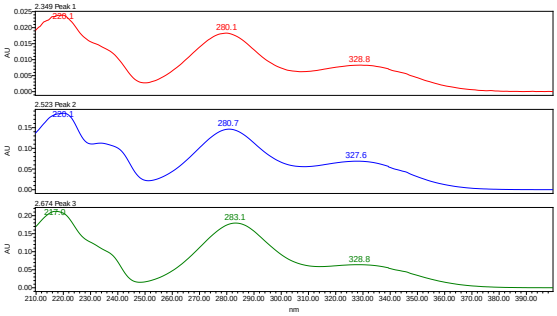


| | Retention Time | Area | % Area | Height |
|---|---|---|---|---|
| 1 | 2.349 | 9326 | 6.25 | 7385 |
| 2 | 2.522 | 64221 | 43.04 | 66319 |
| 3 | 2.674 | 75678 | 50.71 | 92174 |

## No Enzyme Control

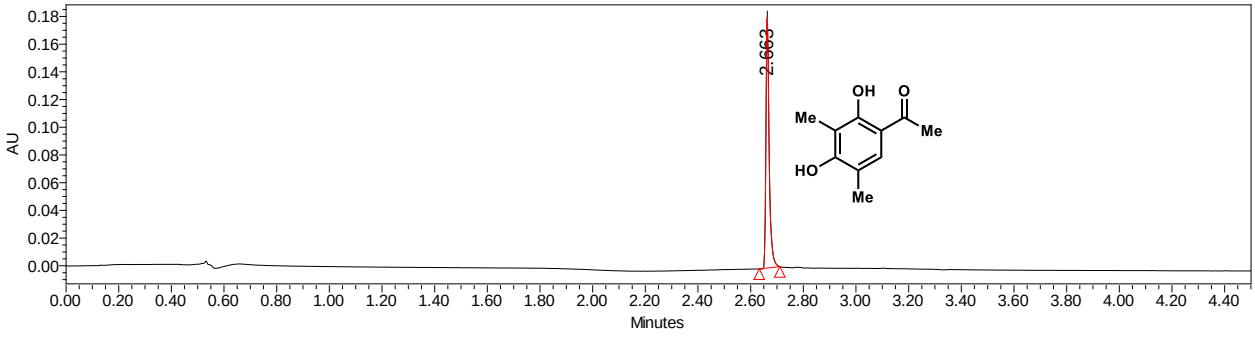


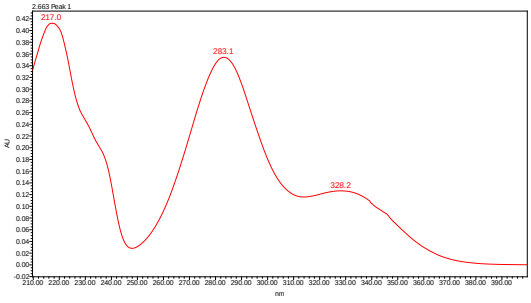


| | Retention Time | Area | % Area | Height |
|---|---|---|---|---|
| 1 | 2.663 | 155114 | 100.00 | 180974 |

**Figure 2.S45. Benzylic hydroxylation of 2.44 by ClaD.**
PDA traces of enzymatic reaction and control reaction.

## With ClaD

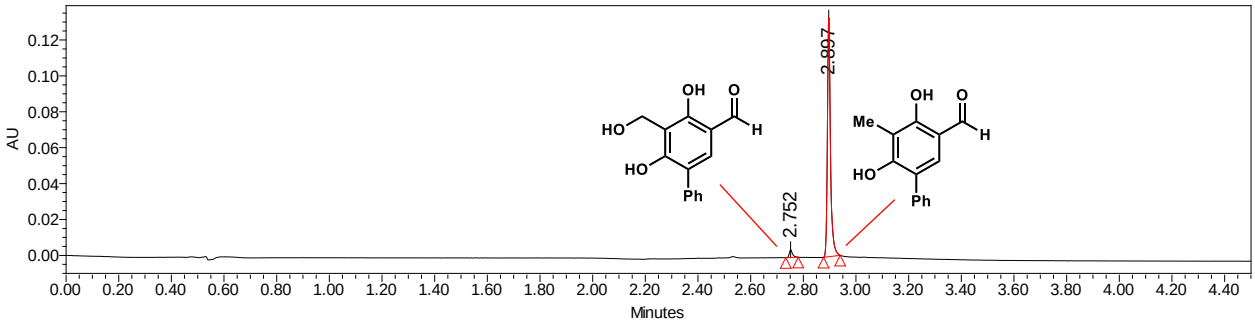


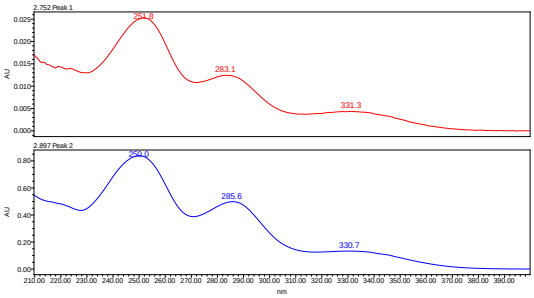


| | Retention Time | Area | % Area | Height |
|---|---|---|---|---|
| 1 | 2.752 | 3621 | 3.26 | 4362 |
| 2 | 2.897 | 107598 | 96.74 | 133020 |

## No Enzyme Control

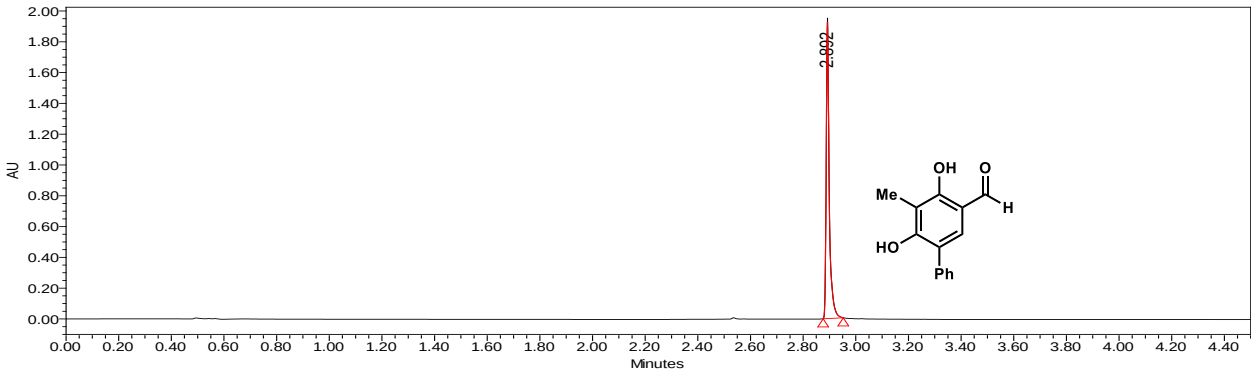


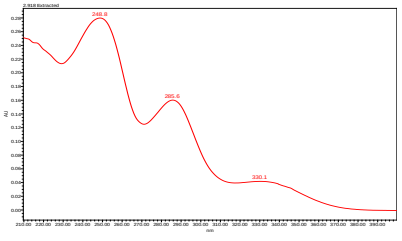


| | Retention Time | Area | % Area | Height |
|---|---|---|---|---|
| 1 | 2.892 | 96616 | 100.00 | 127279 |

**Figure 2.S46. Benzylic hydroxylation of 2.45 by ClaD.**
PDA traces of enzymatic reaction and control reaction.

## With ClaD

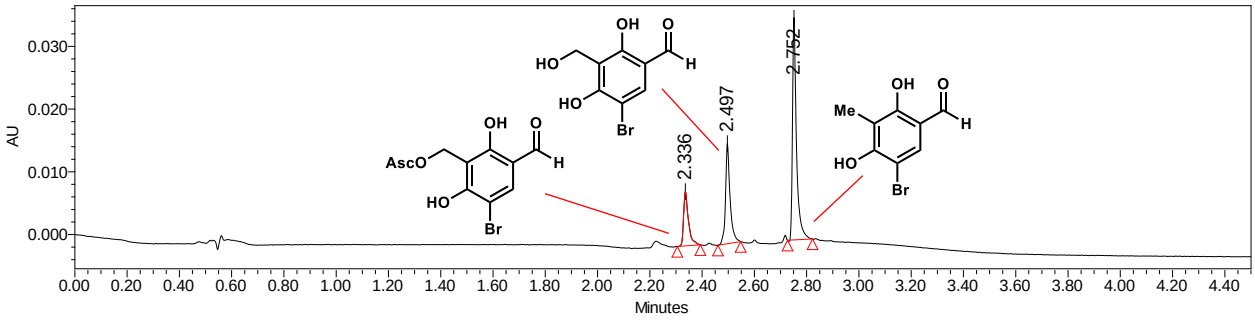


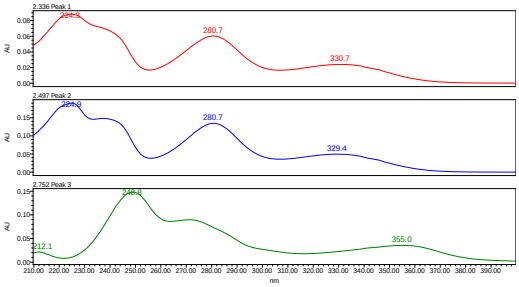


| | Retention Time | Area | % Area | Height |
|---|---|---|---|---|
| 1 | 2.336 | 11217 | 16.48 | 8670 |
| 2 | 2.497 | 19302 | 28.36 | 15961 |
| 3 | 2.752 | 37533 | 55.15 | 35440 |

## No Enzyme Control

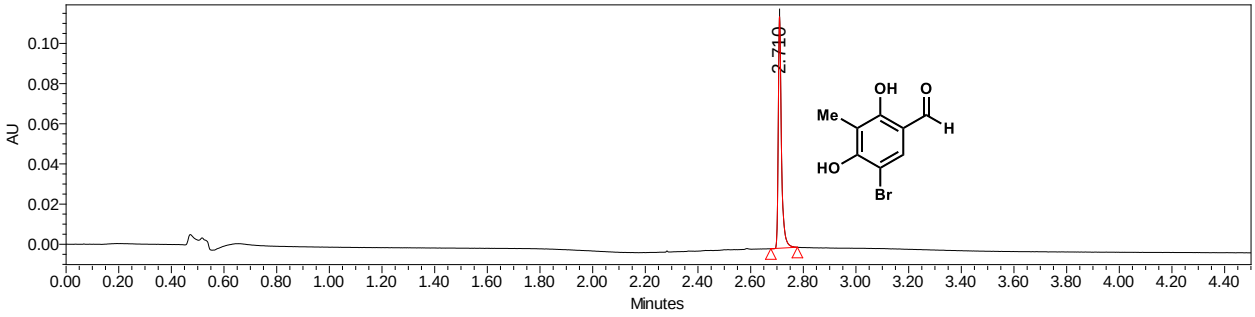


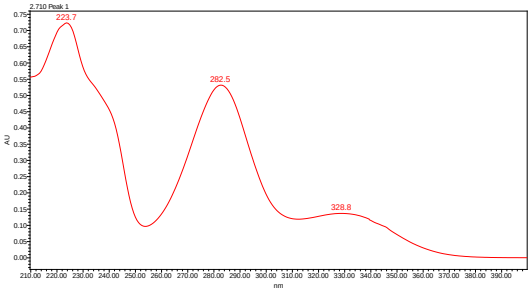


| | Retention Time | Area | % Area | Height |
|---|---|---|---|---|
| 1 | 2.710 | 97130 | 100.00 | 115426 |

**Figure 2.S47. Benzylic hydroxylation of 2.33 by ClaD.**
PDA traces of enzymatic reaction and control reaction.

## With ClaD

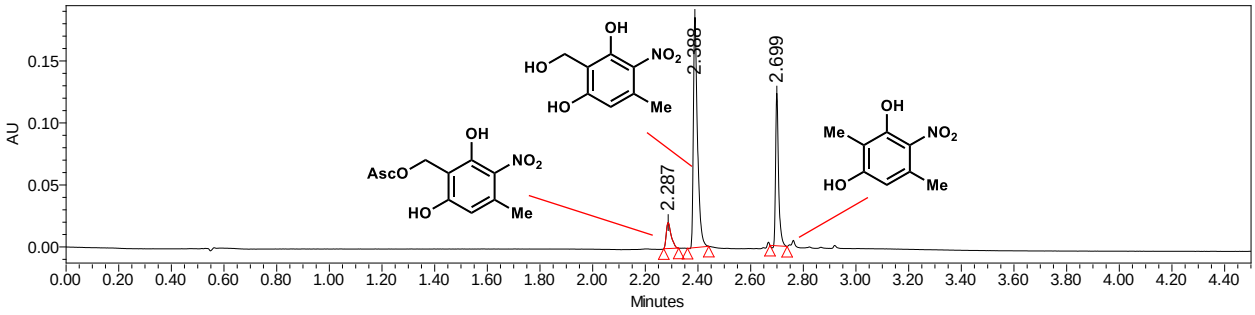


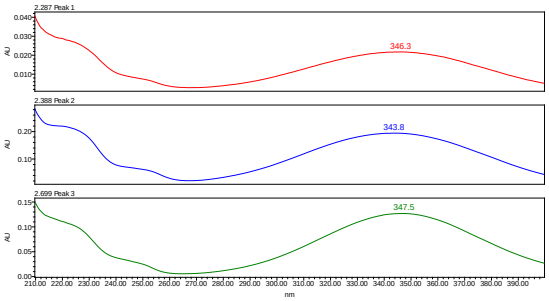


| | Retention Time | Area | % Area | Height |
|---|---|---|---|---|
| 1 | 2.287 | 27135 | 8.36 | 20949 |
| 2 | 2.388 | 200637 | 61.84 | 185589 |
| 3 | 2.699 | 96692 | 29.80 | 122972 |

## No Enzyme Control

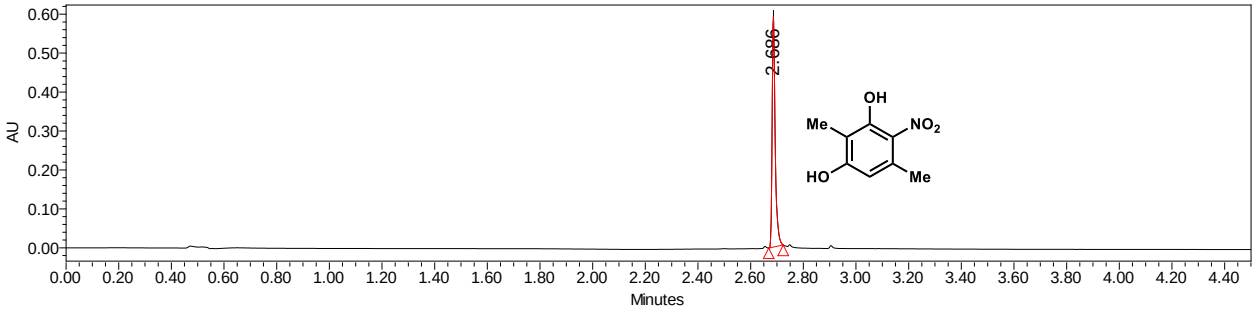


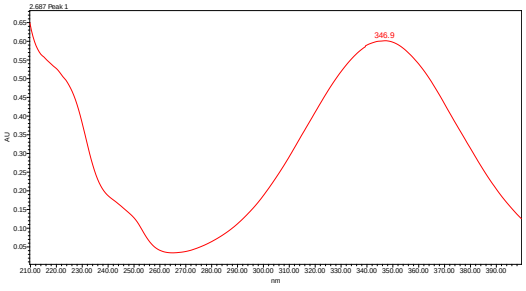


| | Retention Time | Area | % Area | Height |
|---|---|---|---|---|
| 1 | 2.686 | 475366 | 100.00 | 592606 |

**Figure 2.S48. Benzylic hydroxylation of 2.37 by ClaD.**
PDA traces of enzymatic reaction and control reaction.

## With ClaD

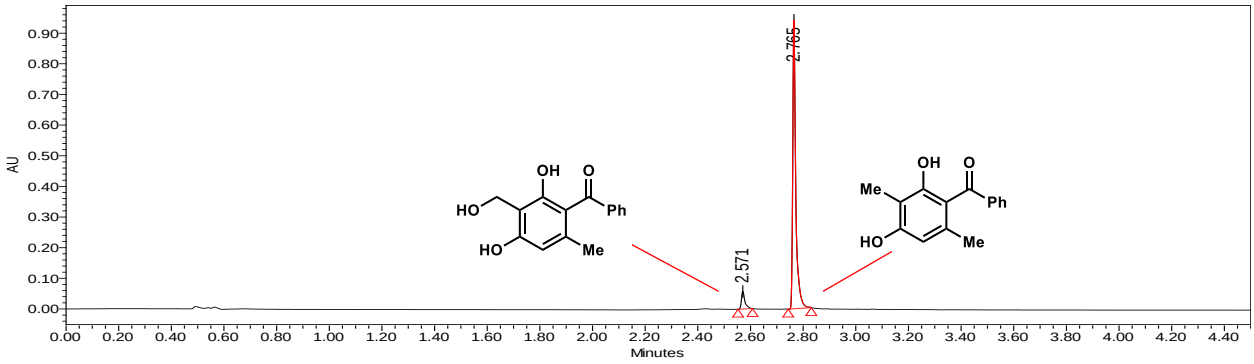


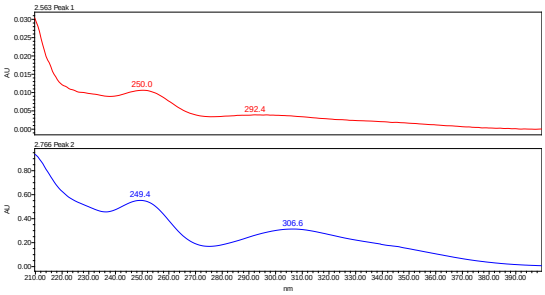


| | Retention Time | Area | % Area | Height |
|---|---|---|---|---|
| 1 | 2.571 | 52992 | 6.57 | 57801 |
| 2 | 2.765 | 754098 | 93.43 | 941895 |

## No Enzyme Control

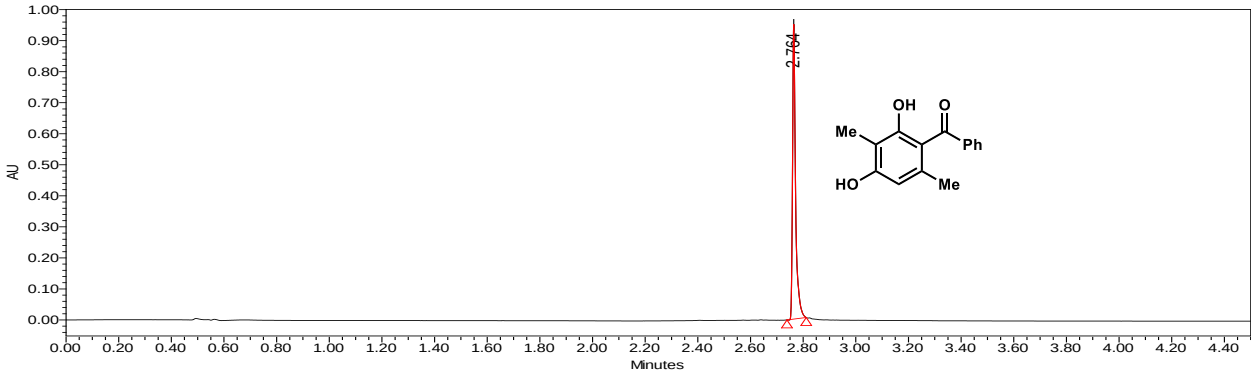


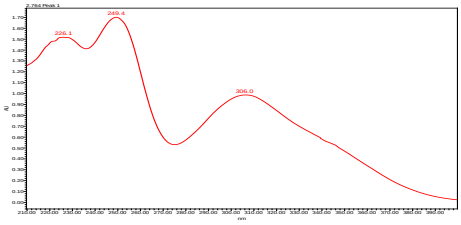


| | Retention Time | Area | % Area | Height |
|---|---|---|---|---|
| 1 | 2.764 | 764260 | 100.00 | 949653 |

**Figure 2.S49. Benzylic hydroxylation of 2.S12 by ClaD.**
PDA traces of enzymatic reaction and control reaction.

## With ClaD

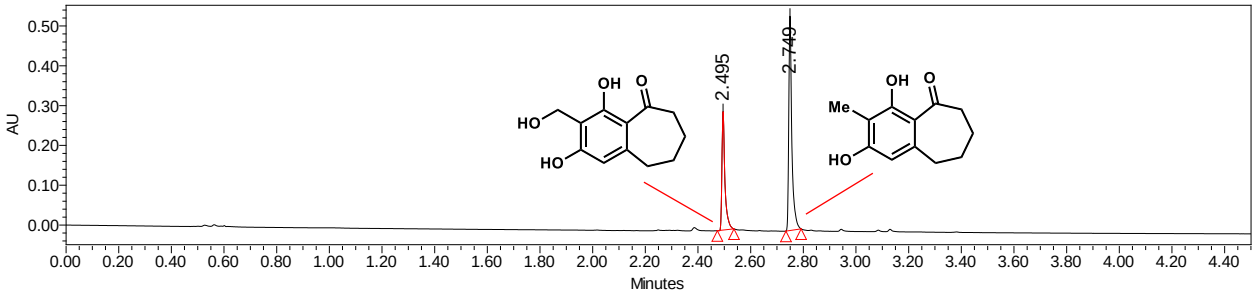


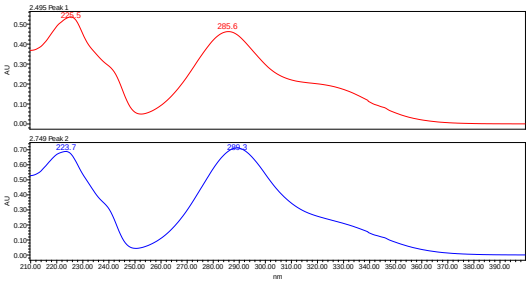


| | Retention Time | Area | % Area | Height |
|---|---|---|---|---|
| 1 | 2.495 | 234136 | 35.21 | 297866 |
| 2 | 2.749 | 430771 | 64.79 | 538897 |

## No Enzyme Control

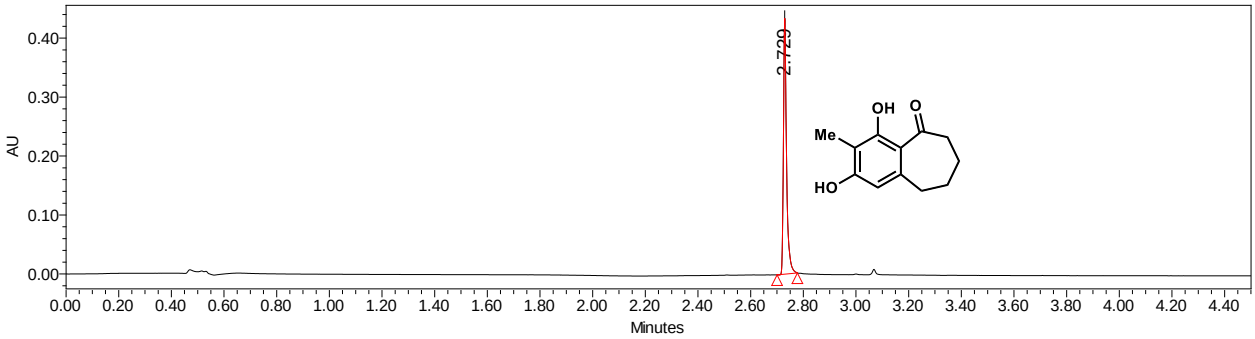


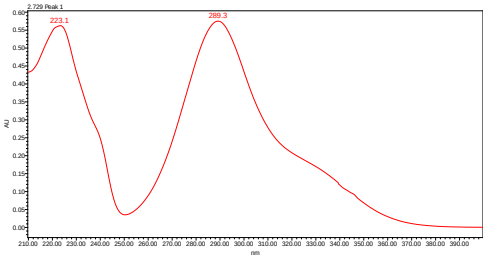


| | Retention Time | Area | % Area | Height |
|---|---|---|---|---|
| 1 | 2.729 | 354920 | 100.00 | 434150 |

**Figure 2.S50. Benzylic hydroxylation of 2.38 by ClaD.**
PDA traces of enzymatic reaction and control reaction.

## With ClaD

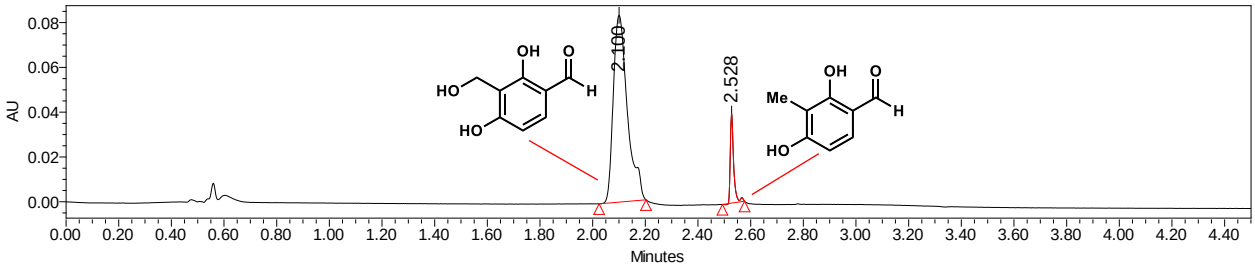


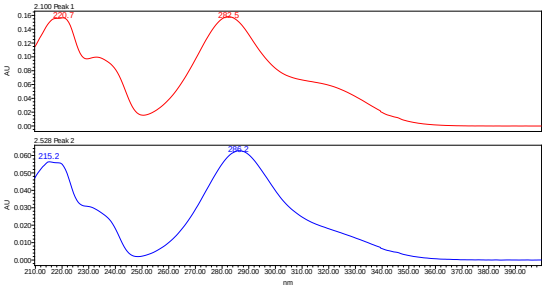


| | Retention Time | Area | % Area | Height |
|---|---|---|---|---|
| 1 | 2.100 | 311160 | 89.76 | 83400 |
| 2 | 2.528 | 35513 | 10.24 | 39781 |

## No Enzyme Control

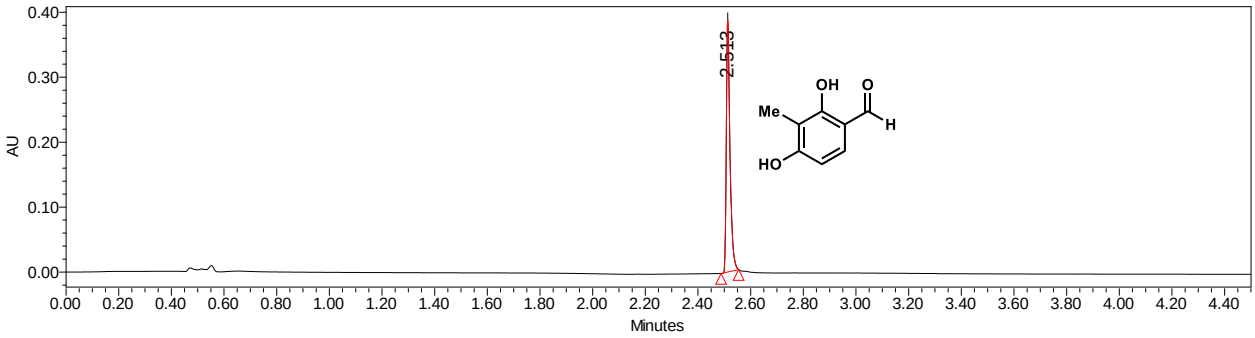


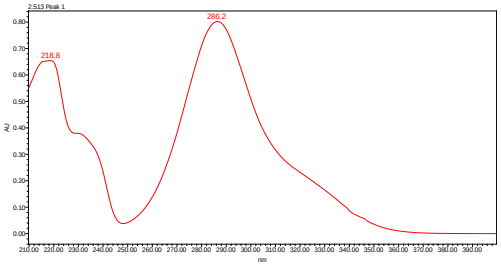


| | Retention Time | Area | % Area | Height |
|---|---|---|---|---|
| 1 | 2.513 | 374802 | 100.00 | 389926 |

**Figure 2.S51. Benzylic hydroxylation of 2.49 by ClaD.**
PDA traces of enzymatic reaction and control reaction.

## With ClaD

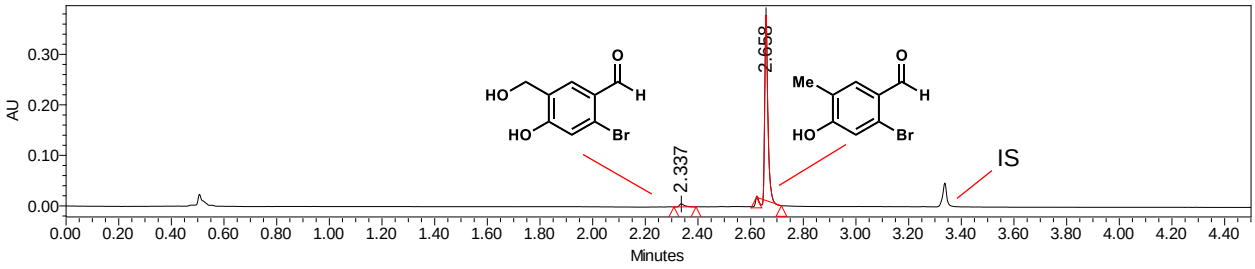


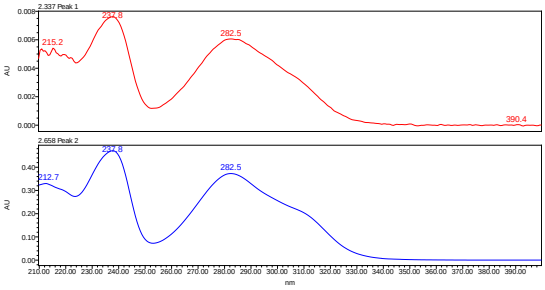


| | Retention Time | Area | % Area | Height |
|---|---|---|---|---|
| 1 | 2.337 | 7645 | 2.40 | 5967 |
| 2 | 2.658 | 310583 | 97.60 | 366569 |

## No Enzyme Control

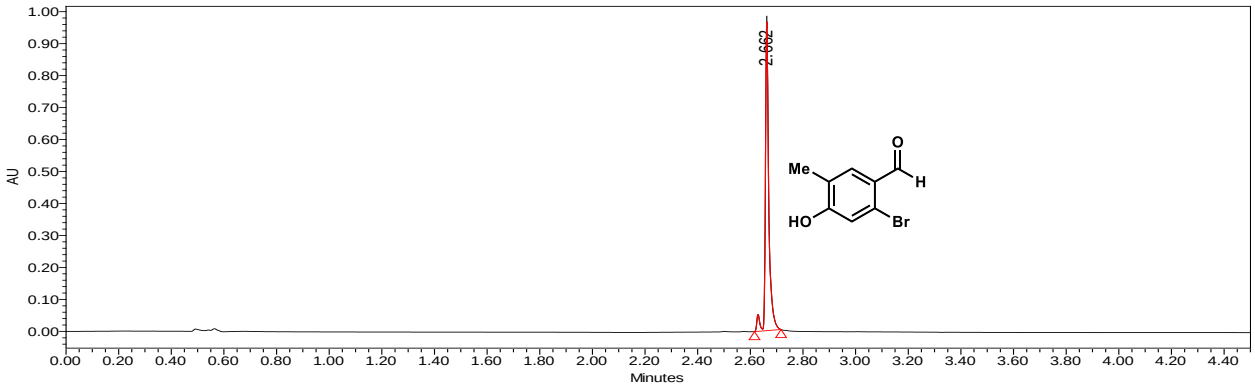


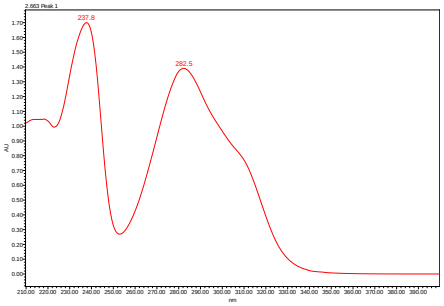


| | Retention Time | Area | % Area | Height |
|---|---|---|---|---|
| 1 | 2.662 | 880367 | 100.00 | 965611 |

**Figure 2.S52. Benzylic hydroxylation of 2.48 by ClaD.**
PDA traces of enzymatic reaction and control reaction.

## With ClaD

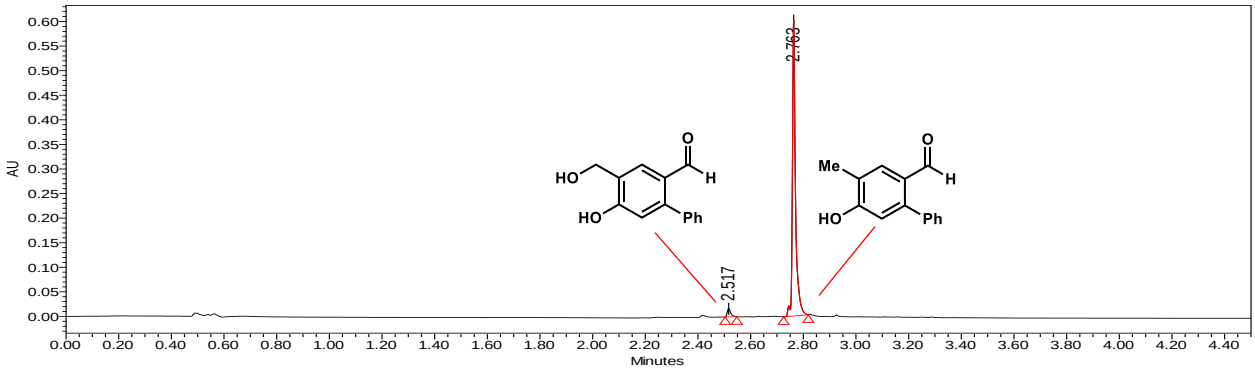


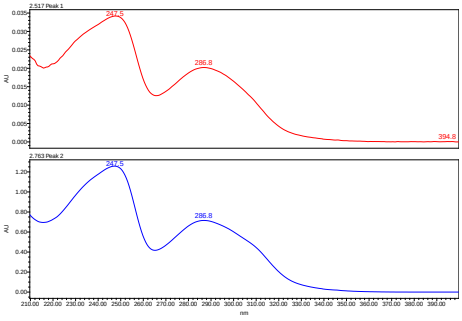


| | Retention Time | Area | % Area | Height |
|---|---|---|---|---|
| 1 | 2.517 | 15034 | 2.97 | 16459 |
| 2 | 2.763 | 491458 | 97.03 | 601297 |

## No Enzyme Control

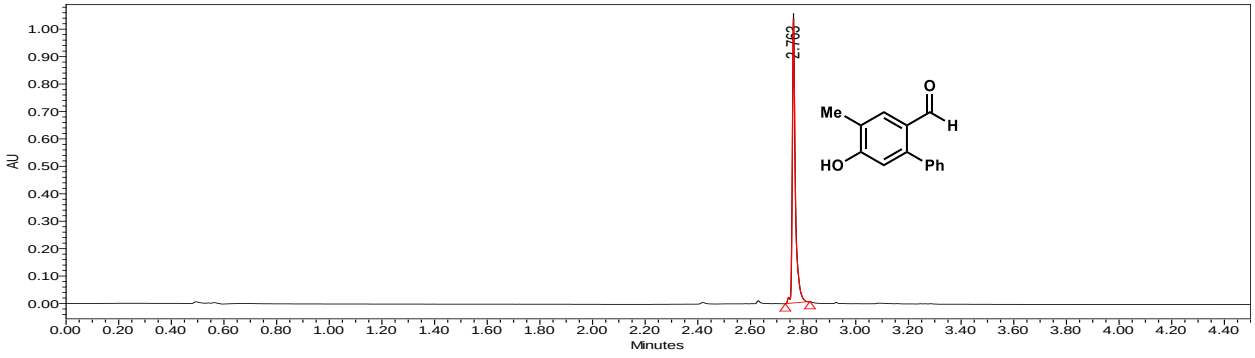


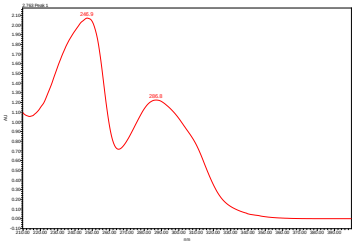

| | Retention Time | Area | % Area | Height |
|---|---|---|---|---|
| 1 | 2.763 | 832443 | 100.00 | 1034833 |

**Figure 2.S53. Benzylic hydroxylation of 2.47 by ClaD.**
PDA traces of enzymatic reaction and control reaction.

## With ClaD

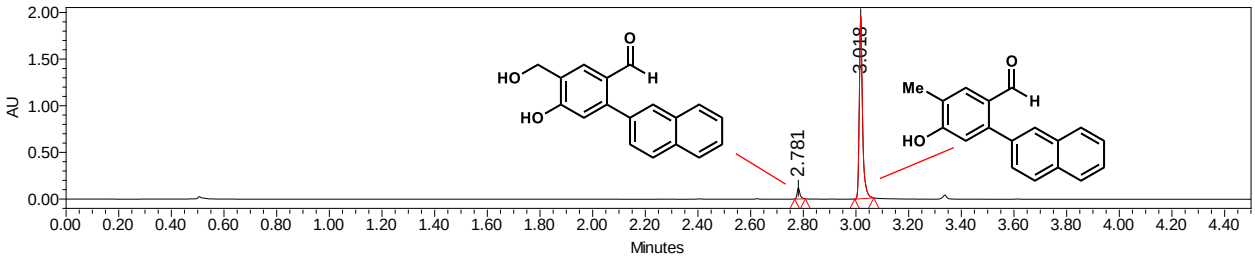


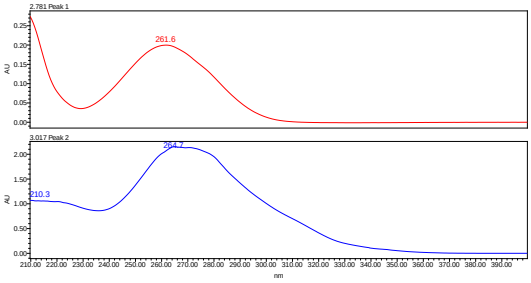


| | Retention Time | Area | % Area | Height |
|---|---|---|---|---|
| 1 | 2.781 | 87888 | 5.00 | 117285 |
| 2 | 3.018 | 1668633 | 95.00 | 1956582 |

## No Enzyme Control

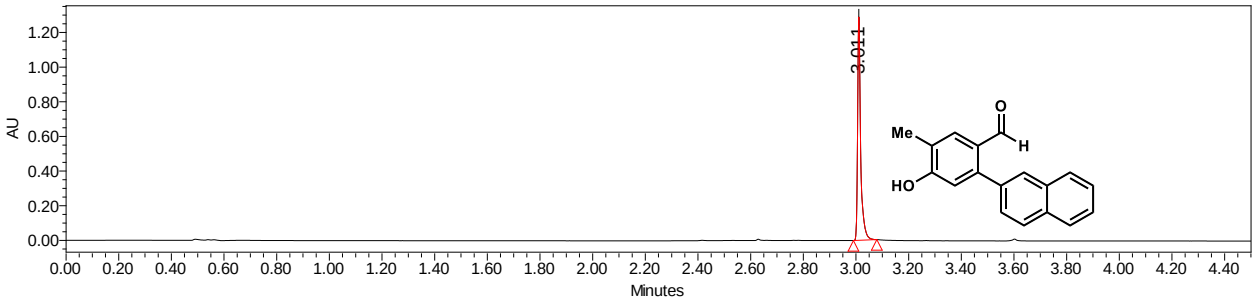


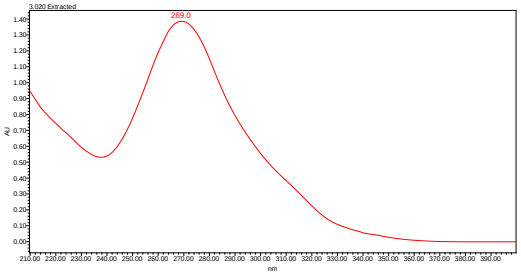


| | Retention Time | Area | % Area | Height |
|---|---|---|---|---|
| 1 | 3.011 | 1033281 | 100.00 | 1288141 |

**Figure 2.S54. Benzylic hydroxylation of 2.S10 by ClaD.**
PDA traces of enzymatic reaction and control reaction.

## With ClaD

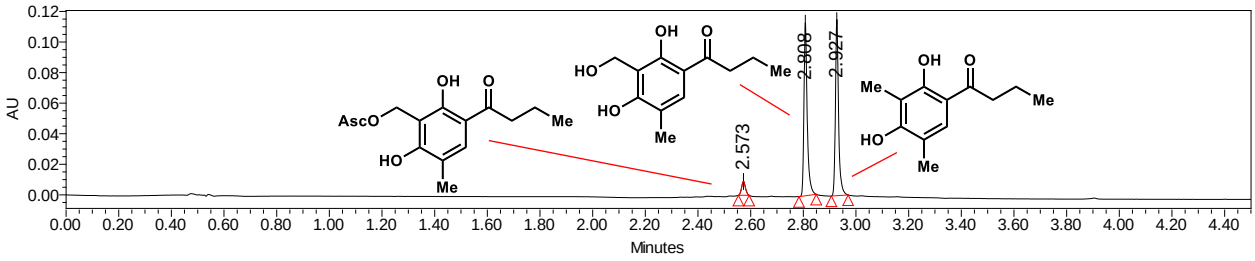


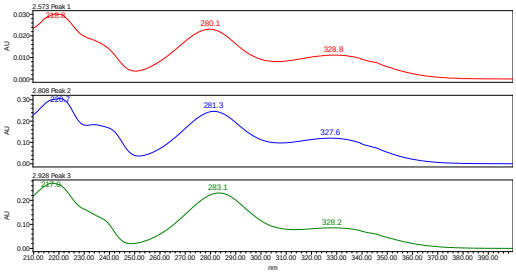


| | Retention Time | Area | % Area | Height |
|---|---|---|---|---|
| 1 | 2.573 | 9363 | 4.62 | 9119 |
| 2 | 2.808 | 97837 | 48.29 | 113182 |
| 3 | 2.927 | 95393 | 47.09 | 115398 |

## No Enzyme Control

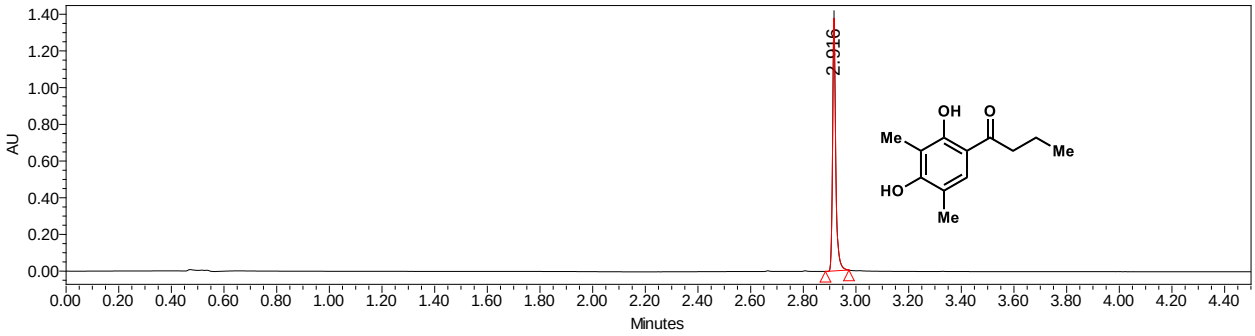


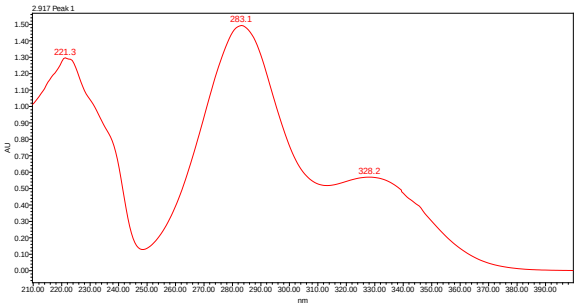


| | Retention Time | Area | % Area | Height |
|---|---|---|---|---|
| 1 | 2.916 | 1139767 | 100.00 | 1378357 |

**Figure 2.S55. Benzylic hydroxylation of 2.S11 by ClaD.**
PDA traces of enzymatic reaction and control reaction.

## With ClaD

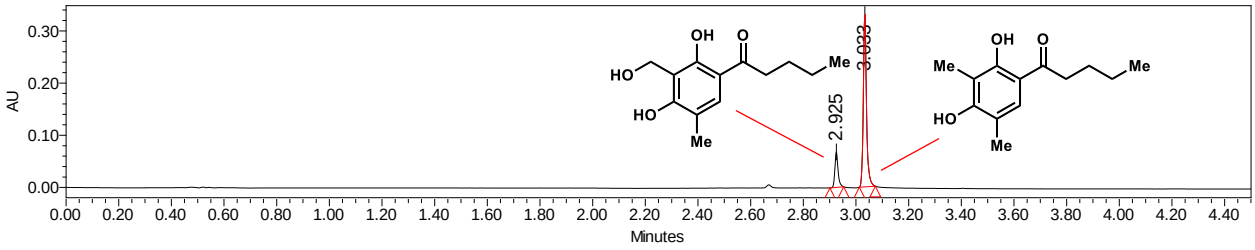


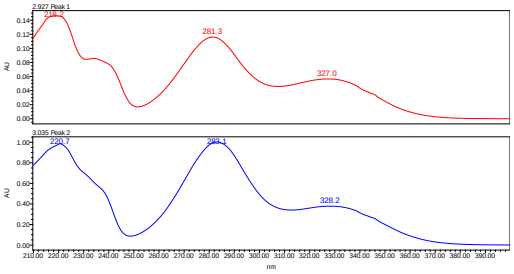


| | Retention Time | Area | % Area | Height |
|---|---|---|---|---|
| 1 | 2.927 | 39775 | 12.60 | 48177 |
| 2 | 3.035 | 275823 | 87.40 | 338915 |

## No Enzyme Control

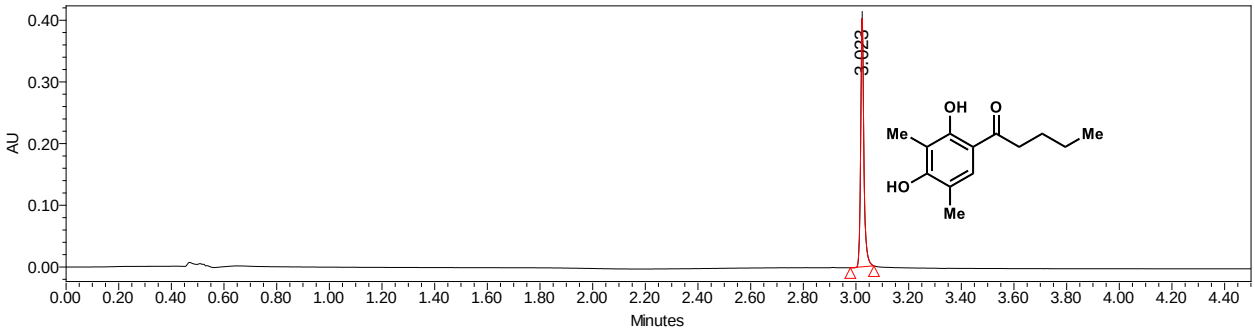


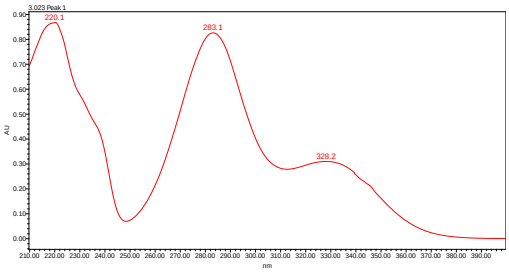


| | Retention Time | Area | % Area | Height |
|---|---|---|---|---|
| 1 | 3.023 | 339980 | 100.00 | 402647 |

**Figure 2.S56. Benzylic hydroxylation of 2.43 by ClaD.**
PDA traces of enzymatic reaction and control reaction.

## With ClaD

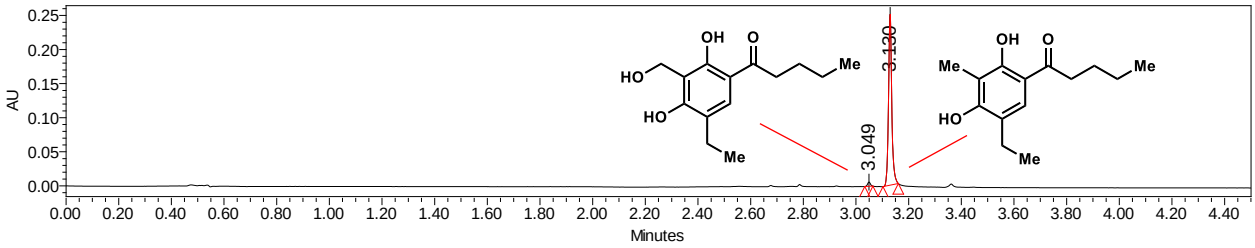


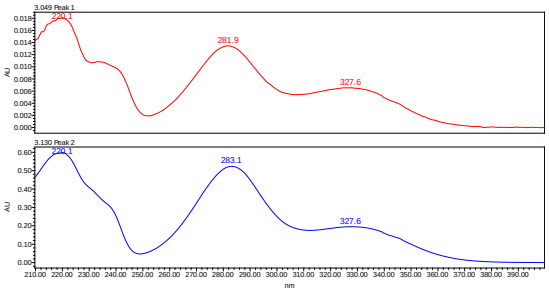


| | Retention Time | Area | % Area | Height |
|---|---|---|---|---|
| 1 | 3.049 | 4714 | 2.15 | 6257 |
| 2 | 3.130 | 215026 | 97.85 | 251237 |

## No Enzyme Control

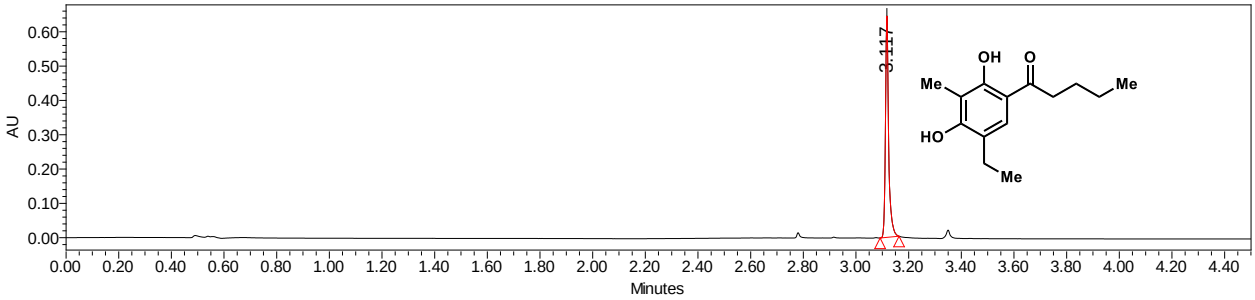


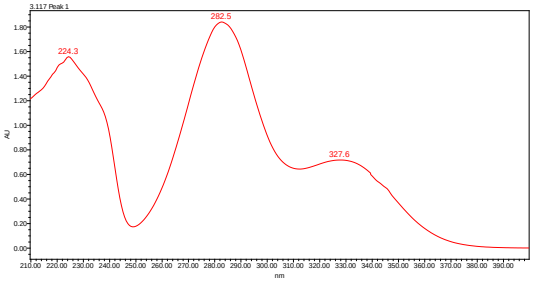


| | Retention Time | Area | % Area | Height |
|---|---|---|---|---|
| 1 | 3.117 | 543126 | 100.00 | 645051 |

**Figure 2.S57. Benzylic hydroxylation of 2.S13 by ClaD.**
PDA traces of enzymatic reaction and control reaction.

## With ClaD

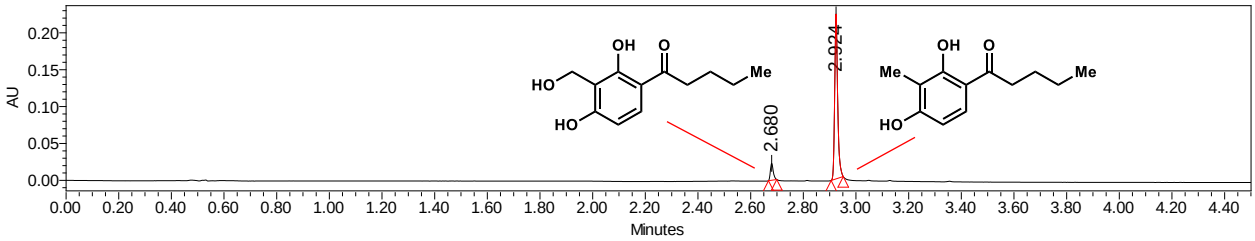


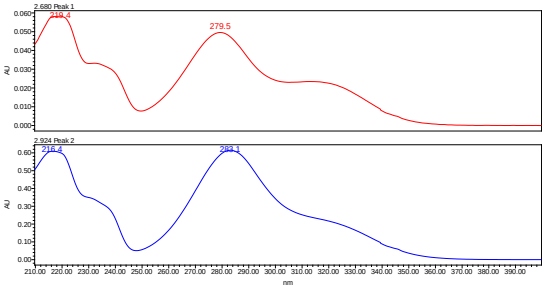


| | Retention Time | Area | % Area | Height |
|---|---|---|---|---|
| 1 | 2.680 | 17449 | 9.10 | 23001 |
| 2 | 2.924 | 174322 | 90.90 | 223470 |

## No Enzyme Control

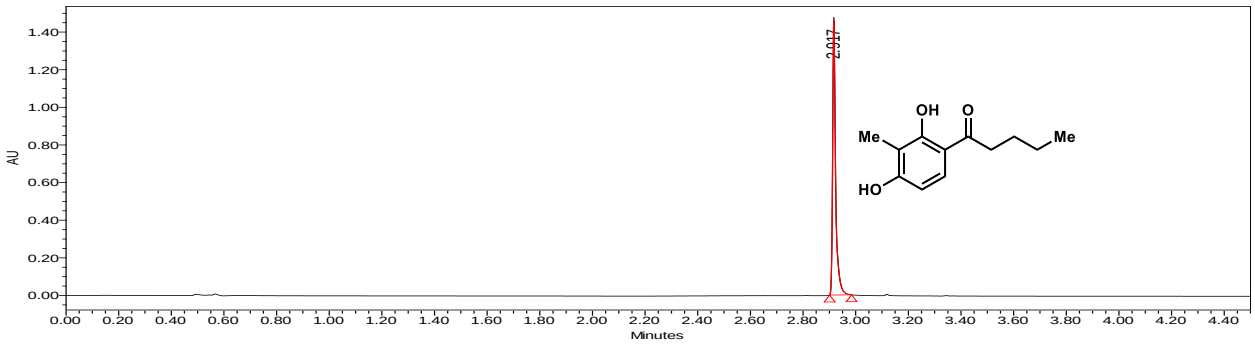


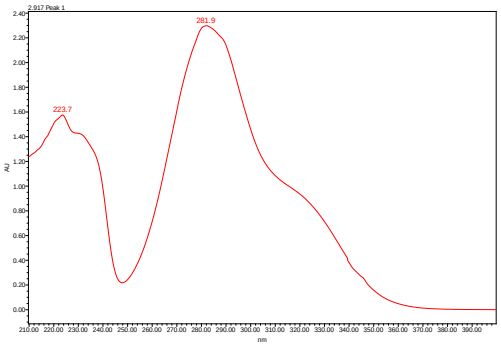


| | Retention Time | Area | % Area | Height |
|---|---|---|---|---|
| 1 | 2.917 | 1167633 | 100.00 | 1462896 |

**Figure 2.S58. Benzylic hydroxylation of 2.S8 by ClaD.**
PDA traces of enzymatic reaction and control reaction.

## With ClaD

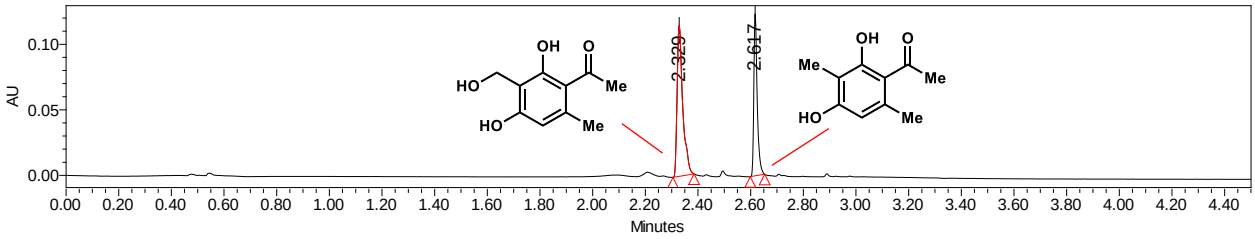


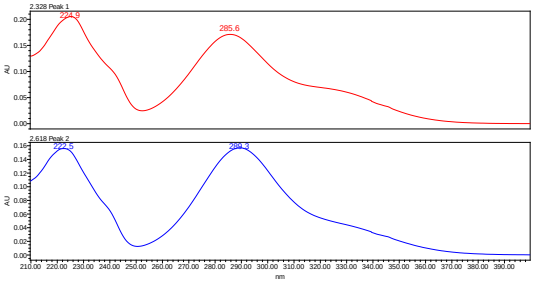


| | Retention Time | Area | % Area | Height |
|---|---|---|---|---|
| 1 | 2.329 | 171376 | 61.01 | 115246 |
| 2 | 2.617 | 109536 | 38.99 | 123736 |

## No Enzyme Control

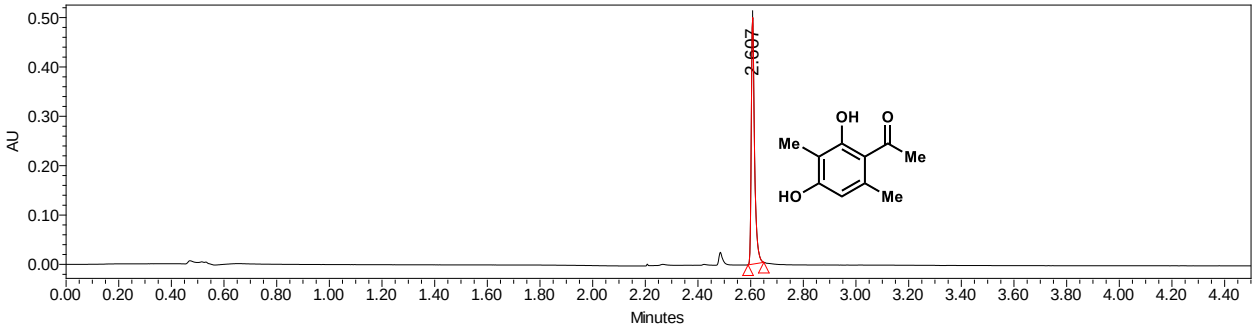


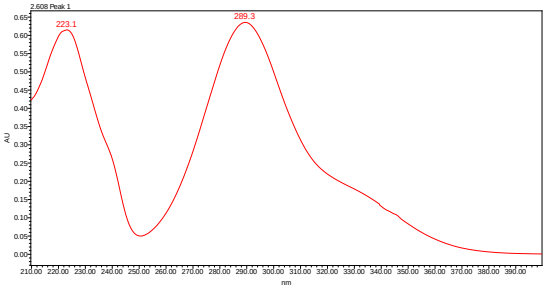


| | Retention Time | Area | % Area | Height |
|---|---|---|---|---|
| 1 | 2.607 | 428890 | 100.00 | 499813 |

**Figure 2.S59. Benzylic hydroxylation of 2.99 by ClaD.**
PDA traces of enzymatic reaction and control reaction.

## With ClaD

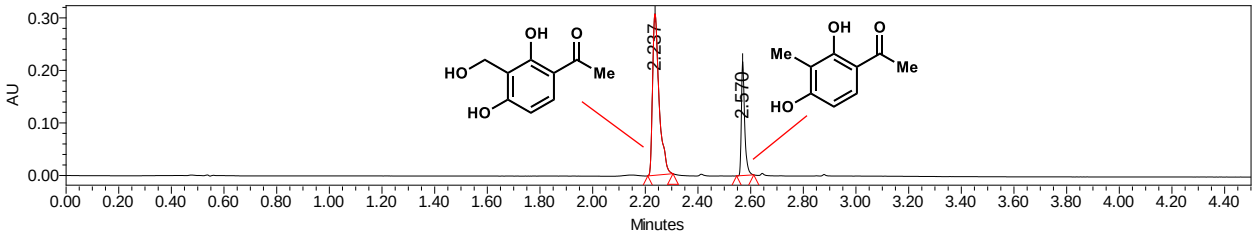


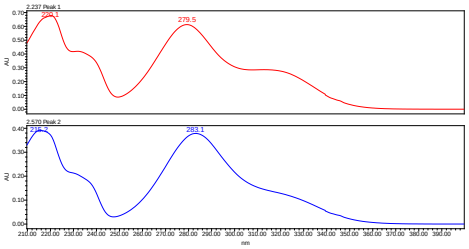


| | Retention Time | Area | % Area | Height |
|---|---|---|---|---|
| 1 | 2.237 | 531242 | 73.92 | 307152 |
| 2 | 2.570 | 187452 | 26.08 | 217040 |

## No Enzyme Control

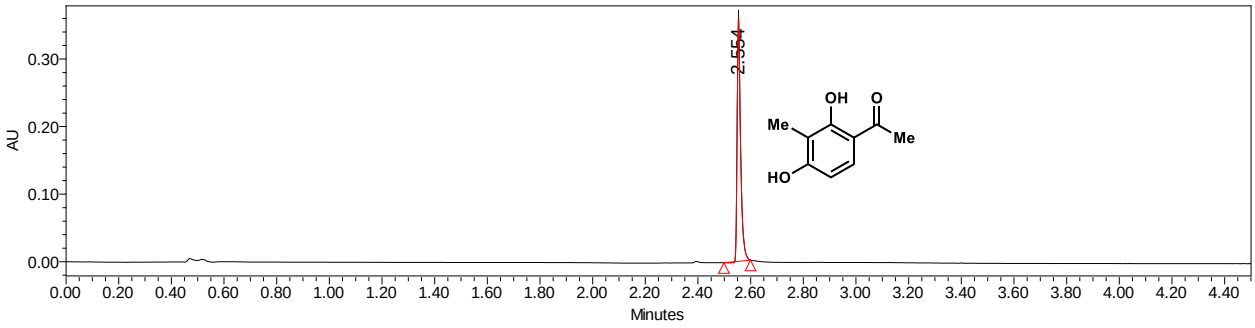


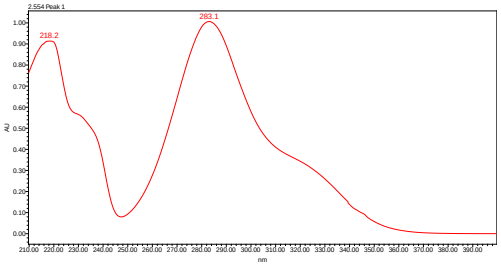


| | Retention Time | Area | % Area | Height |
|---|---|---|---|---|
| 1 | 2.554 | 329611 | 100.00 | 360497 |

**Figure 2.S60. Benzylic hydroxylation of 2.41 by ClaD.**
PDA traces of enzymatic reaction and control reaction.

## With ClaD

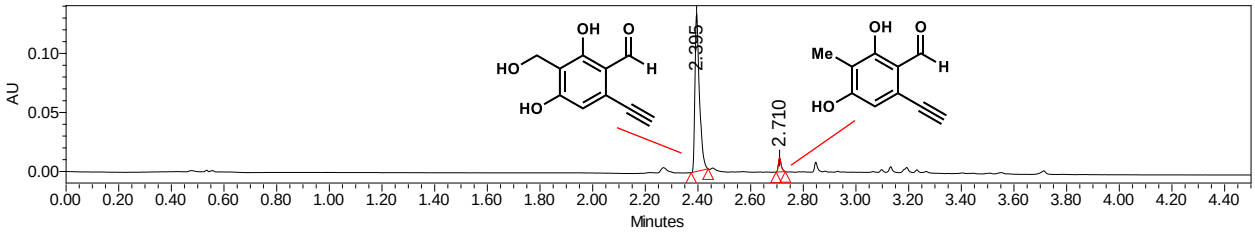


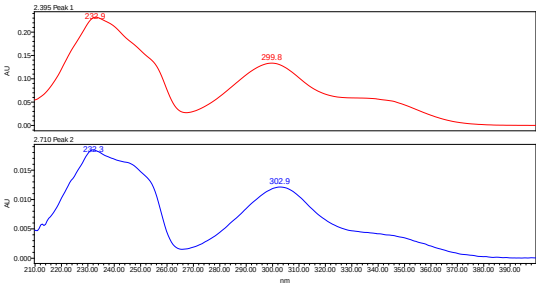


| | Retention Time | Area | % Area | Height |
|---|---|---|---|---|
| 1 | 2.395 | 156338 | 95.35 | 132623 |
| 2 | 2.710 | 7617 | 4.65 | 10921 |

## No Enzyme Control

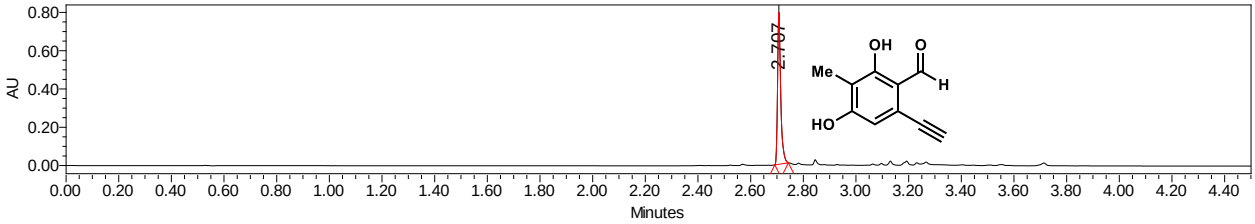


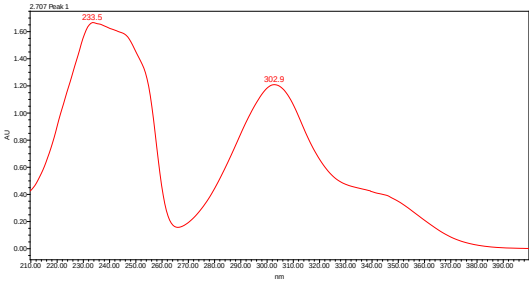


| | Retention Time | Area | % Area | Height |
|---|---|---|---|---|
| 1 | 2.707 | 658162 | 100.00 | 794410 |

**Figure 2.S61. Benzylic hydroxylation of 2.46 by ClaD.**
PDA traces of enzymatic reaction and control reaction.

## With ClaD

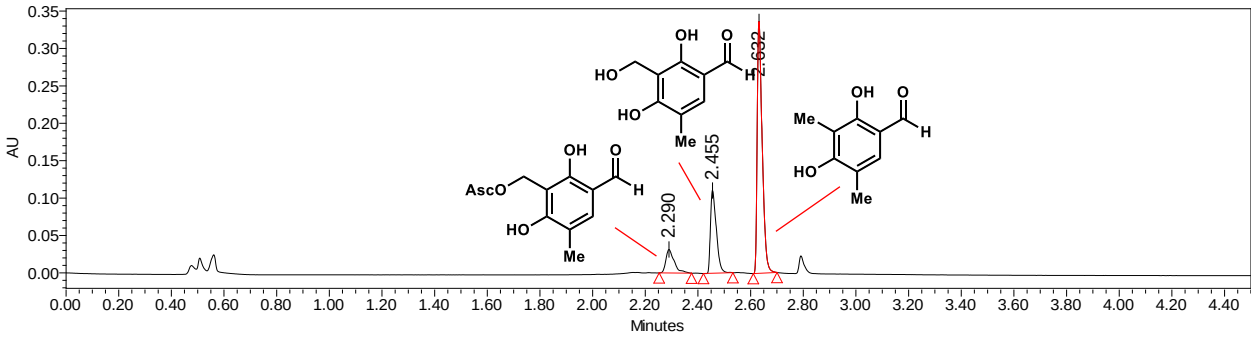


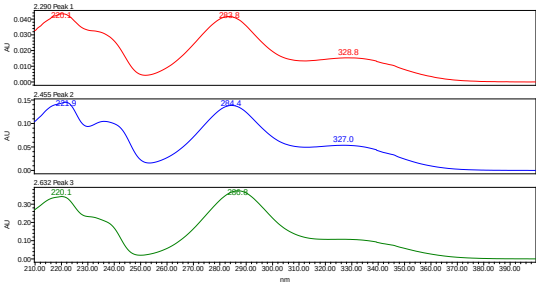


| | Retention Time | Area | % Area | Height |
|---|---|---|---|---|
| 1 | 2.290 | 69105 | 10.09 | 31515 |
| 2 | 2.455 | 170675 | 24.92 | 110968 |
| 3 | 2.632 | 445078 | 64.99 | 336764 |

## No Enzyme Control

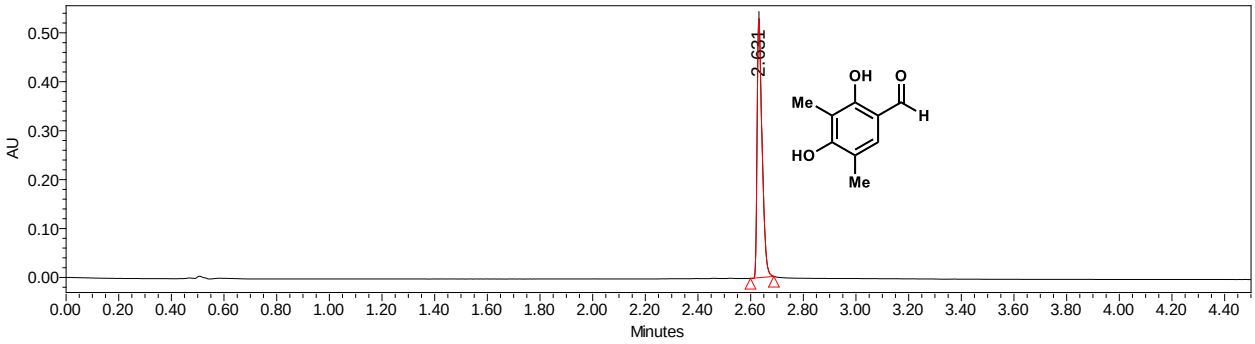


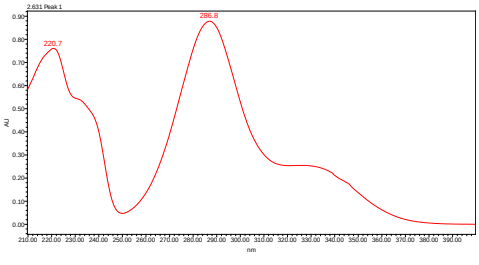


| | Retention Time | Area | % Area | Height |
|---|---|---|---|---|
| 1 | 2.631 | 693251 | 100.00 | 530045 |

**Figure 2.S62. Benzylic hydroxylation of 2.42 by ClaD.**
PDA traces of enzymatic reaction and control reaction.

## With ClaD

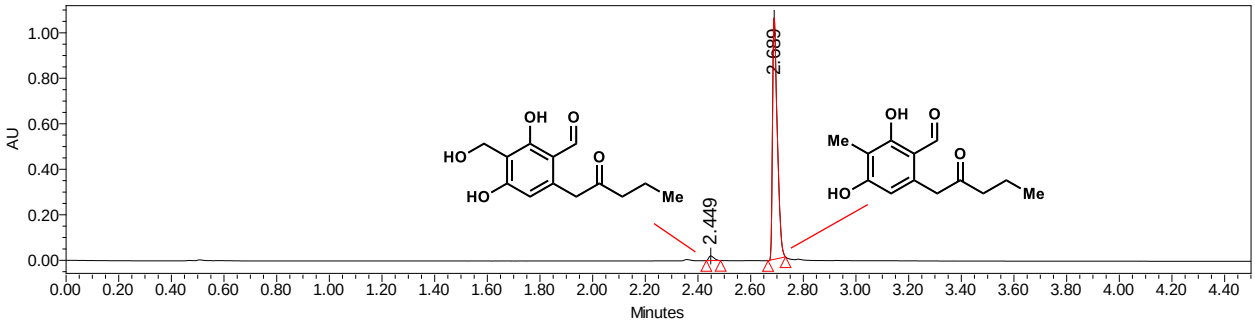


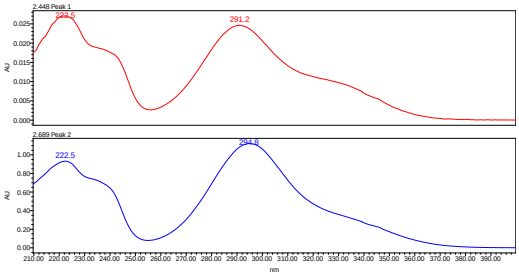


| | Retention Time | Area | % Area | Height |
|---|---|---|---|---|
| 1 | 2.449 | 28624 | 2.10 | 20551 |
| 2 | 2.689 | 1331934 | 97.90 | 1061826 |

## No Enzyme Control

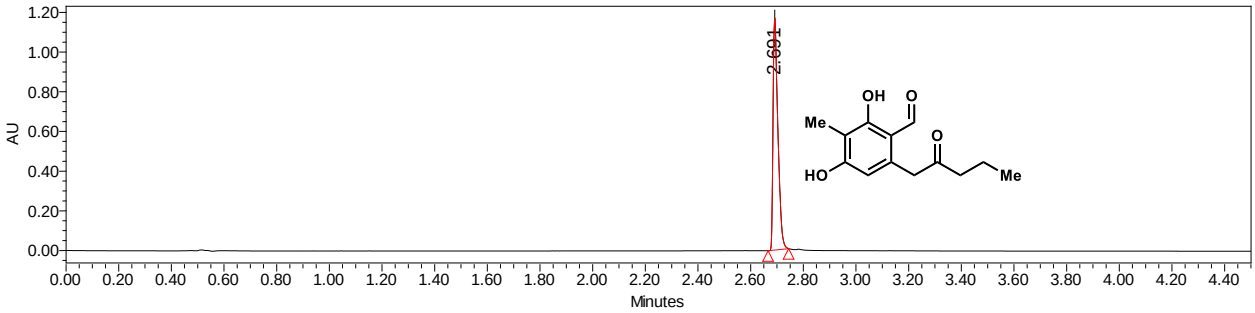


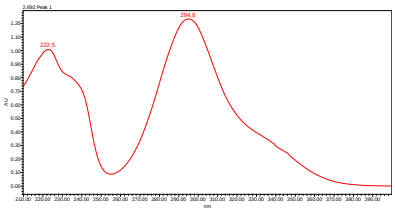


| | Retention Time | Area | % Area | Height |
|---|---|---|---|---|
| 1 | 2.691 | 1488761 | 100.00 | 1169965 |

**Figure 2.S63. Characterization of ascorbate adduct from reaction of 2.45 with ClaD.** PDA traces of enzymatic reaction and isolated ascorbate product.

## Reaction with ClaD

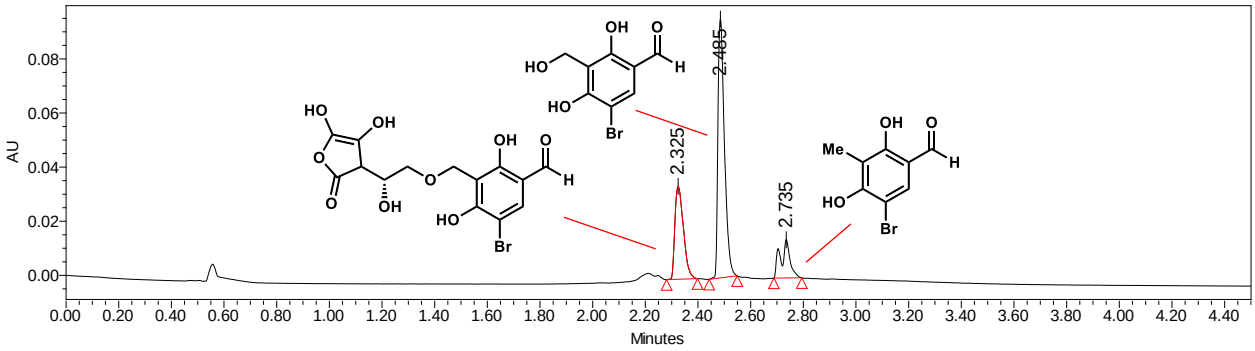


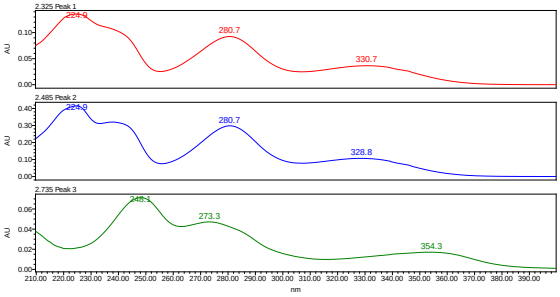


| | Retention Time | Area | % Area | Height |
|---|---|---|---|---|
| 1 | 2.325 | 77133 | 27.84 | 34356 |
| 2 | 2.485 | 164615 | 59.42 | 95691 |
| 3 | 2.735 | 35309 | 12.74 | 14164 |

## Isolated adduct

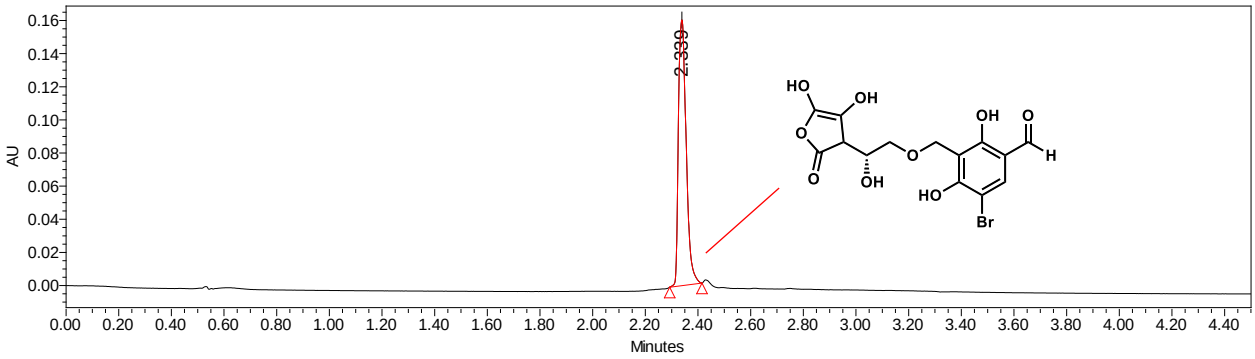


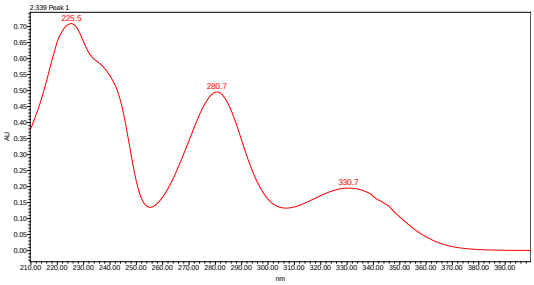


| | Retention Time | Area | % Area | Height |
|---|---|---|---|---|
| 1 | 2.339 | 328663 | 100.00 | 161313 |

## Part IX. UPLC traces for CitB or ClaD benzylic functionalization cascade reactions

**Figure 2.S64. Generation of 2.30 by *in situ* functionalization of benzylic alcohol 2.27.**
PDA traces of enzymatic reaction analyzed at 300 nm.

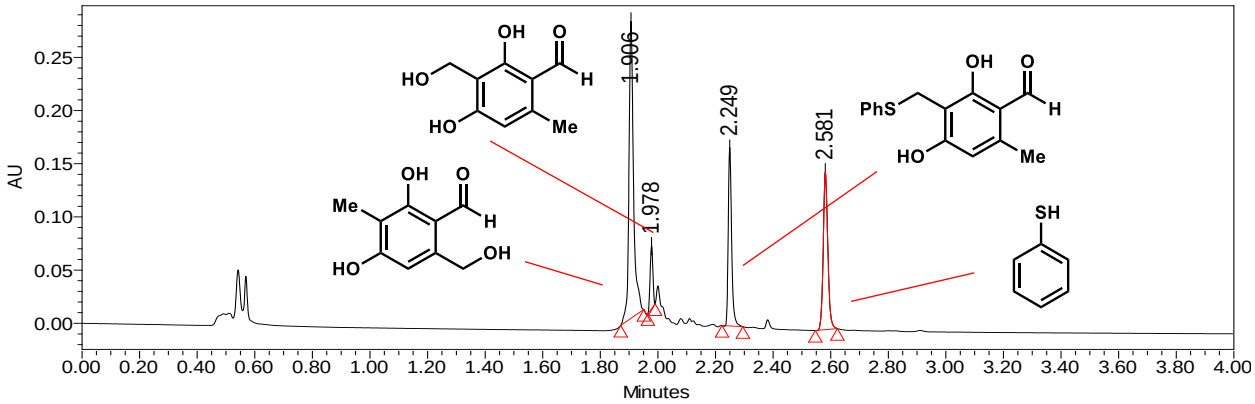


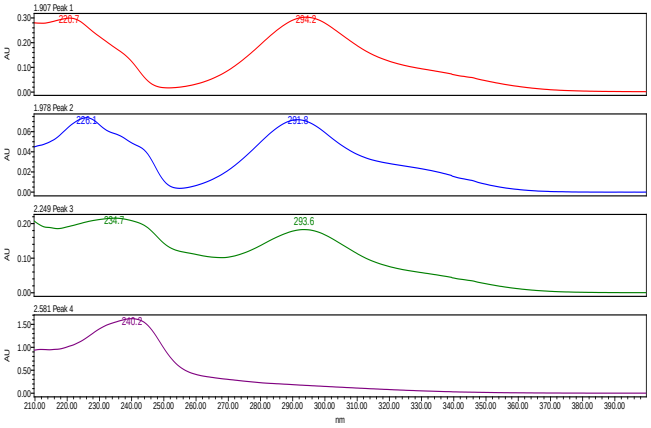


| | Retention Time | Area | % Area | Height |
|---|---|---|---|---|
| 1 | 1.906 | 309186 | 47.62 | 279592 |
| 2 | 1.978 | 39410 | 6.07 | 59128 |
| 3 | 2.249 | 136155 | 20.97 | 167599 |
| 4 | 2.581 | 164504 | 25.34 | 148190 |

## Product Standard

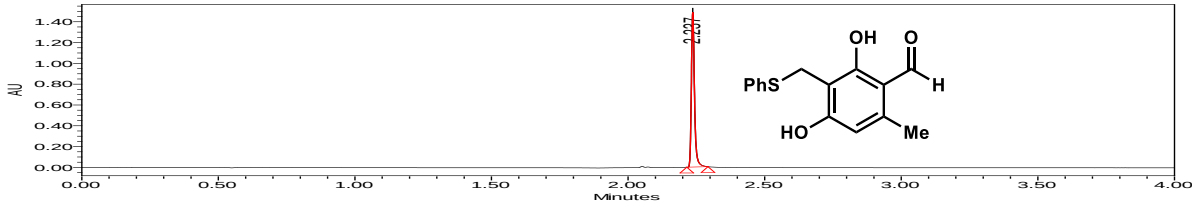


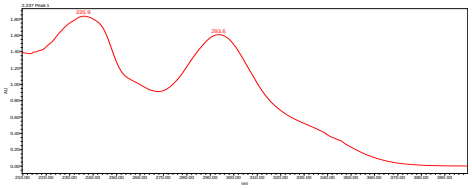

| | Retention Time | Area | % Area | Height |
|---|---|---|---|---|
| 1 | 2.237 | 1179174 | 100.00 | 1486508 |

**Figure 2.S65. Generation of 2.81 by *in situ* functionalization of benzylic alcohol 2.27.**
PDA traces of enzymatic reaction analyzed at 300 nm.

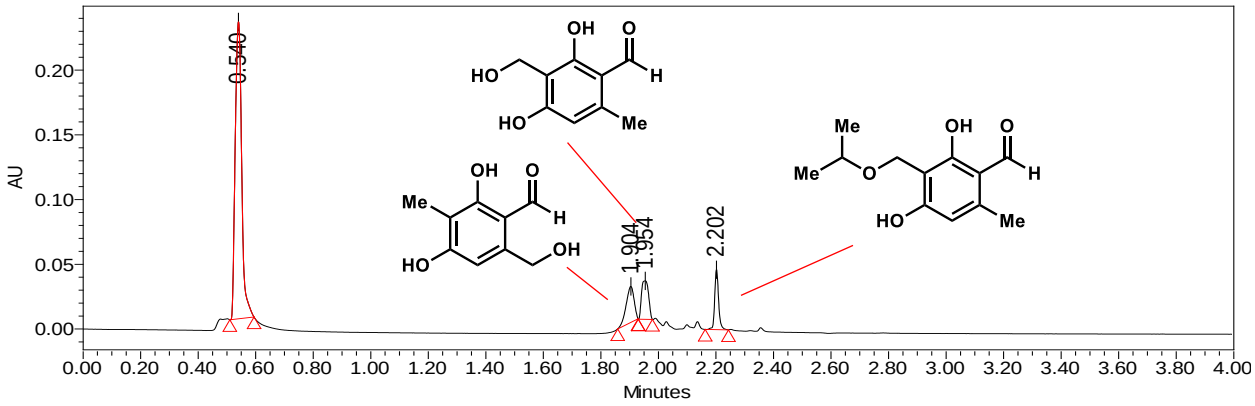


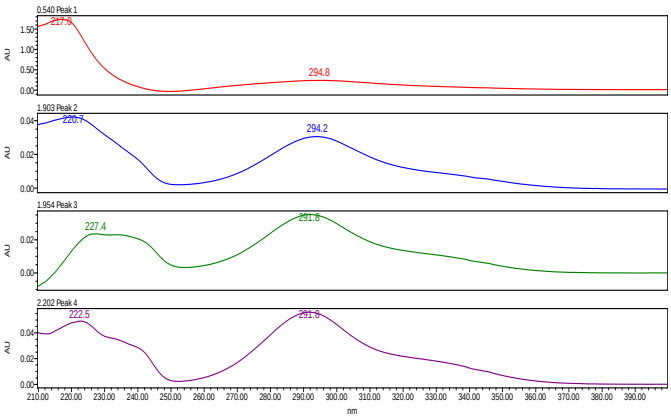


| | Retention Time | Area | % Area |
|---|---|---|---|
| 1 | 0.540 | 358000 | 70.88 |
| 2 | 1.904 | 53153 | 10.52 |
| 3 | 1.954 | 50460 | 9.99 |
| 4 | 2.202 | 43458 | 8.60 |

## Product Standard

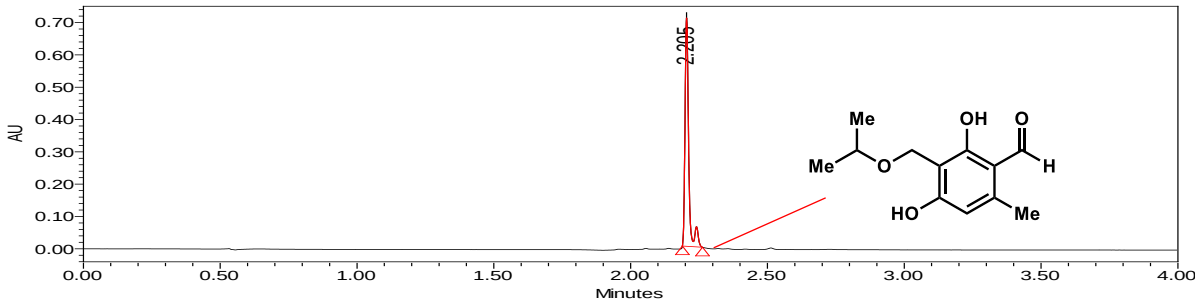


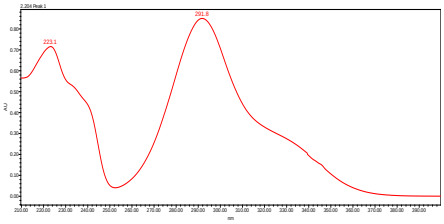


| | Retention Time | Area | % Area |
|---|---|---|---|
| 1 | 2.205 | 663414 | 100.00 |

**Figure 2.S66. Generation of 2.80 by *in situ* functionalization of benzylic alcohol 2.27.**
PDA traces of enzymatic reaction analyzed at 300 nm.

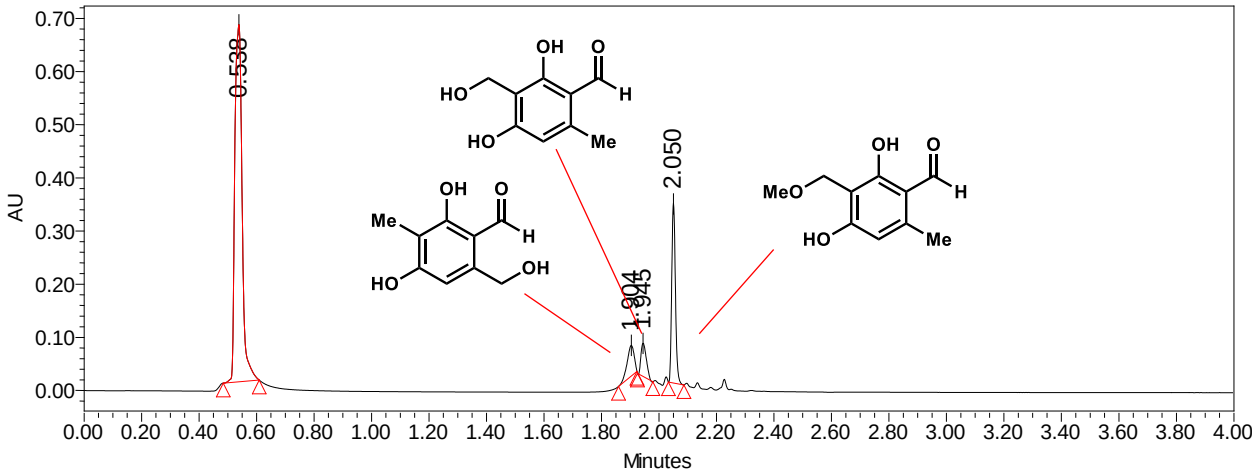


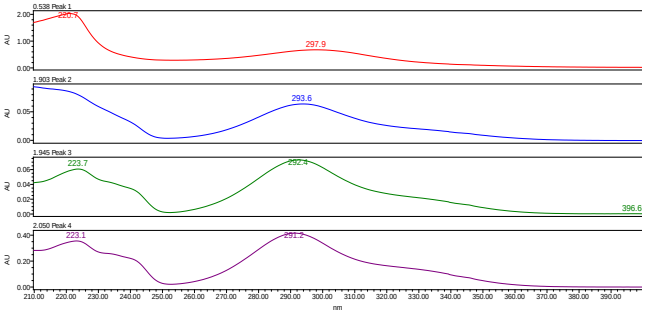


| | Retention Time | Area | % Area | Height |
|---|---|---|---|---|
| 1 | 0.538 | 1178917 | 71.01 | 671933 |
| 2 | 1.904 | 97978 | 5.90 | 57828 |
| 3 | 1.945 | 82146 | 4.95 | 62552 |
| 4 | 2.050 | 301185 | 18.14 | 338785 |

## Product Standard

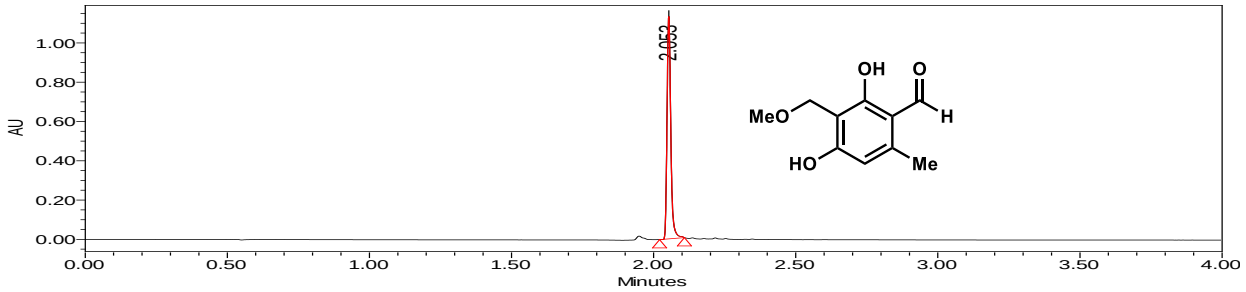


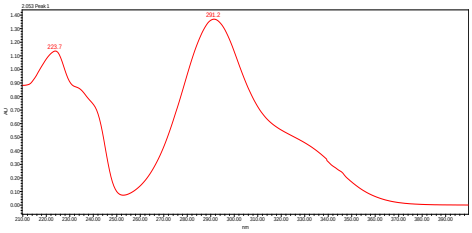


| | Retention Time | Area | % Area | Height |
|---|---|---|---|---|
| 1 | 2.053 | 1038651 | 100.00 | 1131436 |

**Figure 2.S67. Generation of 2.82 by *in situ* functionalization of benzylic alcohol 2.27.**
PDA traces of enzymatic reaction analyzed at 300 nm.

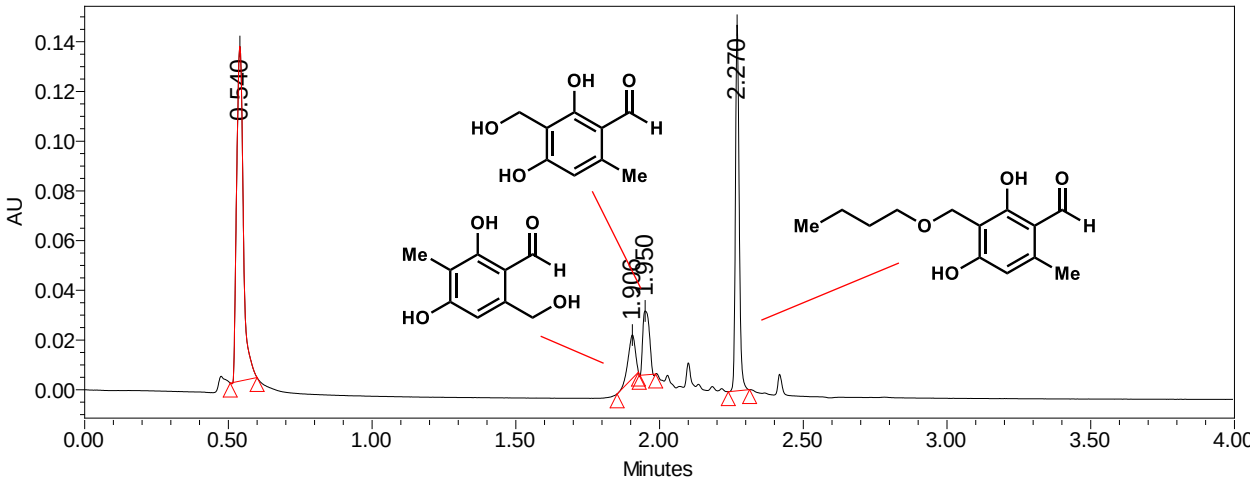


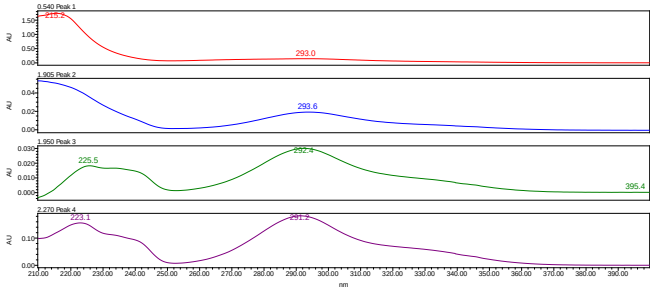

| | Retention Time | Area | % Area | Height |
|---|---|---|---|---|
| 1 | 0.540 | 217704 | 51.57 | 134654 |
| 2 | 1.906 | 30105 | 7.13 | 17480 |
| 3 | 1.950 | 41174 | 9.75 | 25714 |
| 4 | 2.270 | 133156 | 31.54 | 147141 |

## Product Standard

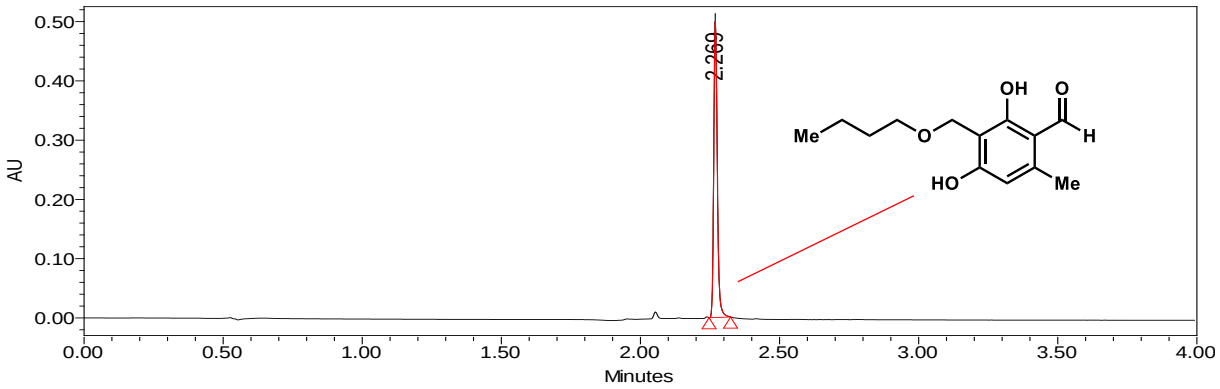


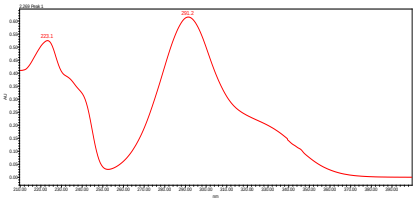

| | Retention Time | Area | % Area | Height |
|---|---|---|---|---|
| 1 | 2.269 | 445637 | 100.00 | 499328 |

**Figure 2.S68. Generation of 2.84 by *in situ* functionalization of benzylic alcohol 2.27.**
PDA traces of enzymatic reaction analyzed at 300 nm.

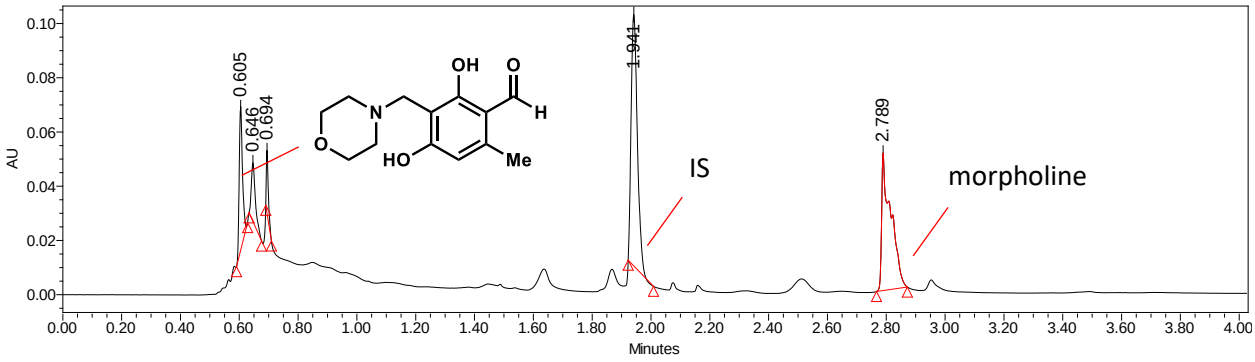


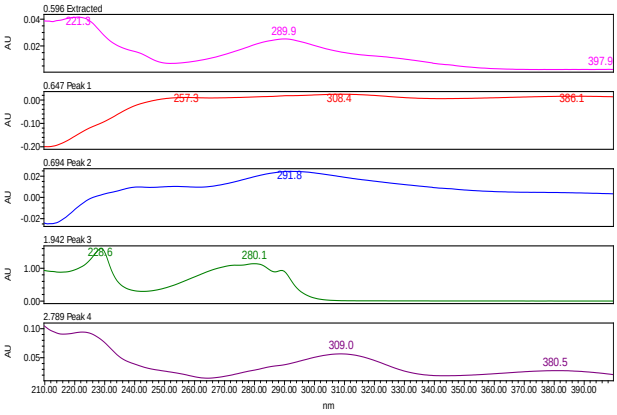


| | Retention Time | Area | % Area |
|---|---|---|---|
| 1 | 0.605 | 37602 | 10.48 |
| 2 | 0.646 | 27255 | 7.60 |
| 3 | 0.694 | 22399 | 6.24 |
| 4 | 1.941 | 163933 | 45.70 |
| 5 | 2.789 | 107496 | 29.97 |

**Product Standard (300 nm)**

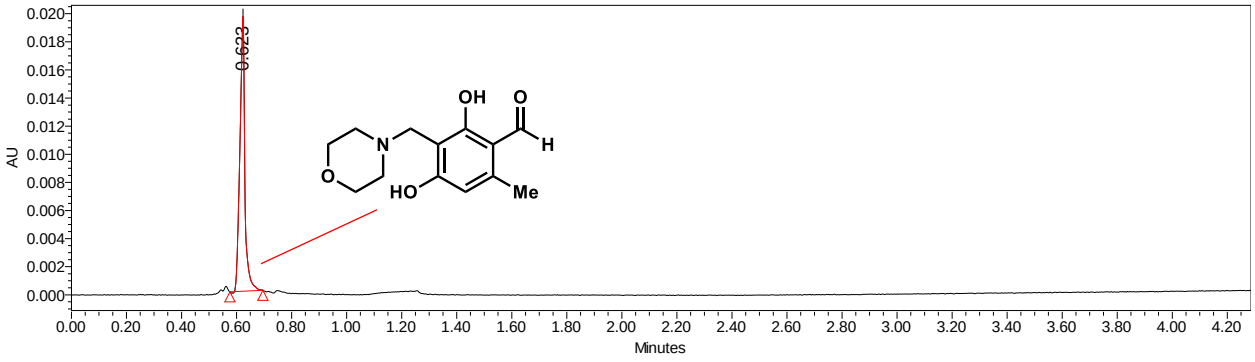


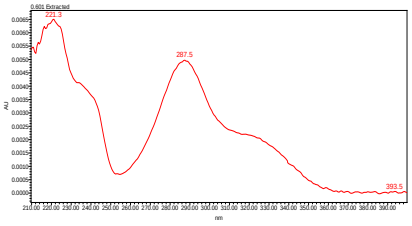


| | Retention Time | Area | % Area |
|---|---|---|---|
| 1 | 0.623 | 24886 | 100.00 |

**Figure 2.S69. Generation of 2.85 and 2.86 by *in situ* functionalization of benzylic alcohol 2.27.** PDA traces of enzymatic reaction analyzed at 300 nm.

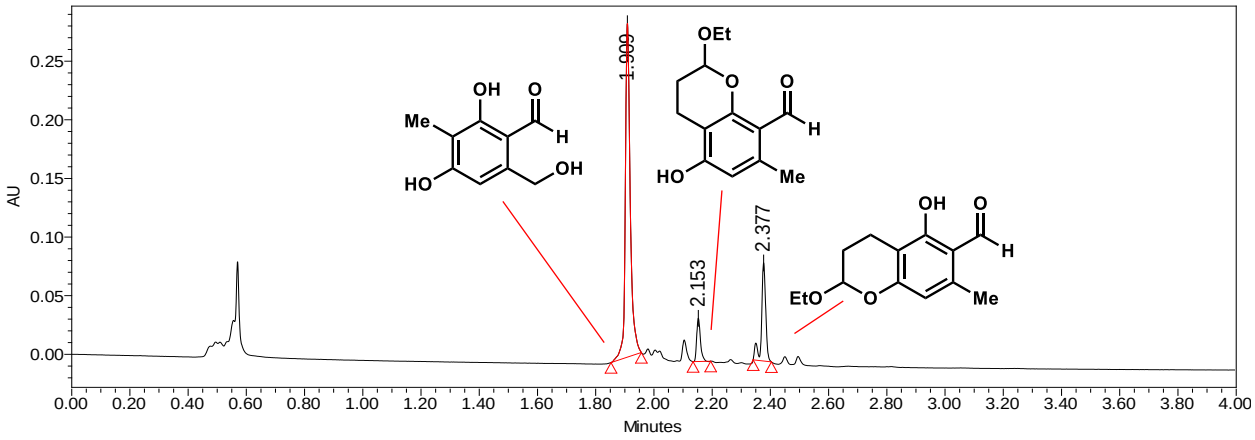


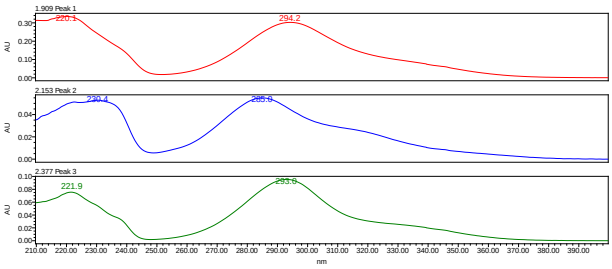


| | Retention Time | Area | % Area | Height |
|---|---|---|---|---|
| 1 | 1.909 | 337063 | 73.92 | 284770 |
| 2 | 2.153 | 33190 | 7.28 | 36905 |
| 3 | 2.377 | 85721 | 18.80 | 83776 |

**Product Standard A (300 nm)**

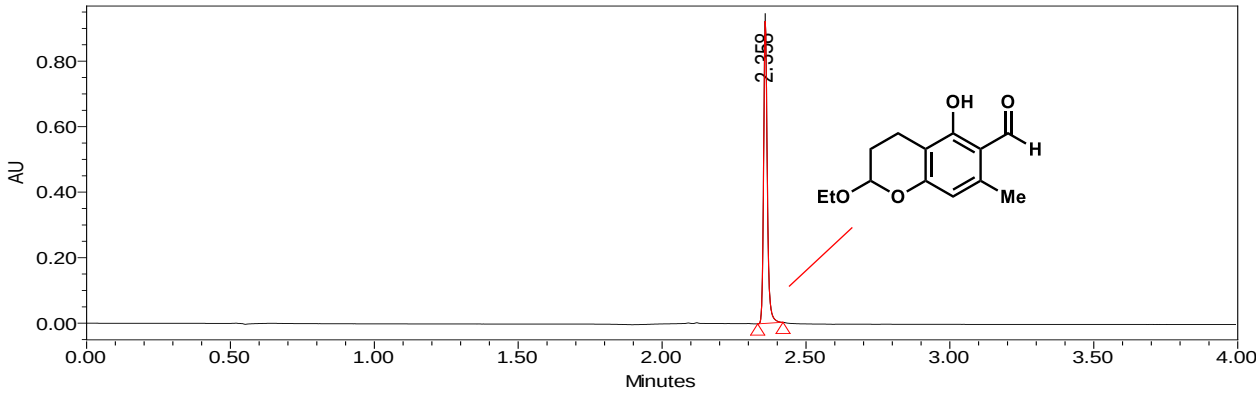


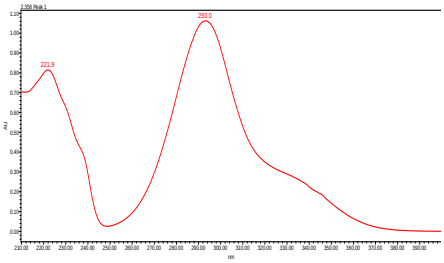


| | Retention Time | Area | % Area | Height |
|---|---|---|---|---|
| 1 | 2.358 | 623683 | 100.00 | 736773 |

## Product Standard B (300 nm)

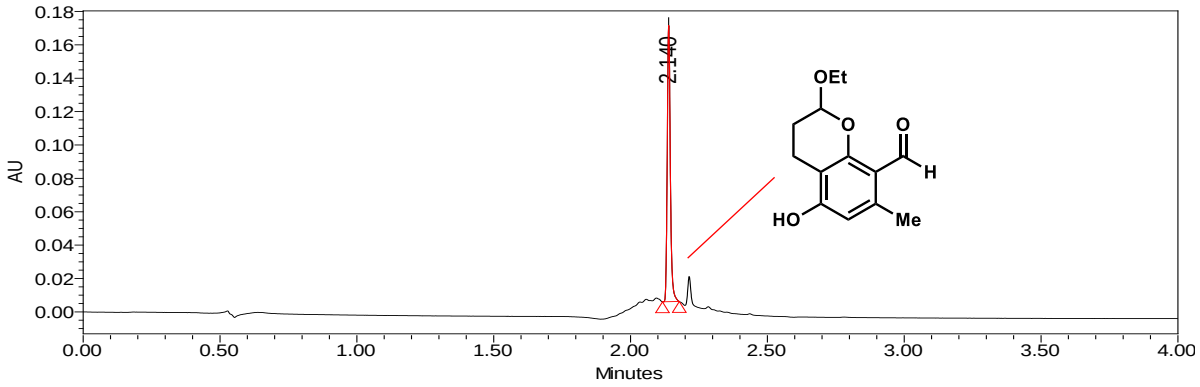


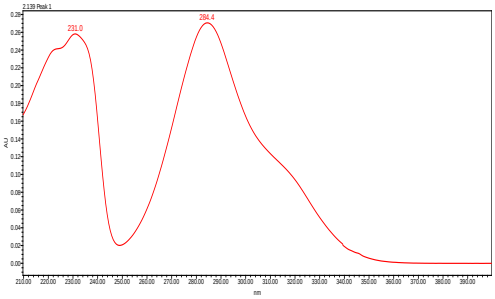


| | Retention Time | Area | % Area | Height |
|---|---|---|---|---|
| 1 | 2.140 | 129934 | 100.00 | 165772 |

**Figure 2.S70. Generation of 2.87 and 2.88 by *in situ* functionalization of benzylic alcohol 2.27.** PDA traces of enzymatic reaction analyzed at 300 nm.

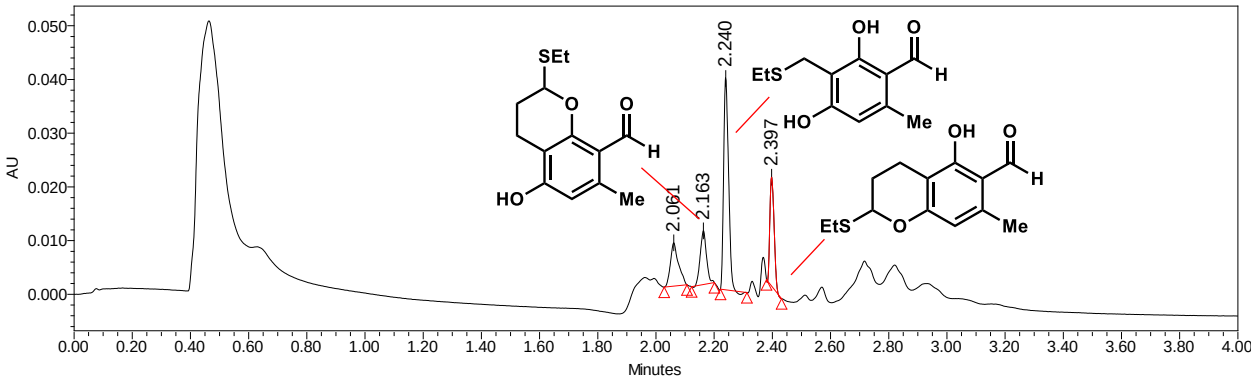


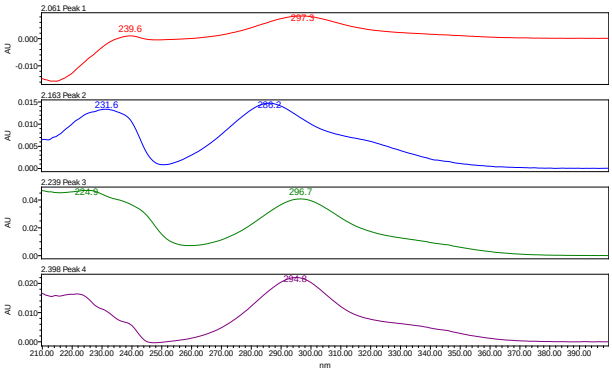


| | Retention Time | Area | % Area | Height |
|---|---|---|---|---|
| 1 | 2.061 | 15479 | 15.72 | 8080 |
| 2 | 2.163 | 15048 | 15.28 | 10019 |
| 3 | 2.240 | 47127 | 47.86 | 39579 |
| 4 | 2.397 | 20805 | 21.13 | 20289 |

## Product Standard A (300 nm)

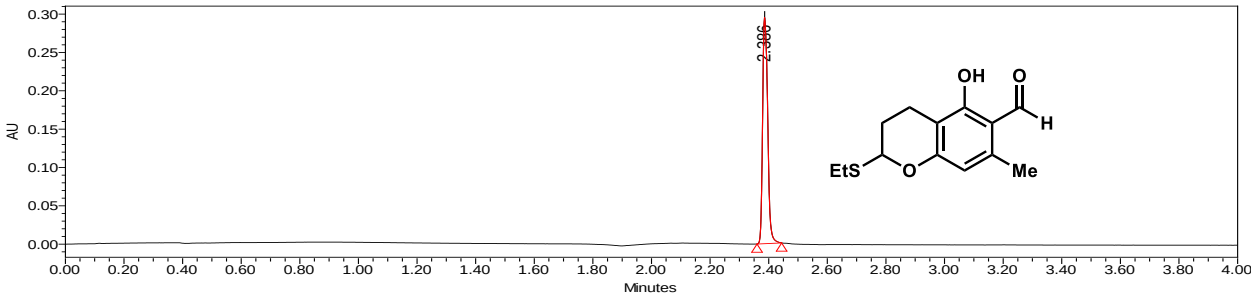


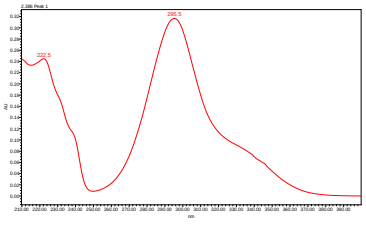

## Product Standard B (280 nm)

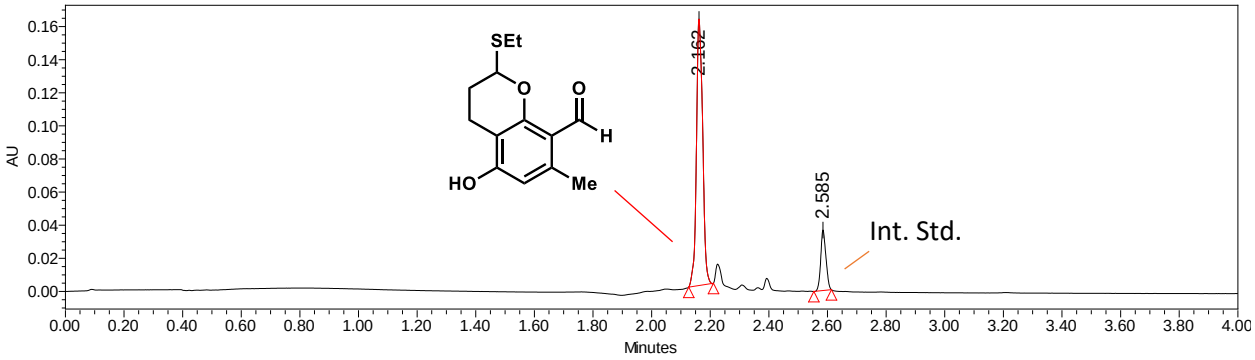


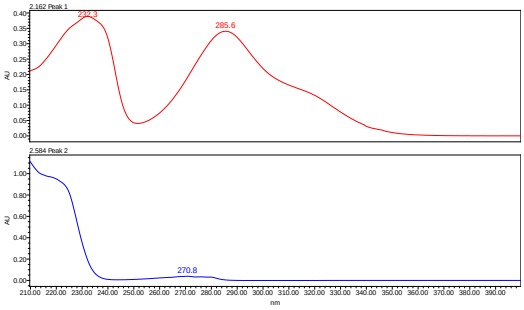


| | Retention Time | Area | % Area | Height |
|---|---|---|---|---|
| 1 | 2.162 | 237852 | 84.14 | 160927 |
| 2 | 2.585 | 44841 | 15.86 | 36598 |

**Figure 2.S71. Generation of 2.89 and 2.90 by *in situ* functionalization of benzylic alcohol 2.27.** PDA traces of enzymatic reaction analyzed at 300 nm.

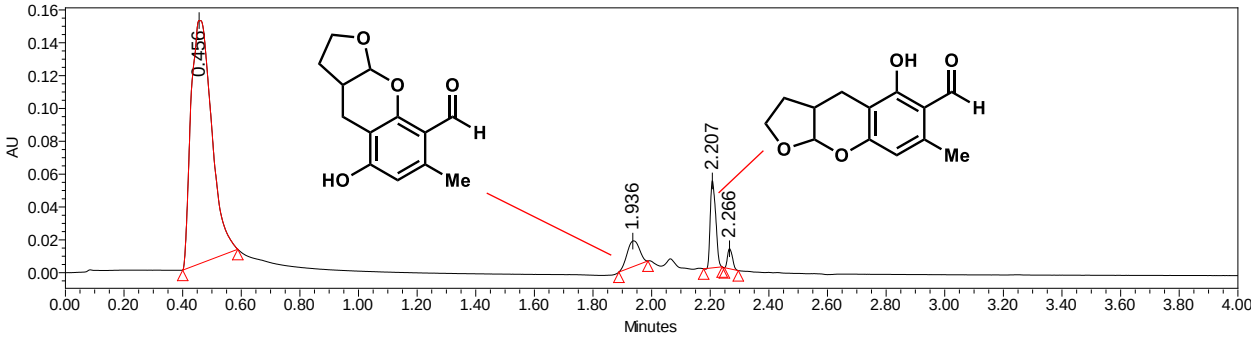


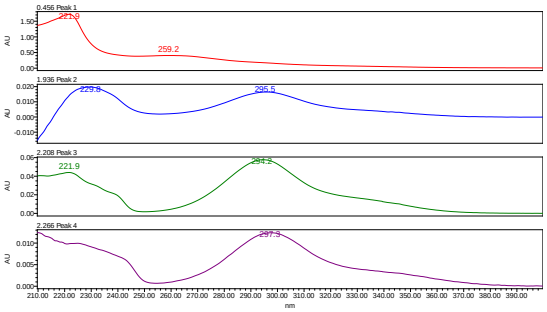


| | Retention Time | Area | % Area | Height |
|---|---|---|---|---|
| 1 | 0.456 | 727787 | 84.98 | 148137 |
| 2 | 1.936 | 45573 | 5.32 | 15630 |
| 3 | 2.207 | 68820 | 8.04 | 53066 |
| 4 | 2.266 | 14250 | 1.66 | 12202 |

**Product Standard A (300 nm)**

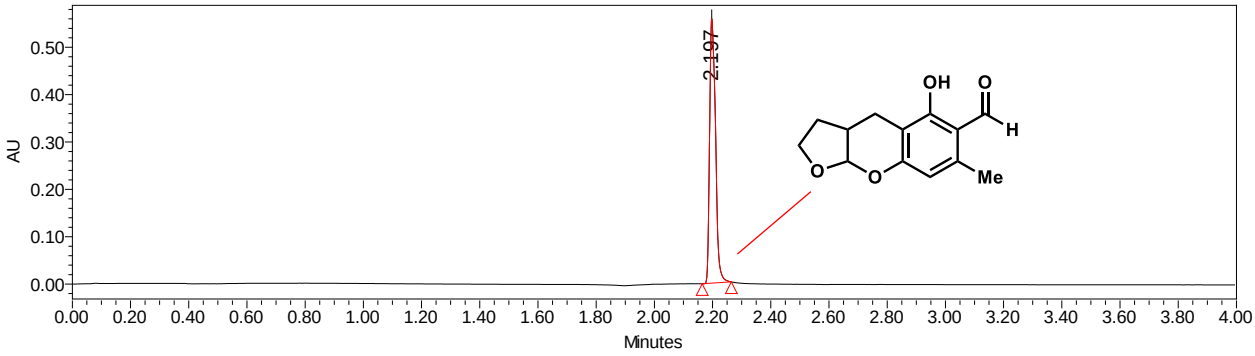


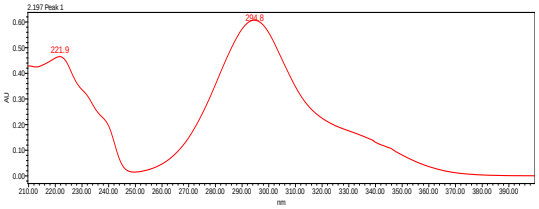


| | Retention Time | Area | % Area | Height |
|---|---|---|---|---|
| 1 | 2.197 | 786523 | 100.00 | 559085 |

**Figure 2.S72. Synthesis of (-)-xyloketal D (2.25) and the diastereomer of (-)-xyloketal D 2.101 by *in situ* functionalization of benzylic alcohol 2.68.**
PDA traces of enzymatic reaction analyzed at 300 nm.

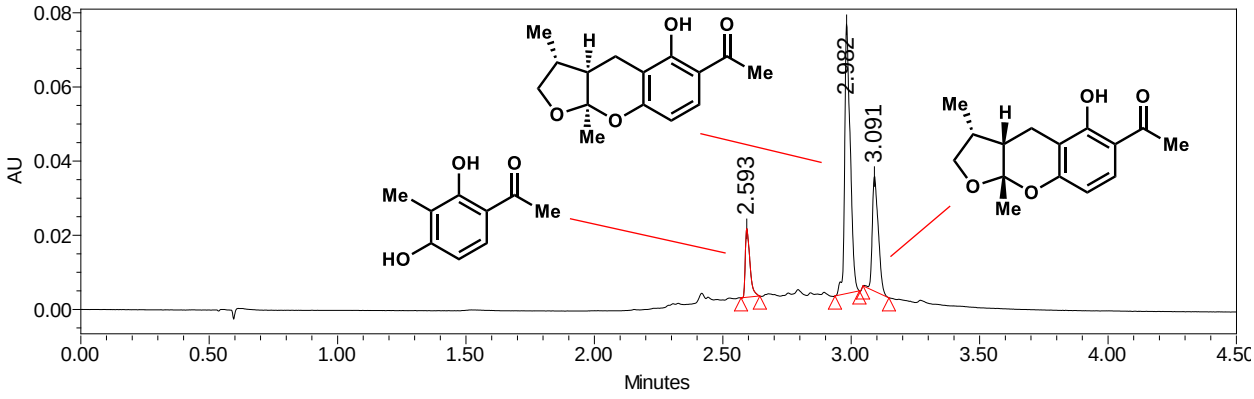


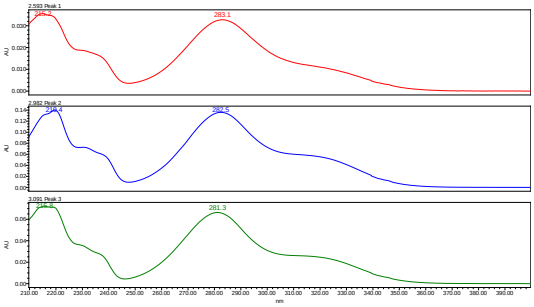

| | Retention Time | Area | % Area | Height |
|---|---|---|---|---|
| 1 | 2.594 | 15629 | 11.31 | 12596 |
| 2 | 2.982 | 81309 | 58.82 | 57927 |
| 3 | 3.091 | 41299 | 29.88 | 25902 |

**Product standard: (-)-xyloketal D**

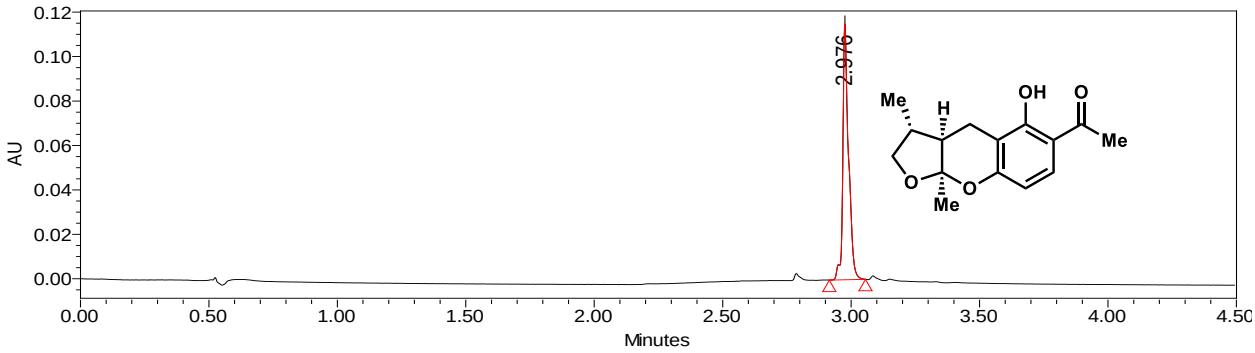


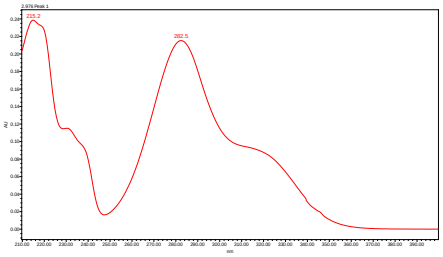

| | Retention Time | Area | % Area | Height |
|---|---|---|---|---|
| 1 | 2.976 | 177894 | 100.00 | 115101 |

**Product standard: diastereomer of (-)-xyloketal D**

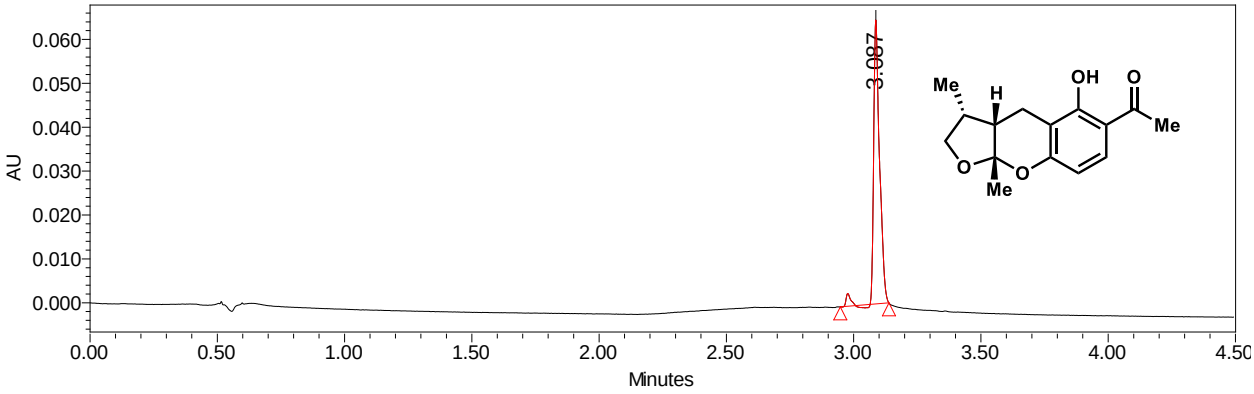


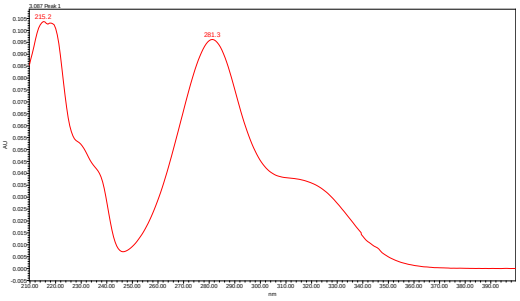


| | Retention Time | Area | % Area | Height |
|---|---|---|---|---|
| 1 | 3.087 | 108813 | 100.00 | 64723 |

**Part X. LC/MS traces for CitB benzylic functionalization cascade reactions**

**Figure 2.S73. Generation of 2.93 and 2.94 by in situ functionalization of benzylic alcohol 2.27.**

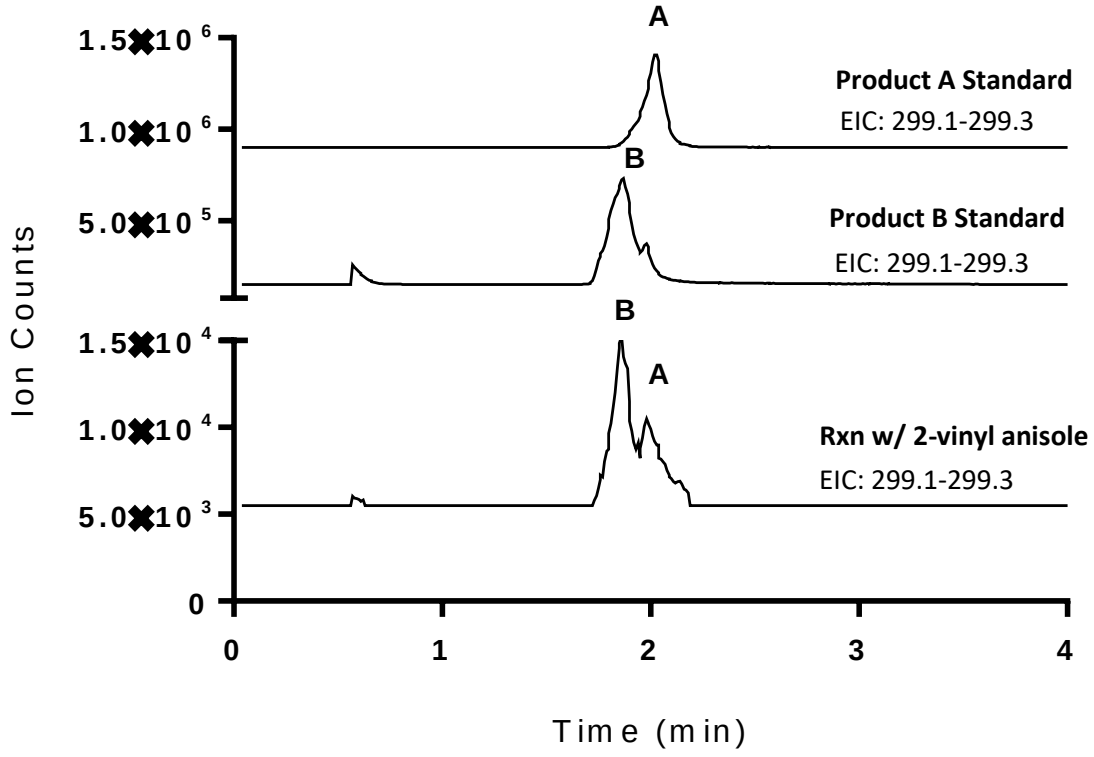


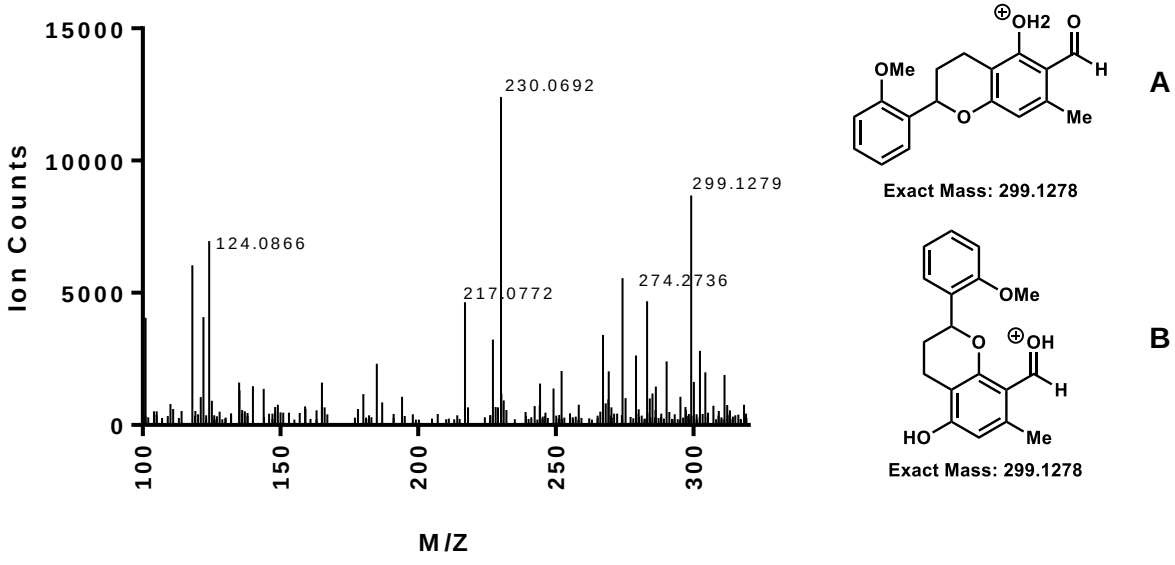


**Mass spectrum of reaction with 2-vinylanisole**

**Figure 2.S74. Generation of 2.91 and 2.92 by in situ functionalization of benzylic alcohol 2.27**.

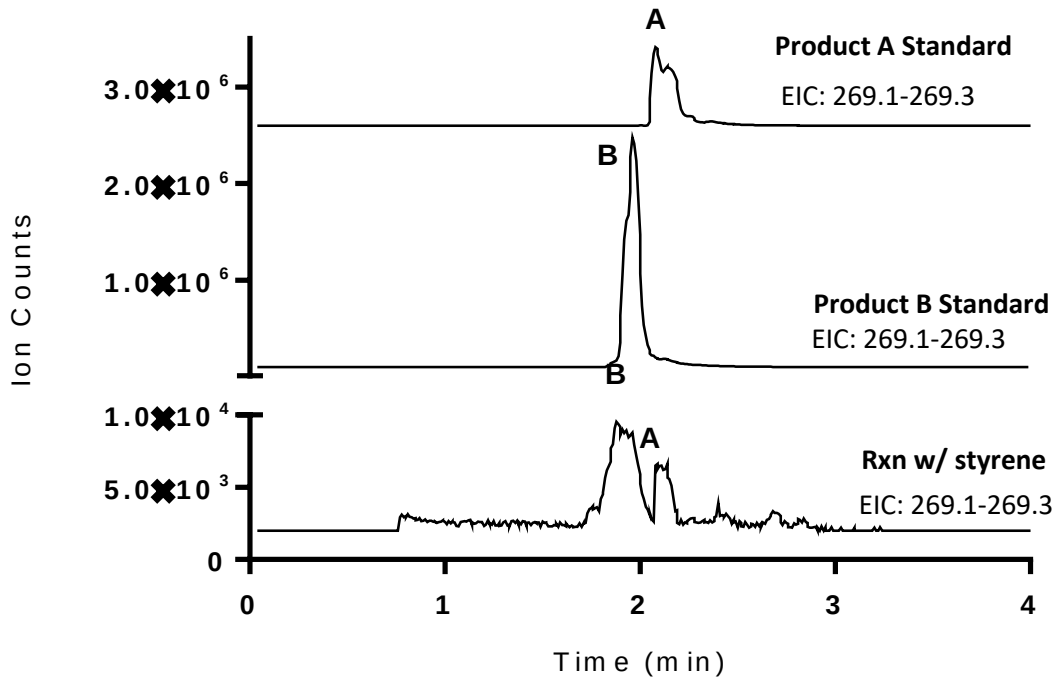


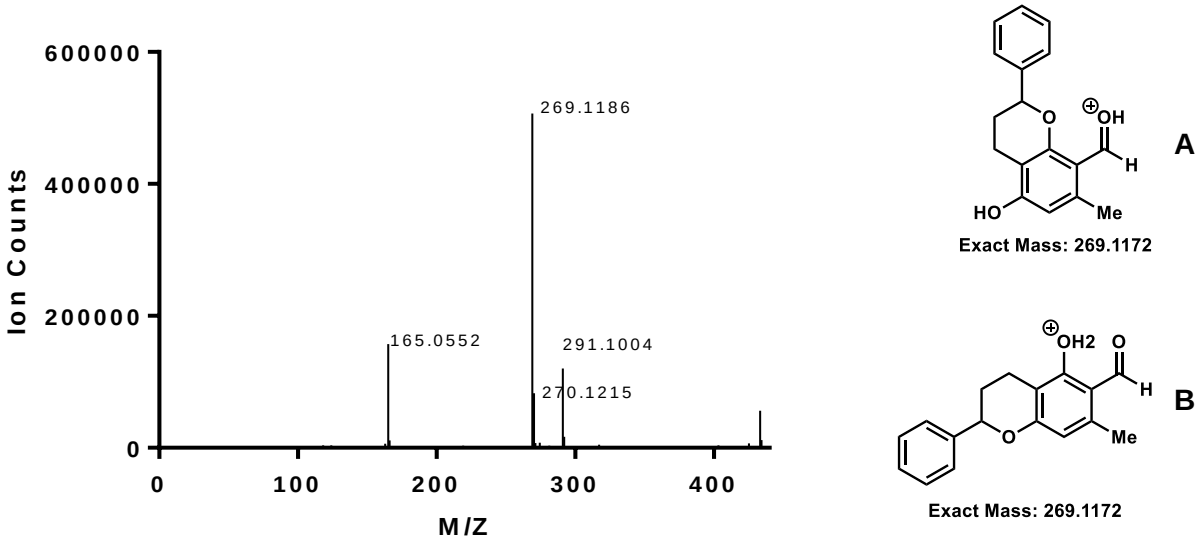


**Mass spectrum of reaction with styrene**

**Figure 2.S75. Generation of 2.95 and 2.96 by in situ functionalization of benzylic alcohol 2.27.**

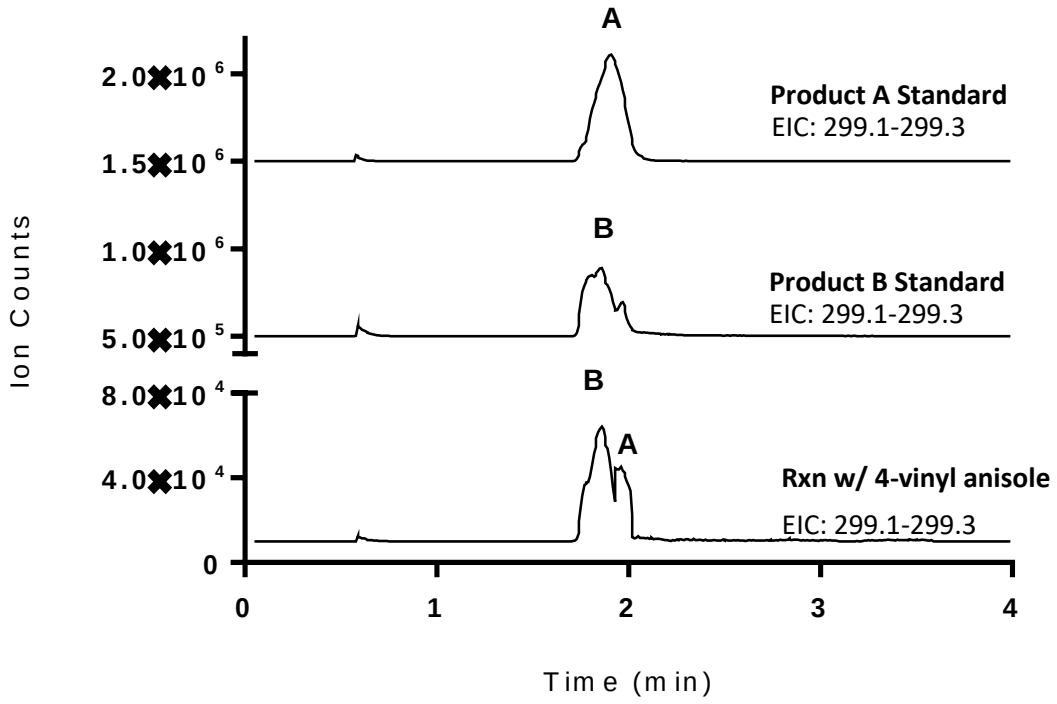


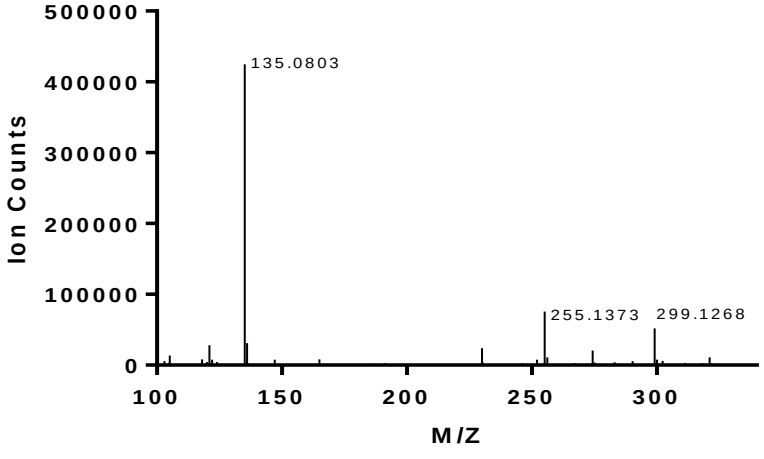


Mass spectrum of reaction with 4-vinyl anisole

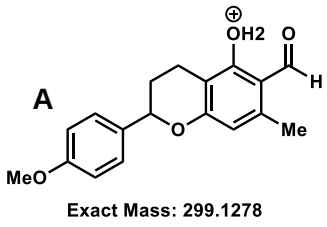


Exact Mass: 299.1278

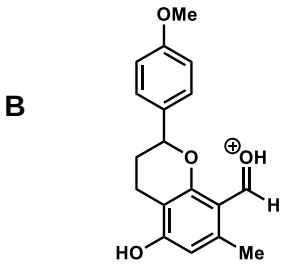


Exact Mass: 299.1278

**Part XI. LC/MS traces for peptide functionalization reactions**

Sequence of peptides used in this study:

Peptide A. Ac-Tyr-βAla-Phe-Ala-Glu-Arg-Arg-Phe-Cys-Pro-Phe-Ala-Glu-Arg-$NH_2$

Peptide B. Ac-Tyr-βAla-Phe-Ala-Glu-Arg-Arg-Phe-Lys-Pro-Phe-Ala-Glu-Arg-$NH_2$

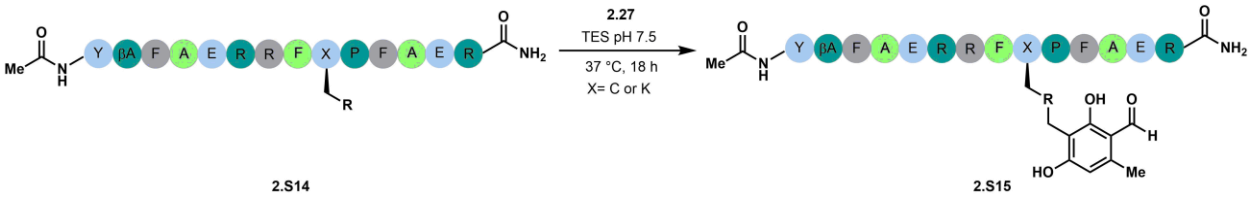


**Figure 2.S76. Functionalization of peptides with CitB-generated benzylic alcohol 2.27.**

**Analytical-scale peptide reactions:** Each reaction contained 50 mM TES buffer pH 7.5 (2.5 µL of a 1 M solution), 50 µM peptide (1 µL of a 2.5 mM stock in DMSO), 200 µM (4 equiv) benzylic alcohol (**2.27**, 1 µL of a 10 mM stock in DMSO) and Milli-Q water to a final volume of 50 µL. Reactions were performed (in duplicate) at 37 °C for 18 h before diluting the reaction with Milli-Q water (with 1% v/v formic acid) to a final concentration of 10 µM peptide. Reactions were analyzed by LC/MS using the method described below for peptide analysis. Peptide reactions were quantified by analyzing the extracted ion chromatogram for the area under the curve (AUC) for product/total AUC (product AUC + starting material AUC). All reactions were performed in duplicate and percent conversion determined as an average of those trials.

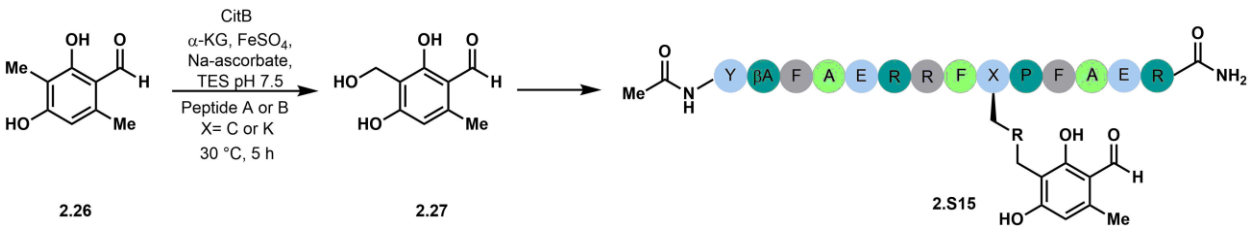


**Figure 2.S77. One-pot CitB-catalyzed hydroxylation and peptide functionalization.**

**Procedure for one-pot CitB-catalyzed hydroxylation and peptide functionalization reactions:** CitB-catalyzed benzylic functionalization and *in situ* peptide functionalization was performed under the following conditions: 50 µL total reaction volume, 1 µM CitB, 50 mM TES (pH 7.5), 0.2 mM substrate, 0.4 mM α-ketoglutaric acid, 8 mM sodium ascorbate, 0.1 mM ferrous sulfate, 50 µM peptide, and Milli-Q water to obtain a total volume of 50 µL. The reaction was incubated for 5 h at 37°C before the addition of 200 µL 1% (v/v) formic acid in water to quench the reaction. The reactions were then analyzed by LC/MS (Q-TOF) using the method described below for peptide analysis. Peptide reactions were quantified by analyzing the extracted ion chromatogram for the area under the curve (AUC) for product/total AUC (product AUC + starting material AUC). All reactions were performed in duplicate and conversion determined as an average of those trials.

**LC-MS analysis of peptide reactions:** Peptide reactions were quenched with 1% (v/v) formic acid in dd$H_2O$ before analysis by LC/MS on an Agilent 1290 Series Infinity HPLC with a 6545 Series Quadrupole-Time-of-Flight mass spectrometer. Samples were analyzed on a Phenomenex Aeris 3.6 µm WIDEPORE C4 column (2.1 x 50 mm) under the following conditions: mobile phase (solvent A: dd$H_2O$ + 0.1% trifluoroacetic acid; solvent B: acetonitrile + 0.1% trifluoroacetic acid) gradient elution over 6 min (5% to 100% solvent B).

**Peptides and potential product masses**

**Peptide A:** Peptide **2.97** with ligandable cysteine residue

Ac-Tyr-βAla-Phe-Ala-Glu-Arg-Arg-Phe-Cys-Pro-Phe-Ala-Glu-Arg-$NH_2$

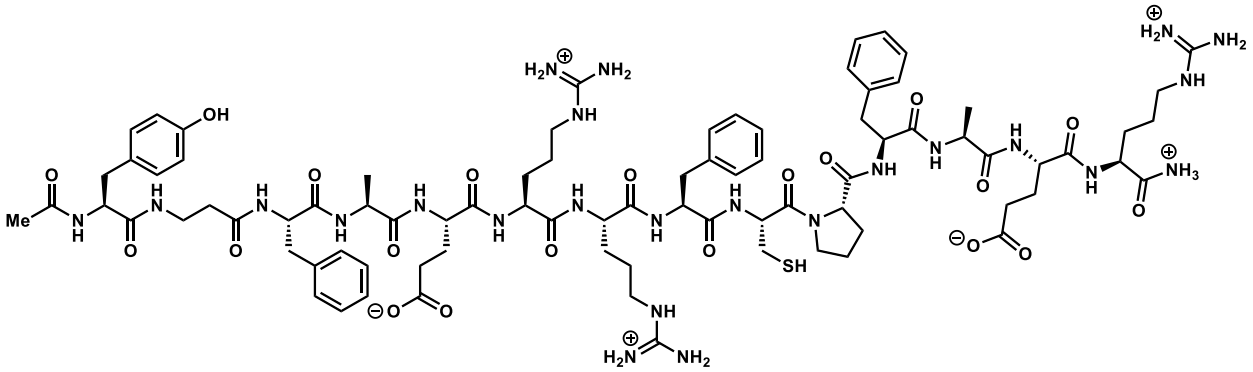


**Liganded peptide A:** Peptide **2.97** liganded with benzylic alcohol **2.27**.

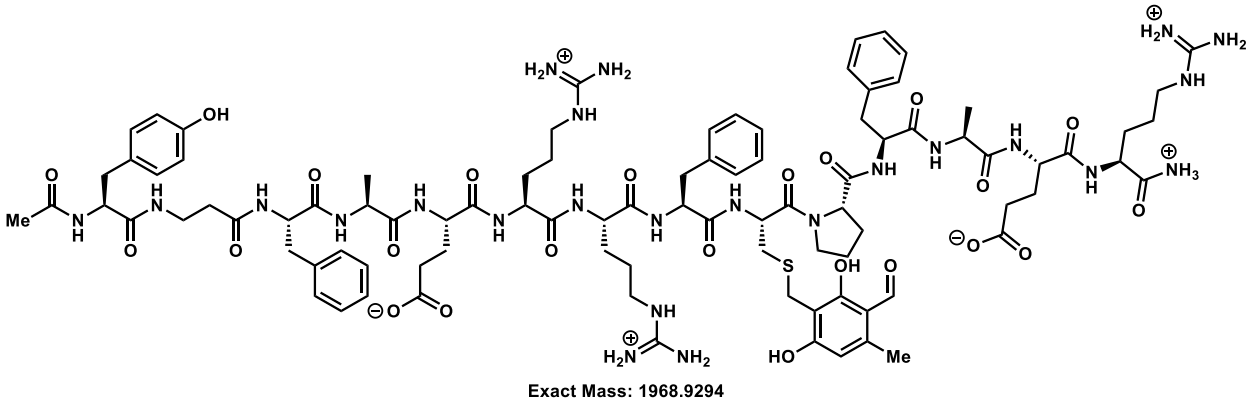

**Peptide B:** Peptide **without** ligandable cysteine residue (**2.S14**)

Ac-Tyr-βAla-Phe-Ala-Glu-Arg-Arg-Phe-Lys-Pro-Phe-Ala-Glu-Arg-$NH_2$

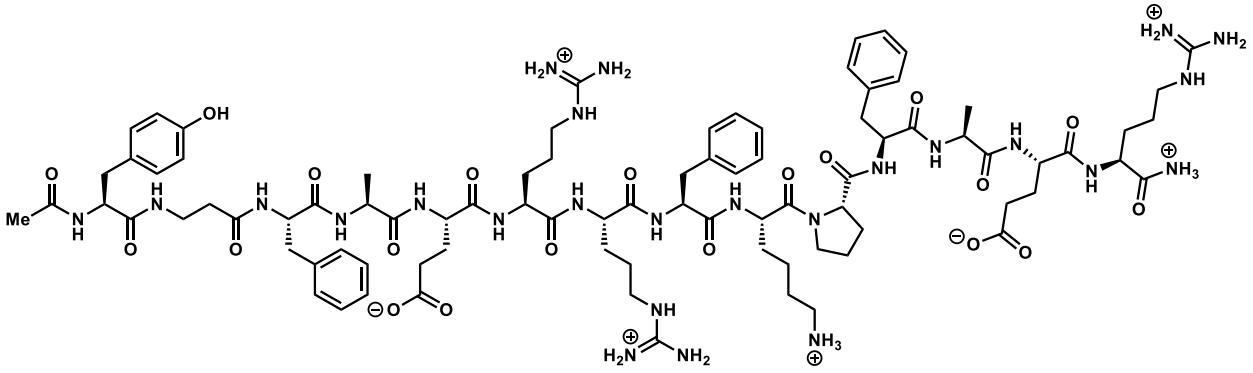

Exact Mass: 1830.9751

**Liganded Peptide B (imine condensation):** Peptide B liganded (**2.S15**) with benzylic alcohol **2.27**.

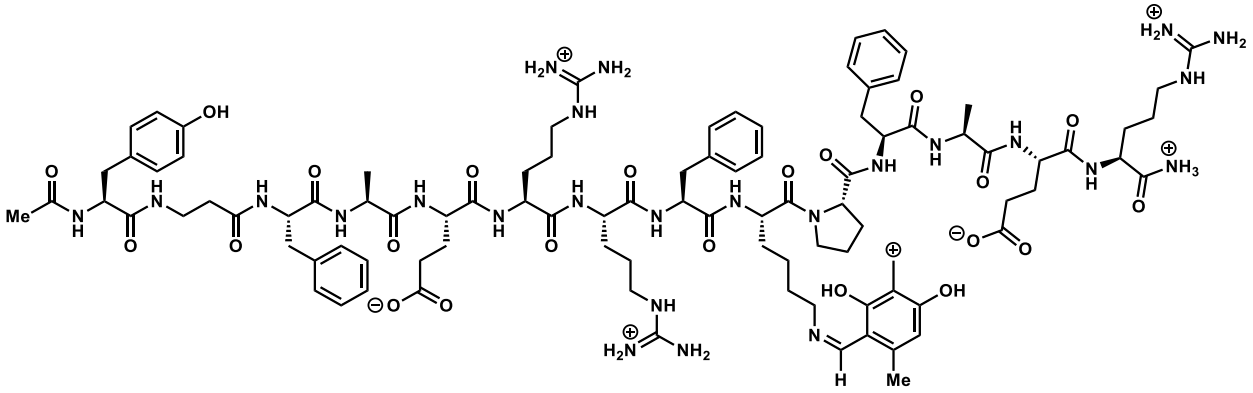

Exact Mass: 1977.0119

**Liganded peptide B (*ortho*-quinone methide):** Peptide B liganded (**2.S16**) with benzylic alcohol **2.27**.

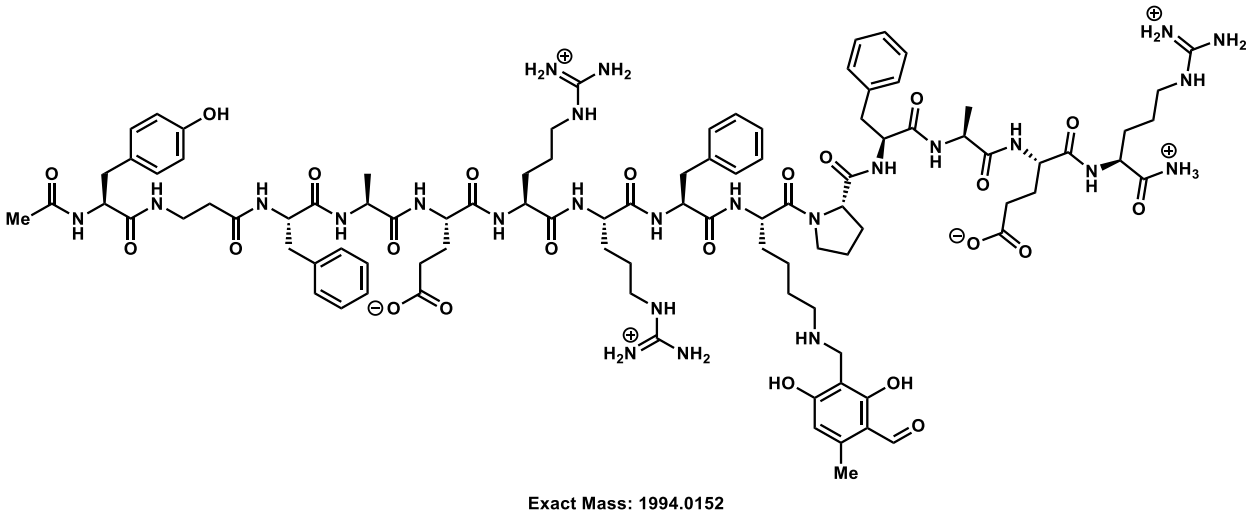


**Table 2.S2.** Calculated and observed peptide masses for peptide MS

| **Peptide** | **Predicted [M+H] mass** | **Predicted [(M/2Z)+H] mass** | **Observed mass (Deconvoluted)** |
|---|---|---|---|
| **Peptide A** | 1804.8820 | 902.4410 | 1804.870 |
| **Peptide A-liganded** | 1968.9294 | 984.4647 | 1968.919 |
| **Peptide B** | 1830.9751 | 915.4876 | 1830.860 |
| **Peptide B-liganded (imine condensation)** | 1977.0119 | 988.5059 | Not observed |
| **Peptide B-liganded (*o*-QM addition)** | 1994.0152 | 997.0076 | Not observed |

## LC-MS traces for peptide functionalization reactions

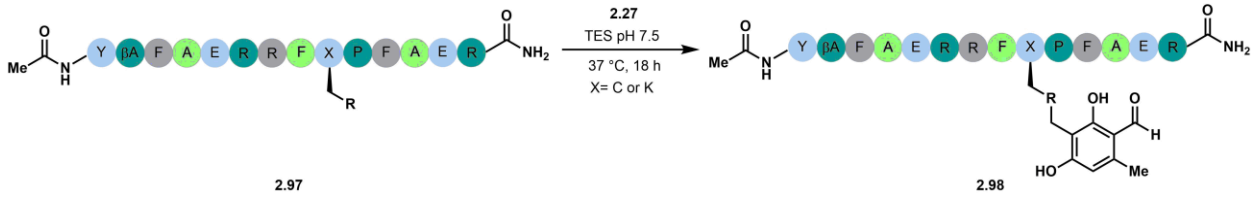


**Figure 2.S78. Functionalization of Peptide A (2.97) with benzylic alcohol 2.27.**
Extracted ion chromatograms (EICs) for expected product and starting material masses.

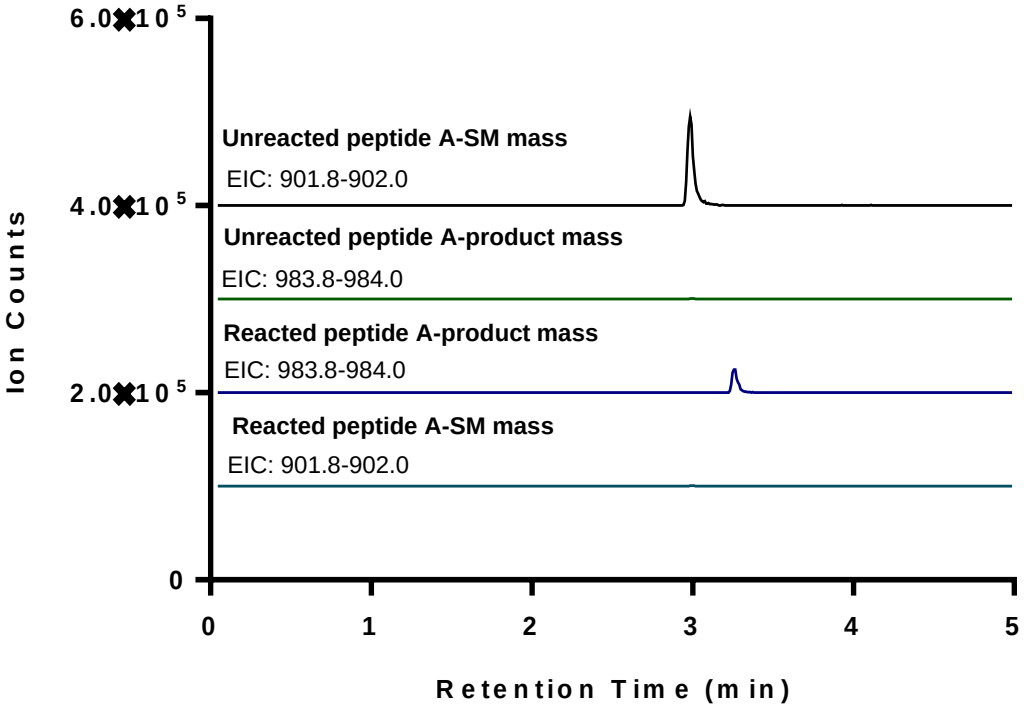

**Figure 2.S79. Functionalization of Peptide B (2.S14) with benzylic alcohol 2.27.**
Extracted ion chromatograms (EICs) for expected product and starting material masses.

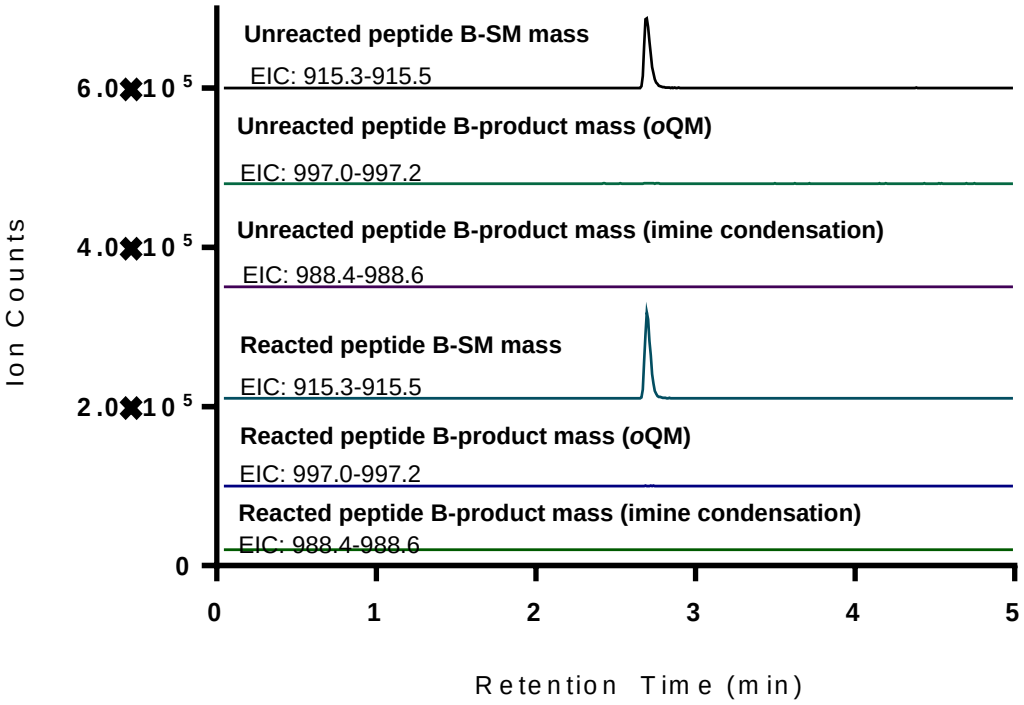

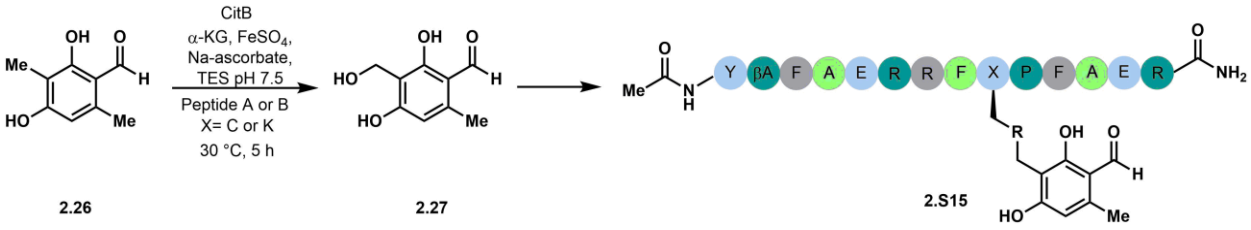


**Figure 2.S80. *In situ* functionalization of Peptide A (2.97) with CitB-generated benzylic alcohol 2.27.**
Extracted ion chromatograms (EICs) for expected product and starting material masses.

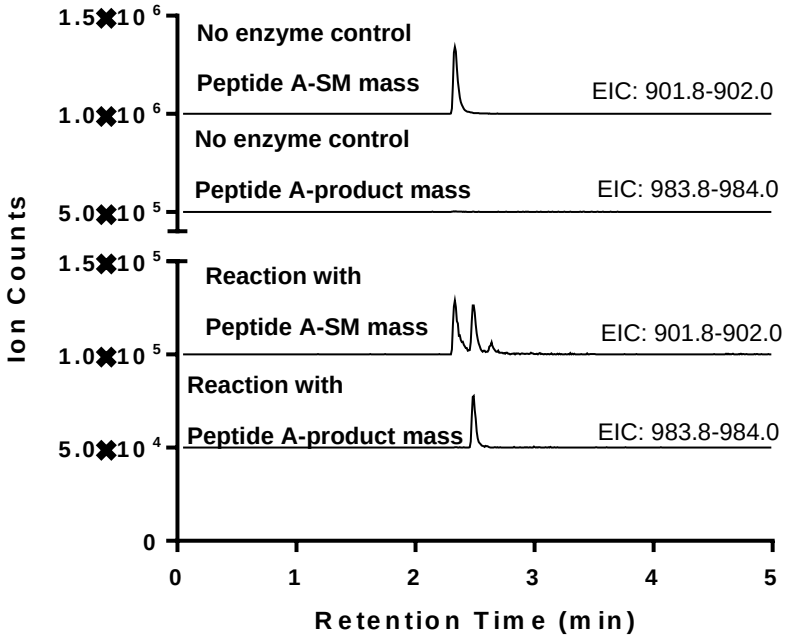

**Figure 2.S81. *In situ* functionalization of Peptide B (2.S14) with CitB-generated benzylic alcohol 2.27.**
Extracted ion chromatograms (EICs) for expected product and starting material masses.

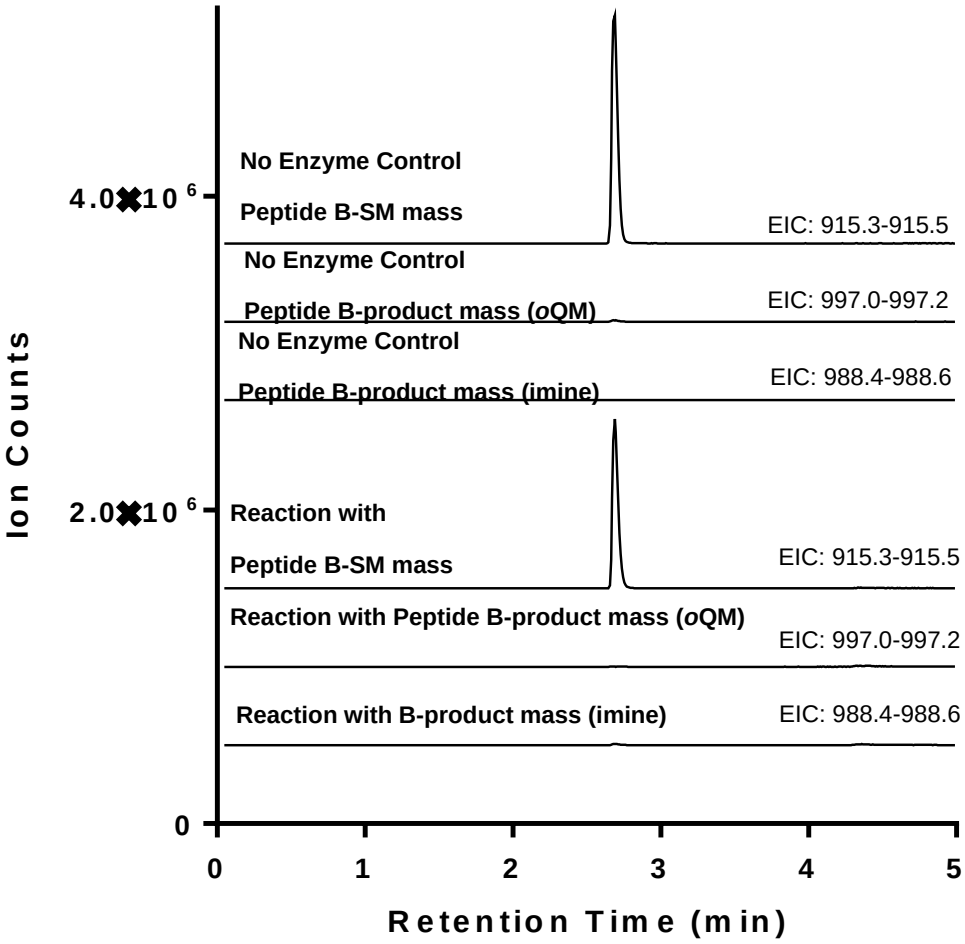

## Part XII. $^{1}H$ and $^{13}C$ NMR Spectra of Compounds

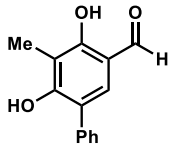


600 MHz, $CD_3OD$




150 MHz, $CD_3OD$

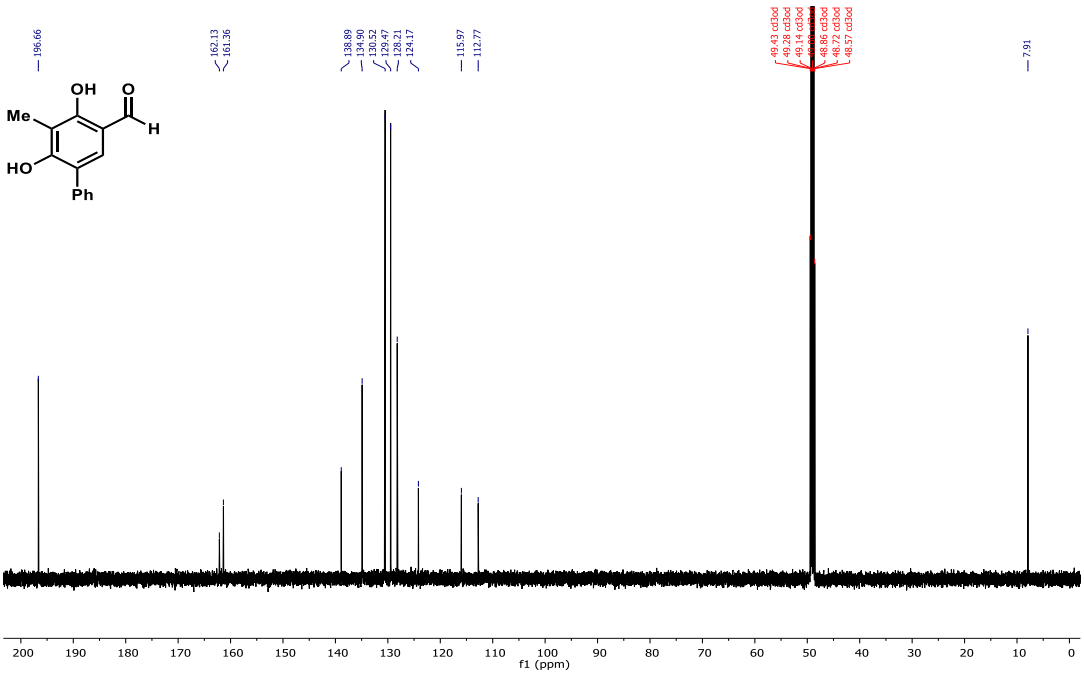

600 MHz, $CD_3OD$

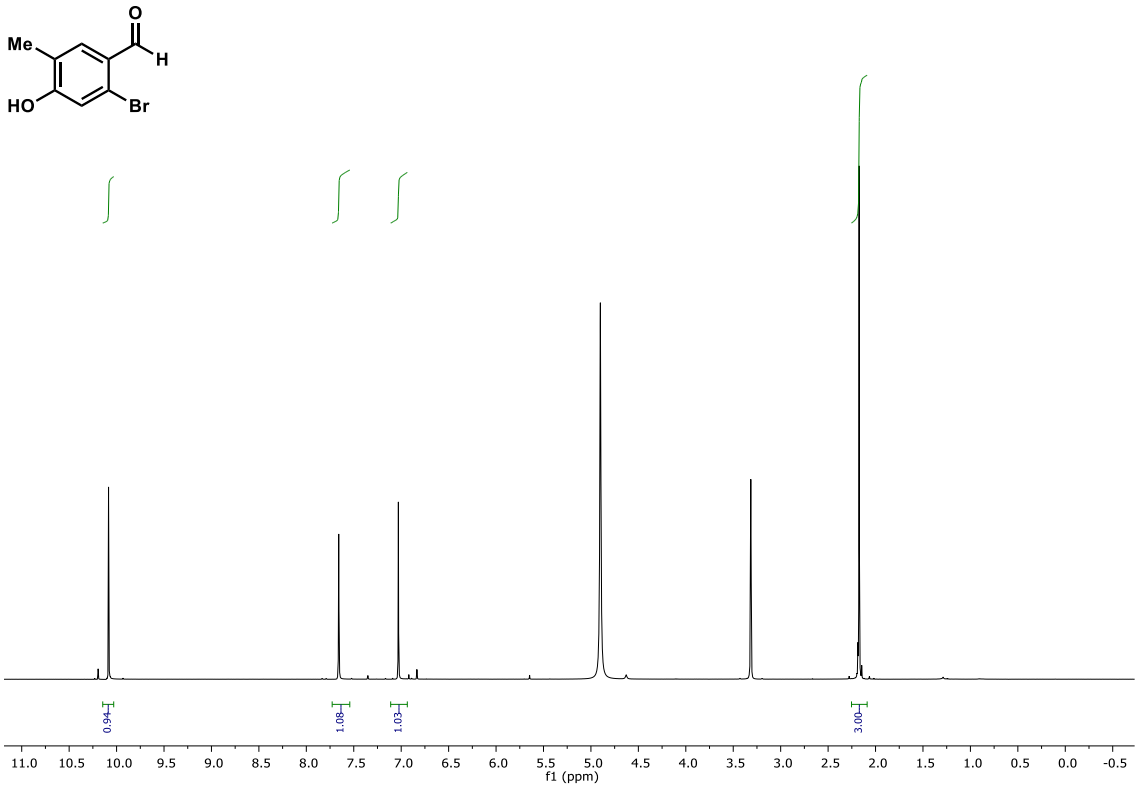


150 MHz, $CD_3OD$

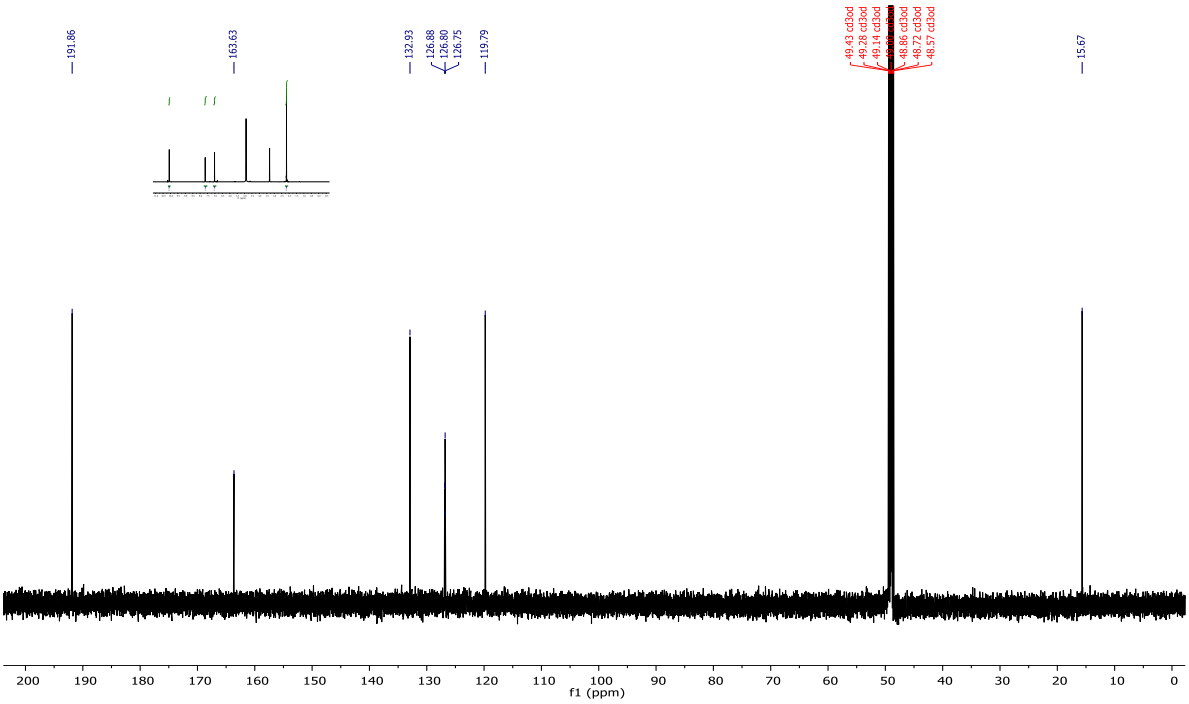

600 MHz, $CD_3OD$

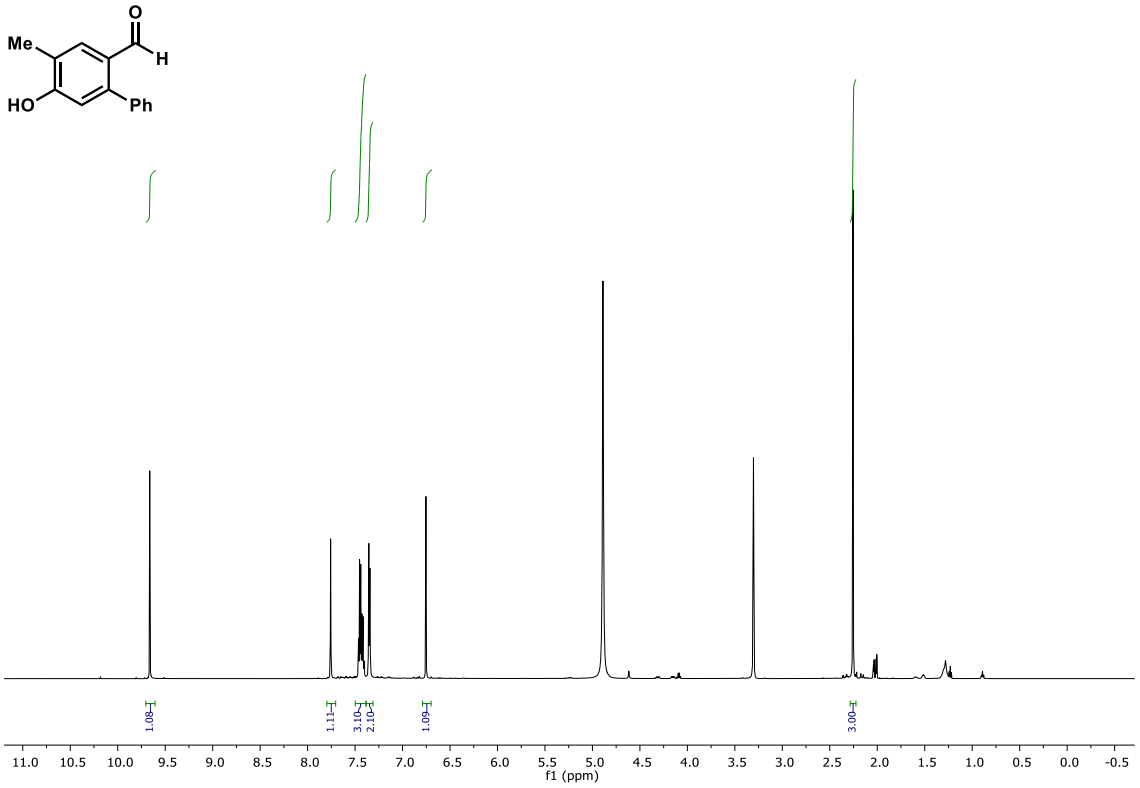


150 MHz, $CD_3OD$

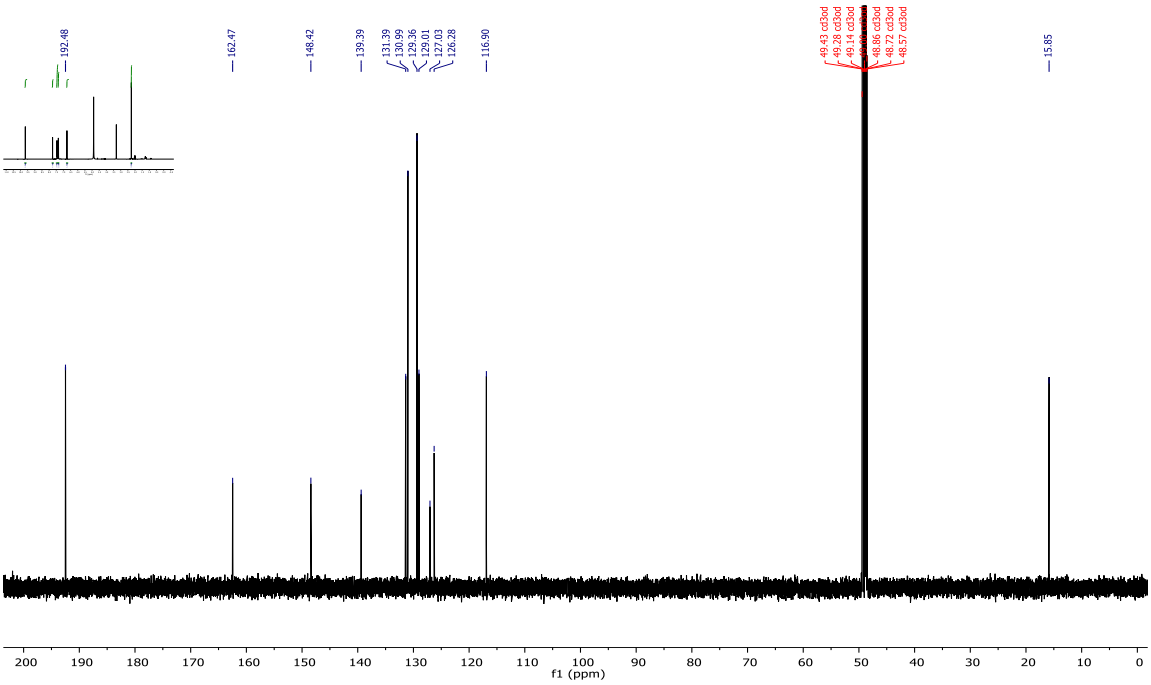

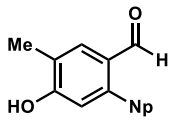


600 MHz, $CD_3OD$

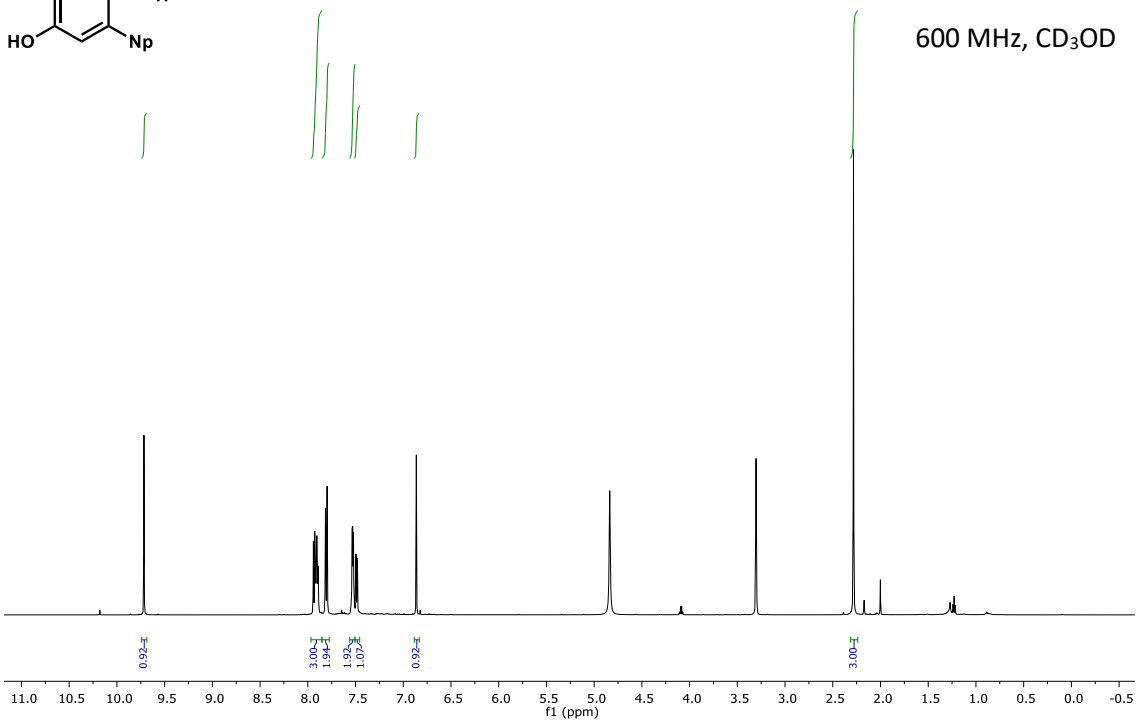


150 MHz, $CD_3OD$

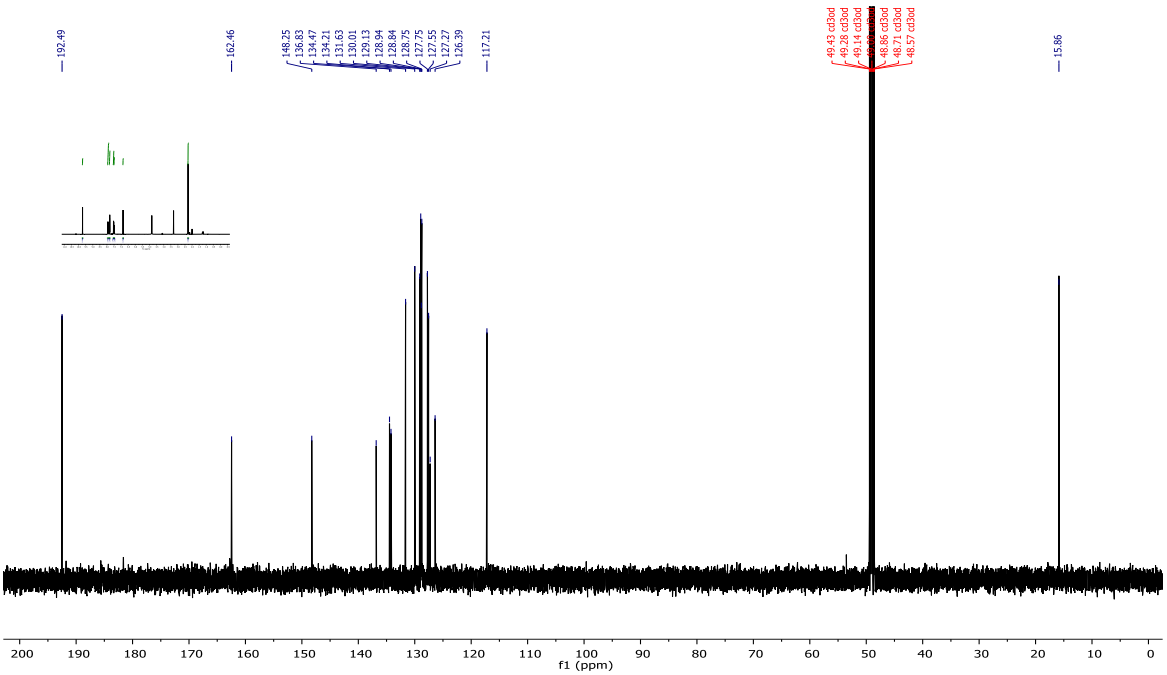

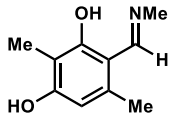


600 MHz, $CDCl_3$

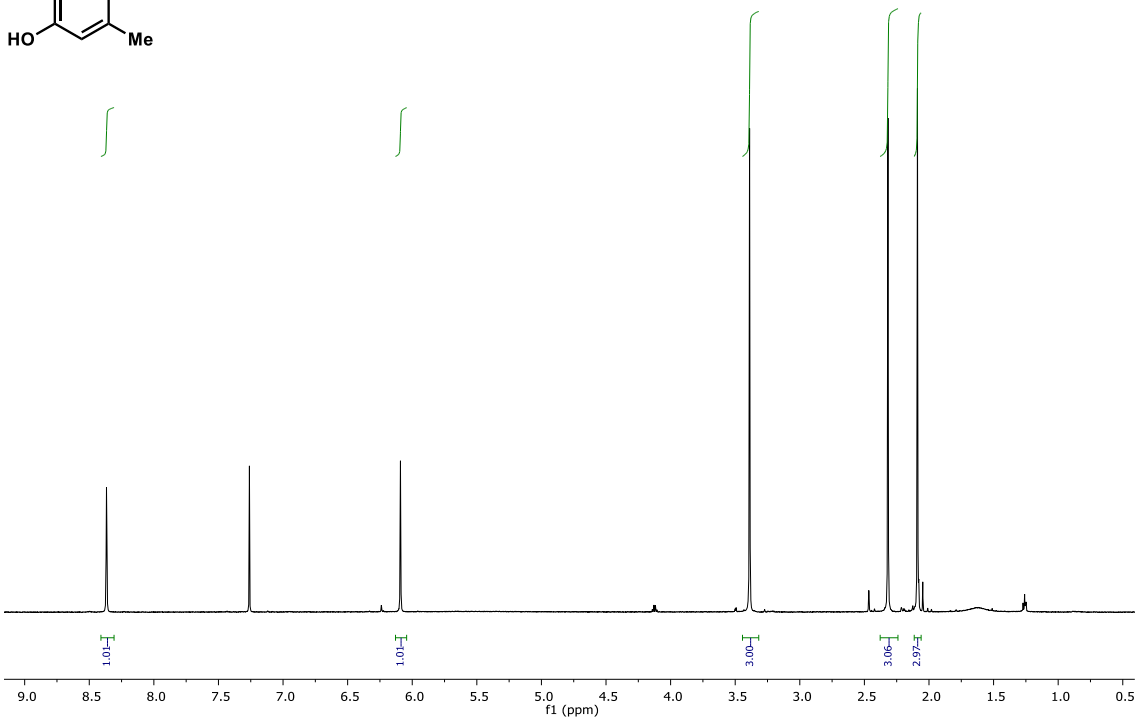


150 MHz, $CDCl_3$

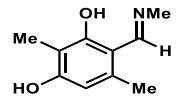

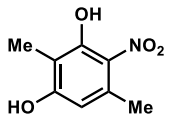


600 MHz, $CD_3OD$

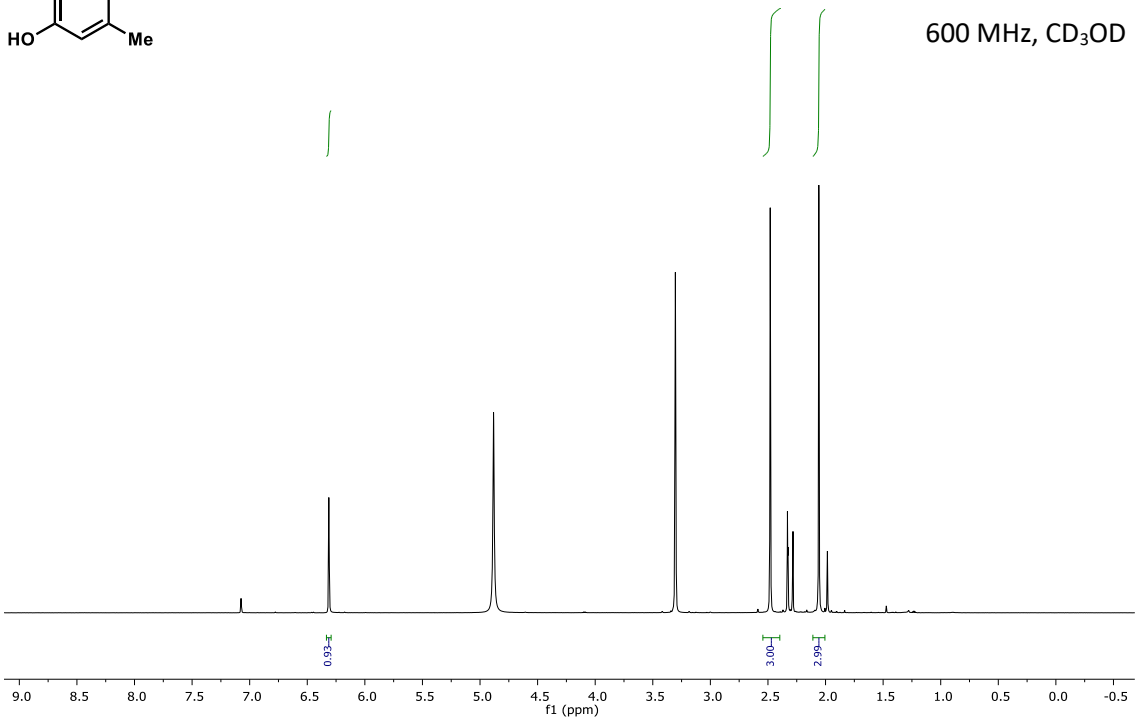

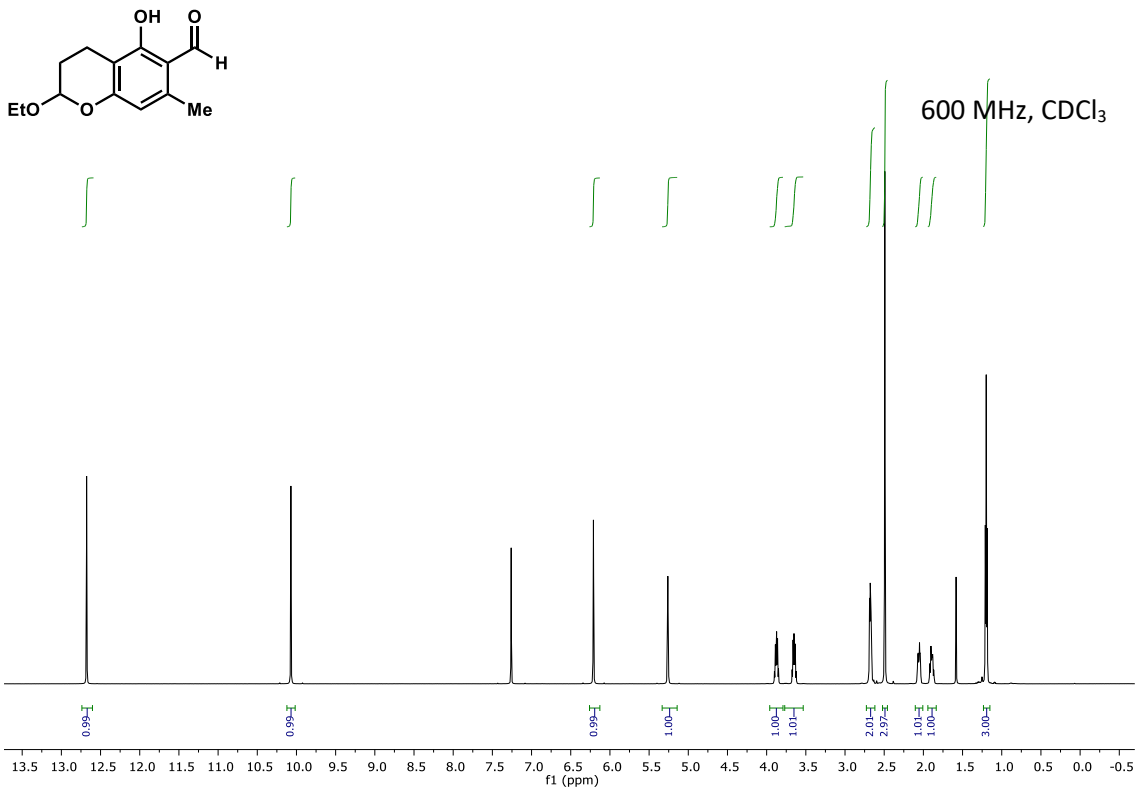
OH
O
H
EtO
O
Me
600 MHz, CDCl3
0.99
0.99
0.99
1.00
1.00
1.01
2.01
2.97
1.01
1.00
3.00
13.5 13.0 12.5 12.0 11.5 11.0 10.5 10.0 9.5 9.0 8.5 8.0 7.5 7.0 6.5 6.0 5.5 5.0 4.5 4.0 3.5 3.0 2.5 2.0 1.5 1.0 0.5 0.0 -0.5
f1 (ppm)

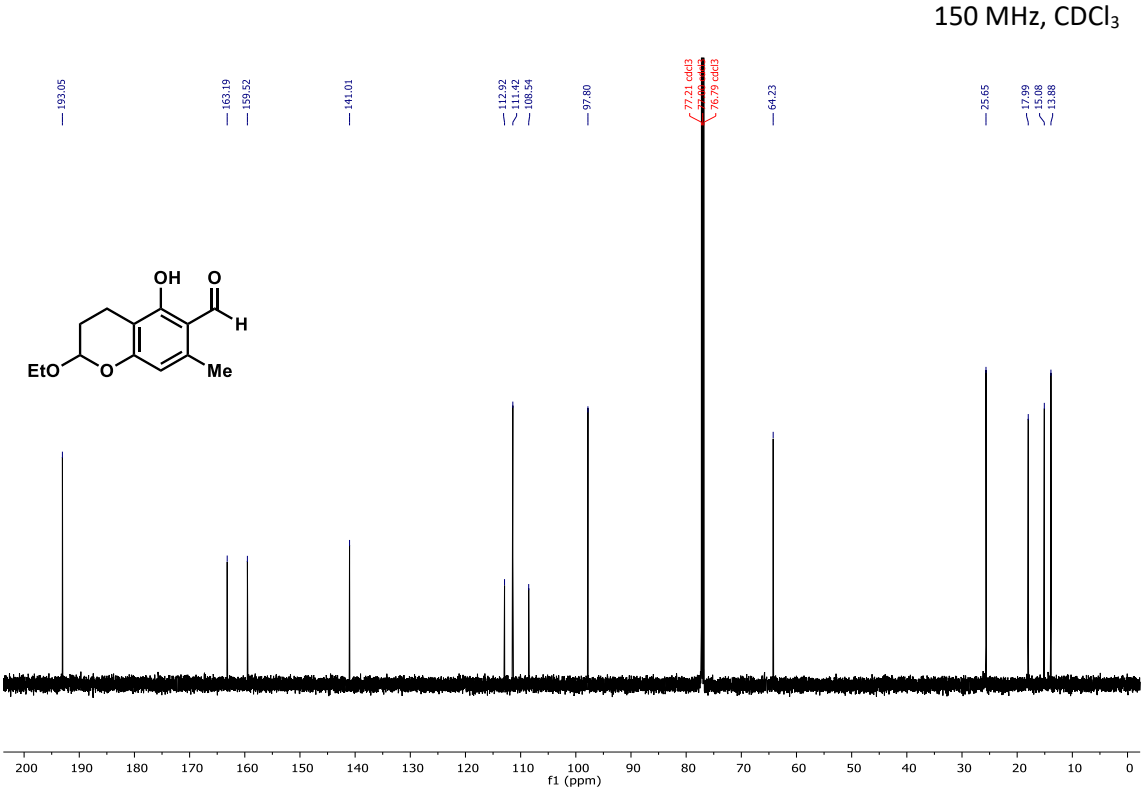
150 MHz, CDCl3
193.05
163.19
159.52
141.01
112.92
111.42
108.54
97.80
77.21 cdcl3
76.79 cdcl3
64.23
25.65
17.99
15.08
13.88
OH
O
H
EtO
O
Me
200 190 180 170 160 150 140 130 120 110 100 90 80 70 60 50 40 30 20 10 0
f1 (ppm)

600 MHz, $CDCl_3$

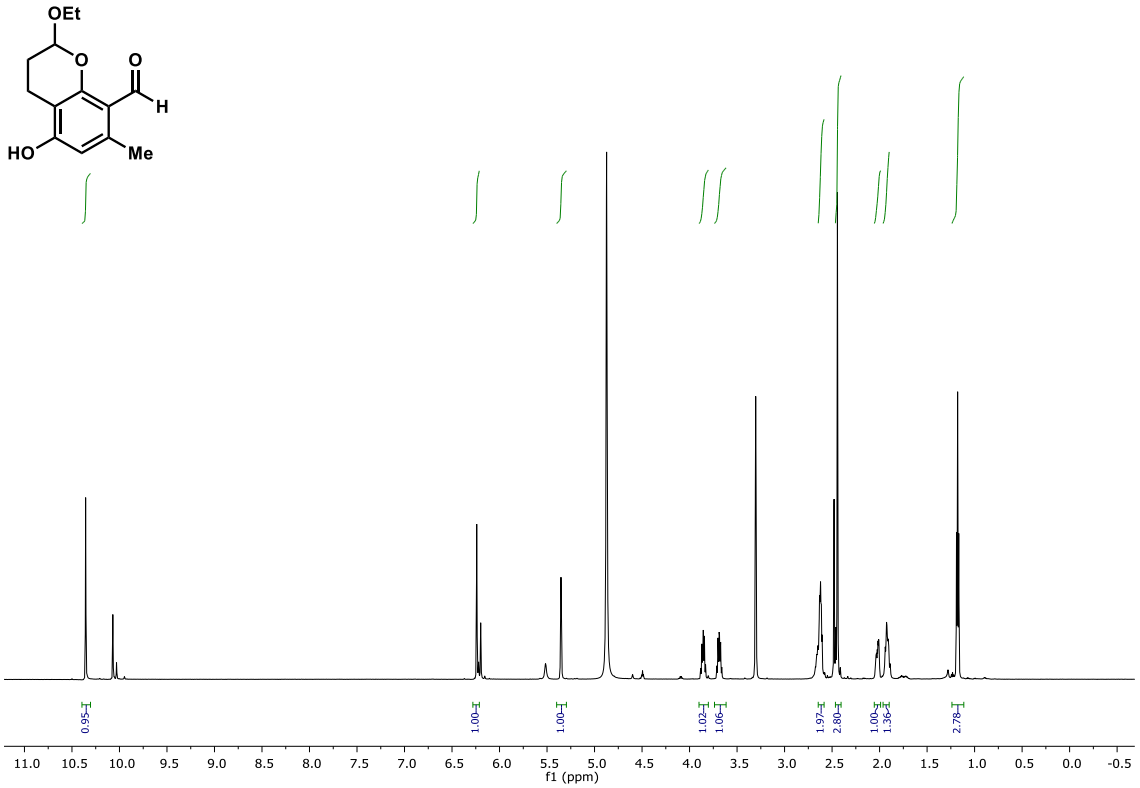


150 MHz, $CDCl_3$

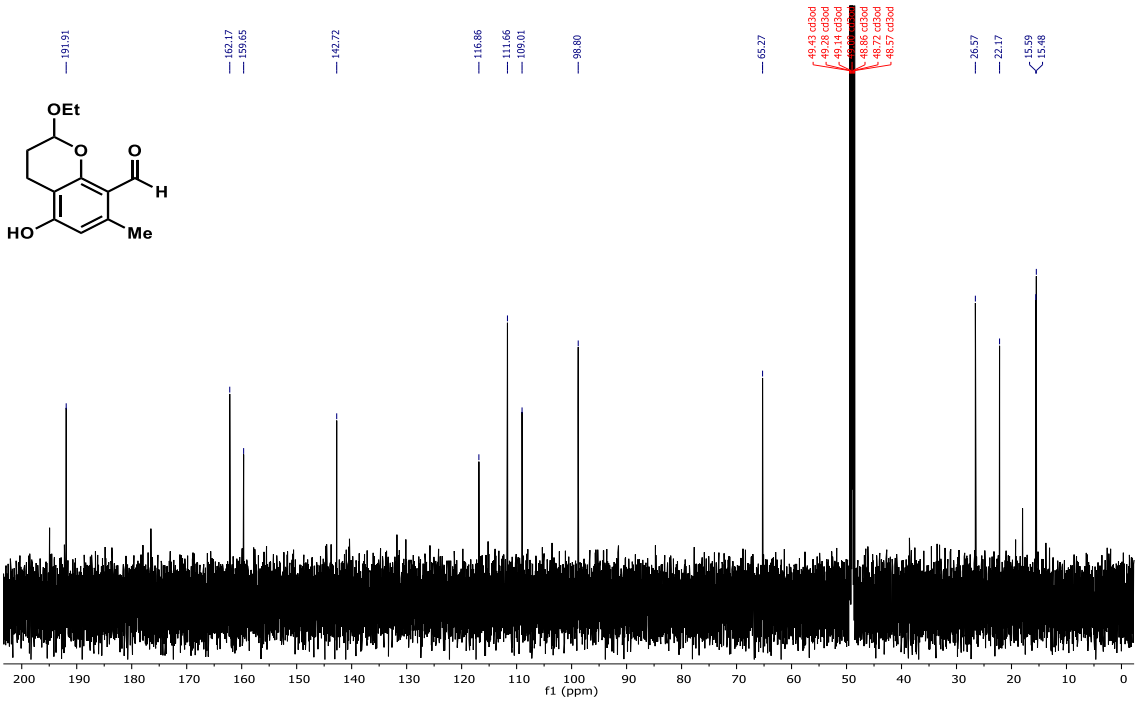

600 MHz, $CD_3OD$

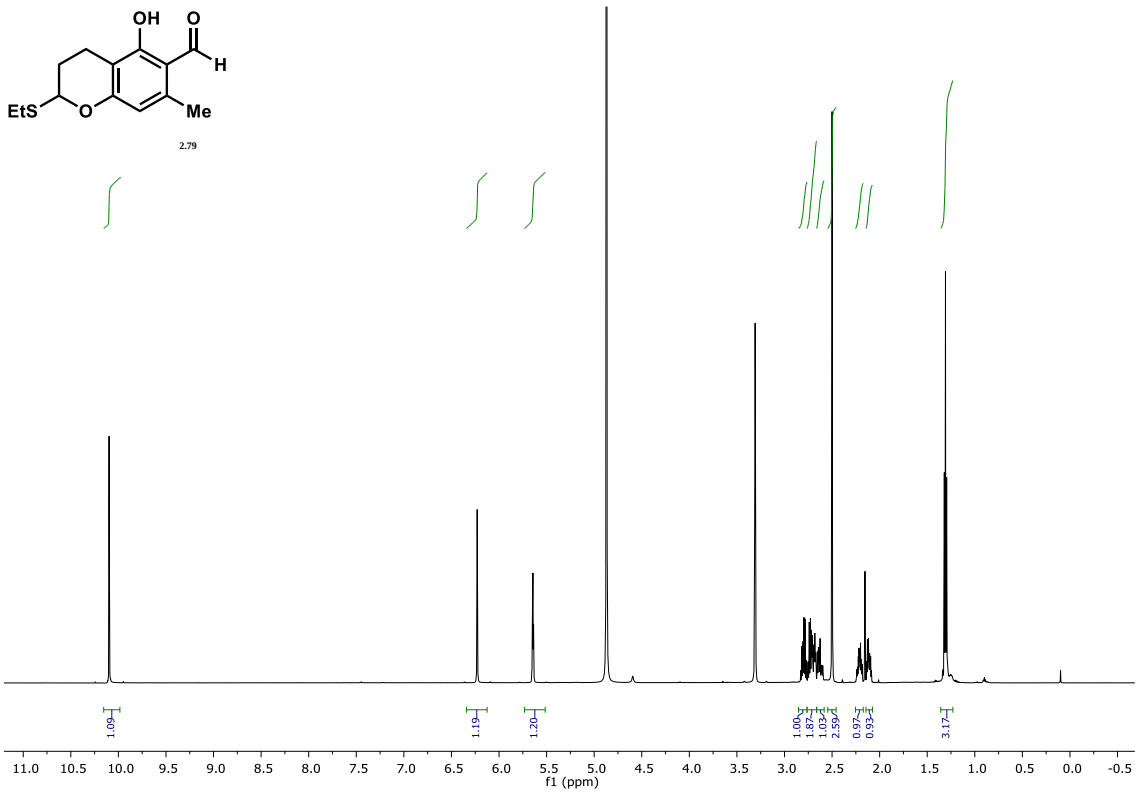


150 MHz, $CD_3OD$

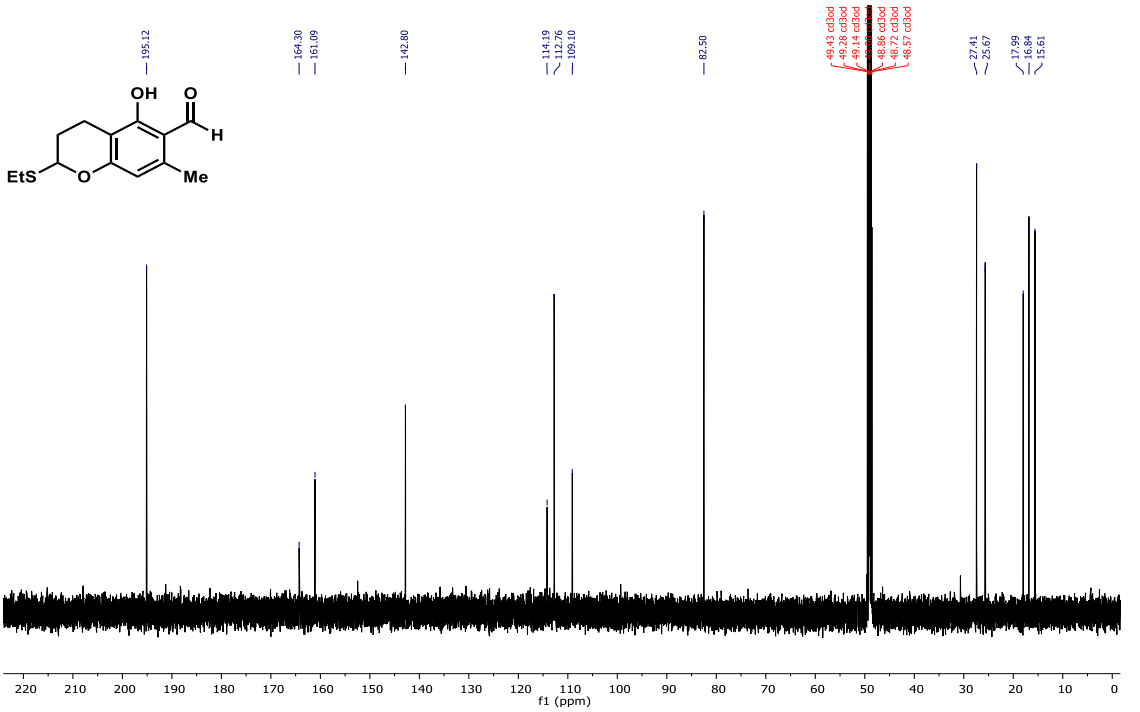

600 MHz, $CDCl_3$

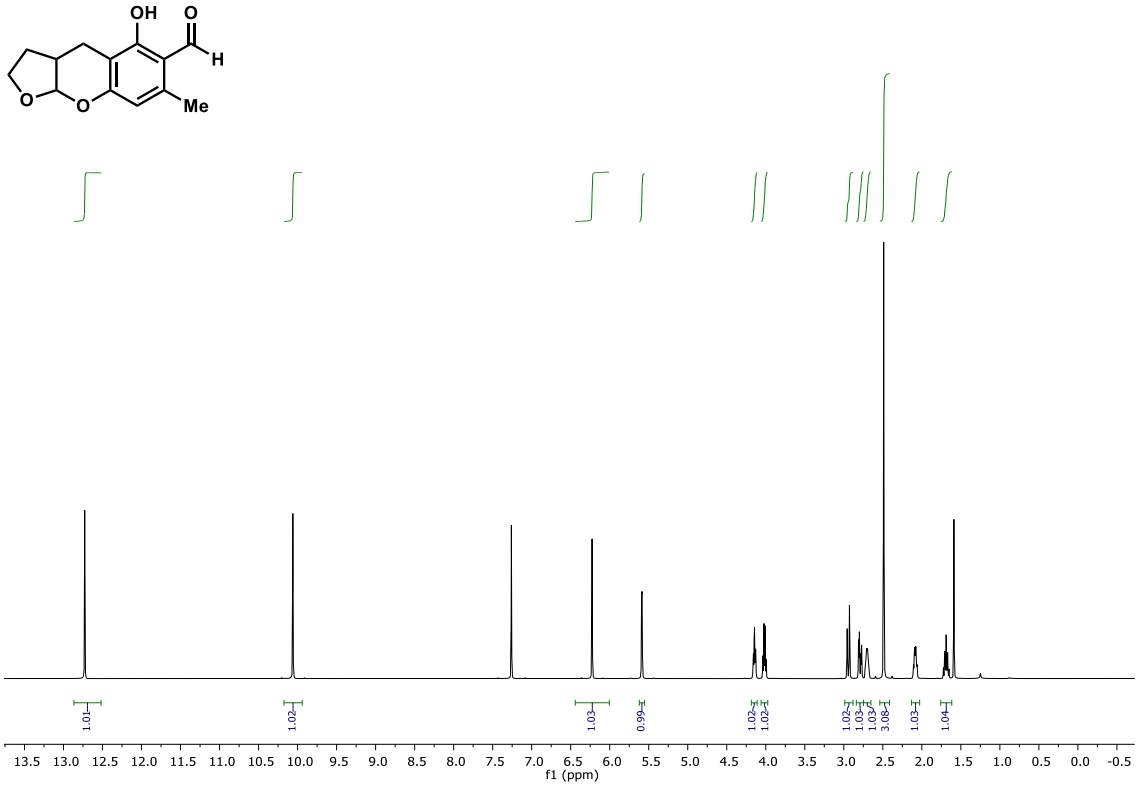


150 MHz, $CDCl_3$

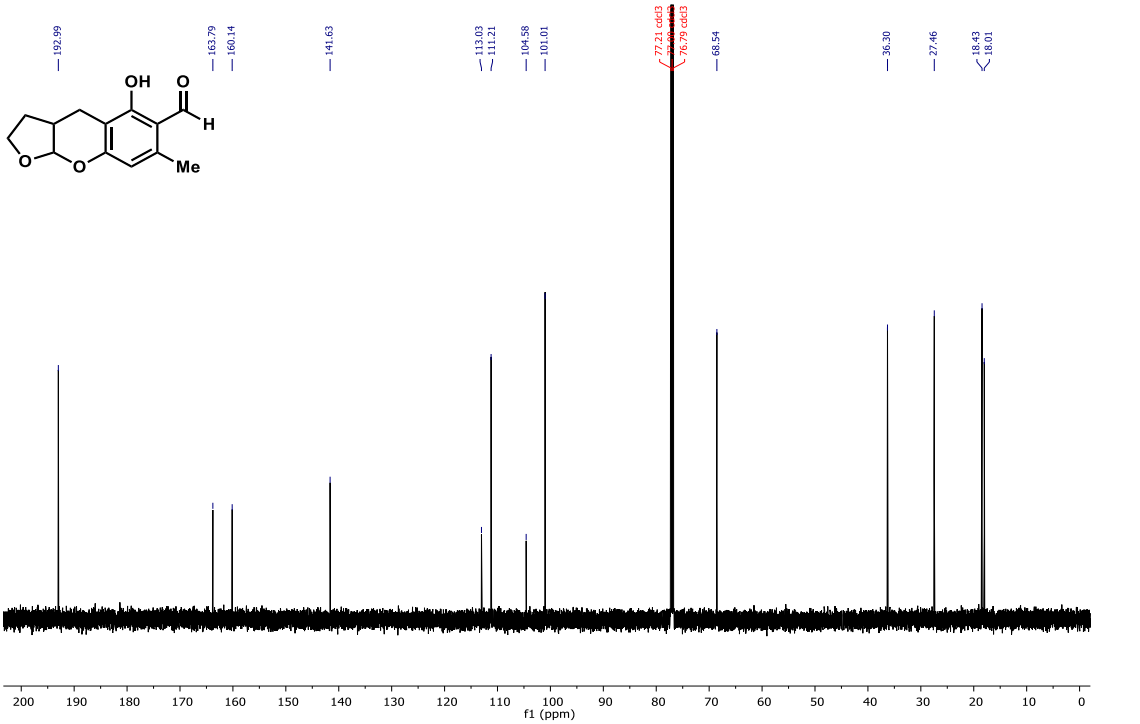

600 MHz, $CDCl_3$

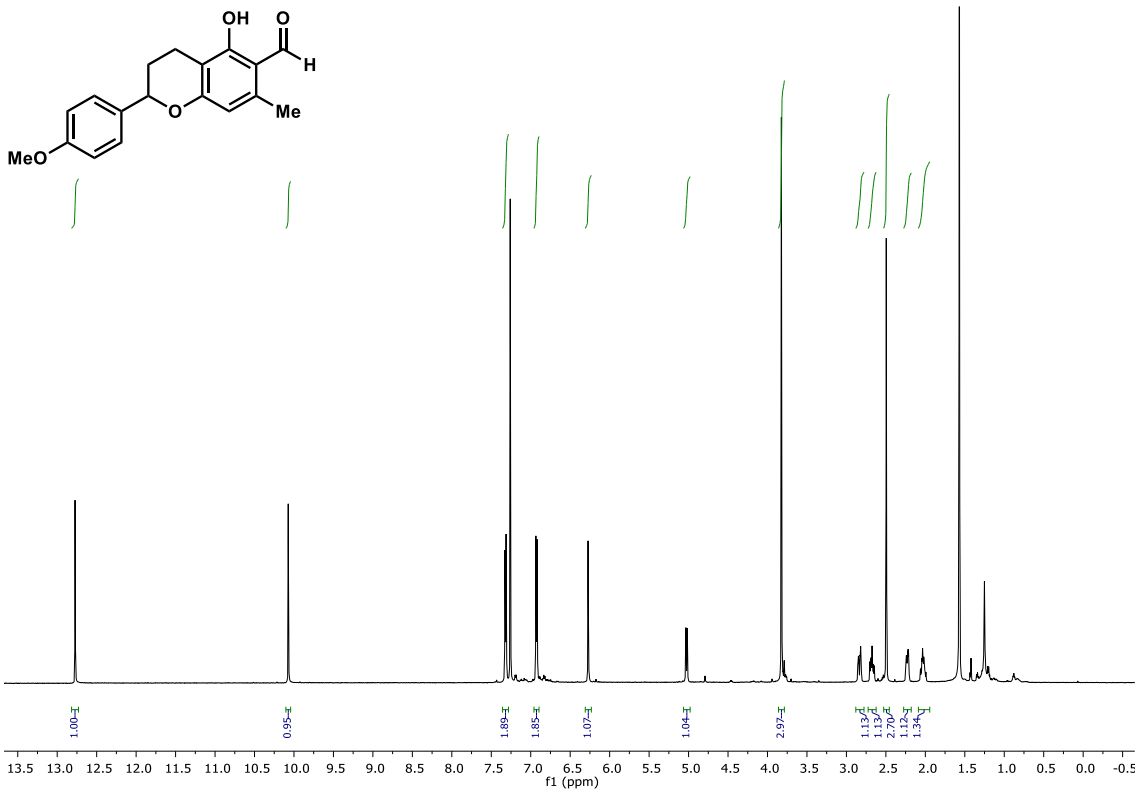


150 MHz, $CDCl_3$

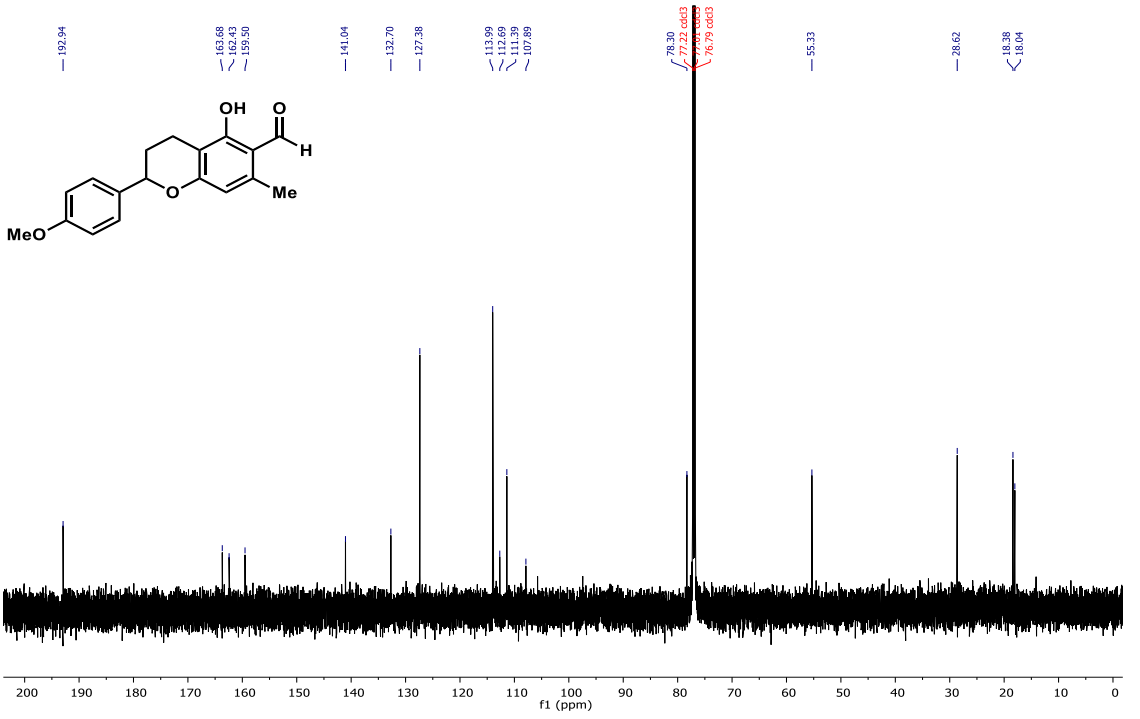

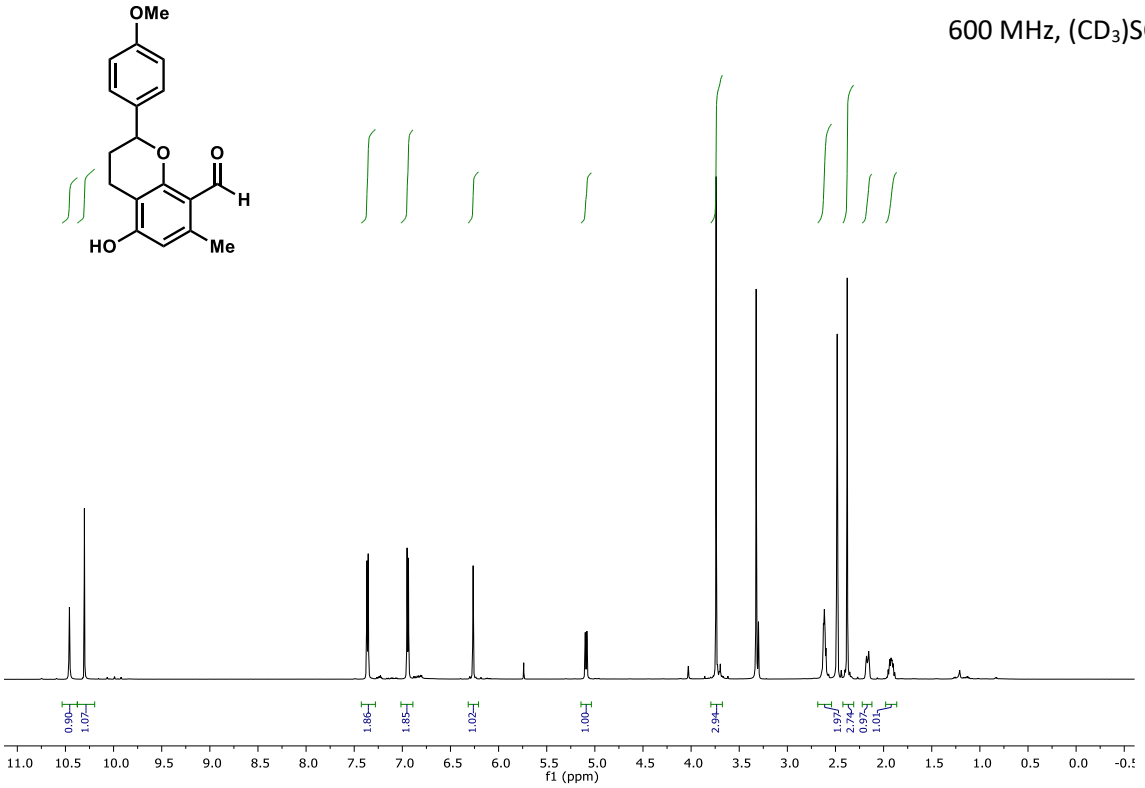
OMe
O
O
H
HO
Me
600 MHz, (CD3)SO
0.90
1.07
1.86
1.85
1.02
1.00
2.94
1.97
2.74
0.97
1.01
11.0 10.5 10.0 9.5 9.0 8.5 8.0 7.5 7.0 6.5 6.0 5.5 5.0 4.5 4.0 3.5 3.0 2.5 2.0 1.5 1.0 0.5 0.0
f1 (ppm)

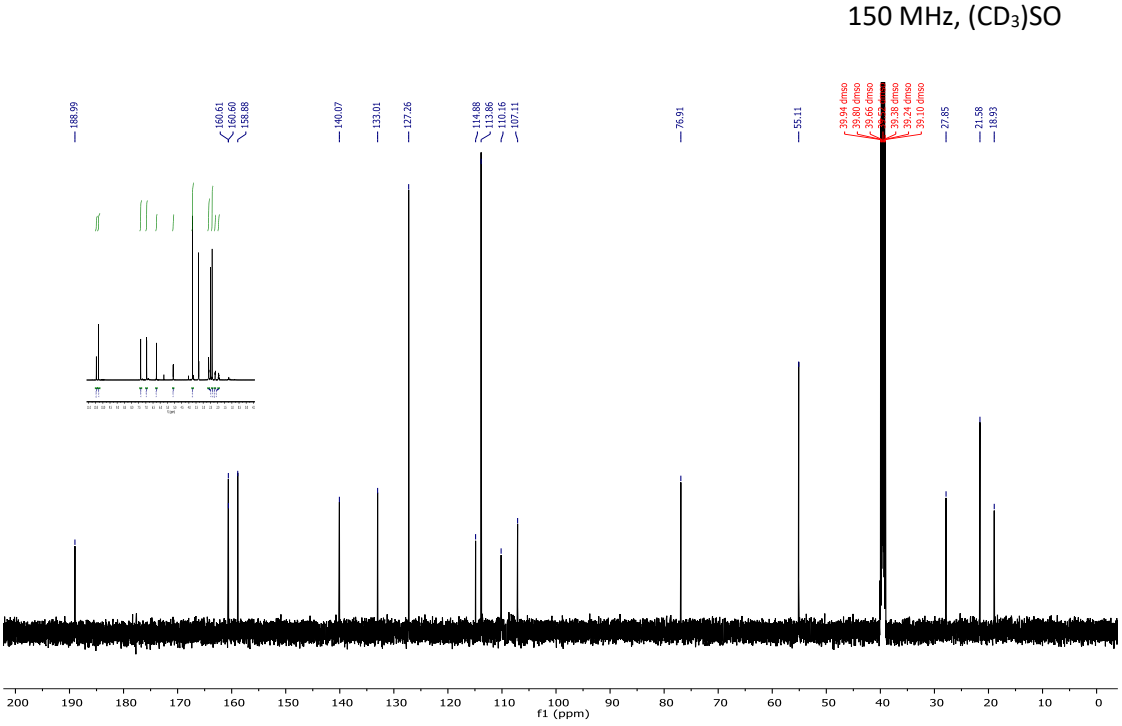
150 MHz, (CD3)SO
188.99
160.61
160.60
158.88
140.07
133.01
127.26
114.88
113.86
110.16
107.11
76.91
55.11
39.94 dmso
39.80 dmso
39.66 dmso
39.52 dmso
39.38 dmso
39.24 dmso
39.10 dmso
27.85
21.58
18.93
200 190 180 170 160 150 140 130 120 110 100 90 80 70 60 50 40 30 20 10 0
f1 (ppm)

600 MHz, $CDCl_3$

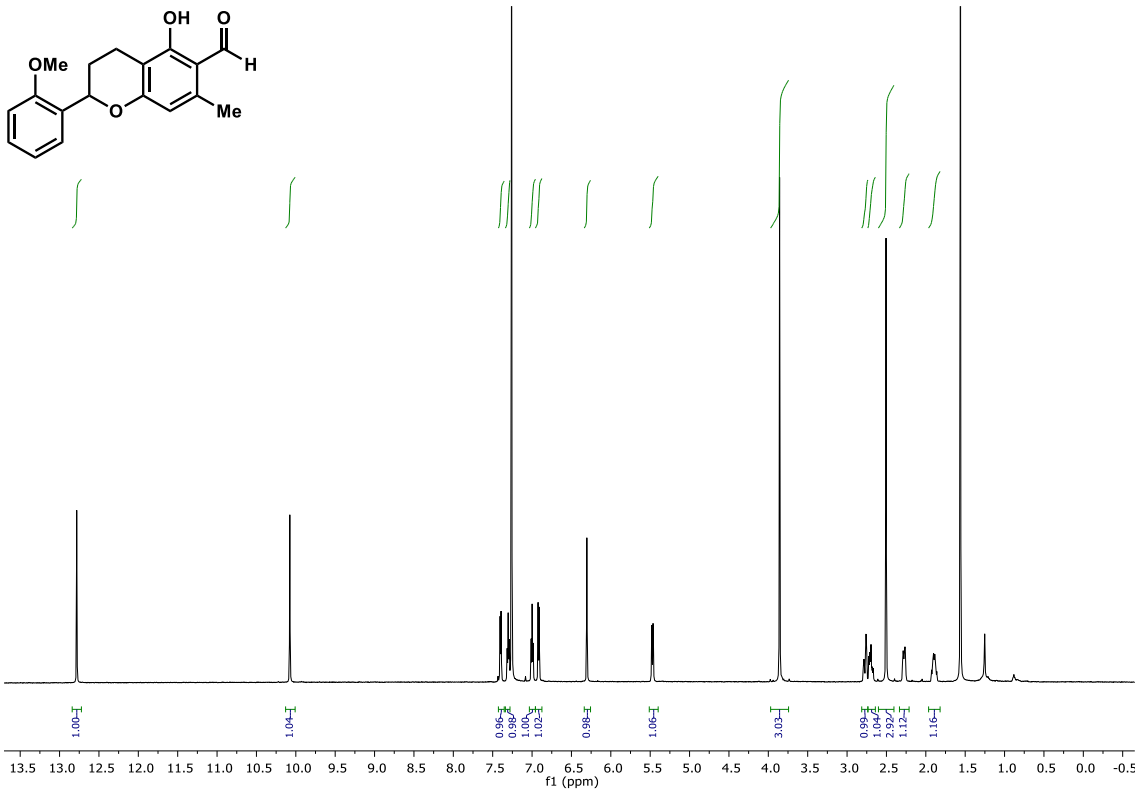


150 MHz, $CDCl_3$

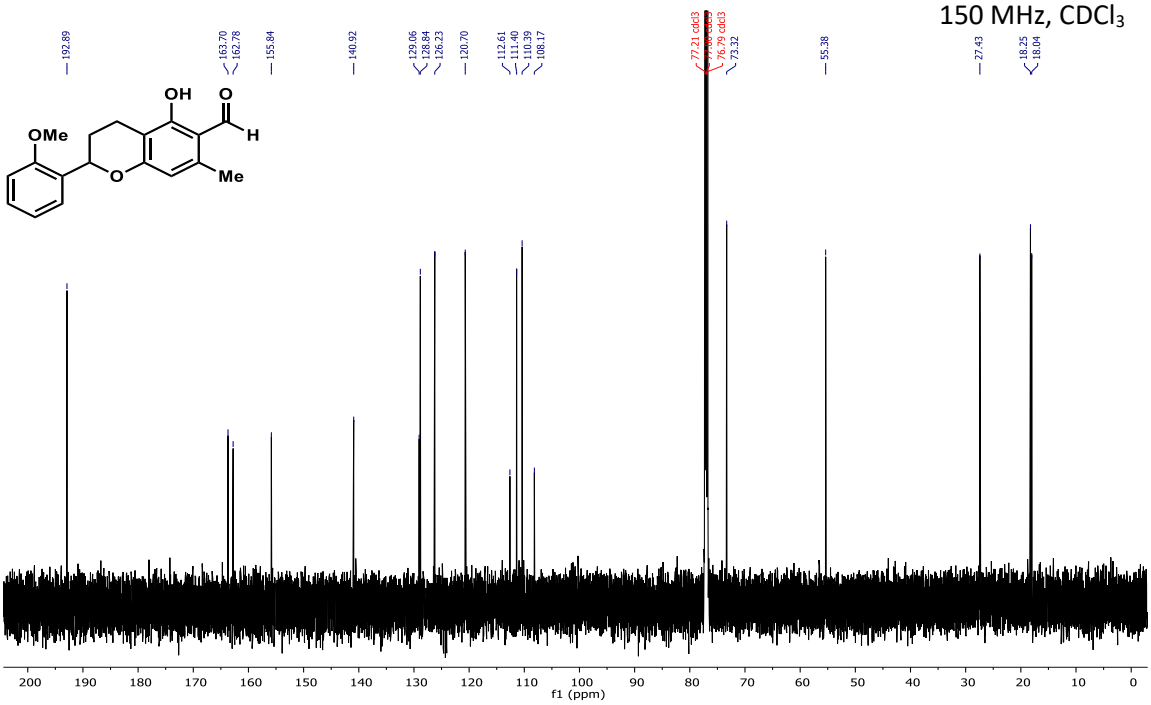

600 MHz, $CD_3OD$

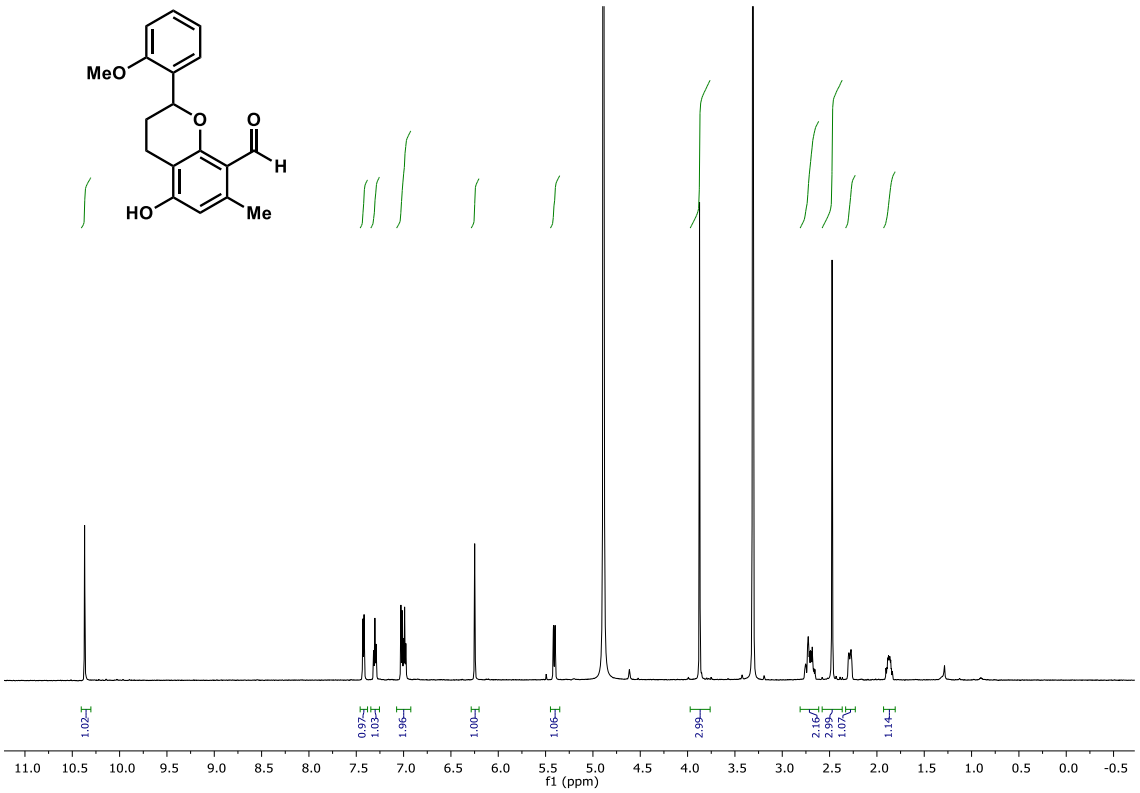


150 MHz, $CD_3OD$

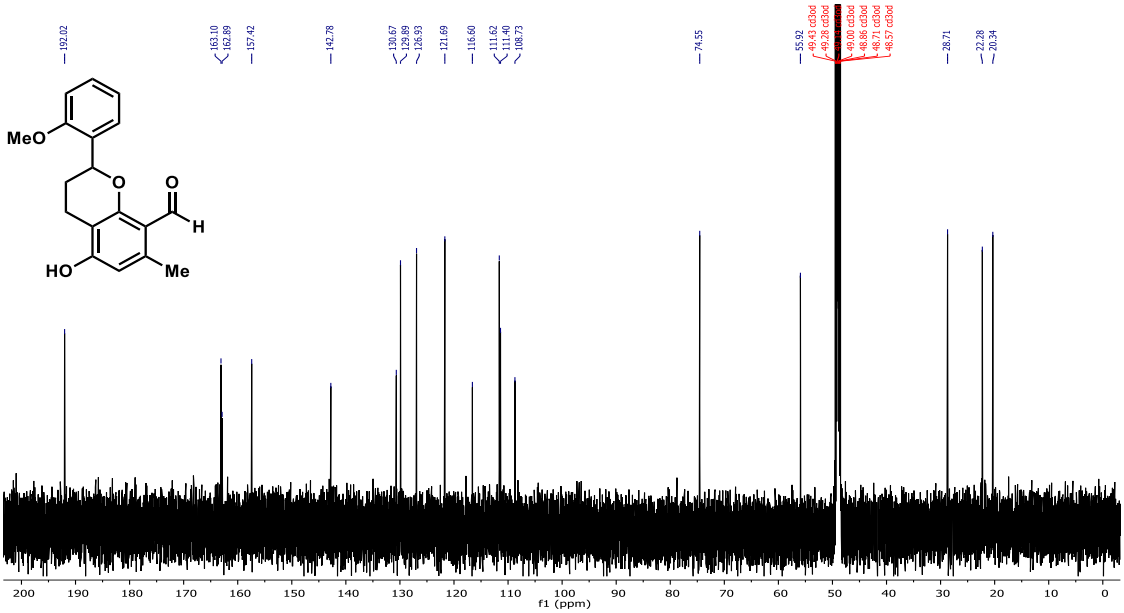

600 MHz, $CDCl_3$

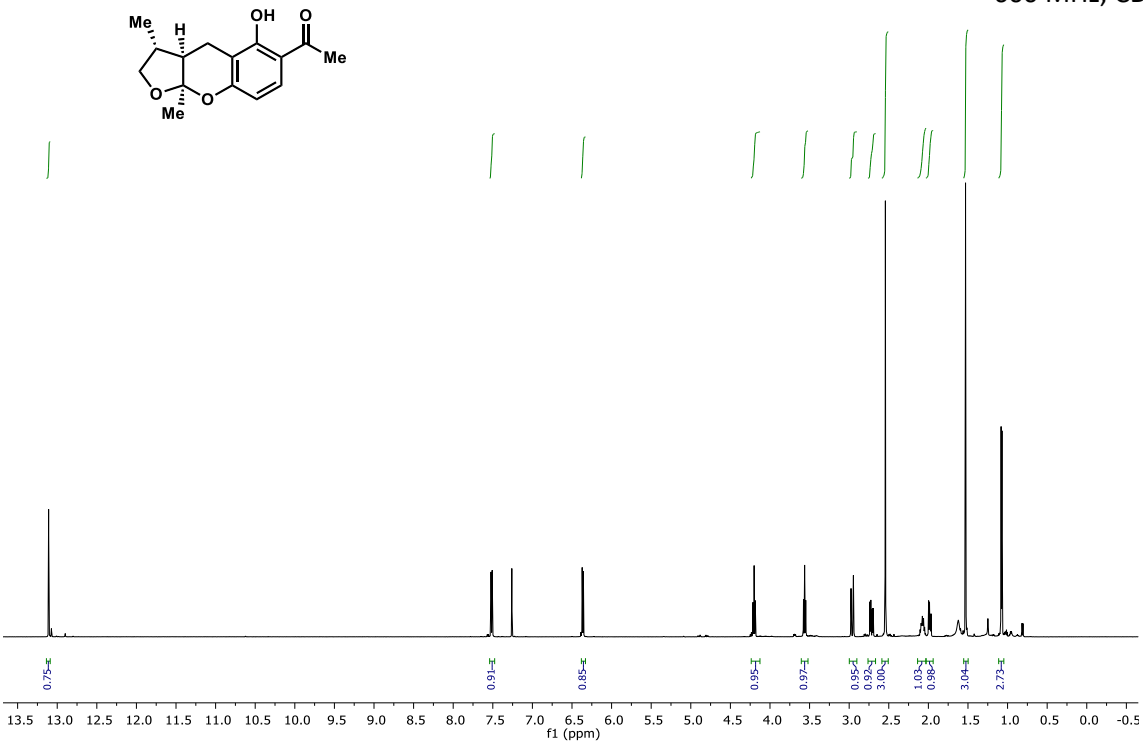


150 MHz, $CDCl_3$

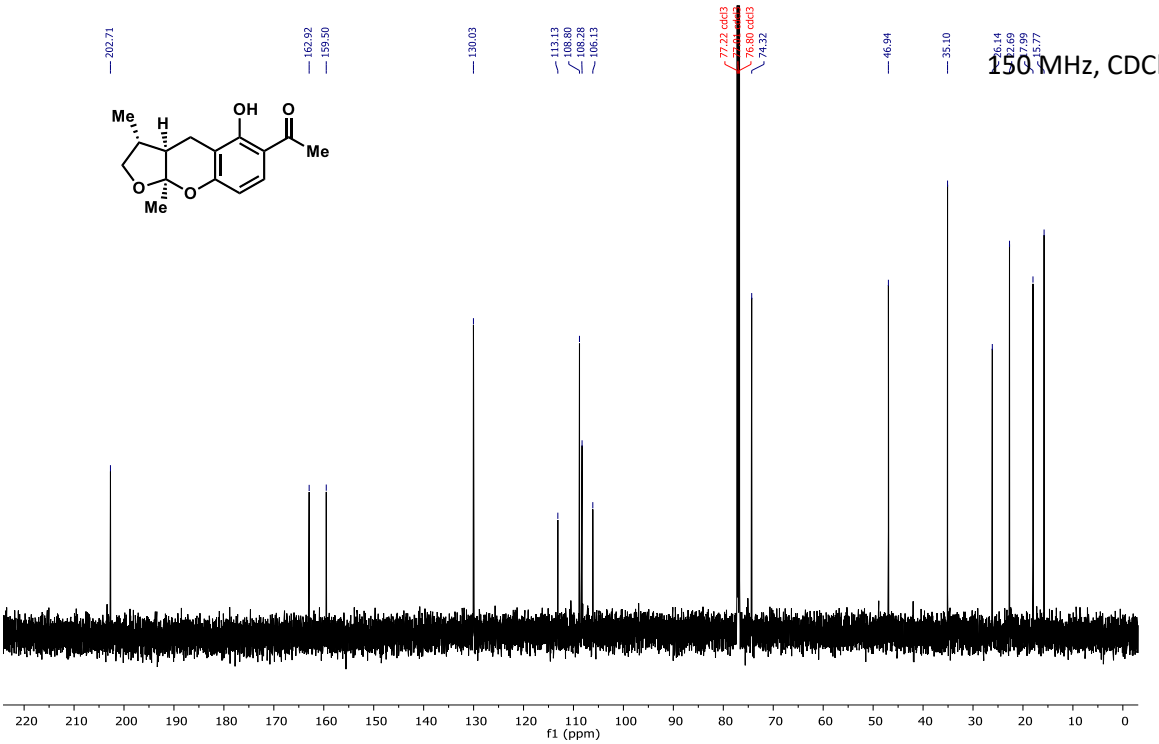

400 MHz, $CD_3OD$

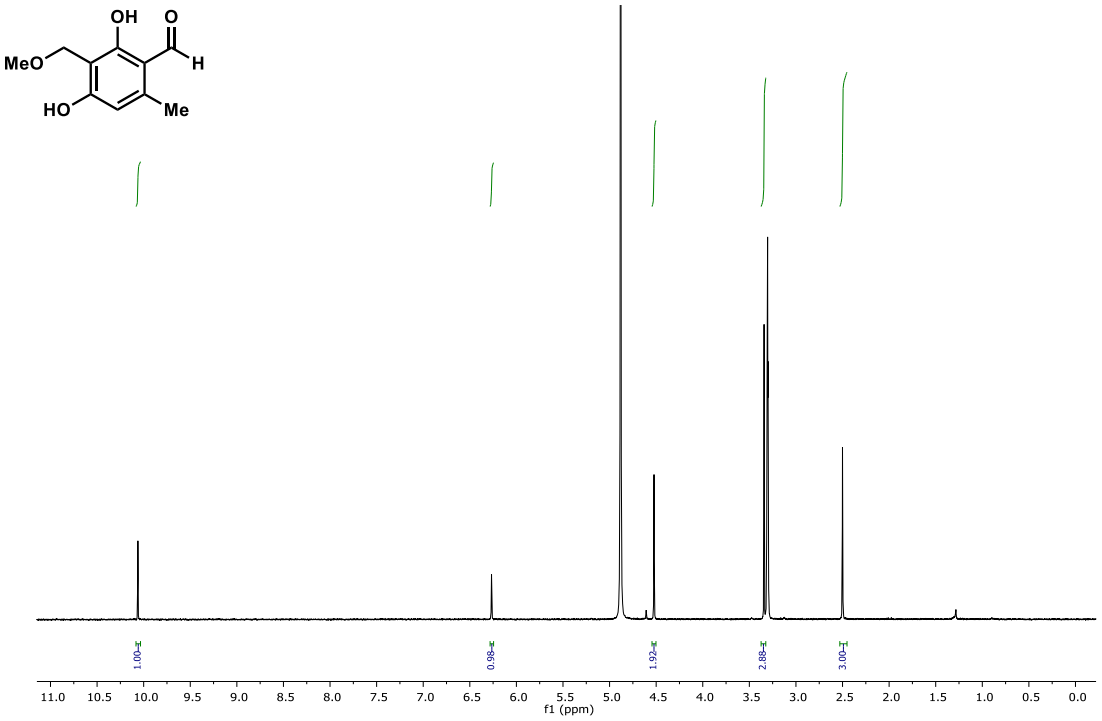


150 MHz, $CD_3OD$

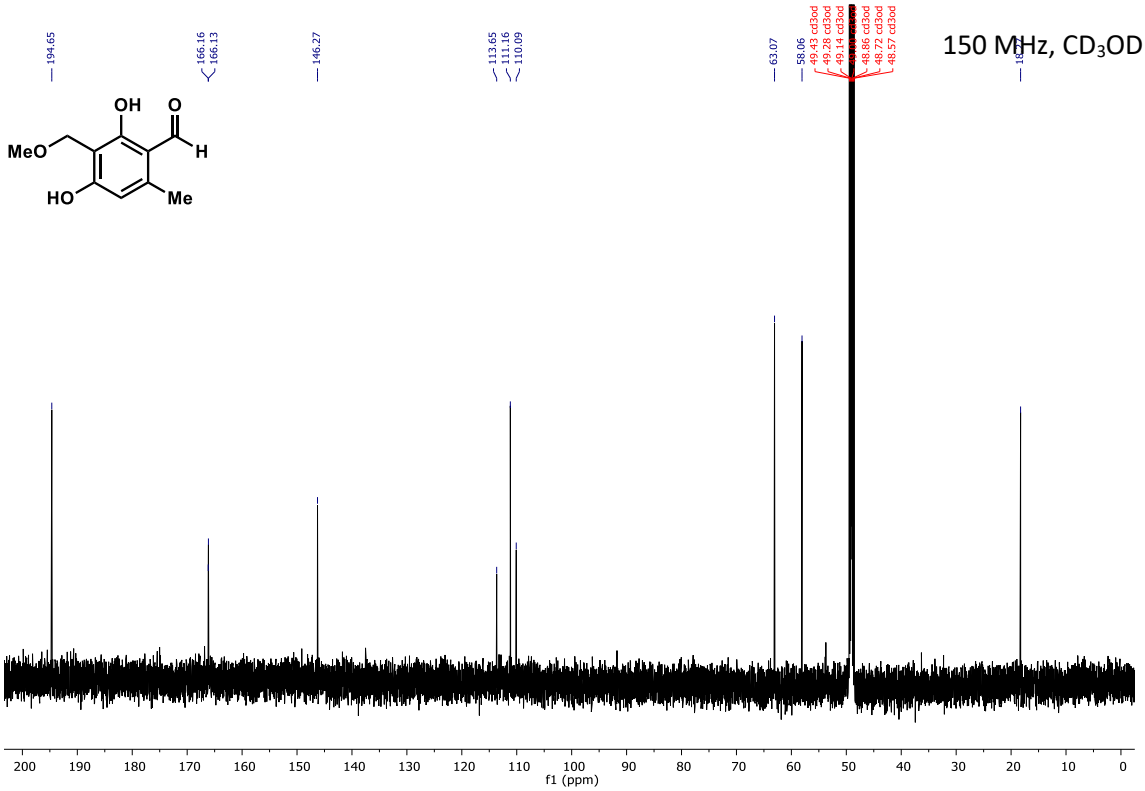

600 MHz, $CD_3OD$

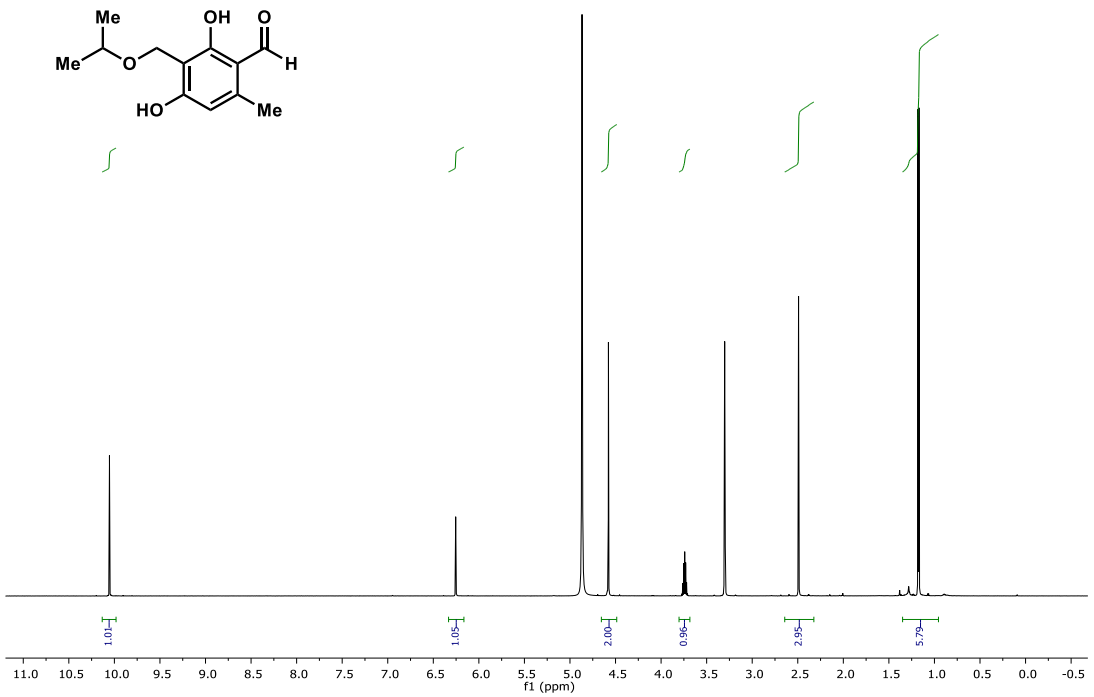


150 MHz, $CD_3OD$

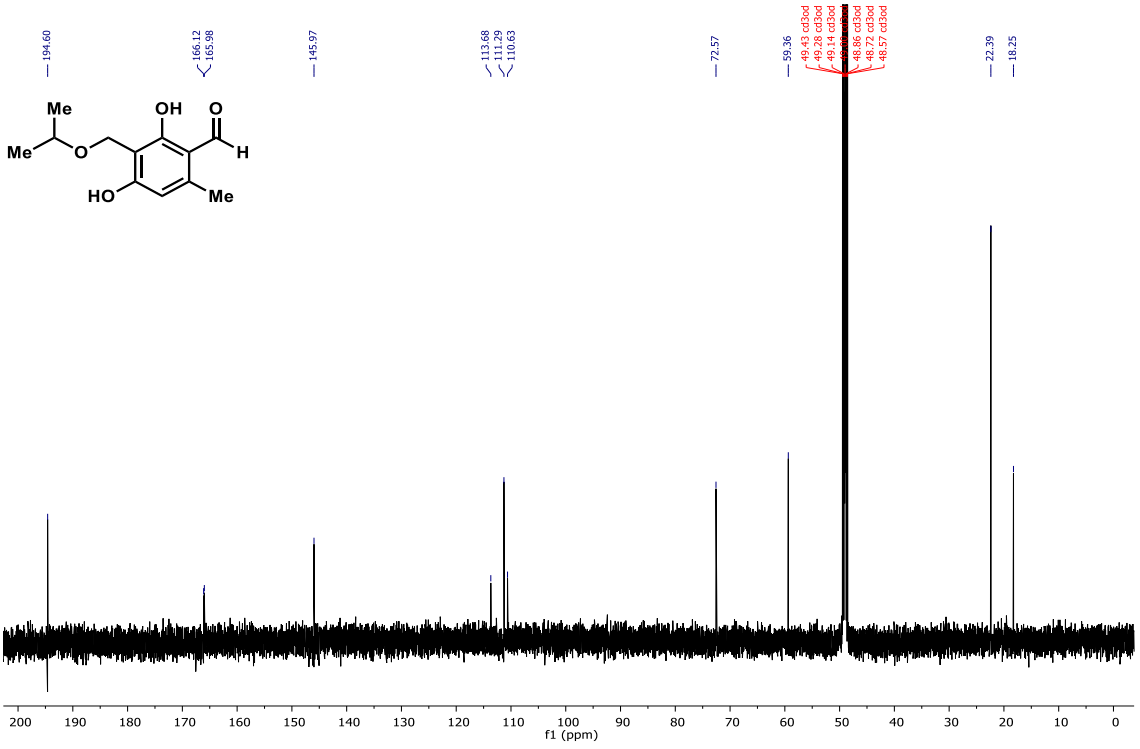

600 MHz, $CD_3OD$

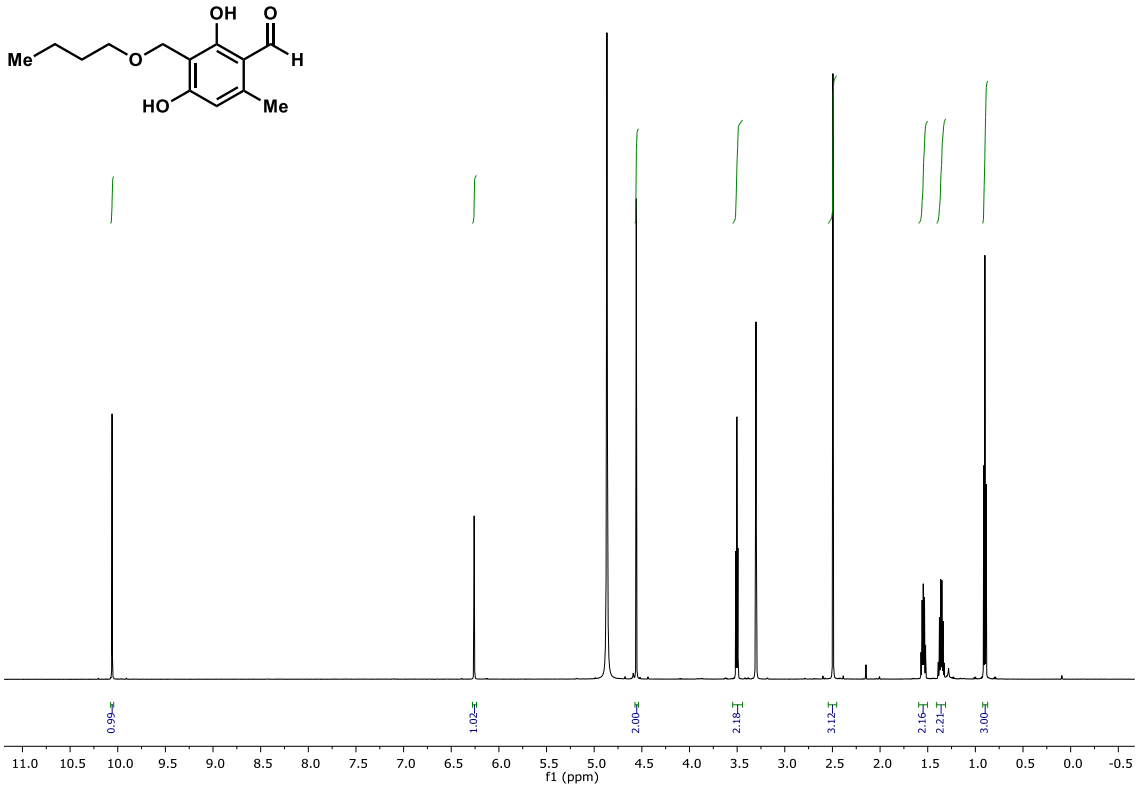


150 MHz, $CD_3OD$

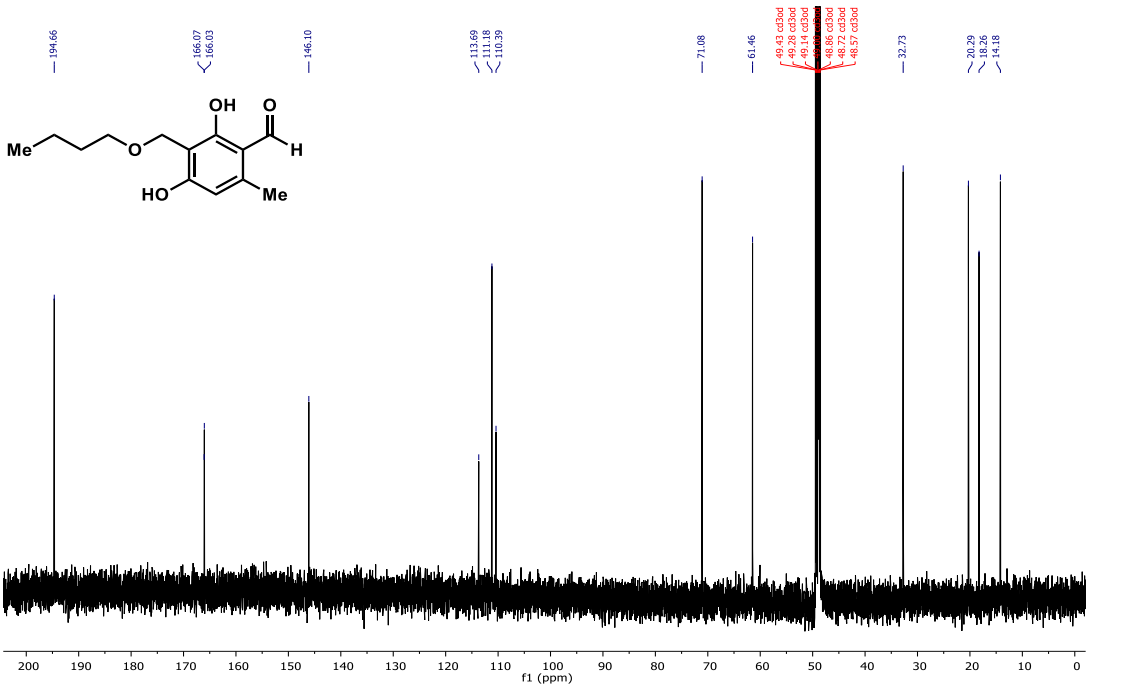

400 MHz, $CD_3OD$

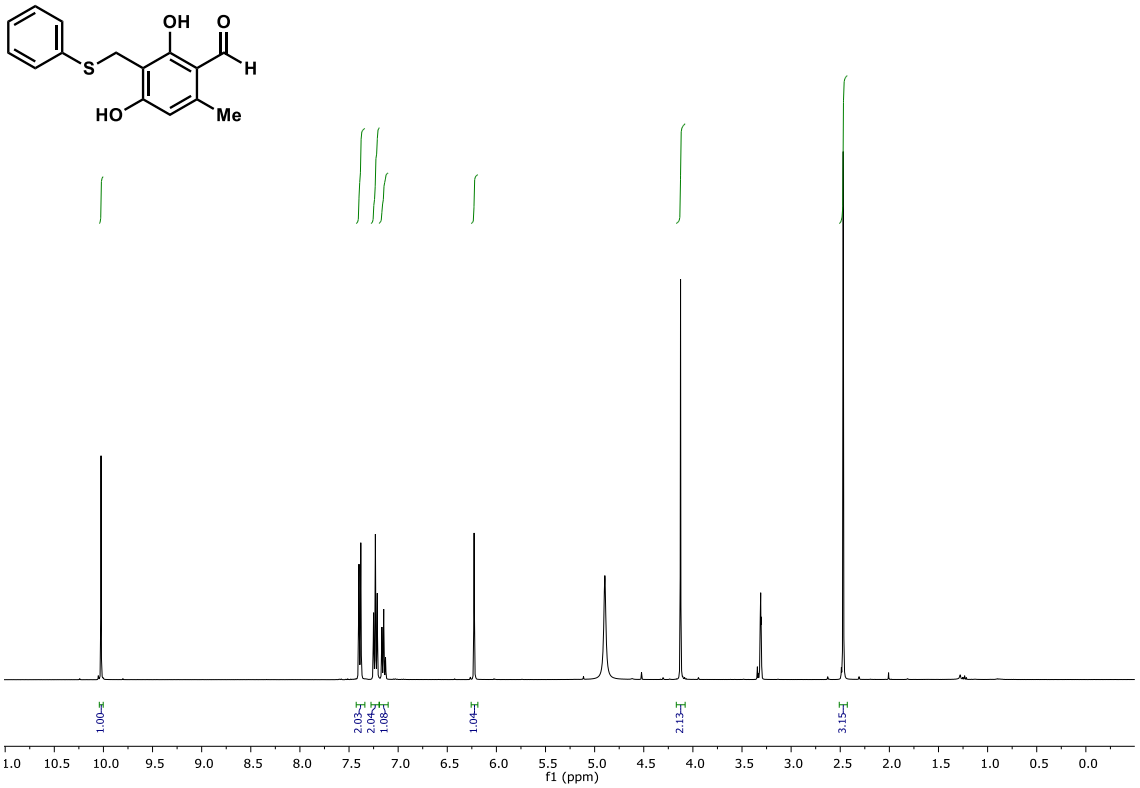


150 MHz, $CD_3OD$

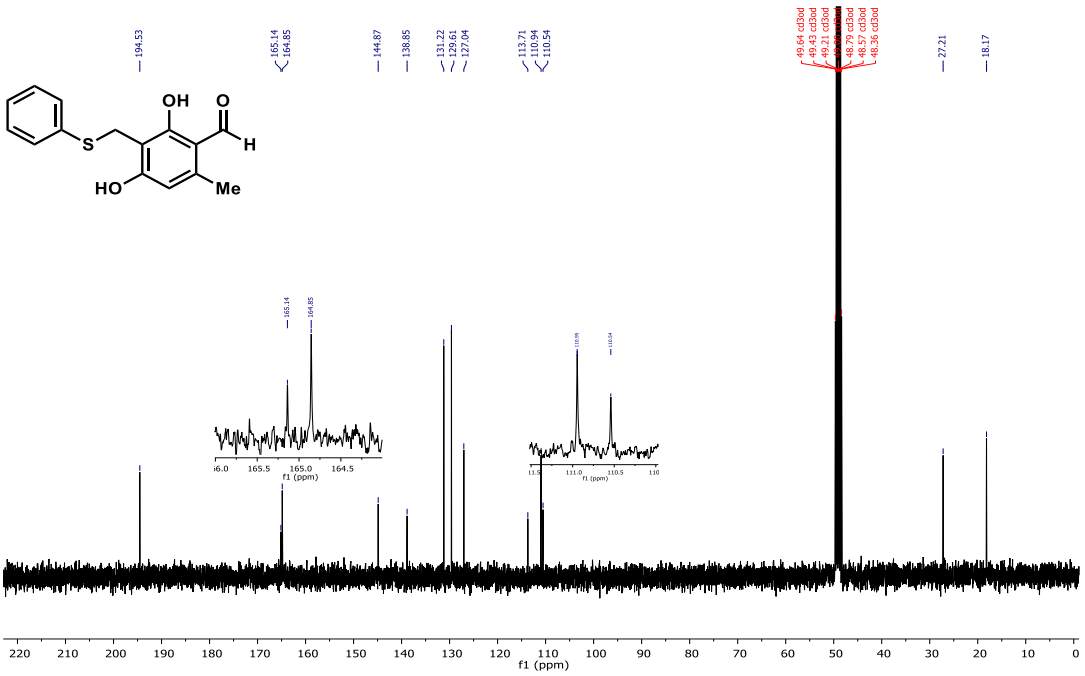

600 MHz, $CD_3OD$

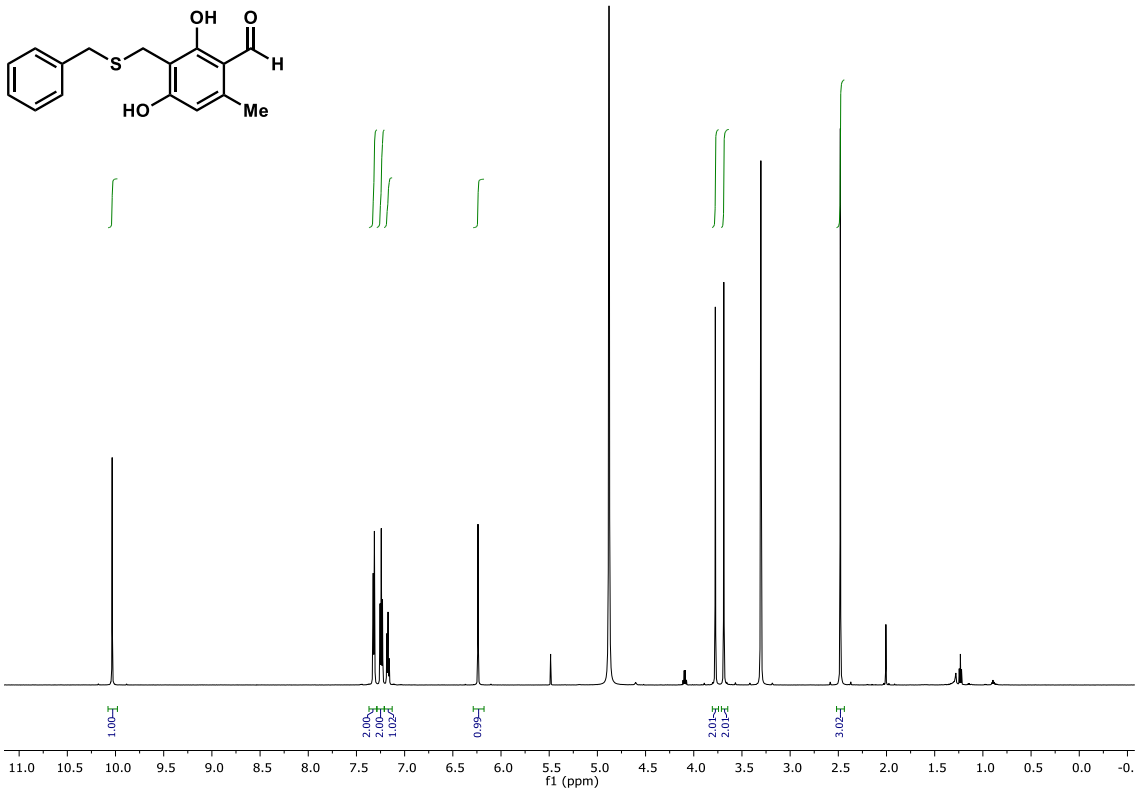


150 MHz, $CD_3OD$

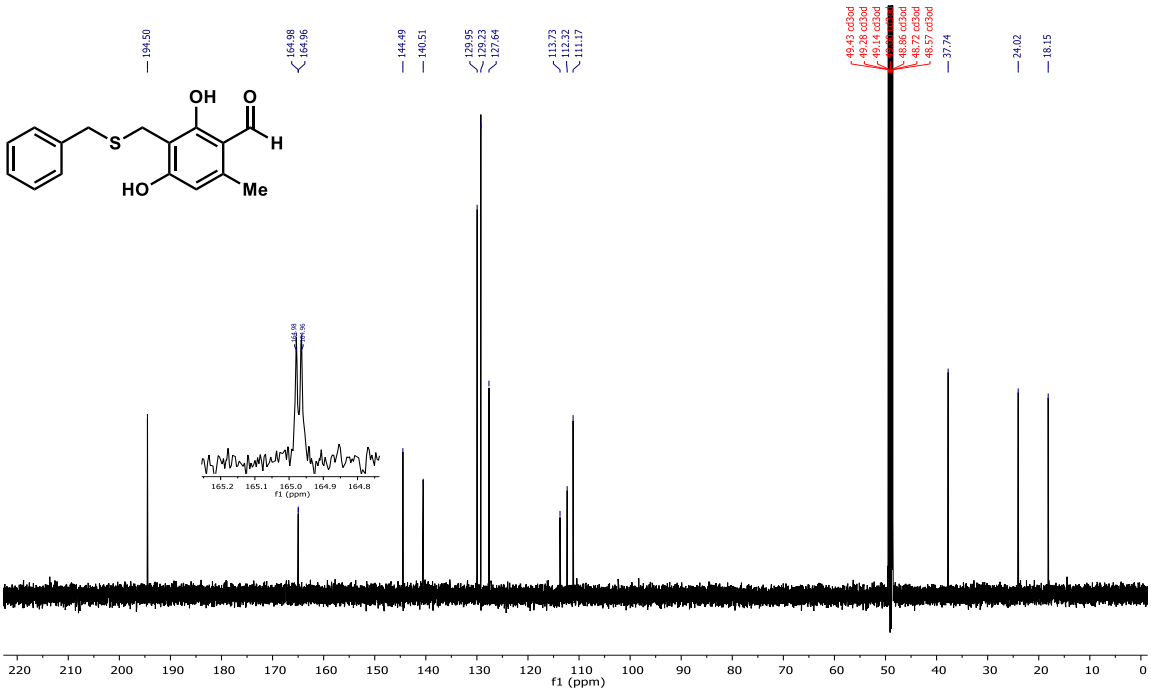

600 MHz, $CD_3OD$

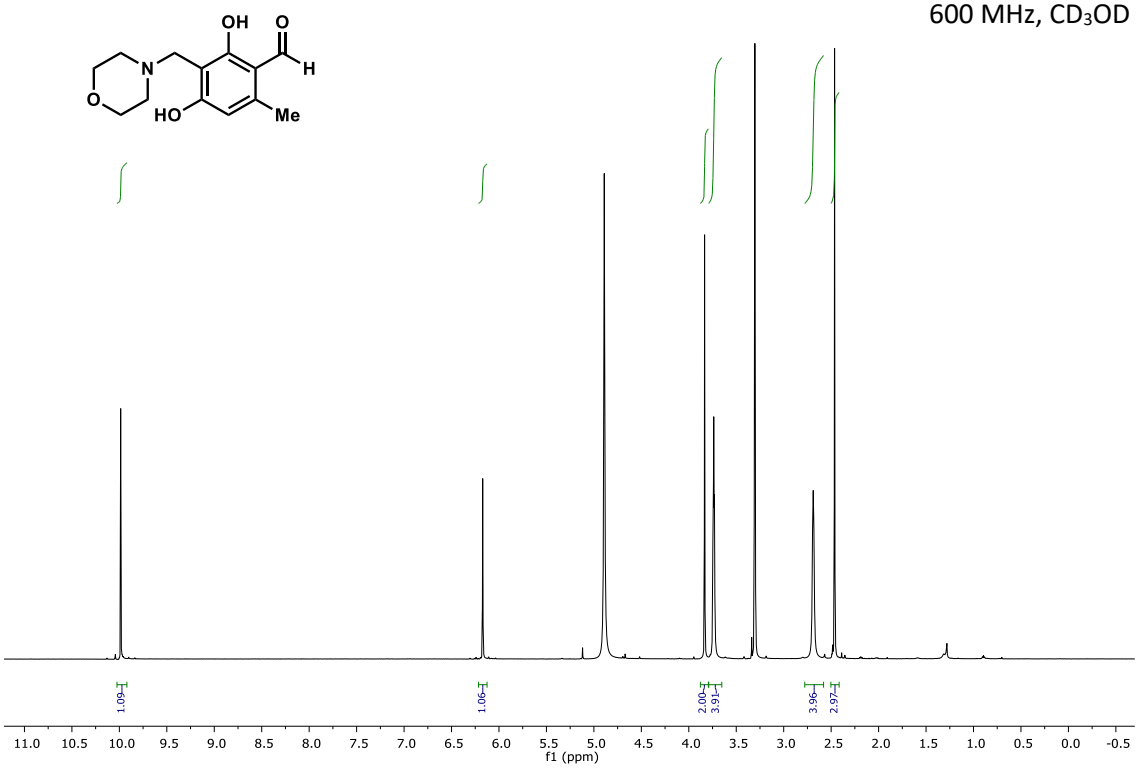


150 MHz, $CD_3OD$

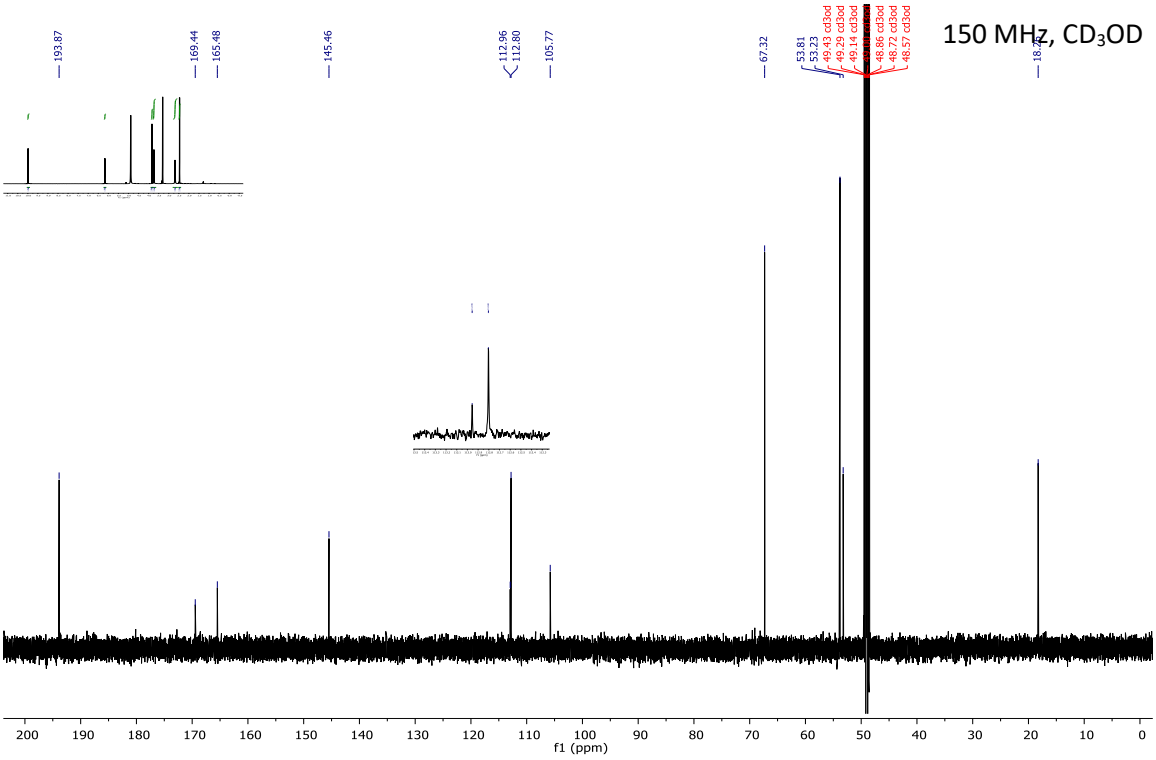

400 MHz, $CD_3OD$

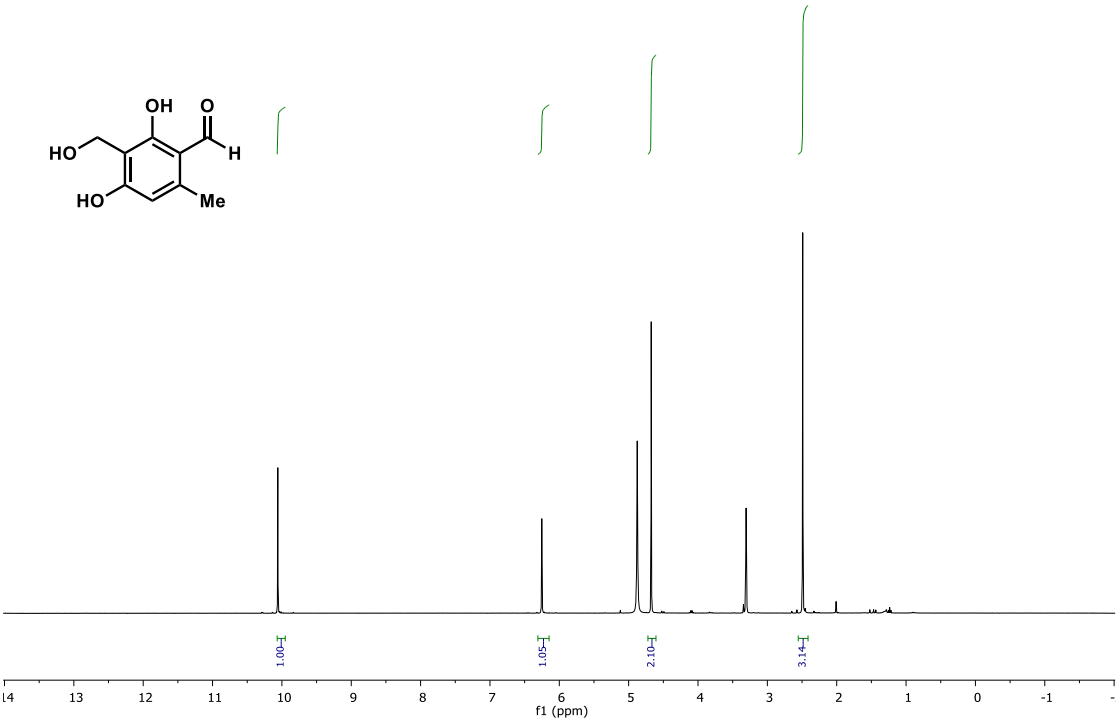


150 MHz, $CD_3OD$

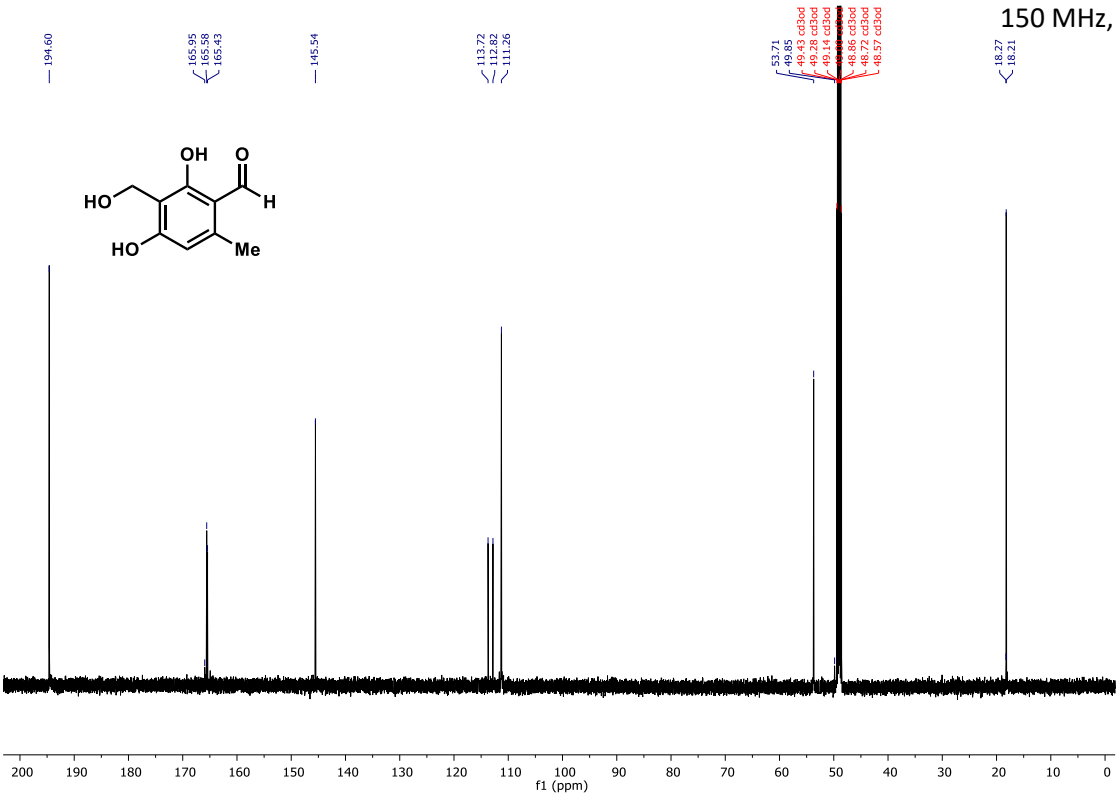

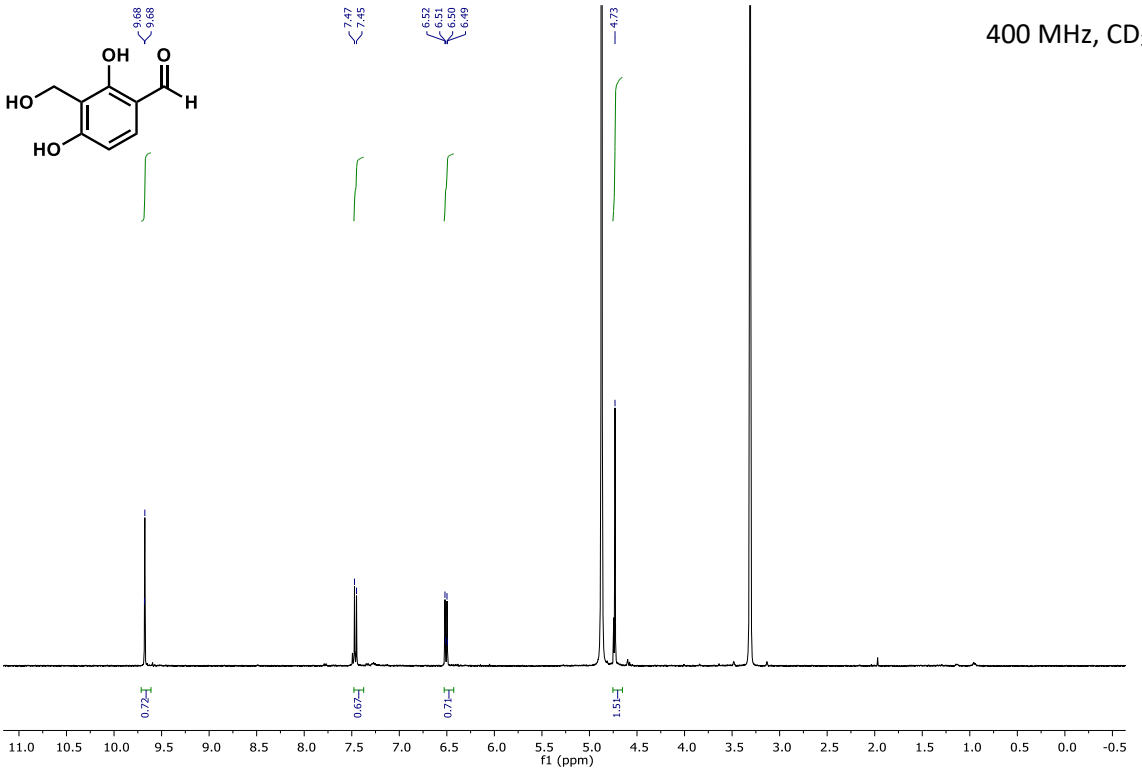


400 MHz, $CD_3OD$

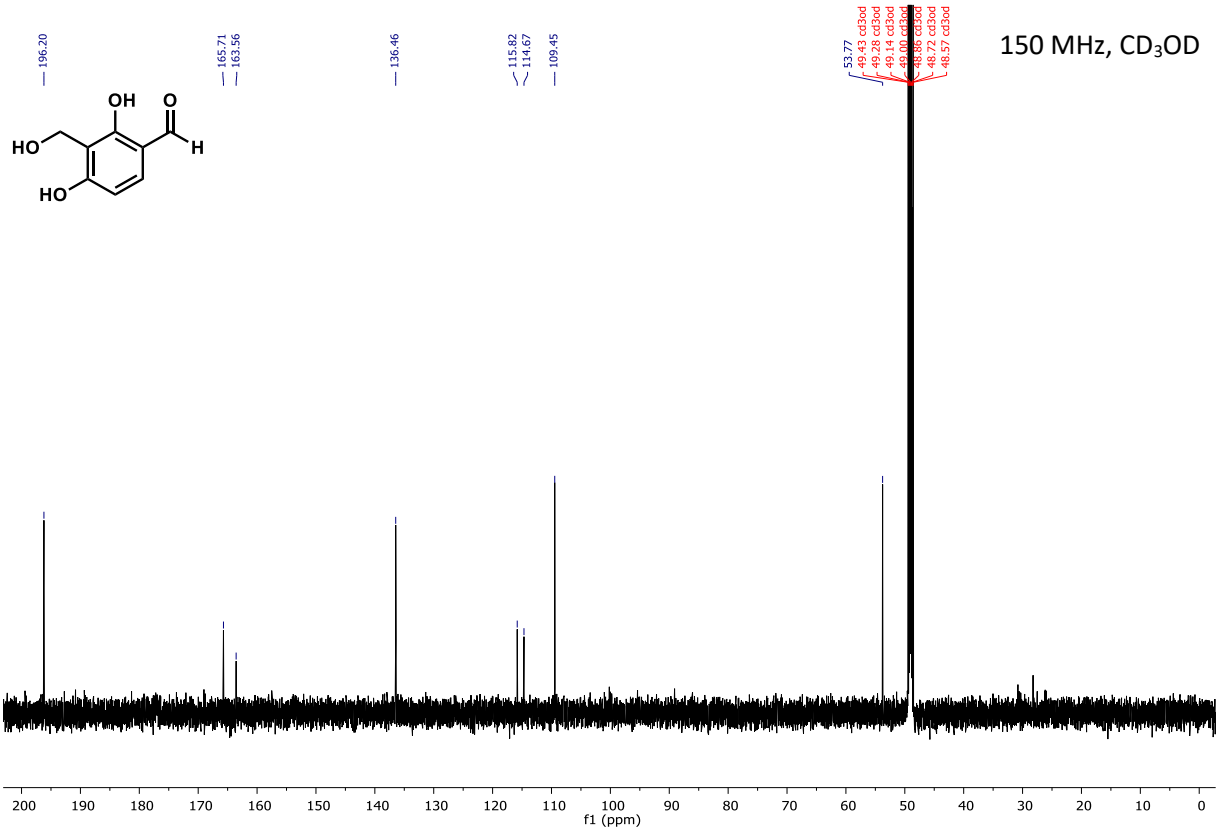


150 MHz, $CD_3OD$

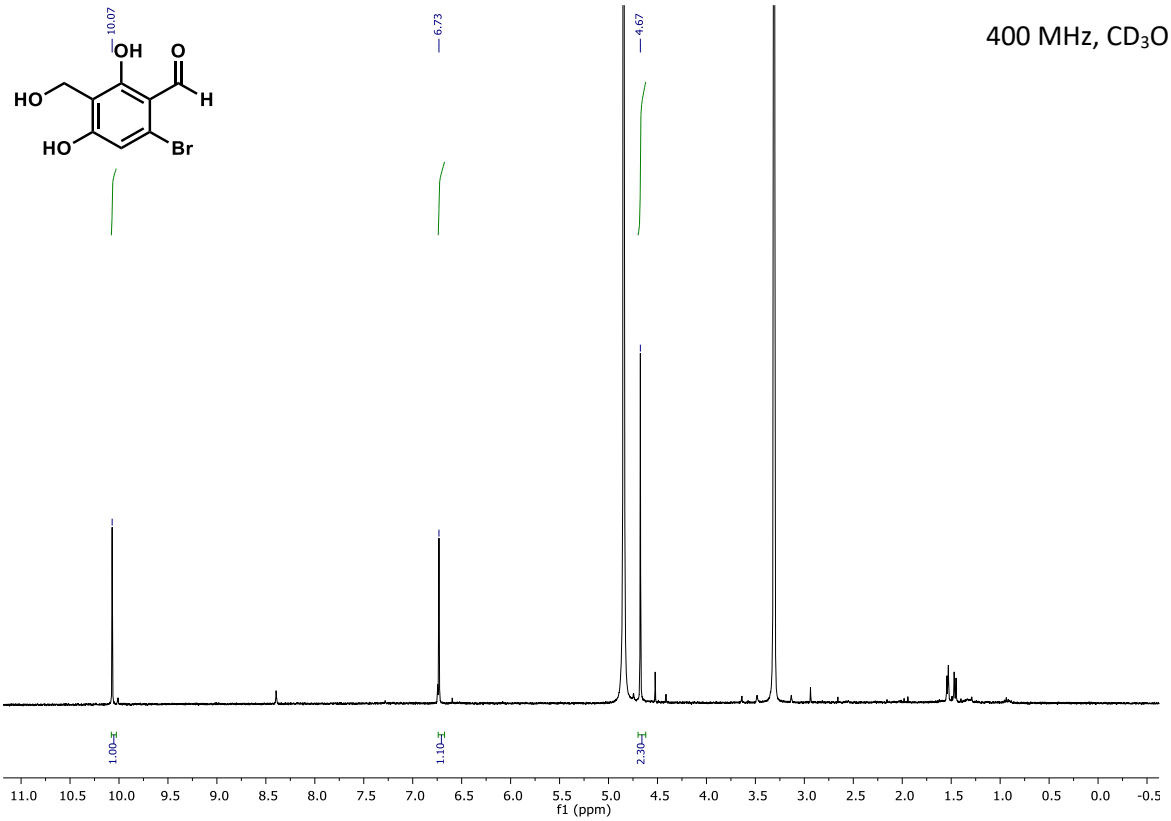


400 MHz, $CD_3OD$

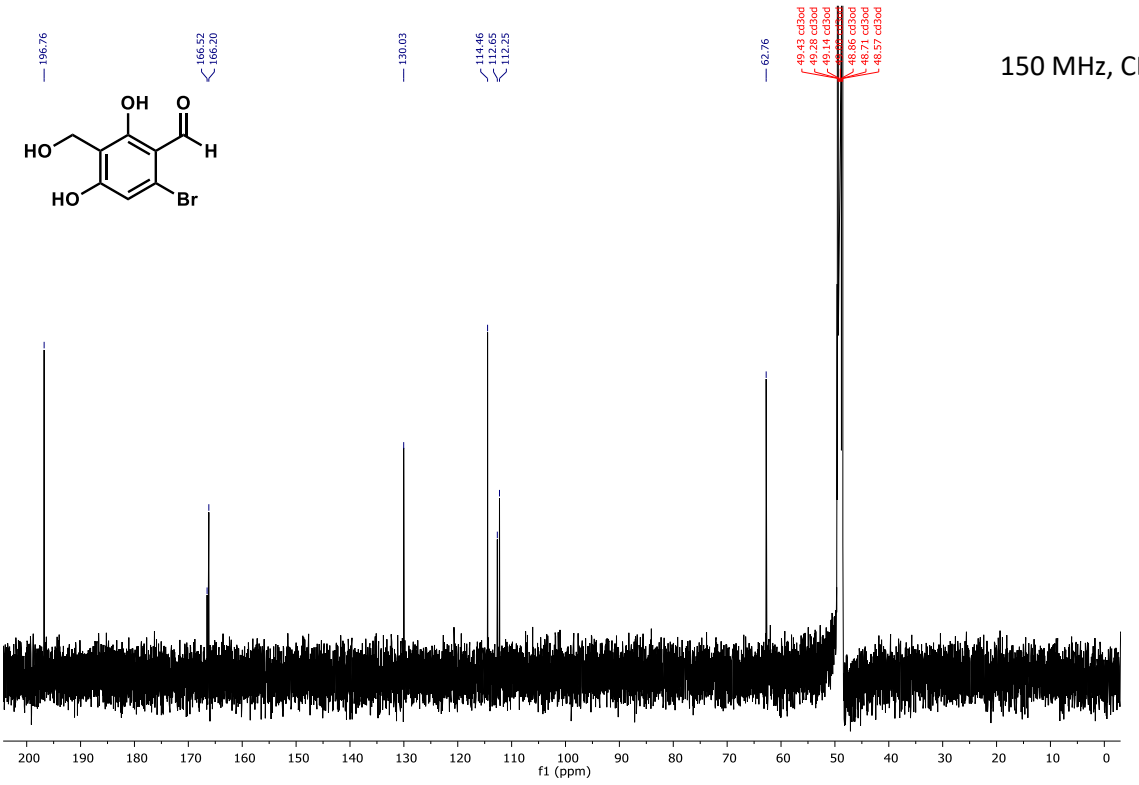


150 MHz, $CD_3OD$

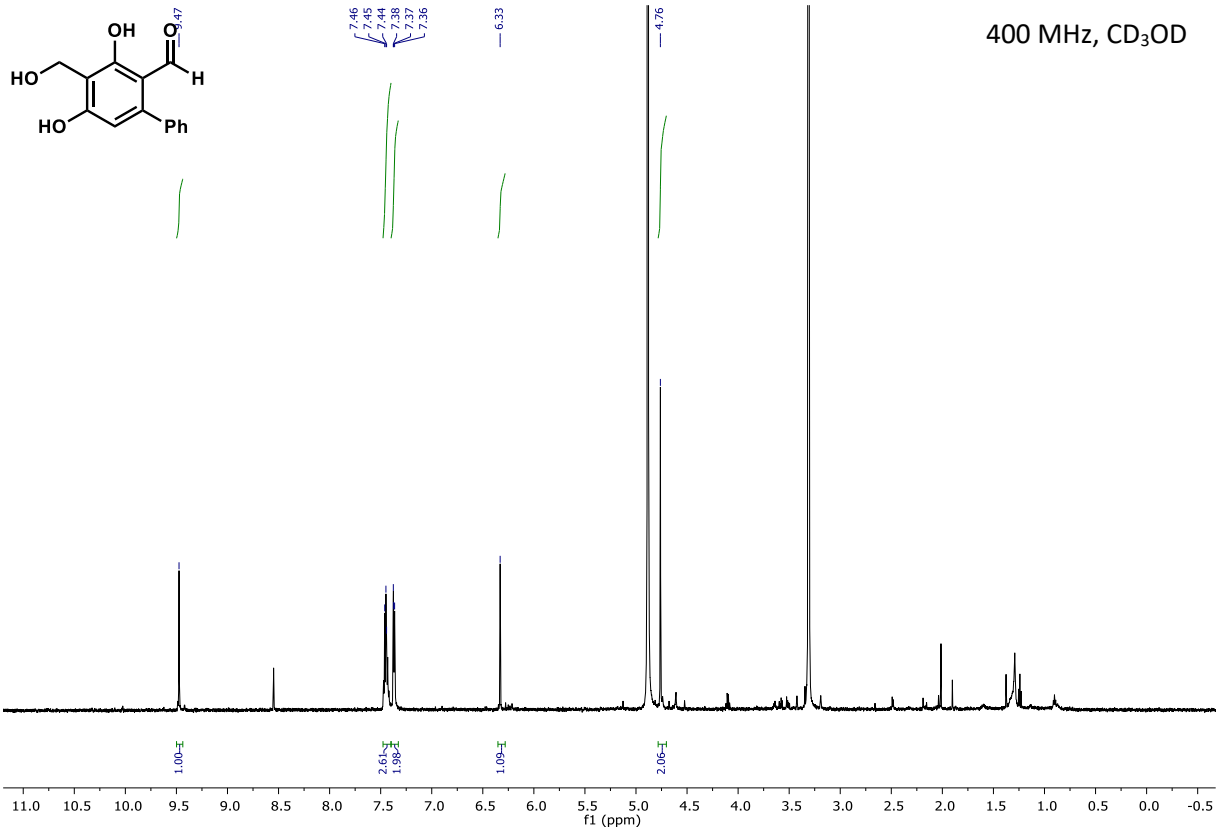
OH
O
HO
H
HO
Ph
9.47
7.46
7.45
7.44
7.38
7.37
7.36
6.33
4.76
1.00
2.61
1.98
1.09
2.06
11.0 10.5 10.0 9.5 9.0 8.5 8.0 7.5 7.0 6.5 6.0 5.5 5.0 4.5 4.0 3.5 3.0 2.5 2.0 1.5 1.0 0.5 0.0 -0.5
f1 (ppm)
400 MHz, CD3OD

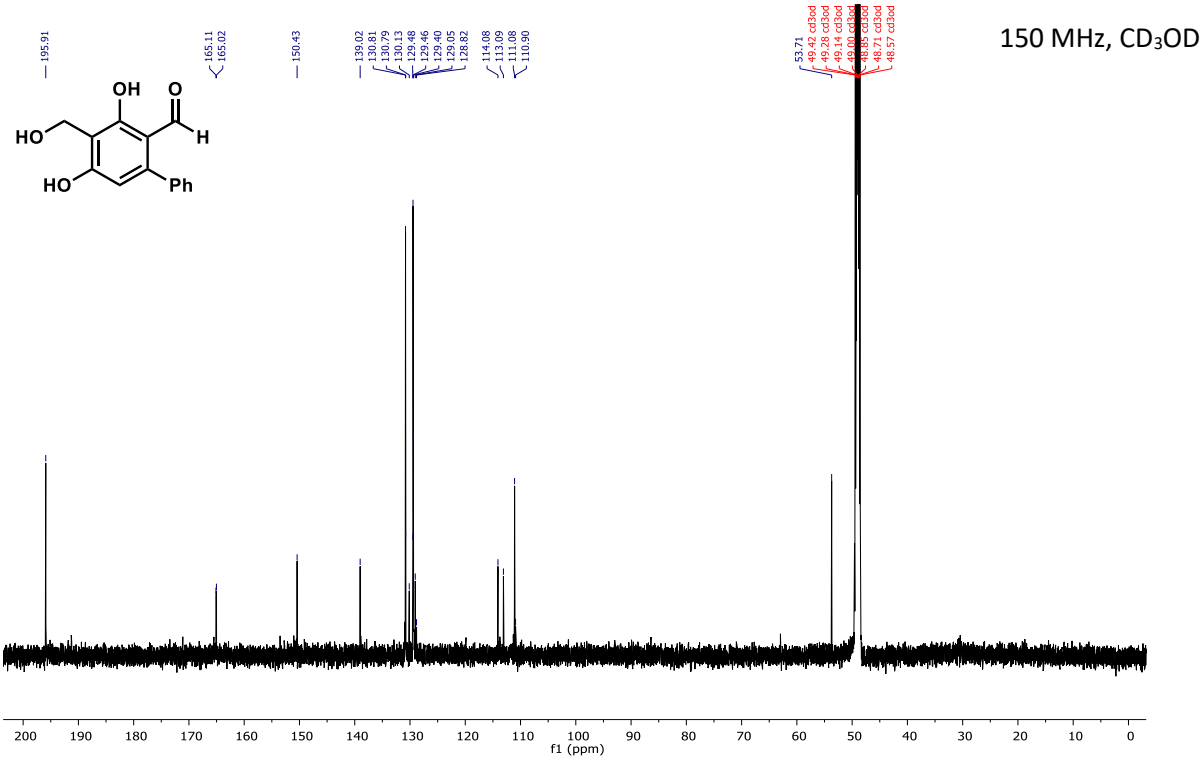
OH
O
HO
H
HO
Ph
195.91
165.11
165.02
150.43
139.02
130.81
130.79
130.13
129.48
129.46
129.40
129.05
128.82
114.08
113.09
111.08
110.90
53.71
49.42 cd3od
49.28 cd3od
49.14 cd3od
49.00 cd3od
48.85 cd3od
48.71 cd3od
48.57 cd3od
200 190 180 170 160 150 140 130 120 110 100 90 80 70 60 50 40 30 20 10 0
f1 (ppm)
150 MHz, CD3OD

400 MHz, $CD_3OD$

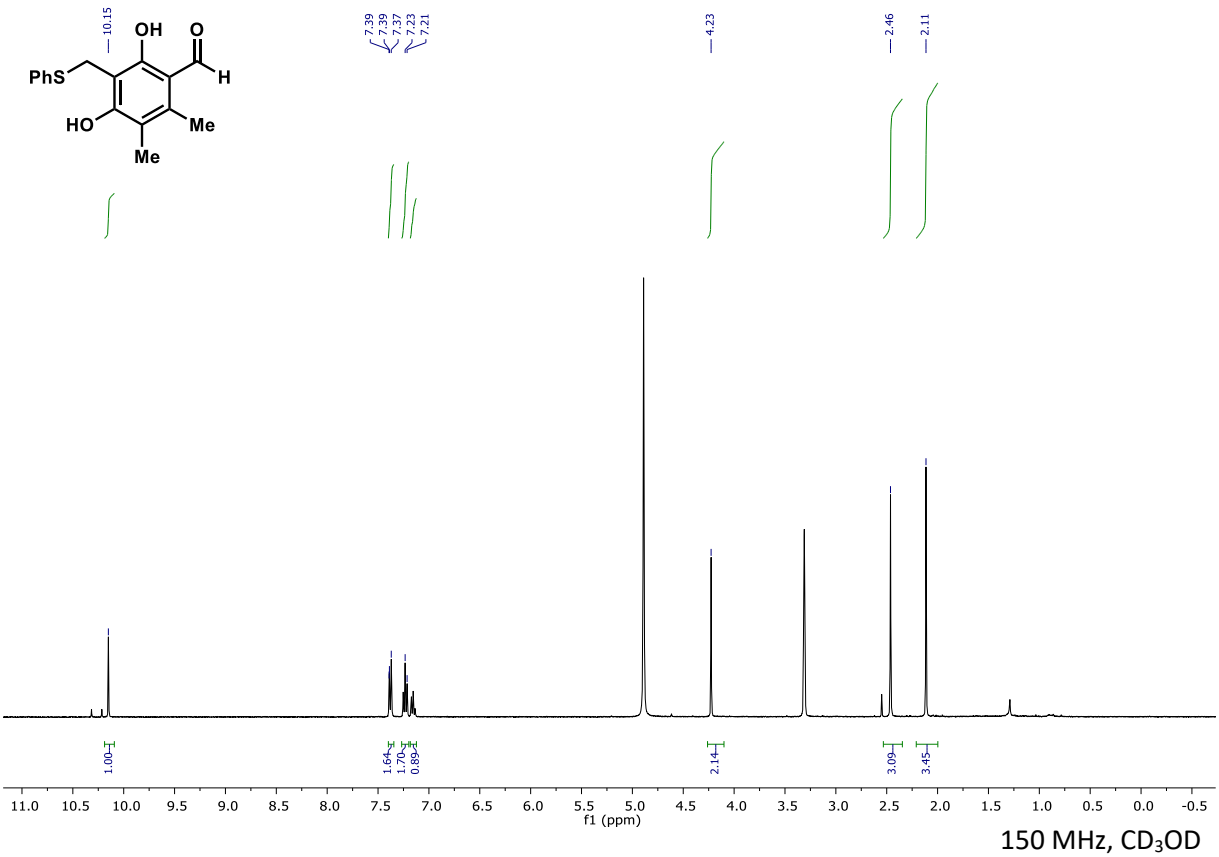


150 MHz, $CD_3OD$

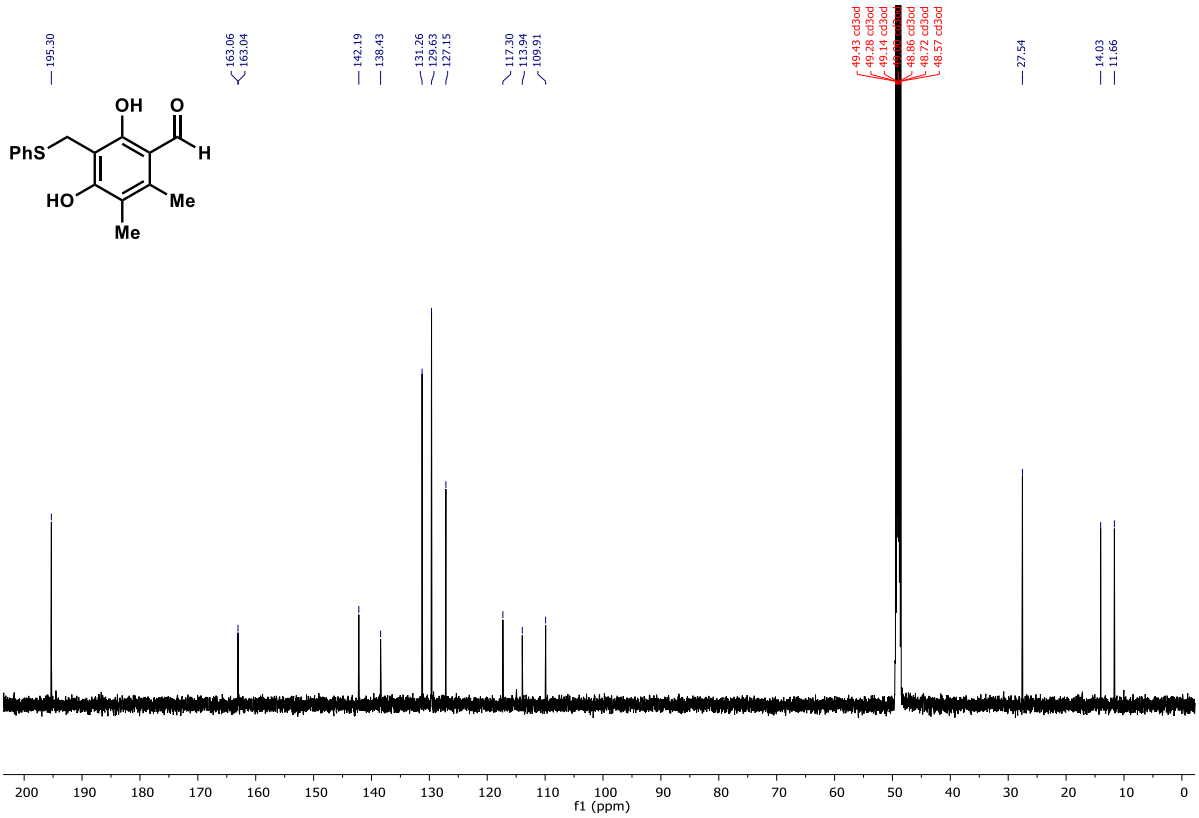
195.30
163.06
163.04
142.19
138.43
131.26
129.63
127.15
117.30
113.94
109.91
49.43 cd3od
49.28 cd3od
49.14 cd3od
48.86 cd3od
48.72 cd3od
48.57 cd3od
27.54
14.03
11.66
OH
O
PhS
H
HO
Me
Me
200
190
180
170
160
150
140
130
120
110
100
90
80
70
60
50
40
30
20
10
0
f1 (ppm)

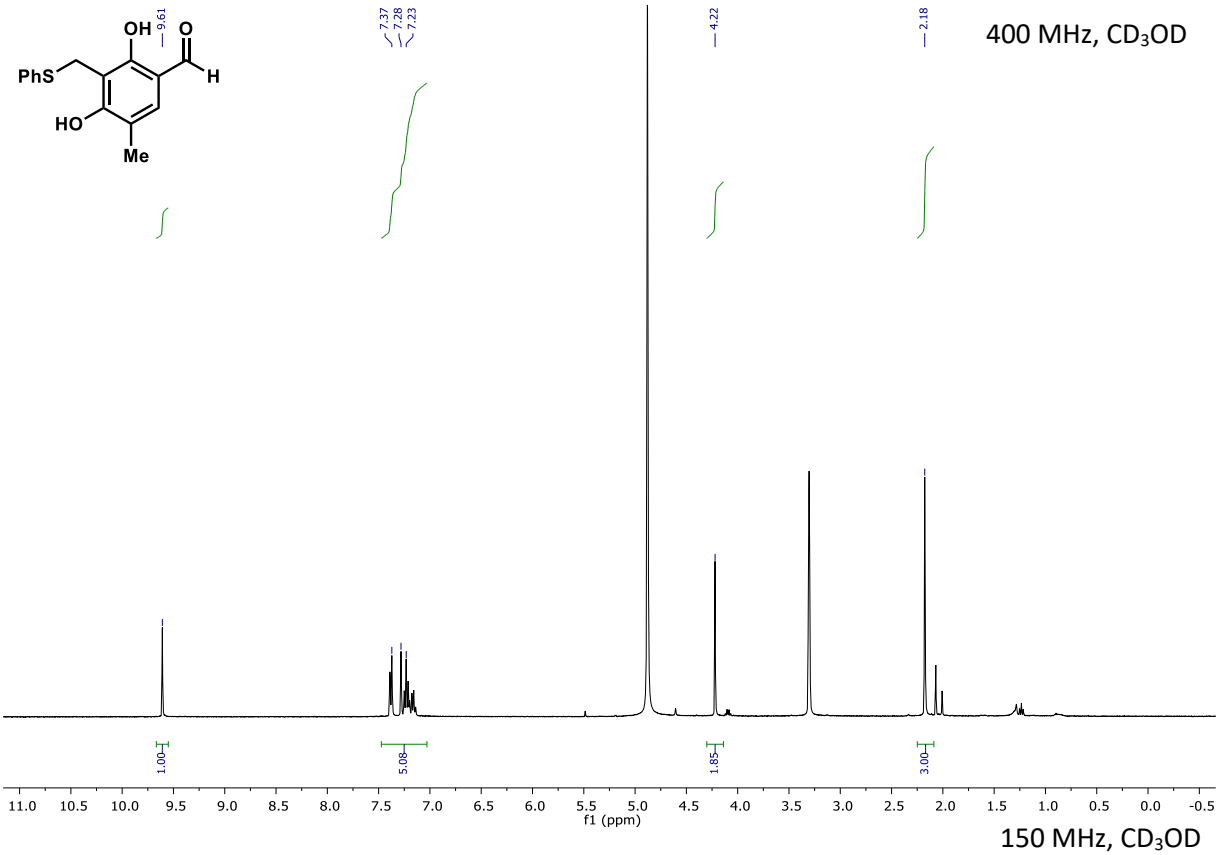
OH
O
PhS
H
HO
Me
9.61
7.37
7.28
7.23
4.22
2.18
400 MHz, CD3OD
1.00
5.08
1.85
3.00
f1 (ppm)

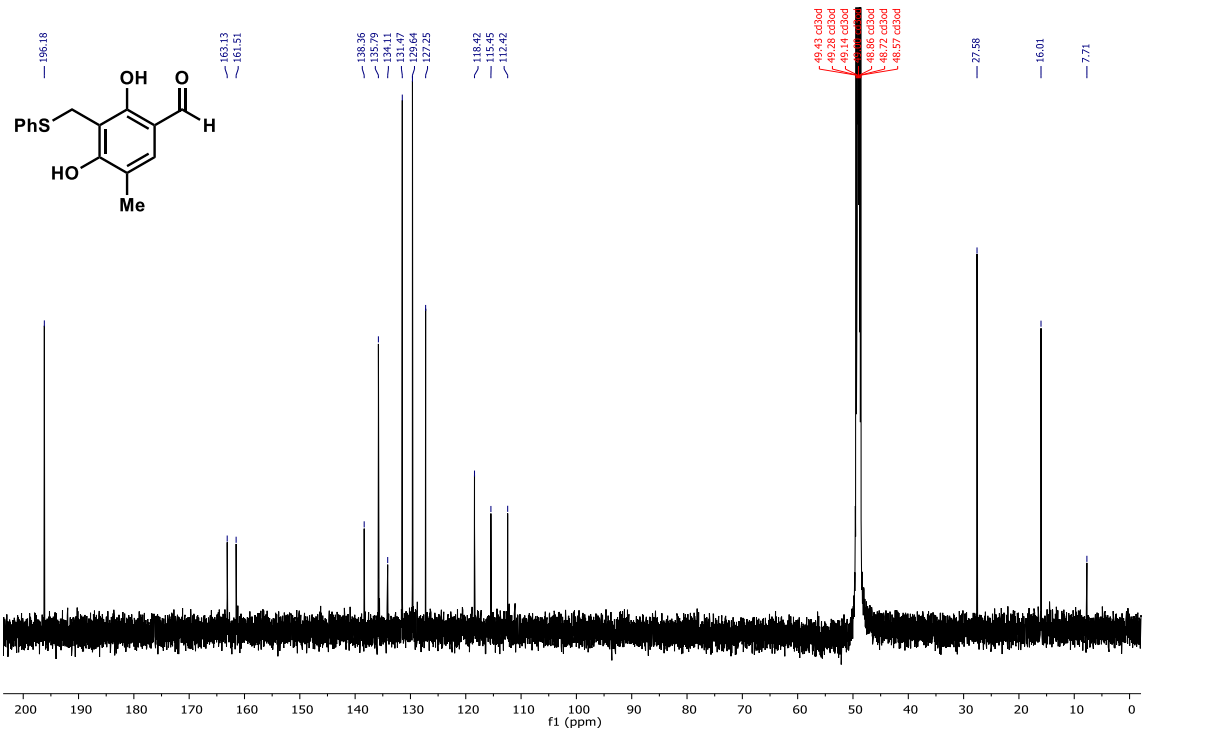
150 MHz, CD3OD
OH
O
PhS
H
HO
Me
196.18
163.13
161.51
138.36
135.79
134.11
131.47
129.64
127.25
118.42
115.45
112.42
49.43 cd3od
49.28 cd3od
49.14 cd3od
48.86 cd3od
48.72 cd3od
48.57 cd3od
27.58
16.01
7.71
f1 (ppm)

400 MHz, $CD_3OD$

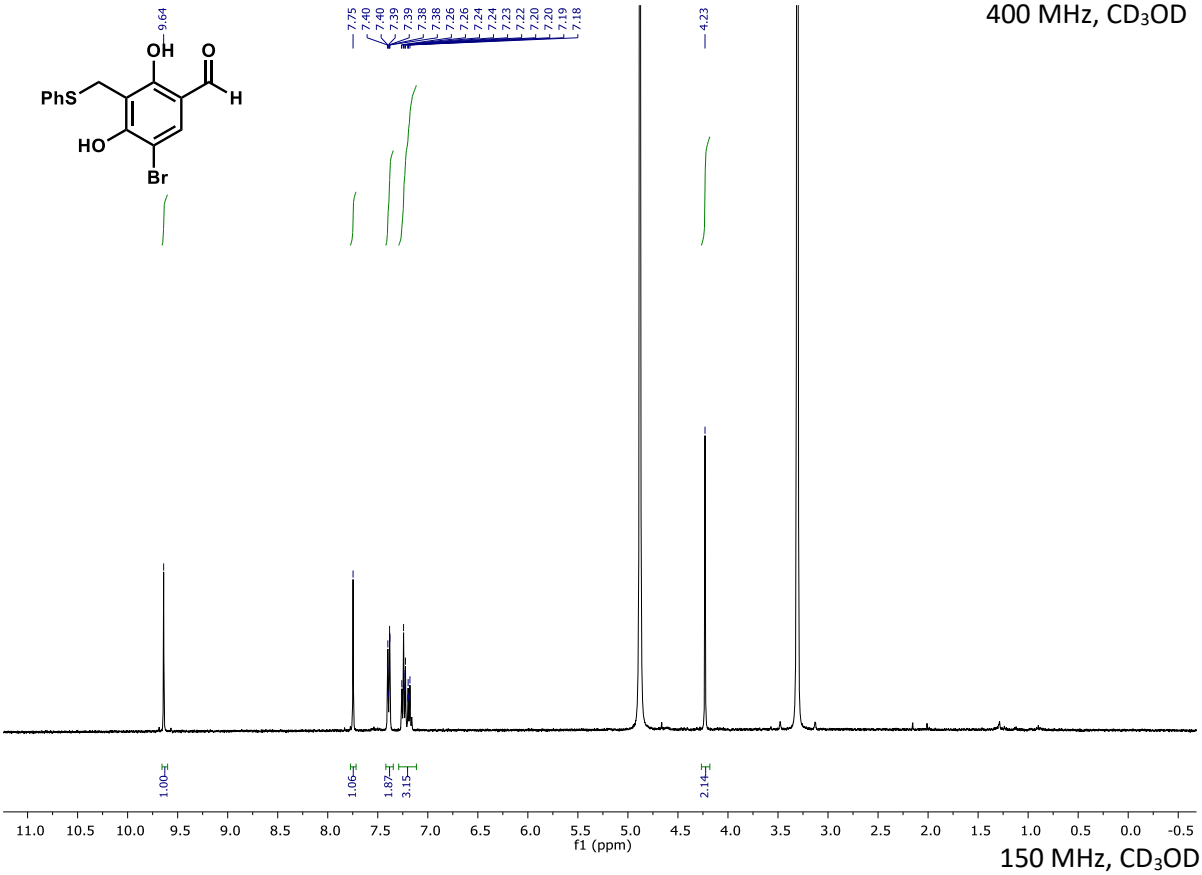


150 MHz, $CD_3OD$

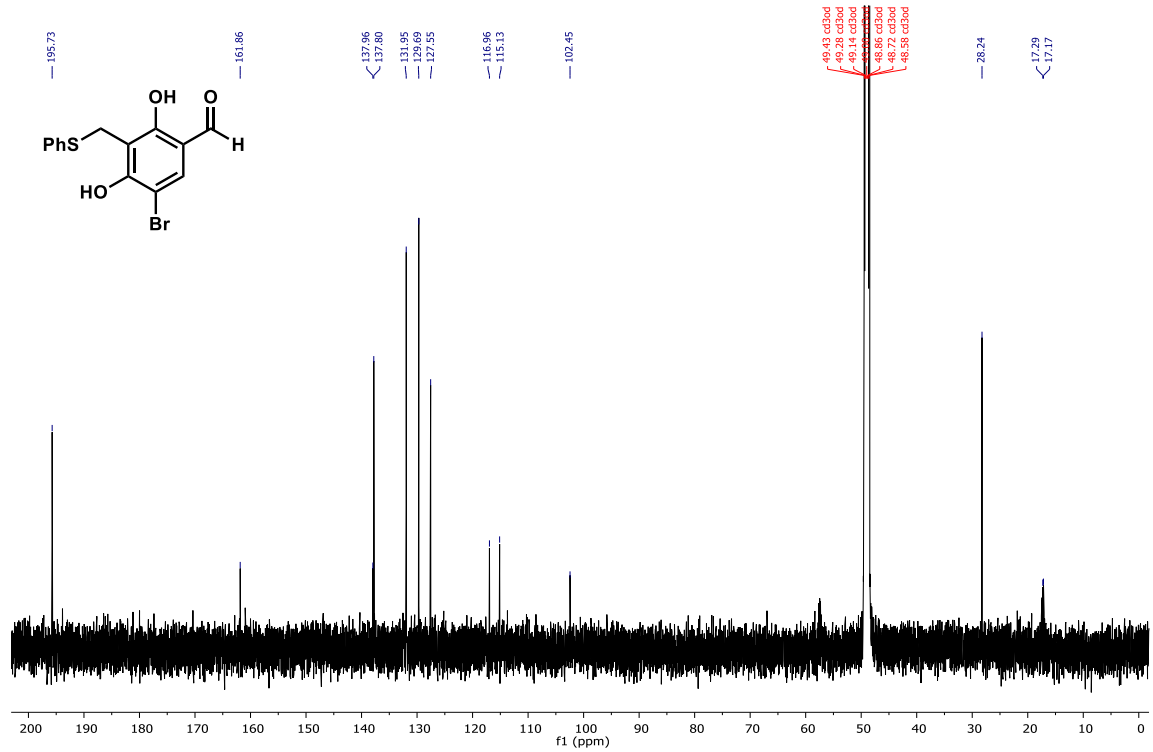

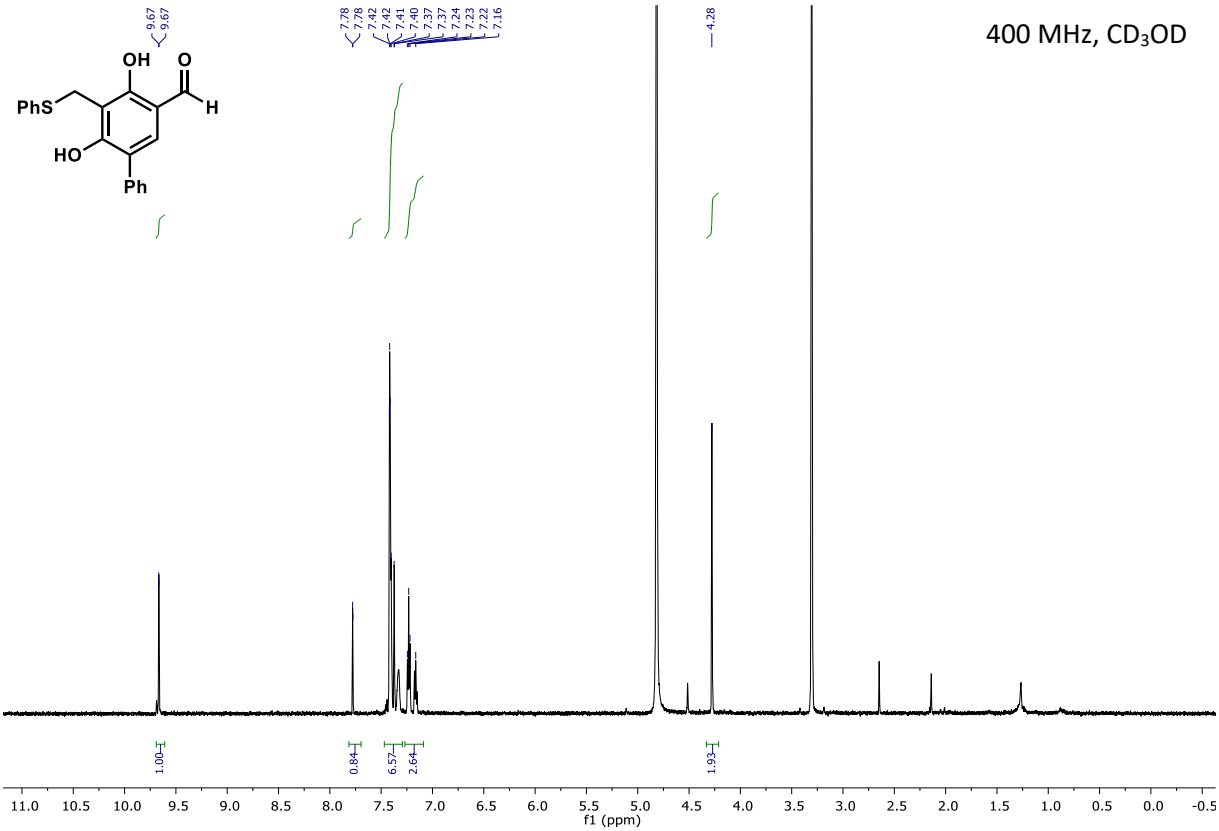
400 MHz, CD3OD
OH
O
H
PhS
HO
Ph
9.67
9.67
7.78
7.78
7.42
7.42
7.41
7.40
7.37
7.37
7.24
7.23
7.22
7.16
4.28
1.00
0.84
6.57
2.64
1.93
f1 (ppm)

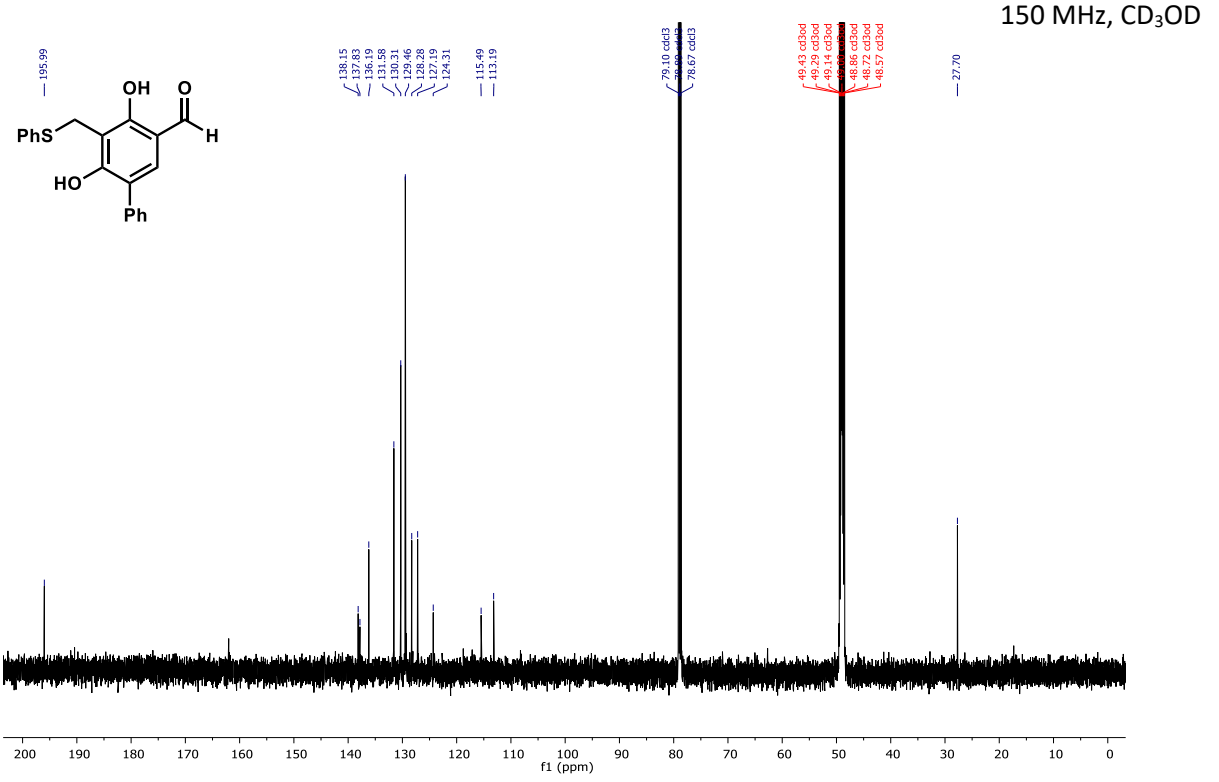
150 MHz, CD3OD
OH
O
H
PhS
HO
Ph
195.99
138.15
137.83
136.19
131.58
130.31
129.46
128.28
127.19
124.31
115.49
113.19
79.10 cdcl3
78.67 cdcl3
49.43 cd3od
49.29 cd3od
49.14 cd3od
48.86 cd3od
48.72 cd3od
48.57 cd3od
27.70
f1 (ppm)

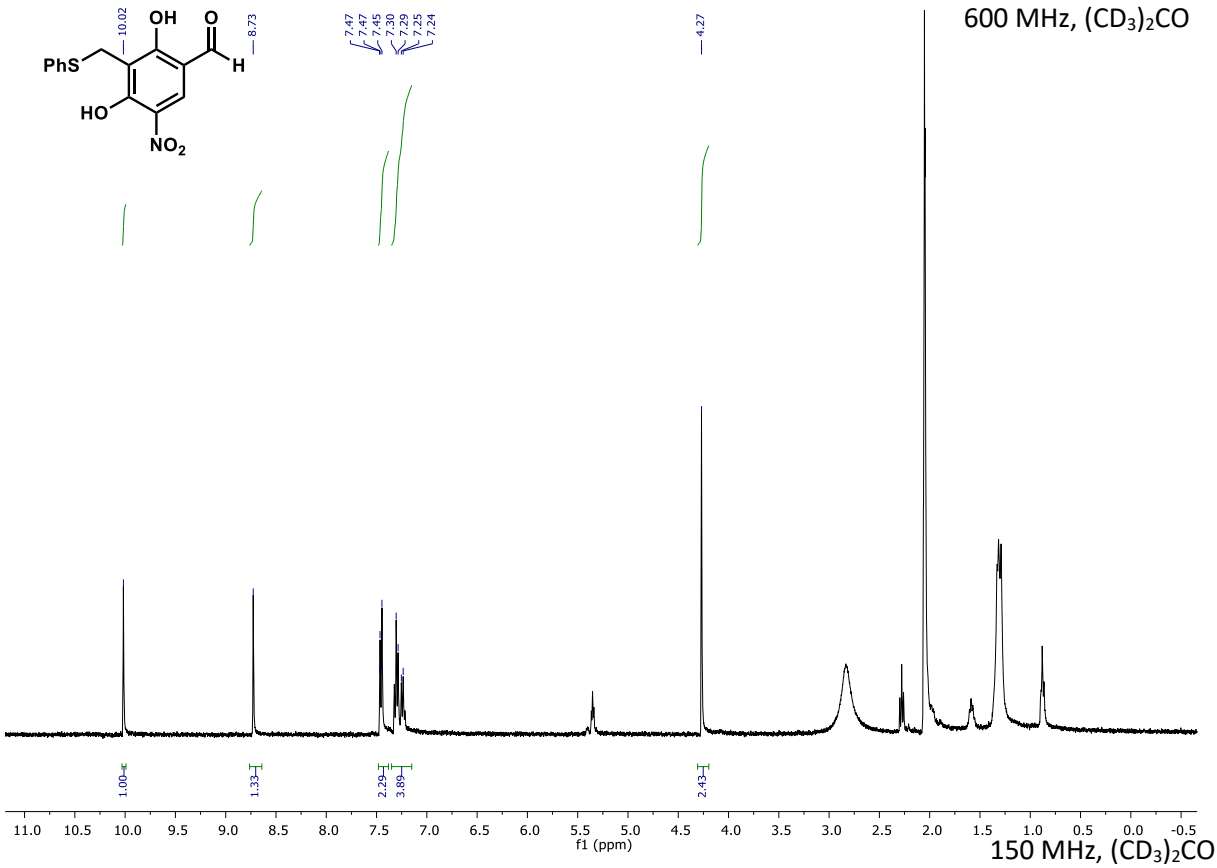
600 MHz, (CD3)2CO
OH
O
H
PhS
HO
NO2
10.02
8.73
7.47
7.47
7.45
7.30
7.29
7.25
7.24
4.27
1.00
1.33
2.29
3.89
2.43
f1 (ppm)

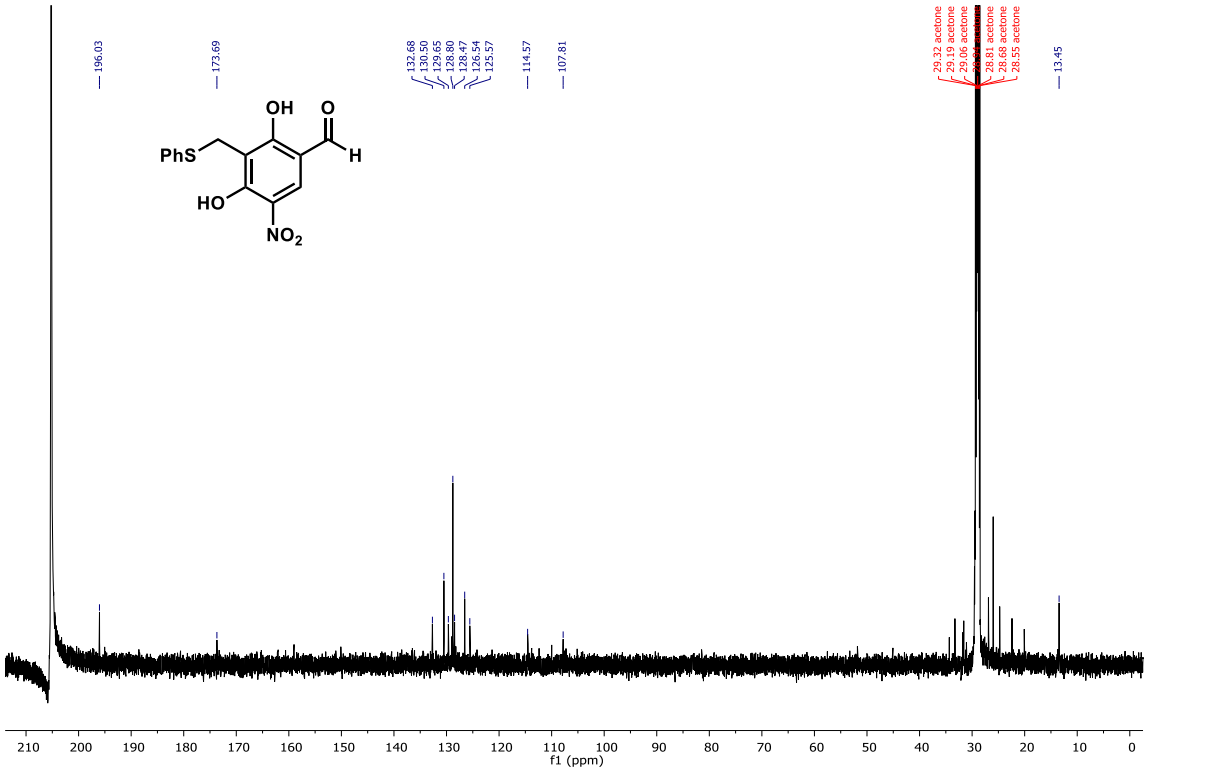
150 MHz, (CD3)2CO
OH
O
H
PhS
HO
NO2
196.03
173.69
132.68
130.50
129.65
128.80
128.47
126.54
125.57
114.57
107.81
29.32 acetone
29.19 acetone
29.06 acetone
28.61 acetone
28.48 acetone
28.35 acetone
13.45
f1 (ppm)

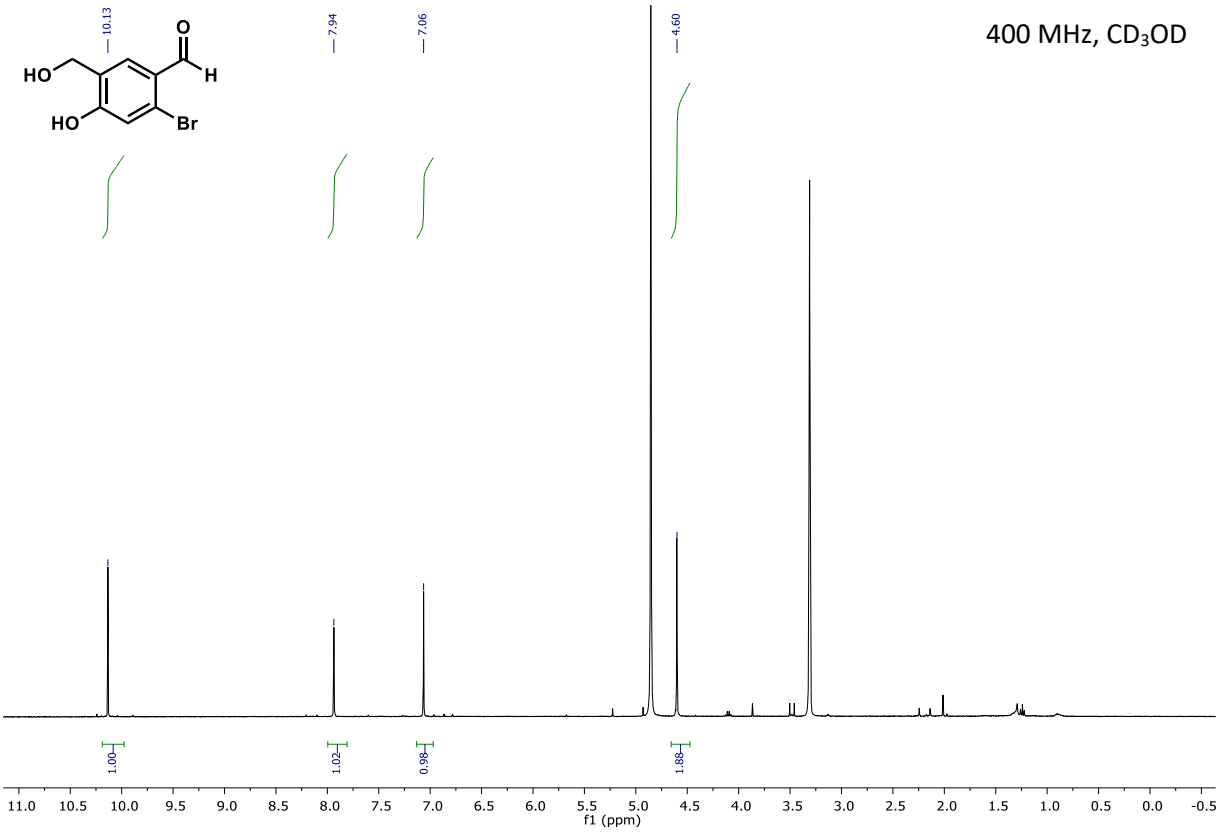
10.13
7.94
7.06
4.60
HO
O
H
HO
Br
400 MHz, CD3OD
1.00
1.02
0.98
1.88
11.0 10.5 10.0 9.5 9.0 8.5 8.0 7.5 7.0 6.5 6.0 5.5 5.0 4.5 4.0 3.5 3.0 2.5 2.0 1.5 1.0 0.5 0.0 -0.5
f1 (ppm)

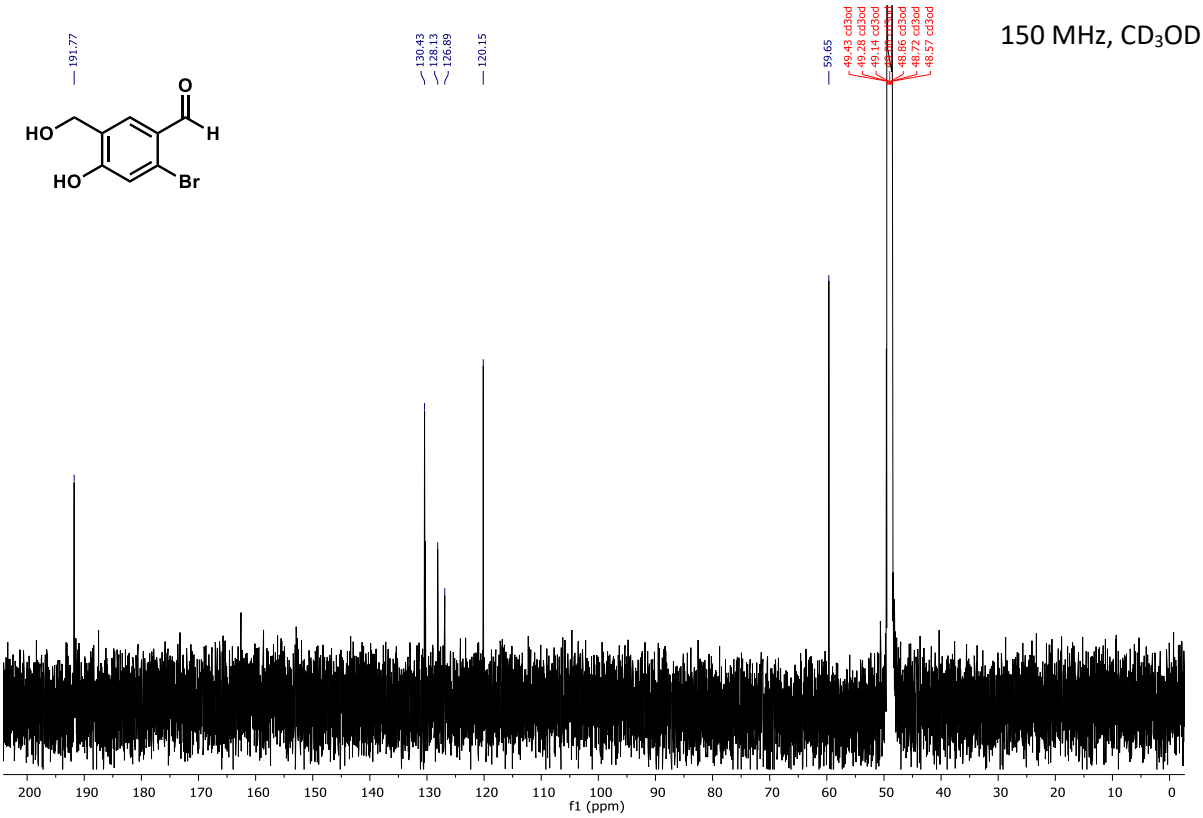
150 MHz, $CD_3OD$
191.77
130.43
128.13
126.89
120.15
59.65
49.43 cd3od
49.28 cd3od
49.14 cd3od
49.00 cd3od
48.86 cd3od
48.72 cd3od
48.57 cd3od
HO
O
H
HO
Br
200 190 180 170 160 150 140 130 120 110 100 90 80 70 60 50 40 30 20 10 0
f1 (ppm)

400 MHz, $CD_3OD$

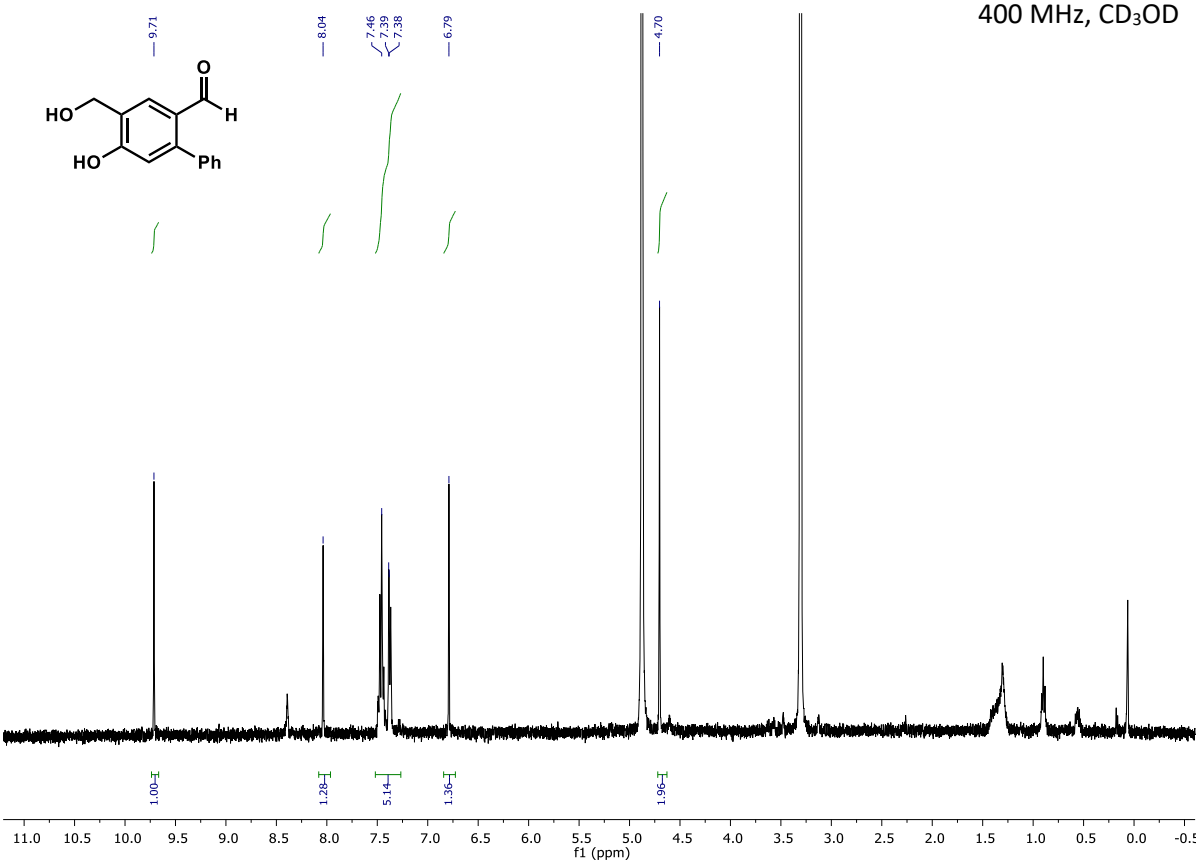


150 MHz, $CD_3OD$

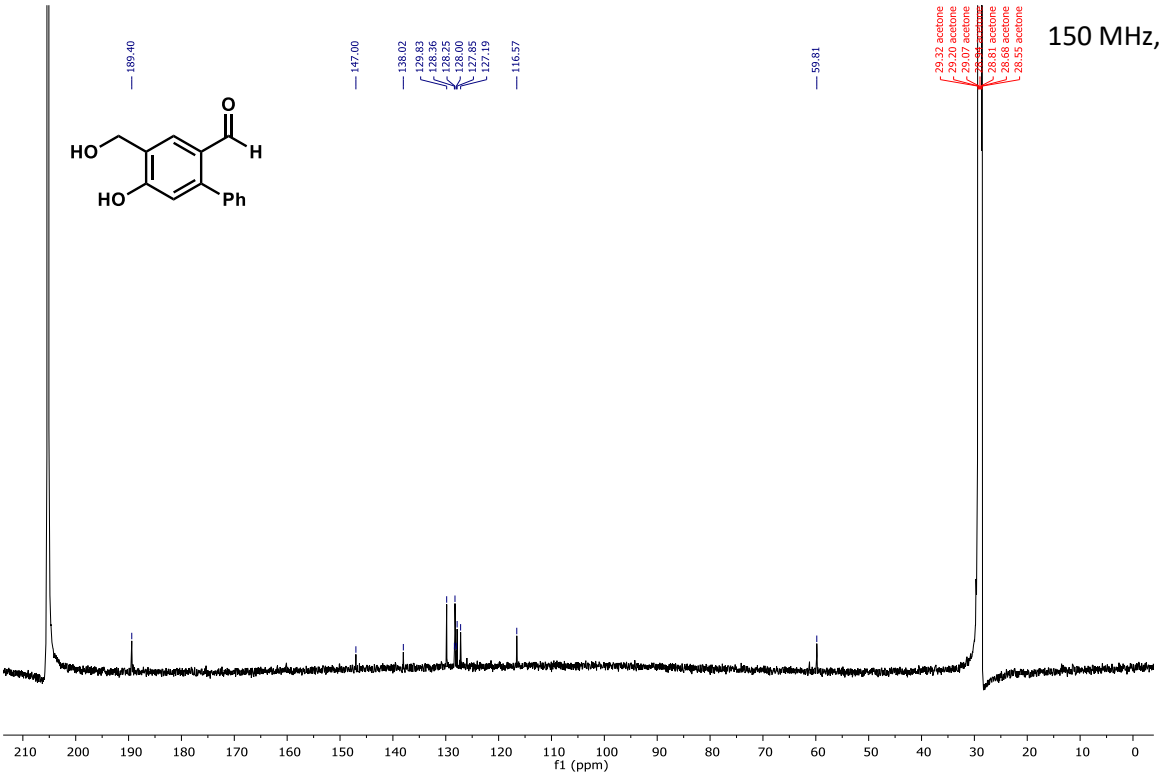

600 MHz, $(CD_3)_2CO$

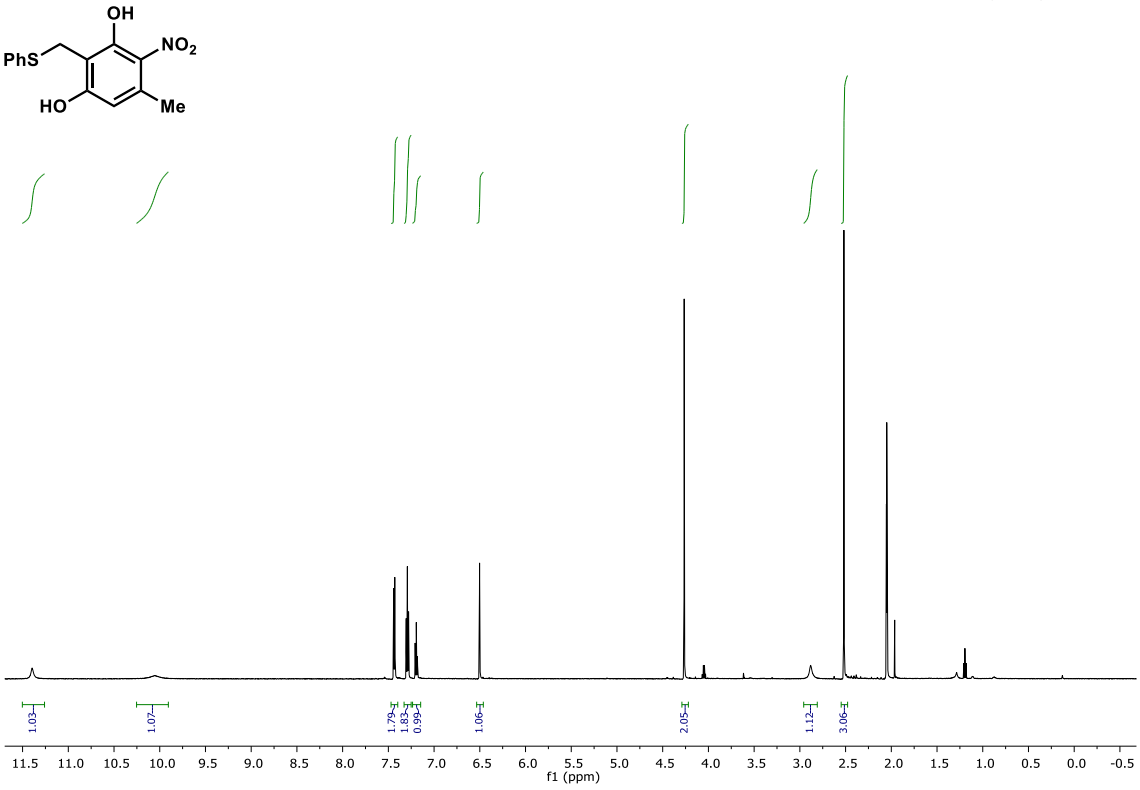


150 MHz, $(CD_3)_2CO$

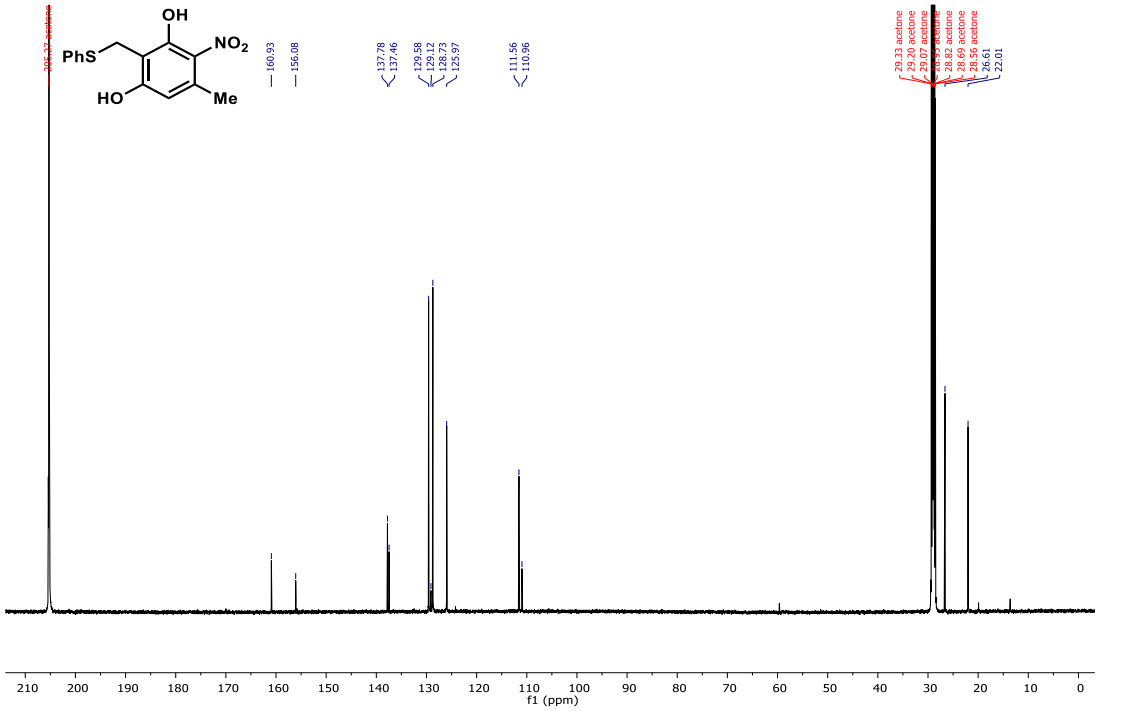

600 MHz, $CD_3OD$

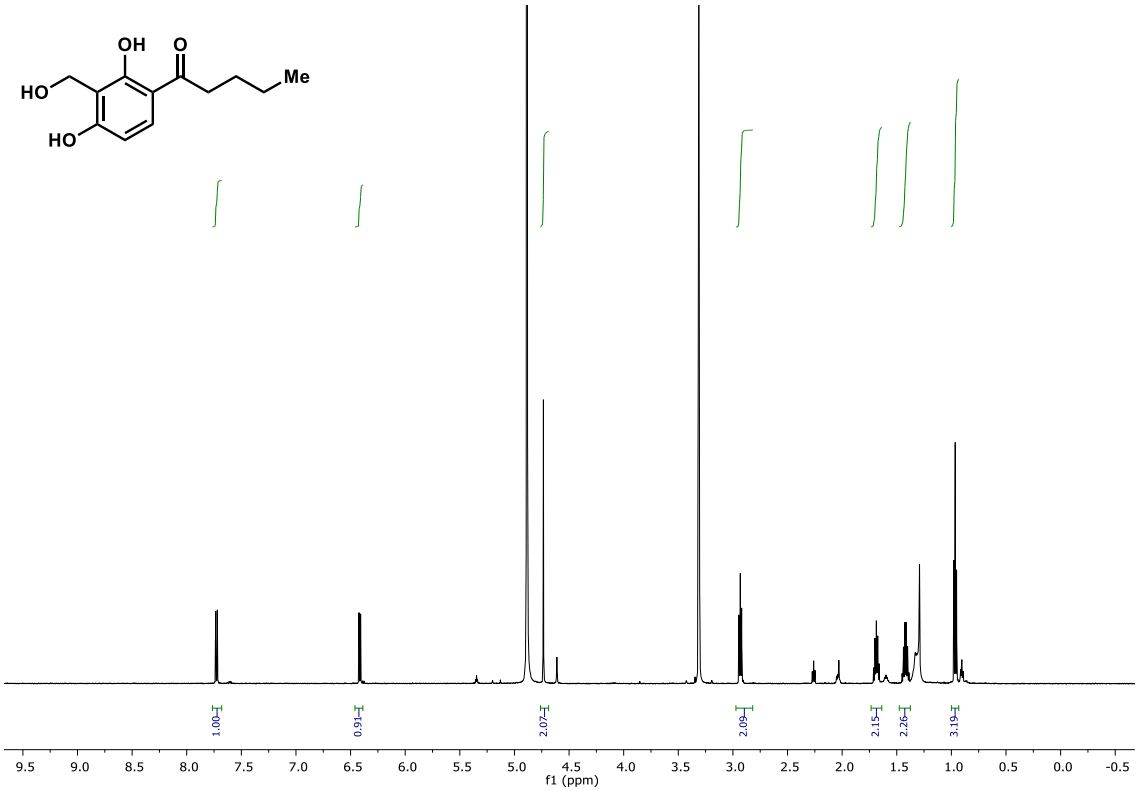


150 MHz, $CD_3OD$

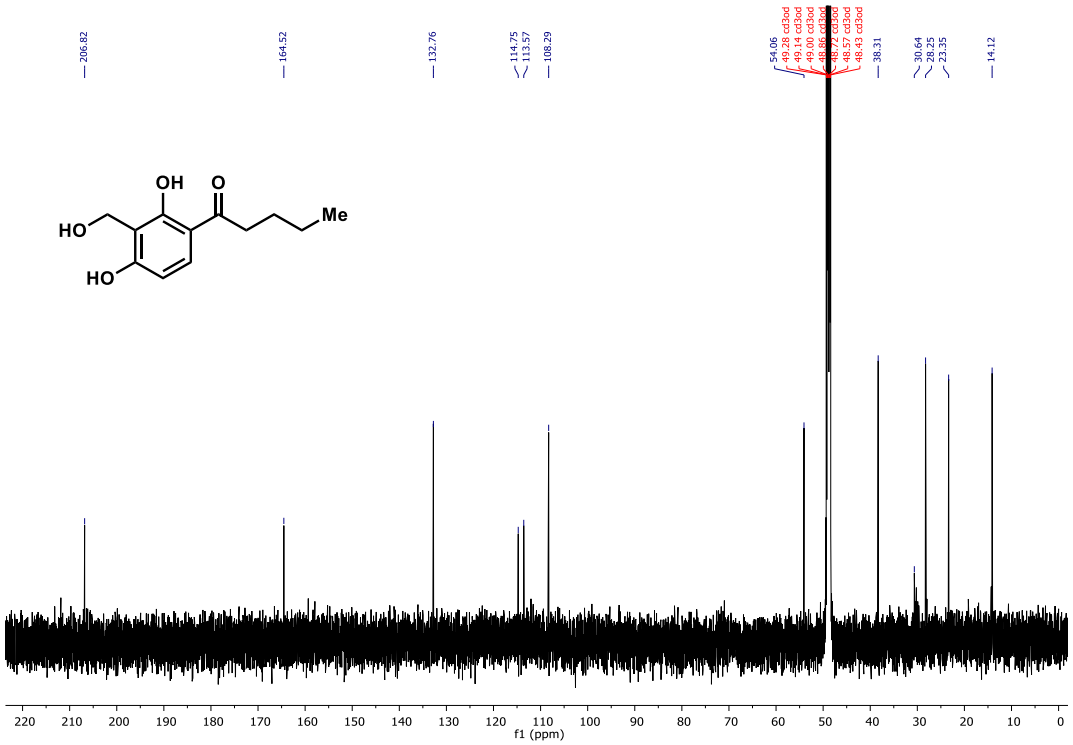

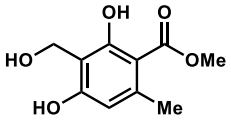


600 MHz, $CD_3OD$




150 MHz, $CD_3OD$

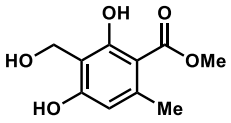

400 MHz, $CD_3CN$

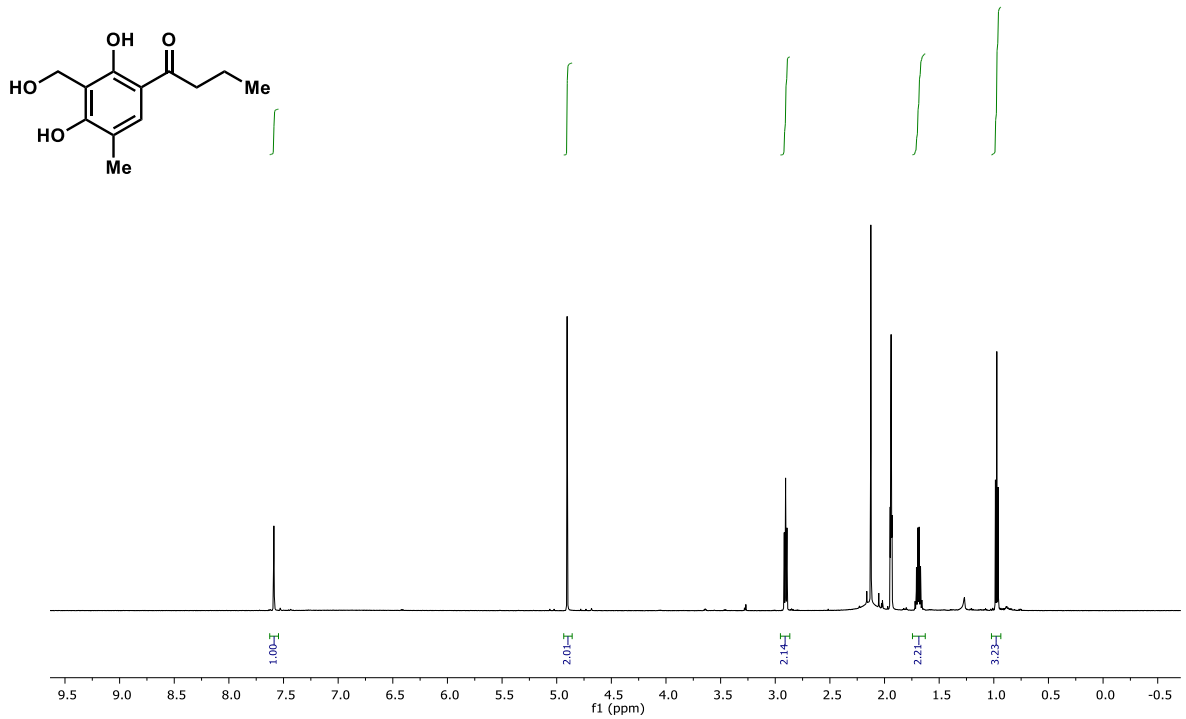


100 MHz, $CD_3CN$

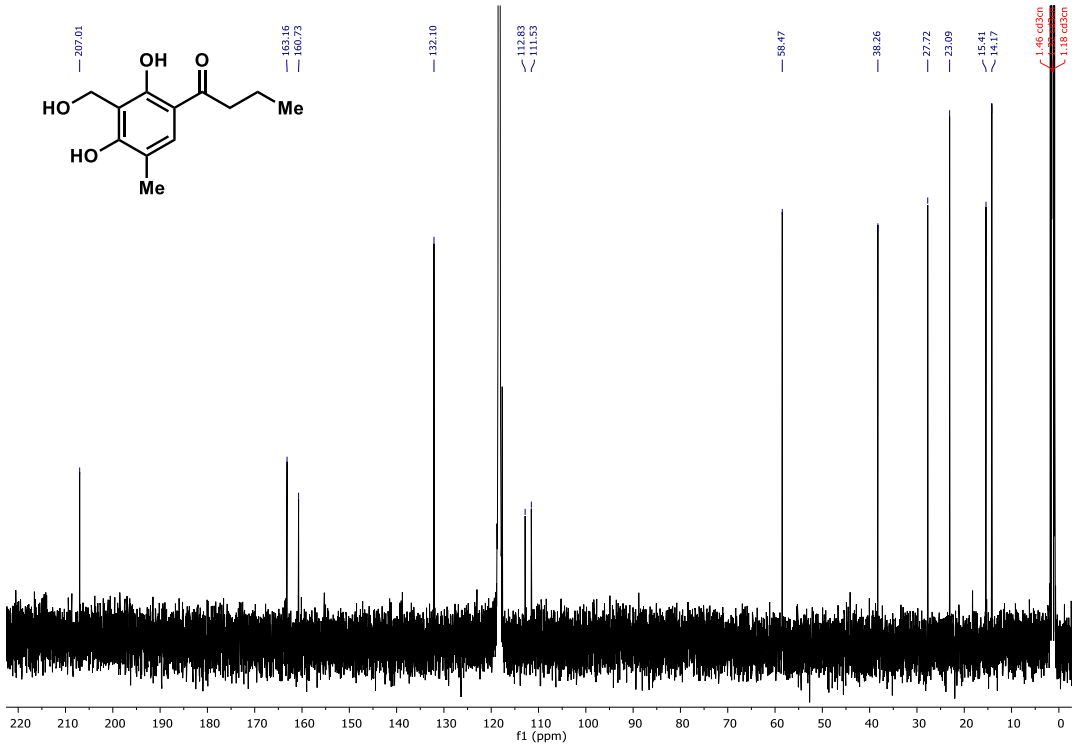

400 MHz, $CD_3CN$

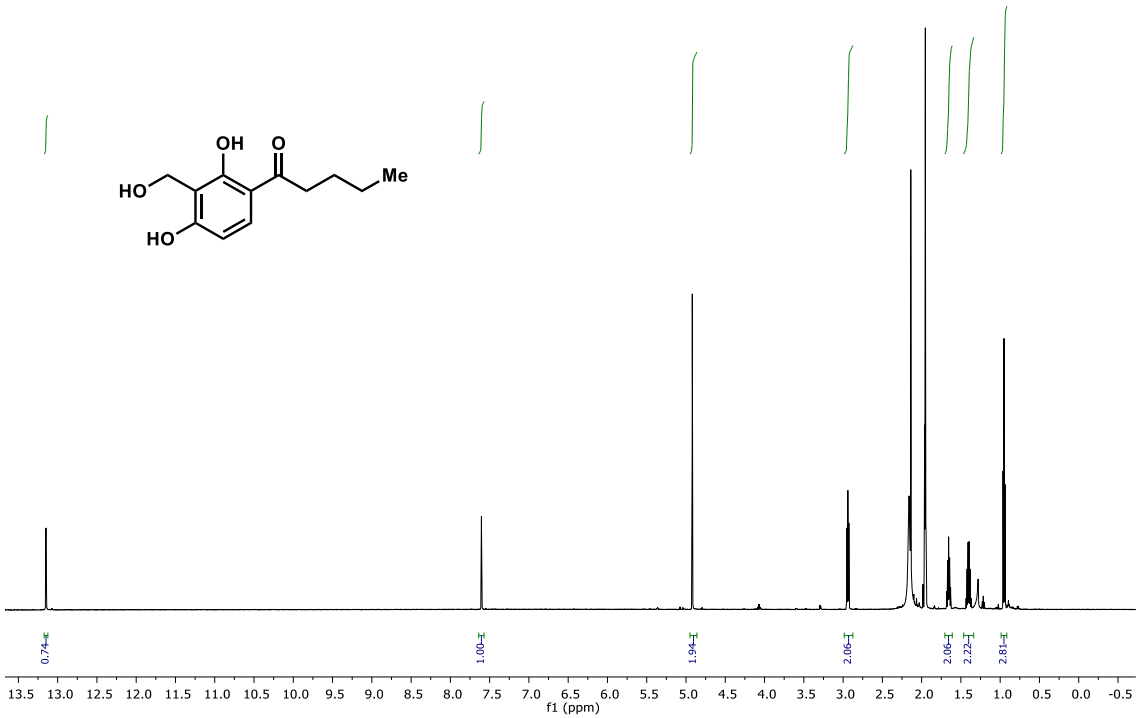


100 MHz, $CD_3CN$

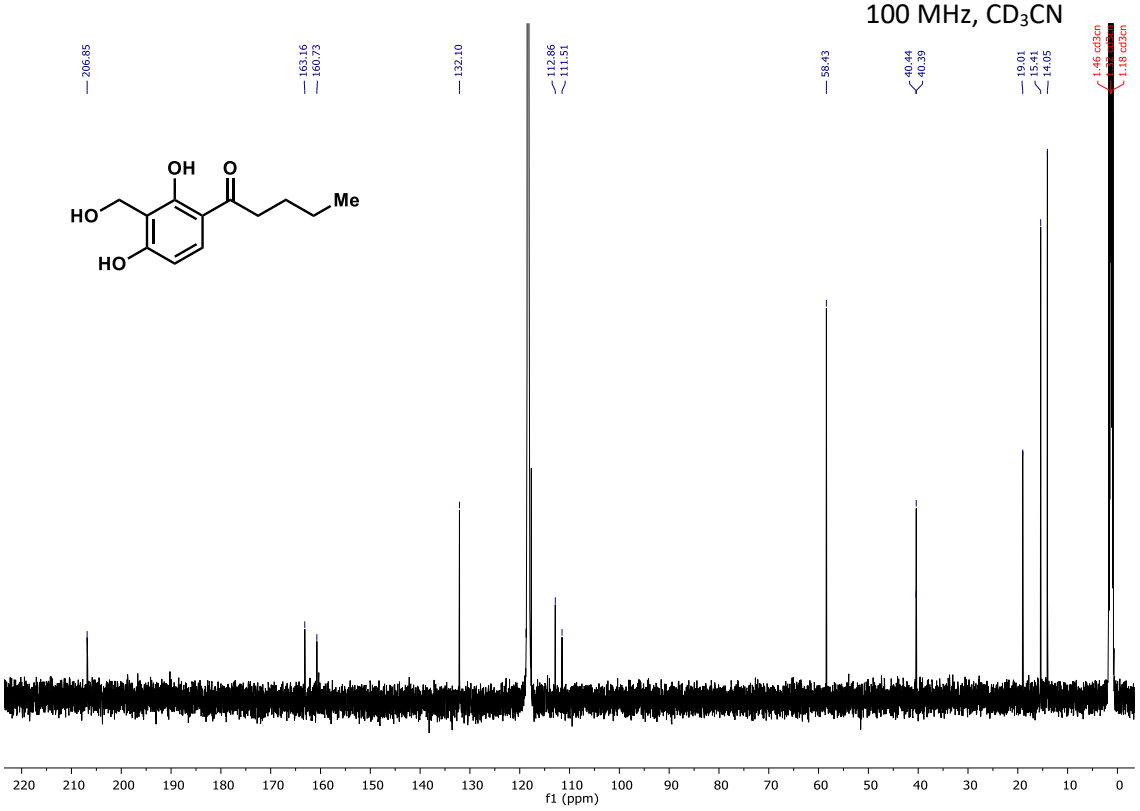

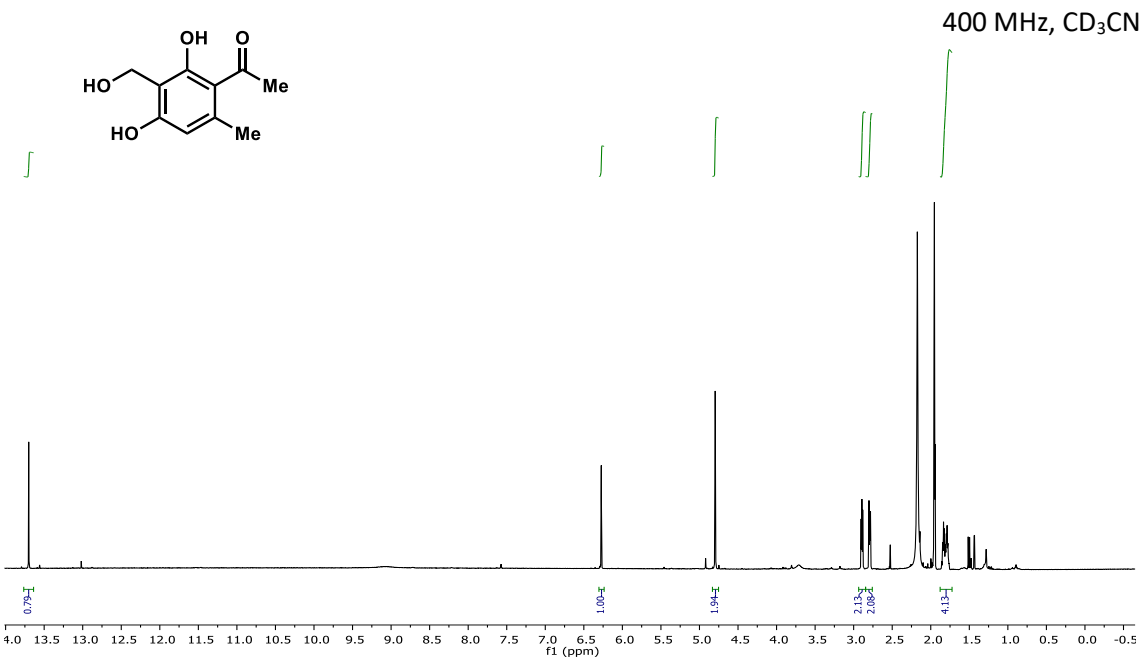
OH
O
HO
Me
HO
Me
400 MHz, CD3CN
0.79
1.00
1.94
2.13
2.08
4.13
f1 (ppm)

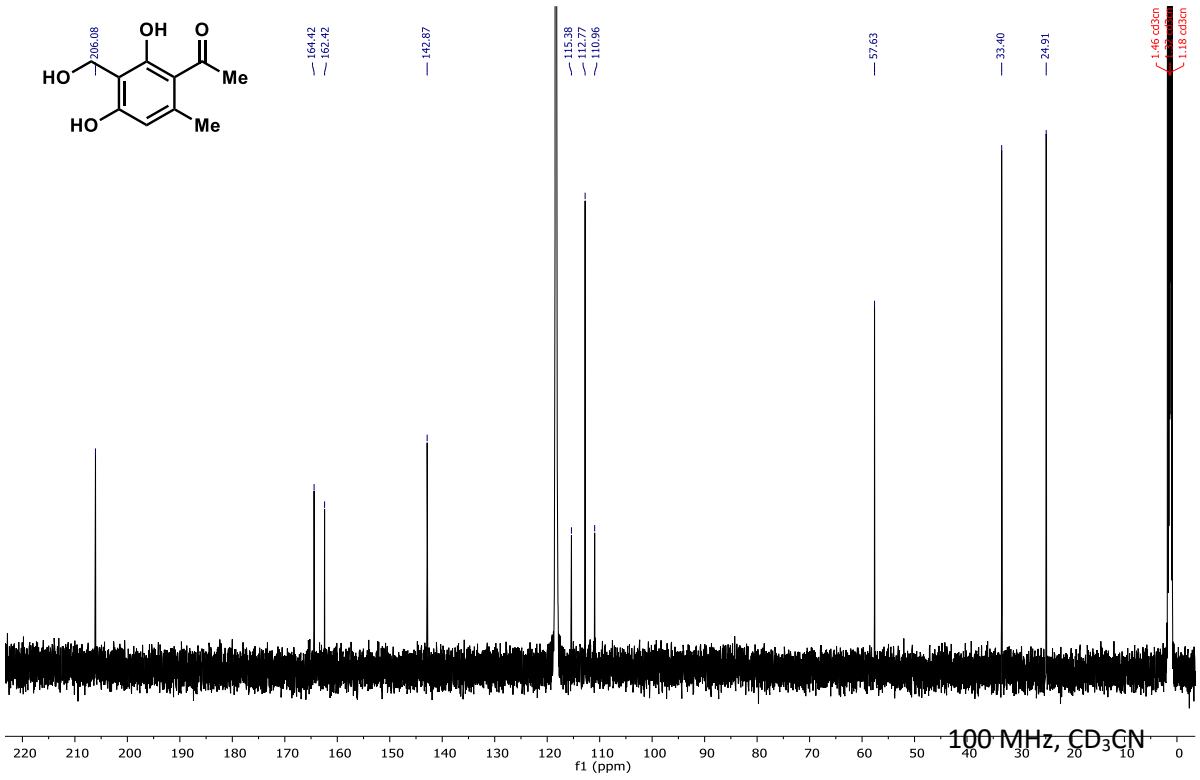
OH
O
HO
Me
HO
Me
206.08
164.42
162.42
142.87
115.38
112.77
110.96
57.63
33.40
24.91
1.46 cd3cn
1.18 cd3cn
100 MHz, CD3CN
f1 (ppm)

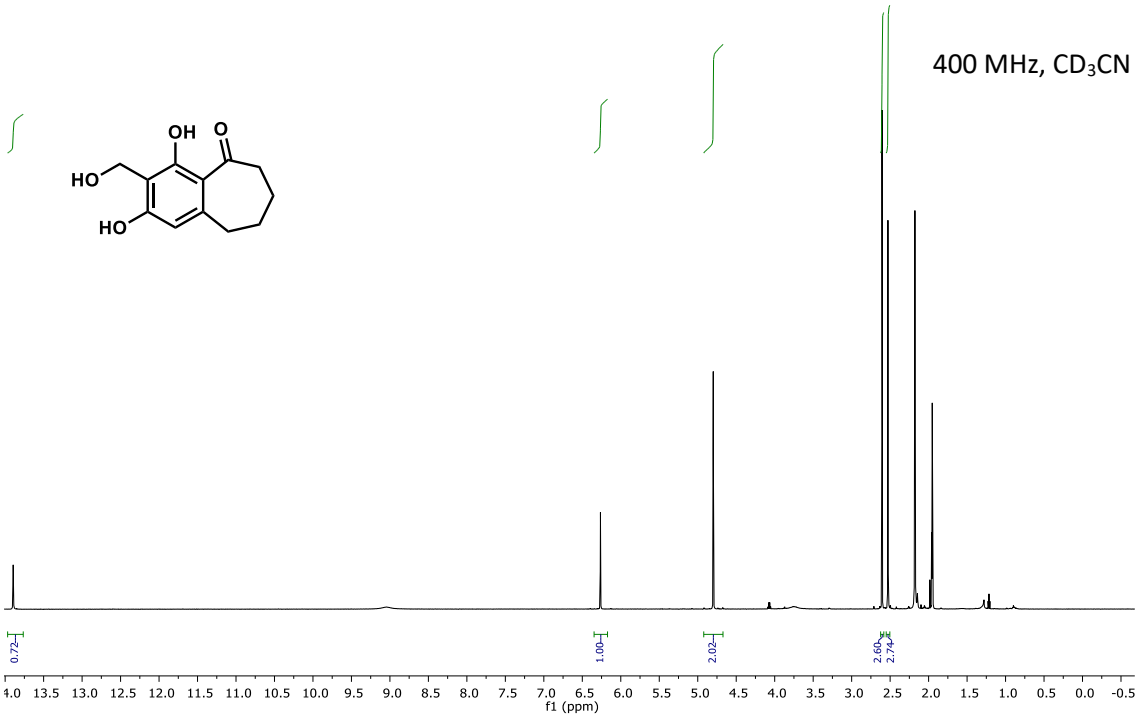
400 MHz, CD3CN
OH
O
HO
HO
0.72
1.00
2.02
2.60
2.74
f1 (ppm)

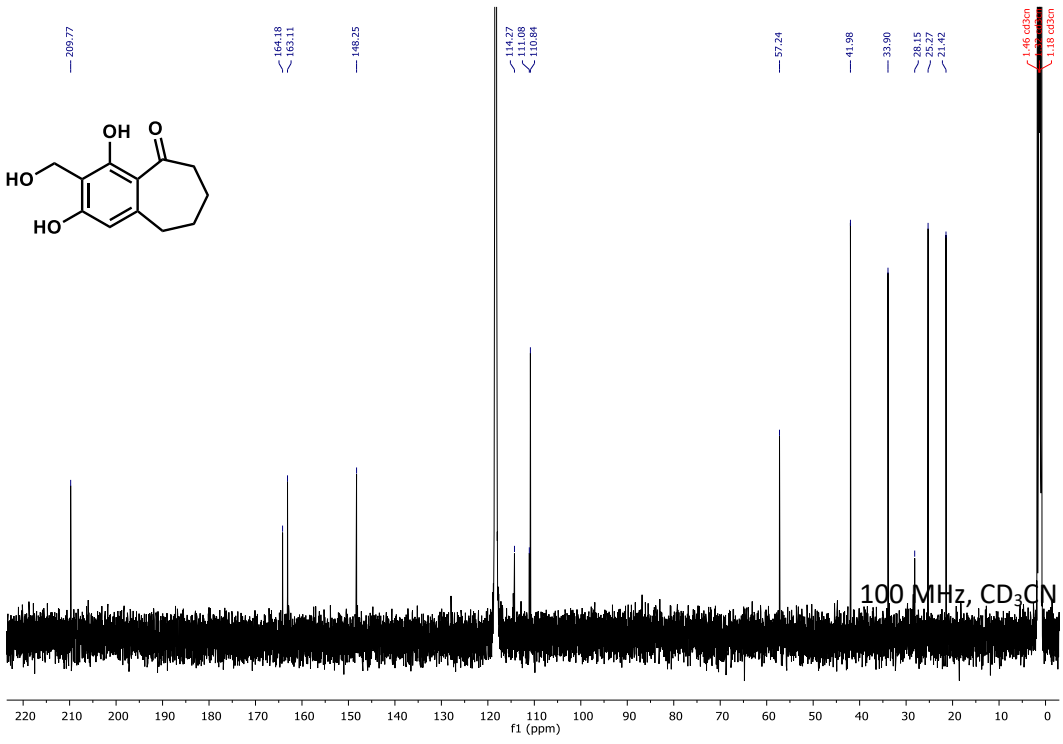
209.77
164.18
163.11
148.25
114.27
111.08
110.84
57.24
41.98
33.90
28.15
25.27
21.42
1.46 cd3cn
1.18 cd3cn
OH
O
HO
HO
100 MHz, CD3CN
f1 (ppm)

400 MHz, $CD_3CN$

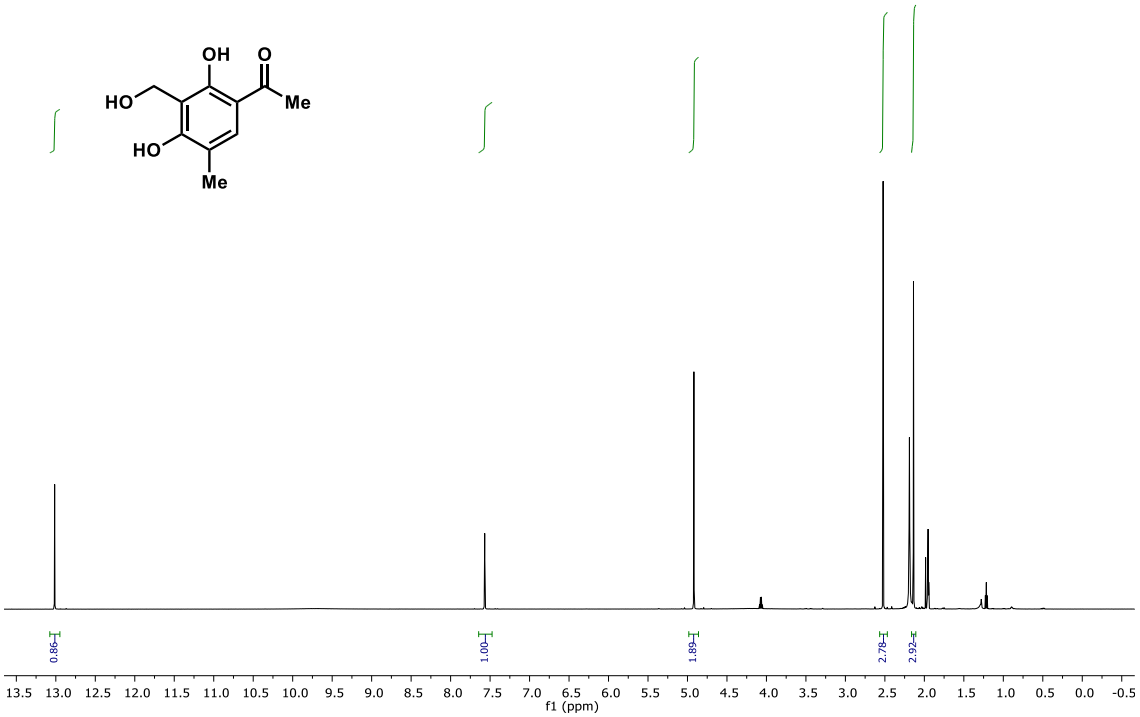


100 MHz, $CD_3CN$

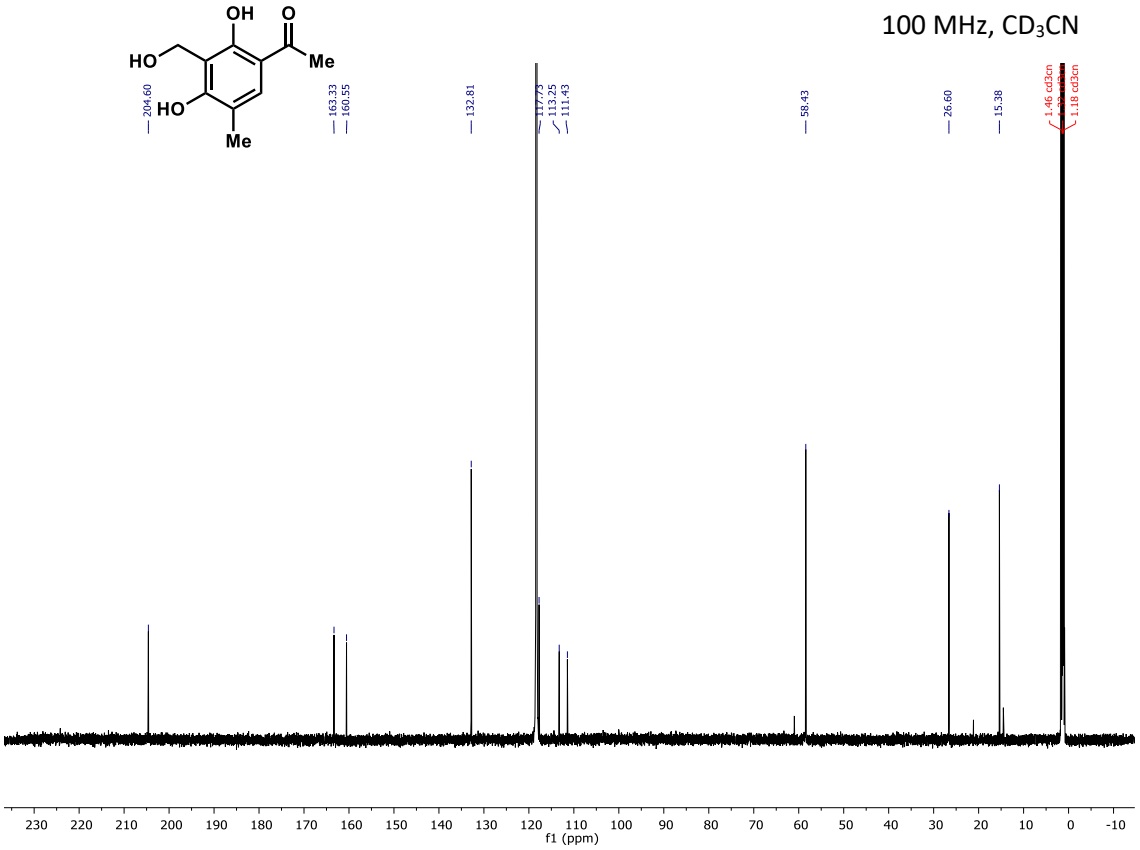

400 MHz, $CD_3CN$

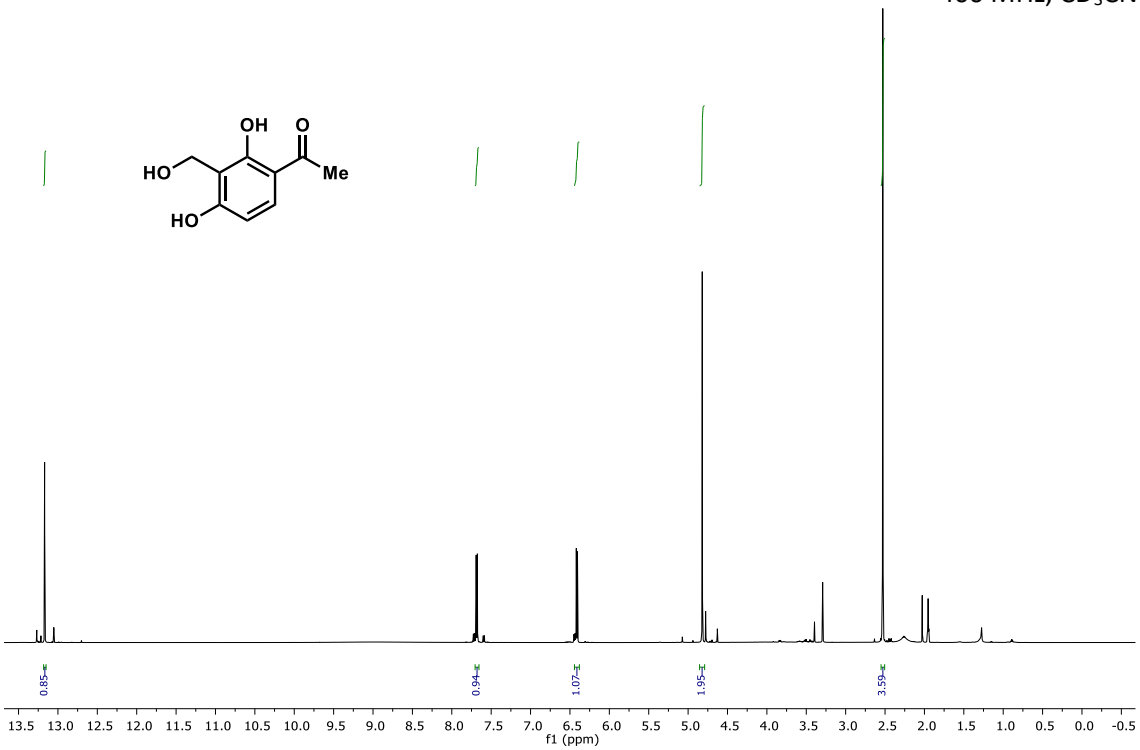


100 MHz, $CD_3CN$

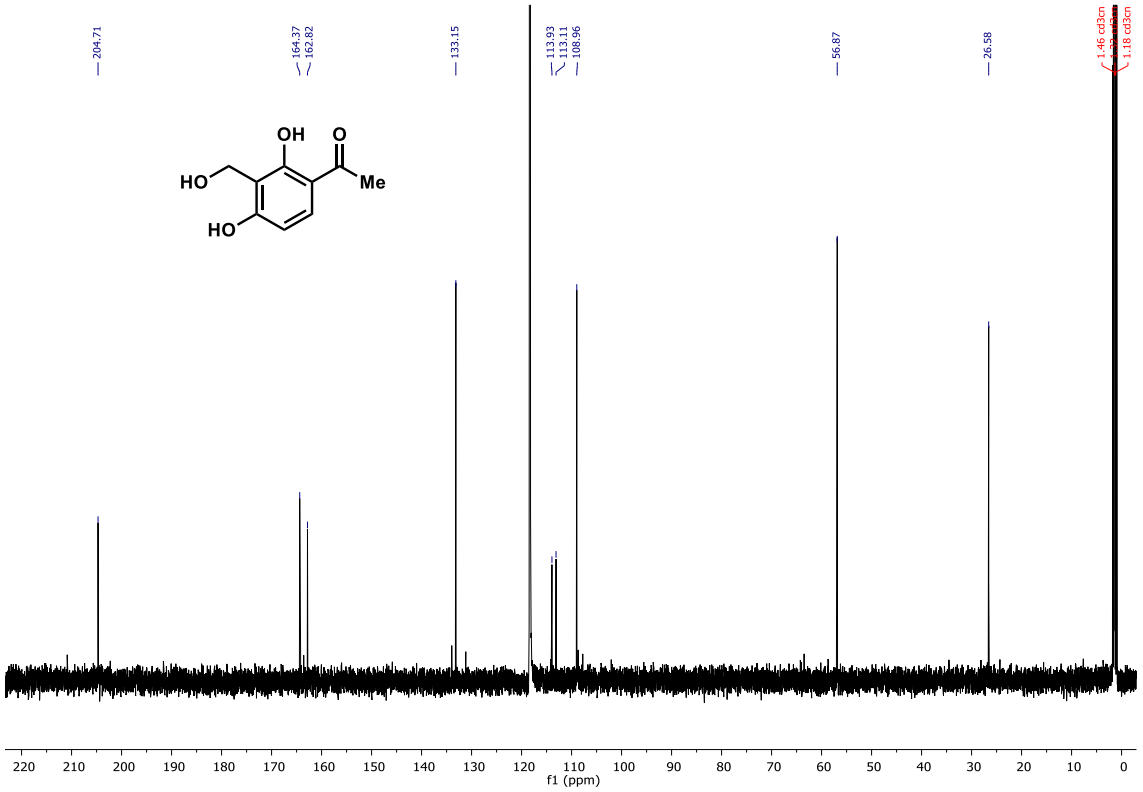

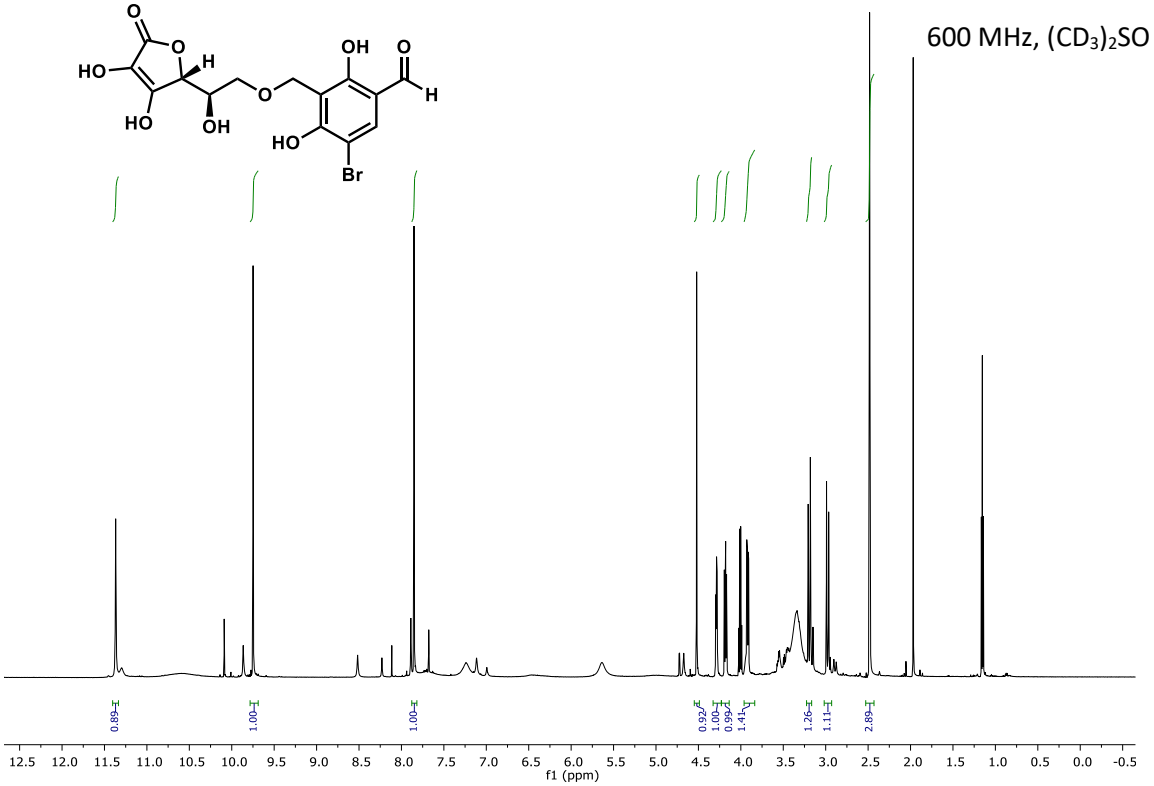
600 MHz, (CD3)2SO
HO
O
O
H
OH
O
H
HO
OH
O
OH
HO
Br
0.89
1.00
1.00
0.92
1.00
0.99
1.41
1.26
1.11
2.89
12.5 12.0 11.5 11.0 10.5 10.0 9.5 9.0 8.5 8.0 7.5 7.0 6.5 6.0 5.5 5.0 4.5 4.0 3.5 3.0 2.5 2.0 1.5 1.0 0.5 0.0 -0.5
f1 (ppm)

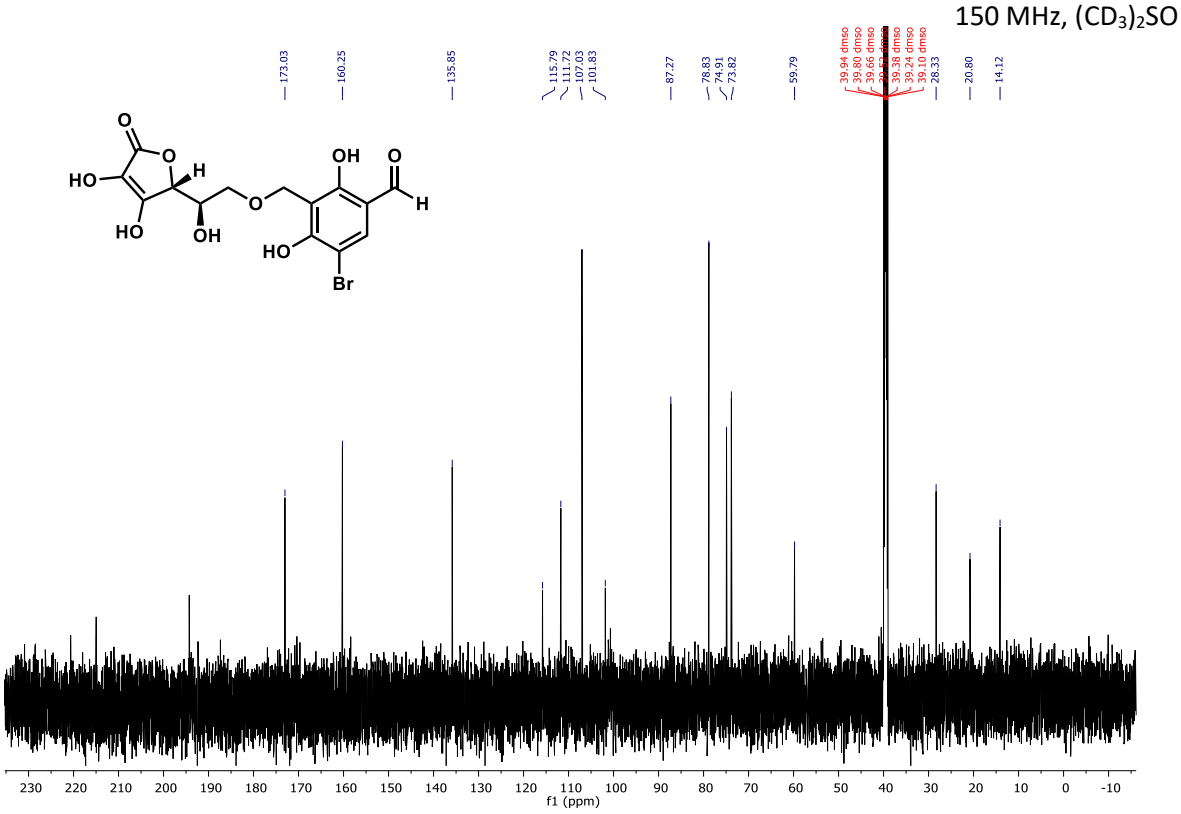
150 MHz, (CD3)2SO
173.03
160.25
135.85
115.79
111.72
107.03
101.83
87.27
78.83
74.91
73.82
59.79
39.94 dmso
39.80 dmso
39.66 dmso
39.52 dmso
39.38 dmso
39.24 dmso
39.10 dmso
28.33
20.80
14.12
HO
O
O
H
OH
O
H
HO
OH
O
OH
HO
Br
230 220 210 200 190 180 170 160 150 140 130 120 110 100 90 80 70 60 50 40 30 20 10 0 -10
f1 (ppm)

**Part XIII. Computational analysis of benzylic functionalization reactions**

**General computational information:** All geometries and frequency computations were obtained using the unrestricted B3LYP density functional[73-74] and 6-311++G** basis set.[75-76] Reaction pathways were calculated using the single-ended growing string method.[77] All ground state geometries were confirmed to have no imaginary frequencies, and transition states were confirmed to have one imaginary frequency. Solvent corrections were performed using the SMD implicit solvent model (water)[78-79] and the cc-pVTZ basis set.[80-85] Reported energies are Gibbs free energies in solvent with gas-phase entropy and enthalpy corrections (at 298.15 K). Most simulations were performed using the Q-Chem 4.0 package,[86] except for the solvent computations, which were performed using ORCA 4.0.[87] *Computations performed by Kevin Skinner.*

**Thermodynamics of *ortho*-quinone methide generation and inverse-electron demand Diels-Alder (IEDDA) reactions:** Figure 2.S68 depicts the potential energy diagram for the formation of the two possible *ortho*-quinone methides that can be accessed for benzylic alcohol **2.27**, and their subsequent reactions with ethyl vinyl ether or styrene. The model predicts moderate barriers for *ortho*-quinone methide generation and IEDDA reactions. Concerted, late transition states are seen for *ortho*-quinone methide generation (Figure 2.S69). For the C1 *ortho*-quinone methide, bonds between atoms $H1_a$ and $O1_a$ (C1-hydroxyl), $H2_a$ and $O2_a$ (water), and $O3_a$ and C7 (benzylic alcohol) are broken. Bonds between $H1_a$ and $O2_a$ (water) and $H2_a$ and $O3_a$ (new water) are formed. For C3 *ortho*-quinone methide, bonds between atoms $H1_b$ and $O1_b$ (C1-hydroxyl), $H2_b$ and $O2_b$ (water), and $O3_b$ and C7 (benzylic alcohol) are broken. Bonds between $H1_a$ and $O2_a$ (water) and $H2_a$ and $O3_a$ (new water) are formed. For the IEDDA reactions, the model shows concerted, asynchronous transition states for the IEDDA reactions (Figure 2.S70). For reactions with ethyl

vinyl ether, changes in bond length are no greater than 0.996 Å (Table 2.S3). Reactions with styrene afford maximal bond length changes of 1.270 Å.

**Table 2.S3.** Changes in C-C and C-O bond lengths during IEDDA reactions with **2.27**.

| Structure | Bond | Change in Bond Length (Å) |
|---|---|---|
| $TS2_{Ia}$ | C-C | 0.985 |
| | C-O | 0.541 |
| $TS2_{IIa}$ | C-C | 0.996 |
| | C-O | 0.573 |
| $TS2_{Ib}$ | C-C | 1.270 |
| | C-O | 0.815 |
| $TS2_{IIb}$ | C-C | 1.212 |
| | C-O | 0.768 |

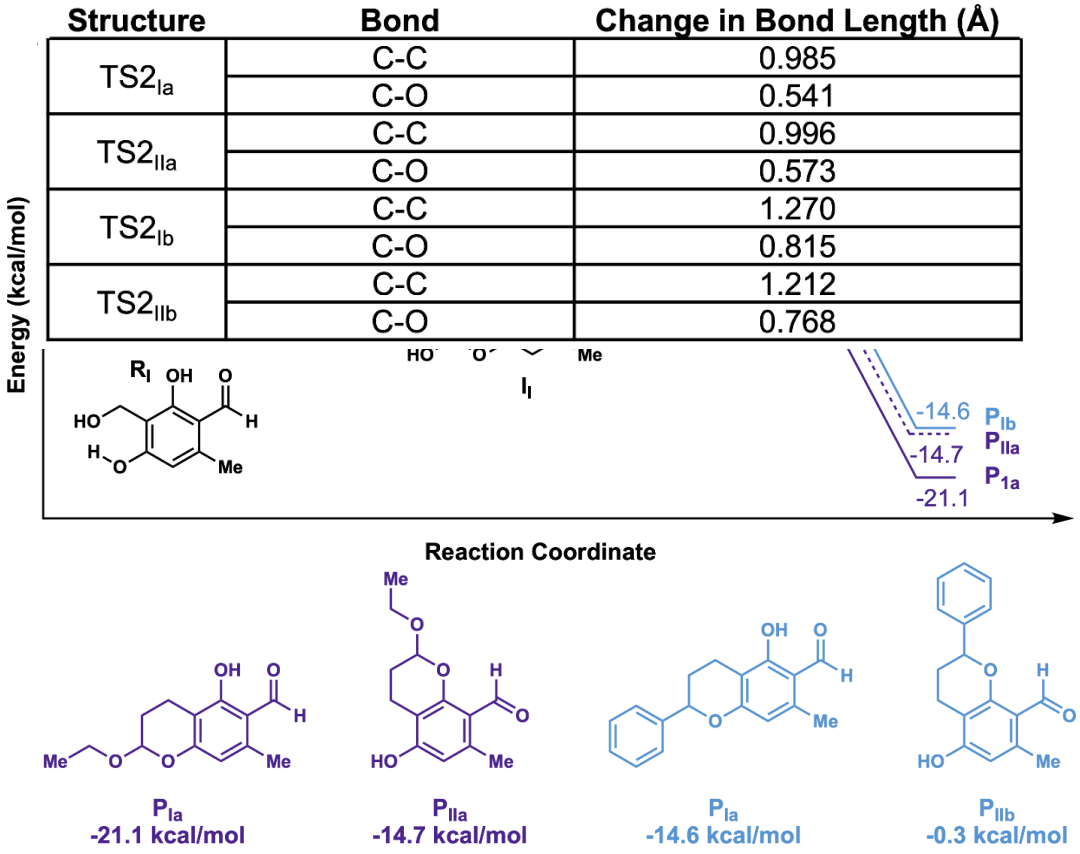


**Figure 2.S82. Potential energy diagram for *ortho*-quinone methide (black) generation, and the subsequent IEDDA reactions with ethyl vinyl ether (purple) and styrene (light blue).**

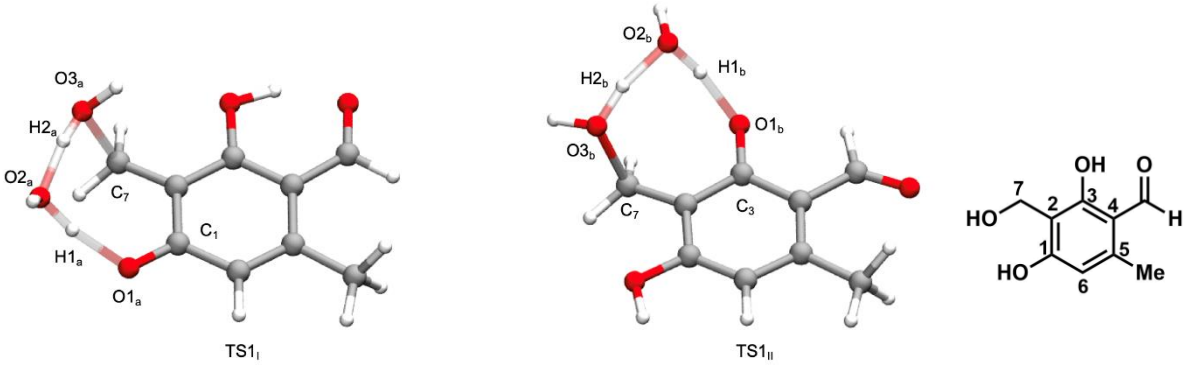


**Figure 2.S83. 3D representations of transition states for both C1 and C3 *ortho*-quinone methides ($I_I$ and $I_{II}$ respectively).**

Both $TS_I$ and $TS_{II}$ structures undergo concerted, late stage transition states. Starting material (benzyl alcohol **2.27**) is depicted on the far right with the relevant carbons labelled.

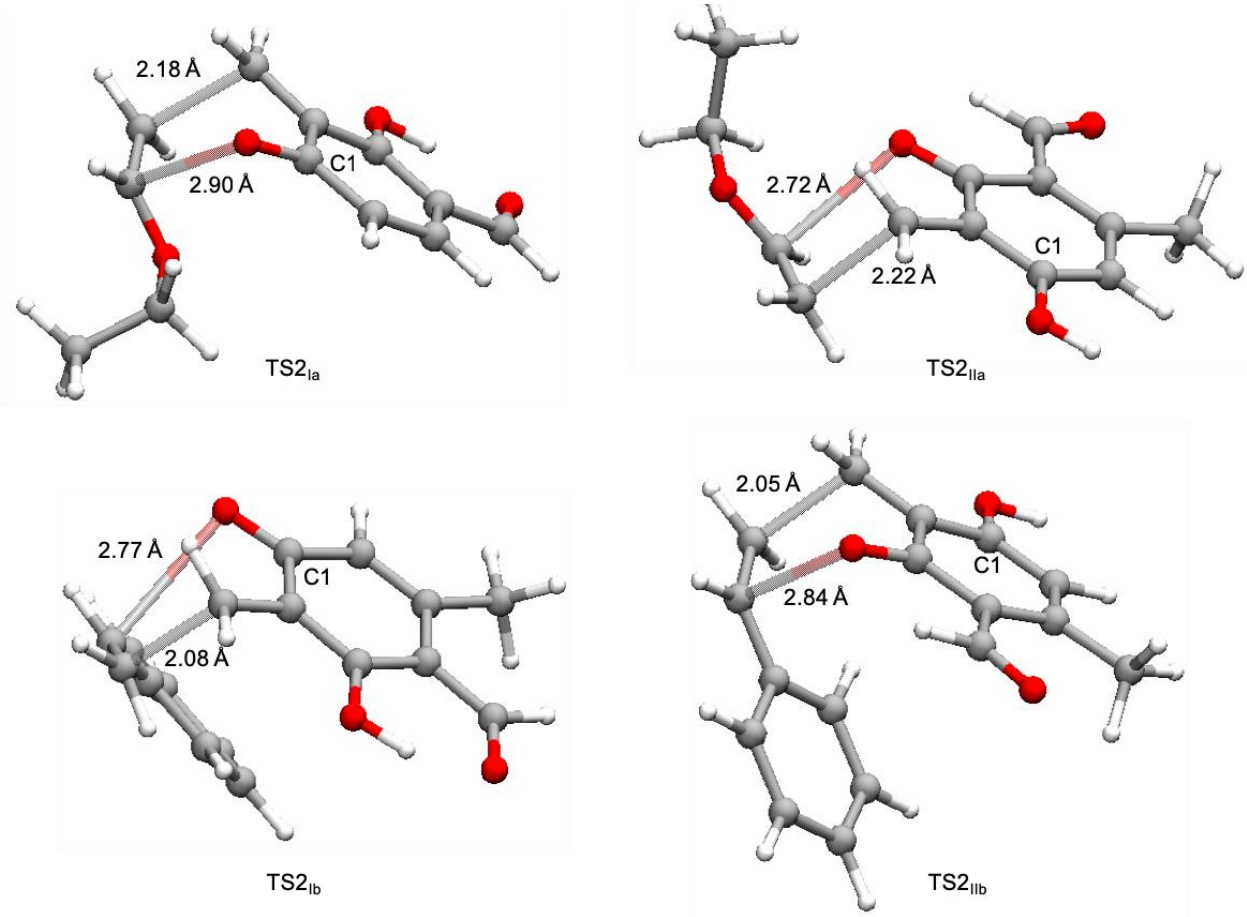


**Figure 2.S84. Transition states for IEDDA reactions between $I_I$ (left) and $I_{II}$ (right) *ortho*-quinone methides with ethyl vinyl ether (top) and styrene (bottom).**

C-C distances are shorter than C-O distances for all transition states, which indicate asynchronous transition states.

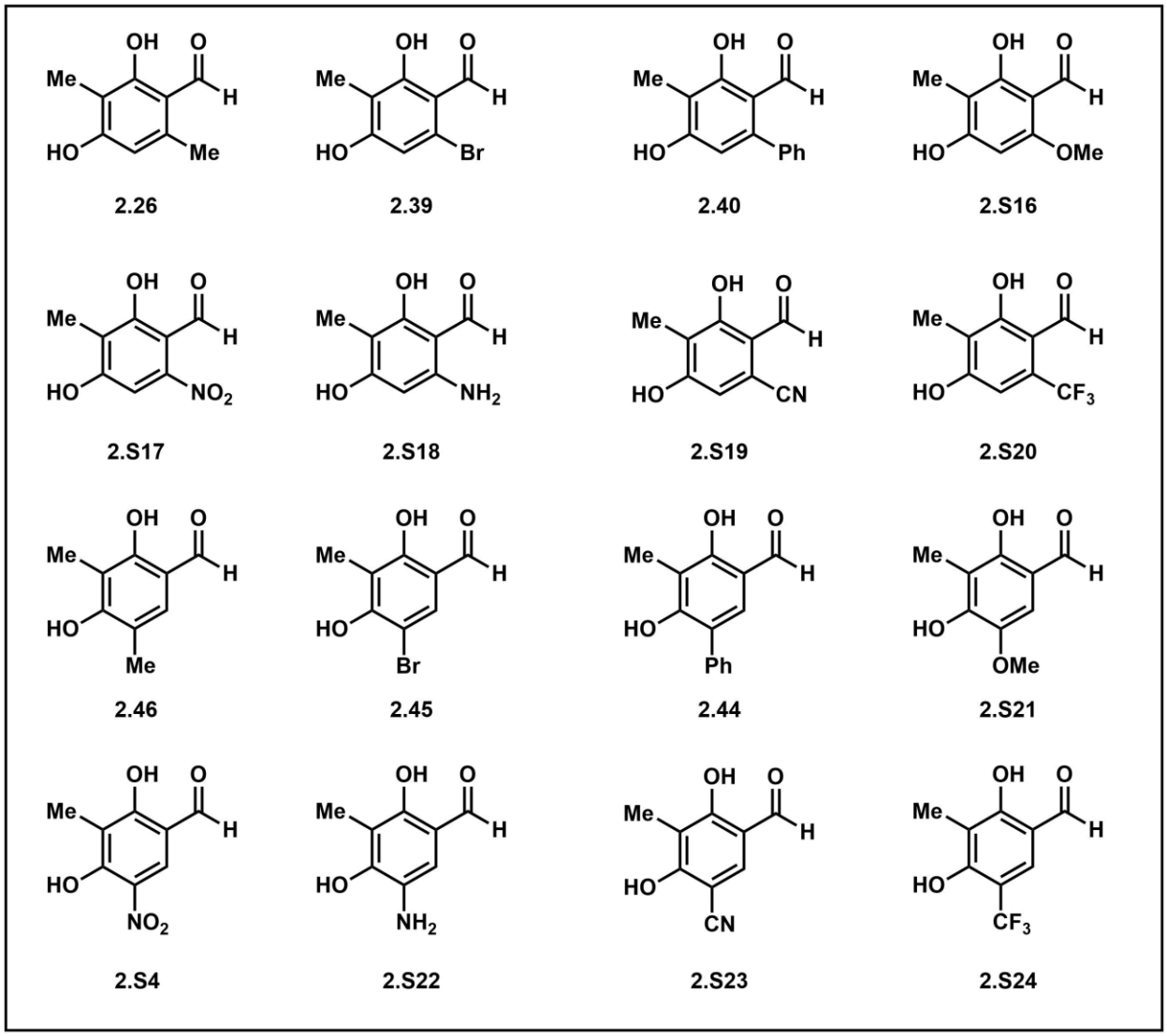


**Figure 2.S85. Substrate panel used to develop thermodynamic relationships between starting material and products.**

**Thermodynamic analysis of CitB-hydroxylated products:** Experimental evidence from preparative-scale reactions with CitB suggested that benzylic alcohol products with C6-substitutents (**2.57-2.61** and **2.70**), particularly with electron-withdrawing substituents, were difficult to isolate without further elaboration to products downstream of *ortho*-quinone methide formation under the conditions of the CitB reaction. C5-substituted resorcinol products (**2.27** and **2.54-2.56**) did not typically exhibit this behavior under the same conditions. We conducted an

analysis of the Gibbs free energies of CitB-generated benzylic alcohols of a panel of substrates (**2.26**, **2.39**-**2.40**, **2.44**-**2.46**, and **2.S4**, **2.S16**-**2.S24**) to examine the impact of substitution pattern on benzylic alcohol stability. This analysis was carried out by comparing the Gibbs free energy for the benzylic alcohol products to their respective starting materials ($\Delta G_t$). Mass balance was achieved by using a truncated 2-His-1-Asp non-heme iron system (Figure 2.S85).

The $\Delta G_t$ of C6-substituted benzylic alcohols were spread over a relatively wide range of 5.1 kcal/mol, while the energies of the C5-substituted benzylic alcohols were nearly isoenergetic, with a range of 0.3 kcal/mol. This data indicated that the relative energies of these products was influenced by their substitution pattern. Further, we noted that benzylic alcohols containing inductively electron-withdrawing substituents in the C6-position generally tended to have higher energies, whereas the benzylic alcohol containing an inductively electron-donating substituent (R = methyl) had the lowest Gibbs free energy value in this substrate panel. This general trend is in agreement with our experimental observations, as **2.S4**, which contains a nitro group at the C6 position, was quite reactive and difficult to isolate. Even upon isolation of the thiophenol adduct (**2.61**), we were required to use a non-nucleophilic NMR solvent for characterization, as MeOD quickly exchanged with thiophenol on the time-scale required for obtaining a $^1$H NMR. In

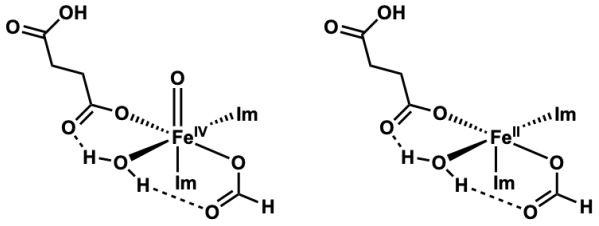


**Figure 2.S86. Truncated 2-His-1-Asp non-heme iron system used for all thermodynamic calculations.**
Structure on left represents [$Fe^{IV}$] species and the structure on the right represents the [$Fe^{II}$] species. These structures were included to maintain atom balance between starting materials and benzylic alcohol products.

comparison, the analogous compound bearing a methyl group at C6 (**2.76**) could be transferred in MeOH and did not exchange with MeOD in the time required for full NMR characterization. To further investigate these observations, the Gibbs energies of thiophenol were analyzed in the same manner as the benzylic alcohol products. Through this analysis, we determined that thiophenol adducts of each CitB-hydroxylated product were lower in energy than their benzylic alcohol precursors (Figure 2.S88-2.S89). We also observed that the C6-nitro thiophenol adduct (**2.61**) had a relatively high Gibbs energy, which supported our observations that **2.76** exhibited reduced stability when compared to other isolated thiophenol adducts.

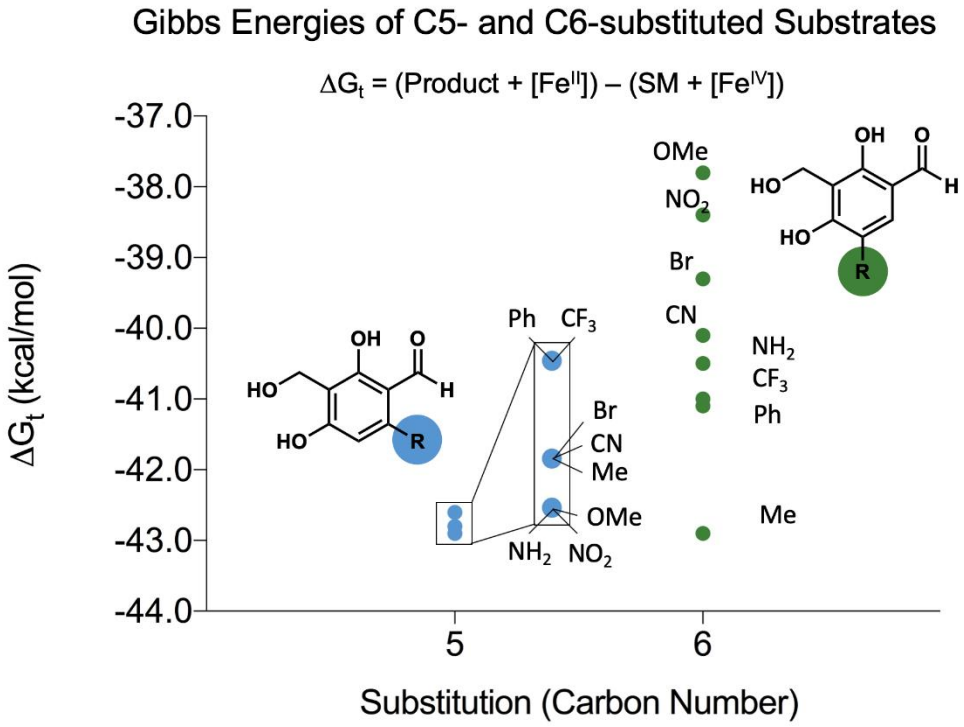


**Figure 2.S87. Calculated thermodynamics ($\Delta G_t$) of benzyl alcohol products, compared to their respective starting materials (SM).**
$\Delta G_t$ = (Product + [$Fe^{II}$]) – (SM + [$Fe^{IV}$]). Blue circles represent C5-substituted substrates and range from -43.6 to -43.9 kcal/mol. Green circles represent C6-substituted substrates and range from -37.8 to -42.9 kcal/mol.

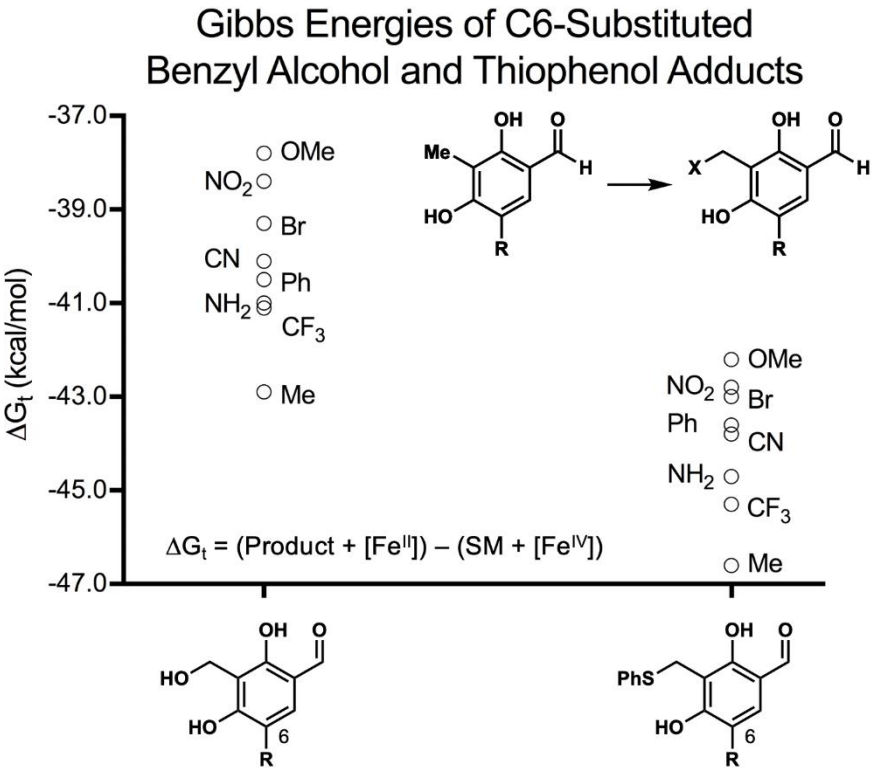


**Figure 2.S88. Thermodynamic comparison of C6-substituted benzylic alcohols (left) and thiophenol products (right).**

All thiophenol products are lower in energy than the corresponding benzyl alcohol precursor. $\Delta G_t$ = (Product + [$Fe^{II}$]) – (SM + [$Fe^{IV}$]).

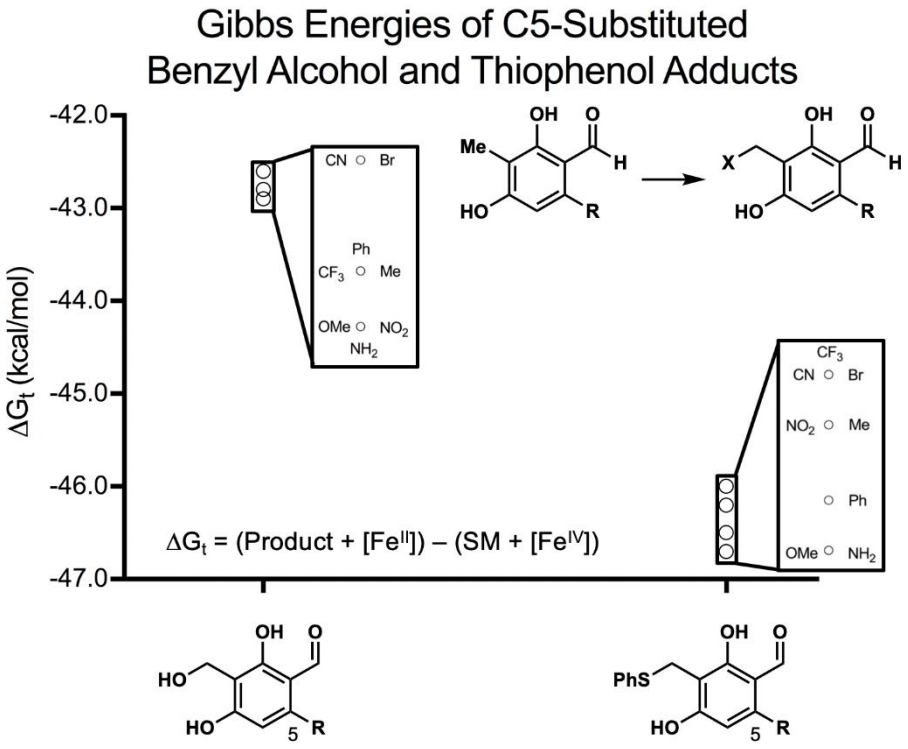


**Figure 2.S89. Thermodynamic comparison of C5-substituted benzylic alcohols (left) and thiophenol products (right), compared to their respective starting material (SM).**
All thiophenol products are lower in energy than their benzylic alcohol precursors. $\Delta G_t$ = (Product + $[Fe^{II}]$) – (SM + $[Fe^{IV}]$).

**Multivariable linear regression Hammett plot analysis:** Intrigued by the apparent relationship between the free energy of C6-substituted substrates and the electronics of their substituents, we sought to define their Hammett relationship, which compares various electronic parameters (Hammett constants) based on substitution on an aryl ring. A relationship was found between the Hammett inductive ($\sigma_I$) and resonance ($\sigma_R$) constants and the Gibbs free energy of ($\Delta G_c$) (Figure 2.S90). When plotting $\Delta G_c$ against $\Delta G_t$, we observe a correlation with an $R^2$ of 0.7537. This correlation provides further support that electronics at the C6 position have an influence on the stability of the benzylic alcohol. An analysis of the coefficients of the regression reveals that $\sigma_I$ has the larger coefficient than $\sigma_R$ 7.7 and -4.7, respectively, and therefore is the most influential

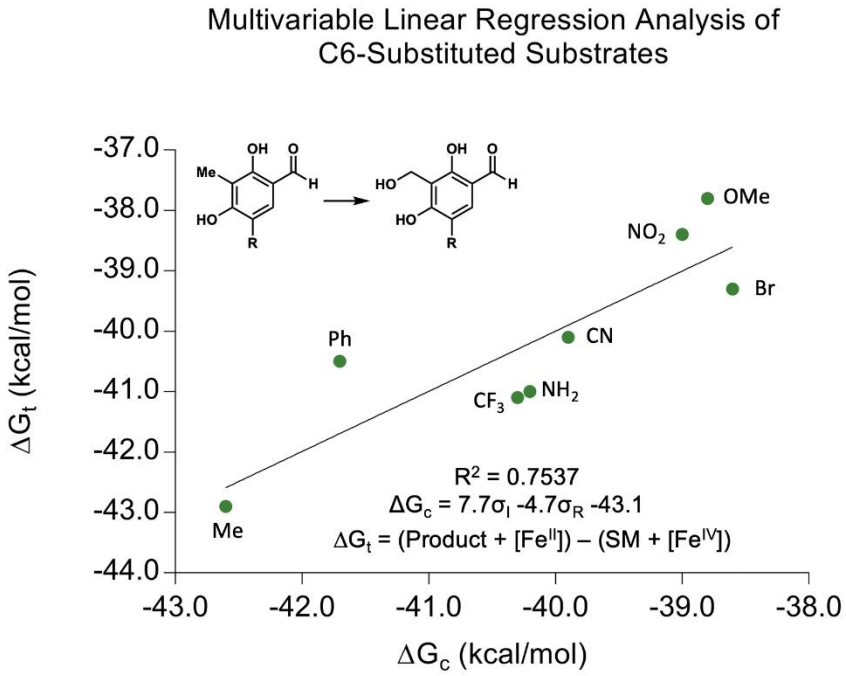


**Figure 2.S90. Multivariable linear regression plot of combined inductive ($\sigma_I$) and resonance ($\sigma_R$).**
Hammett constants against calculated thermodynamics of C6-substituted substrates ($\Delta G_t$). $\Delta G_t$ = (Product + [$Fe^{II}$]) – (SM + [$Fe^{IV}$]). A trend can be observed from inductively electron donating to inductively electron withdrawing. $R^2$ = 0.7537.

factor. Inspection of the $\sigma_I$ and $\sigma_R$ graphs against $\Delta G_t$ also confirms this conclusion (Figures 2.S91-2.S92).

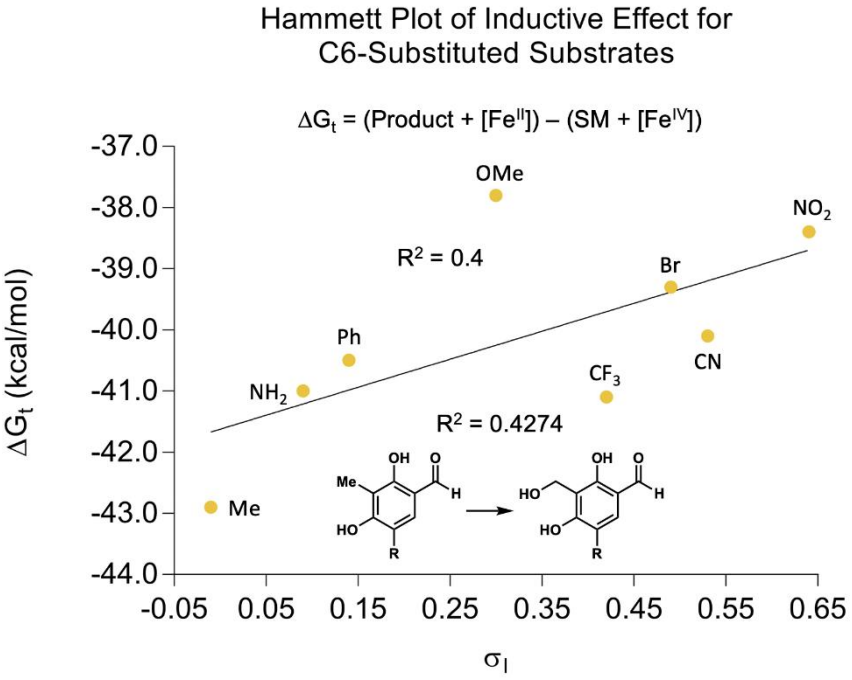


**Figure 2.S91. Plot of the inductive Hammett constant ($\sigma_I$) against calculated thermodynamics.**
($\Delta G_t$) of C6-substituted benzyl alcohol products compared to their respective starting materials. $\Delta G_t$ = (Product + [$Fe^{II}$]) – (SM + [$Fe^{IV}$]). $\Delta G_t$ ranges from -37.8 to -42.9 kcal/mol. $R^2$ = 0.424.

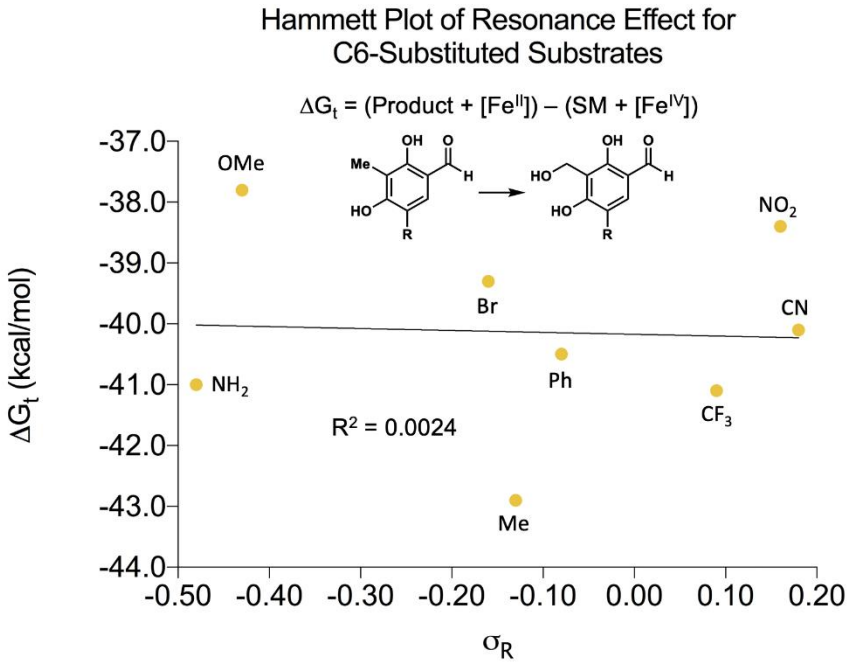


**Figure 2.S92. Plot of the resonance Hammett constant ($\sigma_R$) against calculated thermodynamics (ΔGt) of C6-substituted benzyl alcohol products compared to their respective starting materials.**

$\Delta G_t$ = (Product + [$Fe^{II}$]) – (SM + [$Fe^{IV}$]). ΔGt ranges from -37.8 to -42.9 kcal/mol. $R^2$ = 0.0024.

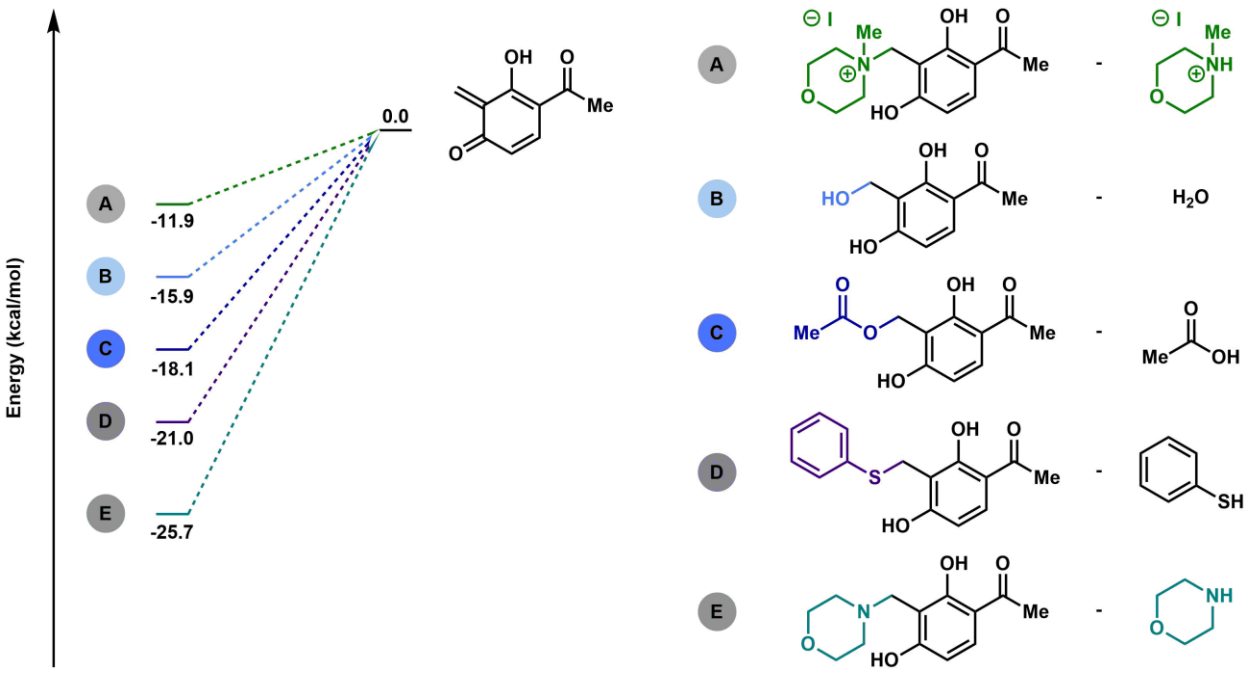


**Figure 2.S93. Thermodynamic comparison of *ortho*-quinone methide precursors with a range of common leaving groups substituted at the *o*-phenolic benzylic position.**
This data shows that the benzylic alcohol (A) is higher in energy than other common leaving groups. This data also clearly shows why methylation of the morpholine adduct precursor used by Wilson and co-workers was necessary to observe *ortho*-quinone methide activity. Overall, this provides evidence as to why our enzymatically generated benzylic alcohol precursors can be used to access the *ortho*-quinone methide intermediates under such mild conditions.

**Part XIV. XYZ coordinates of ortho-quinone methide and IEDDA transition states**

$TS1_I$

H -4.9499456400 0.3051135600 0.4113060800

O -4.0414247800 0.1905241200 0.7316649200

H -3.7185704200 -0.7262253000 0.3535210500

C -2.8443859800 0.9804196500 -0.5535490500

H -2.8982343300 2.0398600900 -0.3262081000

H -3.4872014400 0.6268288300 -1.3533284500

O -2.8288415100 -1.7275963500 -0.3955920400

C -1.6393397800 0.2946932000 -0.3241739200

C -1.6906807200 -1.1569398800 -0.3862488800

O -0.4306888600 2.2663872900 0.1749792500

C -0.4274093000 0.9491992800 0.0104875200

C -0.4491738100 -1.8726385800 -0.3458470700

H -0.4907395000 -2.9525904900 -0.4402619200

H 0.5310208000 2.5221409900 0.3669362800

C 0.7392063900 -1.2273708300 -0.1049139400

C 0.7792546300 0.2024476000 0.0963095000

H 2.4888134500 -1.9392928100 0.9623600200

H 1.8051811700 -3.0951191200 -0.1884324400

C 2.0123708200 -2.0365368800 -0.0196777200

C 1.9892074500 0.9210841300 0.3723851700

O 2.0474349200 2.1565959800 0.5528138500

H 2.7457984200 -1.7139288300 -0.7673807000

H 2.9269280300 0.3453623700 0.4282085900

$TS1_{II}$

C 0.7609422300 0.1826692100 -0.1350069500

C -0.4964908500 0.8856089700 -0.1546474000

C -1.7258848300 0.1103971800 -0.1903379600

C -1.6772023100 -1.2857305800 0.0411133300

C -0.4530291600 -1.9336355000 0.1110299500

C 0.7594621700 -1.2197443900 0.0026149300

C -2.9128524600 0.8306537100 -0.4052586300

O -2.8796925500 2.1523788000 0.9999659900

O -2.8619882500 -1.9446020500 0.1171147800

O -0.6028285200 2.1579348100 -0.0720095800

C 2.0424029900 -2.0078820400 0.0633685700

C 1.9809787700 0.9937082200 -0.2035304900

O 3.1315683400 0.5696553400 -0.1979127100

H -3.8689494900 0.3410491300 -0.2553586700

H -3.4167840300 2.9079700900 0.7141229600

H -2.6927820400 -2.8869331400 0.2528852400

H -2.8928470200 1.6279710000 -1.1413423900

H -1.9066230500 2.3524182000 0.6613052800

H -0.4226526100 -3.0137369500 0.2324542800

H 1.8382503600 -3.0715753300 0.2132115500

H 2.6245371300 -1.8785628000 -0.8535223400

H 2.6898093800 -1.6438364000 0.8650917200

H 1.7830838200 2.0797994900 -0.2703474600

$TS2_{Ia}$

C -1.0362475800 0.3915354700 0.1127718900

C -2.0615369900 0.1378212700 1.0725993800

C -0.0597492100 -0.5883230500 -0.1641720100

C -0.1436962400 -1.8527799200 0.5091458900

C -1.1368341600 -2.1592796100 1.3890075100

C -2.1783460900 -1.1933113900 1.6999297900

H 0.6267831200 -2.5891380300 0.2836518800

H -1.1929744200 -3.1267625300 1.8779376600

C 0.9834671200 -0.3028425800 -1.1064803500

O 1.1034419600 0.7706324200 -1.7268151700

H 1.7244237900 -1.1066493800 -1.2807559800

O -1.0156784200 1.5790666500 -0.4947504200

O -3.1598839500 -1.4608426800 2.4283619100

C -3.0138825700 1.0977774500 1.4049750700

C -4.8437205100 0.8224115400 0.2447003600

H -2.8993381100 2.1125795500 1.0398365400

H -3.5530445300 0.9572028600 2.3335939000

C -5.0492786600 -0.5187795500 0.4351395700

H -4.4274862700 1.1631770900 -0.6973280000

H -5.4492681200 1.5227910700 0.8086404500

O -4.4938790600 -1.3977908900 -0.3844311100

H -5.5876000600 -0.9092717700 1.2958225800

H -0.2157145800 1.5704210300 -1.1031544200

C -4.6185120300 -2.8028294300 -0.0320072100

C -5.9827659900 -3.3543429000 -0.4152536300

H -6.0193004800 -4.4268427800 -0.1937596800

H -6.1754384200 -3.2159495900 -1.4839817400

H -6.7875383900 -2.8692274800 0.1482685500

H -4.3983097600 -2.8995740300 1.0356854600

H -3.8207333900 -3.2869228100 -0.5986686500

$TS2_{Ib}$

C -1.1226393400 0.4771206900 0.3527469300

C -2.2120106100 0.4039241900 -0.5616932000

C -0.2721416300 -0.6349971700 0.5572912100

C -0.5632216800 -1.8842882200 -0.1275907300

C -1.6552283100 -1.9951897400 -0.9387664200

C -2.5544406700 -0.8830068400 -1.1847780000

C 0.3396985900 -3.0794168800 0.0769665800

H -1.8947797700 -2.9328825600 -1.4310999600

C 0.8369690300 -0.4834008500 1.4561665900

O 1.1044273600 0.5629569700 2.0851172100

H 1.4981615000 -1.3533427900 1.6032346900

O -0.9197703700 1.6337977300 0.9874699100

O -3.5984034500 -0.9780117400 -1.8632513500

C -3.0365223100 1.4960453100 -0.8593276500

C -4.7863019700 1.4571353000 0.2066467100

H -3.5597654200 1.4417813800 -1.8070949000

H -2.7357836400 2.4810870700 -0.5160489400

C -5.3160086700 0.1829797300 0.0818792700

H -5.2571192100 2.2592739200 -0.3545150600

H -4.3441247900 1.7631078100 1.1497444700

H -5.9832313000 -0.0217203700 -0.7505884600

C -5.0291217300 -0.9304689700 0.9534445900

H -0.0944095300 1.5010391800 1.5532405600

C -4.1049026600 -0.8441494500 2.0185403000

C -5.6864753500 -2.1629981300 0.7358036800

C -5.4513617600 -3.2529684300 1.5606200500

C -3.8625849800 -1.9445608200 2.8364557600

C -4.5375094300 -3.1466547000 2.6166736400

H -3.5778012800 0.0842896400 2.2106592500

H -3.1469792800 -1.8624805800 3.6496698400

H -5.9708757900 -4.1901963800 1.3821240800

H -4.3514799500 -4.0005532800 3.2623996900

H -6.3790517300 -2.2482040000 -0.0972220800

H 1.3710855200 -2.8674232400 -0.2315179500

H -0.0162700300 -3.9314923200 -0.5080897500

H 0.3768056300 -3.3872254700 1.1295924300

$TS2_{IIa}$

C 1.3663481200 0.8862776400 0.6794257500

C 0.0739675900 0.2354337600 0.4151188100

C 2.5765996900 0.2267469900 0.1966877000

C 2.4802819100 -0.9561587200 -0.5451555000

C 1.2131151800 -1.5167931600 -0.8471165000

C 0.0446510800 -0.9313547000 -0.4041025500

H 1.1694713700 -2.4318909900 -1.4346299900

C 3.8507670900 0.8734376600 0.5186424700

O 4.9682919300 0.4846176100 0.1917999100

H 3.7360883000 1.7979606900 1.1151505700

O 1.3780583500 1.9979432800 1.2647325000

C -1.0779428100 0.8384189000 0.9101031300

C -1.5987970800 2.6437180000 -0.2694298100

H -0.9843355900 1.4793521800 1.7778721000

H -2.0401297600 0.3659645400 0.7446094300

C -0.6136810000 3.4930963900 0.1635385600

H -2.5926116100 2.7234478700 0.1599288100

H -1.5153371900 2.2134381700 -1.2596314300

O -0.7734149800 4.2077050900 1.2686333100

H 0.3389360100 3.5847645800 -0.3505804700

O -1.1831846400 -1.4448259400 -0.6912279800

C 3.6987185500 -1.6796834700 -1.0634888100

H 4.2822048600 -1.0396443400 -1.7325871100

H 3.4101751500 -2.5902761800 -1.5982089600

H 4.3800075700 -1.9397816200 -0.2481818200

H -1.0699674400 -2.2492892900 -1.2225538500

C 0.3763652800 4.9034843100 1.8129863000

C 0.5525250800 4.5074021000 3.2669427700

H 0.1696705700 5.9738690300 1.7043239400

H 1.2621005100 4.6405793500 1.2286608100

H -0.3588723600 4.7066594500 3.8403023000

H 1.3707554400 5.0874505200 3.7089355200

H 0.7994148600 3.4449303200 3.3295001100

$TS2_{IIb}$

C 1.0776353600 1.8739808300 -0.3393770100

C -0.0114023500 1.0045305600 0.1353536500

C 2.4492733000 1.3772349000 -0.2320166900

C 2.6918462100 0.1186801100 0.3232158500

C 1.6193084300 -0.6691403600 0.8216167000

C 0.3124637500 -0.2302909000 0.7637797400

H 1.8426930700 -1.6405329100 1.2590520500

C 3.5071395600 2.2606430600 -0.7310854500

O 4.7116308300 2.0253189700 -0.7242610900

H 3.1265411400 3.2153802900 -1.1387416700

O 0.7817387000 3.0092089400 -0.7772632500

C -1.3132370300 1.4913287000 -0.0067980000

C -1.7338153000 2.9518040500 1.4151011700

H -2.1494701300 0.8475312200 0.2473228700

H -1.4633571200 2.2024051300 -0.8101354200

C -0.7023248000 3.8754775400 1.3924754300

H -1.8237642500 2.2635336400 2.2501405100

H -2.6773182100 3.2315585800 0.9558029900

C 0.4977034200 3.8195029000 2.1962047100

H -0.7780233700 4.7180259100 0.7109601700

O -0.7302737900 -0.9531443600 1.2645062000

C 4.0826983400 -0.4566886400 0.4345712100

H 4.5569438300 -0.5368651100 -0.5484770500

H 4.0563829700 -1.4464955000 0.9017815800

H 4.7355387700 0.2006925500 1.0163531100

H -0.3897157100 -1.7907372700 1.6179999800

C 0.7927955400 2.7304215000 3.0440297000

C 1.4274425000 4.8814311400 2.1255758100

C 2.5916237400 4.8634750900 2.8807909900

C 1.9676044100 2.7101969200 3.7913817200

C 2.8670510700 3.7751089100 3.7174798900

H 2.1826248600 1.8603216000 4.4331784800

H 3.7817299400 3.7575060500 4.3034370700

H 1.2230721700 5.7155843200 1.4594676600

H 3.2936566800 5.6896618800 2.8133536600

H 0.1002894900 1.8989377500 3.1198977500

## 2.7 References


(1) Ueberbacher, B. T.; Hall, M.; Faber, K., Electrophilic and nucleophilic enzymatic cascade reactions in biosynthesis. *Nat. Prod. Rep.* **2012,** *29* (3), 337-50.

(2) Hashimoto, T.; Kuzuyama, T., Mechanistic insights into Diels-Alder reactions in natural product biosynthesis. *Curr. Opin. Chem. Biol.* **2016,** *35*, 117-123.

(3) Walsh, C. T.; Moore, B. S., Enzymatic Cascade Reactions in Biosynthesis. *Angew. Chem. Intl. Ed.* **2019,** *58* (21), 6846-6879.

(4) Bai, W. J.; David, J. G.; Feng, Z. G.; Weaver, M. G.; Wu, K. L.; Pettus, T. R., The domestication of ortho-quinone methides. *Acc. Chem. Res.* **2014,** *47* (12), 3655-64.

(5) Singh, M. S.; Nagaraju, A.; Anand, N.; Chowdhury, S., ortho-Quinone methide (o-QM): a highly reactive, ephemeral and versatile intermediate in organic synthesis. *RSC Adv.* **2014,** *4* (99), 55924-55959.

(6) Van De Water, R. W.; Pettus, T. R. R., o-Quinone methides: intermediates underdeveloped and underutilized in organic synthesis. *Tetrahedron* **2002,** *58* (27), 5367-5405.

(7) Willis, N. J.; Bray, C. D., ortho-Quinone Methides in Natural Product Synthesis. *Chem. Eur. J.* **2012,** *18* (30), 9160-9173.

(8) Fan, J.; Liao, G.; Kindinger, F.; Ludwig-Radtke, L.; Yin, W. B.; Li, S. M., Peniphenone and Penilactone Formation in Penicillium crustosum via 1,4-Michael Additions of ortho-Quinone Methide from Hydroxyclavatol to gamma-Butyrolactones from Crustosic Acid. *J. Am. Chem. Soc.* . **2019**, *141*, (10), 4225-4229.

(9) Wang, J.; Liu, P.; Wang, Y.; Wang, H.; Li, J.; Zhuang, Y.; Zhu, W., Antimicrobial Aromatic Polyketides from Gorgonian-Associated Fungus, Penicillium commune 518. *Chin. J. Chem.* **2012,** *30* (6), 1236-1242.

(10) Liao, G.; Fan, J.; Ludwig-Radtke, L.; Backhaus, K.; Li, S.-M., Increasing Structural Diversity of Natural Products by Michael Addition with ortho-Quinone Methide as the Acceptor. *J. Org. Chem.* **2020,** *85* (2), 1298-1307.

(11) George, J. H.; Baldwin, J. E.; Adlington, R. M., Enantiospecific, Biosynthetically Inspired Formal Total Synthesis of (+)-Liphagal. *Org. Lett.* **2010,** *12* (10), 2394-2397.

(12) Pepper, H. P.; Kuan, K. K. W.; George, J. H., Synthesis of a Liphagal–Frondosin C Hybrid and Speculation on the Biosynthesis of the Frondosins. *Org. Lett.* **2012,** *14* (6), 1524-1527.

(13) Chapman, O. L.; Engel, M. R.; Springer, J. P.; Clardy, J. C., Total synthesis of carpanone. *J. Am. Chem. Soc.* **1971,** *93* (24), 6696-6698.

(14) Brophy, G. C.; Mohandas, J.; Slaytor, M.; Sternhell, S.; Watson, T. R.; Wilson, L. A., Novel lignans from a cinnamomum sp. from bougainville. *Tetrahedron Lett.* **1969,** *10* (59), 5159-5162.

(15) Spence, J. T.; George, J. H., Total Synthesis of Peniphenones A-D via Biomimetic Reactions of a Common o-Quinone Methide Intermediate. *Org. Lett.* **2015,** *17* (24), 5970-5973.

(16) Takao, K.; Noguchi, S.; Sakamoto, S.; Kimura, M.; Yoshida, K.; Tadano, K., Total Synthesis of (+)-Cytosporolide A via a Biomimetic Hetero-Diels-Alder Reaction. *J. Am. Chem. Soc.* **2015,** *137* (50), 15971-7.

(17) Lumb, J.-P.; Choong, K. C.; Trauner, D., ortho-Quinone Methides from para-Quinones: Total Synthesis of Rubioncolin B. *J. Am. Chem. Soc.* **2008,** *130* (29), 9230-9231.

(18) Liao, D.; Li, H.; Lei, X., Efficient Generation of ortho-Quinone Methide: Application to the Biomimetic Syntheses of (±)-Schefflone and Tocopherol Trimers. *Org. Lett.* **2012,** *14* (1), 18-21.

(19) Uyanik, M.; Nishioka, K.; Kondo, R.; Ishihara, K., Chemoselective oxidative generation of ortho-quinone methides and tandem transformations. *Nat. Chem.* **2020,** *12* (4), 353-362.

(20) Pettigrew, J. D.; Freeman, R. P.; Wilson, P. D., Total synthesis of (–)-xyloketal D and its enantiomer: Confirmation of absolute stereochemistry. *Can. J. Chem.* **2004,** *82* (11), 1640-1648.

(21) Spence, J. T. J.; George, J. H., Biomimetic Total Synthesis of *ent*-Penilactone A and Penilactone B. *Org. Lett.* **2013,** *15* (15), 3891-3893.

(22) Basha, R. S.; Chen, C. W.; Reddy, D. M.; Lee, C. F., Iodine-Mediated Direct Generation of o-Quinone Methides at Room Temperature: A Facile Protocol for the Synthesis of ortho-Hydroxybenzyl Thioethers. *Chem. Asian J.* **2018,** *13* (17), 2475-2483.

(23) Zhou, D.; Yu, X.; Zhang, J.; Wang, W.; Xie, H., Organocatalytic Asymmetric Formal [4 + 2] Cycloaddition of in Situ Oxidation-Generated ortho-Quinone Methides and Aldehydes. *Org. Lett.* **2018,** *20* (1), 174-177.

(24) Reichl, K. D.; Smith, M. J.; Song, M. K.; Johnson, R. P.; Porco, J. A., Jr., Biomimetic Total Synthesis of (+/-)-Griffipavixanthone via a Cationic Cycloaddition-Cyclization Cascade. *J. Am. Chem. Soc.* **2017,** *139* (40), 14053-14056.

(25) More, A. A.; Ramana, C. V., o-Quinone Methides via Oxone-Mediated Benzofuran Oxidative Dearomatization and Their Intramolecular Cycloaddition with Carbonyl Groups: An Expeditious Construction of the Central Tetracyclic Core of Integrastatins, Epicoccolide A, and Epicocconigrone A. *Org. Lett.* **2016,** *18* (3), 612-615.

(26) Gebauer, K.; Reuss, F.; Spanka, M.; Schneider, C., Relay Catalysis: Manganese(III) Phosphate Catalyzed Asymmetric Addition of beta-Dicarbonyls to ortho-Quinone Methides Generated by Catalytic Aerobic Oxidation. *Org Lett* **2017,** *19* (17), 4588-4591.

(27) Wong, Y. F.; Wang, Z.; Hong, W.-X.; Sun, J., A one-pot oxidation/cycloaddition cascade synthesis of 2,4-diaryl chromans via ortho -quinone methides. *Tetrahedron* **2016,** *72* (22), 2748-2751.

(28) Lam, H. C.; Spence, J. T.; George, J. H., Biomimetic Total Synthesis of Hyperjapones A-E and Hyperjaponols A and C. *Angew. Chem. Int. Ed. Engl.* **2016**, *55* (35), 10368-71.

(29) Lie, F.; Chen, Y.; Wang, Z.; Li, Z., Enantioselective benzylic hydroxylation of indan and tetralin with Pseudomonas monteilii TA-5. *Tetrahedron: Asymmetry* **2009,** *20* (10), 1206-1211.

(30) Yongzheng, C.; Felicia, L.; Zhi, L., Enantioselective Benzylic Hydroxylation with Pseudomonas monteilii TA-5: A Simple Method for the Syntheses of (R)-Benzylic Alcohols Containing Reactive Functional Groups. *Adv. Synth. & Catal.* **2009,** *351* (13), 2107-2112.

(31) Limberger, R. P.; Ursini, C. V.; Moran, P. J. S.; Rodrigues, J. A. R., Enantioselective benzylic microbial hydroxylation of indan and tetralin. *J. Mol. Catal. B: Enzym.* **2007,** *46* (1), 37-42.

(32) Dai, S.; Wu, J.; Wang, Z.; Chen, Y.; Li, Z., Highly chemo- and regio-selective hydroxylations of o- and m-substituted toluenes to benzyl alcohols with Cellulosimicrobium cellulans EB-8-4. *Tetrahedron* **2010,** *66* (34), 6919-6923.

(33) Uzura, A.; Katsuragi, T.; Tani, Y., Stereoselective oxidation of alkylbenzenes by fungi. *J. Biosci. Bioengin.* **2001,** *91* (2), 217-221.

(34) Yadav, S.; Yadav, R. S. S.; Yadava, S.; Yadav, K. D. S., Stereoselective hydroxylation of ethylbenzene to (R)-1-phenylethanol using mycelia of Aspergillus niger as catalyst. *Catal. Commun.* **2011,** *12* (9), 781-784.

(35) Alexander, D.; Maria, W. A.; Tsvetan, K.; Andrea, M. C.; Erika, T.; Martin, S.; Joëlle, R. A.; Ulrich, S., An Enzymatic Route to α-Tocopherol Synthons: Aromatic Hydroxylation of Pseudocumene and Mesitylene with P450 BM3. *Chem. Eur. J.* **2017,** *23* (71), 17981-17991.

(36) Anja, E.; Łukasz, G.; Susanne, H.; P., K. P.; J., T. N.; Jürgen, P.; L., F. S., Enantioselective Benzylic Hydroxylation Catalysed by P450 Monooxygenases: Characterisation of a P450cam Mutant Library and Molecular Modelling. *ChemBioChem* **2016,** *17* (5), 426-432.

(37) Driscoll, J. P.; Kornecki, K.; Wolkowski, J. P.; Chupak, L.; Kalgutkar, A. S.; O'Donnell, J. P., Bioactivation of Phencyclidine in Rat and Human Liver Microsomes and Recombinant P450 2B Enzymes: Evidence for the Formation of a Novel Quinone Methide Intermediate. *Chem. Res. Toxicol.* **2007,** *20* (10), 1488-1497.

(38) Du, L.; Dong, S.; Zhang, X.; Jiang, C.; Chen, J.; Yao, L.; Wang, X.; Wan, X.; Liu, X.; Wang, X.; Huang, S.; Cui, Q.; Feng, Y.; Liu, S.-J.; Li, S., Selective oxidation of aliphatic C–H bonds in alkylphenols by a chemomimetic biocatalytic system. *Proc. Nat'l. Acad. Sci.* **2017,** *114* (26), E5129-E5137.

(39) Kelly, P. P.; Eichler, A.; Herter, S.; Kranz, D. C.; Turner, N. J.; Flitsch, S. L., Active site diversification of P450cam with indole generates catalysts for benzylic oxidation reactions. *Beilstein J. Org. Chem.* **2015,** *11*, 1713-1720.

(40) Li, A.; Wu, S.; Adams, J. P.; Snajdrova, R.; Li, Z., Asymmetric epoxidation of alkenes and benzylic hydroxylation with P450tol monooxygenase from Rhodococcus coprophilus TC-2. *Chem. Commun.* **2014,** *50* (63), 8771-8774.

(41) Neufeld, K.; Marienhagen, J.; Schwaneberg, U.; Pietruszka, J., Benzylic hydroxylation of aromatic compounds by P450 BM3. *Green Chem.* **2013,** *15* (9), 2408-2421.

(42) Suzuki, K.; Stanfield, J. K.; Shoji, O.; Yanagisawa, S.; Sugimoto, H.; Shiro, Y.; Watanabe, Y., Control of stereoselectivity of benzylic hydroxylation catalysed by wild-type cytochrome P450BM3 using decoy molecules. *Catal. Sci. & Technol.* **2017,** *7* (15), 3332-3338.

(43) Hall, E. A.; Sarkar, M. R.; Bell, S. G., The selective oxidation of substituted aromatic hydrocarbons and the observation of uncoupling via redox cycling during naphthalene oxidation by the CYP101B1 system. *Catal. Sci. & Technol.* **2017,** *7* (7), 1537-1548.

(44) Zwick, C. R.; Renata, H., Evolution of Biocatalytic and Chemocatalytic C–H Functionalization Strategy in the Synthesis of Manzacidin C. *J. Org. Chem.* **2018,** *83* (14), 7407-7415.

(45) Dror, A.; Fishman, A., Engineering non-heme mono- and dioxygenases for biocatalysis. *Comput. Struct. Biotechnol. J.* **2012,** *2* (3), e201209011.

(46) Herr, C. Q.; Hausinger, R. P., Amazing Diversity in Biochemical Roles of Fe(II)/2-Oxoglutarate Oxygenases. *Trends Biochem. Sci.* **2018**.

(47) Martinez, S.; Hausinger, R. P., Catalytic Mechanisms of Fe(II)- and 2-Oxoglutarate-dependent Oxygenases. *J. Biol. Chem.* **2015,** *290* (34), 20702-11.

(48) Nakamura, H.; Matsuda, Y.; Abe, I., Unique chemistry of non-heme iron enzymes in fungal biosynthetic pathways. *Nat. Prod. Rep.* **2018,** *35* (7), 633-645.

(49) He, Y.; Cox, R. J., The molecular steps of citrinin biosynthesis in fungi. *Chem. Sci.* **2016,** *7* (3), 2119-2127.

(50) Zang, Y.; Song, X.; Li, C.; Ma, J.; Chu, S.; Liu, D.; Ren, Q.; Li, Y.; Chen, N.; Zhang, D., Pyrano[3,2-a]carbazole alkaloids as effective agents against ischemic stroke in vitro and in vivo. *Eur. J. Med. Chem.* **2018,** *143*, 438-448.

(51) Carter, D. V.; Charlton, P. T.; Fenton, A. H.; Housley, J. R.; Lessel, B., The Preparation and the Antibacterial and Antifungal Properties of some substituted benzyl alchohols. *J. Pharm. Pharmacol.* **1958,** *10* (S1), 149-159.

(52) Li, L.; Liu, Y.; Wang, Q., Regioselective Oxidative Dehydrogenation under Nonenzymatic Conditions: A Synthetic Route to Gossypol. *Eur. J. Org. Chem.* **2013,** *2013* (35), 8014-8021.

(53) Cort, A. D.; Mandolini, L.; Panaioli, S., Selective One-Pot Oxidation of Methylarenes to Benzyl Alcohols with the Copper(II)-Peroxydisulfate System. *Synth. Commun.* **1988,** *18* (6), 613-616.

(54) Baciocchi, E.; Mandolini, L.; Rol, C., Oxidation by metal ions. 6. Intramolecular selectivity in the side-chain oxidation of p-ethyltoluene and isodurene by cobalt(III), cerium(IV), and manganese(III). *J. Org. Chem.* **1980,** *45* (19), 3906-3909.

(55) Vece, V.; Jakkepally, S.; Hanessian, S., Total Synthesis and Absolute Stereochemical Assignment of the Insecticidal Metabolites Yaequinolones J1 and J2. *Org. Lett.* **2018,** *20* (14), 4277-4280.

(56) Yang, B.; Gao, S., Recent advances in the application of Diels–Alder reactions involving o-quinodimethanes, aza-o-quinone methides and *o*-quinone methides in natural product total synthesis. *Chem. Soc. Rev.* **2018,** *47* (21), 7926-7953.

(57) Arumugam, S.; Popik, V. V., Photochemical Generation and the Reactivity of o-Naphthoquinone Methides in Aqueous Solutions. *J. Am. Chem. Soc.* **2009,** *131* (33), 11892-11899.

(58) Baker Dockrey, S. A.; Lukowski, A. L.; Becker, M. R.; Narayan, A. R. H., Biocatalytic site- and enantioselective oxidative dearomatization of phenols. *Nat. Chem.* **2017,** *10*, 119.

(59) de Carvalho, C. C. C. R., Whole cell biocatalysts: essential workers from Nature to the industry. *Microb. Biotech.* **2017,** *10* (2), 250-263.

(60) Wachtmeister, J.; Rother, D., Recent advances in whole cell biocatalysis techniques bridging from investigative to industrial scale. *Curr. Opin. Biotechnol.* **2016,** *42*, 169-177.

(61) Baker Dockrey, S. A.; Doyon, T. J.; Perkins, J. C.; Narayan, A. R. H., Whole-cell biocatalysis platform for gram-scale oxidative dearomatization of phenols. *Chem. Biol. & Drug Des.* **2018**, *93*, 1207-1213.

(62) deGruyter, J. N.; Malins, L. R.; Baran, P. S., Residue-Specific Peptide Modification: A Chemist's Guide. *Biochemistry* **2017,** *56* (30), 3863-3873.

(63) Spicer, C. D.; Davis, B. G., Selective chemical protein modification. *Nat. Commun.* **2014,** *5*, 4740.

(64) Hoyt, E. A.; Cal, P. M. S. D.; Oliveira, B. L.; Bernardes, G. J. L., Contemporary approaches to site-selective protein modification. *Nat. Rev. Chem.* **2019,** *3* (3), 147-171.

(65) Kolmel, D. K.; Kool, E. T., Oximes and Hydrazones in Bioconjugation: Mechanism and Catalysis. *Chem. Rev.* **2017,** *117* (15), 10358-10376.

(66) Agten, S. M.; Dawson, P. E.; Hackeng, T. M., Oxime conjugation in protein chemistry: from carbonyl incorporation to nucleophilic catalysis. *J. Pept. Sci.* **2016,** *22* (5), 271-9.

(67) Rashidian, M.; Kumarapperuma, S. C.; Gabrielse, K.; Fegan, A.; Wagner, C. R.; Distefano, M. D., Simultaneous Dual Protein Labeling Using a Triorthogonal Reagent. *J. Am. Chem. Soc.* **2013,** *135* (44), 16388-16396.

(68) Lin, Y.; Wu, X.; Feng, S.; Jiang, G.; Luo, J.; Zhou, S.; Vrijmoed, L. L. P.; Jones, E. B. G.; Krohn, K.; Steingröver, K.; Zsila, F., Five Unique Compounds: Xyloketals from Mangrove Fungus Xylaria sp. from the South China Sea Coast. *J. Org. Chem.* **2001,** *66* (19), 6252-6256.

(69) Krohn, K.; Riaz, M.; Flörke, U., Synthesis of Xyloketals, Natural Products from the Mangrove Fungus Xylaria sp. *Eur. J. Org. Chem.* **2004,** *2004* (6), 1261-1270.

(70) Panda, B.; Sarkar, T. K., Gold catalysis: regio- and stereoselective total synthesis of xyloketals D and G and the related natural product alboatrin. *J. Org. Chem.* **2013,** *78* (6), 2413-21.

(71) Abood, A.; Al-Fahad, A.; Scott, A.; Hosny, A. E.-D. M. S.; Hashem, A. M.; Fattah, A. M. A.; Race, P. R.; Simpson, T. J.; Cox, R. J., Kinetic characterisation of the FAD dependent monooxygenase TropB and investigation of its biotransformation potential. *RSC Adv.* **2015,** *5* (62), 49987-49995.

(72) Backus, K. M.; Correia, B. E.; Lum, K. M.; Forli, S.; Horning, B. D.; González-Páez, G. E.; Chatterjee, S.; Lanning, B. R.; Teijaro, J. R.; Olson, A. J.; Wolan, D. W.; Cravatt, B.

F., Proteome-wide covalent ligand discovery in native biological systems. *Nature* **2016,** *534*, 570.

(73) Becke, A. D., Density-functional thermochemistry. III. The role of exact exchange. *J. Chem. Phys.* **1993,** *98* (7), 5648-5652.

(74) Lee, C.; Yang, W.; Parr, R. G., Development of the Colle-Salvetti correlation-energy formula into a functional of the electron density. *Phys. Rev. B* **1988,** *37* (2), 785-789.

(75) Krishnan, R.; Binkley, J. S.; Seeger, R.; Pople, J. A., Self-consistent molecular orbital methods. XX. A basis set for correlated wave functions. *J. Chem. Phys.* **1980,** *72* (1), 650-654.

(76) Clark, T.; Chandrasekhar, J.; Spitznagel, G. W.; Schleyer, P. V. R., Efficient diffuse function-augmented basis sets for anion calculations. III. The 3-21+G basis set for first-row elements, Li–F. *J. Comput. Chem.* **1983,** *4* (3), 294-301.

(77) Zimmerman, P. M., Single-ended transition state finding with the growing string method. *J. Comput. Chem.* **2015,** *36* (9), 601-611.

(78) Marenich, A. V.; Olson, R. M.; Kelly, C. P.; Cramer, C. J.; Truhlar, D. G., Self-Consistent Reaction Field Model for Aqueous and Nonaqueous Solutions Based on Accurate Polarized Partial Charges. *J. Chem. Theor. Comput.* **2007,** *3* (6), 2011-2033.

(79) Marenich, A. V.; Cramer, C. J.; Truhlar, D. G., Universal Solvation Model Based on Solute Electron Density and on a Continuum Model of the Solvent Defined by the Bulk Dielectric Constant and Atomic Surface Tensions. *J. Phys. Chem. B* **2009,** *113* (18), 6378-6396.

(80) Jr., T. H. D., Gaussian basis sets for use in correlated molecular calculations. I. The atoms boron through neon and hydrogen. *J. Chem. Phys.* **1989,** *90* (2), 1007-1023.

(81) Kendall, R. A.; Jr., T. H. D.; Harrison, R. J., Electron affinities of the first-row atoms revisited. Systematic basis sets and wave functions. *J. Chem. Phys.* **1992,** *96* (9), 6796-6806.

(82) Woon, D. E.; Jr., T. H. D., Gaussian basis sets for use in correlated molecular calculations. III. The atoms aluminum through argon. *J. Chem. Phys.* **1993,** *98* (2), 1358-1371.

(83) Woon, D. E.; Jr., T. H. D., Gaussian basis sets for use in correlated molecular calculations. IV. Calculation of static electrical response properties. *J. Chem. Phys.* **1994,** *100* (4), 2975-2988.

(84) Wilson, A. K.; Woon, D. E.; Peterson, K. A.; Jr., T. H. D., Gaussian basis sets for use in correlated molecular calculations. IX. The atoms gallium through krypton. *J. Chem. Phys.* **1999,** *110* (16), 7667-7676.

(85) Balabanov, N. B.; Peterson, K. A., Systematically convergent basis sets for transition metals. I. All-electron correlation consistent basis sets for the 3d elements Sc–Zn. *J. Chem. Phys.* **2005,** *123* (6), 064107.

(86) Shao, Y et al. Advances in molecular quantum chemistry contained in the Q-Chem 4 program package. *Mol. Phys.* **2015,** *113* (2), 184-215.

(87) Neese, F., The ORCA program system. *WIREs Comput. Molec. Sci.* **2012,** *2* (1), 73-78.

# Chapter 3: Chemoenzymatic Synthesis of γ-hydroxytropolones and Tropolone Meroterpenoids

## 3.1 Introduction

Secondary metabolites produced by plants and microorganisms often possess important biological activities which can be leveraged in the development of novel pharmaceuticals.[1-4] Thorough evaluation of these valuable molecular properties requires facile access to a source of the natural product through synthesis of the target compound or fermentation of the producing organism to isolate useful quantities of product.[1-3, 5] However, difficulties in culturing many metabolite-producing organisms, as well as associated challenges in the isolation of the natural products, present a major roadblock in generating a suitable quantity of product for further experimentation.[3, 6] In addition, many natural product scaffolds represent challenging synthetic targets, requiring intensive efforts to design and execute a scalable synthetic campaign.[7-8] In comparison, Nature has developed direct and efficient routes to access these complex molecules. Biosynthetic enzymes within host organisms regularly perform selective reactions to produce secondary metabolites in rapid fashion from bioavailable base materials.[9] These enzymes offer numerous advantages for the construction of complex scaffolds, including exquisite selectivity profiles and sustainable reaction conditions.[9-11] Despite the broad potential of enzymes to improve natural product synthesis, these catalysts remain largely underdeveloped as synthetic tools, particularly for complex transformations and rearrangements.[4, 12] Biocatalytic transformations which are most commonly leveraged for synthetic purposes include amidation, carbonyl/imine

reduction and hydrolytic reactions, providing great advantages for the selective construction of complex molecules.[12] However, to further expand the synthetic toolbox available to organic chemists and develop new approaches for natural product synthesis, diverse enzymatic transformations must be explored for their synthetic potential. Enzymes which perform complexity-generating reactions can possess the ability to construct synthetically-useful targets, with distinct advantages over existing synthetic methods.[4, 12] For example, enzymes which selectively control the fate of a reactive intermediate, such as a radical or cation, often proceed with a reactivity that is fundamentally divergent from small molecule catalysts.[13-14] Diverse enzyme classes, including cyclases,[15] Diels-Alderases,[14] and polyketide synthases[13] leverage this ability to generate products with great selectivity. The enzyme active site provides three-dimensional control over the bond formation steps, leading to a particular outcome.[13] Such selectivity is often unmatched by small molecule methods, which can require extensive substrate engineering to produce the desired transformation. Therefore, the detailed characterization of enzymes which perform complex, synthetically-challenging reactions can lead to the development of novel biocatalytic reactions to construct natural products.[16-17]

Tropolones are a class of natural products which are difficult to access through synthesis or biological fermentation. These compounds are structurally-diverse metabolites containing a 7-membered aromatic ring with an α-hydroxyketone moiety.[18-19] Tropolones are produced within bacteria, fungi and plants and often possess unique biological activities including antiviral,[20-22] antifungal,[23-26] antibacterial,[25, 27] anticancer[28-36] and anthelmintic[37] properties. However, a thorough investigation of the biological activities of many tropolones has been limited by roadblocks in accessing these natural product cores, many of which have not yet been targeted for total synthesis.[18] Synthetic efforts to access tropolones are complicated by challenges in directly

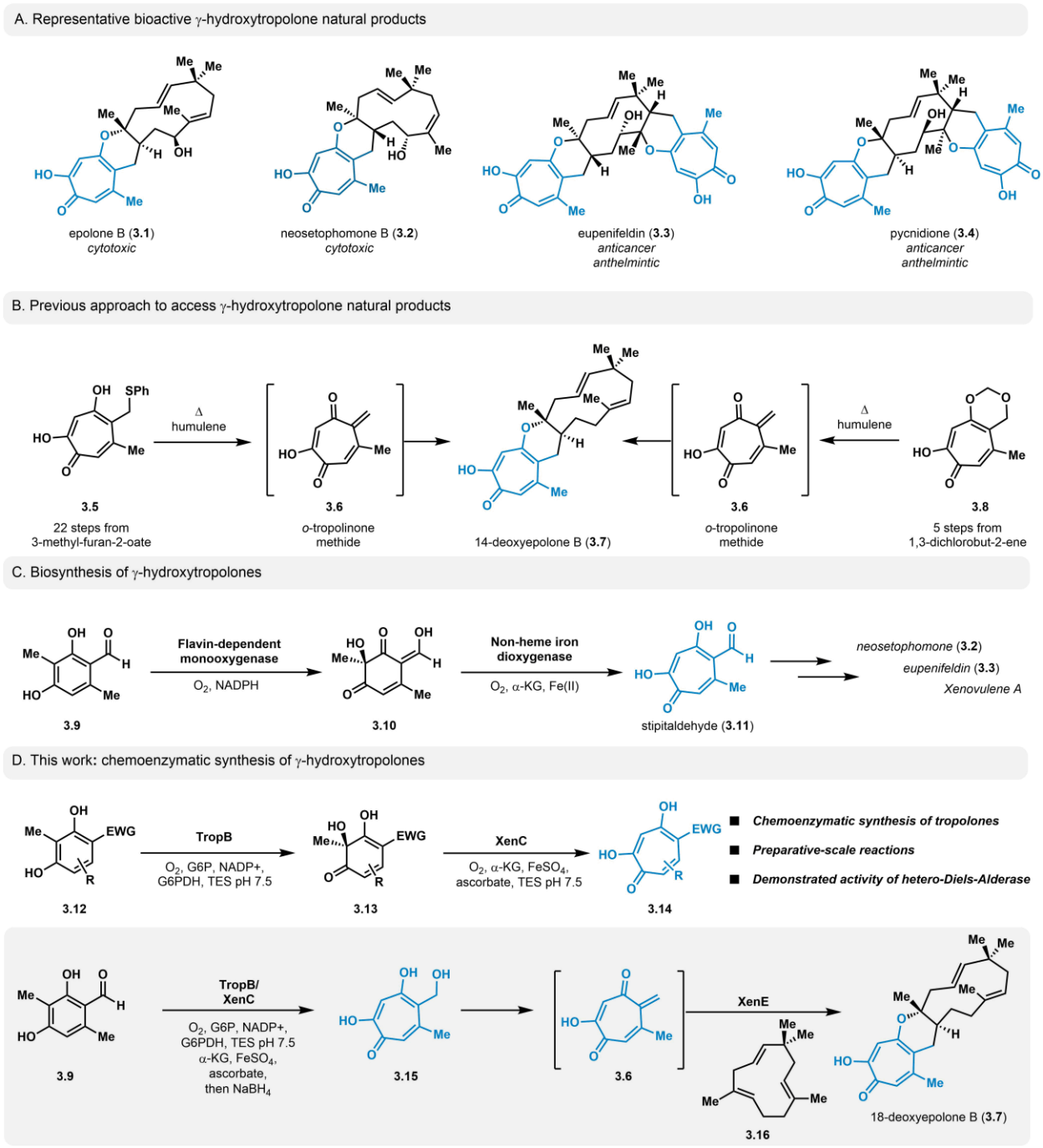


**Figure 3.1. Synthesis and biosynthesis of tropolone natural products.**
A. Representative tropolone meroterpenoids possessing biological activities. B. Previous syntheses of 18-deoxyepolone B. C. Abbreviated biosynthesis of γ-hydroxytropolone natural products. D. This work: development of a chemoenzymatic route to tropolone products.

producing the 7-membered aromatic core with the desired substitution pattern to match the natural

product of interest (Figure 3.2).[18-19] Early efforts to synthesize tropolones focused on direct oxidation of substituted cycloheptatrienes or tropones, generating the tropolone core (Figure 3.2A, see **3.17**-**3.19**).[38-40] However, this approach proved synthetically intractable, as direct oxidation often proceeded with poor selectivity, leading to complex product mixtures and reduced yields.[18] Other early tropolone natural product syntheses leveraged existing tropolone natural product cores to generate new tropolone metabolites (Figure 3.2B).[18, 41-43] For example, a formal total synthesis of colchicine was achieved through elaboration of the commercially-available natural product purpurogallin (**3.20**) to desacetamidocolchicine (**3.21**).[41-42] However, this approach requires access to a variety of tropolone natural product cores, which is limited due to challenges in obtaining tropolone metabolites from source organisms.[18] Tropolones have also been constructed through ring-closing metathesis (RCM) or cyclization reactions, enabling late-stage tropolone formation and allowing greater flexibility in substrate design (Figure 3.2C).[18, 44-46] Despite these advantages, late-stage access to tropolones still requires extensive substrate design considerations, leading to lengthy, linear reaction sequences with few opportunities for the development of divergent synthetic routes.[18] In addition, some methods can suffer from poor regioselectivity in the cyclization step, a common challenge in the synthesis of medium-sized rings.[47] The most common synthetic tactic to access tropolones involves rearrangements from smaller rings, such as the Büchner reaction (see **3.24**-**3.26**), the de Mayo fragmentation, and [5+2] cycloadditions (Figure 3.2D).[18, 48] As with ring-closing reactions, these methods also require specific substrate design considerations to achieve the intended transformation.[18-19] Consequently, ring expansion approaches to access tropolone natural products vary widely depending on the target structure, obfuscating efforts to achieve a generalized method for tropolone synthesis.[47-48] Therefore, the development of direct synthetic routes to access diverse tropolone natural products and their

derivatives remains a major challenge in synthetic chemistry. We aimed to address this challenge by leveraging Nature's tools for the construction of tropolone natural products and their analogs through a scalable chemoenzymatic process.

We envisioned an approach which utilizes a two-enzyme cascade reaction involving a flavin-dependent monooxygenase and an α-KG-dependent NHI enzyme which directly produce tropolone natural products in native fungal tropolone biosynthesis (Figure 3.1C). This ring expansion reaction has been studied in multiple fungal species and has been identified as an intermediate step in the biosynthesis of the secondary metabolites xenovulene A and eupenifeldin (**3.30**), among others (Figure 3.3).[49-51] In this biosynthetic pathway, a non-reducing polyketide synthase (PKS) is responsible for the synthesis of β-orcinaldehyde (**3.9**) which then undergoes a site- and stereoselective oxidative dearomatization reaction catalyzed by a flavin-dependent monooxygenase to produce diene **3.10** (Figure 3.1C).[49-52] Following this step, an α-KG-dependent NHI enzyme performs an oxidative ring expansion reaction, resulting in the formation of

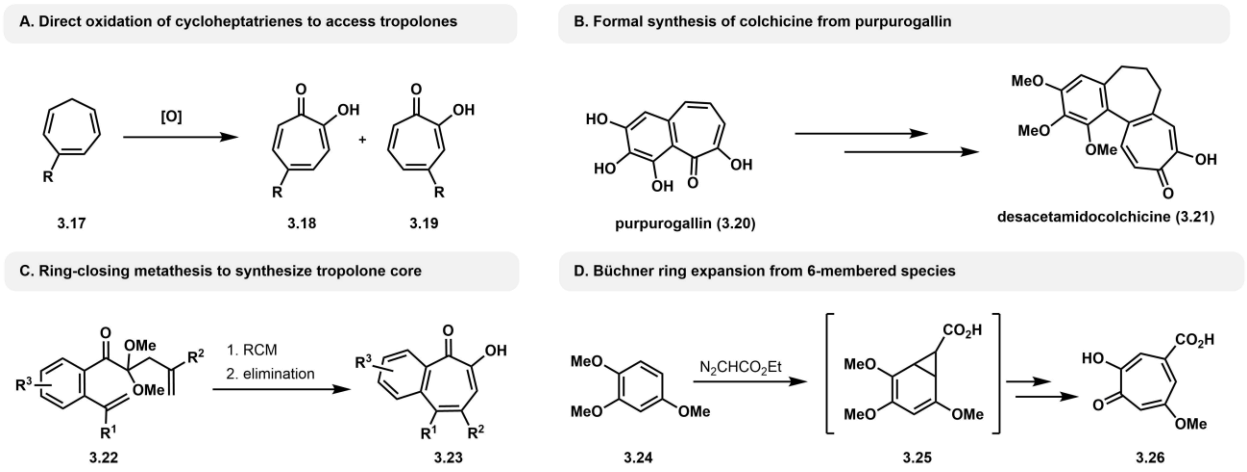


**Figure 3.2. Synthetic approaches to accessing the tropolone core.**
A. Direct oxidation of cycloheptatrienes to access the tropolone core. B. Formal synthesis of colchicine from tropolone natural product purpurogallin (3.20). C. Ring closing metathesis (RCM) to access the tropolone core. D. Büchner ring expansion reaction to generate tropolone core from 6-memebered species.

stipitaldehyde (**3.11**), which serves as the common branch point in the biosynthesis of related natural products (Figure 3.3).[49-53] While many tropolone biosynthetic pathways remain unexplored, a variety of bioactive tropolones possess the γ-hydroxytropolone core present in stipitaldehyde (**3.11**), suggesting that this ring expansion cascade is conserved in the biosynthesis of numerous tropolone natural products.[50] We aimed to leverage this enzymatic sequence for the synthesis of a variety of substituted tropolones. We also envisioned that this cascade could allow facile access to a bioactive class of tropolone natural products known collectively as tropolone meroterpenoids.

As a result of the wide-ranging challenges in tropolone synthesis, only two synthetic groups have achieved successful construction of tropolone meroterpenoid cores. The Baldwin group accessed the deoxy-form of the natural product epolone B (**3.7**) through a 21-step synthesis of a phenylthioether-substituted tropolone **3.5**, which served as a precursor to an *o*-tropolinone methide (*o*-TM) species.[54] This intermediate then underwent a racemic inverse electron-demand Diels-Alder (IEDDA) reaction with α-humulene (**3.16**) to generate the desired product, 18-deoxy-epolone B (**3.7**).[54] A thesis from the Sarlah group recently reported a strategy involving a de Mayo

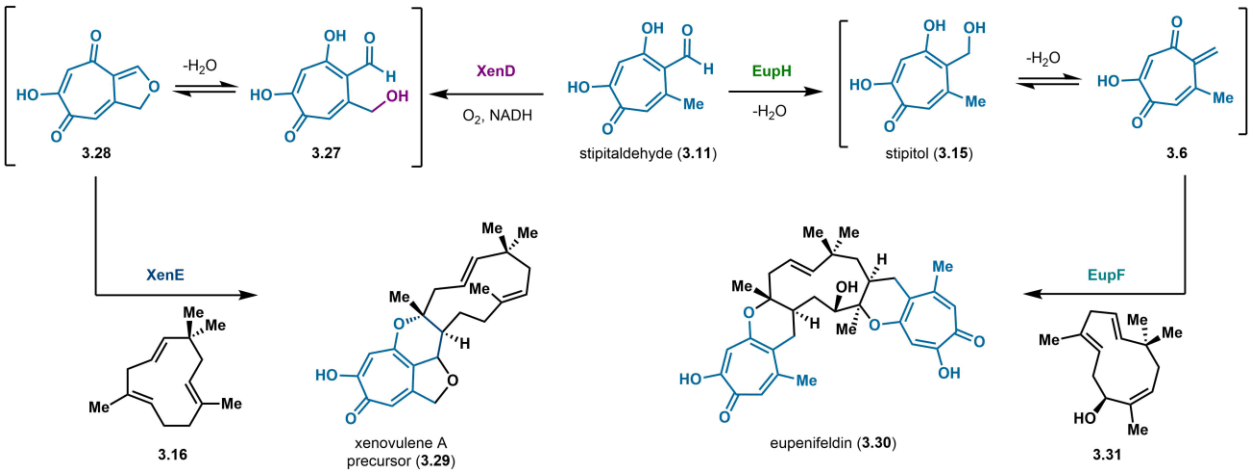


**Figure 3.3. Biosynthesis of tropolone meroterpenoid natural products**.

fragmentation to directly produce the *o*-TM precursor **3.8** in a 6-step sequence from 1,3-chlorobut-2-ene.[55] The elaboration of **3.8** was again accomplished by a racemic IEDDA reaction with α-humulene (**3.16**), generating the desired product in a more direct fashion.[55] We envisioned pursuing a chemoenzymatic route to 18-deoxyepolone B (**3.7**), leveraging the advantages of a biocatalytic platform for the direct synthesis of the tropolone core. Similar to the approach taken by Baldwin and Sarlah, we aimed to exploit the reactive nature of *o*-TM intermediate **3.6**, performing an IEDDA reaction with α-humulene to construct the desired tropolone product (Figure 3.1D). To generate *o*-TM precursor **3.6**, we anticipated that stipitol (**3.15**), a proposed intermediate in eupenifeldin (**3.30**) biosynthesis (Figure 3.3), could be directly accessed by chemical reduction of stipitaldehyde (**3.11**).[50] We further aimed to develop a one-pot, two-enzyme oxidative dearomatization and ring expansion reaction platform to produce stipitaldehyde (**3.11**) from β-orcinaldehyde (**3.9**), providing a direct, chemoenzymatic approach to accessing the tropolone core. This reaction platform would leverage a flavin-dependent monooxygenase, TropB for the site- and stereoselective oxidative dearomatization of **3.9** to generate *o*-quinol **3.10**, followed by an oxidative ring expansion reaction catalyzed by an α-KG-dependent NHI dioxygenase to produce stipitaldehyde (**3.11**). This proposed route takes advantage of the reactivity of stipitol (**3.15**) to serve as a precursor to an *o*-TM, enabling rapid access to tropolone meroterpenoid natural product cores. In addition, we hypothesized that a hetero-Diels-Alderase, XenE (Figure 3.3), which was previously characterized *in vivo* in the biosynthesis of xenovulene A, could be leveraged for the enantioselective synthesis of 18-deoxyepolone B (**3.7**) from **3.15**, representing the first selective synthesis of this product.[50] A related biosynthetic pathway was recently characterized by Chen et al. for the *in vivo* synthesis of neosetophomone B using the hetero-Diels-Alderase EupF to achieve the reported selectivity, demonstrating the synthetic utility of this approach.[56] Through our

proposed chemoenzymatic reaction platform, we aimed to construct a scalable biocatalytic method for the direct and selective synthesis of 18-deoxyepolone B (**3.7**), as well as other tropolone natural product derivatives.

### 3.2 Identification of candidate NHI dioxygenase for ring expansion reactions

Toward the development of a direct chemoenzymatic route for the synthesis of tropolones, we first sought to identify a biocatalyst capable of efficiently accessing tropolones through a one-pot, two-enzyme oxidative dearomatization and ring expansion process. As the enzyme TropC had been previously shown to perform a ring expansion reaction, we used the TropC amino acid sequence as a starting point for identifying homologs which could engage in the same ring expansion reactions.[49] An initial basic local alignment tool (BLAST) search of the National Center for Biotechnology Information (NCBI) database yielded several NHI dioxygenases sharing

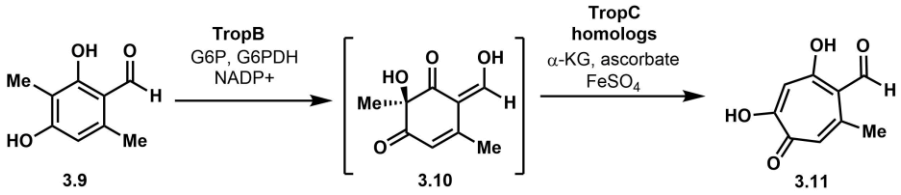


| Entry | Species | % ID with TropC (*T. stipitatus*) | Substrate conversion |
|---|---|---|---|
| **1** | *T. stipitatus* (TropC) | 100% | 90% |
| **2** | *S. strictum* (XenC) | 54% | 98% |
| **3** | *P. freii* | 56% | 74% |
| **4** | *Hypoxylon sp.* | 63% | 37% |

**Table 3.1. Comparison of TropC homologs in one-pot reaction with substrate 3.9**
Reaction conditions: 2 mM substrate, 10 μM TropC, 5 μM TropB or AzaH, 50 mM TES pH 7.5, 5 mM α-ketoglutaric acid (α-KG), 4 mM sodium ascorbate, 0.1 mM ferrous sulfate ($FeSO_4$), 5 mM glucose-6-phosphate (G6P), 0.1 mM nicotinamide adenine diphosphate (NADP+), 0.1 U/mL glucose-6-phosphate dehydrogenase (G6PDH), 30 °C. Conversion to product was quantified by LC-MS analysis.

sequence identity with TropC (Table 3.1). To ensure that these unannotated sequences were indeed functional homologs of TropC, we then confirmed the presence of a TropB homolog within the gene cluster of the species of interest. From this set of sequence results, we selected three homologs sharing various levels of sequence identity with TropC. These genes were ordered from Twist Biosciences in pET-28a expression vectors. The constructs were transformed into BL21(DE3) *E. coli*, expressed and purified using the standard conditions described in Section 3.8 of this chapter. All of the homologous enzymes were soluble and were used in subsequent reactions to assess their relative performance in a one-pot oxidative dearomatization/ring expansion process. Our group has previously demonstrated the substrate promiscuity of flavin-dependent monooxygenase TropB in performing site- and stereo-selective oxidative dearomatization of resorcinols. Taking advantage of this selective reaction, we established a modular, one-pot platform in which TropB-catalyzed dearomatization was allowed to proceed until completion, followed by the addition of each NHI dioxygenase and the cofactors α-KG, sodium ascorbate and ferrous sulfate heptahydrate. Under the same reaction conditions, TropC homologs performed with varied efficiency. After 3 h, the reaction was quenched with methanol, and the product conversions were analyzed by LC-MS. For all homologs tested, we observed conversion of compound **3.10** to stipitaldehyde. However, the most effective enzyme in catalyzing this ring expansion reaction was the NHI dioxygenase from the fungus *S. strictum* known as XenC. Recently, XenC has been shown to catalyze the formation of stipitaldehyde natively in the context of xenovulene A biosynthesis, demonstrating that **3.10** is the native substrate for the enzyme.[51] Encouragingly, this biocatalyst converted nearly all of substrate **3.10** to stipitaldehyde (**3.11**) in this one-pot process. As a result of this superior performance, we chose to conduct subsequent studies with XenC.

### 3.3 Scope of oxidative dearomatization and ring expansion platform

We first explored the ability of NHI dioxygenase XenC to convert *ortho*-quinols (such as **3.13**) to γ-hydroxytropolones in a one-pot oxidative dearomatization/ring expansion cascade. Tropolones possessing synthetically-tractable functional handles, such as aldehydes, halogens, alkynes and nitro groups, were produced with good conversion (51-96% conversion, Figure 3.5, **3.33-3.35**, **3.42**). The diversity of functional groups which were incorporated in the final tropolone products provide the ability to achieve a divergent synthesis of complex tropolones following a simple chemoenzymatic synthesis of the core structure. In addition, we explored the feasibility of generating tropolone structures which were substituted at the C3 (**3.37**) and C7 (**3.38**) positions respectively. The resulting tropolones were generated with moderate to good conversion over two

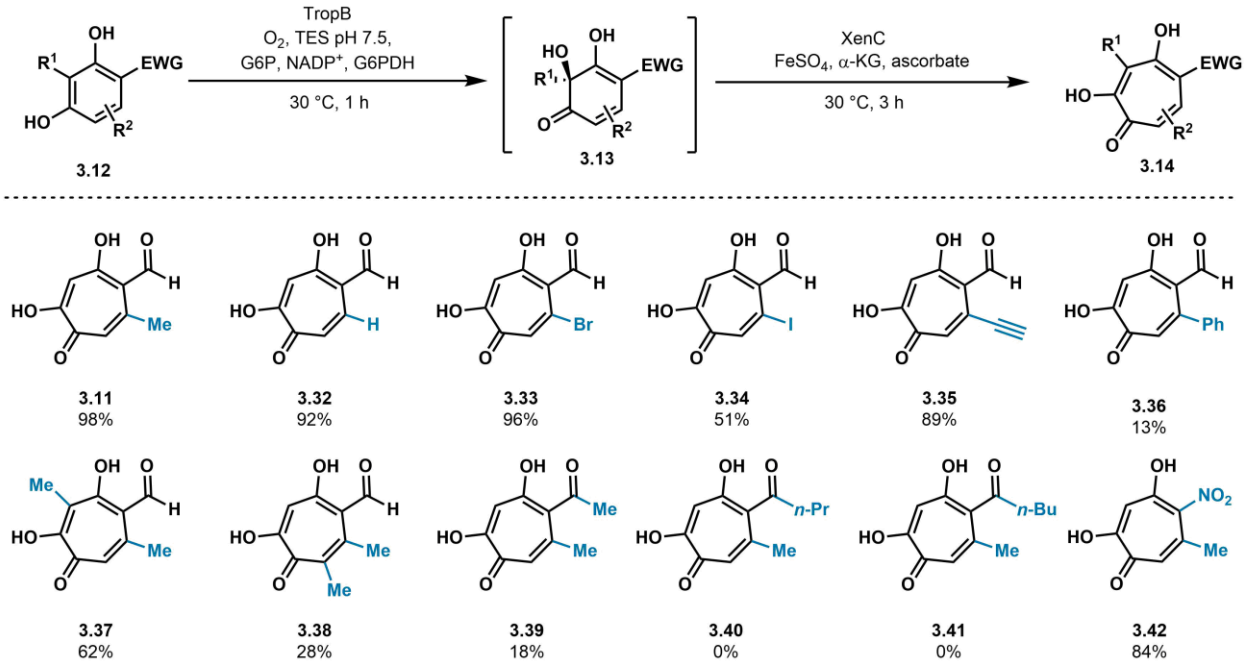


**Figure 3.4. Substrate scope for XenC-catalyzed ring expansion.**
Reaction conditions: 2 mM substrate, 10 μM TropC, 5 μM TropB or AzaH, 50 mM TES pH 7.5, 5 mM α-ketoglutaric acid (α-KG), 4 mM sodium ascorbate, 0.1 mM ferrous sulfate ($FeSO_4$), 5 mM glucose-6-phosphate (G6P), 0.1 mM nicotinamide adenine diphosphate (NADP+), 0.1 U/mL glucose-6-phosphate dehydrogenase (G6PDH), 30 °C. Conversion to product was quantified by LC-MS analysis.

steps, demonstrating the ability of XenC to generate tropolones possessing non-native substitution patterns. The C5 aldehyde of stipitaldehyde (**3.11**) could also be replaced with a similar sized electron-withdrawing group, such as a methyl ketone (**3.39**) or nitro group (**3.42**), although with reduced conversion over two steps. However, larger ketones, such as *n*-propyl (**3.40**) or *n*-butyl (**3.41**) were not converted by XenC through this reaction sequence, suggesting a limitation in the size of substrates able to achieve productive binding in the XenC active site. Encouragingly, other large, bulky tropolones, such as phenyl tropolone **3.36** were produced, but with lower conversion compared to smaller tropolones, again suggesting a limitation of XenC to catalyze ring expansion of larger substrates. However, this limitation is overshadowed by the ability of XenC to generate tropolones with a broad array of functional handles which can be used to produce more complex tropolone structures from accessible precursors.

### 3.4 Preparative-scale oxidative dearomatization and ring expansion

In order to test the synthetic utility of this chemoenzymatic one-pot tropolone synthesis platform, we performed milligram-scale synthesis of several tropolones. One-pot reactions with TropB and XenC were performed in a sequenced fashion. The initial TropB dearomatization reaction was allowed to reach full conversion (typically 1-2 h) before the addition of XenC and the necessary cofactors ferrous sulfate, sodium ascorbate and α-KG. This sequenced approach resulted in improved conversion of material through the initial dearomatization reaction, which was notably less efficient with the addition of XenC cofactors when attempting reactions under cascade conditions. Following the addition of XenC, each reaction was incubated at 30 °C for 4 h and the conversion was monitored by LC-MS.

Initial efforts to isolate stipitaldehyde (**3.11**) from the crude product mixture were met with challenges related to the reactivity of the tropolone with proteinaceous materials, particularly as proteins were denatured in the presence of organic solvents used for liquid-liquid extraction of biocatalytic products. Following the denaturation of enzyme, the brown tropolone material could be visually identified as being located within the debris of denatured enzyme and initial yields of stipitaldehyde were correspondingly low (12% yield) despite high conversion through the reaction sequence (68% conversion). Based on these observations, we anticipated that the electrophilic aldehyde group of the natural product core could participate in condensation reactions with enzymatic lysine residues or free N-terminal amines, yielding an enzyme-tropolone complex. Challenges associated with handling tropolones have been similarly documented in the literature.[38] Trace metal contamination has led to isolation challenges due to the affinity of tropolones for divalent metal ions.[38, 42] In addition, tropolones are well-known inhibitors of numerous metalloenzymes, generating stable enzyme-tropolone complexes that have been characterized by X-ray crystallography.[19-20, 22, 57-58] Our attempts to extract this crude enzymatic material indicated that tropolone materials trapped within this complex could not be liberated in the presence of myriad solvent combinations, under basic or acidic conditions, or under aqueous high temperature (60-100 °C) conditions. To circumvent this issue, we evaluated possible extraction procedures involving *in situ* protection of the tropolone and remaining enzymatic materials in the crude biocatalytic mixture. Attempted acylation of the crude mixture using acetic anhydride in the presence of pyridine yielded monoacylated tropolones as detected by LC-MS. However, attempted isolation of acylated material through extraction under acidic conditions yielded only unprotected tropolone in slightly higher yields, indicating that the installed acyl group was labile. We then attempted an *in situ* methylation procedure using dimethylsulfate (20 equiv) at a pH of 10-11

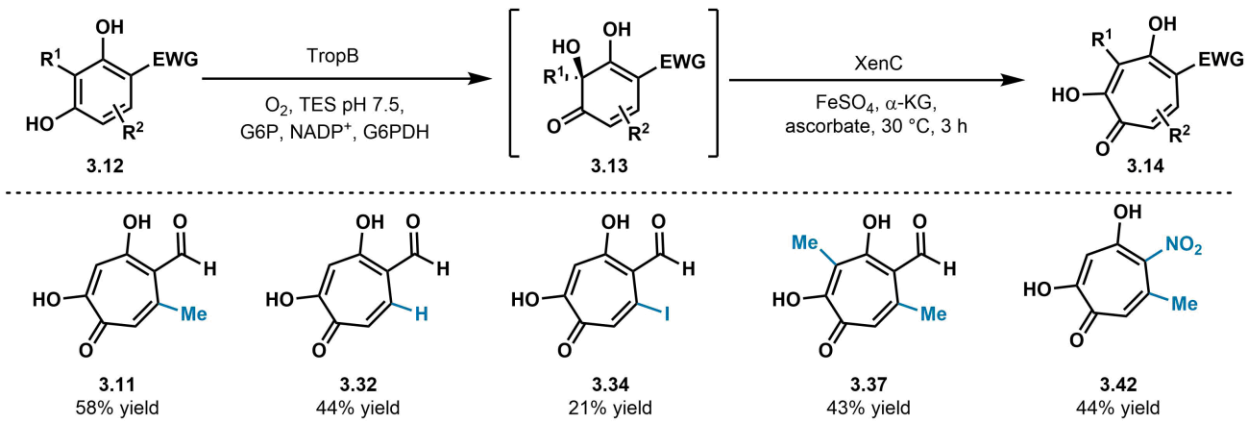


**Figure 3.5. Preparative-scale XenC-catalyzed ring expansion.**
Reaction conditions: 2.5 mM substrate, 10 μM TropC, 5 μM TropB, 50 mM TES pH 7.5, 5 mM α-ketoglutaric acid (α-KG), 4 mM sodium ascorbate, 0.2 mM ferrous sulfate ($FeSO_4$), 5 mM glucose-6-phosphate (G6P), 0.1 mM nicotinamide adenine diphosphate (NADP+), 0.1 U/mL glucose-6-phosphate dehydrogenase (G6PDH), 30 °C.

maintained by potassium carbonate (40 equiv). Full methylation of the tropolone mixture could be achieved under these conditions, yielding two methyl protected tautomers[38] of stipitaldehyde in 52% yield. We further desired to determine if this methylation procedure could be leveraged for isolation of unprotected tropolones by capping nucleophilic amines within the crude enzymatic material of the biocatalytic mixture. Analytical-scale isolation experiments demonstrated that methylation with only 4 mol % dimethylsulfate under basic conditions yielded unprotected stipitaldehyde (**3.11**) with a minor amount of protected stipitaldehyde, whereas controls without the addition of dimethylsulfate yielded no detectable stipitaldehyde (see Section 3.8 Experimental for details). This demonstrated that *in situ* methylation enabled isolation of unprotected stipitaldehyde and circumvented apparent reactivity between XenC and aldehyde-containing tropolone products.

Following the procedure for *in situ* methylation of the crude enzymatic materials, tropolones **3.11**, **3.32**, **3.34**, **3.37** and **3.42** were synthesized, isolated, and characterized using the one-pot TropB/XenC reaction (Figure 3.6). XenC native product stipitaldehyde (**3.11**) was

generated in moderate yield along with 3-methylated tropolone **3.11** and 6-desmethyl tropolone **3.32**. 5-nitro- (**3.42**) and 6-iodo-tropolone **3.34** was also generated in moderate yields, providing an additional functional handle for potential tropolone modification reactions.

### 3.5 Synthesis of (+/-)-18-deoxyepolone B

After demonstrating that rapid, preparative-scale biocatalytic synthesis of tropolones could be achieved using the XenC ring expansion reaction, we aimed to elaborate XenC products to more complex natural products, including **3.7**. The *ortho*-phenolic aldehyde moiety in stipitaldehyde (**3.11**) set the stage to access *ortho*-tropolinone methide (*o*-TM) species **3.6**. We envisioned that this reactive *o*-TM could be accessed by borohydride reduction of stipitaldehyde (**3.11**) to produce tropolonic alcohol **3.15**, a proposed biosynthetic precursor to form *o*-TM **3.6**. We also anticipated that heating alcohol **3.15** in the presence of α-humulene (**3.16**), would enable *in situ* formation of *o*-TM **3.6** and inverse electron demand Diels Alder (IEDDA) reaction with the C1-C2 double bond

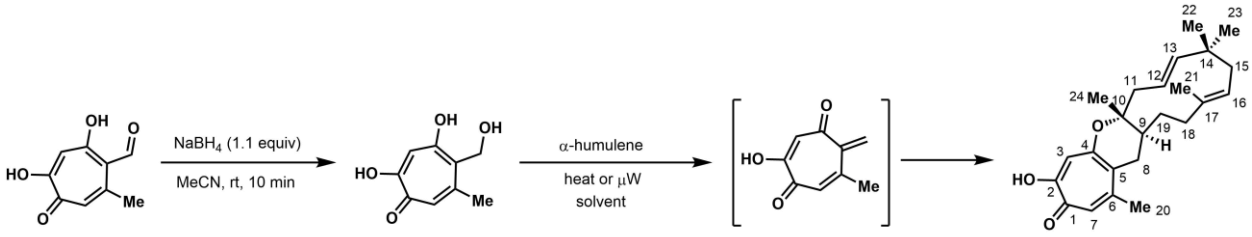


| Entry | Condition | Equiv of α-humulene | Conversion to 3.7 |
|---|---|---|---|
| **1** | 80 °C for 12 h (1:1 MeCN/$H_2O$) | 2.0 | 42% |
| **2** | 80 °C for 12 h (1:1 DMSO/benzene) | 2.0 | 84% |
| **3** | μW, 80 °C for 15 min (1:1 DMSO/benzene) | 2.0 | 92% |
| **4** | μW, 80 °C for 60 min (1:1 DMSO/benzene) | 2.0 | >99% |

**Table 3.2 Optimization of conditions for thermal IEDDA reaction between 3.15 and α-humulene (3.16).**

of the α-humulene macrocycle. This reaction would directly deliver the racemic form of 18-deoxyepolone B (**3.7**, Figure 3.7)

Initial experiments to generate stipitol (**3.15**) through sodium borohydride reduction of stipitaldehyde (**3.11**) were successful, yielding the *o*-TM precursor in an 84% yield on milligram scale (Figure 3.7). The tropolone was then used in analytical-scale IEDDA reactions with α-humulene. We subjected stipitol (**3.15**) to thermal IEDDA conditions (80 °C for 18 h) in a solvent mixture of acetonitrile and water (1:1). These conditions resulted in direct formation of a product matching the expected mass of 18-deoxyepolone B. However, conversion to the product was quite low, requiring additional optimization of reaction conditions. Table 3.2 describes the conditions screened in this optimization process, including the development of microwave conditions, which reduced reaction times significantly to around 1 h for complete substrate conversion. In addition, the use of DMSO and benzene (1:1) improved the solubility of α-humulene, improving the overall conversion under thermal conditions. These idealized conditions were applied to microwave reactions, generating 18-deoxyepolone B (**3.7**) with >99% conversion of the starting material observed in 1 h. Efforts are ongoing to isolate the product from preparative-scale reactions.

### 3.6 XenE-catalyzed synthesis of 18-deoxyepolone B

In addition to our efforts to thermally generate 18-deoxyepolone B, we sought to characterize the activity of putative Diels-Alderase XenE[51] in a [4+2] reaction between stipitol (**3.15**) and α-humulene (**3.16**) to produce 18-deoxyepolone B (Figure 3.8, **3.7**). Early efforts to achieve productive catalysis were challenging, as no previous *in vitro* activity was reported for this enzyme. We first evaluated the activity of XenE in performing a hetero-Diels-Alder reaction under near neutral pH conditions (pH = 7.2). Stipitol (**3.15**) was incubated with 0.4 mol % XenE in the

presence of 2 equiv α-humulene. MeCN (10 % v/v in water) was used in these reactions to improve solubility of α-humulene. However, under these initial reaction conditions, we did not observe substrate conversion. Screening pH conditions using a citrate-KPi buffer system, we observed a significant increase in conversion of starting material (95%) near pH 5.8 (Table 3.3). Under these conditions we observed the greatest percentage of substrate conversion to produce 18-deoxyepolone B, demonstrating that conditions for hetero-Diels-Alderase activity could be

optimized for product formation. Furthermore, the product generated by XenE in this reaction eluted at the same reaction time and with the same extracted ion mass as the product generated in thermal IEDDA reactions, suggesting that the hetero-Diels-Alderase-catalyzed reaction is likely

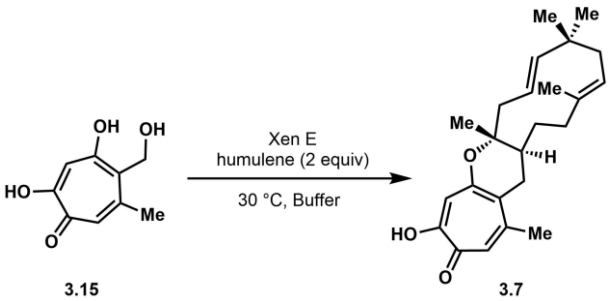


3.15 3.7

| Entry | Buffer (50 mM) | Reaction pH | Conversion to 3.7 |
|---|---|---|---|
| **1** | Citrate-KPi | 4.8 | 29% |
| **2** | Citrate-KPi | 5.0 | 72% |
| **3** | Citrate-KPi | 5.2 | 87% |
| **4** | Citrate-KPi | 5.4 | 87% |
| **5** | Citrate-KPi | 5.6 | 89% |
| **6** | Citrate-KPi | 5.8 | 95% |
| **7** | Citrate-KPi | 6.0 | 84% |
| **8** | Citrate-KPi | 6.2 | 82% |
| **9** | Citrate-KPi | 6.4 | 70% |
| **10** | TES-HCl | 6.6 | 62% |
| **11** | TES-HCl | 6.8 | 38% |
| **12** | TES-HCl | 7.0 | 0% |
| **13** | TES-HCl | 7.2 | 0% |

**Table 3.3 Optimization of reaction conditions for XenE-catalyzed hetero-Diels-Alderase reaction between 3.15 and α-humulene.**

producing an identical product. Efforts to generate this product on preparative-scale are ongoing. We anticipate that full characterization of this product will provide valuable information on the enantioselectivity of the hetero-Diels-Alderase reaction catalyzed by XenE. This route can potentially deliver the first enantioselective synthesis of 18-deoxyepolone B (**3.7**), illustrating the synthetic utility of this biocatalytic platform.

### 3.7 Conclusions

In this work, we have demonstrated the potential for NHI dioxygenases to synthesize tropolone natural product analogs through a two-enzyme oxidative dearomatization and ring expansion reaction sequence. We have applied this biocatalytic platform to the preparative-scale synthesis of a variety of tropolone natural product derivatives, demonstrating the synthetic potential of these transformations. Furthermore, we have leveraged the chemoenzymatic synthesis of the natural product stipitaldehyde (**3.11**) to construct 18-deoxyepolone B under thermal and enzymatic conditions. This represents the first successful demonstration of the activity of hetero-Diels-Alderase XenE *in vitro*, illustrating the potential to apply hetero-Diels-Alderases for the synthesis of natural products. We aim to further characterize the activity of XenE through preparative-scale reactions with stipitol (**3.15**), enabling characterization of the enantioselectivity of this reaction. In addition, our work provides a novel and direct route to the synthesis of tropolones, improving on existing synthetic methods by harnessing the potential of Nature's chemical toolbox to efficiently access bioactive molecules.

## 3.8 Experimental

### I. Substrate synthesis

**General Information:** All reagents were used as received unless otherwise noted. Reactions were carried out under a nitrogen atmosphere using standard Schlenk techniques unless otherwise noted. Solvents were degassed and dried over aluminum columns on an MBraun solvent system (Innovative Technology, inc., Model PS-00-3). Reactions were monitored by thin layer chromatography using Millipore 60 F254 pre-coated silica TLC plates (0.25 mm) which were visualized using UV, *p*-anisaldehyde, CAM, DNP, or bromocresol green stains. Flash column chromatography was performed using Machery-Nagel 60 μm (230-400 mesh) silica gel. All compounds purified by column chromatography were sufficiently pure for use in further experiments unless otherwise indicated. $^{1}H$ and $^{13}C$ NMR spectra were obtained in $CDCl_3$ at rt (25 °C), unless otherwise noted, on Varian 400 MHz or Varian 600 MHz spectrometers. Chemical shifts of $^{1}H$ NMR spectra were recorded in parts per million (ppm) on the δ scale. High resolution electrospray mass spectra were obtained on an Agilent 1290 Series Infinity II HPLC with a 6230 Series Time-of-Flight mass spectrometer or an Agilent 1290 Series Infinity HPLC with a 6545 Series Quadrupole-Time-of-Flight mass spectrometer. UPLC-PDA spectrometric traces were obtained on a Waters Aquity H-class instrument.

### Part II. Plasmid and protein information

**Plasmid:** The genes encoding *xenC* (listed as "L3" in *Sarcocladium strictum*, MG736817.1) and *xenE* (listed as "asR5" in *Sarcocladium strictum*, AOA2U8U2M1.1) were codon-optimized for overexpression in *E. coli* and synthesized by Twist Biosciences. The synthesized sequences were each cloned by Twist biosciences into a pET-28a vector containing the T7 expression system,

kanamycin resistance, and N-terminal 6xHis-tag encoded upstream from the insert gene. No further modifications to these plasmid constructs were necessary. Information regarding the *tropB* plasmid has been published by our group previously.[59]

**Codon-Optimized *xenC* Sequence (including 6 x His Tag)**

ATGGGCAGCAGCCATCATCATCATCATCACAGCAGCGGCCTGGTGCCGCGCGGCAGCCATATGG
CTAGCATGACTGGTGGACAGCAAATGGGTCGCGGATCCGAATTCATGGGCAGTTTGACCGACAA
TGCCGCGATTCCCACCGTGGATATCTCGGCGTTCTTAGATCCTAATGCCTCGCAGGAGGCACGT
CAGGACGTTGTGAATGCGATGTCGAATGCCTGCCACGTATATGGTTTTTTCAATCTGGCGGGTC
ATGGCATTCCACAAGAGACCTTGCGCGAAGCATTCGAACTTAATAAGATGTTTTTCGCCTTGCC
AGAGGAATCAAAAAAAGAAGTGTTGATTAGTAAGTCAATCGGACAATCATTCCGTGGTTACGAG
CCGCCCGGCATCCAGACACATCACAAGGGCCTTCTTCCCGATATTAAAGAGACGTTCATGGTCG
GGCGTGAAGTACCGCTTGACGACCCTGATTGTGGCACATTCTCAACGGGTCCCAACCTTTGGCC
CTCATCTTTACCGAAAGAGAAATTTCAGGACCGCATCATGGCTTACCAGGGTAGCATGTTAGAA
CTTGTAAAGAATATTCTTGCTATTTTGGCACAAGGGCTGCCAAAGGAATGGGGATGCTCACCGA
CCGTTTTCAACTCTTTATTGGATAAGCCGAGTATTCCAATGCGTTTCTTACACTACGCCCCCGT
CCCCTCACAACTTGAAGATGTACGCCAGTTTGGGGTAGCTGACCACACTGACTTTGGTTGTGTA
AGTATTTTGTTGCAGGAGCCCGGAACTTCGGGCTTAGAGGTCTACTATCCCCCGTCGGACTCGT
GGATTCCTGTCCCAGTTATCGACGATGGATTCGTGATCAACATGGGTGATATGATGCAACGTTA
CACCGGGGGATATTACCGCTCAGCTCGCCATCGCGTCCTTACAAACCGCGAGAAACATCGTCAC
AGTGTGGCGTTTTTTCTGAATGGGAACTTGGGATTAAAGGCGAAGGCTTTAGATGGCAGCGAAA
CGGAGACAGTAGTTGGAGATTGGATTCGCGGGCGTCTGATTGACACTATGGGACAGACGGGGAA
GTTATTGCAGCGTGAGAGTCCGAAACCGGTAGTACTGCCG

**XenC Protein Sequence (including 6 x His Tag)**

MGSSHHHHHHSSGLVPRGSHMASMTGGQQMGRGSEFMGSLTDNAAIPTVDISAFLDPNASQEAR
QDVVNAMSNACHVYGFFNLAGHGIPQETLREAFELNKMFFALPEESKKEVLISKSIGQSFRGYE
PPGIQTHHKGLLPDIKETFMVGREVPLDDPDCGTFSTGPNLWPSSLPKEKFQDRIMAYQGSMLE
LVKNILAILAQGLPKEWGCSPTVFNSLLDKPSIPMRFLHYAPVPSQLEDVRQFGVADHTDFGCV
SILLQEPGTSGLEVYYPPSDSWIPVPVIDDGFVINMGDMMQRYTGGYYRSARHRVLTNREKHRH
SVAFFLNGNLGLKAKALDGSETETVVGDWIRGRLIDTMGQTGKLLQRESPKPVVLP

**Codon-optimized *tropC* homolog sequence (*P. freii*) (including 6 x His Tag)**

ATGGGCAGCAGCCATCATCATCATCATCACAGCAGCGGCCTGGTGCCGCGCGGCAGCCATATGG
CTAGCATGACTGGTGGACAGCAAATGGGTCGCGGATCCGAATTCATGACTATCAGCGCGGAGAC
TATTCCAACAGTTGATTTGTCCCCCTGGCTTAACCCCGATGCGAGTGAAGAGGCAAAGGATGCA
GTCGTAAAAGCCGTATCCCATGCGTGCAGCACCTACGGCTTCTTCAATCTTGTCGGCCACGGGA
TCCCAGTGGAGGCTCAAAATAAAATCTTTGAGTGTAGCAAGGAGTTTTTTGACTTGCCATTGAA
CGAGAAGATGAAAGTTTCTGTCGATAAATCATTGGGAAAGAGCTTTCGCGGGTATGAACCCAGT
CGTATCCAGACCCATCAGGAAGGGCTTTTGCCGGATACAAAGGAATGTTTCATCACCGGGGCAG
AAACCCCCGCCGATCACCCGGACGCAGGTAAATTCAGTACGGGCCCTAACTTATGGCCTGGTAC

CCTTCCAGATGAGAACTTCCGTCAGCCAGTGATGGAGTATCGTGCGCGTATGTTGGACCTGGTT
GGCATCCTGATTAAGATTCTGGGTCAGGGTTTACCTAAAGCGTGGGGGTATTCGCCTGACGTTC

TTAACGATATCCTTATCAACCCATCGATTCCTATGCGTCTTCTTCATTACGCTCCCGAGACAAA
CATCGACCCACGCCAGTTCGGAGTAGGCGACCACACCGATTTCGGCTGTGTCTCAATCTTGCTT
CAGCAAGCGAACACGAAGGGATTAGAAGTTTGGTATCCATTAACGAAAACGTGGATTCCCGTCC
CCGTAGTCGAGAATGCTTTTGTGATTAACATGGGCGATACGATGCATCGCTGGACGGGGGGTCA
CTATCGTTCTGCACGTCACCGCGTTCTGATTTCTGGTAACCGCCGCTACTCTGTCGCATTTTTT
CTTAACGGCAACCTTAATTTGAAAATTAAACCGCTGGATGGTAGCGGGGAGGAAGCCTCTGTCG
GTGAACATATCAACTTACGTTTGGCCCACACCCTGGGT

**TropC homolog (*P. freii*) Protein Sequence (including 6 x His Tag)**

MGSSHHHHHHSSGLVPRGSHMASMTGGQQMGRGSEFMTISAETIPTVDLSPWLNPDASEEAKDA
VVKAVSHACSTYGFFNLVGHGIPVEAQNKIFECSKEFFDLPLNEKMKVSVDKSLGKSFRGYEPS
RIQTHQEGLLPDTKECFITGAETPADHPDAGKFSTGPNLWPGTLPDENFRQPVMEYRARMLDLV
GILIKILGQGLPKAWGYSPDVLNDILINPSIPMRLLHYAPETNIDPRQFGVGDHTDFGCVSILL
QQANTKGLEVWYPLTKTWIPVPVVENAFVINMGDTMHRWTGGHYRSARHRVLISGNRRYSVAFF
LNGNLNLKIKPLDGSGEEASVGEHINLRLAHTLG

**Codon-optimized *tropC* homolog sequence (*Hypoxylon sp.*) (including 6 x His Tag)**

ATGGGCAGCAGCCATCATCATCATCATCACAGCAGCGGCCTGGTGCCGCGCGGCAGCCATATGG
CTAGCATGACTGGTGGACAGCAAATGGGTCGCGGATCCGAATTCATGGGAAGTATCGAAAAGAT
TCCGGAAACAGCCCCGGATGCTATCCCTACTGTTGACATCTCTCCATTTACAGACCCGAATGCC
AGTGAAGAGGCAAAAAACGCTGTAGTGGATGCCGTCCGTCATGCGTGTACAACATATGGCTTCT
TTTACCTGGCTGGCCACGGAGTGTCTGCGGAACAGCGTGAAGGCATTTTGAACTGTGCGAAAAA
ATTTTTTGAACTGCCGCAGGAGGAACGTATGGACGTCTGGATTGGAAAGAGCATGGGCAAGTCA
TTTCGCGGTTATGAACCCCCAGGCATCCAGACCCACCAGAAAGGCCTTCTTCCTGATATTAAGG
AATGCTTCATTATTGGGCATGAAGTGCCGGCGGATGACCCGGAAGCAGGGACCTTTTCGACCGG
CCCCAATTTGTGGCCGAAGAATCTGAAAGACGAGGAGTTTCGTACACCGATCATGGATTATCAA
GCTACAATGTTAGCCCTGTCGAAAGTTCTTCTGAAGATTTTGGCTCGCGGGCTTCCCAAAGCGT
GGGGTCATCCCCCCAACGTCATGGATGAATTTGCTGTTAATCCATCTATGCCAATGCGTCTTCT
GCACTATGCCCCGCAGGAGGTCCTGGATGAACGTCAATTCGGTGTTGGAGATCACACTGATTTT
GGAGGCATCGCAATCTTATTGCAGGAAATGAATACCAAGGGACTTGAAGTATGGTACCCCCCGA
CAGAGACATGGATTCCGGTTCCGCCGAAGGAGAACACATATGTTATCAACATGGGAGACATGAT
GCAAAAATGGACCGCTGGTTATTACCGTTCCGCCCGCCACCGCGTCATCACTAGCGGTACCAAC
CACCGTTACTCCGTCCCATGGTTTTTGAATGGCCAGTTGAAATTGAAATGTCAGAGCCTTGACG
GCTCCGGGGTAGAAACCATTGTAGGCGAGCACATCCGCCAACGTCTTATTGCGACAATGCCGGA
GGCTGGTAAGGCCTTACGC

**TropC homolog (*Hypoxylon sp.*) Protein Sequence (including 6 x His Tag)**

MGSSHHHHHHSSGLVPRGSHMASMTGGQQMGRGSEFMGSIEKIPETAPDAIPTVDISPFTDPNA
SEEAKNAVVDAVRHACTTYGFFYLAGHGVSAEQREGILNCAKKFFELPQEERMDVWIGKSMGKS
FRGYEPPGIQTHQKGLLPDIKECFIIGHEVPADDPEAGTFSTGPNLWPKNLKDEEFRTPIMDYQ
ATMLALSKVLLKILARGLPKAWGHPPNVMDEFAVNPSMPMRLLHYAPQEVLDERQFGVGDHTDF

GGIAILLQEMNTKGLEVWYPPTETWIPVPPKENTYVINMGDMMQKWTAGYYRSARHRVITSGTN
HRYSVPWFLNGQLKLKCQSLDGSGVETIVGEHIRQRLIATMPEAGKALR

**Codon-optimized *xenE* sequence (including 6 x His Tag)**

ATGGGCAGCAGCCATCATCATCATCATCACAGCAGCGGCCTGGTGCCGCGCGGCAGCCATATGG
CTAGCATGACTGGTGGACAGCAAATGGGTCGCGGATCCGAATTCATGCGCCGCTCCTTCTTAAT
AAGTGCGGCATTAGGGTTGTCCATGTCAACCCCTGCCCTTGCCGCCTCAATCCAGTCTGTCTTA
GGGTACCTGCGCCCGACGTCGCACCACCATGCCCCTTGCGCTGACGATGTTGTTTTGAAACAGT
CTGCCGGGTCAGACTCCGCCGCTCCCGACCCTCTTCCTTCCAGAGTTGTTCACAACTGGCCAAA
CGGGACGTGGATAGAGAACATTTCTGTTCGCCCAAATGGCAACTTACTGGTCAGCCAATCCACG
CCACGTGGACGCGTTTGGCAGGTAAAGGAGCCGTGGTTGGATGAGCCTAAGGTGGAGTTGGCGT
ATGATTTTGATGAATGGGTAGATAGAATAATTGGGATAGGTGAGACCACACCTGACAAGTATGT
CGTGGTGGGGTCCCGTTTTTACTCCCTTGATCCCCAGTCTTCGCAAGTGGAGCGGACCTTCTGC
GCAATGGAGCTGGATTTTACCAAAGGGGAGAAACCTTCGGCTCGGCTGGTCGCTCGGTTTCCTC
ATGCAAACCTTTTGCAAAGTGTTAGTGCACTTCCTTGGGATCGCAGCGTCGTTTTAATCTCTGA
CCAGTACTTGTTACATCCCCGTGCCGACTGGGAAGATTTGACGCCCGGCCCTGGTCAAATCTGG
AGATTAGACACGAAGACAGGTCACCACGAAATTGTTATGACCAACTACGCCGAGATGAACACCA
CCTATAATCACGGCTTAGATGTTGGGATTAACGGGATCAAAATCCACGGAGATCATCTGTATTG
GATCAATATGGATACGGGGGGAGCTTATAGAGTCCGTATAGATAAGTATGGCTACCCCACTCCG
TTGAATGCAGTACCCGAAACGTTGGGCGTGGCGGAGGATGCTTTGTGGGACGACTTTGCCATGC
ATGGTACCCGTATCGGCGAAGAAAGCGACGATACTACGATGTTTGCTACTTCCATCGTAAACTT
GATGGCAATCTCTCCTGAGAACGGCACCATCGTTCCGTTGGCAGGTGTAGGAACGTCCGAACCT
ATGGGTTTTCCAGGCCCCACTTCTGCTCAATTCGGTCGCACTGAAAAGGATAGCCATATACTTT
ATGTAACAGGGAAATTGTTCAACGTGCCCCCGTCAATCCGGGACGTGGTCATACAGGGGTGGGT
GAGAGCGATAGACACTACCGGGTTTCACTTTTAAATGCGCCGCTCCTTCTTAATAAGTGCGGCA
TTAGGGTTGTCCATGTCAACCCCTGCCCTTGCCGCCTCAATCCAGTCTGTCTTAGGGTACCTGC
GCCCGACGTCGCACCACCATGCCCCTTGCGCTGACGATGTTGTTTTGAAACAGTCTGCCGGGTC
AGACTCCGCCGCTCCCGACCCTCTTCCTTCCAGAGTTGTTCACAACTGGCCAAACGGGACGTGG
ATAGAGAACATTTCTGTTCGCCCAAATGGCAACTTACTGGTCAGCCAATCCACGCCACGTGGAC
GCGTTTGGCAGGTAAAGGAGCCGTGGTTGGATGAGCCTAAGGTGGAGTTGGCGTATGATTTTGA
TGAATGGGTAGATAGAATAATTGGGATAGGTGAGACCACACCTGACAAGTATGTCGTGGTGGGG
TCCCGTTTTTACTCCCTTGATCCCCAGTCTTCGCAAGTGGAGCGGACCTTCTGCGCAATGGAGC
TGGATTTTACCAAAGGGGAGAAACCTTCGGCTCGGCTGGTCGCTCGGTTTCCTCATGCAAACCT
TTTGCAAAGTGTTAGTGCACTTCCTTGGGATCGCAGCGTCGTTTTAATCTCTGACCAGTACTTG
TTACATCCCCGTGCCGACTGGGAAGATTTGACGCCCGGCCCTGGTCAAATCTGGAGATTAGACA
CGAAGACAGGTCACCACGAAATTGTTATGACCAACTACGCCGAGATGAACACCACCTATAATCA
CGGCTTAGATGTTGGGATTAACGGGATCAAAATCCACGGAGATCATCTGTATTGGATCAATATG
GATACGGGGGGAGCTTATAGAGTCCGTATAGATAAGTATGGCTACCCCACTCCGTTGAATGCAG
TACCCGAAACGTTGGGCGTGGCGGAGGATGCTTTGTGGGACGACTTTGCCATGCATGGTACCCG
TATCGGCGAAGAAAGCGACGATACTACGATGTTTGCTACTTCCATCGTAAACTTGATGGCAATC
TCTCCTGAGAACGGCACCATCGTTCCGTTGGCAGGTGTAGGAACGTCCGAACCTATGGGTTTTC
CAGGCCCCACTTCTGCTCAATTCGGTCGCACTGAAAAGGATAGCCATATACTTTATGTAACAGG
GAAATTGTTCAACGTGCCCCCGTCAATCCGGGACGTGGTCATACAGGGGTGGGTGAGAGCGATA
GACACTACCGGGTTTCACTTTTAA

**XenE Protein Sequence (including 6 x His Tag)**

MGSSHHHHHHSSGLVPRGSHMASMTGGQQMGRGSEFMRRSFLISAALGLSMSTPALAASIQSVL
GYLRPTSHHHAPCADDVVLKQSAGSDSAAPDPLPSRVVHNWPNGTWIENISVRPNGNLLVSQST
PRGRVWQVKEPWLDEPKVELAYDFDEWVDRIIGIGETTPDKYVVVGSRFYSLDPQSSQVERTFC
AMELDFTKGEKPSARLVARFPHANLLQSVSALPWDRSVVLISDQYLLHPRADWEDLTPGPGQIW
RLDTKTGHHEIVMTNYAEMNTTYNHGLDVGINGIKIHGDHLYWINMDTGGAYRVRIDKYGYPTP
LNAVPETLGVAEDALWDDFAMHGTRIGEESDDTTMFATSIVNLMAISPENGTIVPLAGVGTSEP
MGFPGPTSAQFGRTEKDSHILYVTGKLFNVPPSIRDVVIQGWVRAIDTTGFHF

**Protein Overexpression and Purification:** The plasmid containing *xenC* was transformed using standard heat-shock protocols for chemically competent *E. coli* into BL21(DE3) cells. The plasmid containing XenE was transformed into LEMO(DE3) cells. Overexpression of *xenC* and *xenE* was achieved using 4% glycerol (v/v) Terrific Broth (TB) in 2.8 L flasks. 500 mL portions of autoclaved media were inoculated with 5 mL of overnight culture prepared from a single colony in Luria Broth (LB) and 100 μg/mL kanamycin (Gold Biotechnology). Cultures were grown at 37 °C and 200 rpm until the optical density (at 600 nm) reached 0.8. The cultures were then cooled to 20 °C for 20 min for *xenC* expression (16 °C for *xenE* expression) and protein expression was induced with 0.2 mM isopropyl-β-D-1-thiogalactopyranoside (IPTG, Gold Biotechnology). Expression was continued at 20 °C overnight for *xenC* and 16 °C overnight for *xenE* (approx. 18 h) at 200 rpm. The typical yield for one 500 mL culture cell pellet (wet cell pellet) was ~25 g.

**General Purification Procedure:** 50-60 g of cell pellet was resuspended in 250 mL of lysis buffer containing 50 mM Tris HCl (pH 7.4 for XenC, pH 8.0 for XenE), 300 mM NaCl, 10 mM imidazole and 10% glycerol. The mixture was homogenized using a handheld dounce homogenizer. Approximately 1 mg/mL lysozyme (Gold Biotechnology) was added prior to 1 h incubation on a rocker held at 4 °C. Cells were lysed by sonication of the total cell lysate in 100 mL batches on ice. Each cycle of sonication was 10 s sonication, followed by a 20 s rest period, for a total of 6

min at 60% power. The total cell lysate was centrifuged at 45,000 x g for 30 min and the supernatant was removed. The cell lysate was then batch-bound to 3 mL of Ni-NTA resin (Thermo) for 1 h at 4 °C with gentle rocking. The supernatant was filtered through a fritted 50 mL plastic column (Gold Biotechnologies) to isolate the Ni-NTA resin. The resin was washed with 100 mL of wash buffer containing 50 mM Tris HCl (pH 7.4 for XenC, pH 8.0 for XenE), 300 mM NaCl, 25 mM imidazole and 10% glycerol. The protein was then eluted using 15 mL of an elution buffer containing 50 mM Tris HCl (pH 7.4 for XenC, pH 8.0 for XenE), 300 mM NaCl, 250 mM imidazole and 10% glycerol. The eluted protein was concentrated to a volume of 2.5 mL using a 30 KDa molecular weight cutoff ultrafiltration device (Amicon). The concentrated protein was desalted using a PD-10 desalting column that was pre-equilibrated with a storage buffer containing 50 mM Tris HCl (pH 7.4 for XenC, pH 8.0 for XenE), 300 mM NaCl, and 10% glycerol. The protein was eluted from the column with 3.5 mL of storage buffer, before flash freezing in liquid nitrogen and storage at -80 °C. Protein concentration was determined by the A280 absorbance method using a Nanodrop spectrophotometer. The concentration was corrected using the estimated extinction coefficient from the ProtParam tool on the Expasy server. **Average yield:** 80-100 mg/L of XenC. 20-30 mg/L of XenE. Flavin-dependent monooxygenase TropB was expressed and purified using the construct and conditions reported previously and is found within the supplementary information of the cited reference.[59]

**Figure 3.S1.** SDS-PAGE gel of purified TropC

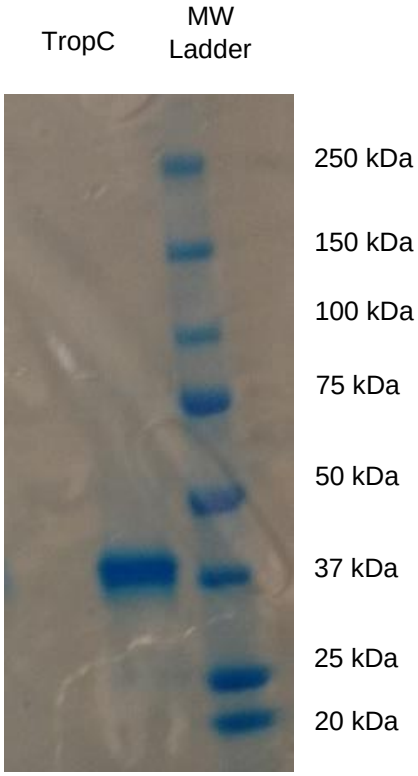


**Figure 3.S2.** SDS-PAGE gel of purified TropC homologs

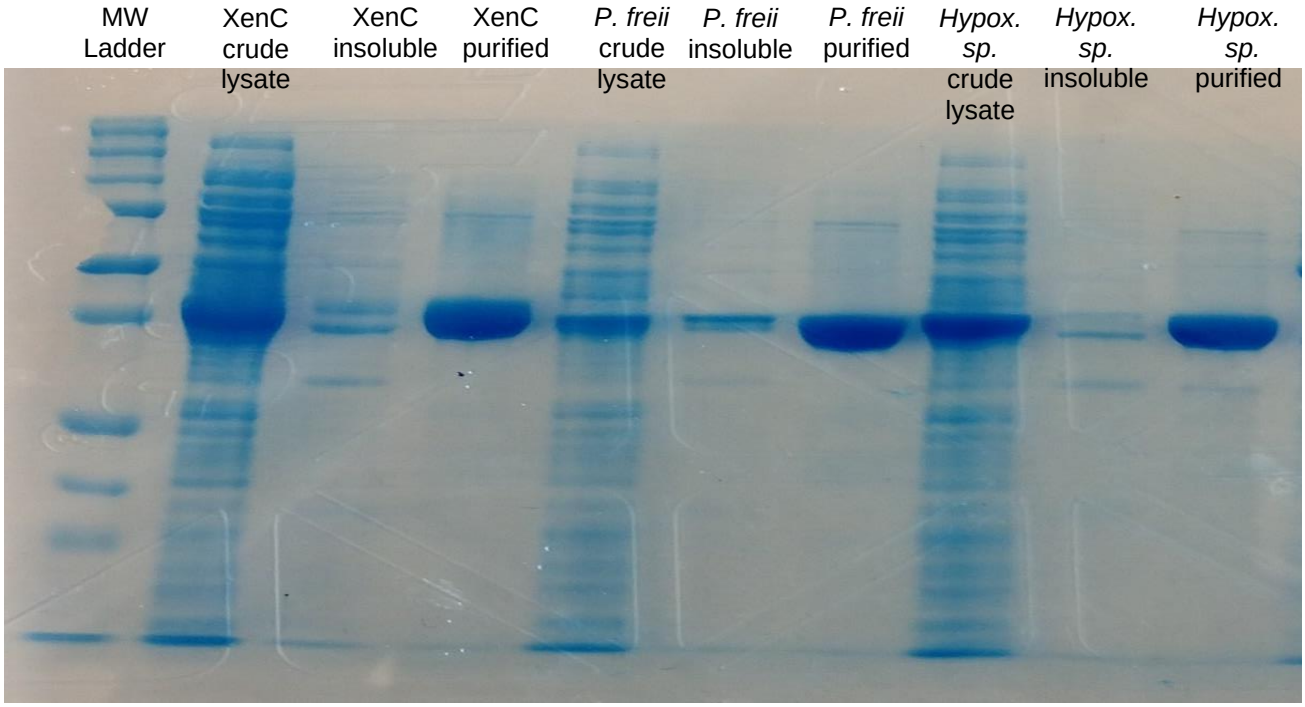

**Part III. Biocatalytic reactions and products**

**Stock solutions:** Stock solutions of each substrate (50 mM) were prepared by dissolving the substrate in DMSO (analytical grade). Stock solutions of α-ketoglutaric acid (125 mM), ferrous sulfate (10 mM) and sodium ascorbate (50 mM) were freshly prepared in MQ water before each use, stored on ice, and used within 3 h. Aliquots of glucose-6-phosphate (G6P, 500 mM), glucose-6-phosphate dehydrogenase (G6PDH, 100 U/mL), and nicotinamide adenine dinucleotide (NADP+, 100 mM) were prepared and stored at -20 °C before use. Aliquots of XenC were stored at -80 °C.

***In vitro*** **analytical-scale cascade ring expansion reactions:** Cascade oxidative dearomatization/ring expansion reactions were performed as follows. Each reaction contained 50 mM TES buffer pH 7.5 (2.5 μL, 1 M), 2.0 mM substrate (2.0 μL, 50 mM in MeOH), 5 μM TropB (4 μL, 124 μM), 10 μM XenC (or homolog), 5 mM G6P (0.5 μL, 500 mM), 1 mM NADP+ (0.5 μL, 100 mM), 5 mM α-ketoglutaric acid (2 μL, 125 mM), 0.1 mM ferrous sulfate (0.5 μL, 10 mM), 4 mM sodium ascorbate (4 μL, 50 mM) and Milli-Q water to a final volume of 50 μL. Reactions were carried out at 30 °C for 3 h and quenched by the addition of 3 volumes of methanol containing 600 μM 2,6-dimethoxytoluene as an internal standard. Precipitated biomolecules were pelleted by centrifugation (17,000 x g, 20 min). The supernatant was analyzed by LC-TOF MS and conversion obtained by comparison to calibration curves of each substrate.

***In vitro*** **analytical-scale XenE-catalyzed Diels-Alder reactions:** XenE-catalyzed Diels-Alder reactions were performed as follows. Each reaction contained 50 mM TES buffer pH 6.8 (2.5 μL, 1M), 2 mM stipitol (2.0 μL, 50 mM in MeOH), 4 mM α-humulene (4.0 μL, 50 mM in MeOH), Reactions were carried out at 30 °C for 18 h and quenched by the addition of 3 volumes of

methanol containing 600 μM 2,6-dimethoxytoluene as an internal standard. Precipitated biomolecules were pelleted by centrifugation (17,000 x g, 20 min). The supernatant was analyzed by LC-TOF MS and conversion obtained by comparison to calibration curves of each substrate.

**Determination of percent conversion:** Percent conversion was determined by analysis of each reaction after 3 h. LC/MS spectrometric analysis was performed on an Agilent 1290 Series Infinity II HPLC with a 6230 Series Time-of-Flight (TOF) mass spectrometer, using a Phenomenex Kinetex (1.7 μm C18, 2.1 x 150 mm) column under the following conditions: mobile phase (Solvent A: deionized water + 0.1% formic acid; Solvent B: acetonitrile + 0.1% formic acid) 5% to 100% solvent B over 2 min, 100% solvent B for 2 min; flow rate: 0.4 mL/min. Based on the calibration curves of the starting materials, the percent conversion of the substrate to tropolone product was calculated with $AUC_{substrate}/AUC_{internal\ standard}$. *In vitro* reactions were performed and analyzed in triplicate with reported conversions as an average of those trials.

**General procedure for *in vitro* milligram-scale reactions:** Except where otherwise noted, preparative-scale enzymatic reactions were conducted on 20-100 mg of each substrate under the following conditions: 2.5 mM substrate, 50 mM TES buffer pH 7.5, 5 mM α-ketoglutaric acid, 0.1 mM ferrous sulfate, 8 mM sodium ascorbate, and 10 μM XenC. Reactions were performed in Erlenmeyer flasks of appropriate volume to achieve proper oxygenation (at least 3 times reaction volume) at 30 °C. Reaction progress was monitored at hourly intervals by analysis of a 50 μL

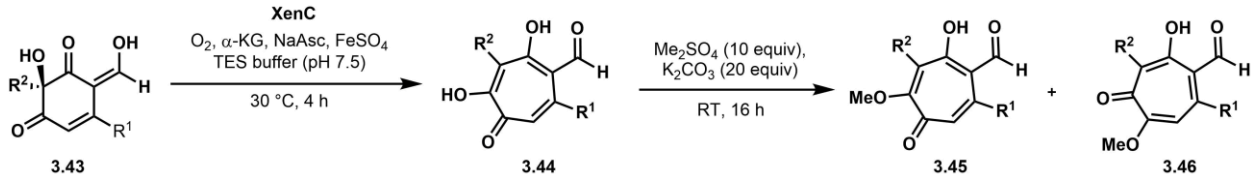


**Figure 3.S3. *In situ* methylation of XenC-generated products.**

aliquot by LC-TOF MS. The aliquot was processed in the manner described for *in vitro* analytical scale determination of reaction conversion.

***In situ* methylation procedure:** Products of enzymatic reactions were isolated following methylation of the tropolone vinylogous acid moiety to improve yields and ensure compound stability. Following completion of the milligram-scale enzymatic ring expansion reaction, the pH of the crude reaction mixture was increased to >10 by the addition of $K_2CO_3$ while the mixture was stirred at room temperature. 20 equiv of dimethylsulfate was added via syringe and the crude mixture was stirred for 16 h. The pH of the reaction was routinely monitored and more $K_2CO_3$ was added when necessary to maintain a pH greater than 9-10. Reaction conversion was monitored by LC-TOF MS. An identical procedure was used isolate unmethylated tropolones (by capping nucleophilic residues in XenC following the reaction), except that 0.4 equiv of dimethylsulfate was used. The methylation was allowed to proceed for 2 h before workup and isolation (see isolation procedure).

**Isolation procedure:** Following *in situ* methylation, the reaction mixture was acidified to pH 2.0 with 0.1 M HCl. The organic materials were extracted from the aqueous layer with ethyl acetate (3 x 50 mL). The organic fractions were pooled and concentrated under reduced pressure to yield a crude mixture. Products were purified from this crude mixture by preparative HPLC.

**Purification by preparative HPLC:** For purification of milligram-scale reactions, the resulting crude mixture was taken up in a 50:50 mixture of milli-Q water:acetonitrile (2 mL). The product(s) were purified from this mixture by preparative HPLC using a Phenomenex Kinetex 5 μm C18, 150 x 21.2 mm column under the following conditions: mobile phase (Solvent A: deionized water +

0.1% formic acid; Solvent B: acetonitrile + 0.1% formic acid) 5% to 100% solvent B over 13 min, 100% solvent B for 4 min; flow rate: 11.5 mL/min.

**Products of biocatalytic ring expansion**

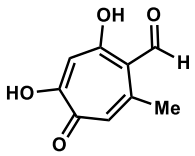


3.11

**2,4-dihydroxy-7-methyl-5-oxocyclohepta-1,3,6-triene-1-carbaldehyde (stipitaldehyde) (3.11)**

The title compound was synthesized according to the general procedure for milligram-scale enzymatic ring expansion with XenC. The reaction was performed with 100 mg of starting material. Purification by preparative HPLC afforded 57 mg (58% yield) of the title compound as an orange solid. **$^{1}$H NMR** (400 MHz, MeOD) δ 10.12 (s, 1H), 6.83 (s, 1H), 6.81 (s, 1H), 2.65 (s, 3H); **$^{13}$C NMR** (150 MHz, MeOD) δ 196.67, 177.19, 175.40, 165.67, 150.70, 125.04, 115.01, 110.49, 24.87; **HR-ESI-MS**: m/z calcd for $C_9H_8O_4^+$ $[M+H]^+$: 181.0495, found: 181.0497.

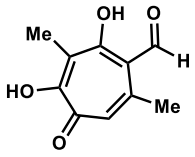


3.37

**2,4-dihydroxy-3,7-dimethyl-5-oxocyclohepta-1,3,6-triene-1-carbaldehyde (3.37)**

The title compound was synthesized according to the general procedure for milligram-scale enzymatic ring expansion with XenC. The reaction was performed with 20 mg of starting material. Purification by preparative HPLC afforded 8 mg (43% yield) of the title compound as a tan solid. **$^{1}$H NMR** (400 MHz, MeOD) 10.12 (s, 1H), 6.85 (s, 1H), 2.64 (s, 3H), 2.33 (s, 3H); **$^{13}$C NMR** (150 MHz, MeOD) δ 197.19, 161.39, 150.18, 141.63, 124.10, 109.59, 105.56, 24.66, 11.23; **HR-ESI-MS**: m/z calcd for $C_9H_8O_4^+$ $[M+H]^+$: 195.0652, found: 195.0657.

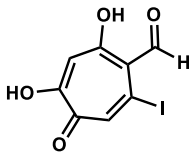


3.34

**2,4-dihydroxy-7-iodo-5-oxocyclohepta-1,3,6-triene-1-carbaldehyde (3.34)**

The title compound was synthesized according to the general procedure for milligram-scale enzymatic ring expansion with XenC. The reaction was performed with 20 mg of starting material. Purification by preparative HPLC afforded 4 mg (20% yield) of the title compound as a yellow solid. **$^{1}$H NMR** (400 MHz, MeOD) δ 10.31 (s, 1H), 7.10 (s, 1H), 6.84 (s, 1H); **HR-ESI-MS**: m/z calcd for $C_9H_8O_4^+$ $[M+H]^+$: 292.9305, found: 292.9309.

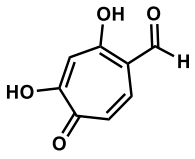


3.32

**2,4-dihydroxy-5-oxocyclohepta-1,3,6-triene-1-carbaldehyde (3.32)**

The title compound was synthesized according to the general procedure for milligram-scale enzymatic ring expansion with XenC. The reaction was performed with 20 mg of starting material. Purification by preparative HPLC afforded 8.7 mg (44% yield) of the title compound as a yellow solid. **$^{1}$H NMR** (400 MHz, MeOD) δ 9.80 (s, 1H), 7.21 (d, $J_{HH}$ = 8.0, 1H), 6.97 (s, 1H), 6.89 (d, $J_{HH}$ = 8.0, 1H); **$^{13}$C NMR** (150 MHz, MeOD) δ 196.72, 142.13, 135.51, 114.40, 113.43, 110.27, 110.25, 100.59; **HR-ESI-MS**: m/z calcd for $C_9H_8O_4^+$ $[M+H]^+$: 167.0339, found: 167.0348.

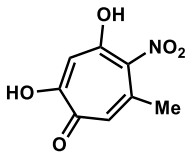


3.42

**2,4-dihydroxy-6-methyl-5-nitrocyclohepta-2,4,6-trien-1-one (3.42)**

The title compound was synthesized according to the general procedure for milligram-scale enzymatic ring expansion with XenC. The reaction was performed with 20 mg of starting material. Purification by preparative HPLC afforded 8.5 mg (44% yield) of the title compound as a yellow solid. **$^{1}$H NMR** (400 MHz, MeOD) δ 6.90 (s, 1H), 6.89 (s, 1H), 2.30 (s, 3H); **$^{13}$C NMR** (150 MHz, MeOD); **HR-ESI-MS**: m/z calcd for $C_9H_8O_4^+$ $[M+H]^+$: 198.0397, found: 198.0394.

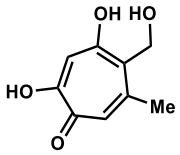


3.15

**2,4-dihydroxy-5-(hydroxymethyl)-6-methylcyclohepta-2,4,6-trien-1-one (stipitol) (3.15)**

The title compound was synthesized by sodium borohydride reduction of stipitaldehyde (**3.11**). 10 mg (0.06 mmol) of stipitaldehyde was suspended in 1 mL total volume of MeCN and water (1:1) in a 20 mL scintillation vial with a stir bar. 1.1 equiv of sodium borohydride (122 μL of a 500 mM solution in water) was added at rt and allowed to stir for 10 min. The resulting solution was directly injected on preparative HPLC to afforded 8.5 mg (84% yield) of the title compound as a light yellow residue. **$^{1}$H NMR** (400 MHz, $CD_3CN$) δ 8.10 (s, 1H), 7.03 (s, 1H), 6.89 (s, 1H), 4.63 (s, 2H), 2.48 (s, 3H); **HR-ESI-MS**: m/z calcd for $C_9H_8O_4^+$ $[M+H]^+$: 181.0495, found: 181.0497.

## Part IV. Substrate and product standard curves

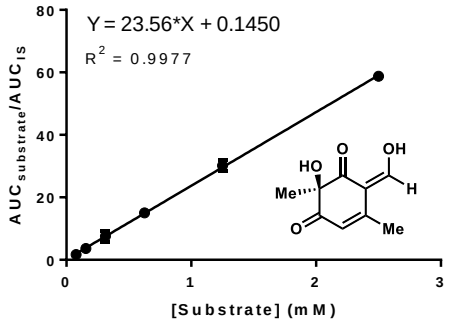


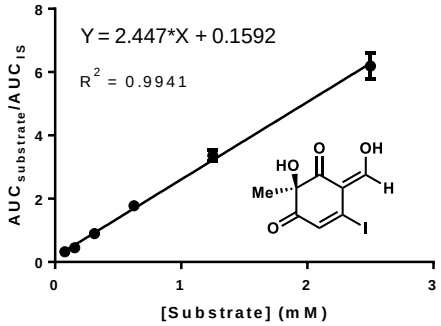


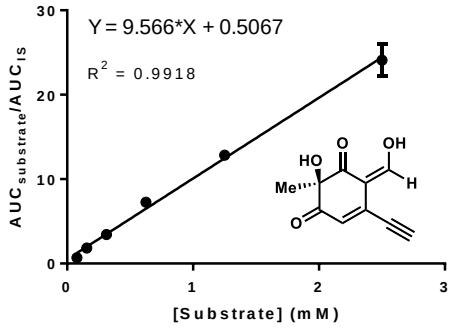


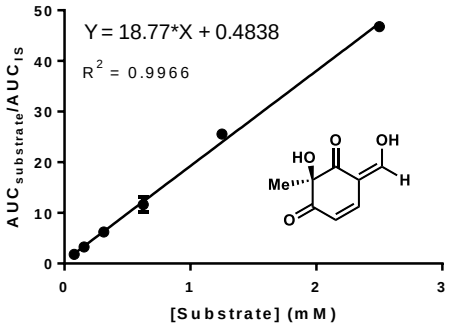


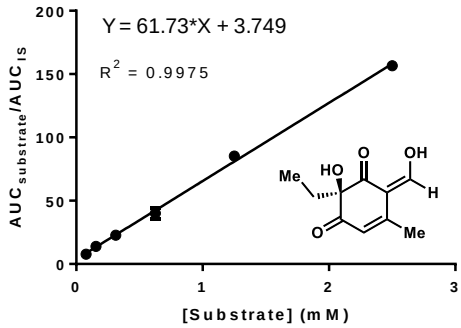


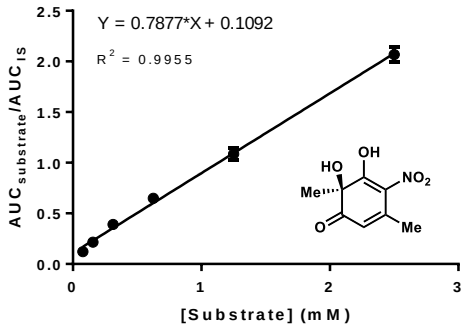

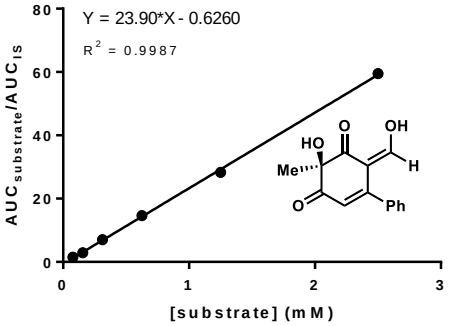
Y = 23.90*X - 0.6260
R2 = 0.9987
AUCsubstrate/AUCIS
[substrate] (mM)
HO
Me
O
OH
H
Ph

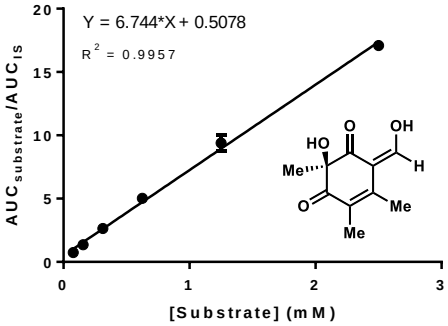
Y = 6.744*X + 0.5078
R2 = 0.9957
AUCsubstrate/AUCIS
[Substrate] (mM)
HO
Me
O
OH
H
Me
Me

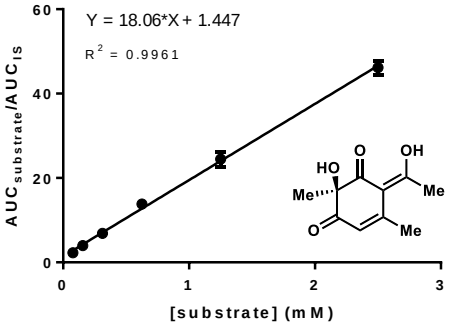
Y = 18.06*X + 1.447
R2 = 0.9961
AUCsubstrate/AUCIS
[substrate] (mM)
HO
Me
O
OH
Me
Me

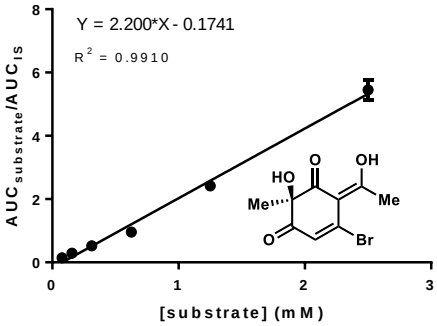
Y = 2.200*X - 0.1741
R2 = 0.9910
AUCsubstrate/AUCIS
[substrate] (mM)
HO
Me
O
OH
Me
Br

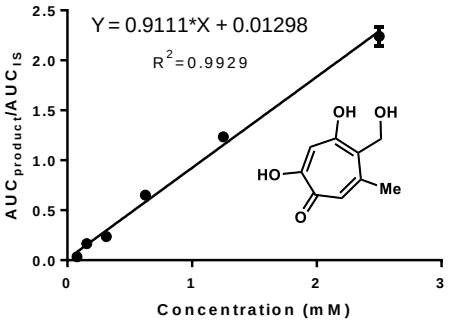
Y = 0.9111*X + 0.01298
R2=0.9929
AUCproduct/AUCIS
Concentration (mM)
OH
OH
HO
Me
O

**Figure 3.S4.** LC/MS traces for one-pot TropB/XenC cascade to generate product **3.11**.

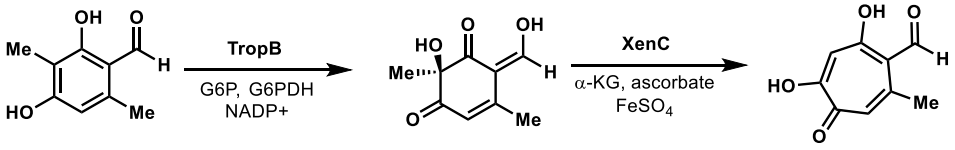


**Reaction with TropB and XenC**

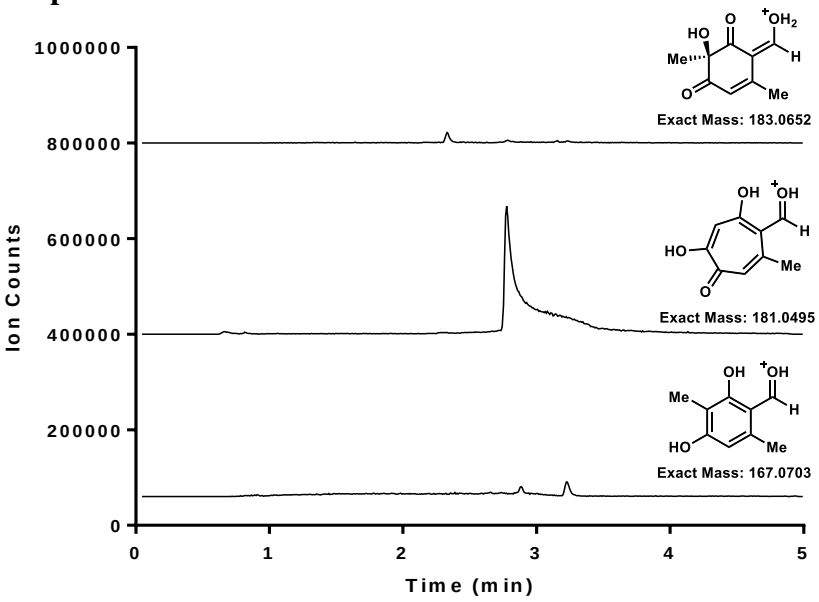


**Reaction with TropB only**

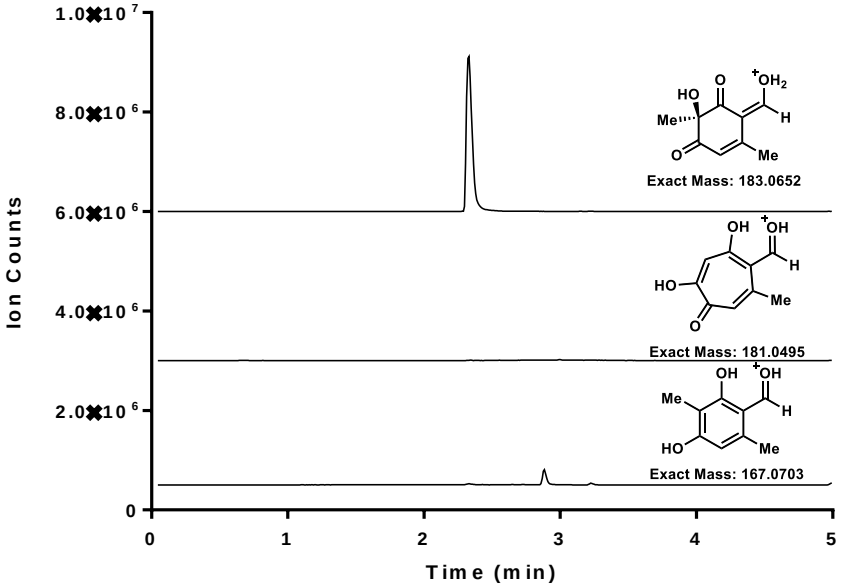

**No enzyme control**

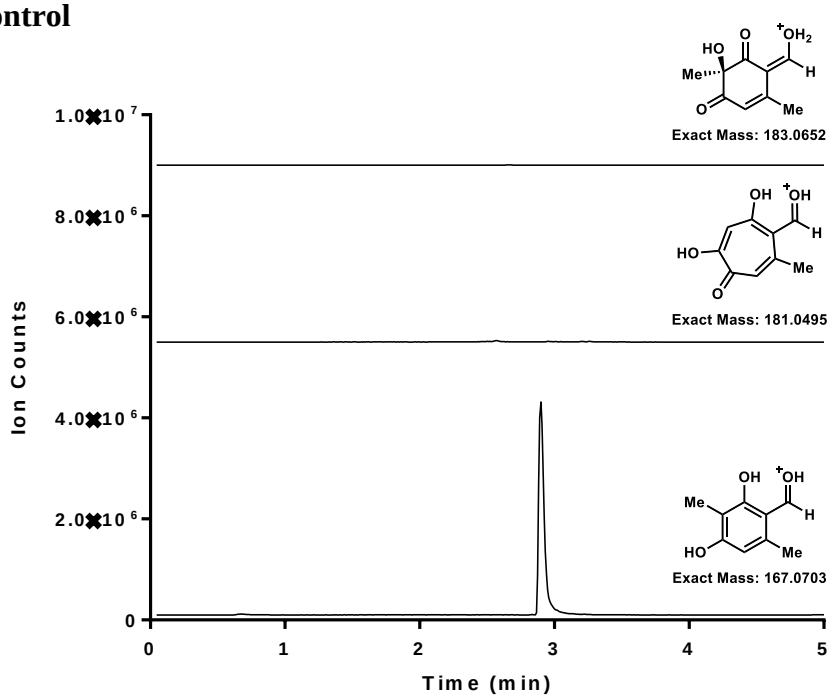


**Mass spectrum of tropolone product**

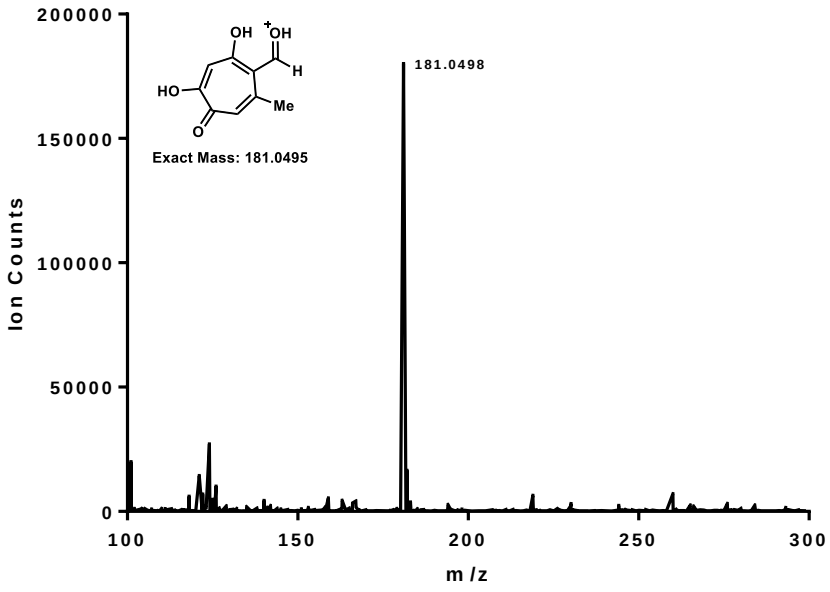

**Figure 3.S5.** LC/MS traces for one-pot TropB/XenC cascade to generate product **3.32**.

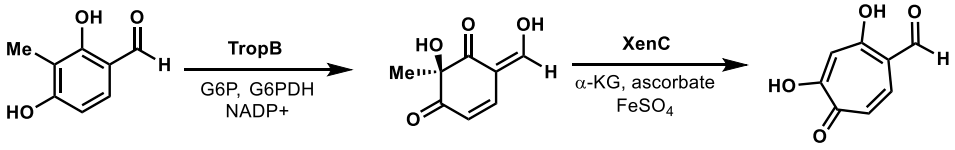


**Reaction with TropB and XenC**

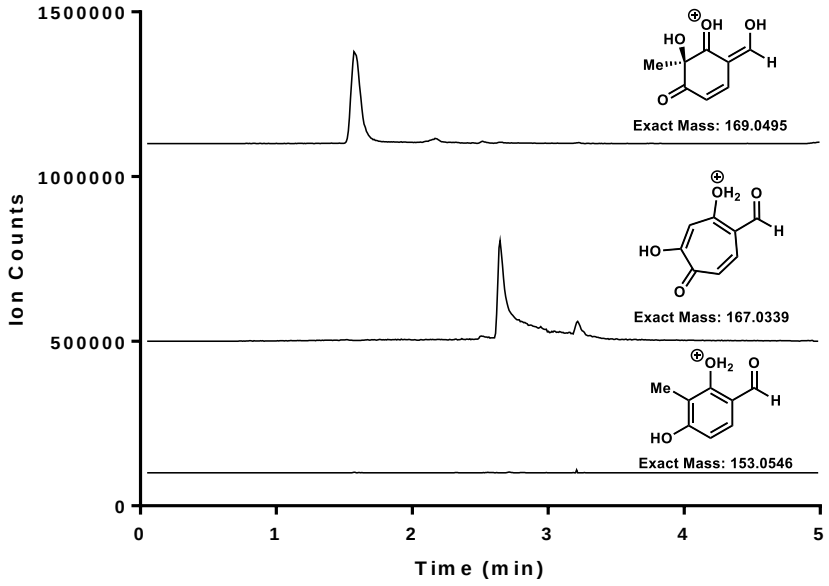


**Reaction with TropB only**

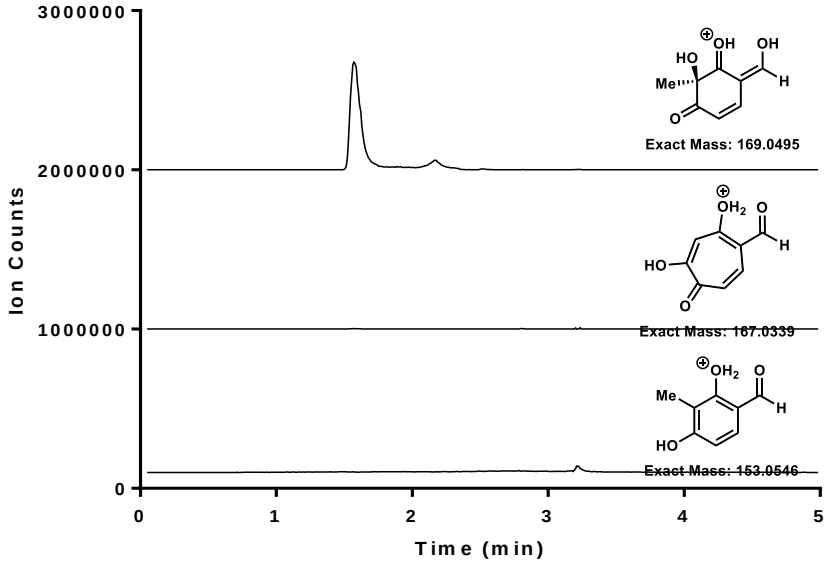

## No enzyme control

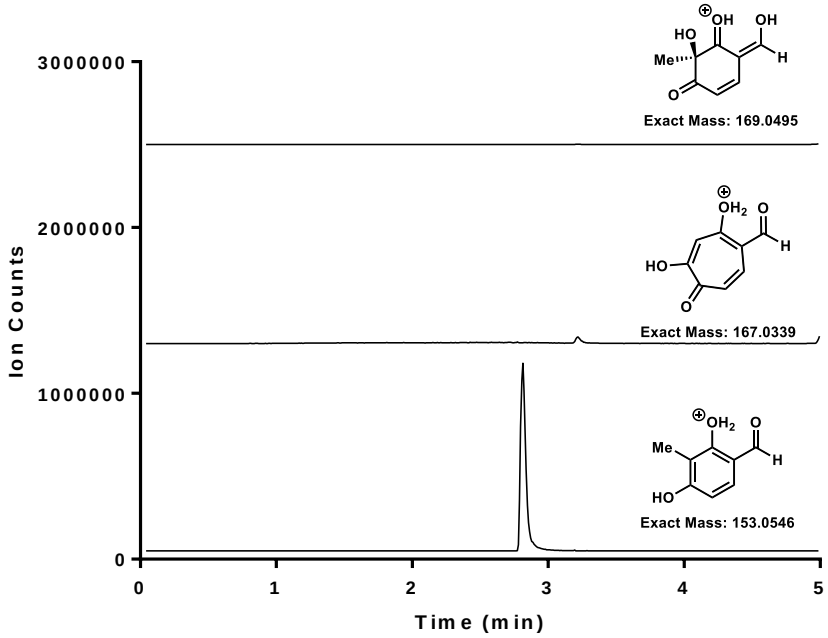


## Mass spectrum of tropolone product

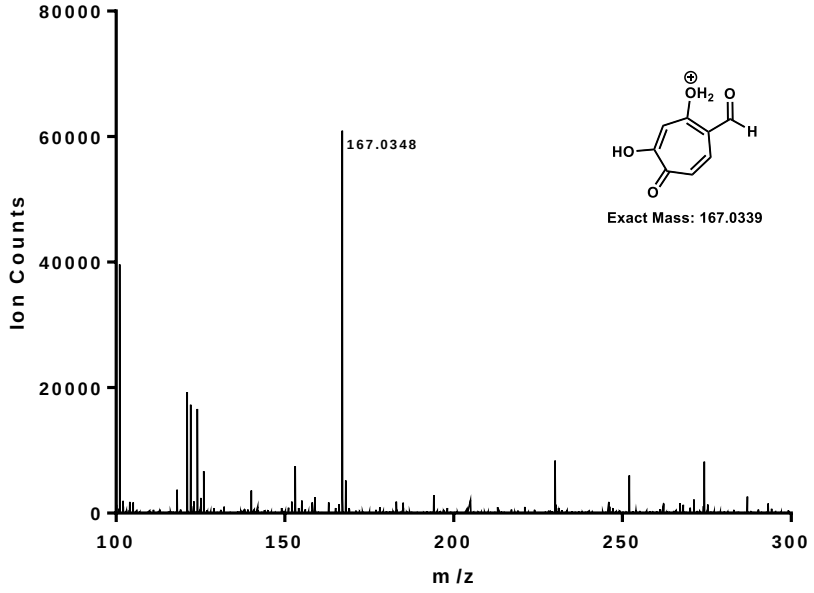

**Figure 3.S6.** LC/MS traces for one-pot TropB/XenC cascade to generate product **3.37**.

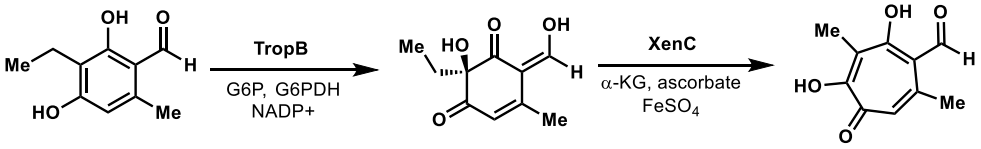


**Reaction with TropB and XenC**

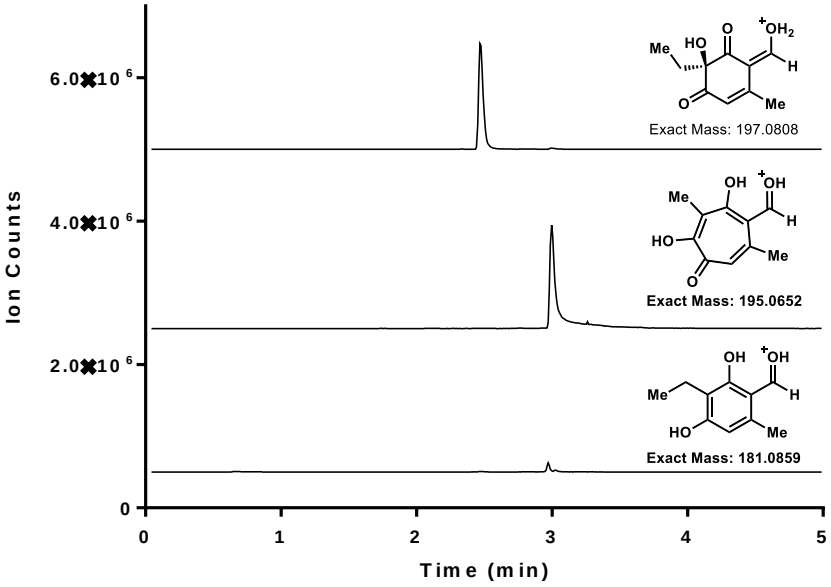


**Reaction with TropB only**

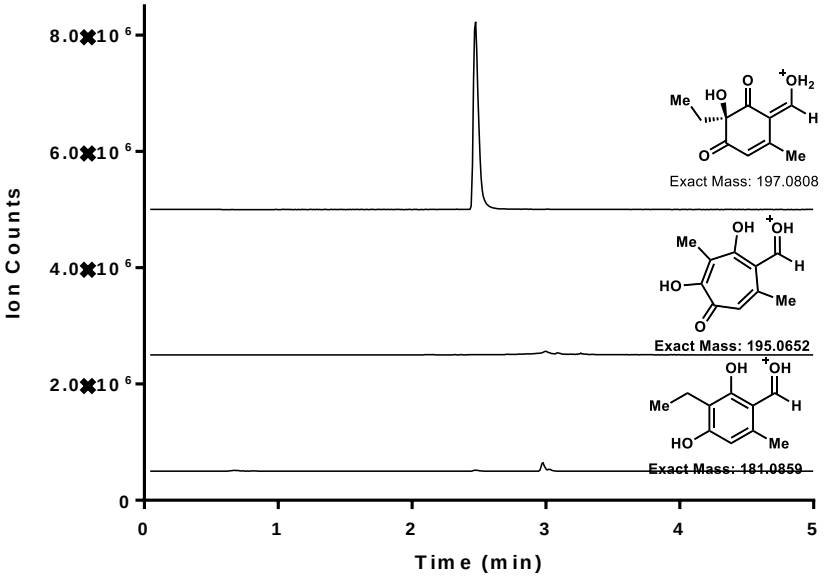

**No enzyme control**

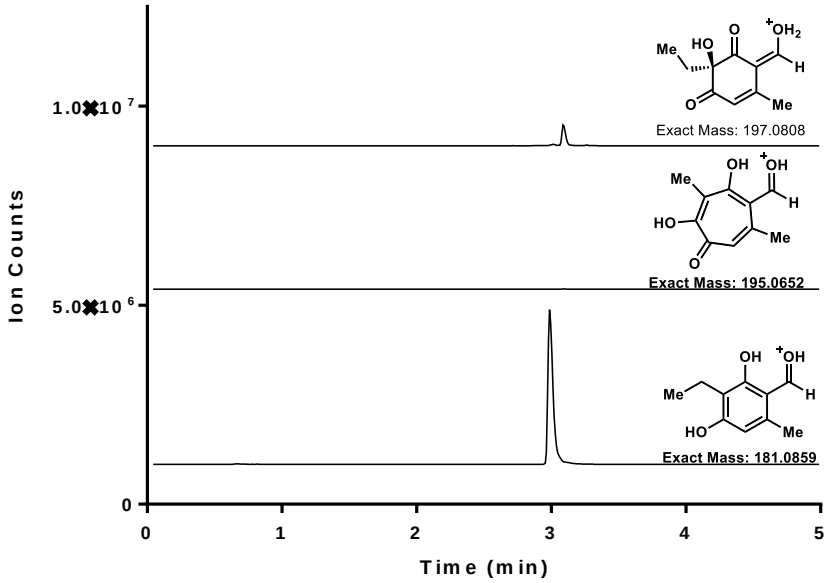


**Mass spectrum of tropolone product**

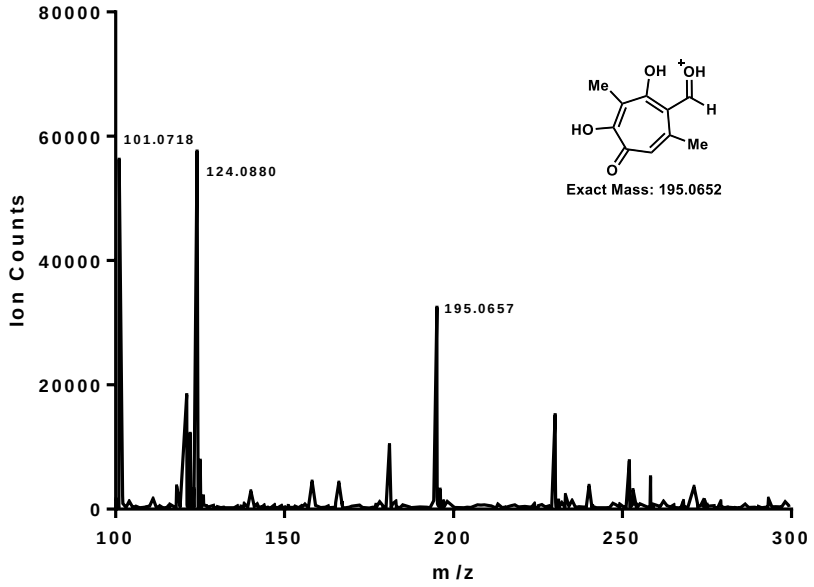

**Figure 3.S7.** LC/MS traces for one-pot TropB/XenC cascade to generate product **3.39**.

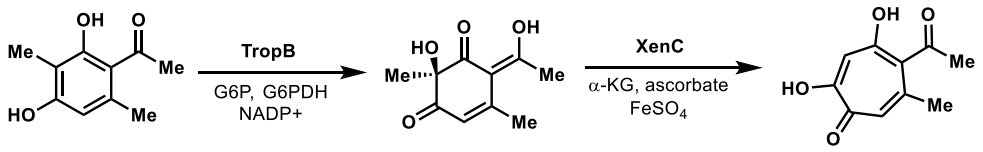


**Reaction with TropB and XenC**

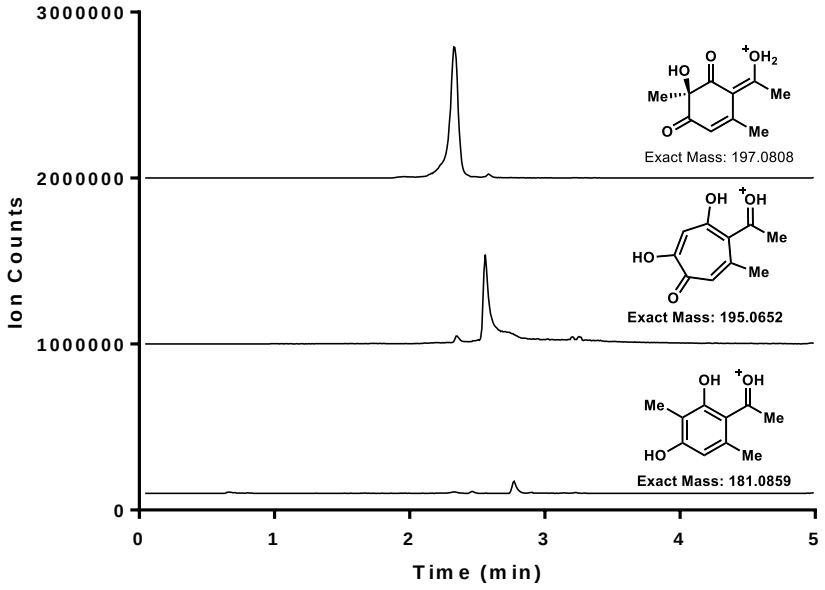


**Reaction with TropB only**

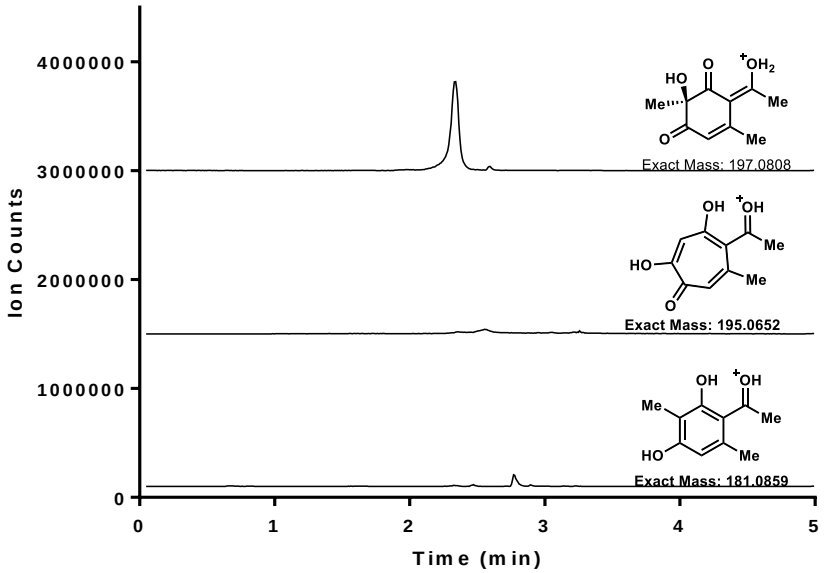

**No enzyme control**

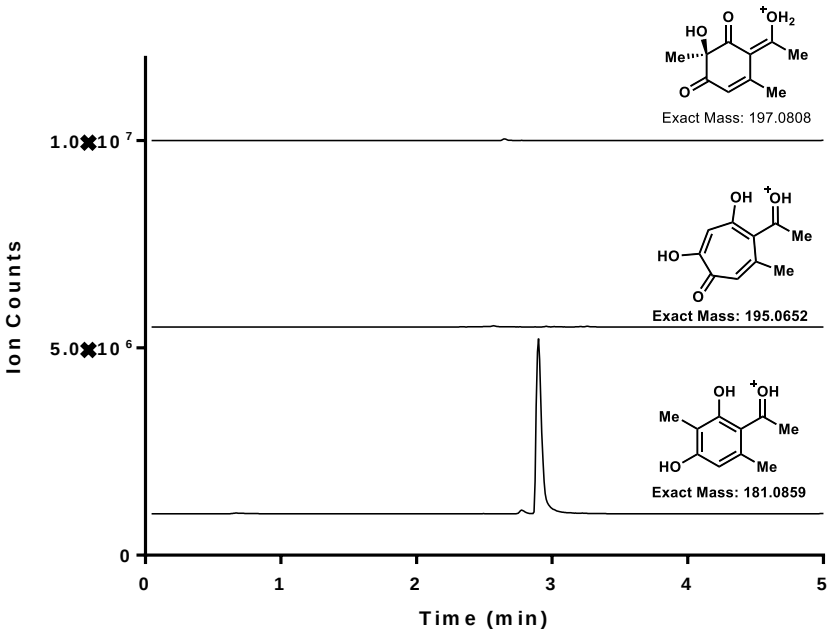


**Mass spectrum of tropolone compound**

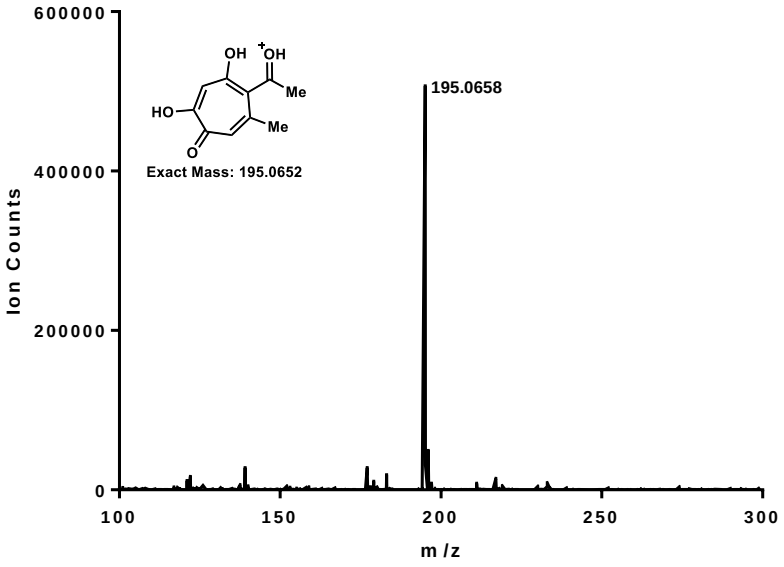

**Figure 3.S8.** LC/MS traces for one-pot TropB/XenC cascade to generate product **3.34**.

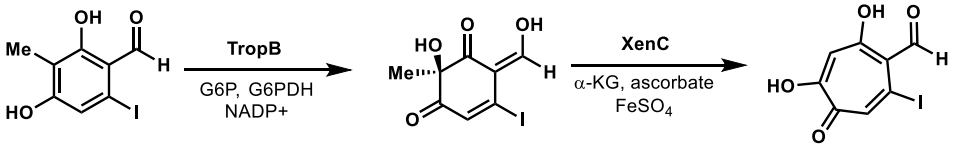


**Reaction with TropB and XenC**

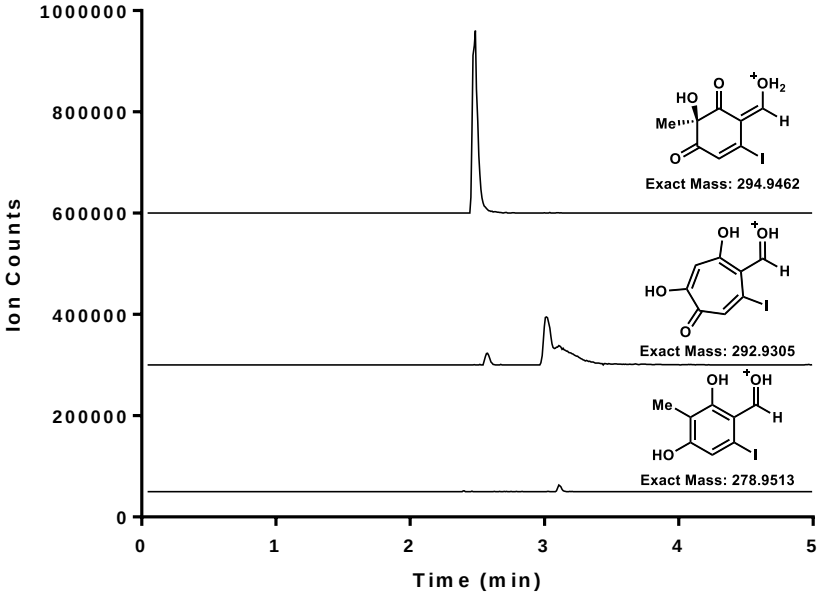


**Reaction with TropB only**

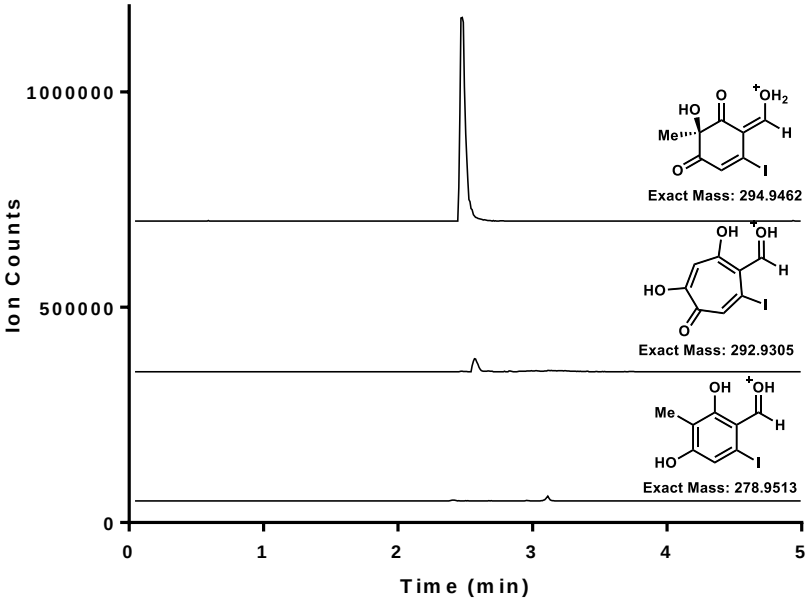

## No enzyme control

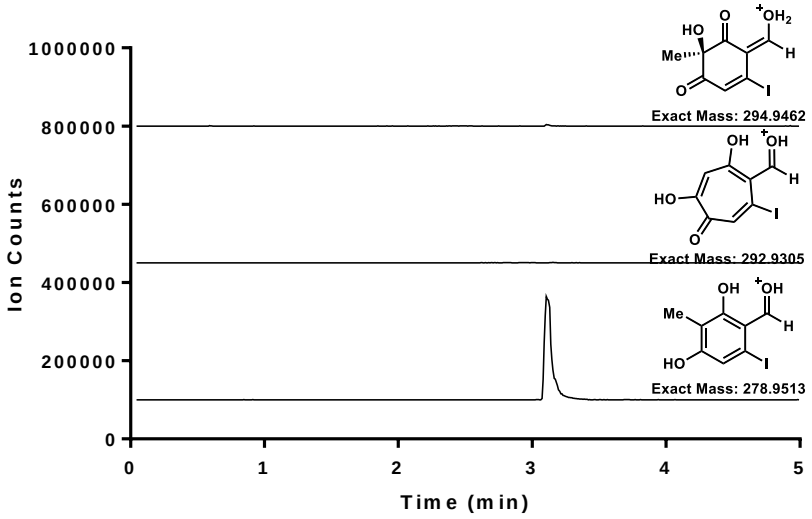


## Mass spectrum of tropolone product

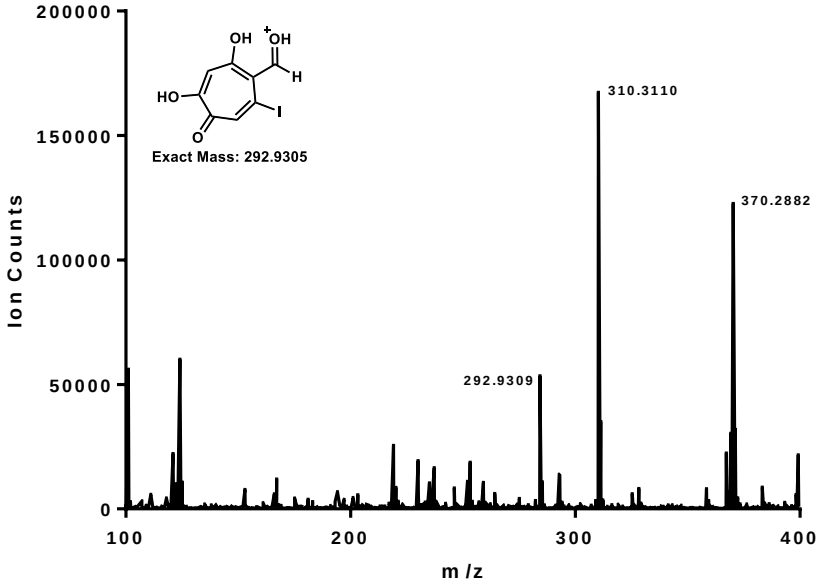

**Figure 3.S9.** LC/MS traces for one-pot TropB/XenC cascade to generate product **3.35**.

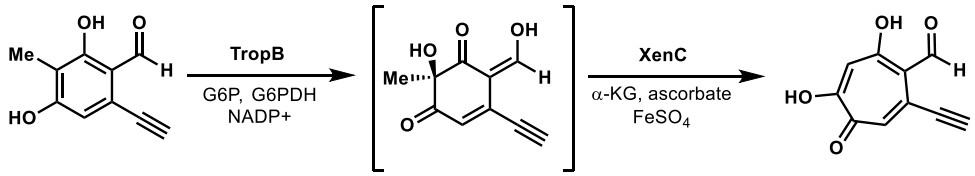


**Reaction with TropB and XenC**

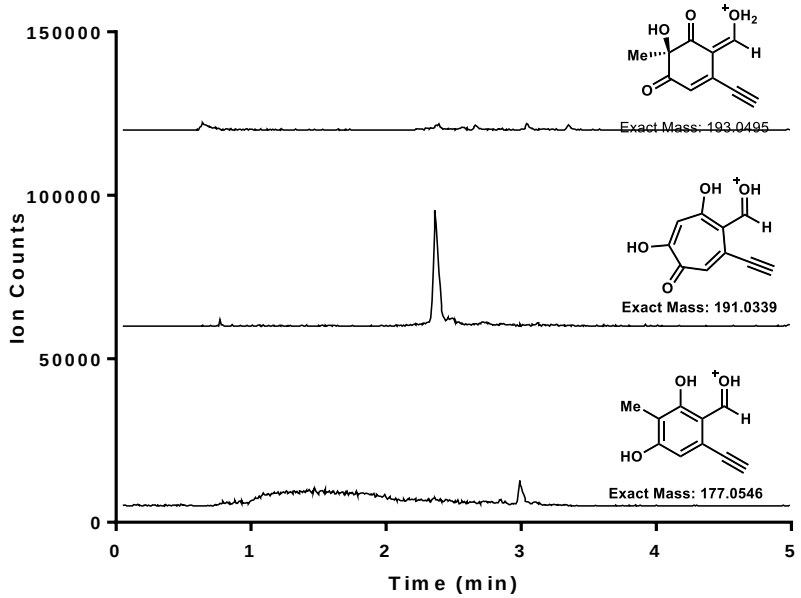


**Reaction with TropB only**

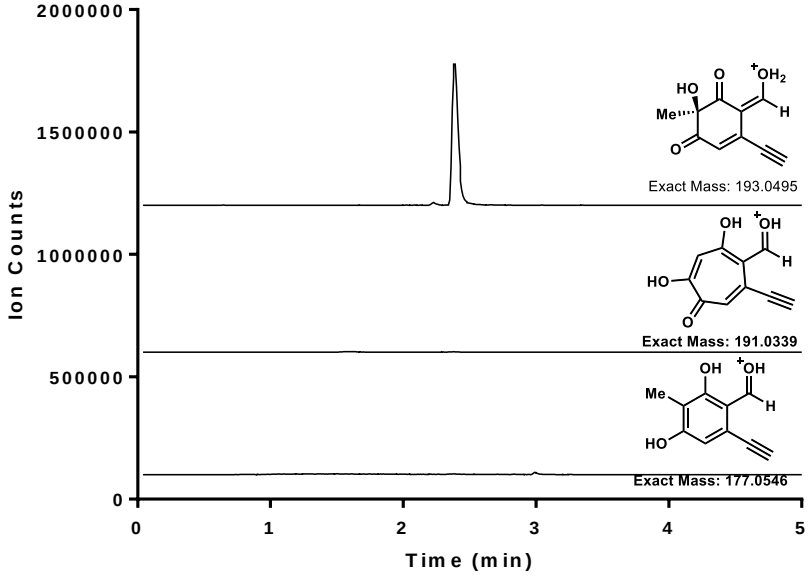

## No enzyme control

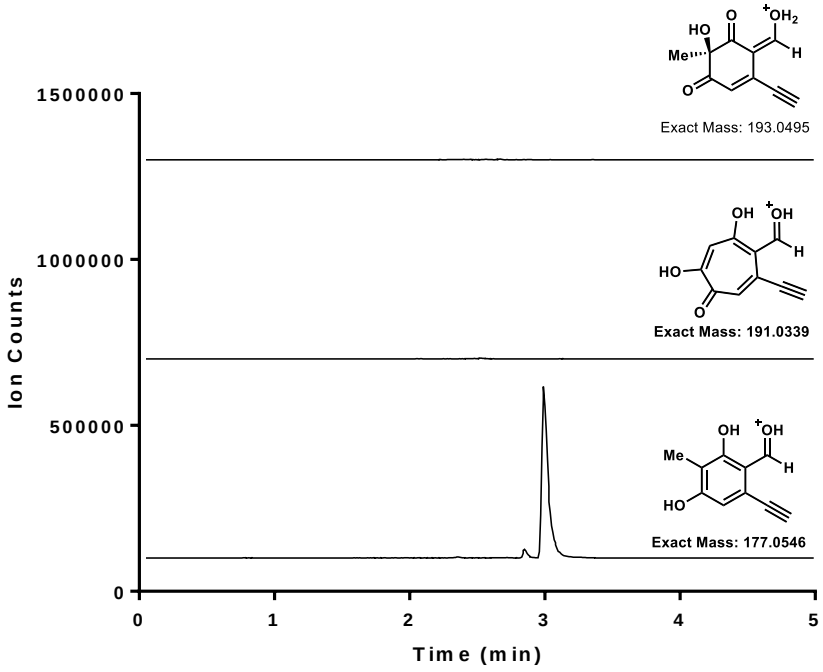


## Mass spectrum of tropolone compound

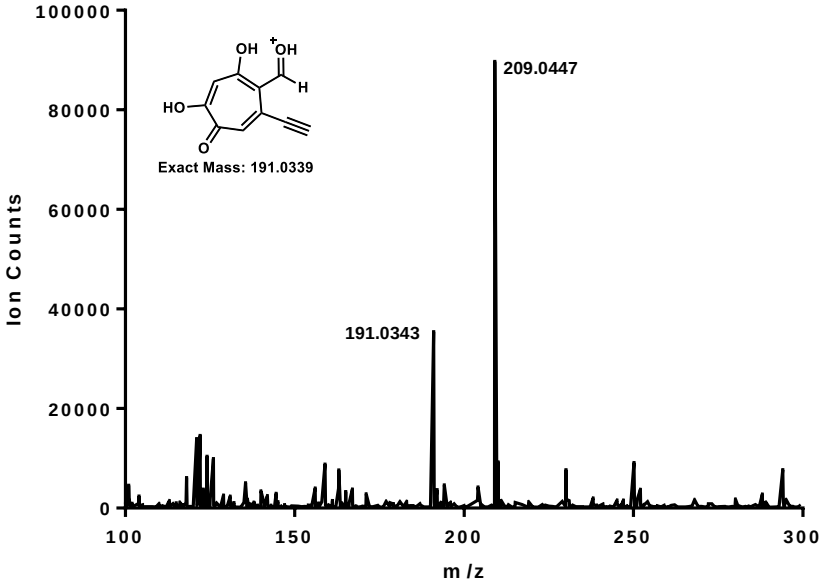

**Figure 3.S10.** LC/MS traces for one-pot TropB/XenC cascade to generate product **3.36**.

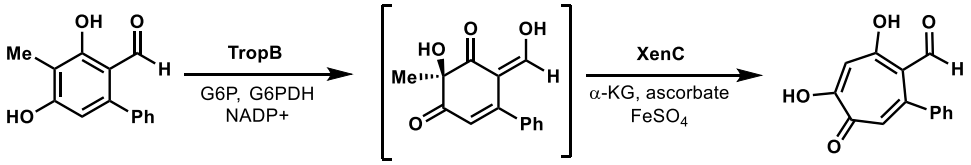


**Reaction with TropB and XenC**

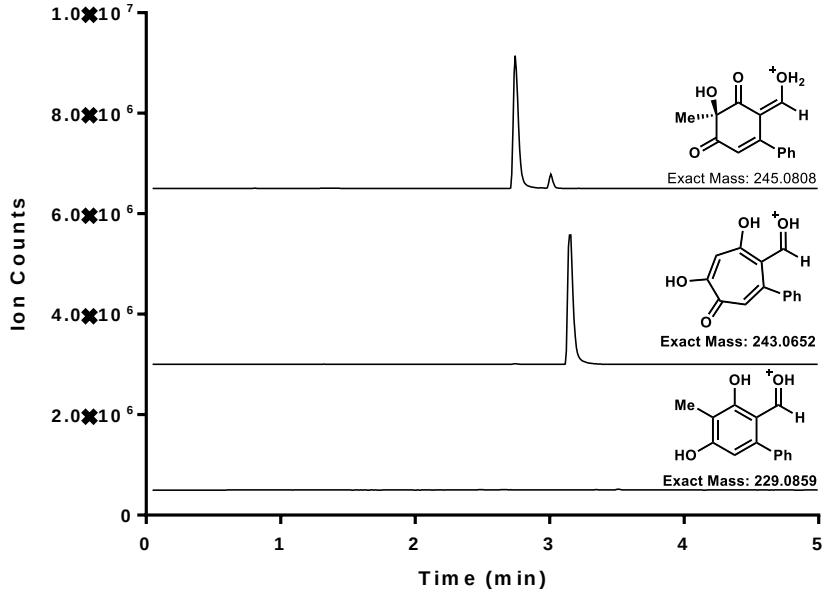


**Reaction with TropB only**

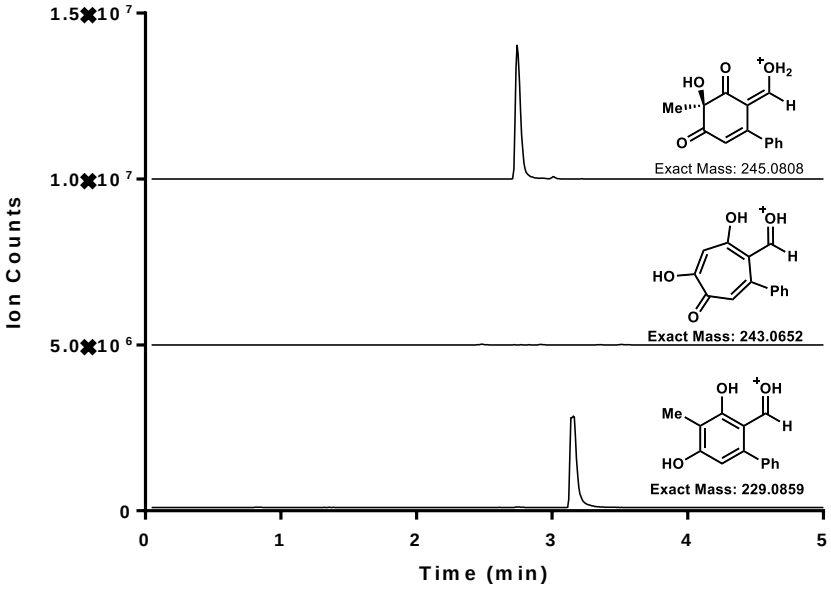

## No enzyme control

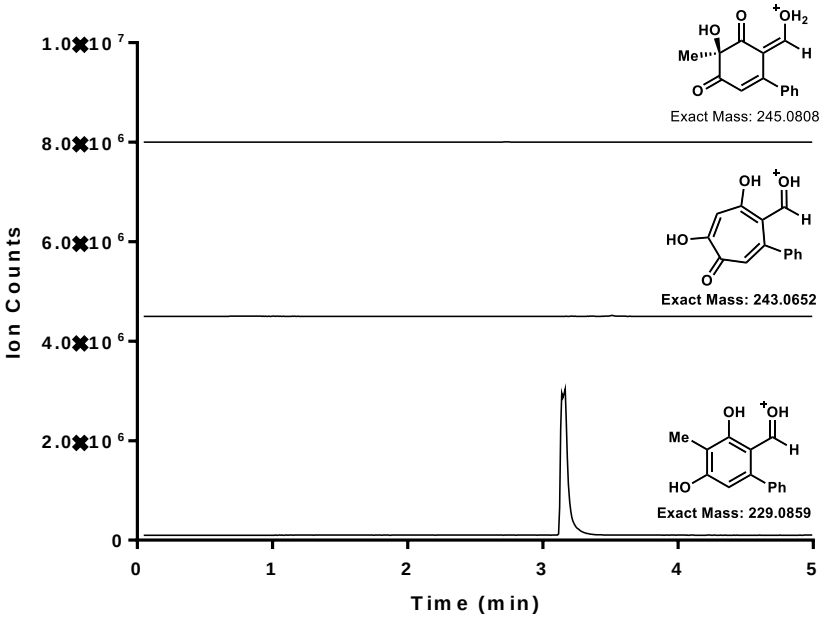


## Mass spectrum of tropolone compound

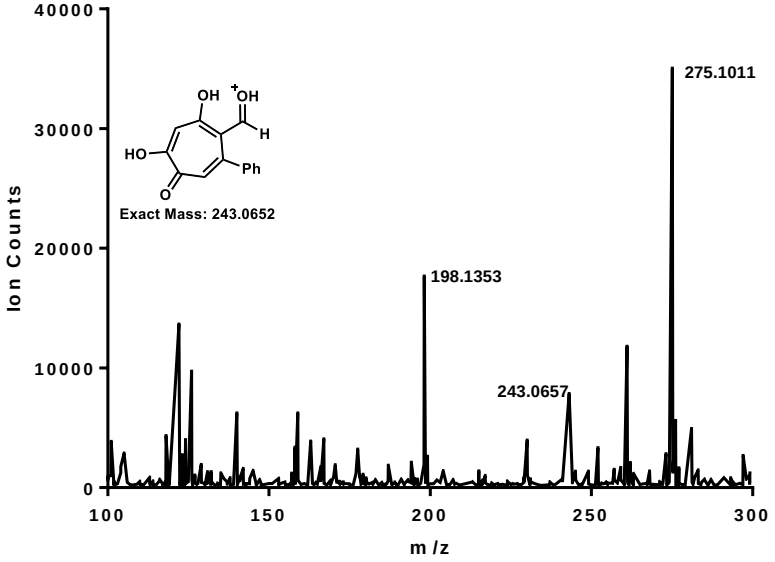

**Figure 3.S11.** LC/MS traces for one-pot TropB/XenC cascade to generate product **3.33**.

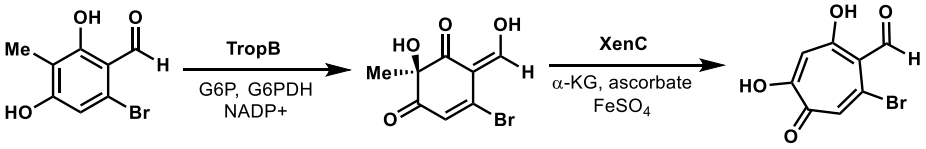


**Reaction with TropB and XenC**

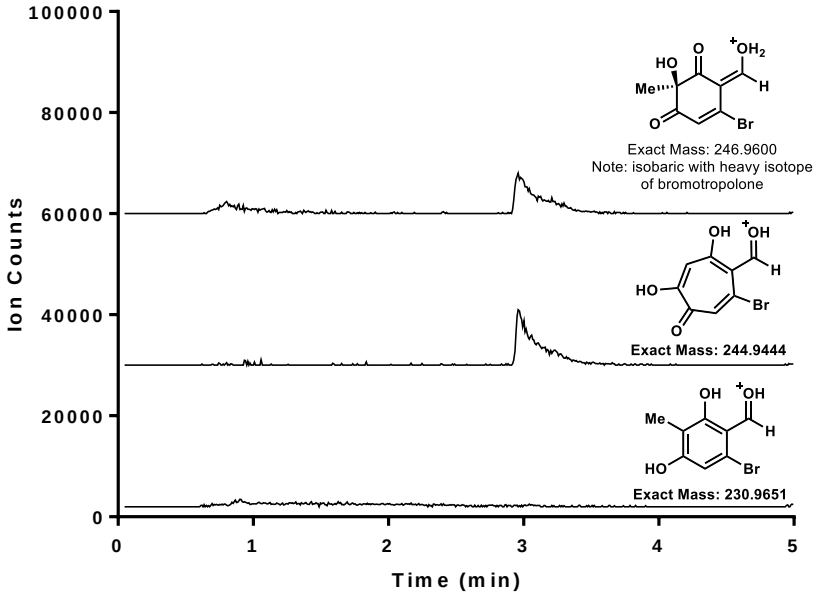


**Reaction with TropB only**

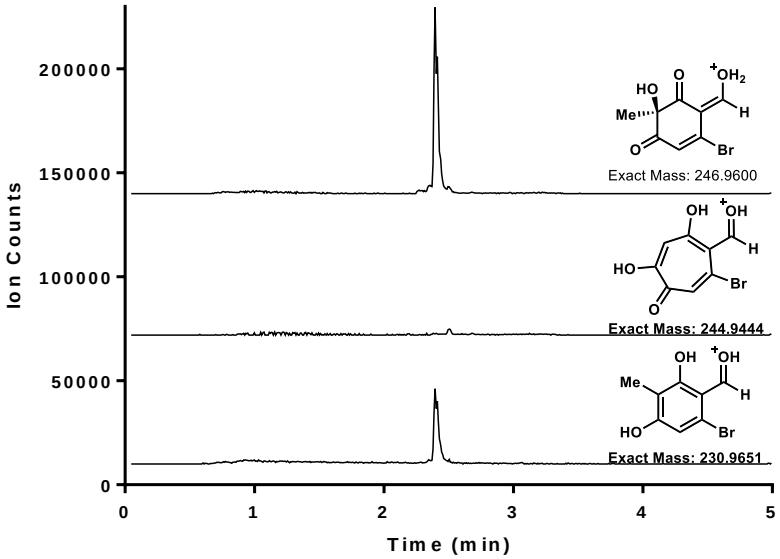

**No enzyme control**

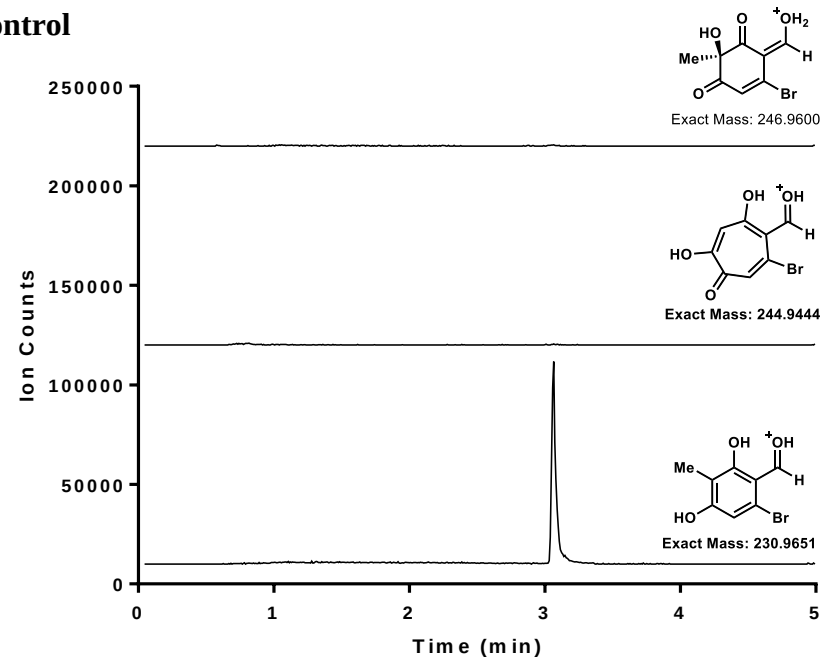


**Mass spectrum of tropolone compound**

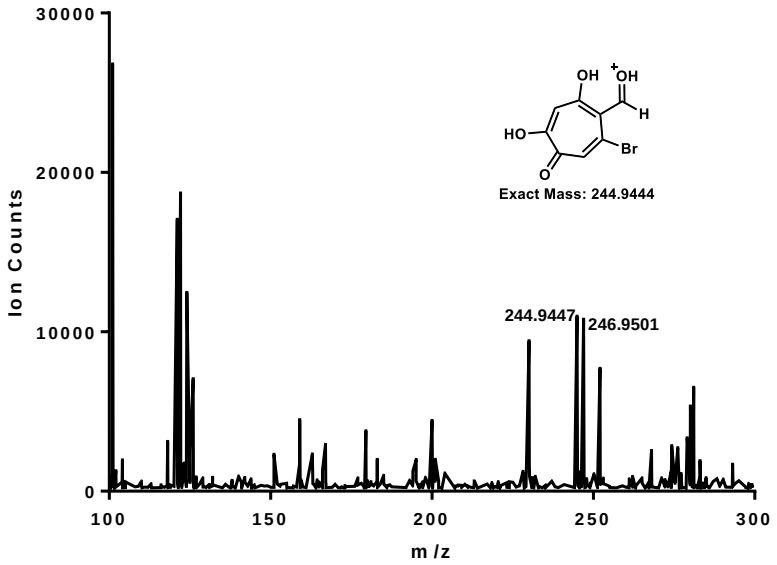

**Figure 3.S12.** LC/MS traces for one-pot TropB/XenC cascade to generate product **3.38**.

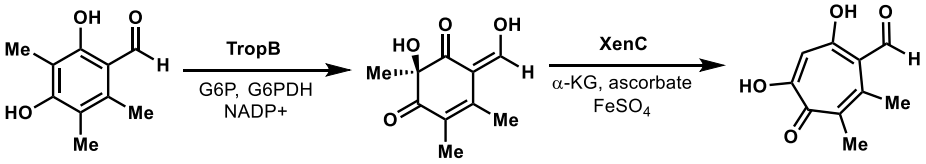


**Reaction with TropB and XenC**

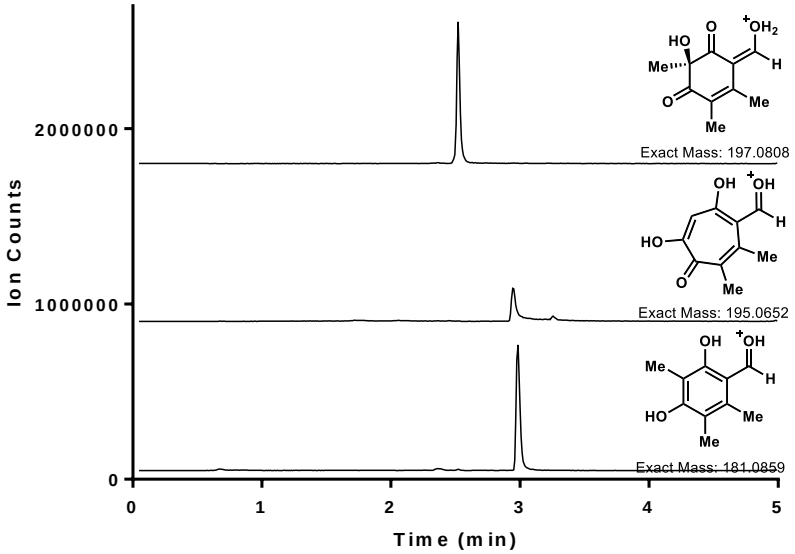


**Reaction with TropB only**

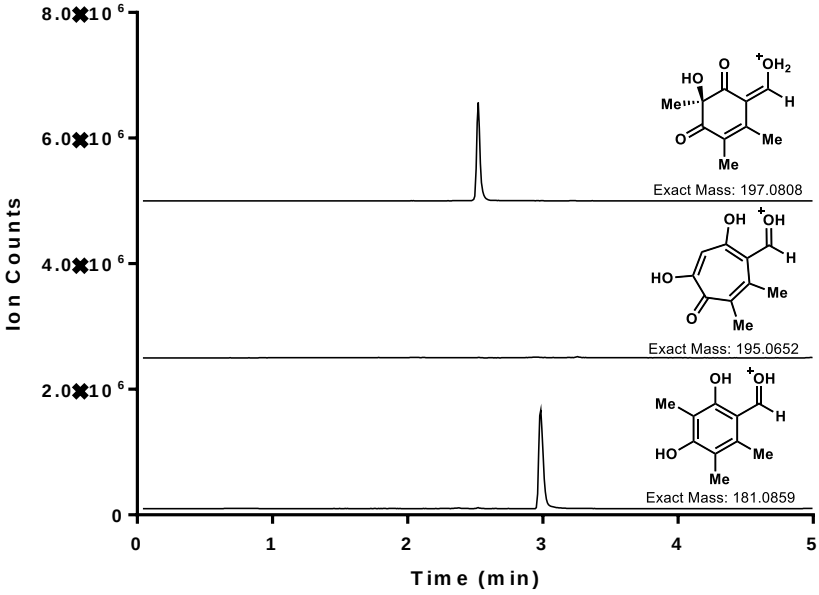

## No enzyme control

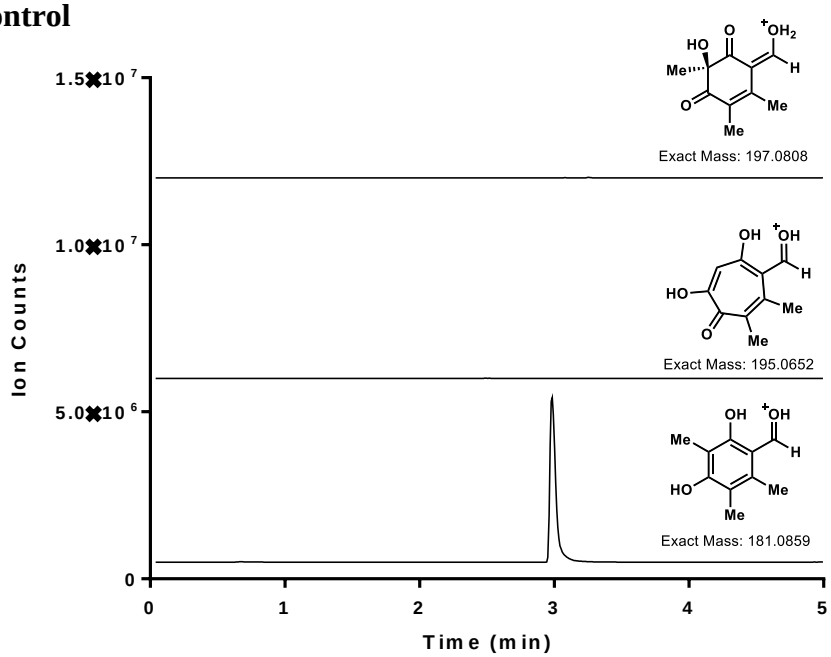


## Mass spectrum of tropolone compound

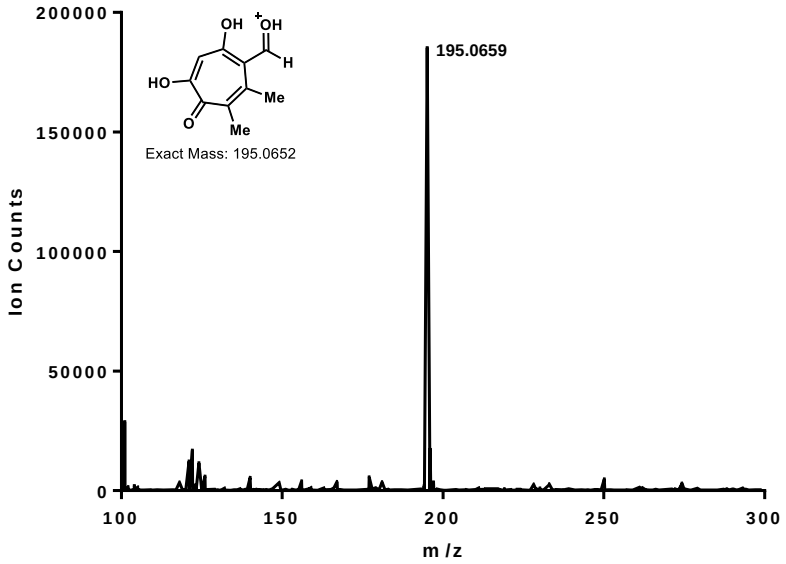

**Figure 3.S13. LC/MS traces for one-pot TropB/XenC cascade to generate product 3.42.**

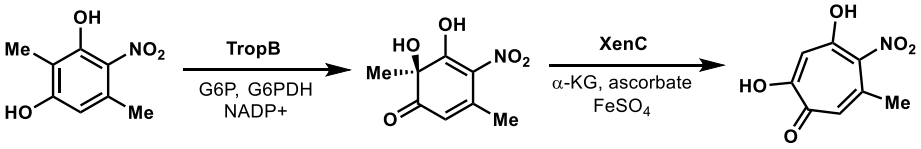


**Reaction with TropB and XenC**

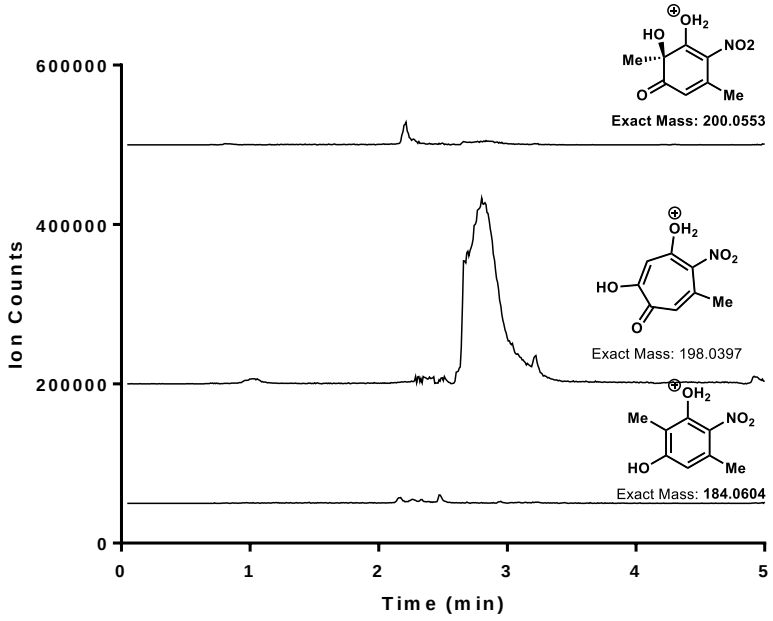


**Reaction with TropB only**

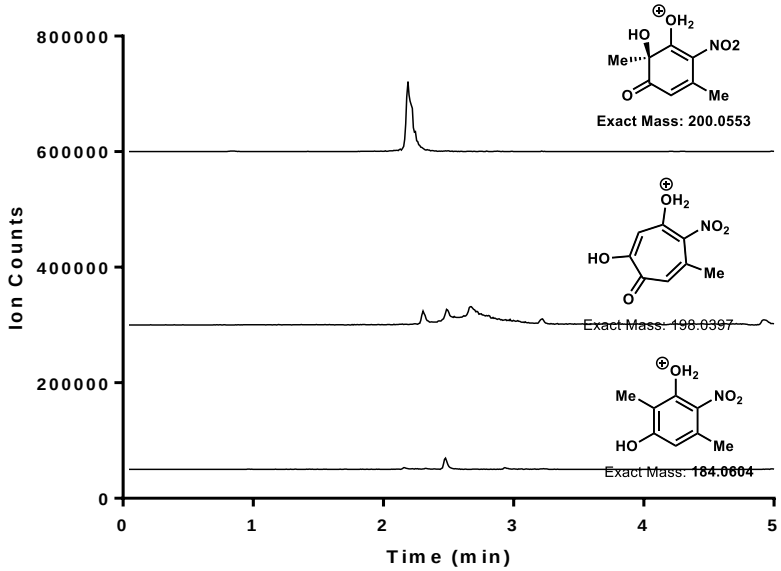

## No enzyme control

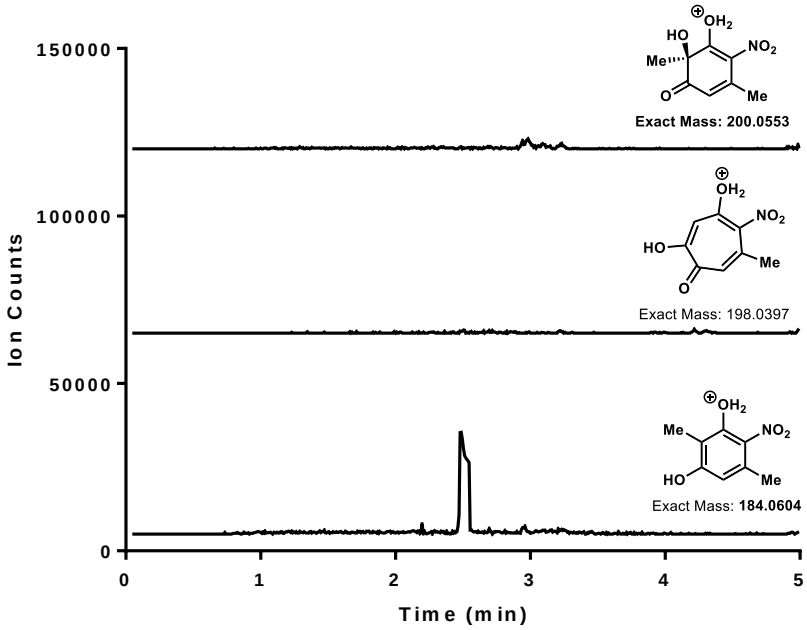


## Mass spectrum of tropolone compound

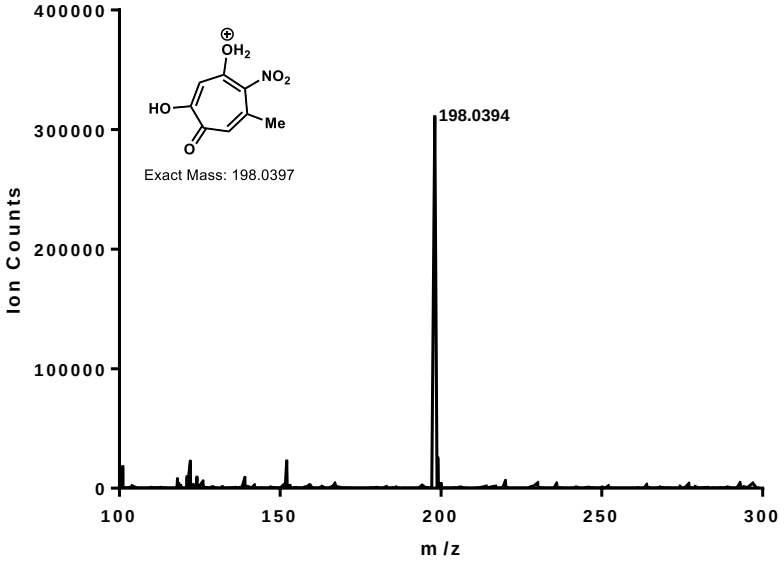

**Part VI. Reactions with tropolone products**

**Figure 3.S14. LC/MS traces for Diels-Alder reaction to generate product 3.7.**

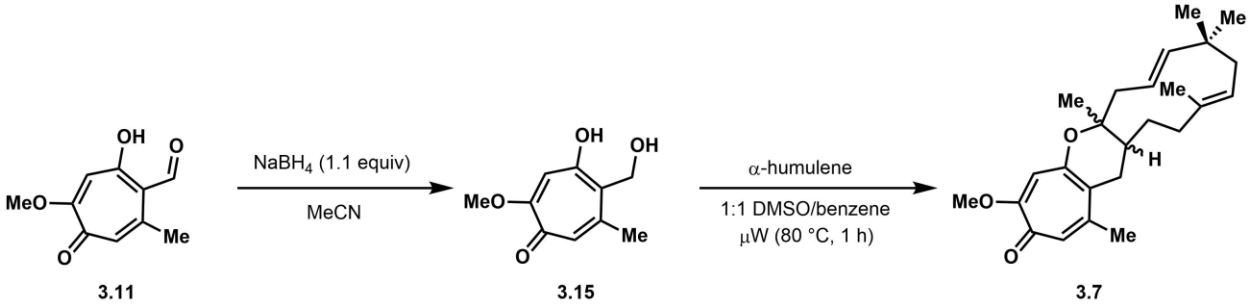


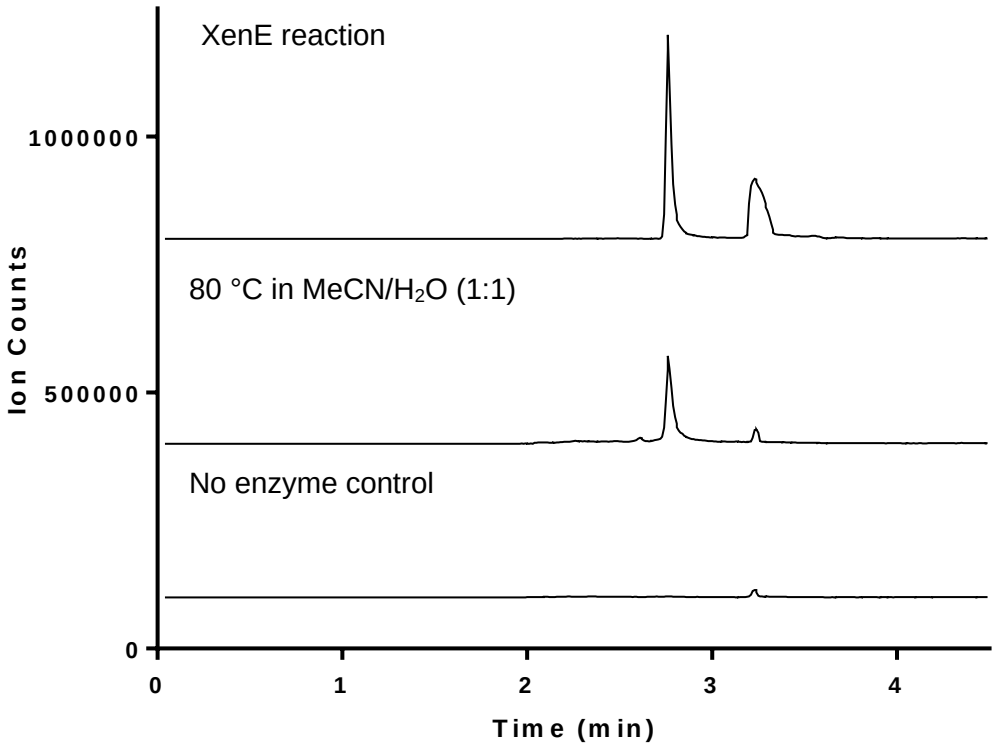

## Part VI. NMR Spectra

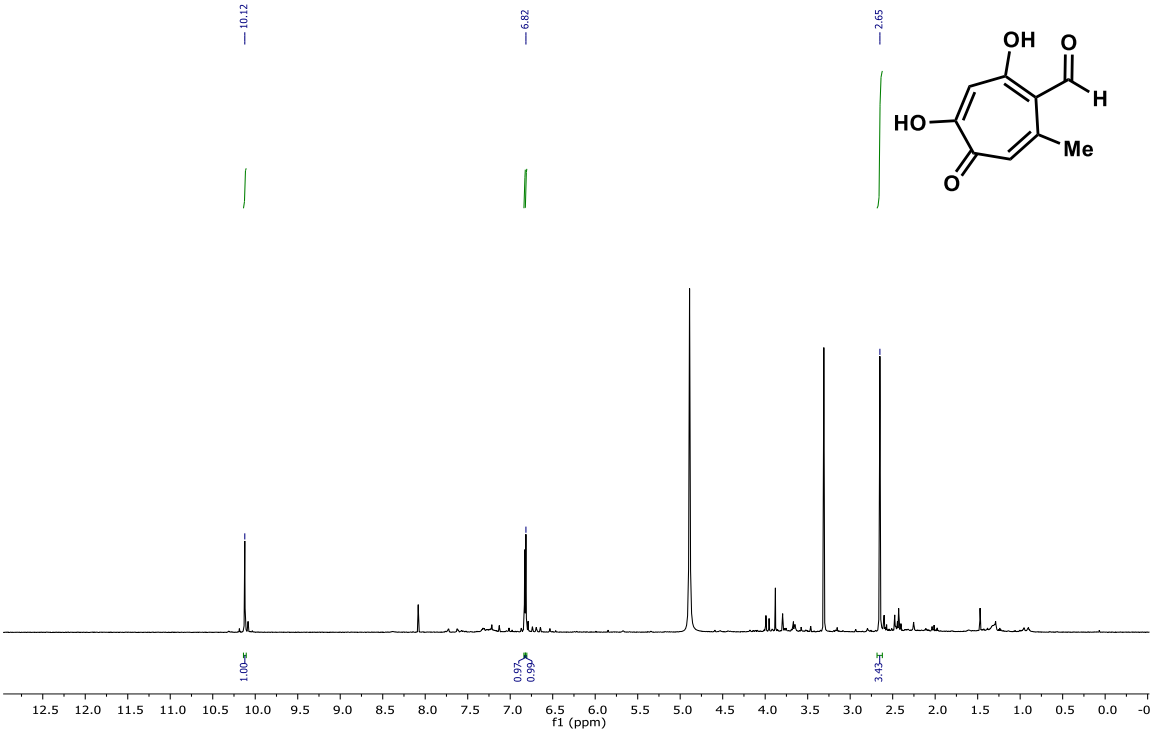


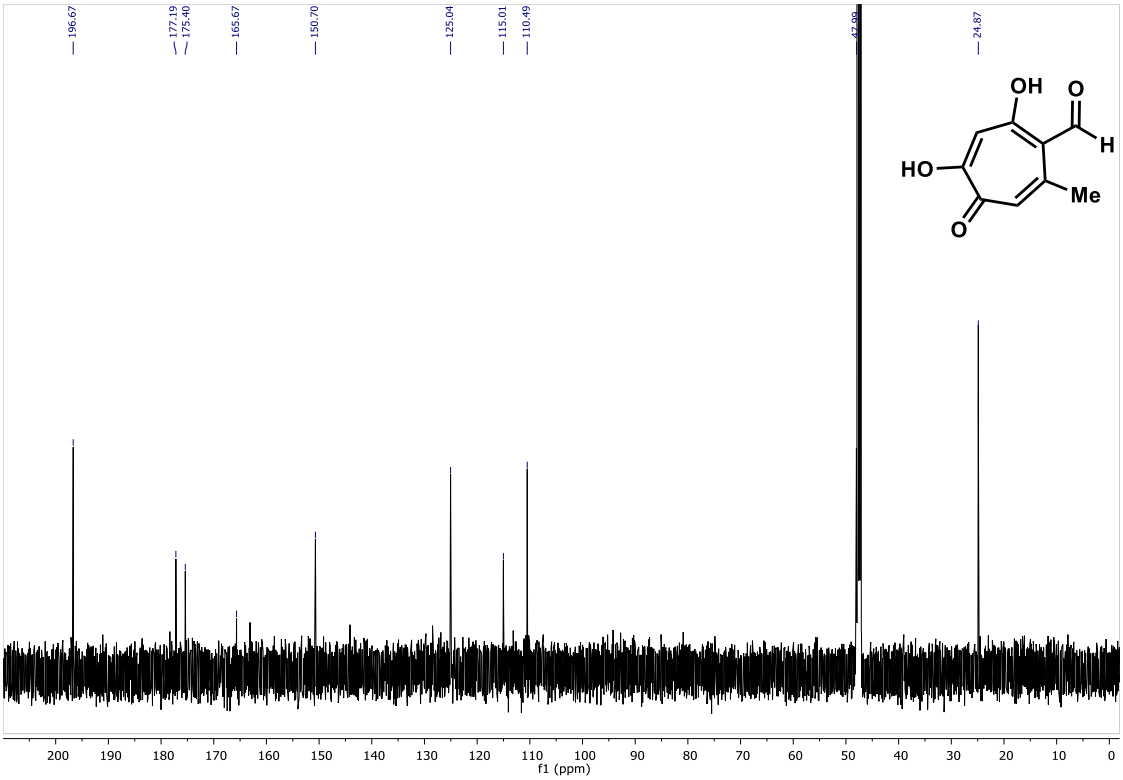

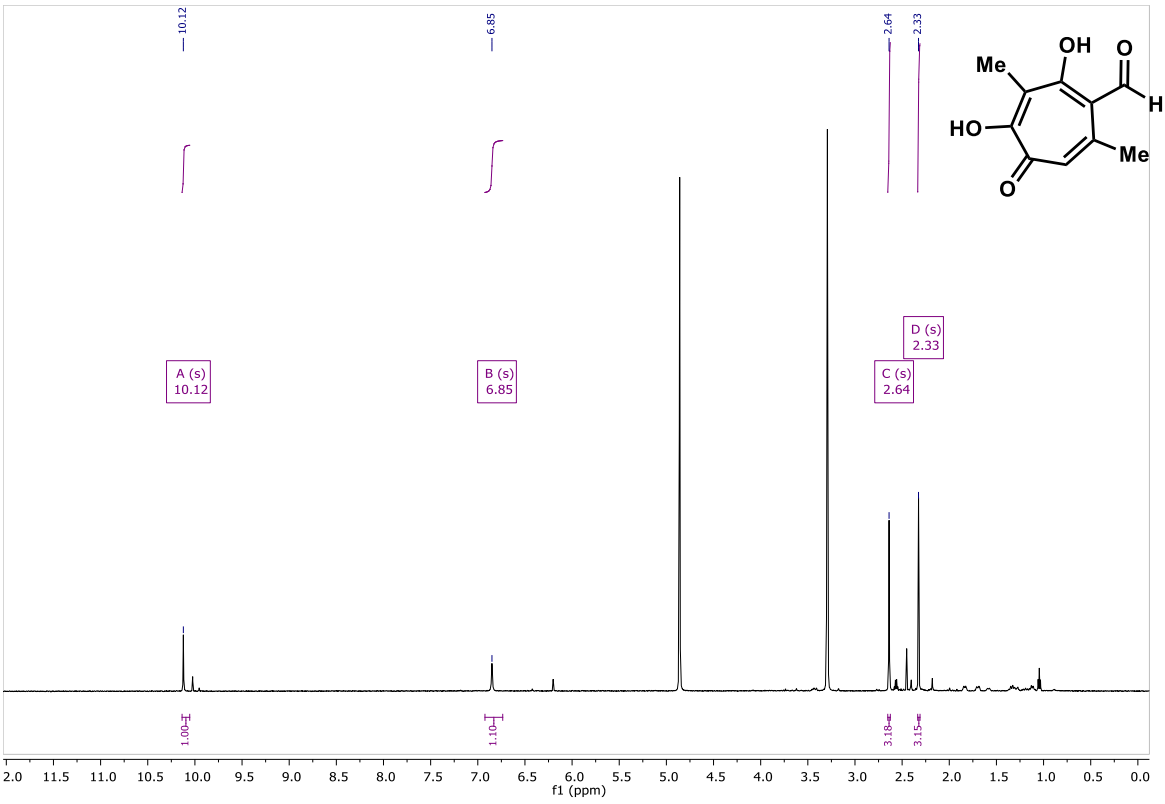
10.12
6.85
2.64
2.33
OH
O
Me
H
HO
Me
O
A (s)
10.12
B (s)
6.85
C (s)
2.64
D (s)
2.33
1.00
1.10
3.18
3.15
f1 (ppm)

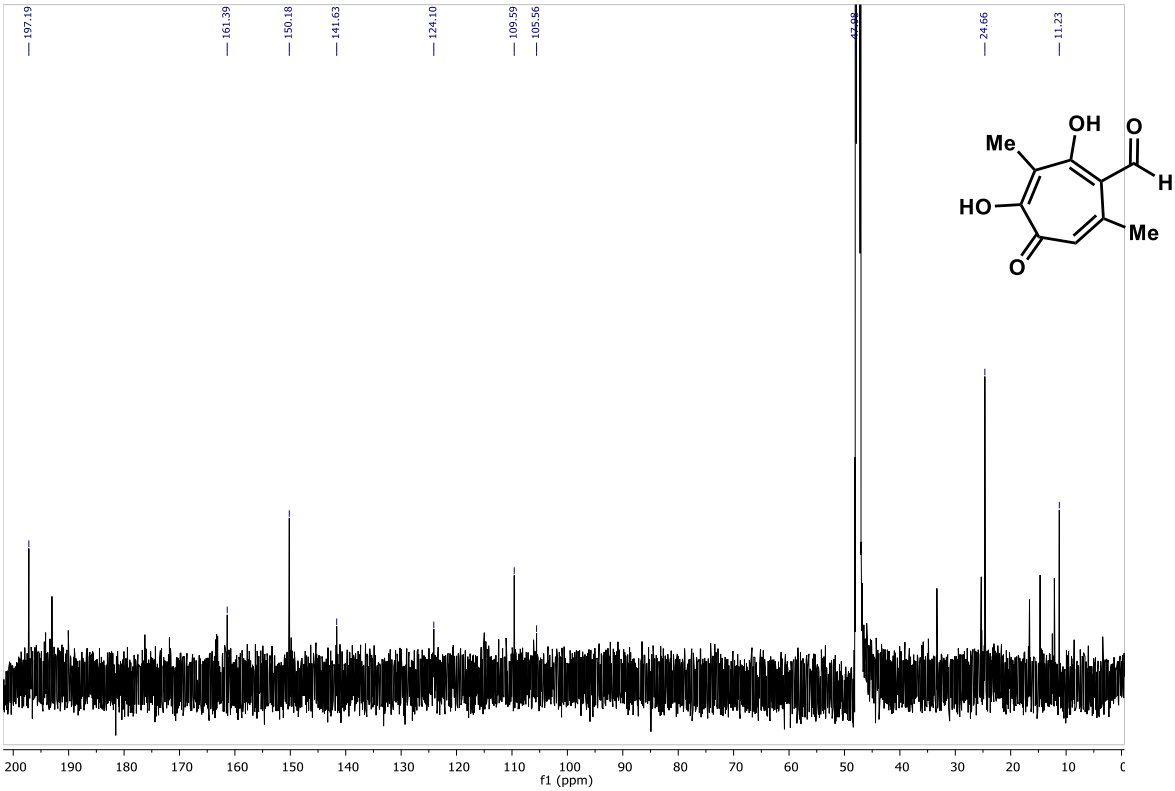
197.19
161.39
150.18
141.63
124.10
109.59
105.56
42.68
24.66
11.23
OH
O
Me
H
HO
Me
O
f1 (ppm)

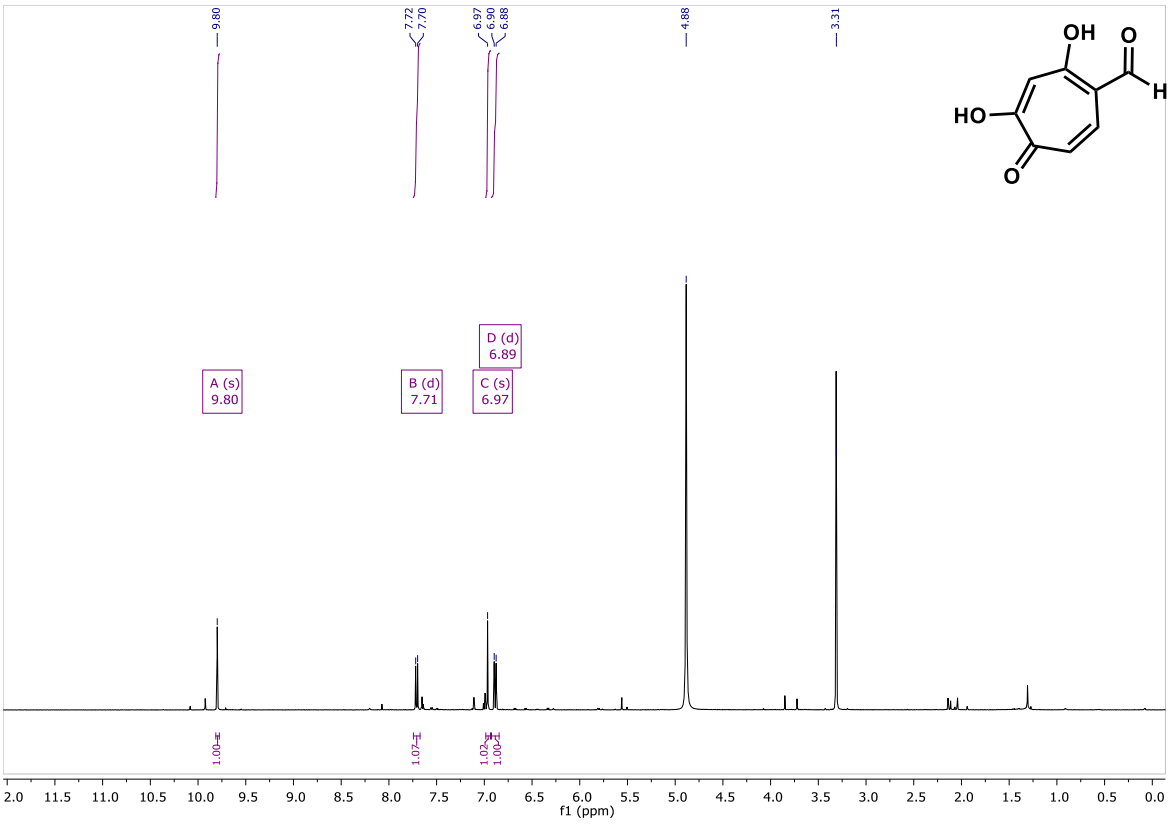
9.80
7.72
7.70
6.97
6.90
6.88
4.88
3.31
OH
O
H
HO
O
A (s)
9.80
B (d)
7.71
C (s)
6.97
D (d)
6.89
1.00
1.07
1.02
1.00
f1 (ppm)

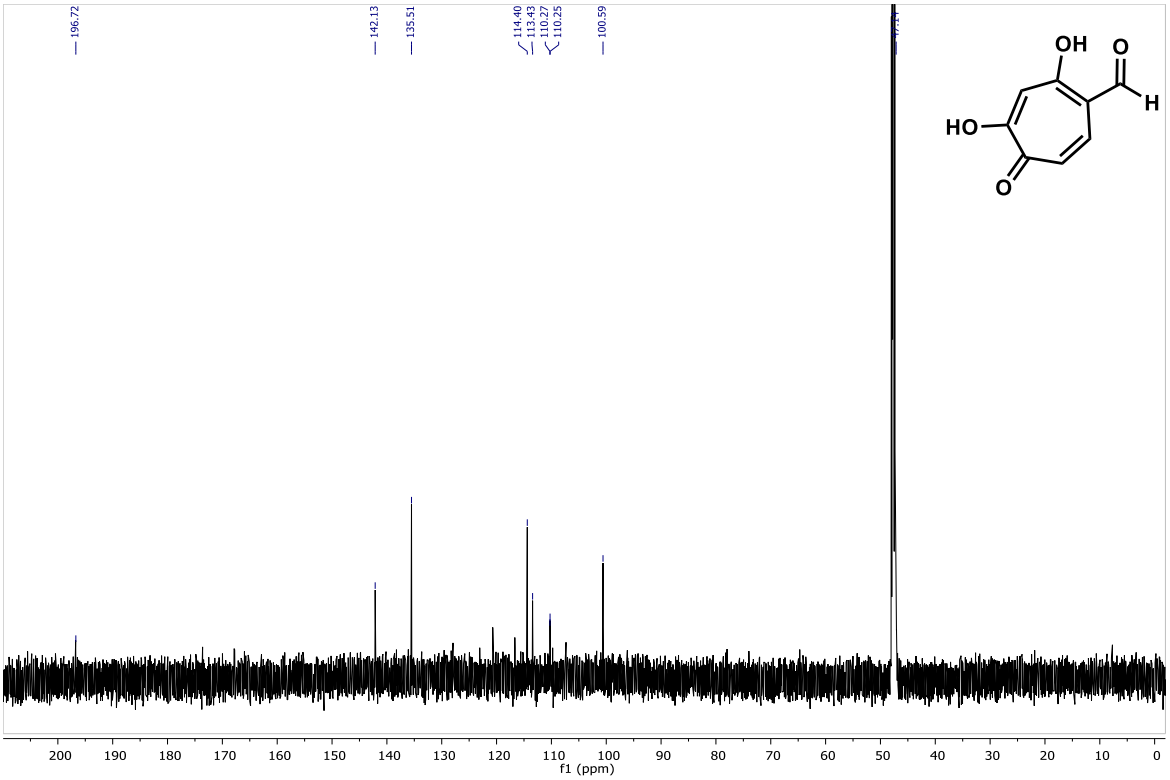
196.72
142.13
135.51
114.40
113.43
110.27
110.25
100.59
OH
O
H
HO
O
f1 (ppm)

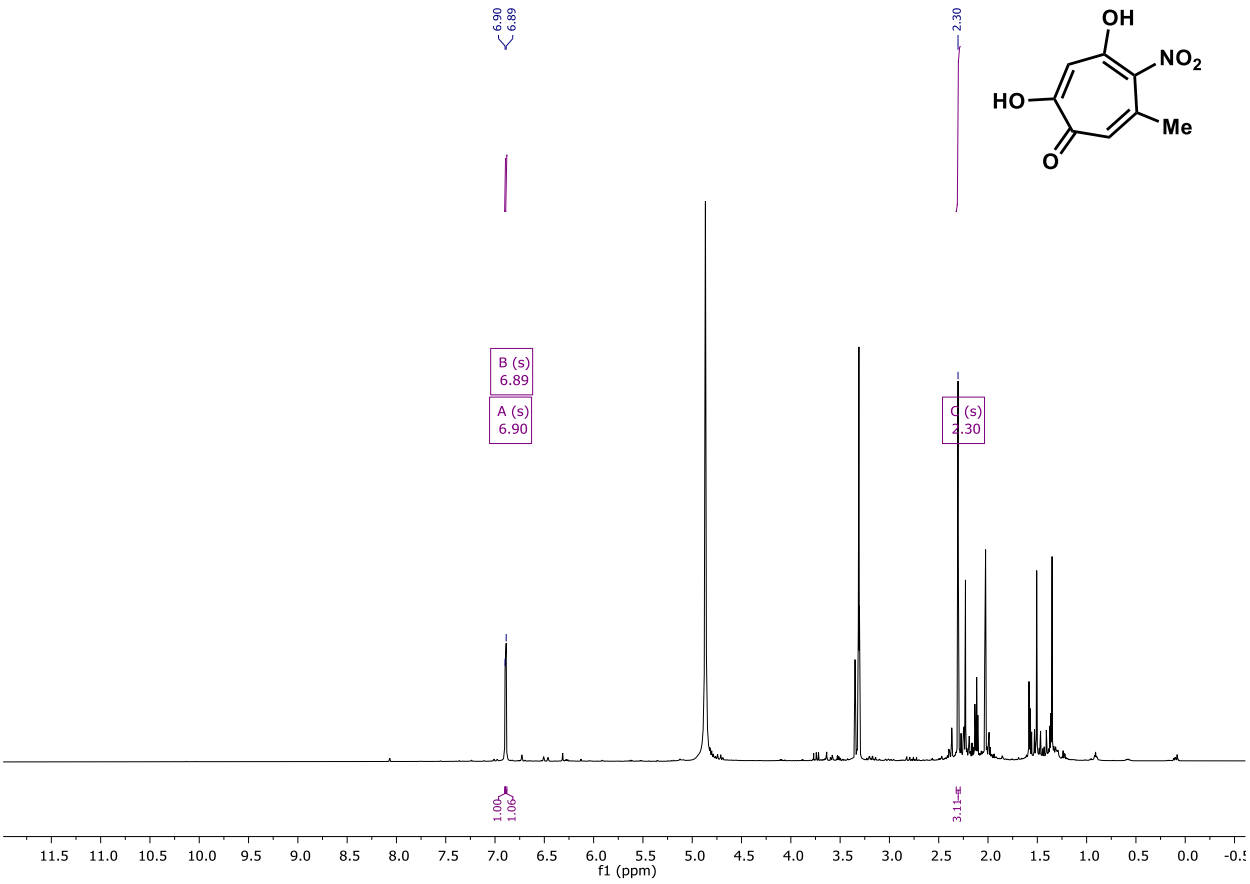
6.90
6.89
2.30
OH
NO2
HO
Me
O
B (s)
6.89
A (s)
6.90
C (s)
2.30
1.00
1.06
3.11
f1 (ppm)

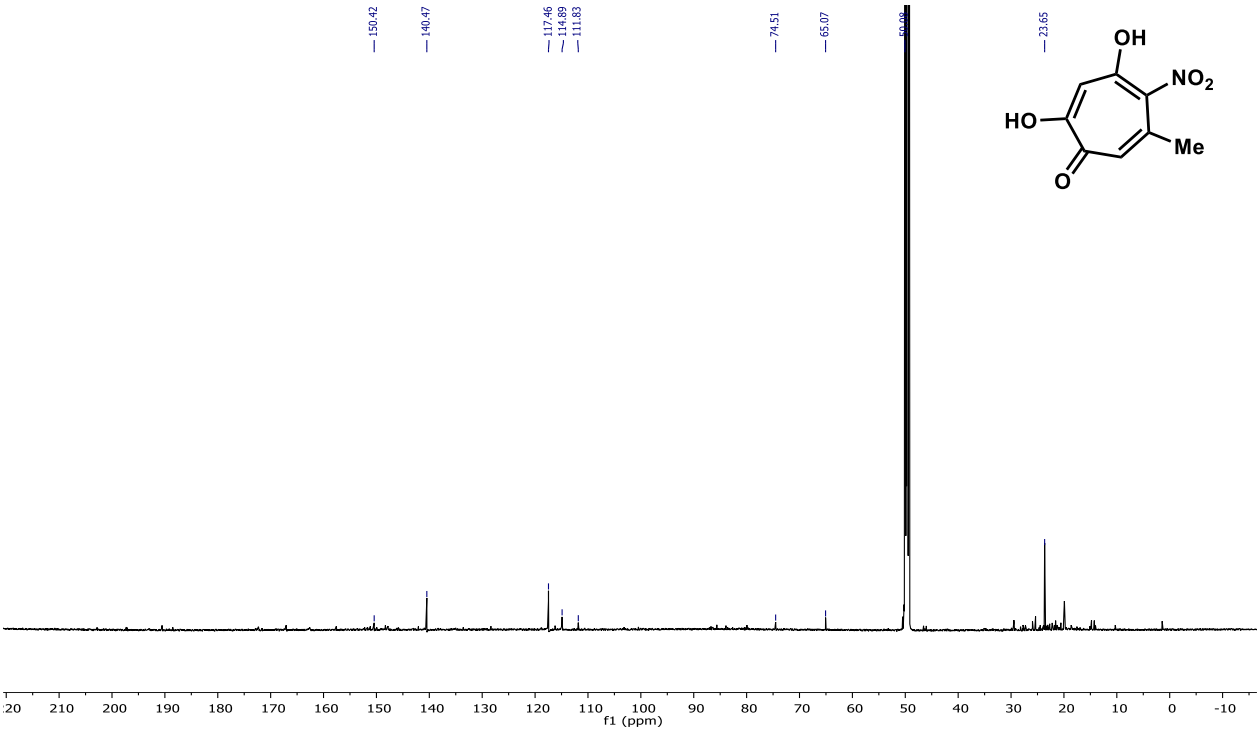
150.42
140.47
117.46
114.89
111.83
74.51
65.07
50.00
23.65
OH
NO2
HO
Me
O
f1 (ppm)

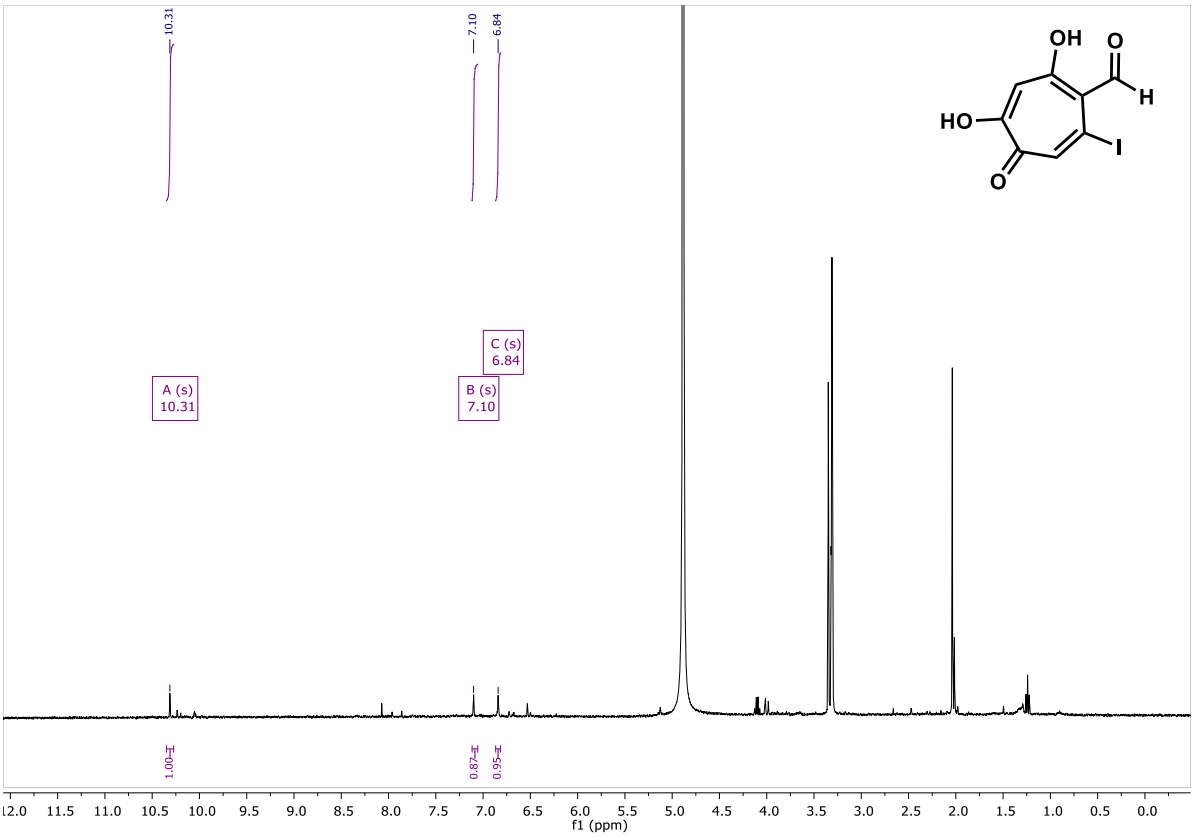
10.31
7.10
6.84
OH
O
H
HO
I
O
C (s)
6.84
A (s)
10.31
B (s)
7.10
1.00
0.87
0.95
f1 (ppm)

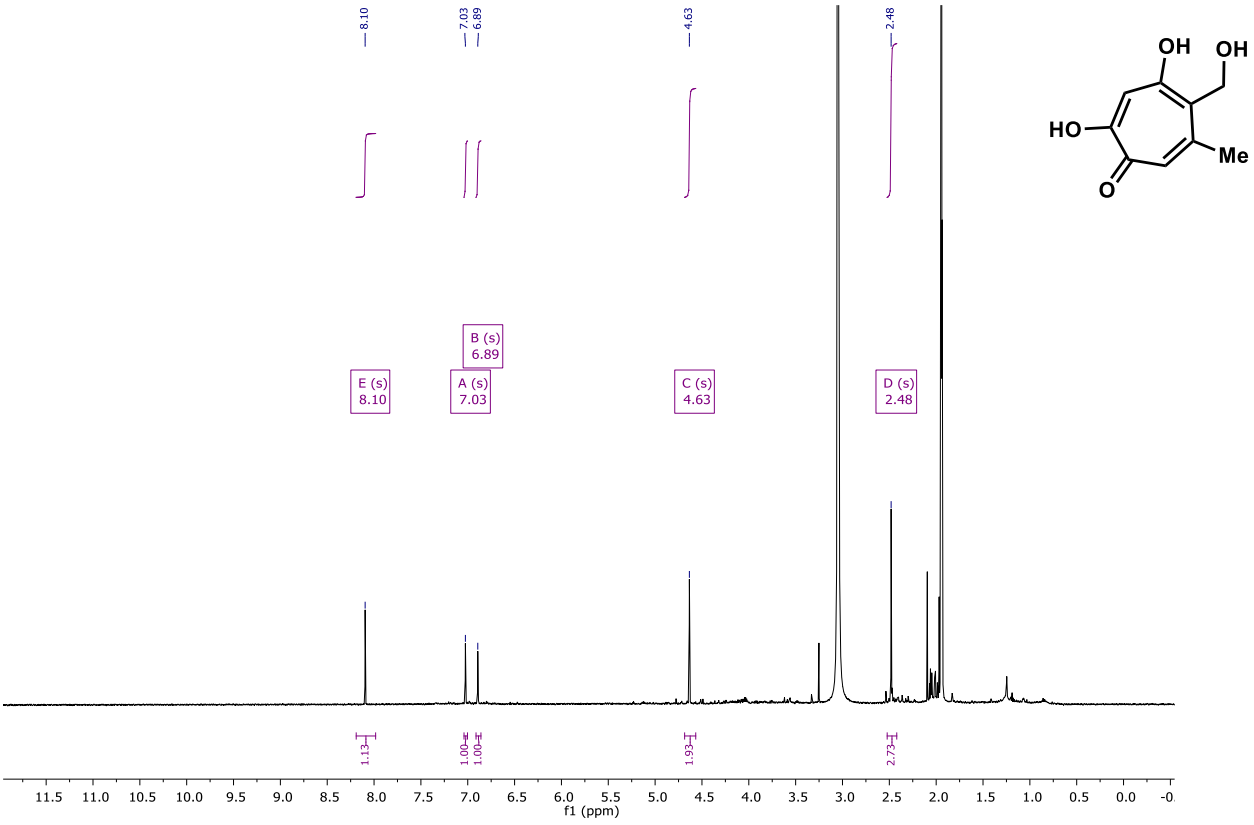
8.10
7.03
6.89
4.63
2.48
OH
OH
HO
Me
O
B (s)
6.89
E (s)
8.10
A (s)
7.03
C (s)
4.63
D (s)
2.48
1.13
1.00
1.00
1.93
2.73
f1 (ppm)

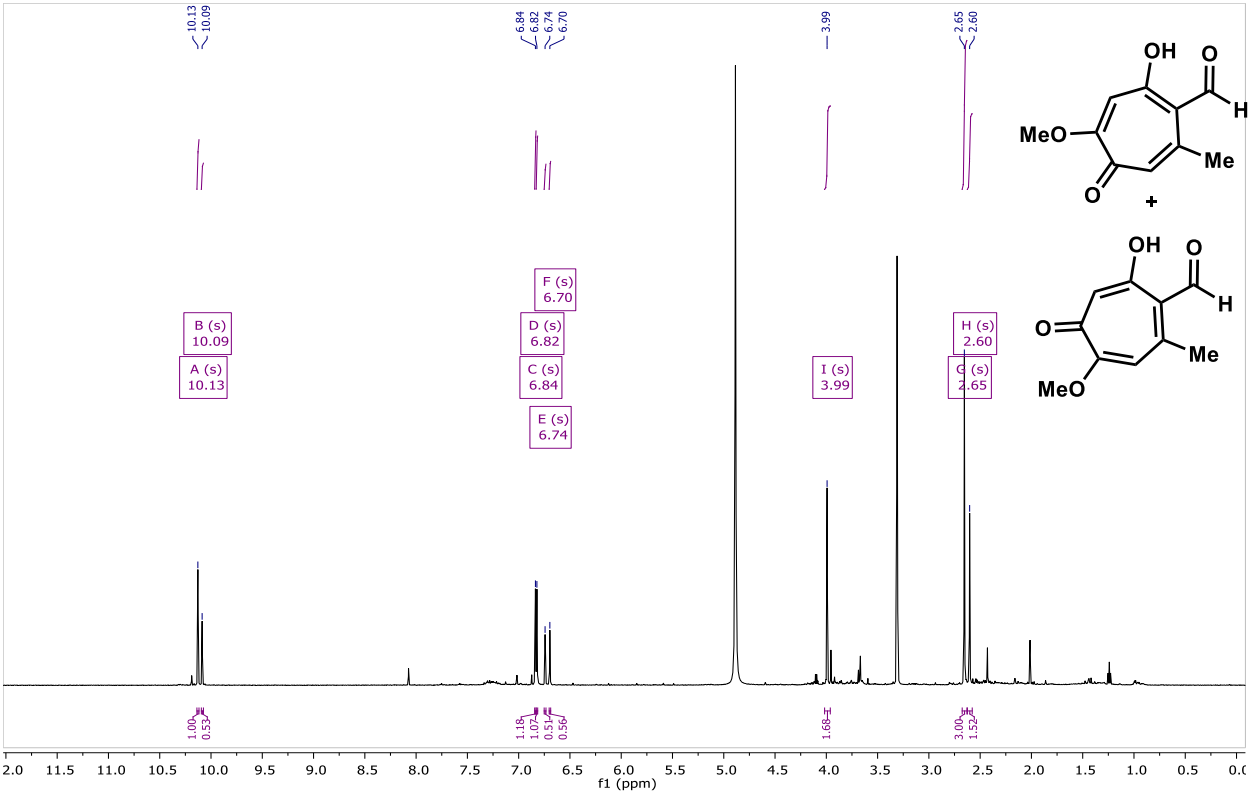
10.13
10.09
6.84
6.82
6.74
6.70
3.99
2.65
2.60
OH
O
H
MeO
Me
O
+
OH
O
H
O
Me
MeO
F (s)
6.70
B (s)
10.09
D (s)
6.82
H (s)
2.60
A (s)
10.13
C (s)
6.84
I (s)
3.99
G (s)
2.65
E (s)
6.74
1.00
0.53
1.18
1.07
0.51
0.56
1.68
3.00
1.52
f1 (ppm)

## 3.9 References


(1) Newman, D. J.; Cragg, G. M.; Kingston, D. G. I., Chapter 5 - Natural Products as Pharmaceuticals and Sources for Lead Structures. In *The Practice of Medicinal Chemistry (Fourth Edition)*, Wermuth, C. G.; Aldous, D.; Raboisson, P.; Rognan, D., Eds. Academic Press: San Diego, 2015; pp 101-139.

(2) Newman, D. J.; Cragg, G. M., Natural Products as Sources of New Drugs from 1981 to 2014. *J. Nat. Prod.* **2016,** *79* (3), 629-661.

(3) Beutler, J. A., Natural Products as a Foundation for Drug Discovery. *Curr. Protoc. Pharmacol.* **2009,** *46* (1), 9.11.1-9.11.21.

(4) Devine, P. N.; Howard, R. M.; Kumar, R.; Thompson, M. P.; Truppo, M. D.; Turner, N. J., Extending the application of biocatalysis to meet the challenges of drug development. *Nat. Rev. Chem.* **2018,** *2* (12), 409-421.

(5) Truppo, M. D., Biocatalysis in the Pharmaceutical Industry: The Need for Speed. *ACS Med. Chem. Lett.* **2017,** *8* (5), 476-480.

(6) Bucar, F.; Wube, A.; Schmid, M., Natural product isolation – how to get from biological material to pure compounds. *Nat. Prod. Rep.* **2013,** *30* (4), 525-545.

(7) Baran, P. S., Natural Product Total Synthesis: As Exciting as Ever and Here To Stay. *J. Am. Chem. Soc.* **2018,** *140* (14), 4751-4755.

(8) Hong, J., Natural Product Synthesis at the Interface of Chemistry and Biology. *Chem. Eur. J.* **2014,** *20* (33), 10204-10212.

(9) Bommarius, A. S., Biocatalysis: A Status Report. *Annu. Rev. Chem. Biomol. Engin.* **2015,** *6* (1), 319-345.

(10) Wells, A.; Meyer, H.-P., Biocatalysis as a Strategic Green Technology for the Chemical Industry. *ChemCatChem* **2014,** *6* (4), 918-920.

(11) Wohlgemuth, R., Biocatalysis—key to sustainable industrial chemistry. *Curr. Opin. Biotechnol.* **2010,** *21* (6), 713-724.

(12) Bornscheuer, U. T.; Huisman, G. W.; Kazlauskas, R. J.; Lutz, S.; Moore, J. C.; Robins, K., Engineering the third wave of biocatalysis. *Nature* **2012,** *485* (7397), 185-194.

(13) Walsh, C. T.; Moore, B. S., Enzymatic Cascade Reactions in Biosynthesis. *Angew. Chem. Intl. Ed.* **2019,** *58* (21), 6846-6879.

(14) Klas, K.; Tsukamoto, S.; Sherman, D. H.; Williams, R. M., Natural Diels–Alderases: Elusive and Irresistable. *J. Org. Chem.* **2015,** *80* (23), 11672-11685.

(15) Christianson, D. W., Structural and Chemical Biology of Terpenoid Cyclases. *Chem. Rev.* **2017,** *117* (17), 11570-11648.

(16) Li, F.; Zhang, X.; Renata, H., Enzymatic CH functionalizations for natural product synthesis. *Curr. Opin. Chem. Biol.* **2019,** *49*, 25-32.

(17) Rudroff, F.; Mihovilovic, M. D.; Gröger, H.; Snajdrova, R.; Iding, H.; Bornscheuer, U. T., Opportunities and challenges for combining chemo- and biocatalysis. *Nat. Catal.* **2018,** *1* (1), 12-22.

(18) Liu, N.; Song, W.; Schienebeck, C. M.; Zhang, M.; Tang, W., Synthesis of Naturally Occurring Tropones and Tropolones. *Tetrahedron* **2014,** *70* (49), 9281-9305.

(19) Guo, H.; Roman, D.; Beemelmanns, C., Tropolone natural products. *Nat. Prod. Rep.* **2019,** *36* (8), 1137-1155.

(20) Lu, G.; Lomonosova, E.; Cheng, X.; Moran, E. A.; Meyers, M. J.; Le Grice, S. F. J.; Thomas, C. J.; Jiang, J.-k.; Meck, C.; Hirsch, D. R.; D'Erasmo, M. P.; Suyabatmaz, D. M.; Murelli, R. P.; Tavis, J. E., Hydroxylated Tropolones Inhibit Hepatitis B Virus Replication by Blocking Viral Ribonuclease H Activity. *Antimicrob. Agents Chemother.* **2015,** *59* (2), 1070-1079.

(21) Budihas, S. R.; Gorshkova, I.; Gaidamakov, S.; Wamiru, A.; Bona, M. K.; Parniak, M. A.; Crouch, R. J.; McMahon, J. B.; Beutler, J. A.; Le Grice, S. F. J., Selective inhibition of HIV-1 reverse transcriptase-associated ribonuclease H activity by hydroxylated tropolones. *Nucleic Acids Res.* **2005,** *33* (4), 1249-1256.

(22) Miyamoto, D.; Kusagaya, Y.; Endo, N.; Sometani, A.; Seiji, T.; Suzuki, T.; Arima, Y.; Nakajima, K.; Yasuo, S., Thujaplicin–copper chelates inhibit replication of human influenza viruses. *Antivir. Res.* **1998,** *39* (2), 89-100.

(23) Oblak, E. Z.; Bolstad, E. S.; Ononye, S. N.; Priestley, N. D.; Hadden, M. K.; Wright, D. L., The furan route to tropolones: probing the antiproliferative effects of beta-thujaplicin analogs. *Org. Biomol. Chem.* **2012,** *10* (43), 8597-604.

(24) Angawi, R. F.; Swenson, D. C.; Gloer, J. B.; Wicklow, D. T., Malettinin A: a new antifungal tropolone from an unidentified fungal colonist of Hypoxylon stromata (NRRL 29110). *Tetrahedron Lett.* **2003,** *44* (41), 7593-7596.

(25) Silber, J.; Ohlendorf, B.; Labes, A.; Wenzel-Storjohann, A.; Näther, C.; Imhoff, J. F., Malettinin E, an antibacterial and antifungal tropolone produced by a marine Cladosporium strain. *Front. Marine Sci.* **2014,** *1* (35).

(26) Overy, D. P.; Berrue, F.; Correa, H.; Hanif, N.; Hay, K.; Lanteigne, M.; Mquilian, K.; Duffy, S.; Boland, P.; Jagannathan, R.; Carr, G. S.; Vansteeland, M.; Kerr, R. G., Sea foam as a source of fungal inoculum for the isolation of biologically active natural products. *Mycol.* **2014,** *5* (3), 130-144.

(27) Saleh, N. A.; Zwiefak, A.; Mordarski, M.; Pulverer, G., Antibacterial Activity of Selected Tropones and Tropolones. *Zentralbl. Bakteriol. Mikrobiol. Hyg. A* **1988,** *270* (1), 160-170.

(28) Yamato, M.; Hashigaki, K.; Kokubu, N.; Tsuruo, T.; Tashiro, T., Synthesis and antitumor activity of tropolone derivatives. 1. *J. Med. Chem.* **1984,** *27* (12), 1749-1753.

(29) Yamato, M.; Hashigaki, K.; Ishikawa, S.; Kokubu, N.; Inoue, Y.; Tsuruo, T.; Tashiro, T., Synthesis and antitumor activity of tropolone derivatives. 2. *J. Med. Chem.* **1985,** *28* (8), 1026-1031.

(30) Yamato, M.; Hashigaki, K.; Kokubu, N.; Tashiro, T.; Tsuruo, T., Synthesis and antitumor activity of tropolone derivatives. 3. *J. Med. Chem.* **1986,** *29* (7), 1202-1205.

(31) Yamato, M.; Hashigaki, K.; Sakai, J.; Kawasaki, Y.; Tsukagoshi, S.; Tashiro, T., Synthesis and antitumor activity of tropolone derivatives. 4. *J. Med. Chem.* **1987,** *30* (1), 117-120.

(32) Yamato, M.; Hashigaki, K.; Sakai, J.; Takeuchi, Y.; Tsukagoshi, S.; Tashiro, T.; Tsuruo, T., Synthesis and antitumor activity of tropolone derivatives. 5. *J. Med. Chem.* **1987,** *30* (7), 1245-1248.

(33) Yamato, M.; Hashigaki, K.; Yasumoto, Y.; Sakai, J.; Luduena, R. F.; Banerjee, A.; Tsukagoshi, S.; Tashiro, T.; Tsuruo, T., Synthesis and antitumor activity of tropolone derivatives. 6. Structure-activity relationships of antitumor-active tropolone and 8-hydroxyquinoline derivatives. *J. Med. Chem.* **1987,** *30* (10), 1897-1900.

(34) Yamato, M.; Ando, J.; Sakaki, K.; Hashigaki, K.; Wataya, Y.; Tsukagoshi, S.; Tashiro, T.; Tsuruo, T., Synthesis and antitumor activity of tropolone derivatives. 7. Bistropolones containing connecting methylene chains. *J. Med. Chem.* **1992,** *35* (2), 267-273.

(35) Hsiao, C.-J.; Hsiao, S.-H.; Chen, W.-L.; Guh, J.-H.; Hsiao, G.; Chan, Y.-J.; Lee, T.-H.; Chung, C.-L., Pycnidione, a fungus-derived agent, induces cell cycle arrest and apoptosis in A549 human lung cancer cells. *Chem. Biol. Interact.* **2012,** *197* (1), 23-30.

(36) El-Elimat, T.; Raja, H. A.; Ayers, S.; Kurina, S. J.; Burdette, J. E.; Mattes, Z.; Sabatelle, R.; Bacon, J. W.; Colby, A. H.; Grinstaff, M. W.; Pearce, C. J.; Oberlies, N. H., Meroterpenoids from Neosetophoma sp.: A Dioxa[4.3.3]propellane Ring System, Potent Cytotoxicity, and Prolific Expression. *Org. Lett.* **2019,** *21* (2), 529-534.

(37) Ayers, S.; Zink, D. L.; Powell, J. S.; Brown, C. M.; Grund, A.; Bills, G. F.; Platas, G.; Thompson, D.; Singh, S. B., Noreupenifeldin, a Tropolone from an Unidentified Ascomycete. *J. Nat. Prod.* **2008,** *71* (3), 457-459.

(38) Pauson, P. L., Tropones and Tropolones. *Chem. Rev.* **1955,** *55* (1), 9-136.

(39) Doering, W. v. E.; Knox, L. H., Synthesis of Substituted Tropolones. *J. Am. Chem. Soc.* **1953,** *75* (2), 297-303.

(40) Doering, W. v. E.; Knox, L. H., Tropolone. *J. Am. Chem. Soc.* **1951,** *73* (2), 828-838.

(41) Kaneko, S.-i.; Matsui, M., Synthetic Studies on Colchicine-related Tropolones. *Agr. Biol. Chem.* **1968,** *32* (8), 995-1001.

(42) Scott, A. I.; McCapra, F.; Buchanan, R. L.; Day, A. C.; Young, D. W., Total synthesis of colchicine modelled on a biogenetic theory. *Tetrahedron* **1965,** *21* (12), 3605-3631.

(43) Seto, S.; Matsumura, S.; Ro, K., Synthesis of β-Dolabrin from β-Thujaplicin (Hinokitiol). *Chem. Pharm. Bull.* **1962,** *10* (10), 901-905.

(44) Arican, D.; Brückner, R., Syntheses of 3,4-Benzotropolones by Ring-Closing Metatheses. *Org. Lett.* **2013,** *15* (11), 2582-2585.

(45) Mori, M., Synthesis of Natural Products and Related Compounds using Enyne Metathesis. *Adv. Synth. Catal.* **2007,** *349* (1-2), 121-135.

(46) Boyer, F.-D.; Hanna, I., Synthesis of the Tricyclic Core of Colchicine via a Dienyne Tandem Ring-Closing Metathesis Reaction. *Org. Lett.* **2007,** *9* (12), 2293-2295.

(47) Donald, J. R.; Unsworth, W. P., Ring-Expansion Reactions in the Synthesis of Macrocycles and Medium-Sized Rings. *Chem. Eur. J.* **2017,** *23* (37), 8780-8799.

(48) Reisman, S. E.; Nani, R. R.; Levin, S., Buchner and Beyond: Arene Cyclopropanation as Applied to Natural Product Total Synthesis. *Synlett* **2011,** *2011* (17), 2437-2442.

(49) Davison, J.; al Fahad, A.; Cai, M.; Song, Z.; Yehia, S. Y.; Lazarus, C. M.; Bailey, A. M.; Simpson, T. J.; Cox, R. J., Genetic, molecular, and biochemical basis of fungal tropolone biosynthesis. *Proceed. Natl. Acad. Sci.* **2012,** *109* (20), 7642-7647.

(50) Zhai, Y.; Li, Y.; Zhang, J.; Zhang, Y.; Ren, F.; Zhang, X.; Liu, G.; Liu, X.; Che, Y., Identification of the gene cluster for bistropolone-humulene meroterpenoid biosynthesis in Phoma sp. *Fungal. Genet. Biol.* **2019,** *129*, 7-15.

(51) Schor, R.; Schotte, C.; Wibberg, D.; Kalinowski, J.; Cox, R. J., Three previously unrecognised classes of biosynthetic enzymes revealed during the production of xenovulene A. *Nat. Commun.* **2018,** *9* (1), 1963.

(52) Cox, R., Oxidative rearrangements during fungal biosynthesis. *Nat. Prod. Rep.* **2014,** *31* (10), 1405-24.

(53) Cox, R. J.; Al-Fahad, A., Chemical mechanisms involved during the biosynthesis of tropolones. *Curr. Opin. Chem. Biol.* **2013,** *17* (4), 532-6.

(54) Adlington, R. M.; Baldwin, J. E.; Mayweg, A. V. W.; Pritchard, G. J., Biomimetic Cycloaddition Approach to Tropolone Natural Products via a Tropolone Ortho-quinone Methide. *Org. Lett.* **2002,** *4* (17), 3009-3011.

(55) Beemis, C., Synthesis of Sesquiterpene-Tropolones. *Dissertation* **2019**.

(56) Chen, Q.; Gao, J.; Jamieson, C.; Liu, J.; Ohashi, M.; Bai, J.; Yan, D.; Liu, B.; Che, Y.; Wang, Y.; Houk, K. N.; Hu, Y., Enzymatic Intermolecular Hetero-Diels–Alder Reaction in the Biosynthesis of Tropolonic Sesquiterpenes. *J. Am. Chem. Soc.* **2019,** *141* (36), 14052-14056.

(57) Ononye, S. N.; VanHeyst, M. D.; Oblak, E. Z.; Zhou, W.; Ammar, M.; Anderson, A. C.; Wright, D. L., Tropolones As Lead-Like Natural Products: The Development of Potent and Selective Histone Deacetylase Inhibitors. *ACS Med. Chem. Lett.* **2013,** *4* (8), 757-761.

(58) Ismaya, W. T.; Rozeboom, H. J.; Weijn, A.; Mes, J. J.; Fusetti, F.; Wichers, H. J.; Dijkstra, B. W., Crystal Structure of Agaricus bisporus Mushroom Tyrosinase: Identity of the

Tetramer Subunits and Interaction with Tropolone. *Biochemistry* **2011,** *50* (24), 5477-5486.

(59) Baker Dockrey, S. A.; Lukowski, A. L.; Becker, M. R.; Narayan, A. R. H., Biocatalytic site- and enantioselective oxidative dearomatization of phenols. *Nat. Chem.* **2018,** *10* (2), 119-125.

# Chapter 4: Characterization of the Mechanism of Ring Expansion in NHI Enzyme-catalyzed Tropolone Synthesis

## 4.1 Introduction

Enzymes from secondary metabolic pathways catalyze challenging transformations with exquisite control over chemo-, site- and stereoselectivity, directing the synthesis of structurally-complex products from bioavailable starting materials. These transformations often take advantage of the three-dimensional architecture of the enzyme active site to guide reactive intermediates toward formation of the desired product.[1] Biocatalytic control over the fate of reactive intermediates is a common mechanistic archetype in a variety of enzymes such as cyclases, which leverage active site geometries to induce selective cyclization reactions, polyketide synthases that deliver specific products from large, structurally-complex intermediates, Diels-Alderases, which choreograph the relative position of two reactive components to form a stereo-enriched product, and non-heme iron (NHI) dioxygenases, an enzyme class known to catalyze numerous skeletal rearrangements through radical or polar mechanisms.[1-4] In many cases, reactions of identical intermediates generated outside of the enzyme active site proceed in an uncontrolled fashion, leading to racemic products or fundamentally divergent reactivity.[1-2]

In contrast to the selectivity demonstrated by enzyme-mediated transformations, small molecule-enabled transformations often require careful substrate design to achieve a desired rearrangement, adding synthetic steps and reducing the efficiency and sustainability of the

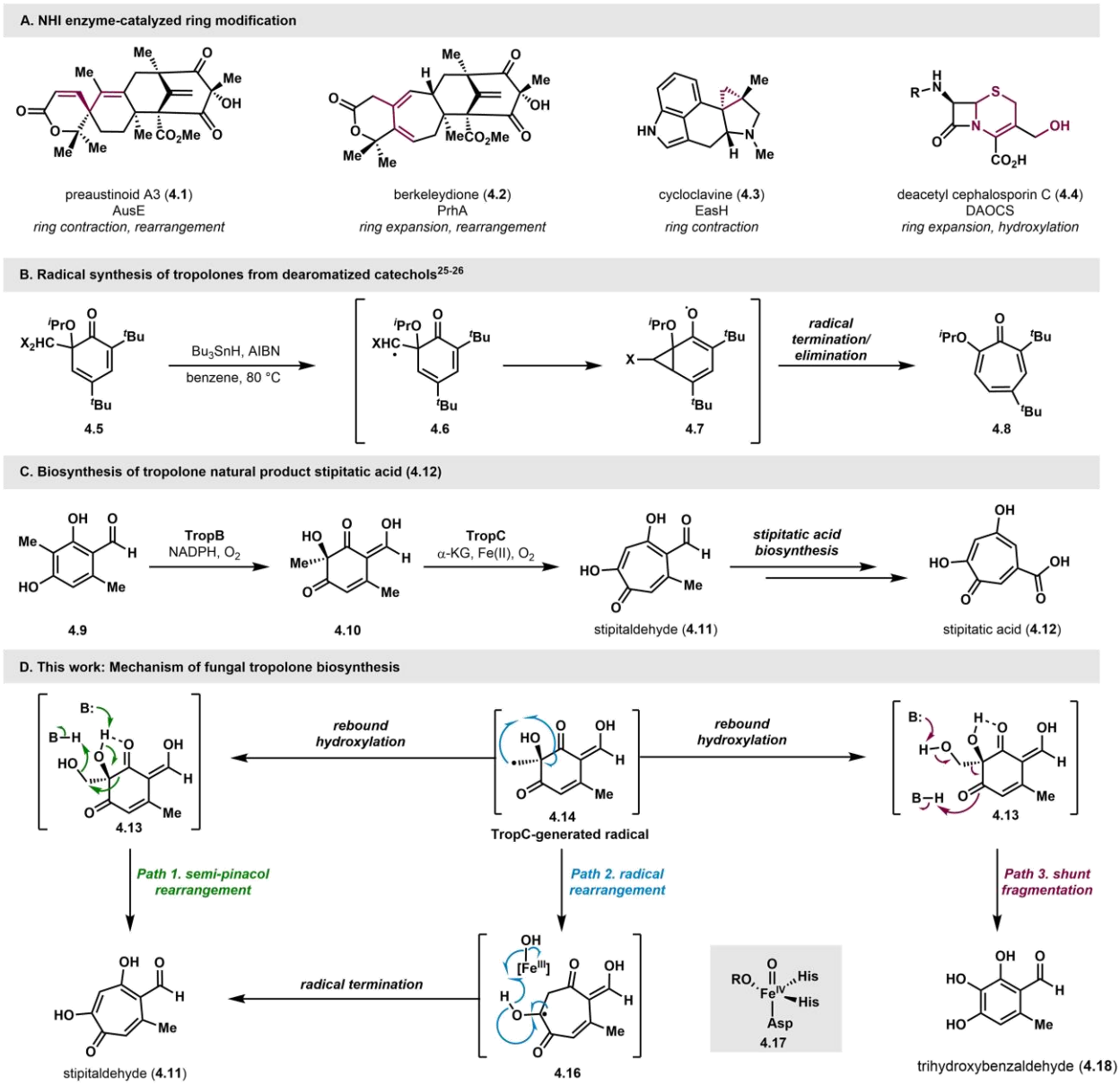


**Figure 4.1. Ring rearrangements in natural product scaffold synthesis and biosynthesis.** A. Ring rearrangement reactions catalyzed by NHI enzymes. B. Radical tropolone synthesis from dearomatized *ortho*-phenols. C. Biosynthesis of stipitaldehyde (**4.11**) on path to fungal tropolone natural products. D. This work: Mechanistic studies of ring expansion in NHI enzyme TropC.

resulting syntheses.[5-6] Radical-based rearrangements are particularly impacted by selectivity challenges, as competing radical pathways often complicate anticipated reaction outcomes.[5-6] As a result, selectivity can be achieved only through optimization of substrate design and reaction

conditions to favor the desired reaction pathway.[5-6] In comparison, biocatalysts operate with precise control over the reaction outcome, enabling highly selective and direct synthesis of natural product scaffolds.[7-9] Therefore, thorough examination of the mechanistic details of enzyme-catalyzed rearrangements is critically important to the development of novel, selective approaches to complex molecule synthesis.

Non-heme iron (NHI) enzymes perform an array of oxidative transformations and rearrangements in secondary metabolism.[4, 10-11] Members of the α-ketoglutarate-dependent family of NHI dioxygenases couple the oxidative decarboxylation of α-ketoglutarate (α-KG) to the activation of molecular oxygen, generating an iron(IV)-oxo species (**4.17**, Figure 4.1D).[12-13] Through this common mechanism of oxygen activation, NHI enzymes catalyze a variety of selective transformations that are often initiated by hydrogen atom abstraction, followed by a variety of processes including hydroxylation, desaturation, halogenation, endoperoxidation, epimerization, ring expansion and ring contraction, among others.[4, 11-13] Understanding how the fate of a radical intermediate is controlled by each catalyst has motivated structural, spectroscopic and computational studies of NHI enzymes. In-depth interrogation of NHI-catalyzed reaction mechanisms has revealed critical enzyme-substrate interactions that dictate the reaction outcome in several cases.[7-9] These studies provide mechanistic detail for several NHI-catalyzed rearrangements, including ring contractions and ring expansions.[14-17] Ring-modifying transformations often proceed through an initial C–H atom abstraction, followed by radical rearrangement and termination by single electron oxidation or hydroxylation to yield product.[7-9, 14-17] The NHI active site architecture dictates the reaction outcome by exerting fine control over events downstream from hydrogen atom abstraction, enabling highly selective transformations.[7-9, 14-17] For example, AusE and PrhA are highly related NHI enzymes (78% sequence ID) that catalyze

divergent transformations on a common substrate to generate preaustinoid A3 (**4.1**) and berkeleydione (**4.2**), respectively (Figure 4.1A).[7-9] Structural and computational studies have shown that minor differences in their active site architecture play a critical role in determining the outcome of the initial enzyme-catalyzed desaturation, ultimately leading to the formation of two distinct natural products through a divergent radical rearrangement process.[7, 9] Similar mechanistic studies found that the NHI-catalyzed biosynthesis of cycloclavine (**4.3**) and deacetoxy-cephalosporin C (**4.4**) proceed through a one-electron reaction pathway, suggesting a common mechanistic architype for ring rearrangements catalyzed by NHI enzymes (Figure 4.1A).[14-16, 18]

Natural products often possess medium-sized rings (7-11 atoms) which can be difficult to access using small molecule techniques. One such class of synthetically-challenging targets are tropolones, a structurally-diverse group of bioactive metabolites with an aromatic cycloheptatriene core structure containing an α-hydroxyketone moiety (see Figure 4.1C, **4.11**).[19-21] Tropolones have been synthesized through a variety of approaches, typically involving ring expansion.[22] These transformations include classic two-electron rearrangements such as the Büchner reaction,[23] the de Mayo fragmentation[24] and [5+2] cycloadditions.[22] In addition, radical-based approaches have been successful in synthesizing tropolones from *ortho*-dearomatized catechols (**4.5**) through a selective radical ring expansion mechanism (Figure 4.1B).[25-26] This approach required pre-functionalization of the arene to ensure that radical initiation occurred at the methyl halide *ipso* to the site of dearomatization, leading to the desired rearrangement (Figure 4.1B).[25-26] While these methods have been successful in enabling ring expansion, they require arduous synthetic efforts to achieve the desired substitution pattern of the tropolone natural product, preventing facile access to the target compound.[22] In contrast, Nature efficiently assembles complex tropolones using available biosynthetic machinery. In fungi, the identification of the stipitatic acid (**4.12**)

biosynthetic gene cluster in *T. stipitatus* provided a blueprint for the assembly of these aromatic seven-membered rings in Nature (Figure 4.1C).[21] Fungal tropolone biosynthesis, in the case of stipitatic acid, commences with polyketide synthase production of 3-methylorcinaldehyde (**4.9**) and subsequent flavin-dependent monooxygenase-mediated oxidative dearomatization.[21, 27] It has been established that the resulting dienone (**4.10**) undergoes an oxidative ring expansion catalyzed by an α-KG-dependent NHI enzyme, TropC, to afford stipitaldehyde (**4.11**). Downstream enzymatic modifications of stipitaldehyde (**4.11**) generate stipitatic acid (**4.12**).[21] Since the identification and characterization of enzymes involved in stipitatic acid biosynthesis, several other tropolone natural products have been shown to proceed through the same oxidative dearomatization/ring expansion cascade to generate the tropolone core.[28-29] Motivated to understand the chemical steps of this powerful transformation, we initiated our studies on the chemistry and mechanism of the TropC-catalyzed ring expansion. In particular, we sought to investigate two transformations which TropC has been shown to catalyze (1) ring expansion to generate stipitaldehyde (**4.11**) and (2) a fragmentation reaction which produces 3-hydroxyorcinaldehyde (**4.18**), a known shunt product in fungal tropolone biosynthesis (Figure 4.1D).

As the fate of a radical intermediate in NHI dioxygenase-catalyzed transformations is critical to the observed reactivity of the enzyme, we envisioned that TropC-catalyzed ring expansion could occur through several possible mechanistic pathways. Cox and coworkers initially proposed that TropC performs a polar ring expansion to produce stipitaldehyde (**4.11**, Figure 4.1D, Path 1).[19-21] Their proposal commences with TropC-mediated C–H atom abstraction on dienone **4.10** to generate radical species **4.14**.[19-21] Subsequent rebound hydroxylation would afford diol **4.13**, which is proposed to undergo a semi-pinacol rearrangement to form stipitaldehyde (**4.11**).

We anticipated that this rearrangement could be assisted by residues in the TropC active site through activation of the alcohol leaving group in diol intermediate **4.13**.[19-21] The proposed ring expansion mechanism is also consistent with the observed formation of a shunt product in this biosynthetic pathway, **4.18**, which is anticipated to arise through loss of formaldehyde and concomitant rearomatization to produce 3-hydroxyorcinaldehyde **4.18** (Figure 4.1D, Path 3).[21] Based on the radical reaction pathways that have been proposed for other ring modifying enzymes, we envisioned an alternative mechanism to arrive at stipitaldehyde in which radical **4.14** directly undergoes ring expansion, followed by radical termination via a single electron oxidation involving the iron(III)-hydroxyl species (Figure 4.1D, Path 2). Under this model, the product generated by the enzyme is determined by the radical termination process which occurs in the active site. If rebound hydroxylation predominates, then 3-hydroxyorcinaldehyde (**4.18**) will be the major product formed. If radical rearrangement is preferred under the reaction conditions, then stipitaldehyde (**4.11**) formation will dominate. To decipher the ring expansion mechanism used by TropC, we aimed to investigate the active site architecture of the enzyme, as well as the reactivity of proposed ring expansion intermediate **4.13**.

### 4.2 Computational analysis of proposed ring expansion pathways

To determine the nature of the TropC-catalyzed ring expansion, a computational analysis of the proposed pathways was carried out by our collaborator Kevin Skinner, under the guidance of Prof. Paul Zimmerman (Figure 4.1D). Through these calculations, we aimed to compare the relative barriers of proposed ring expansion pathways to assess the feasibility of a one- or two-electron ring expansion mechanism. Each mechanistic pathway was evaluated using a small molecule NHI mimetic complex (see Figure 4.S32). We manually performed tautomerization of

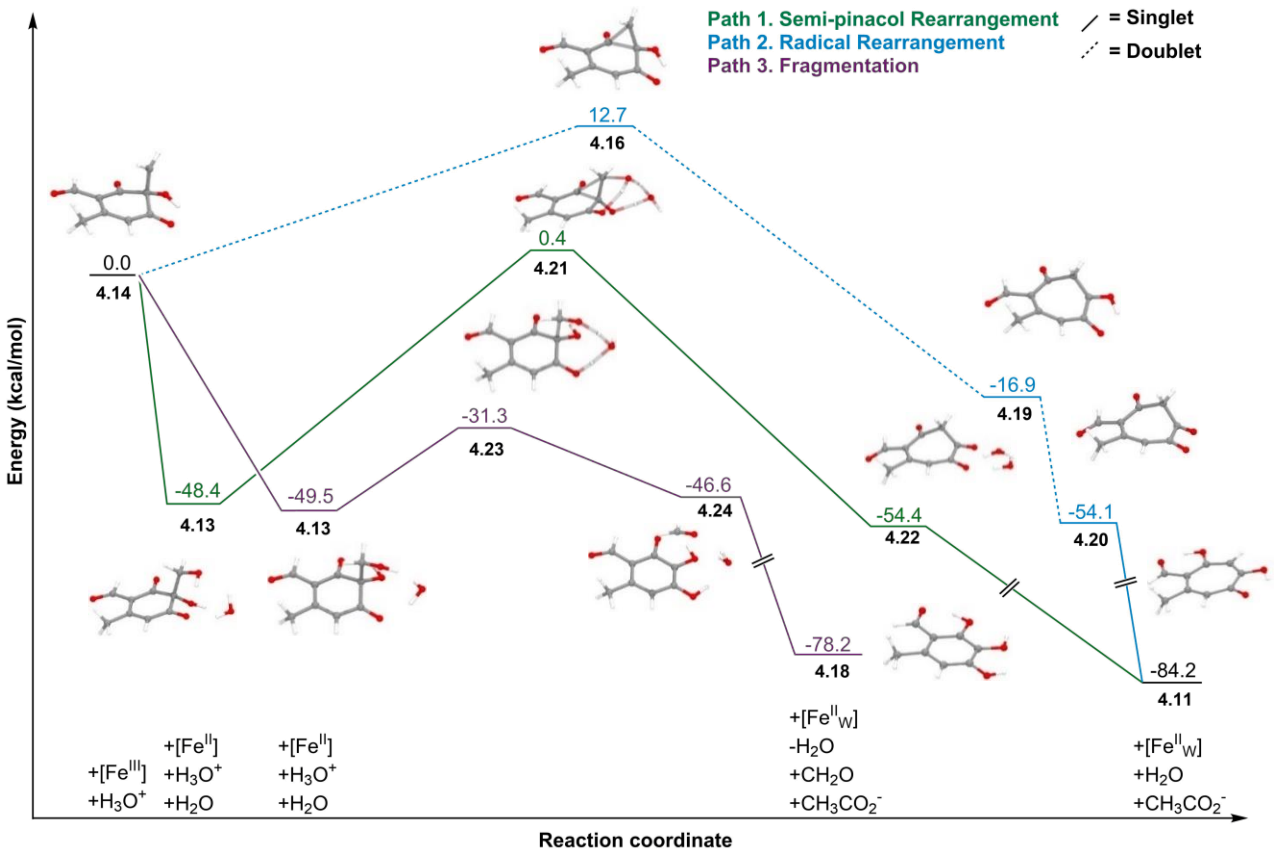


**Figure 4.2. QM calculations for TropC-catalyzed reaction pathways to generate stipitaldehyde (4.11) and 3-hydroxyorcinaldehyde 4.18.** *Analysis performed by Kevin Skinner.*

reaction pathway products to model stipitaldehyde (**4.11**) and the 3-hydroxyorcinaldehyde shunt product **4.18** as protonated, neutral structures, reflecting the enzymatic reaction conditions for TropC-catalyzed ring expansion (pH 7.0). Water molecules were used as proton shuttles to mimic the protonation and deprotonation events that would be facilitated by residues in the enzyme active site.

These computational investigations were initiated using the radical intermediate **4.14** (Figure 4.2), which is the divergence point for each of the pathways along the potential energy surface (PES). We first explored the radical rearrangement (Path 2), which occurs with a barrier of 12.7 kcal/mol (**4.16**). A subsequent H-atom abstraction by an iron(III)-hydroxyl species to

produce the tautomer of stipitaldehyde (**4.11**) was calculated to be barrierless. This calculation was supported by literature precedent which demonstrated that tropolones could be synthesized from *ortho*-dearomatized radicals (Figure 4.1B).[22, 26] We then explored the rebound hydroxylation and semi-pinacol rearrangement (Path 1). As expected, rebound hydroxylation to produce diol **4.13** was found to be a barrierless process in our active site model.[12, 30-31] In an enzyme active site, we anticipate that substrate movement and alignment would be restricted by local residues, resulting in thermodynamic barriers to this process.[12, 30-31] The barrier for the proposed semi-pinacol rearrangement was observed to be excessively high at 48.8 kcal/mol (**4.24**), indicating that this transformation is not likely to occur. These barriers are in agreement with computational analysis by Siegbahn and coworkers examining ring expansion mechanisms of *ortho*-dearomatized phenols, indicating that a semi-pinacol type ring expansion is unlikely to occur in these systems.[32] In comparison, fragmentation to afford an aromatic product from diol **4.13** (Path 3) to produce formaldehyde and 3-hydroxyorcinaldehyde **4.18** was found to be a low barrier process at 18.2 kcal/mol (**4.23**). These calculations suggest that diol **4.13** favorably undergoes fragmentation and rearomatization (Path 3), rather than the proposed semi-pinacol ring expansion (Path 1). The calculated low barrier for Path 3 is supported by experimental observation of 3-hydroxyorcinaldehyde formation during the TropC-catalyzed reaction. Taken together, the QM simulations support our alternative mechanistic proposal in which the radical rearrangement is a kinetically and thermodynamically accessible route towards tropolone formation (Path 2).

### 4.3 X-ray crystal structure of wild-type TropC

Next, we sought experimental evidence to discriminate between the two reaction pathways under consideration for TropC-catalyzed ring expansion. We aimed to further interrogate the

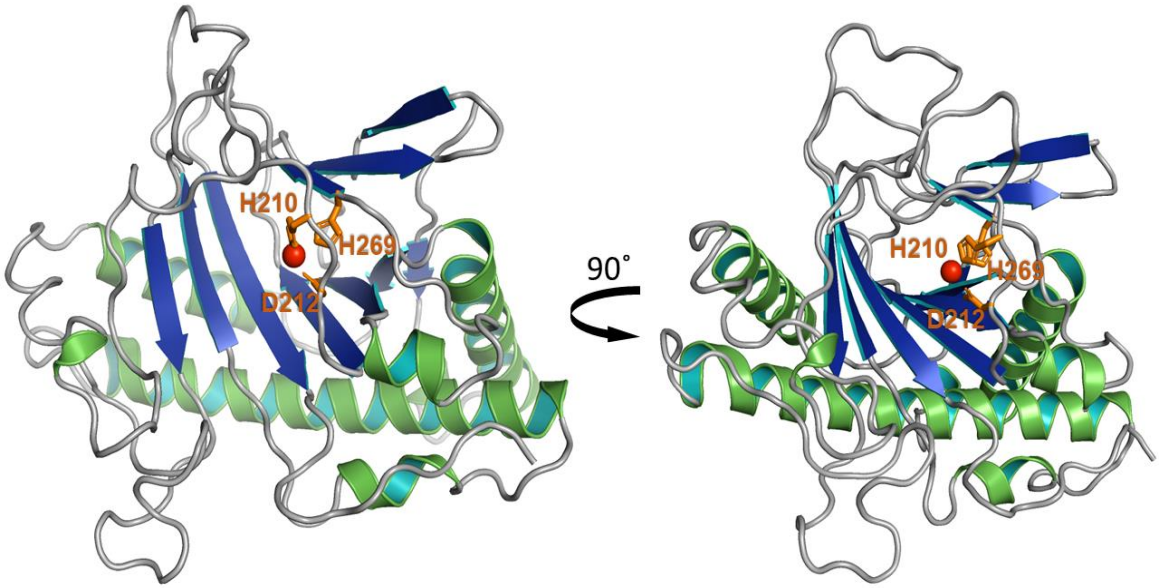


**Figure 4.3. Overall architecture of TropC determined using X-ray crystallography (PDB ID: 6XJJ).**
(Left) Structure of TropC from *T. stipitatus* in ribbon representation. At the core of TropC, the Fe (III) shown with red sphere and side chain of residues, H210, D212 and H269, are shown in stick representation. (Right) Rotated view of crystal structure of TropC and active site located at the center of the protein. *Structure generated by Dr. Leena Mallik and Prof. Markos Koutmos.*

proposed ring expansion mechanisms by performing a detailed mutational analysis of TropC in order to determine if specific active site residues are responsible for catalyzing the ring expansion to the tropolone. To gain structural information, we purified TropC to homogeneity and provided materials to our structural biology collaborators Dr. Leena Mallik and Prof. Markos Koutmos, who obtained TropC crystals using the sitting drop vapor diffusion method (see Section 4.7 Experimental for details). Following data collection, we found that TropC crystallized in the $P3_121$ space group with two molecules of TropC in the asymmetric unit (PDB ID: 6XJJ). The crystal structure of unliganded TropC was solved at a resolution of 2.7 Å with the molecular replacement method using the structure of thymine-7-hydroxylase (T7H) of *Neurospora crassa* as a search model (Figure 4.3).[33] Our analysis of the structural data indicated that TropC adopts a similar

architecture as other α-KG-dependent NHI dioxygenases [34]. The three-dimensional structure of TropC consists of double-stranded β-helix (DSBH or jelly-roll) fold at the core of the protein [34]. The DSBH core of TropC is comprised of ten anti-parallel β-strands, which form two β-sheets, called major and minor β-sheets. Major β-sheets of TropC include β1-5, β8 and β10, and the minor β-sheet consists of β6, β7 and β9 (Figure 4.S29). The exterior of the major β-sheets of the DSBH fold is surrounded by α-helices (α1-3, α5 and α7) to form a compact globular structure.

Structures similar to TropC in the Protein Data Bank (PDB) were explored by using the DALI server (Table 4.S2),[35] revealing the highly similar structures of isopenicillin N synthase from *Pseudomonas aeruginosa* PAO1 (*Pa*IPNS, PDB ID: 6JYV, Z-score: 32.2)[36] and thymine-7-hydroxylase (T7H, PDB ID: 5C3Q, Z-score: 31.8) of *Neurospora crassa*.[36] An overall structural comparison of TropC with *Pa*IPNS and T7H suggested a putative substrate binding site for TropC (Figure 4.S30). Overlaying TropC with T7H revealed several shared residues which define the substrate binding site in the T7H structure (Figure 4.S31).[33] Specifically, residues F284 and F213 align well with two conserved aromatic residues in T7H, F292 and Y217, respectively.[33] F292 and Y217 have been demonstrated as critical for substrate binding and alignment in T7H, with F292 providing π-π stacking interactions that align thymine in the enzyme active site for productive catalysis.[33] The conservation of these aromatic residues in homologs of T7H and their alignment with F284 and F213 in TropC suggests that these residues may play an analogous role in substrate alignment.[33] In addition, bound metal ion was observed in the structure of TropC, which was refined to be Fe. As has been observed with the active site of other α-KG-dependent NHI dioxygenases, our structure demonstrates that the conserved HxD/E…H metal binding residues are involved in interaction with Fe.[33-34, 36] Specifically, our data showed the coordination of

residues H210, D212 and H269 (located at the loop between β4-5 and β9) to the active site Fe atom (Figure 4.3).

### 4.4 Computational modelling of TropC-substrate-cosubstrate complex and alanine-scan of TropC active site

Crystallography experiments yielded vital information on structural features of TropC and enabled further investigation of mechanistic considerations by computational and mutagenic analysis. Toward this goal, we anticipated that an enzyme-substrate complex would provide critical information for determining which active site residues are involved in mediating the ring expansion. To construct a computational substrate-bound model, Kevin Skinner, Dr. Troy Wymore and Prof. Paul Zimmerman modeled the missing electron density from the C-terminus and used an overlaid structure of T7H to establish the coordinates of critical enzyme cofactors, such as α-KG, ferrous iron and substrate (see Section 4.7 Experimental for model construction and simulation details). To prepare the model for substrate binding studies, they performed a molecular mechanics (MM) minimization over 5000 steps. The system was then prepared for a combined quantum mechanics and molecular dynamics (QM/MD) simulation. The system was subjected to three phases of MD simulations in which the system was heated, equilibrated, and sampled for a total of 12 ns to generate an enzyme-substrate-cosubstrate complex with the appropriate geometry and alignment for C–H atom abstraction (see Section 4.7 Experimental for details).

Our analysis of the substrate-bound TropC model revealed that substrate **4.10** was flanked by numerous active site residues that could potentially be involved in substrate binding or catalysis (Figure 4.4C). Residues from the TropC substrate pocket were identified and selected for alanine screening to determine if specific amino acids are critical for the ring expansion process. We

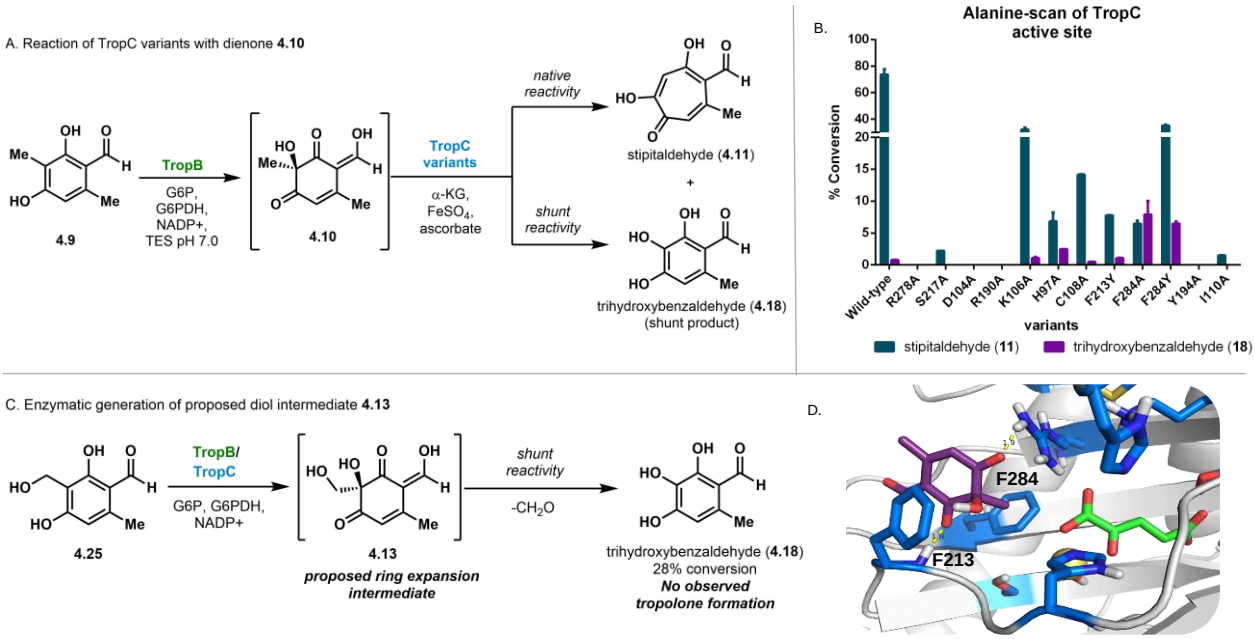


**Figure 4.4. Analysis of TropC variant reactivity and enzymatic synthesis of proposed ring expansion intermediate 4.13.** A. Oxidative dearomatization and ring expansion cascade to generate stipitaldehyde (**4.11**) and 3-hydroxyorcinaldehyde (**4.18**). B. Product profiles observed in alanine-scanning of TropC active site residues. C. Enzymatic synthesis of proposed ring expansion intermediate, diol **4.13**. D. Close-up view of substrate-bound model of TropC with select targeted alanine-scanning residues highlighted in blue, α-KG highlighted in green and the substrate shown in purple.

anticipated that a TropC variant, without the required residue for a polar, semi-pinacol-type ring expansion, would be unable to generate stipitaldehyde (**4.11**), resulting in a change to the ratio of observed enzyme products toward formation of the shunt product, **4.18** (Figure 4.4A). We carried out mutagenesis of twelve active site residues, generating the corresponding alanine variants (Figure 4.4B and Figure 4.S2) as well as variants with isosteric and isoelectronic residues at the same position. These residues were chosen using the substrate-bound TropC model as a guide and were selected for their proximity to the substrate as well as their ability to participate in the proposed reaction pathways. Many of the resulting variants were soluble, but catalytically inactive, suggesting that the structural changes in some variants prevented productive catalysis. Catalytically active variants exhibited reduced enzymatic conversion to products, but the product

profiles were largely unaltered, and stipitaldehyde (**4.11**) remained the major product under the reaction conditions, suggesting that most of the substrate-flanking residues were not involved in catalysis. However, the F284A variant uniquely demonstrated a shift in the product profile to produce nearly equimolar amounts of stipitaldehyde (**4.11**) and 3-hydroxyorcinaldehyde (**4.18**). Analysis of the substrate-bound TropC model suggests that this residue could be important for positioning of the substrate in the active site. This proposed role is analogous to the function of residue F292 in T7H, which has been shown to be critical for binding and alignment of substrate for productive catalysis. The binding mode of substrate **4.10** in the TropC MD simulation demonstrates that F284 and F213 flank the substrate in the active site, potentially guiding the proper alignment for C–H atom abstraction. This proposal is likewise analogous to the reported role of F292 and Y217 in T7H, suggesting a similar function in aligning the TropC substrate to achieve catalysis.[33] To further investigate this hypothesis, we generated the isosteric variant TropC F284Y which reconstituted the ring expansion activity of the enzyme, providing further evidence that F284 is a critical residue for determining the product mixtures generated by TropC. We aimed to further analyze this reaction by generating a TropC F213A variant but were unable to produce soluble protein with this construct. Despite this challenge, the data generated through alanine scanning of the TropC active site suggested that substrate alignment plays a role in determining the product profile of the enzyme. Perturbations of this alignment often result in a change to the products generated by the enzyme, providing clues about the mechanism of the transformation.[7, 9] In particular, substrate alignment relative to the iron(III)-hydroxyl species is key in discriminating whether rebound hydroxylation occurs over other NHI-catalyzed reactivity, such as halogenation.[37] In the context of our TropC model, these observations support the proposed mechanistic pathway for radical ring expansion (Path 1) in which the fate of the radical

(rearrangement versus rebound hydroxylation) determines which product is generated by the enzyme. In addition, mutagenic changes to polar residues did not produce a corresponding shift in the product profile to the production of 3-hydroxyorcinaldehyde **4.18**, suggesting that local acid or base catalysis does not drive a ring expansion mechanism (Figure 4.1D, Path 1).

### 4.5 Chemoenzymatic synthesis of proposed ring expansion intermediate 4.13

We aimed to further interrogate the proposed semi-pinacol rearrangement (Figure 4.1D, Path 1) by evaluating the reactivity of the proposed diol intermediate **4.13**. To generate the target diol in the absence of TropC, a biocatalytic approach was employed using CitB and TropB.[21, 27, 38-40] We aimed to directly synthesize diol **4.13** through oxidative dearomatization of benzylic alcohol **4.25** using TropB. Notably, 3-hydroxyorcinaldehyde **4.18** was detected in these reactions, but diol intermediate **4.13** was not observed, suggesting that the fragmentation reaction described in Path 3 (Figure 4.1D) occurs spontaneously under the reaction conditions. To further probe whether diol **4.13** is a ring expansion intermediate in TropC catalysis, we again performed a TropB-catalyzed oxidative dearomatization of benzylic alcohol **4.25** and included TropC in this reaction. We envisioned that diol **4.13**, when generated *in situ*, could enter the active site of TropC and undergo a ring expansion reaction as proposed in reaction Path 2 (Figure 4.1D). In this reaction, exclusive formation of 3-hydroxyorcinaldehyde (**4.18**) was observed with no stipitaldehyde (**4.11**) detected, suggesting that fragmentation and rearomatization of diol **4.13** is the predominant mode of reactivity observed for this putative intermediate (Figure 4D). In support of this finding, Riess and coworkers noted this same fragmentation and rearomatization reactivity in their attempts to perform ring expansion reactions on *ortho*-dearomatized phenols to produce tropolones (Figure 4.S29).[41] These observations also agree with the computational modelling

which suggests that fragmentation and rearomatization is a low-barrier process (18.2 kcal/mol). Taken together, these data indicate that diol intermediate **4.13** is unlikely to be the correct ring expansion intermediate in the TropC-catalyzed reaction, further suggesting that a radical mechanism (Path 2) leads to tropolone formation in this NHI system.

### 4.6 Conclusions

These experimental observations and QM calculations suggest that TropC-catalyzed ring expansion occurs through a radical-based process (Path 2), rather than the previously proposed rebound hydroxylation/semi-pinacol sequence (Path 1). This mechanistic proposal is supported by structural characterization, modelling and mutagenic analysis of the TropC active site, demonstrating that modification of a residue involved in substrate positioning altered the products generated by the enzyme. These data suggest that substrate positioning in TropC determines which radical termination step predominates: rebound hydroxylation or radical rearrangement followed by single electron transfer. Furthermore, we have demonstrated that rebound hydroxylation generates an intermediate (**4.13**) which does not undergo ring expansion, but rather a fragmentation and rearomatization process to produce 3-hydroxyorcinaldehyde **4.18**. The observed reactivity of intermediate **4.13** illustrates the thermodynamic favorability for rearomatization over ring expansion in *ortho*-dearomatized phenols, as has been documented in previous studies.[32, 41] This revised proposal of radical-based ring expansion is also supported by literature precedent, demonstrating that tropolones can be synthesized from *ortho*-dearomatized radicals. These findings provide strong evidence of a radical-based mechanism for fungal tropolone biosynthesis, representing a major shift in the current understanding of the role of NHI enzymes in this process. In addition, our observations provide new insight into the mechanistic processes harnessed by NHI

enzymes for the selective synthesis of complex molecules. We anticipate that computational studies that consider active site geometries could provide additional insight into the molecular details of these transformations and the observed behavior of TropC variants. Furthermore, we envision that the molecular details of NHI-catalyzed ring expansion can be leveraged to address current challenges in the synthesis of tropolone natural product scaffolds.

## 4.7 Experimental

### Part I. Substrate synthesis information

**General Information:** All reagents were used as received unless otherwise noted. Reactions were carried out under a nitrogen atmosphere using standard Schlenk techniques unless otherwise noted. Solvents were degassed and dried over aluminum columns on an MBraun solvent system (Innovative Technology, inc., Model PS-00-3). Reactions were monitored by thin layer chromatography using Millipore 60 F254 pre-coated silica TLC plates (0.25 mm) which were visualized using UV, *p*-anisaldehyde, CAM, DNP, or bromocresol green stains. Flash column chromatography was performed using Machery-Nagel 60 μm (230-400 mesh) silica gel. All compounds purified by column chromatography were sufficiently pure for use in further experiments unless otherwise indicated. $^{1}H$ and $^{13}C$ NMR spectra were obtained in $CDCl_3$ at rt (25 °C), unless otherwise noted, on Varian 400 MHz or Varian 600 MHz spectrometers. Chemical shifts of $^{1}H$ NMR spectra were recorded in parts per million (ppm) on the δ scale. High resolution electrospray mass spectra were obtained on an Agilent 1290 Series Infinity II HPLC with a 6230 Series Time-of-Flight mass spectrometer or an Agilent 1290 Series Infinity HPLC with a 6545 Series Quadrupole-Time-of-Flight mass spectrometer. UPLC-PDA spectrometric traces were

obtained on a Waters Aquity H-class instrument. IR spectra were recorded on a Perkin-Elmer Spectrum BX FT-IR spectrometer.

Compound **4.9** was prepared and characterized by our lab previously.[39] Details of this characterization can be found in the Supplementary Information of the provided reference.

**Part II. Plasmid and protein information**

**Plasmid:** The genes encoding *tropC* (DAA64706.1), *citB* (KT781075.1), and *tropB* (DAA64700.1) were codon-optimized for overexpression in *E. coli* and synthesized by GeneArt (ThermoFisher). The synthesized sequence was cloned by GeneArt into a pET-151 vector containing the T7 expression system, ampicillin resistance, and N-terminal 6xHis-tag encoded upstream from the insert gene. No further modifications to this plasmid construct were necessary.

**Codon-Optimized *tropC* Sequence (including 6 x His Tag)**

```
ATGCATCATCACCATCACCATGGTAAGCCTATCCCTAACCCTCTCCTCGGTCTCGATTCTACGGAAAACCTGTATTT
TCAGGGAATTGATCCCTTCACCATGAGCATTGGTGATGAAGTTATTCCGACCGTTGATATTAGCGCATGGCTGAGCA
GCACCGCAAGTCCGGAAAGCAAAAACAAAGTTGTTGAAGAAGTTCGTAGCGCCTGCAACAAATATGGCTTTTTTAAC
CTGGTTGGTCATGGTATTCCGGCAGAAGCACGCGAAAAAATCTTTGGTTGTACCAAAAAATTCTTCGACCTGCCGCT
GGAAGAGAAAATGAAAATTTCAGTTGATAAAAGCCTGGGCAAAAGCTTTCGTGGTTATGAACCGAGCCTGATTCAGA
CCCATCAGGATGGTCTGCTGCCGGATACAAAAGAATGTTTTATTACCGGTGCAGAAATCCCTGCAGATCATCCAGAT
GCAGGTAAATTTAGCACCGGTCCGAATCTGTGGCCTGAAGGTCTGAGCGATAAAGAATTTCGTCAGCCGGTTATGGA
ATATCGTGCACTGATGCTGGATCTGGTTAGCACCATTGTTCGTATTCTGGGTCAGGGTATTCATAAAGCATTTGGTC
ATCCGAGTGATGTGCTGAACGATATTCTGATTAATCCGAGCATTCCGATGCGCCTGCTGCATTATGCTCCGCAAGAA
AATCCGGATCCGCGTCAGTTTGGTGTTGGTGATCACACCGATTTTGGTTGTGTTAGCATTCTGCTGCAACAGAAAGG
CACCAAAGGTCTGGAAGTTTGGTATCCGCCTAAAGAAACCTGGATTCCGGTTCCGGTTATTGAAGATGCATTTGTGA
TTAATATGGGCGATACCATGCATCGTTGGACCGGTGGTTATTATCGTAGCGCACGTCATCGTGTGTATATTACAGGT
GAACGTCGTTATAGCGTTGCCTTTTTTCTGAATGGTAACCTGAACCTGAAAATCAAACCGCTGGATGGTAGCGGTGG
TGAAGCAAGCGTTGGTGAACATATTAACAGCCGTCTGGCACATACCCTGGGTGATAATGCAAAATATCTGCGC
```

**TropC Protein Sequence (including 6 x His Tag)**

```
MHHHHHHGKPIPNPLLGLDSTENLYFQGIDPFTMSIGDEVIPTVDISAWLSSTASPESKNKVVEEVRSACNKYGFFN
LVGHGIPAEAREKIFGCTKKFFDLPLEEKMKISVDKSLGKSFRGYEPSLIQTHQDGLLPDTKECFITGAEIPADHPD
AGKFSTGPNLWPEGLSDKEFRQPVMEYRALMLDLVSTIVRILGQGIHKAFGHPSDVLNDILINPSIPMRLLHYAPQE
NPDPRQFGVGDHTDFGCVSILLQQKGTKGLEVWYPPKETWIPVPVIEDAFVINMGDTMHRWTGGYYRSARHRVYITG
ERRYSVAFFLNGNLNLKIKPLDGSGGEASVGEHINSRLAHTLGDNAKYLR
```

**Codon-Optimized *citB* Sequence (including 6 x His Tag)**

ATGCATCATCACCATCACCATGGTAAGCCTATCCCTAACCCTCTCCTCGGTCTCGATTCTACGGAAAACCTGTATTT
TCAGGGAATTGATCCCTTCACCATGCCGATTAGCACCAAAAGCAGCTTTTATCTGCCTGCAGTTGATATTAGCCCGT
ATCTGCAGGATCCGAATAGTGATGCAGCACGTAAAGTTATTGATGATGTTCGTGCAGCATGTACCAGCACCGGTTTT
TTTCAGCTGTTAGGTCATGGTATTAGTCCGGCACTGCAGCAGAGCGTTTTTGCAGCAGCAGCAAAATTCTTTGCACT
GCCGAGTGATGTTAAAAGCCGTTGTCGTAATGTTGGTTTTCGTGGTTATGATCCGATGGCAAGCCAGAGCTATGAAC
TGGGTGTTCTGCCGGATCTGAAAGAAGGTTTTATTGCCGGTAAAGATATTCCGCTGGATGATCCGCGTGTTGCAAGC
CAGCGCTTTTTTATGGGTCAGAATGCATGGCCTCCGAGCGAACTGCTGCCGGAAGCAAATTTTCGTCGTCCGATTGA
AGAATATTATCAGGCAATGCTGAAACTGTGTTGGGTTGTTCTGGATCTGGTTGCAGCAACCCTGCCGTATGGTCCGC
ATGTTTTTGATGAATTCAAAGAAAATGATCCGGCATGTCCGCTGCGTCTGCTGCATTATCCGCCTGCACCGGCACCG
GATGTTGCAAAAGGTCGTCAGCTGGGTAGCAGCGCACATACCGATTTTGGTGCAATTACCCTGCTGTTACAGGATGA
TCATAGCGGTCTGGAAGTTCAGGATTGTGAAACCGGTGAATGGATTGGTGTTCCGCCTAATAAAGATGCCTATGTTG
TTAATCTGGGCGATATGATGAGCCGTATTACCCGTGGTCACTATAAAAGCAGCATTCATCGTGTGATTAACCAGAAT
CTGACCGATCGTTATAGCGTGGTGTTTTTTTTCGATGGCAATCTGGATTATCGTCTGCGTCCTCTGGATCGTGTTGG
TCAGAATTGGGATGAAGAAGATACCCTGACCGTTGAAGAACATATGCTGGAACGTACCACCACCACCTATAATCTGA
AAGTGAAATAA

## CitB Protein Sequence (including 6 x His Tag)

MHHHHHHGKPIPNPLLGLDSTENLYFQGIDPFTMPISTKSSFYLPAVDISPYLQDPNSDAARKVIDDVRAACTSTGF
FQLLGHGISPALQQSVFAAAAKFFALPSDVKSRCRNVGFRGYDPMASQSYELGVLPDLKEGFIAGKDIPLDDPRVAS
QRFFMGQNAWPPSELLPEANFRRPIEEYYQAMLKLCWVVLDLVAATLPYGPHVFDEFKENDPACPLRLLHYPPAPAP
DVAKGRQLGSSAHTDFGAITLLLQDDHSGLEVQDCETGEWIGVPPNKDAYVVNLGDMMSRITRGHYKSSIHRVINQN
LTDRYSVVFFFDGNLDYRLRPLDRVGQNWDEEDTLTVEEHMLERTTTTYNLKVK

## Codon-Optimized *tropB* Sequence

ATGCCTGGTAGCCTGATTGATACCCGTCAGCAGCCGCTGAGCGTTGGTATTGTTGGTGGTGGTATTATTG
GCGTTATTCTGGCAGCAGGTCTGGTTCGTCGTGGTATTGATGTTAAAGTTTTTGAACAGGCACGTGGCTT
TCGTGAAATTGGTGCAGGTATGGCATTTACCGCAAATGCAGTTCGTTGTATGGAAATGCTGGATCCGGCA
ATTGTTTGGGCACTGCGTAGCAGCGGTGCAGTTCCGATTAGCATTGGTGATCATCAGGCCGAAGCACGTG
ATTATCTGCGTTGGGTTGATGGTTATCATGAAAGCAGCAAACGTCTGTATCAGCTGGATGCAGGTATTCG
TGGTTTTGAAGCATGTCGTCGTGATCAGTTTCTGGAAGCACTGGTTAAAGTTCTGCCGGAAGGTATTGTG
GAATGTCAGAAACGTCTGCAGAAAATCCACGAAAAAAACGAAACCGAAAAAGTGACCCTGGAATTTGCAG
ATGGCACCTTTGCACATGTTGATTGTGTTATTGGTGCCGATGGTATTCGTAGCCGTGTTCGTCAGCACCT
GTTTGGTGAAGATAGCCCGTATAGCCATCCGCATTATAGCCATAAATTTGCATTTCGTGGTCTGATCACC
ATGGAAAATGCAATTAGCGCACTGGGCGAAGATAAAGCACGTACCCTGAATATGCATGTTGGTCCGAATG
CACATCTGATTCATTATCCGGTTGCAAATGAAACCATGGTGAATATTGCAGCCTTTGTTAGCGATCCGGA
AGAATGGCCTGATAAACTGAGCCTGGTTGGTCCGGCAACCCGTGAAGAAGCAATGGGTTATTTTGCAAAT
TGGAATCCGGGTCTGCGTGCAGTTCTGGGTTTTATGCCGGAAAATATTGATCGTTGGGCAATGTTCGATA
CCTATGATTATCCGGCACCGTTTTTTAGCCGTGGTAAAATTTGTCTGGTTGGTGATGCAGCACATGCAGC
AGTTCCGCATCATGGTGCCGGTGCATGTATTGGTATTGAAGATGCACTGTGTGCAACCGTTCTGCTGGCA
GAAGTTTTTGTTAGCACCCGTGGCAAAAGCAGCATTGTTCGTAATCGTGCAATTGCCGCAGCATTTGGTA
GCTTTAATGCAGTGCGTCGTGTTCGTGCACAGTGGTTTGTTGATAGCAGCCGTCGTGTTTGTGATCTGTA
TCAACAGCCGGAATGGGCAGATCCGCAGAAACGTATTAAAGCCGAAAATTGCTTCGAAGAGATTAAAGAT
CGCAGCCATAAAATCTGGCACTTCGATTATAACTCCATGCTGCAAGAAGCCATCGAAAAATATCGTCATA
ATATGGGCAGCTAA

## TropB Protein Sequence

MPGSLIDTRQQPLSVGIVGGGIIGVILAAGLVRRGIDVKVFEQARGFREIGAGMAFTANAVRCMEMLDPA
IVWALRSSGAVPISIGDHQAEARDYLRWVDGYHESSKRLYQLDAGIRGFEACRRDQFLEALVKVLPEGIV
ECQKRLQKIHEKNETEKVTLEFADGTFAHVDCVIGADGIRSRVRQHLFGEDSPYSHPHYSHKFAFRGLIT
MENAISALGEDKARTLNMHVGPNAHLIHYPVANETMVNIAAFVSDPEEWPDKLSLVGPATREEAMGYFAN
WNPGLRAVLGFMPENIDRWAMFDTYDYPAPFFSRGKICLVGDAAHAAVPHHGAGACIGIEDALCATVLLA
EVFVSTRGKSSIVRNRAIAAAFGSFNAVRRVRAQWFVDSSRRVCDLYQQPEWADPQKRIKAENCFEEIKD
RSHKIWHFDYNSMLQEAIEKYRHNMGS

**Protein Overexpression and Purification:** The plasmids containing *tropC*, *tropB*, and *citB* were transformed using standard heat-shock protocols for chemically competent *E. coli* into BL21(DE3) cells. Overexpression of these enzymes was achieved using 4% glycerol (v/v) Terrific Broth (TB) in 2.8 L flasks. 500 mL portions of autoclaved media were inoculated with 5 mL of overnight culture prepared from a single colony in Luria Broth (LB) and 100 μg/mL ampicillin (Gold Biotechnology). Cultures were grown at 37 °C and 200 rpm until the optical density (at 600 nm) reached 0.8. The cultures were then cooled to 20 °C for 1 h and protein expression was induced with 0.2 mM isopropyl-β-D-1-thiogalactopyranoside (IPTG, Gold Biotechnology). Expression was continued at 20 °C overnight (approx. 18 h) at 200 rpm. The typical yield for one 500 mL culture cell pellet (wet cell pellet) was ~25-30 g.

**General Considerations:** HisPur nickel-nitrilotriacetic acid resin (Ni-NTA resin) was purchased from Thermo Scientific. Fast protein liquid chromatography (FPLC) purification was conducted on an ÄTKA Pure FPLC system (GE Healthcare) equipped with a HiPrep 16/60 Sephacryl S-200 HR column purchased from GE Healthcare. Proteins were concentrated at 4,500 x g at 4 °C using Amicon centrifuge filters purchased from EMD Millipore.

**General Purification Procedure (for biocatalytic reactions):** 50-60 g of cell pellet was resuspended in 250 mL of lysis buffer containing 50 mM Tris HCl (pH 7.4), 300 mM NaCl, 10 mM imidazole and 10% glycerol. The mixture was homogenized using a handheld dounce homogenizer. Approximately 1 mg/mL lysozyme (Gold Biotechnology) was added prior to 1 h incubation on a rocker held at 4 °C. Cells were lysed by sonication of the total cell lysate in 100 mL batches on ice. Each cycle of sonication was 10 s sonication, followed by a 20 s rest period, for a total of 6 min at 60% power. The total cell lysate was centrifuged at 45,000 x g for 30 min

and the supernatant was removed. The cell lysate was then batch-bound to 3 mL of Ni-NTA resin (Thermo) for 1 h at 4 °C with gentle rocking. The supernatant was filtered through a fritted 50 mL plastic column (Gold Biotechnologies) to isolate the Ni-NTA resin. The resin was washed with 100 mL of wash buffer containing 50 mM Tris HCl (pH 7.4), 300 mM NaCl, 25 mM imidazole and 10% glycerol. The protein was then eluted using 15 mL of an elution buffer containing 50 mM Tris HCl (pH 7.4), 300 mM NaCl, 250 mM imidazole and 10% glycerol. The eluted protein was concentrated to a volume of 2.5 mL using a 30 KDa molecular weight cutoff ultrafiltration device (Amicon). The concentrated protein was desalted using a PD-10 desalting column that was pre-equilibrated with a storage buffer containing 50 mM Tris HCl (pH 7.4), 300 mM NaCl, and 10% glycerol. The protein was eluted from the column with 3.5 mL of storage buffer, before flash freezing in liquid nitrogen and storage at -80 °C. Protein concentration was determined by the A280 absorbance method using a Nanodrop spectrophotometer. The concentration was corrected using the estimated extinction coefficient from the ProtParam tool on the Expasy server ($\varepsilon$ = 1.128). **Average yield:** 60-70 mg/L of TropC. 40-50 mg/L of TropB. 60-70 mg/L of CitB.

**Purification protocols for TropC crystallography:** Initial purification steps are identical to those outlined above. Following purification by Ni-NTA column, the volume of the resulting protein solution was reduced by ultrafiltration (Amicon, 30 KDa weight cutoff) to a volume of 2 mL. The concentrated protein solution was loaded onto a 16/60 Sephacryl S200 HR column at 0.5 mL/min from a 2 mL sample loop using the ÄTKA Pure FPLC system with the size exclusion buffer containing 20 mM Tris HCl (pH 7.4), 1 mM tris(2-carboxyethyl)phosphine (TCEP), and eluted at 0.5 mL/min. Fractions containing TropC were diluted to 1 mg/mL and placed in a dialysis bag

containing 0.1 mg/mL of TEV protease. The TEV protease digestion was allowed to incubate for 18 h at 4 °C in TEV protease dialysis buffer (50 mM TrisHCl, 50 mM NaCl, 0.5 mM EDTA, 1 mM DTT). After completion of the TEV digestion, the protein solution was incubated for 1 h with 1 mL of Ni-NTA resin at 4 °C. The reaction mixture was loaded onto a 50 mL fritted column and the flow through was collected and concentrated to 12 mg/mL. The resulting protein solution was briefly stored at 4 °C and used within 48 h for crystallization procedures (see Part VIII for details).

**Figure 4.S1.** SDS-PAGE gels of purified wild-type TropC and TropC variants (39.95 kDa with 6x His tag)

*Wild-type TropC purified for X-ray crystallography*

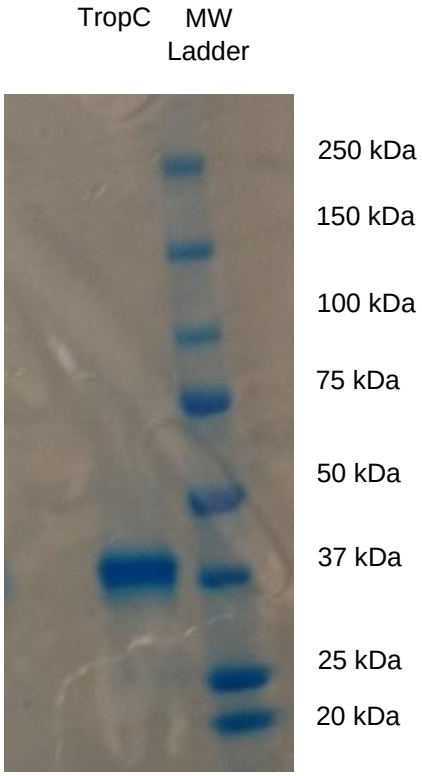

*TropC variants purified for biocatalytic experiments*

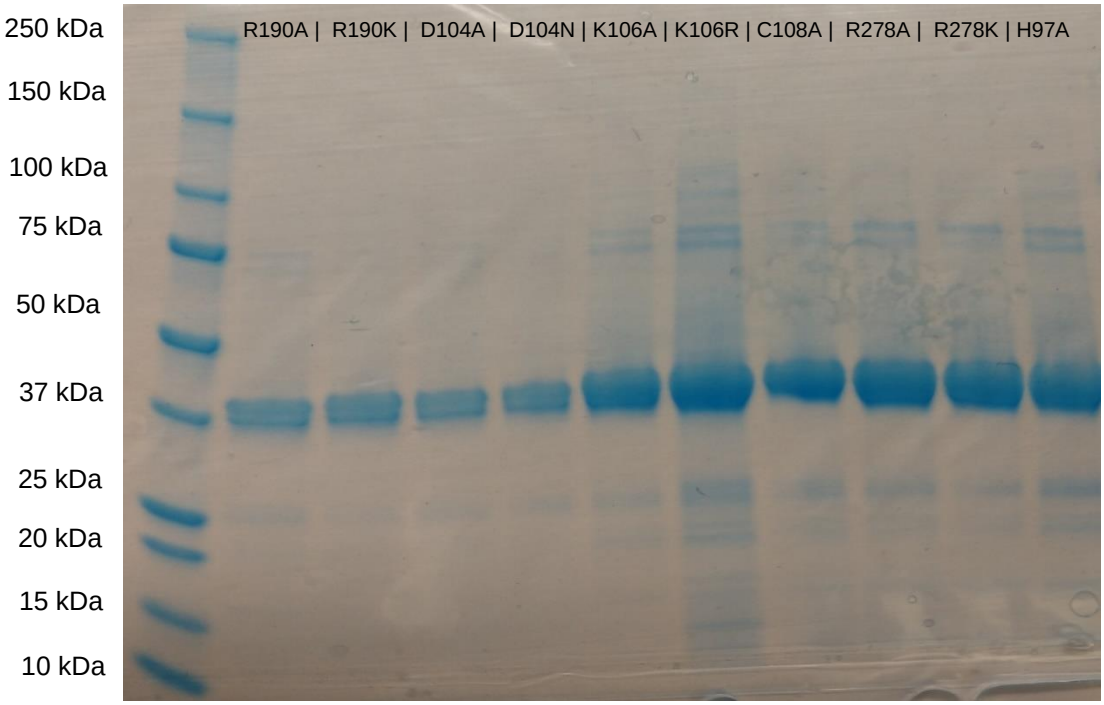


*TropC variants purified for biocatalytic reactions*

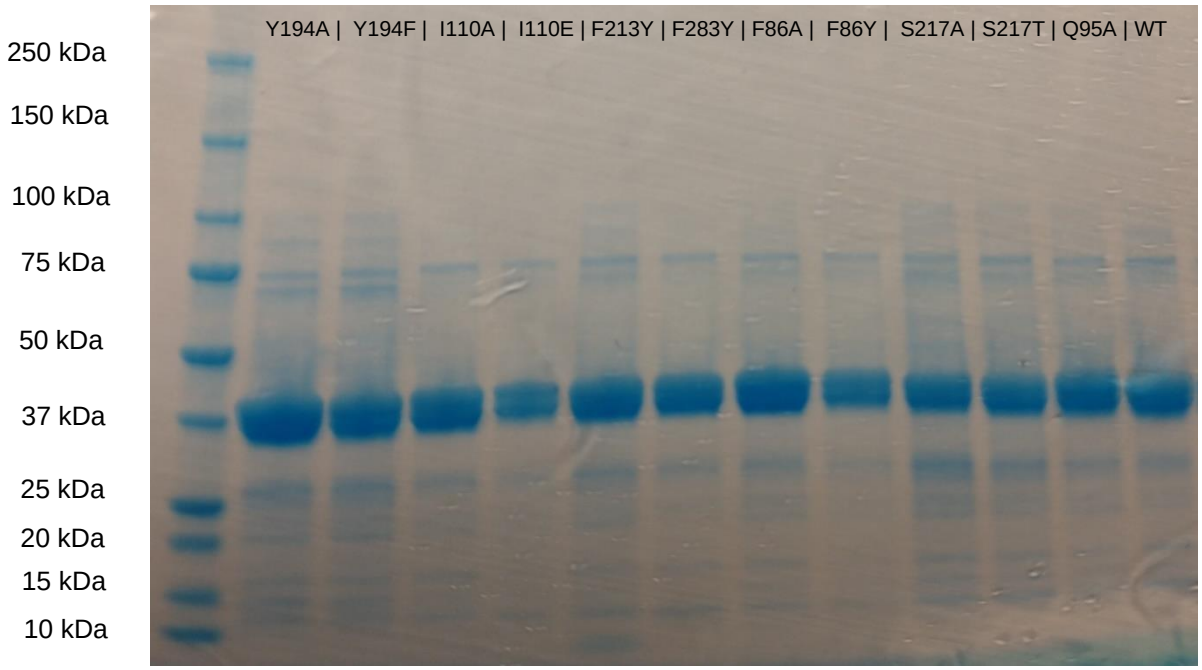

**Part III. Site-directed mutagenesis of TropC**

| TropC variant | Vector | Primer sequence |
|---|---|---|
| TropC Y194A | pET-151 | CGCCTGCTGCAT**GCG**GCTCCGCAAG |
| TropC Y194F | pET-151 | CGCCTGCTGCAT**TTT**GCTCCGCAAGAAAAT |
| TropC R278A | pET-151 | GTATATTACAGGTGAACGT**GCG**TATAGCGTTGCC |
| TropC R278K | pET-151 | GTATATTACAGGTGAACGT**AAA**TATAGCGTTGCC |
| TropC F284A | pET-151 | CGTCGTTATAGCGTTGCC**GCG**TTTCTGAATGGTAAC |
| TropC F284Y | pET-151 | CGTCGTTATAGCGTTGCC**TAT**TTTCTGAATGGTAAC |
| TropC R190A | pET-151 | GAGCATTCCGATG**GCG**CTGCTGCATTATG |
| TropC R190K | pET-151 | CCGAGCATTCCGATG**AAA**CTGCTGCATTATG |
| TropC C108A | pET-151 | CCGGATACAAAAGAA**GCG**TTTATTACCGGTGC |
| TropC H97A | pET-151 | CTGATTCAGACC**GCG**CAGGATGGTCTG |
| TropC K106A | pET-151 | CTGCTGCCGGATACA**GCG**GAATGTTTTATTAC |
| TropC K106R | pET-151 | CTGCTGCCGGATACA**CGT**GAATGTTTTATTACC |
| TropC D104A | pET-151 | GATGGTCTGCTGCCG**GCG**ACAAAAGAATG |
| TropC D104N | pET-151 | GATGGTCTGCTGCCG**AAC**ACAAAAGAATG |
| TropC I110A | pET-151 | CAAAAGAATGTTTT**GCG**ACCGGTGCAGAAATC |
| TropC F86A | pET-151 | GCCTGGGCAAAAGC**GCG**CGTGGTTATGAAC |
| TropC F86Y | pET-151 | GCCTGGGCAAAAGC**TAT**CGTGGTTATGAACCG |
| TropC F213Y | pET-151 | GTTGGTGATCACACCGAT**TAT**GGTTGTGTTAGCATTC |
| TropC Q95A | pET-151 | GAACCGAGCCTGATT**GCG**ACCCATCAGGATGG |
| TropC S217A | pET-151 | CGATTTTGGTTGTGTT**GCG**ATTCTGCTGCAACAG |
| TropC S217T | pET-151 | CGATTTTGGTTGTGTT**ACC**ATTCTGCTGCAACAG |
| TropC-5N (5 residue N-terminal truncation) | pET-151 | GAATTGATCCCTTCACCGAAGTTATTCCGACC |

**Table 4.S1.** Primers used in the generation of TropC variants.

**Whole plasmid mutagenesis procedure:** Variants of TropC were generated via polymerase chain reaction (PCR) using the primers listed above. Substitutions were generated by site-directed mutagenesis of the pET-151-*tropC* parent plasmid. 25 µL PCR reaction mixtures contained 5 x Phusion HF buffer (NEB), 1 ng/µL parent plasmid, 500 nM primer, 200 µM dNTPs, 1% DMSO, and 1 U/µL Phusion HF DNA polymerase (NEB). Mutant plasmid amplification was accomplished using the following procedure. 98 °C (30 s) then a repeating cycle (30 cycles) of the following temperatures: 98 °C (30 s), $T_m$ – 5 °C (30 s), 72 °C (3 min), followed by a final extension at 72 °C for 10 min. Parent plasmid DNA was digested in a 10 µL reaction containing 8 µL PCR product

mixture, 1 μL CutSmart buffer (NEB), and 20 U (1 μL) DpnI endonuclease (NEB). The reaction was incubated at 37 °C for 3 h and transformed into chemically competent DH5-α *E. coli* cells.

**Part IV. Biocatalytic reaction conditions and products**

**Stock solutions:** Stock solutions of each substrate (50 mM) were prepared by dissolving the substrate in DMSO (analytical grade). Stock solutions of α-ketoglutaric acid (125 mM), ferrous sulfate (10 mM) and sodium ascorbate (50 mM) were freshly prepared in MQ water before each use, stored on ice, and used within 3 h. Aliquots of glucose-6-phosphate (G6P, 500 mM), glucose-6-phosphate dehydrogenase (G6PDH, 100 U/mL), and nicotinamide adenine dinucleotide (NADP+, 100 mM) were prepared and stored at -20 °C before use. Aliquots of WT TropC and variants were stored at -80 °C.

***In vitro* analytical-scale TropB/TropC cascade reactions:** Cascade oxidative dearomatization/ring-expansion reactions were performed as follows. Each reaction contained 50 mM TES buffer pH 7.5 (2.5 μL, 1 M), 2.5 mM substrate (2.5 μL, 50 mM), 5 μM TropB, 10 μM TropC, 5 mM glucose-6-phosphate (G6P, 0.5 μL, 500 mM), 1 mM nicotinamide adenine dinucleotide phosphate disodium salt (NADP+, 0.5 μL, 100 mM), 1 U/mL glucose-6-phosphate dehydrogenase (G6PDH, 0.5 μL, 100 U/mL), 5 mM α-ketoglutaric acid (α-KG, 2 μL, 125 mM), 0.1 mM ferrous sulfate ($FeSO_4$, 0.5 μL, 10 mM), 8 mM sodium ascorbate (8 μL, 50 mM) and Milli-Q water to a final volume of 50 μL. Reactions were carried out at 30 °C for 3 h and quenched by the addition of 3 volumes of methanol containing 3.5 mM pentamethyl benzene as an internal standard. Precipitated biomolecules were pelleted by centrifugation (17,000 x g, 20 min). The supernatant was analyzed by UPLC-DAD and conversion obtained by comparison to calibration curves of each product.

***In vitro* analytical-scale TropB reactions:** Analytical-scale oxidative dearomatization reactions were performed as follows. Each reaction contained 50 mM TES buffer pH 7.5 (2.5 μL, 1 M), 2.5 mM substrate (2.5 μL, 50 mM), 5 μM TropB, 5 mM glucose-6-phosphate (G6P, 0.5 μL, 500 mM), 1 mM nicotinamide adenine dinucleotide phosphate disodium salt (NADP+, 0.5 μL, 100 mM), 1 U/mL glucose-6-phosphate dehydrogenase (G6PDH, 0.5 μL, 100 U/mL) and Milli-Q water to a final volume of 50 μL. Reactions were carried out at 30 °C for 3 h and quenched by the addition of 3 volumes of methanol containing 3.5 mM pentamethyl benzene as an internal standard. Precipitated biomolecules were pelleted by centrifugation (17,000 x g, 20 min). The supernatant was analyzed by UPLC-DAD and conversion obtained by comparison to calibration curve of the product.

**Determination of percent yield:** Percent yield of product was determined by analysis of each reaction after 3 h. PDA spectrometric analysis was performed on a Waters Aquity H-Class instrument, using a Phenomenex Kinetex (1.7 μm C18, 2.1 x 150 mm) column under the following conditions: mobile phase (Solvent A: deionized water + 0.1% formic acid; Solvent B: acetonitrile + 0.1% formic acid) 5% to 100% solvent B over 2 min, 100% solvent B for 1 min; flow rate: 0.5 mL/min. Based on the calibration curves of isolated products, the percent yield of stipitaldehyde (**4.11**) was calculated with $AUC_{product}$ (360 nm)/$AUC_{internal\ standard}$ (270 nm). The percent yield of 3-hydroxyorcinaldehyde **4.18** was calculated with $AUC_{product}$ (360 nm)/$AUC_{internal\ standard}$ (270 nm). *In vitro* reactions were performed and analyzed in duplicate, with reported conversions as an average of those trials.

**Procedure for *in vitro* milligram-scale TropB/TropC reactions:** Preparative-scale cascade oxidative dearomatization/ring-expansion reactions were performed on 50 mg scale. Each reaction

contained 50 mM TES buffer pH 7.5, 2.5 mM substrate, 5 μM TropB, 10 μM TropC, 5 mM G6P, 1 mM NADP+, 1 U/mL G6PDH, 5 mM α-KG, 0.1 mM $FeSO_4$, 8 mM sodium ascorbate. TropB-catalyzed oxidative dearomatization was carried out at 30 °C and allowed to proceed to completion (~1 h) before the addition of TropC, α-KG, ascorbate and $FeSO_4$. The reaction was then further incubated at 30 °C for an additional 2 h before workup. Reaction progress was monitored by UPLC-DAD analysis of 50 μL samples, quenched by the addition of 3 volumes of methanol containing 3.5 mM pentamethyl benzene as an internal standard. Precipitated biomolecules were pelleted by centrifugation (17,000 x g, 20 min). The supernatant was analyzed by UPLC-DAD and conversion obtained by comparison to calibration curves of each product. **Isolation procedure:** The reaction mixture was transferred to a separatory funnel and acidified to pH 2.0 with 0.1 M HCl. The organic materials were extracted from the aqueous layer with ethyl acetate (3 x 50 mL). The organic fractions were pooled and concentrated under reduced pressure to yield a crude mixture. This mixture was purified using preparative HPLC according to the procedure listed below.

**Purification by preparative HPLC:** For purification of milligram-scale reactions, the resulting crude mixture was taken up in a 50:50 mixture of milli-Q water:acetonitrile (4 mL). The product(s) were purified from this mixture by preparative HPLC using a Phenomenex Kinetex 5 μm C18, 150 x 21.2 mm column under the following conditions: mobile phase (Solvent A: deionized water + 0.1% formic acid; Solvent B: acetonitrile + 0.1% formic acid) 5% to 100% solvent B over 10 min, 100% solvent B for 4 min; flow rate: 11.5 mL/min. Product elution was monitored at wavelengths corresponding to maximal absorbances for each product: stipitaldehyde (**4.11**) at 360 nm, 3-hydroxyorcinaldehyde (**4.18**) at 300 nm.

**Procedure for *in vitro* milligram-scale CitB reaction:** Preparative-scale enzymatic reactions were conducted on 200 mg scale under the following conditions: 2.5 mM substrate, 50 mM TES buffer pH 7.5, 5 mM α-ketoglutaric acid, 0.1 mM ferrous sulfate, 8 mM sodium ascorbate, 45 mg/mL CitB wet cell pellet. Reactions were performed in Erlenmeyer flasks of appropriate volume to achieve proper oxygenation (at least 3 times reaction volume) and shaken at 100 rpm at 30 °C. Reaction progress was monitored at hourly intervals by analysis of a 50 μL aliquot by UPLC-DAD as described previously.[38] Upon satisfactory conversion of the substrate, the product(s) were isolated in the following manner. **Isolation procedure:** The reaction mixture was transferred to a 50 mL falcon tube and 2 volumes of acetone were added. The mixture was centrifuged at 4,500 x g for 10 min to separate the biomolecule components from the aqueous reaction mixture. The supernatant was removed and acetone removed under reduced pressure. The supernatant was acidified to pH 2.0 with 0.1 M HCl. The organic materials were extracted from the aqueous layer with ethyl acetate (3 x 50 mL). The organic fractions were pooled and concentrated under reduced pressure to yield a crude mixture, which was purified by silica gel chromatography to yield the hydroxylated product.

**Figure 4.S2. Products generated in the reaction of TropC variants with TropB-generated dienone 4.10.**

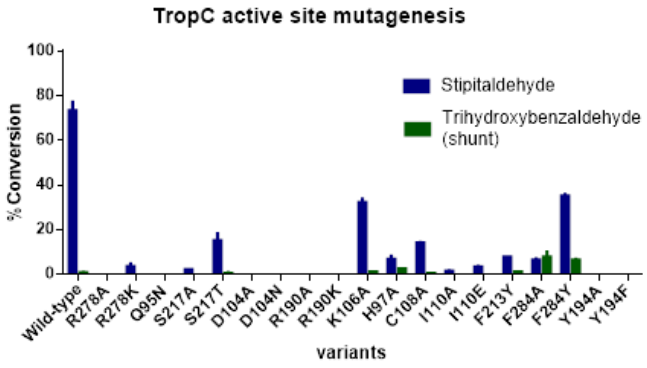

**Biocatalytic reaction products**

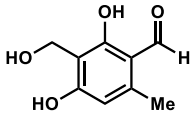


25

**2,4-dihydroxy-3-(hydroxymethyl)-6-methylbenzaldehyde (4.25)**

The title compound was synthesized and characterized previously by our group using a procedure for preparative-scale benzylic hydroxylation reactions with CitB.[38] Purification by flash chromatography afforded 460 mg (84% yield) of the title compound as a white solid. **$^1$H NMR** (400 MHz, MeOD) δ 10.07 (s, 1H), 6.26 (s, 1H), 4.68 (s, 2H), 2.50 (s, 3H); **HR-ESI-MS**: m/z calcd for $C_9H_{11}O_4^+$ $[M+H-H_2O]^+$: 165.0546, found: 165.0544.

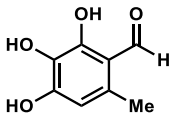


18

**2,3,4-trihydroxy-6-methylbenzaldehyde (3-hydroxyorcinaldehyde 4.18)**

The title compound was synthesized according to the procedure for preparative-scale TropB/TropC reactions. Full characterization for this compound has been reported previously.[21] Purification by preparative HPLC afforded 10.2 mg (20% yield) of the title compound as a yellow solid. **$^1$H NMR** (400 MHz, $CDCl_3$) δ 10.08 (s, 1H), 6.35 (s, 1H), 2.90 (s, 3H). **HR-ESI-MS**: m/z calcd for $C_8H_8O_4^+$ $[M+H]^+$: 169.0495, found: 169.0494.

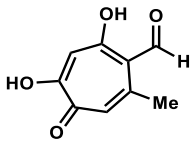


11

**2,4-dihydroxy-7-methyl-5-oxocyclohepta-1,3,6-triene-1-carbaldehyde (stipitaldehyde, 4.11)**

The title compound was synthesized according to the procedure for preparative-scale TropB/TropC reactions. Full characterization for this compound has been reported previously.[21] Purification by preparative HPLC afforded 8 mg (16% yield) of the title compound as an orange solid. **$^1$H NMR** (600 MHz, MeOD) δ 10.13 (s, 1H), 6.83 (s, 1H), 6.82 (s, 1H), 2.65 (s, 3H). **HR-ESI-MS**: m/z calcd for $C_9H_8O_4^+$ $[M+H]^+$: 181.0495, found 181.0497.

**Part V. Product standard curves**

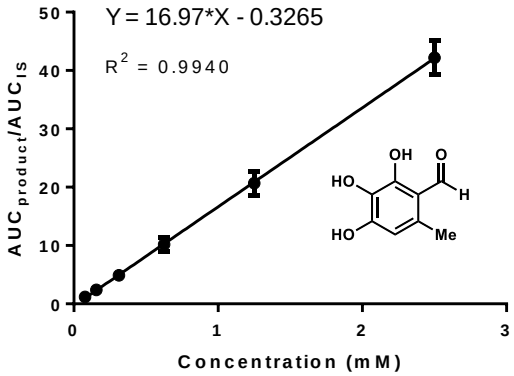


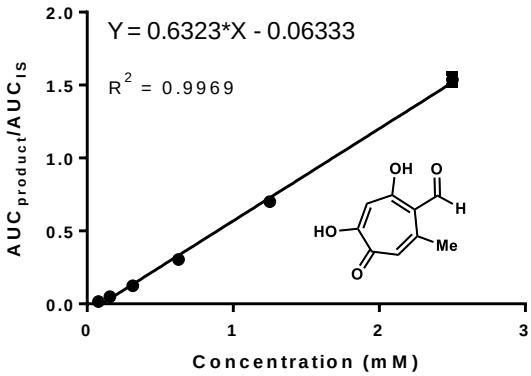

## Part VI. UPLC traces of biocatalytic reactions

**Figure 4.S3. Reaction of wild-type TropC with TropB-generated dienone 4.10.** PDA traces of enzymatic reaction analyzed at 360 nm.

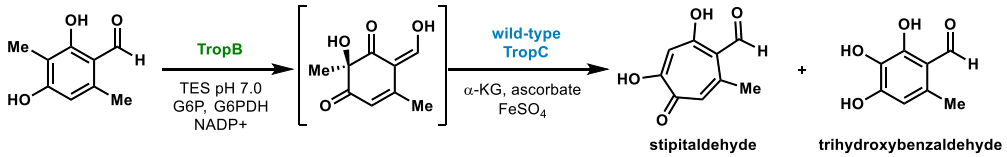


### With TropC

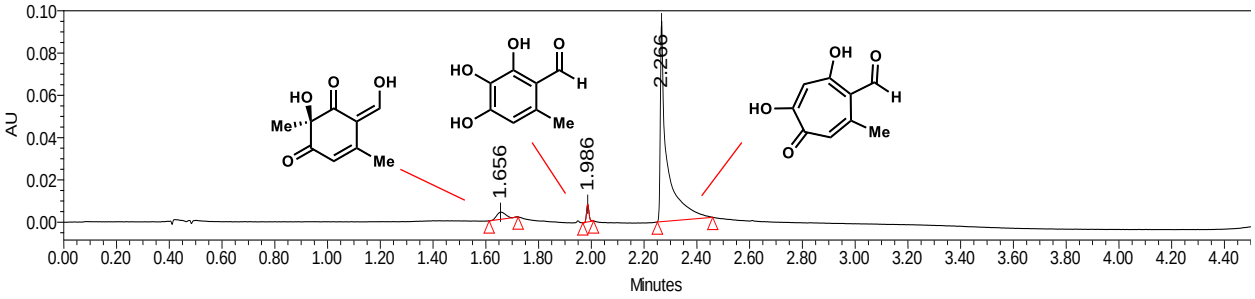


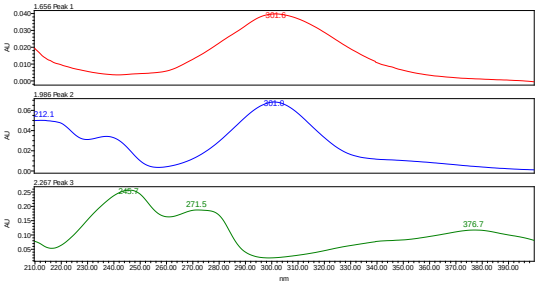

| | Retention Time | Area | % Area | Height |
|---|---|---|---|---|
| 1 | 1.656 | 8022 | 4.49 | 3380 |
| 2 | 1.986 | 5527 | 3.09 | 8463 |
| 3 | 2.266 | 165108 | 92.42 | 95011 |

### TropB only

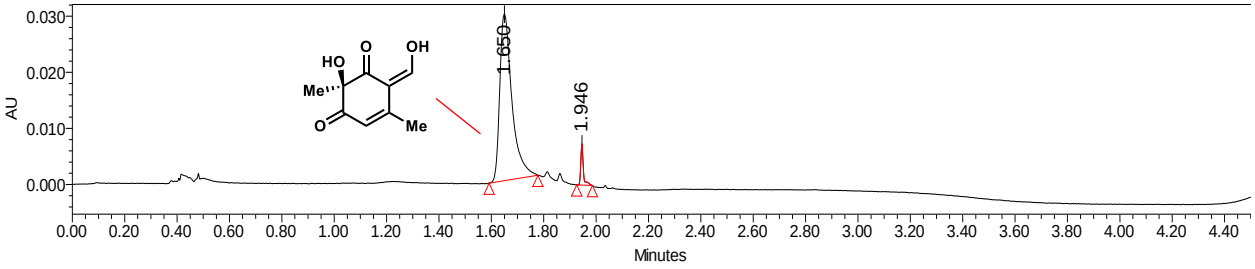


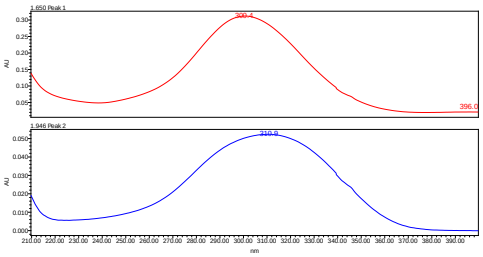

| | Retention Time | Area | % Area | Height |
|---|---|---|---|---|
| 1 | 1.650 | 96047 | 95.01 | 29701 |
| 2 | 1.946 | 5046 | 4.99 | 7337 |

Stipitaldehyde (**4.11**) product standard

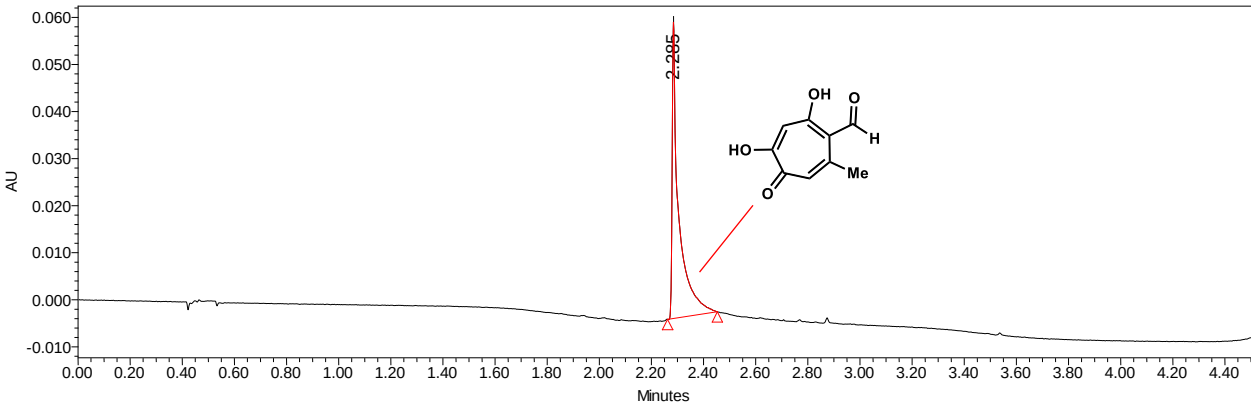


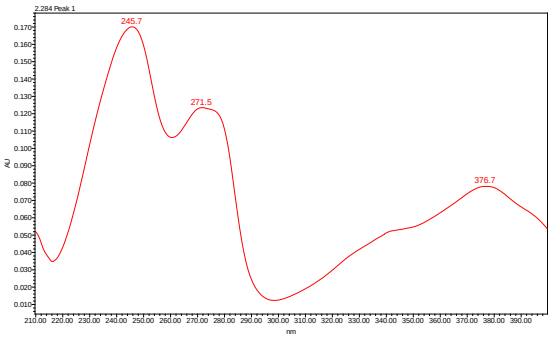


| | Retention Time | Area | % Area | Height |
|---|---|---|---|---|
| 1 | 2.285 | 110190 | 100.00 | 63128 |

3-hydroxyorcinaldehyde (**4.18**) product standard

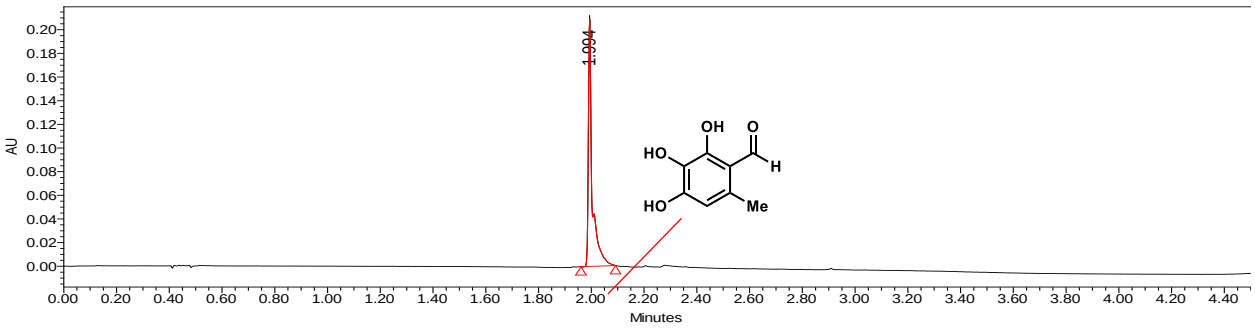


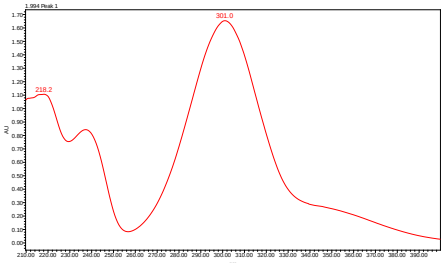


| | Retention Time | Area | % Area | Height |
|---|---|---|---|---|
| 1 | 1.994 | 209222 | 100.00 | 209461 |

**Figure 4.S4. Reaction of TropC R190A with TropB-generated dienone 4.10.** PDA traces of enzymatic reaction analyzed at 360 nm.

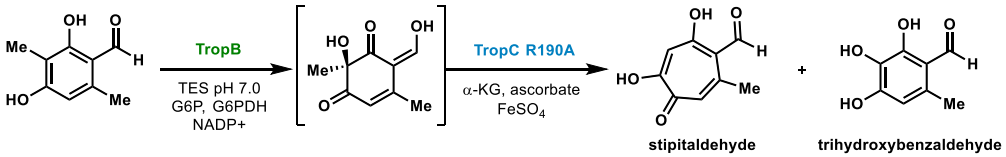


## With TropC

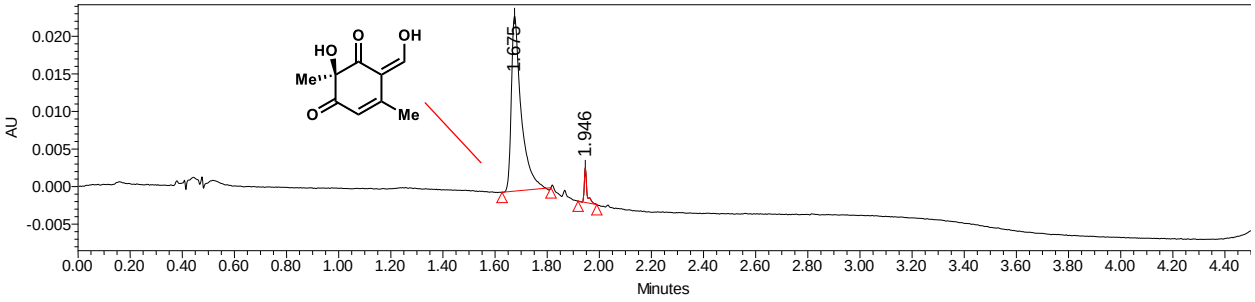


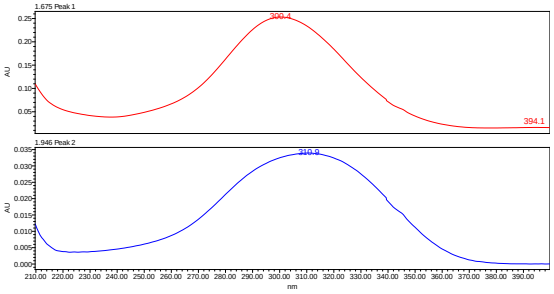


| | Retention Time | Area | % Area | Height |
|---|---|---|---|---|
| 1 | 1.675 | 61537 | 94.92 | 23309 |
| 2 | 1.946 | 3294 | 5.08 | 4602 |

## TropB only

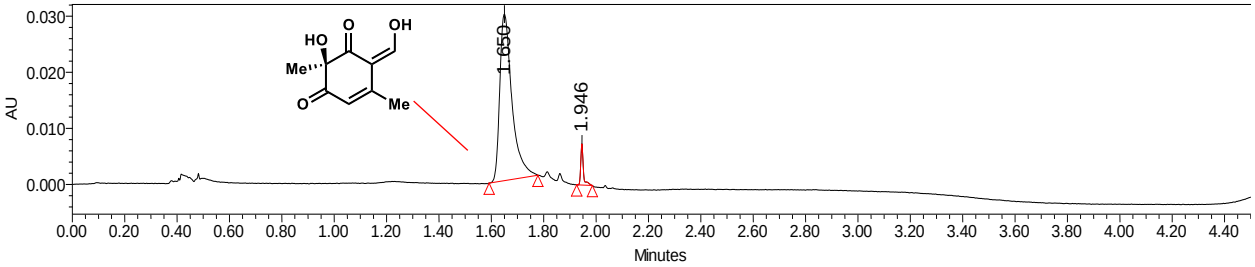


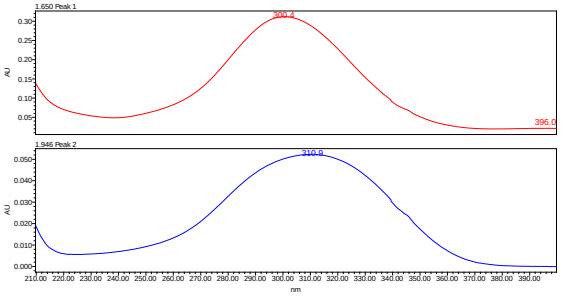


| | Retention Time | Area | % Area | Height |
|---|---|---|---|---|
| 1 | 1.650 | 96047 | 95.01 | 29701 |
| 2 | 1.946 | 5046 | 4.99 | 7337 |

**Figure 4.S5. Reaction of TropC R190K with TropB-generated dienone 4.10.** PDA traces of enzymatic reaction analyzed at 360 nm.

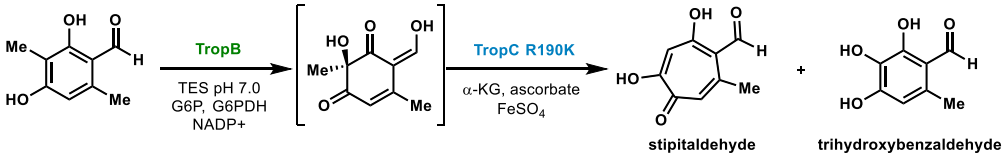


## With TropC

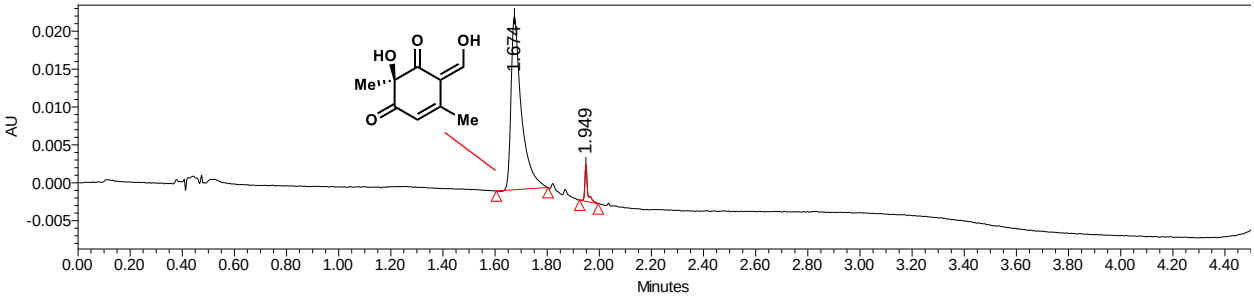


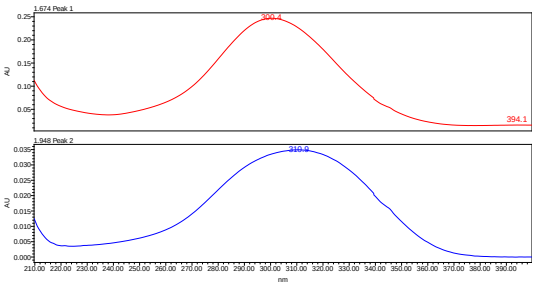

| | Retention Time | Area | % Area | Height |
|---|---|---|---|---|
| 1 | 1.674 | 63799 | 94.66 | 22880 |
| 2 | 1.949 | 3601 | 5.34 | 4825 |

## TropB only

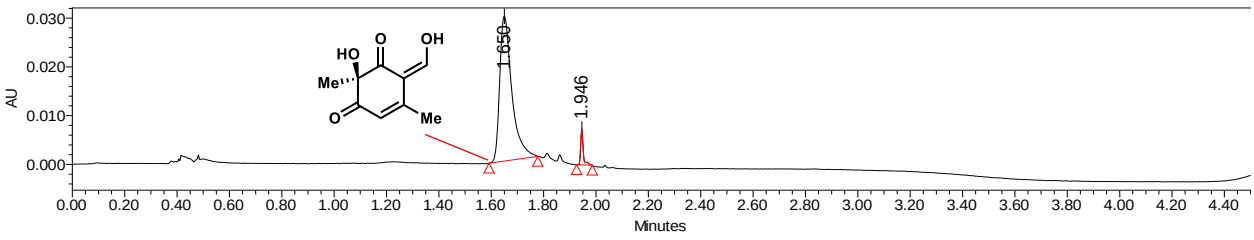


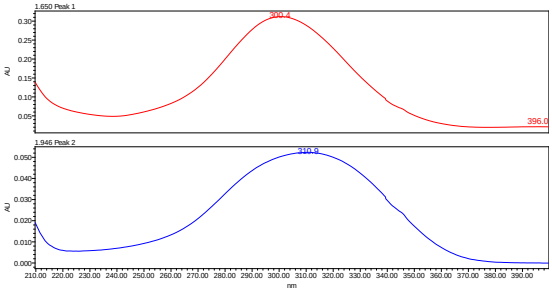

| | Retention Time | Area | % Area | Height |
|---|---|---|---|---|
| 1 | 1.650 | 96047 | 95.01 | 29701 |
| 2 | 1.946 | 5046 | 4.99 | 7337 |

**Figure 4.S6.** Reaction of TropC D104A with TropB-generated dienone **4.10**. PDA traces of enzymatic reaction analyzed at 360 nm.

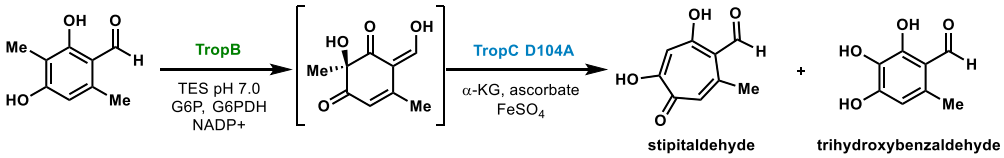


## With TropC

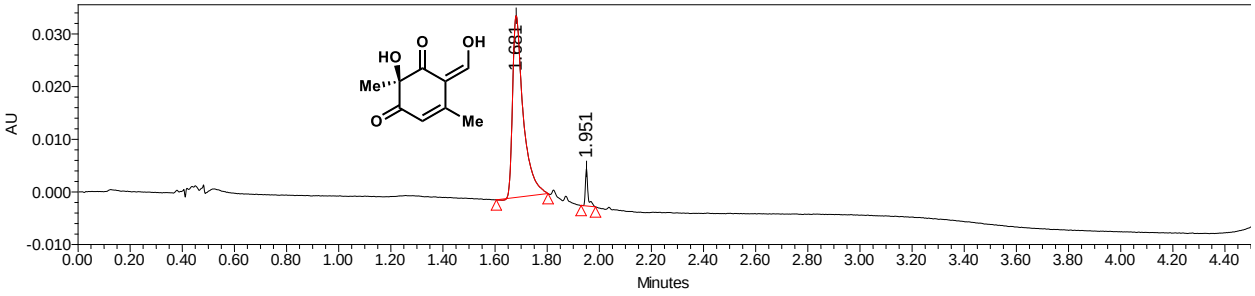


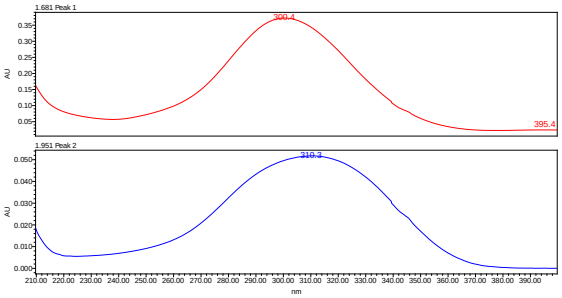

| | Retention Time | Area | % Area | Height |
|---|---|---|---|---|
| 1 | 1.681 | 98240 | 95.26 | 34505 |
| 2 | 1.951 | 4891 | 4.74 | 7063 |

## TropB only

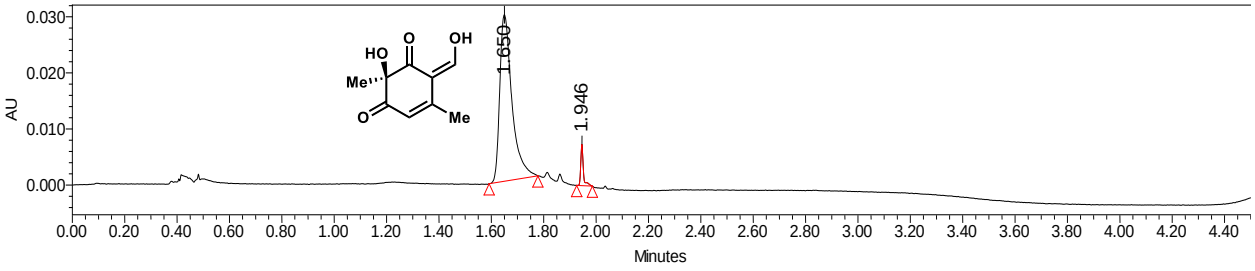


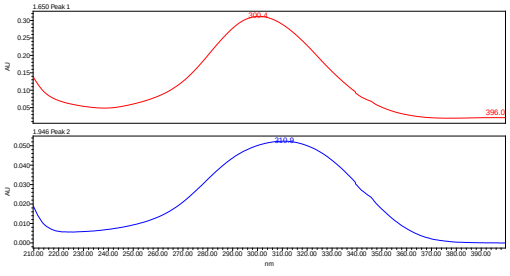

| | Retention Time | Area | % Area | Height |
|---|---|---|---|---|
| 1 | 1.650 | 96047 | 95.01 | 29701 |
| 2 | 1.946 | 5046 | 4.99 | 7337 |

**Figure 4.S7. Reaction of TropC D104N with TropB-generated dienone 4.10.** PDA traces of enzymatic reaction analyzed at 360 nm.

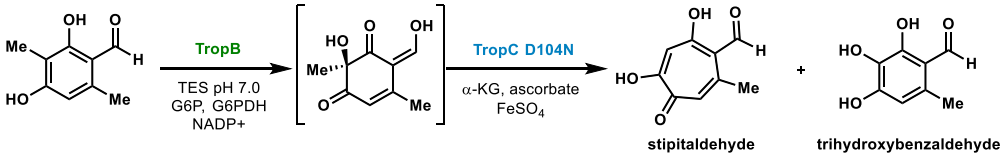


## With TropC

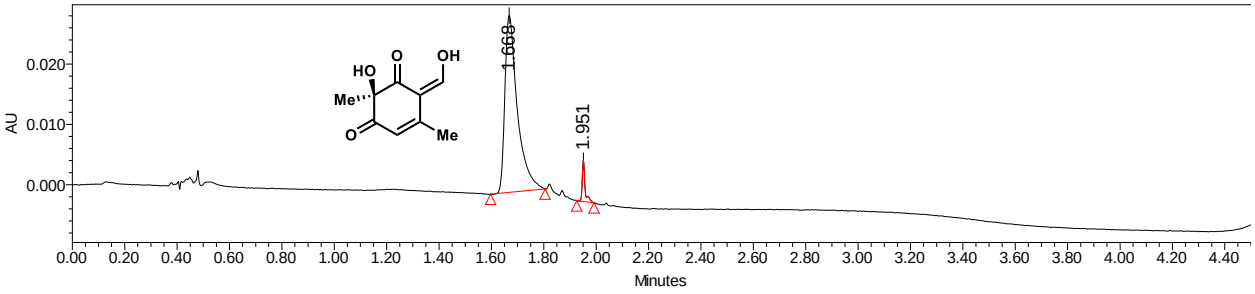


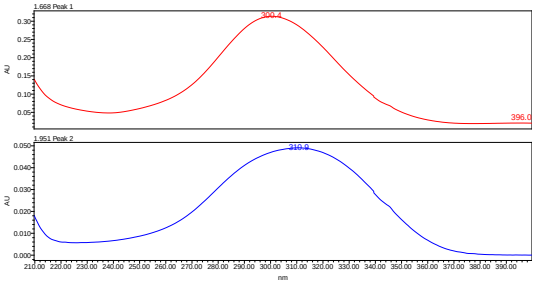

| | Retention Time | Area | % Area | Height |
|---|---|---|---|---|
| 1 | 1.668 | 97336 | 95.10 | 29302 |
| 2 | 1.951 | 5013 | 4.90 | 6842 |

## TropB only

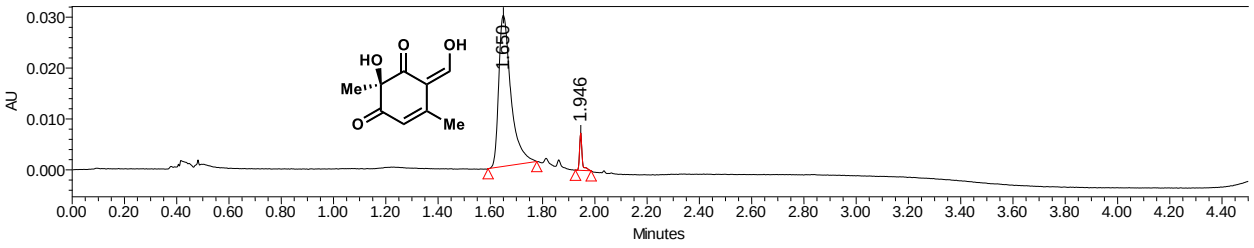


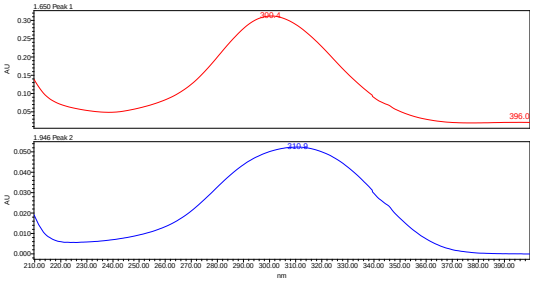

| | Retention Time | Area | % Area | Height |
|---|---|---|---|---|
| 1 | 1.650 | 96047 | 95.01 | 29701 |
| 2 | 1.946 | 5046 | 4.99 | 7337 |

**Figure 4.S8. Reaction of TropC Y194A with TropB-generated dienone 4.10.** PDA traces of enzymatic reaction analyzed at 360 nm.

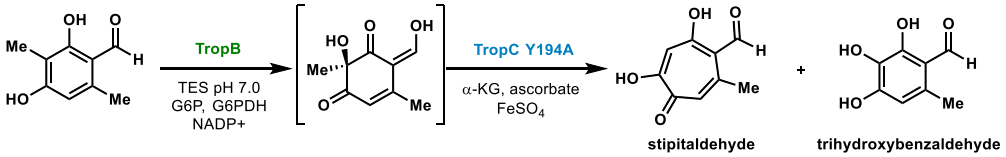


## With TropC

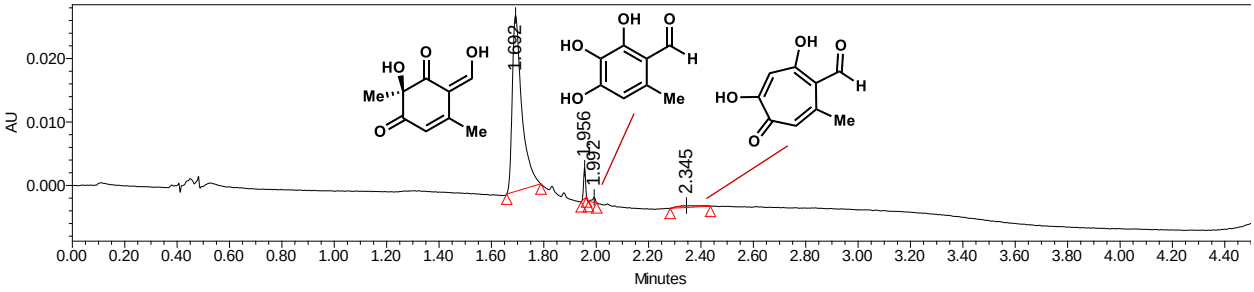


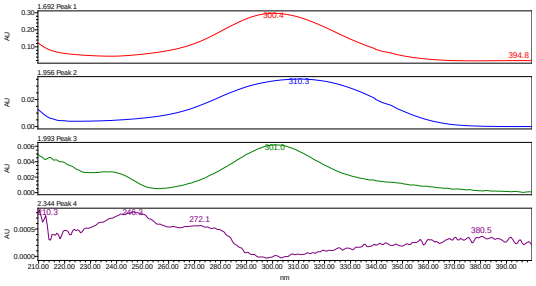

| | Retention Time | Area | % Area | Height |
|---|---|---|---|---|
| 1 | 1.692 | 70681 | 93.73 | 27731 |
| 2 | 1.956 | 2433 | 3.23 | 4819 |
| 3 | 1.992 | 638 | 0.85 | 777 |
| 4 | 2.345 | 1653 | 2.19 | 307 |

## TropB only

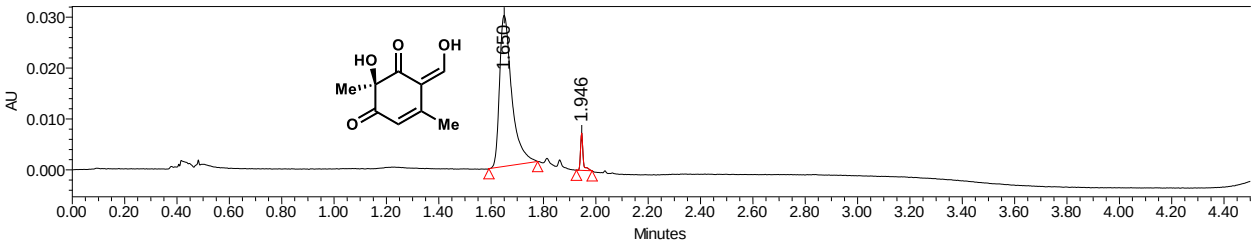


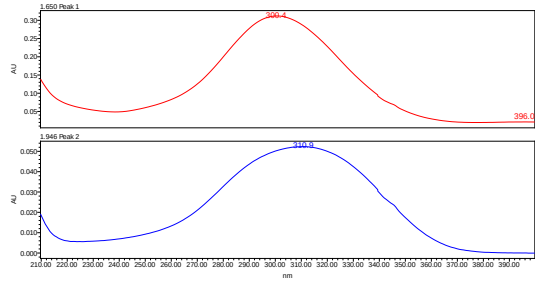

| | Retention Time | Area | % Area | Height |
|---|---|---|---|---|
| 1 | 1.650 | 96047 | 95.01 | 29701 |
| 2 | 1.946 | 5046 | 4.99 | 7337 |

**Figure 4.S9. Reaction of TropC Y194F with TropB-generated dienone 4.10.** PDA traces of enzymatic reaction analyzed at 360 nm.

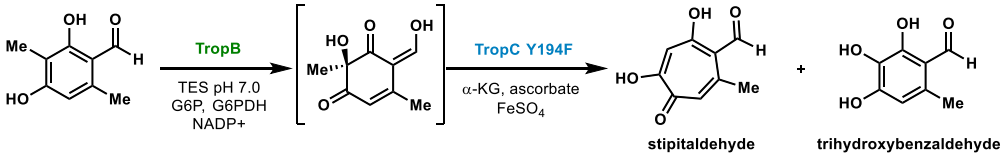


## With TropC

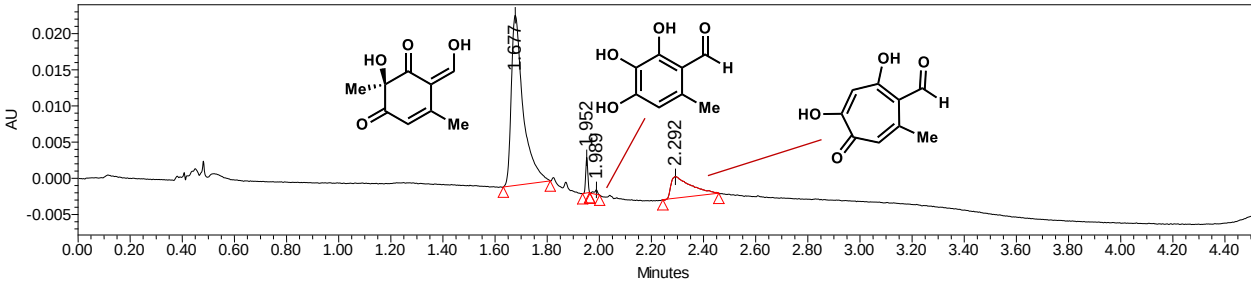


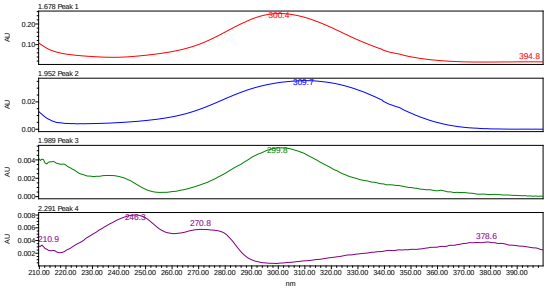

| | Retention Time | Area | % Area | Height |
|---|---|---|---|---|
| 1 | 1.677 | 74618 | 79.52 | 23525 |
| 2 | 1.952 | 2759 | 2.94 | 4890 |
| 3 | 1.989 | 583 | 0.62 | 640 |
| 4 | 2.292 | 15872 | 16.92 | 2962 |

## TropB only

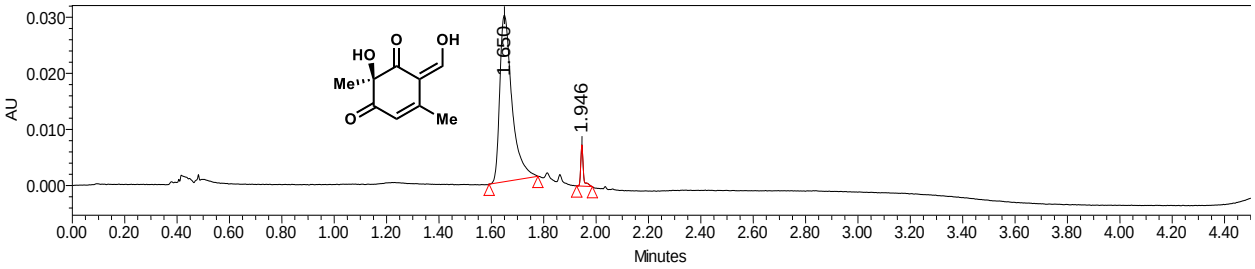


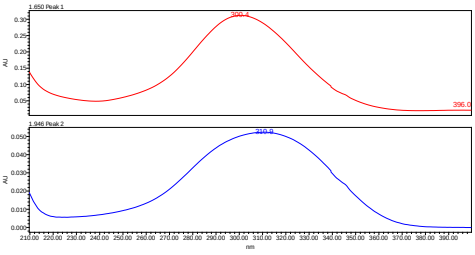

| | Retention Time | Area | % Area | Height |
|---|---|---|---|---|
| 1 | 1.650 | 96047 | 95.01 | 29701 |
| 2 | 1.946 | 5046 | 4.99 | 7337 |

**Figure 4.S10. Reaction of TropC K106A with TropB-generated dienone 4.10.** PDA traces of enzymatic reaction analyzed at 360 nm.

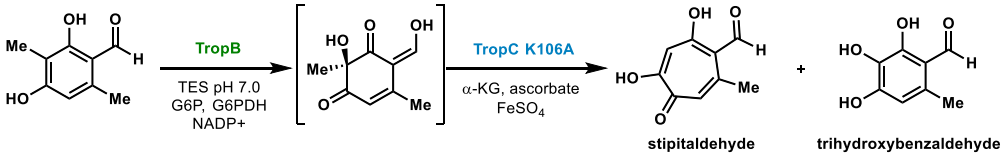


## With TropC

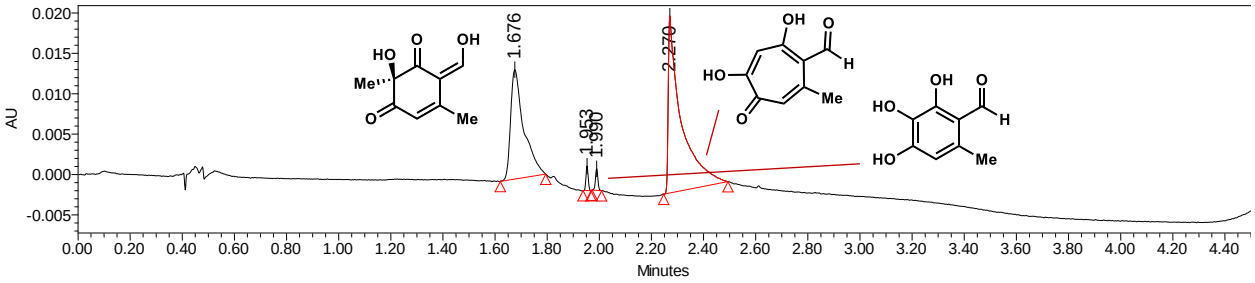


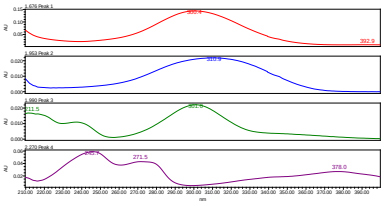

| | Retention Time | Area | % Area | Height |
|---|---|---|---|---|
| 1 | 1.676 | 47508 | 37.52 | 13538 |
| 2 | 1.953 | 1816 | 1.43 | 3056 |
| 3 | 1.990 | 1741 | 1.38 | 2689 |
| 4 | 2.270 | 75547 | 59.67 | 21945 |

## TropB only

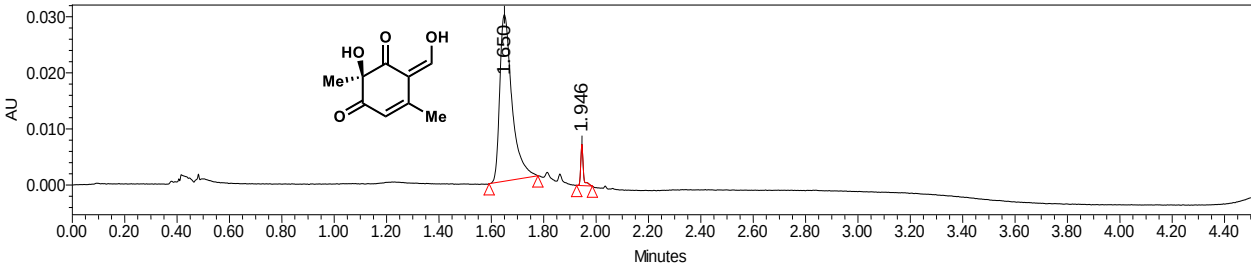


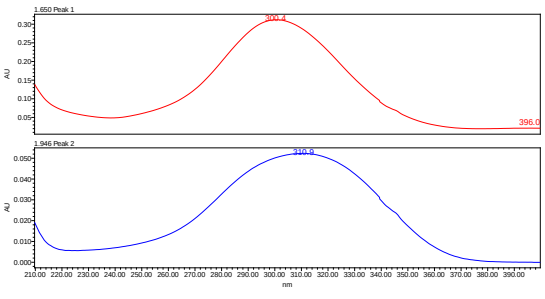

| | Retention Time | Area | % Area | Height |
|---|---|---|---|---|
| 1 | 1.650 | 96047 | 95.01 | 29701 |
| 2 | 1.946 | 5046 | 4.99 | 7337 |

**Figure 4.S11. Reaction of TropC K106R with TropB-generated dienone 4.10.** PDA traces of enzymatic reaction analyzed at 360 nm.

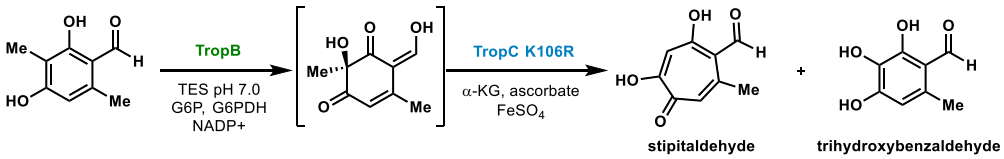


## With TropC

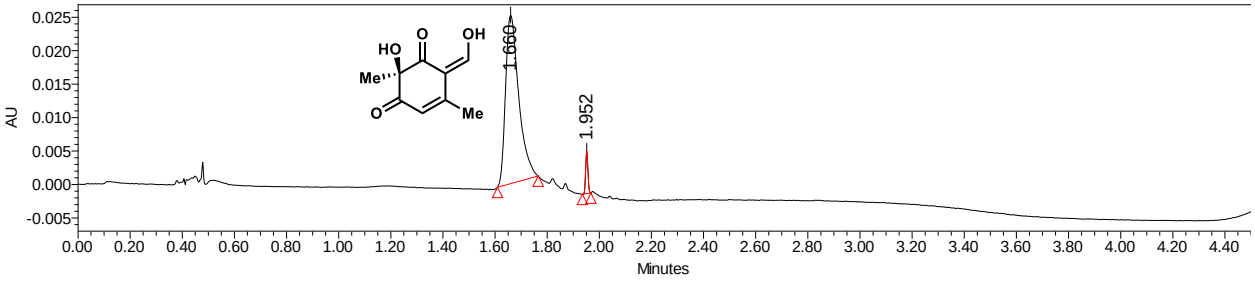


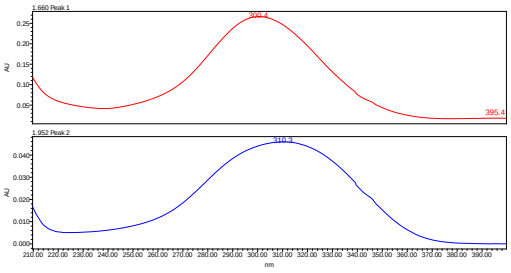

| | Retention Time | Area | % Area | Height |
|---|---|---|---|---|
| 1 | 1.660 | 88528 | 95.85 | 25190 |
| 2 | 1.952 | 3835 | 4.15 | 6351 |

## TropB only

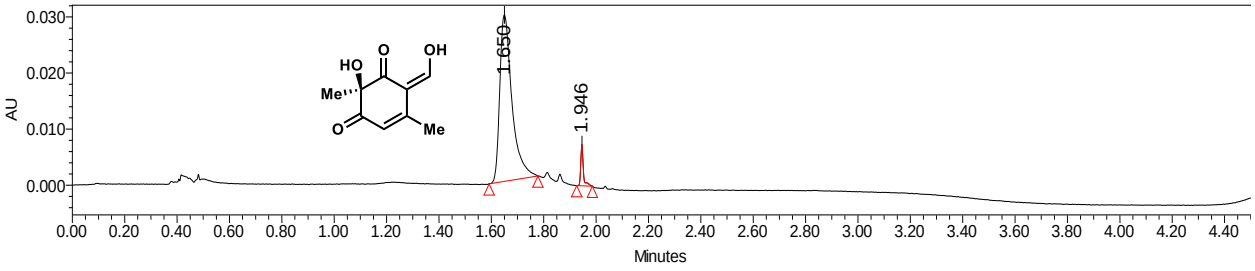


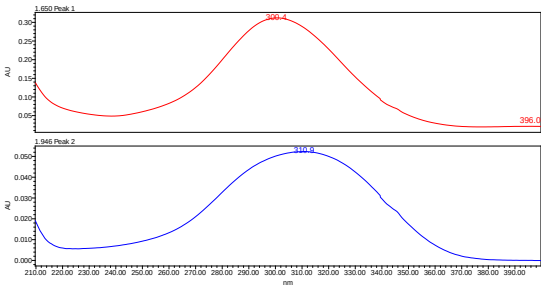

| | Retention Time | Area | % Area | Height |
|---|---|---|---|---|
| 1 | 1.650 | 96047 | 95.01 | 29701 |
| 2 | 1.946 | 5046 | 4.99 | 7337 |

**Figure 4.S12. Reaction of TropC H97A with TropB-generated dienone 4.10.** PDA traces of enzymatic reaction analyzed at 360 nm.

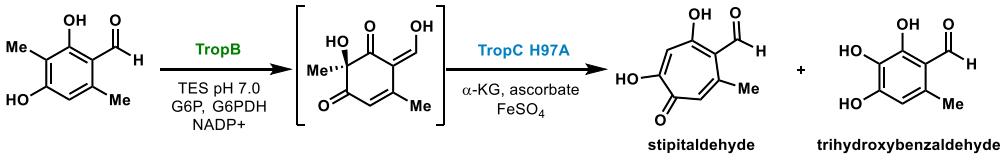


## With TropC

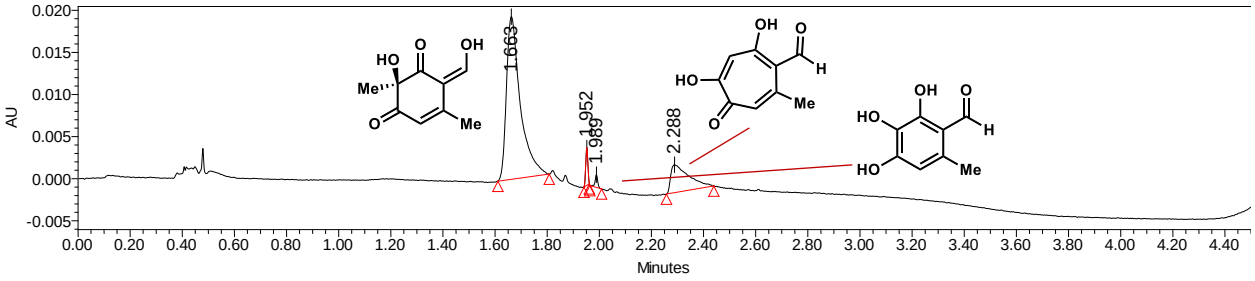


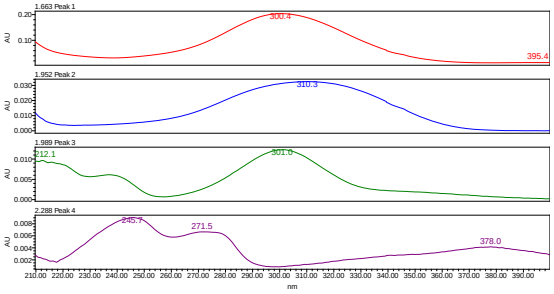


| | Retention Time | Area | % Area | Height |
|---|---|---|---|---|
| 1 | 1.663 | 71366 | 78.57 | 19312 |
| 2 | 1.952 | 2552 | 2.81 | 4487 |
| 3 | 1.989 | 1065 | 1.17 | 1516 |
| 4 | 2.288 | 15843 | 17.44 | 3331 |

## TropB only

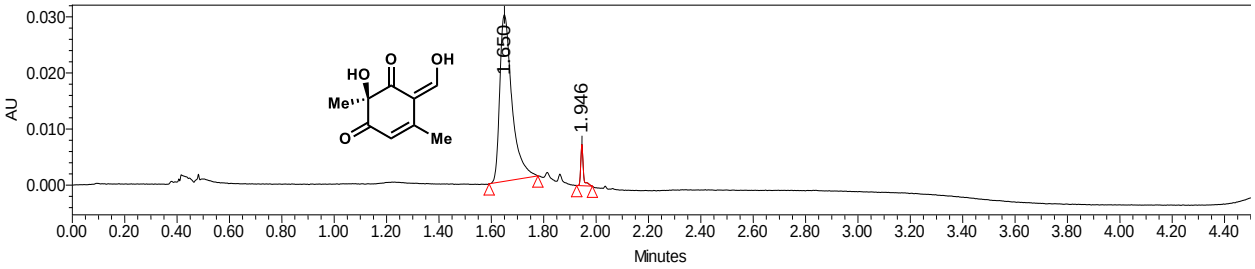


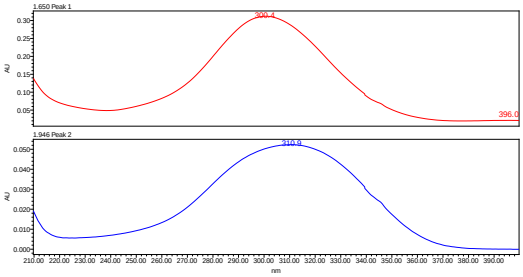


| | Retention Time | Area | % Area | Height |
|---|---|---|---|---|
| 1 | 1.650 | 96047 | 95.01 | 29701 |
| 2 | 1.946 | 5046 | 4.99 | 7337 |

**Figure 4.S13. Reaction of TropC I110A with TropB-generated dienone 4.10.** PDA traces of enzymatic reaction analyzed at 360 nm.

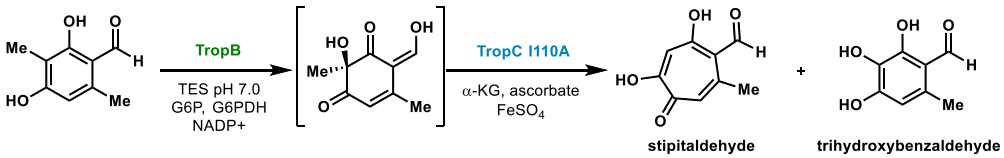


## With TropC

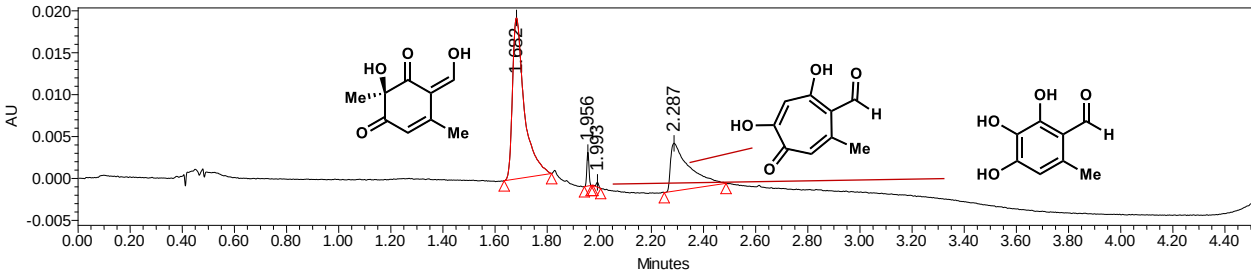


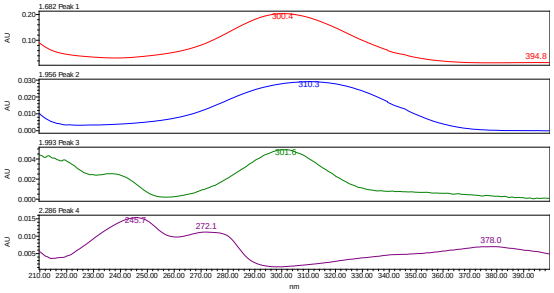


| | Retention Time | Area | % Area | Height |
|---|---|---|---|---|
| 1 | 1.682 | 60457 | 66.12 | 19206 |
| 2 | 1.956 | 2285 | 2.50 | 4020 |
| 3 | 1.993 | 376 | 0.41 | 586 |
| 4 | 2.287 | 28321 | 30.97 | 5705 |

## TropB only

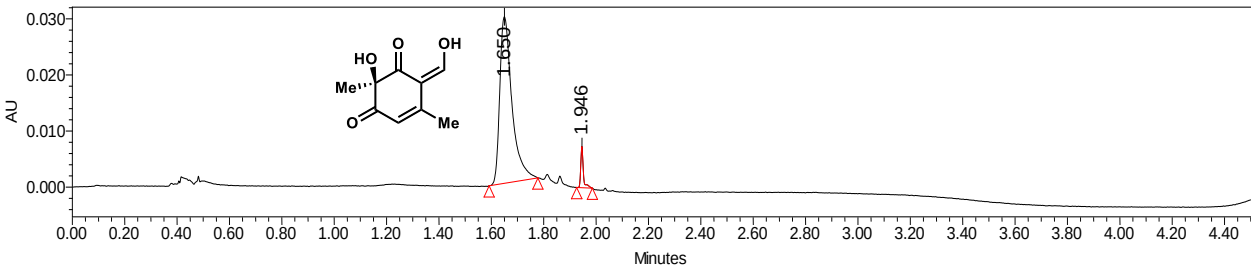


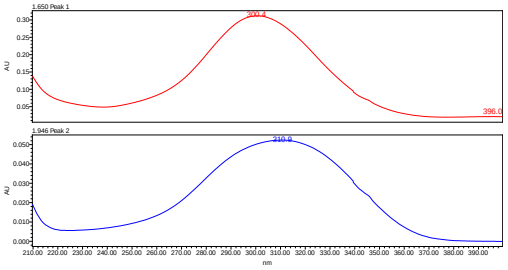


| | Retention Time | Area | % Area | Height |
|---|---|---|---|---|
| 1 | 1.650 | 96047 | 95.01 | 29701 |
| 2 | 1.946 | 5046 | 4.99 | 7337 |

**Figure 4.S14. Reaction of TropC F213Y with TropB-generated dienone 4.10.** PDA traces of enzymatic reaction analyzed at 360 nm.

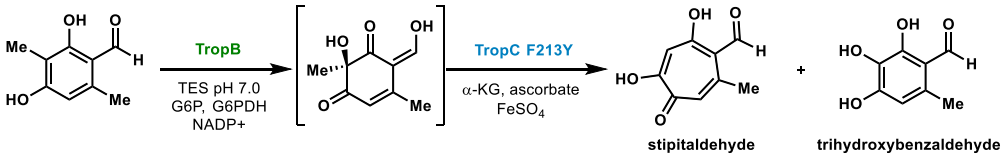


## With TropC

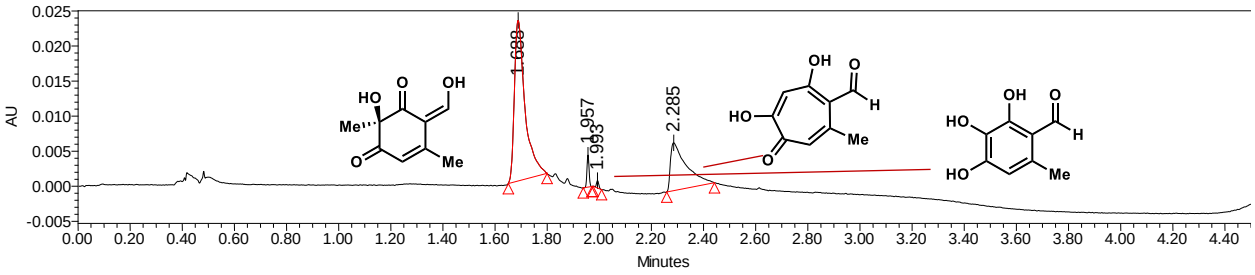


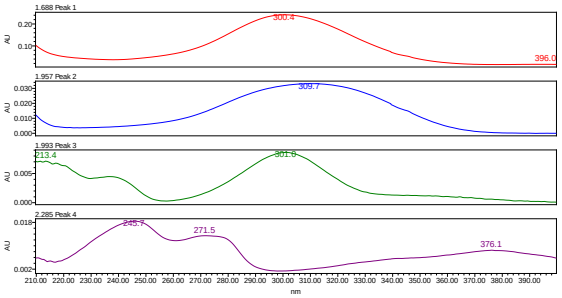

| | Retention Time | Area | % Area | Height |
|---|---|---|---|---|
| 1 | 1.688 | 64855 | 66.86 | 22883 |
| 2 | 1.957 | 2595 | 2.67 | 4564 |
| 3 | 1.993 | 646 | 0.67 | 1063 |
| 4 | 2.285 | 28901 | 29.80 | 6834 |

## TropB only

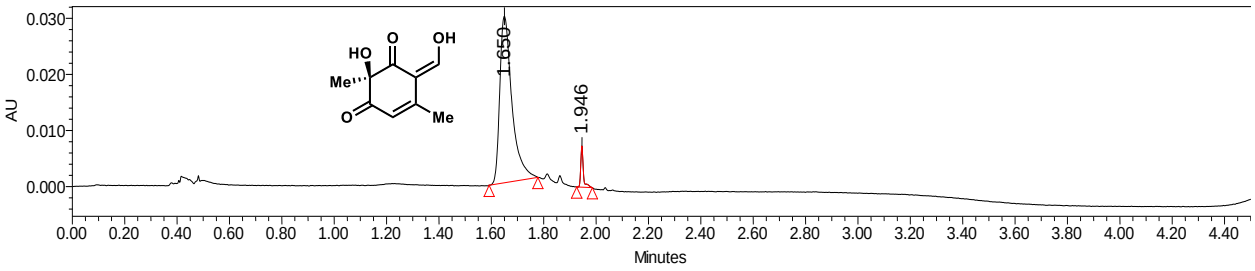


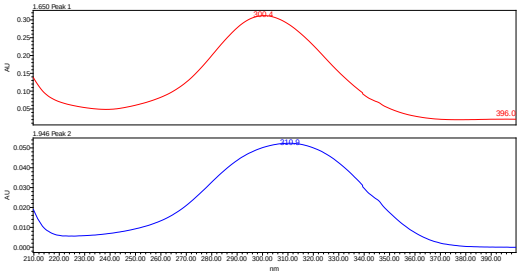

| | Retention Time | Area | % Area | Height |
|---|---|---|---|---|
| 1 | 1.650 | 96047 | 95.01 | 29701 |
| 2 | 1.946 | 5046 | 4.99 | 7337 |

**Figure 4.S15. Reaction of TropC F283A with TropB-generated dienone 4.10.** PDA traces of enzymatic reaction analyzed at 360 nm.

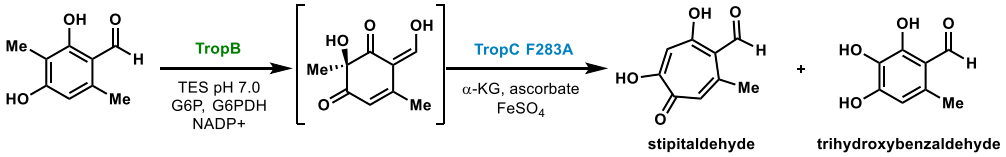


## With TropC

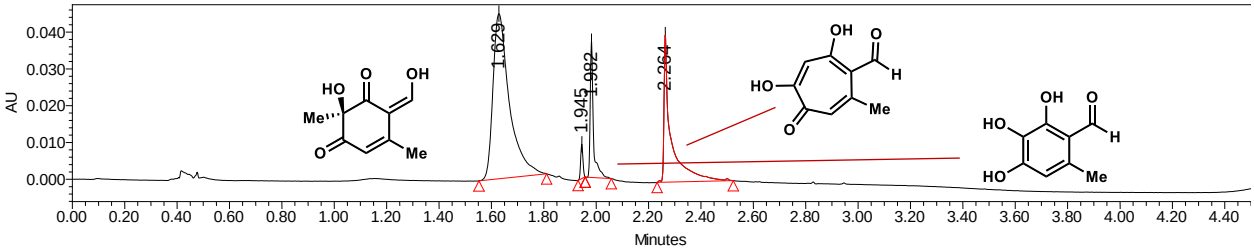


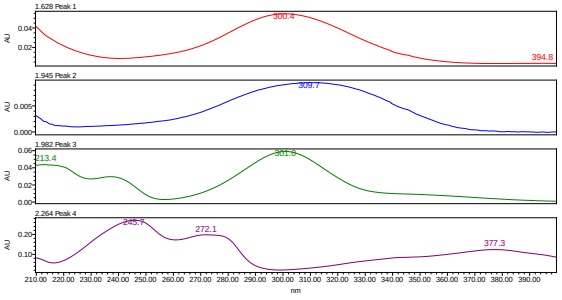


| | Retention Time | Area | % Area | Height |
|---|---|---|---|---|
| 1 | 1.629 | 195814 | 63.48 | 44839 |
| 2 | 1.945 | 5569 | 1.81 | 9326 |
| 3 | 1.982 | 31658 | 10.26 | 37019 |
| 4 | 2.264 | 75432 | 24.45 | 40034 |

## TropB only

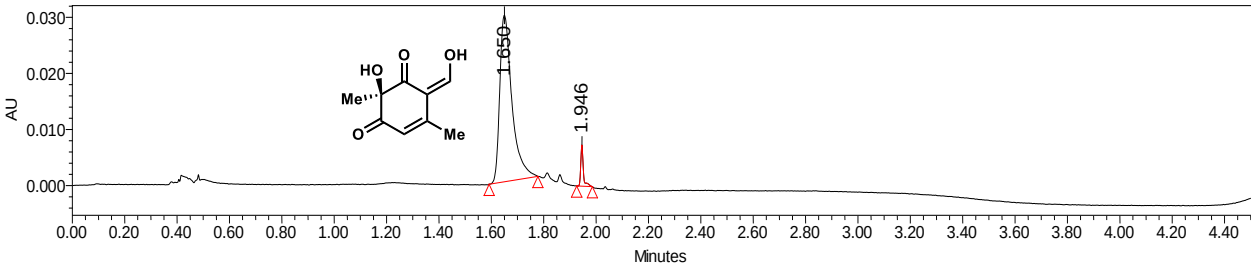


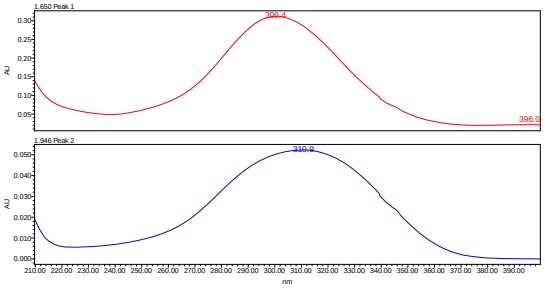


| | Retention Time | Area | % Area | Height |
|---|---|---|---|---|
| 1 | 1.650 | 96047 | 95.01 | 29701 |
| 2 | 1.946 | 5046 | 4.99 | 7337 |

**Figure 4.S16. Reaction of TropC F283Y with TropB-generated dienone 4.10.** PDA traces of enzymatic reaction analyzed at 360 nm.

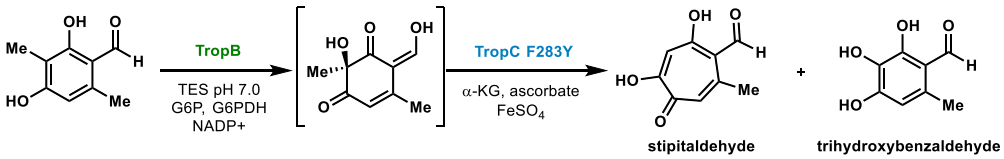


## With TropC

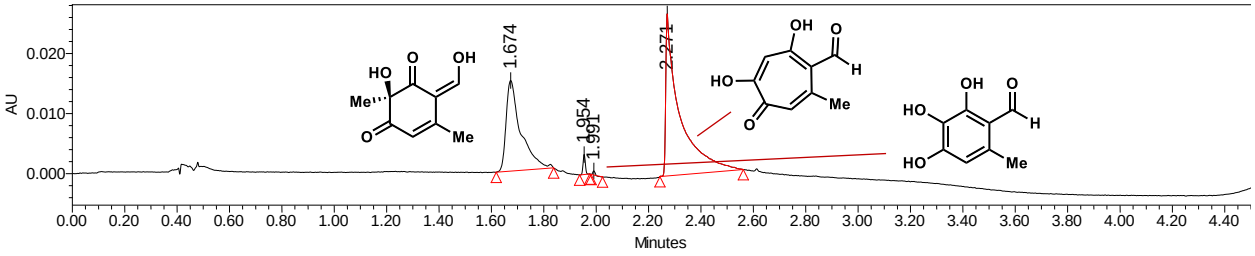


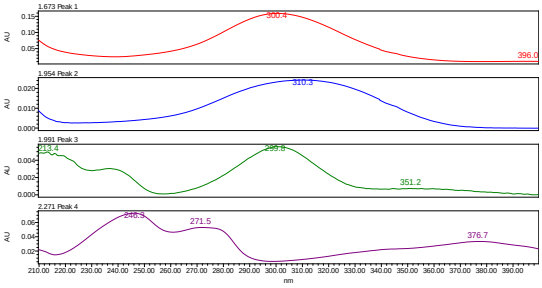

| | Retention Time | Area | % Area | Height |
|---|---|---|---|---|
| 1 | 1.674 | 58765 | 36.59 | 15106 |
| 2 | 1.954 | 1990 | 1.24 | 3339 |
| 3 | 1.991 | 463 | 0.29 | 700 |
| 4 | 2.271 | 99381 | 61.88 | 27052 |

## TropB only

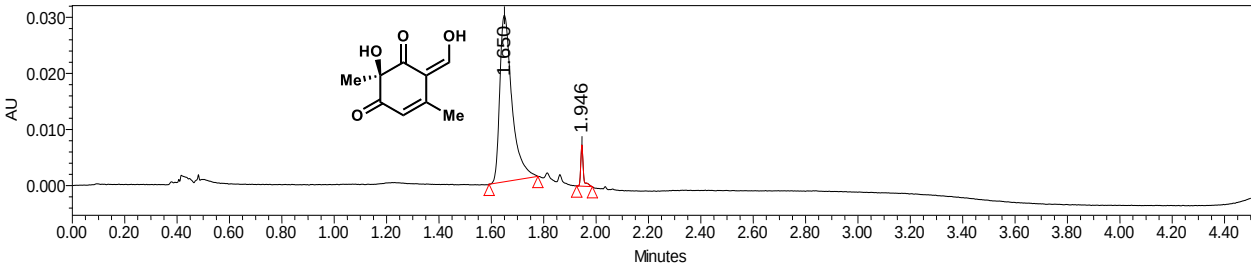


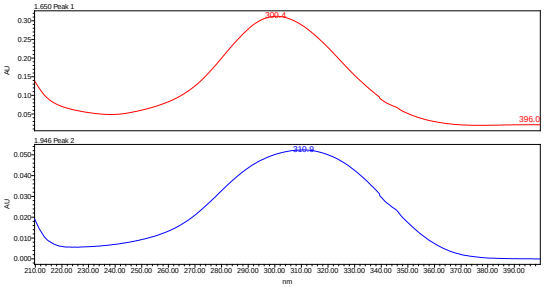

| | Retention Time | Area | % Area | Height |
|---|---|---|---|---|
| 1 | 1.650 | 96047 | 95.01 | 29701 |
| 2 | 1.946 | 5046 | 4.99 | 7337 |

**Figure 4.S17. Reaction of TropC F86A with TropB-generated dienone 4.10.** PDA traces of enzymatic reaction analyzed at 360 nm.

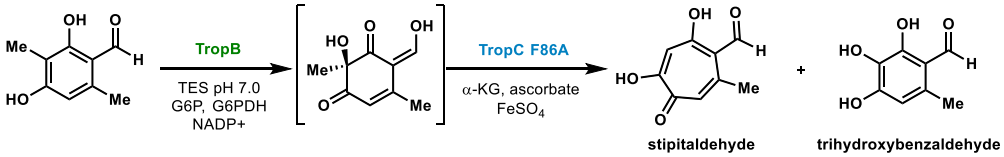


## With TropC

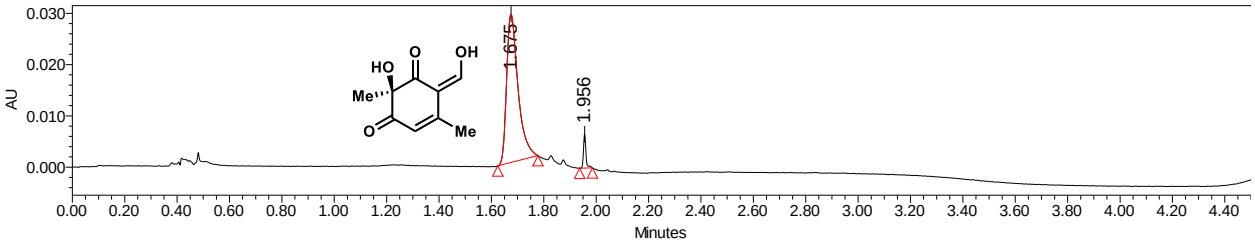


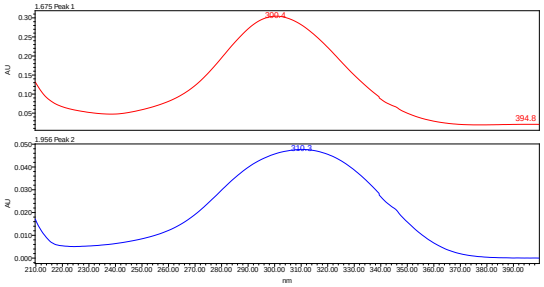

| | Retention Time | Area | % Area | Height |
|---|---|---|---|---|
| 1 | 1.675 | 87718 | 95.29 | 28900 |
| 2 | 1.956 | 4337 | 4.71 | 6627 |

## TropB only

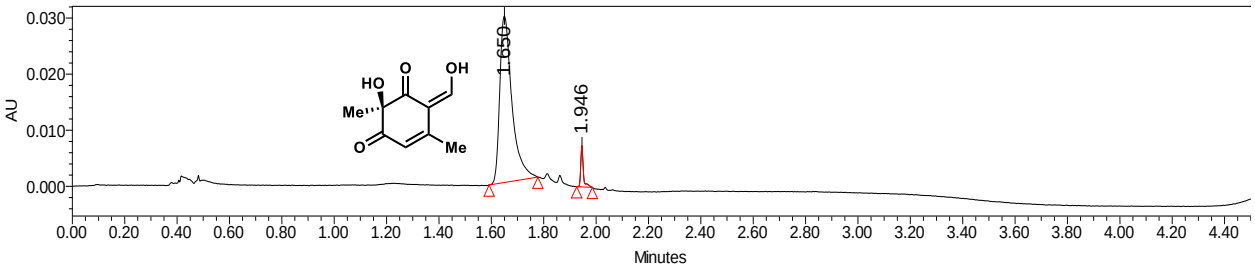


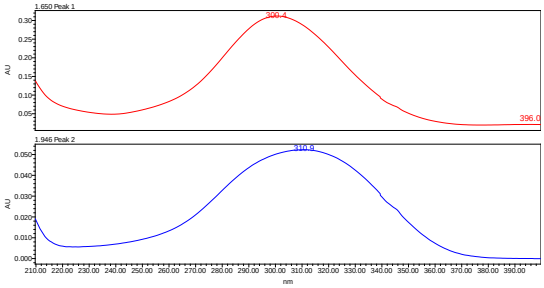

| | Retention Time | Area | % Area | Height |
|---|---|---|---|---|
| 1 | 1.650 | 96047 | 95.01 | 29701 |
| 2 | 1.946 | 5046 | 4.99 | 7337 |

**Figure 4.S18. Reaction of TropC F86Y with TropB-generated dienone 4.10.** PDA traces of enzymatic reaction analyzed at 360 nm.

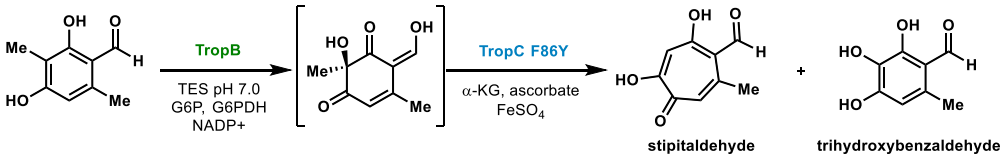


## With TropC

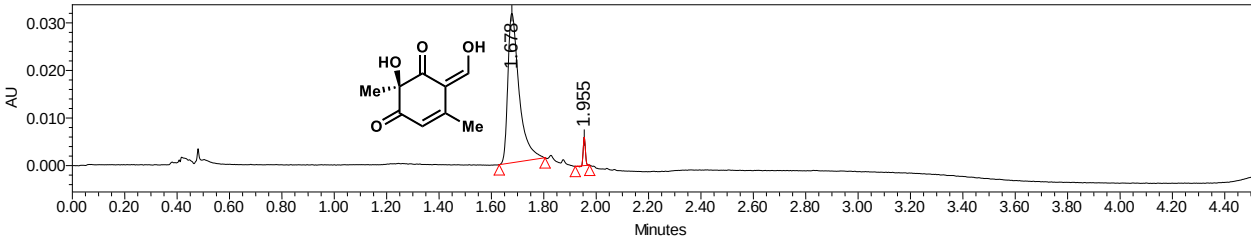


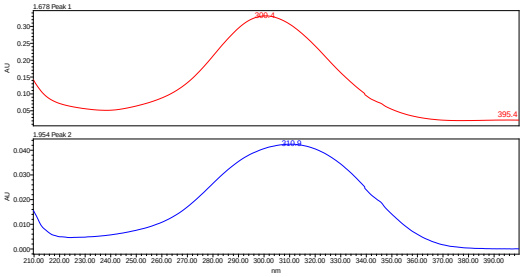

| | Retention Time | Area | % Area | Height |
|---|---|---|---|---|
| 1 | 1.678 | 94345 | 96.33 | 31408 |
| 2 | 1.955 | 3599 | 3.67 | 5966 |

## TropB only

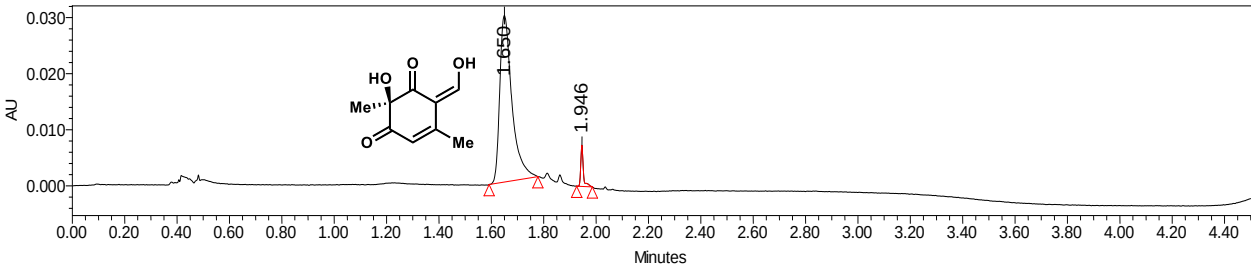


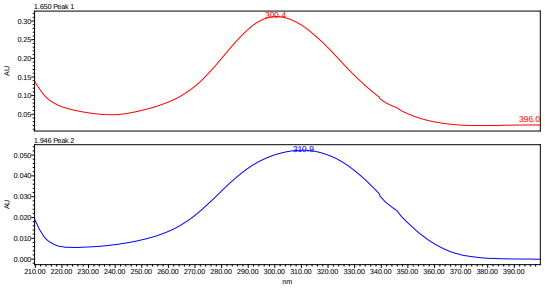

| | Retention Time | Area | % Area | Height |
|---|---|---|---|---|
| 1 | 1.650 | 96047 | 95.01 | 29701 |
| 2 | 1.946 | 5046 | 4.99 | 7337 |

**Figure 4.S19. Reaction of TropC S217A with TropB-generated dienone 4.10.** PDA traces of enzymatic reaction analyzed at 360 nm.

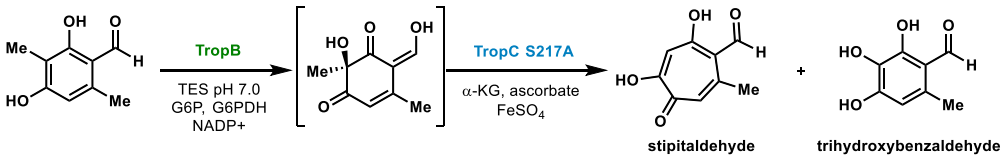


## With TropC

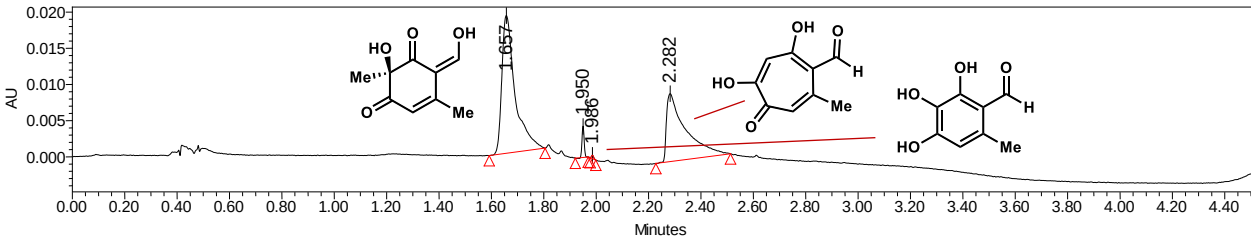


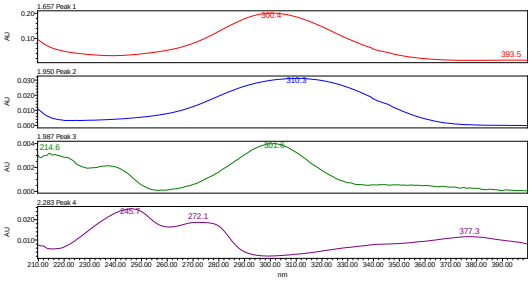

| | Retention Time | Area | % Area | Height |
|---|---|---|---|---|
| 1 | 1.657 | 67041 | 57.09 | 19048 |
| 2 | 1.950 | 2538 | 2.16 | 4320 |
| 3 | 1.986 | 270 | 0.23 | 477 |
| 4 | 2.282 | 47580 | 40.52 | 9389 |

## TropB only

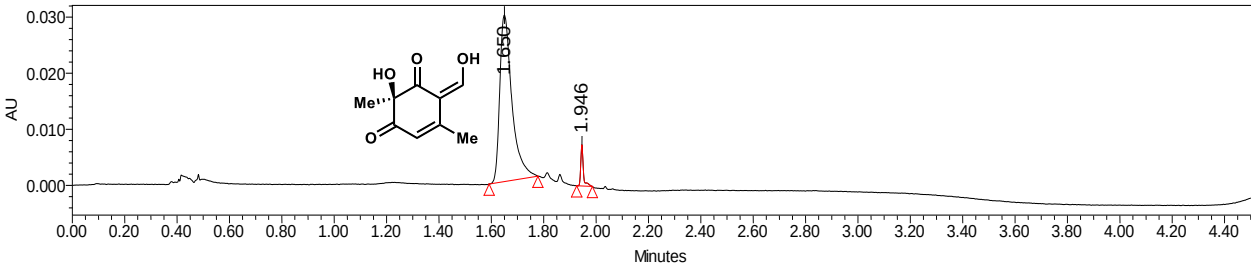


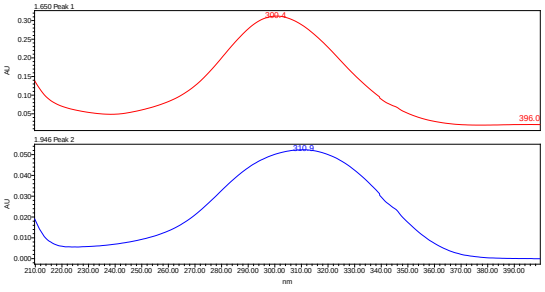

| | Retention Time | Area | % Area | Height |
|---|---|---|---|---|
| 1 | 1.650 | 96047 | 95.01 | 29701 |
| 2 | 1.946 | 5046 | 4.99 | 7337 |

**Figure 4.S20. Reaction of TropC S217T with TropB-generated dienone 4.10.** PDA traces of enzymatic reaction analyzed at 360 nm.

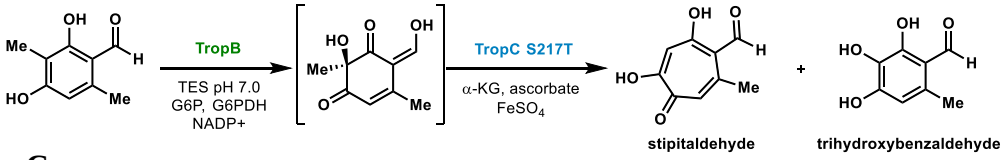


## With TropC

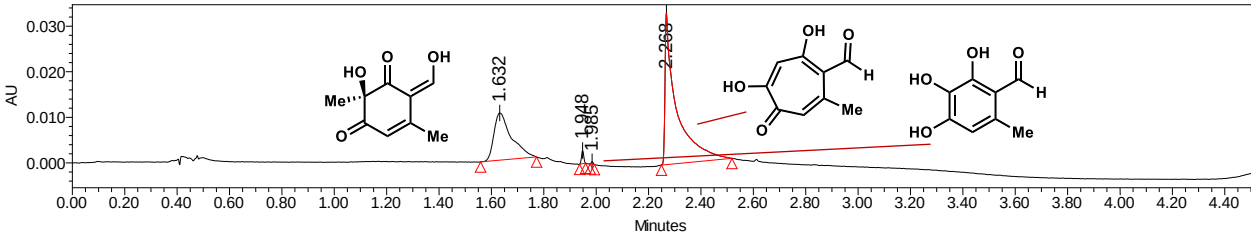


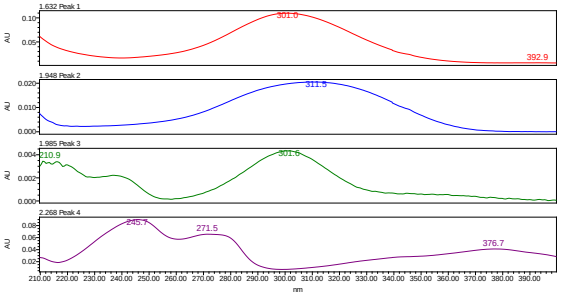

| | Retention Time | Area | % Area | Height |
|---|---|---|---|---|
| 1 | 1.632 | 47777 | 31.65 | 10364 |
| 2 | 1.948 | 1693 | 1.12 | 2886 |
| 3 | 1.985 | 268 | 0.18 | 546 |
| 4 | 2.268 | 101199 | 67.05 | 33239 |

## TropB only

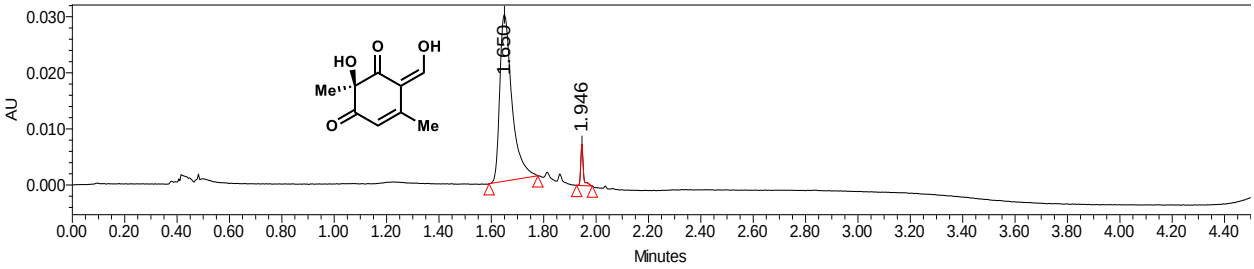


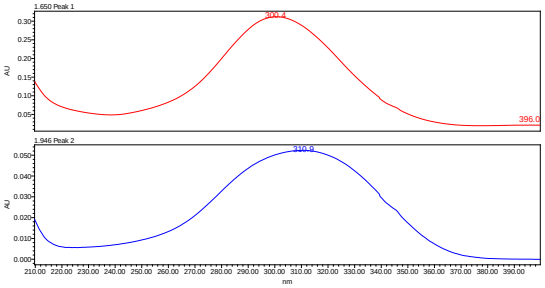

| | Retention Time | Area | % Area | Height |
|---|---|---|---|---|
| 1 | 1.650 | 96047 | 95.01 | 29701 |
| 2 | 1.946 | 5046 | 4.99 | 7337 |

**Figure 4.S21. Reaction of TropC C108A with TropB-generated dienone 4.10.** PDA traces of enzymatic reaction analyzed at 360 nm.

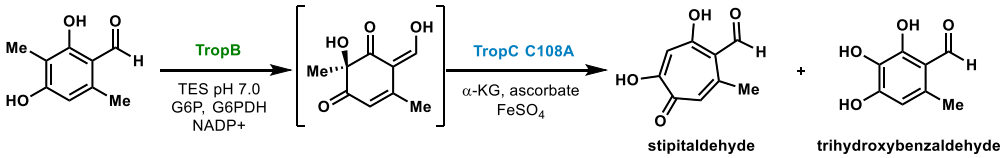


## With TropC

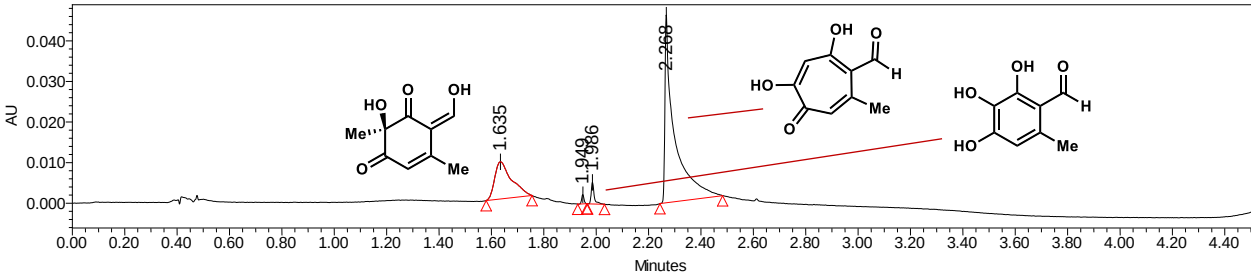


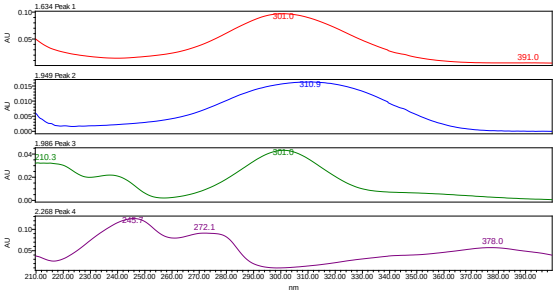

| | Retention Time | Area | % Area | Height |
|---|---|---|---|---|
| 1 | 1.635 | 40674 | 24.93 | 9174 |
| 2 | 1.949 | 1422 | 0.87 | 2302 |
| 3 | 1.986 | 4246 | 2.60 | 5332 |
| 4 | 2.268 | 116799 | 71.59 | 46252 |

## TropB only

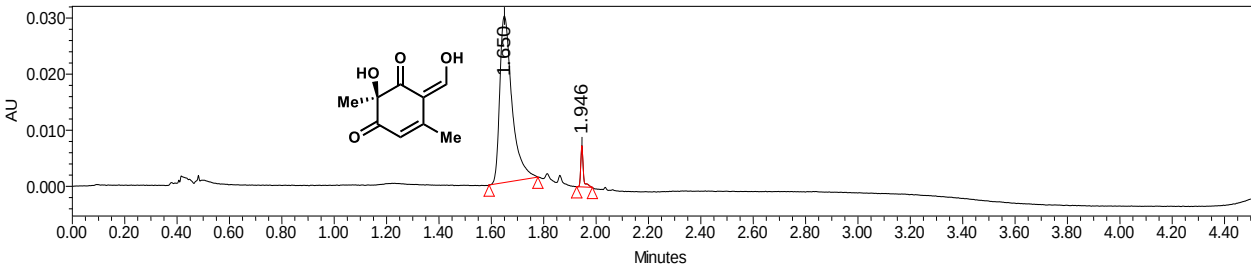


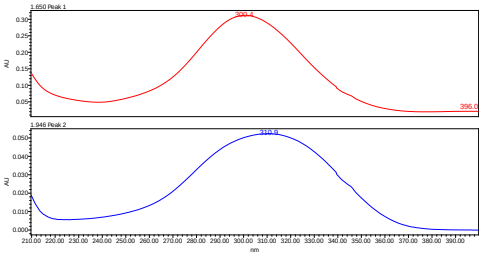

| | Retention Time | Area | % Area | Height |
|---|---|---|---|---|
| 1 | 1.650 | 96047 | 95.01 | 29701 |
| 2 | 1.946 | 5046 | 4.99 | 7337 |

**Figure 4.S22. Reaction of TropC Q95A with TropB-generated dienone 4.10.** PDA traces of enzymatic reaction analyzed at 360 nm.

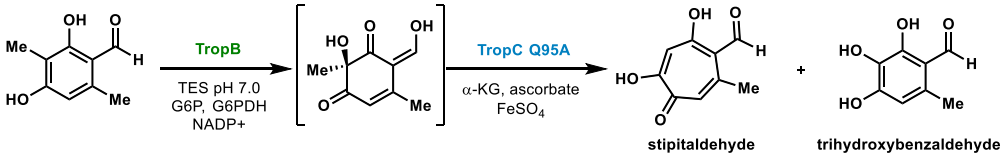


## With TropC

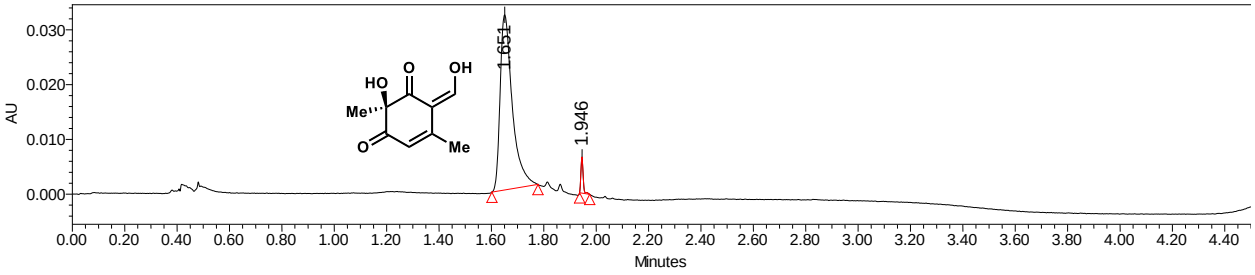


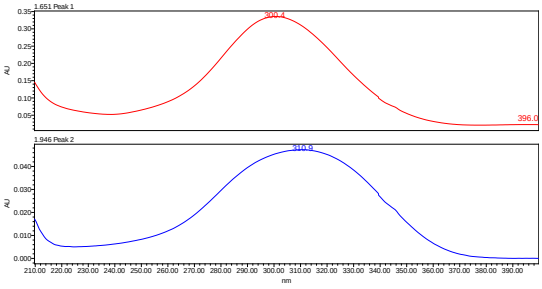

| | Retention Time | Area | % Area | Height |
|---|---|---|---|---|
| 1 | 1.651 | 103456 | 96.37 | 31979 |
| 2 | 1.946 | 3896 | 3.63 | 6593 |

## TropB only

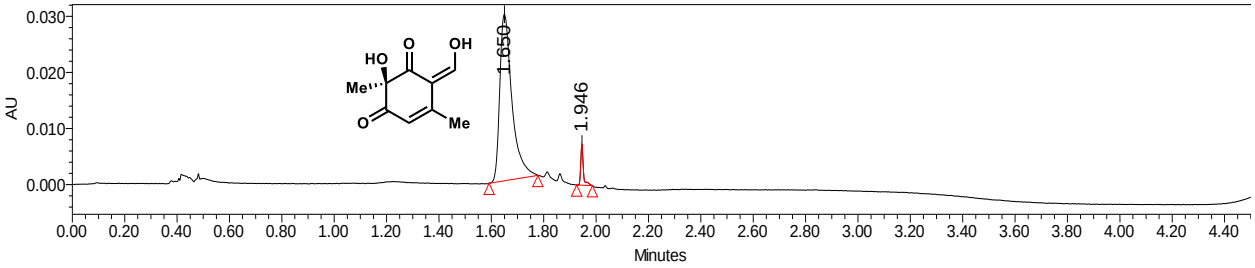


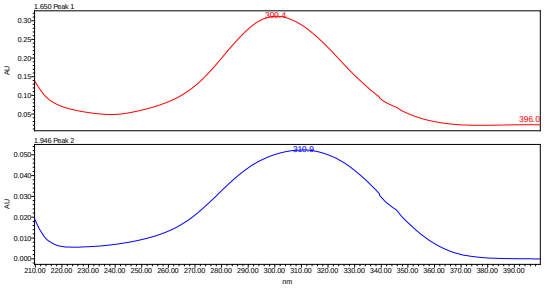

| | Retention Time | Area | % Area | Height |
|---|---|---|---|---|
| 1 | 1.650 | 96047 | 95.01 | 29701 |
| 2 | 1.946 | 5046 | 4.99 | 7337 |

**Figure 4.S23. Reaction of TropC R278A with TropB-generated dienone 4.10.** PDA traces of enzymatic reaction analyzed at 360 nm.

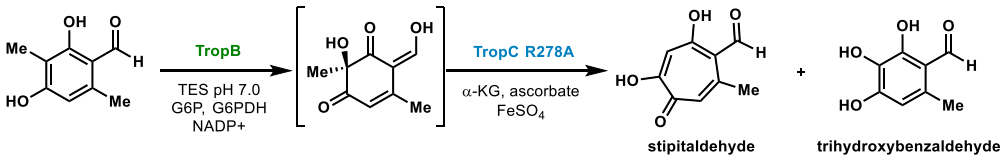


## With TropC

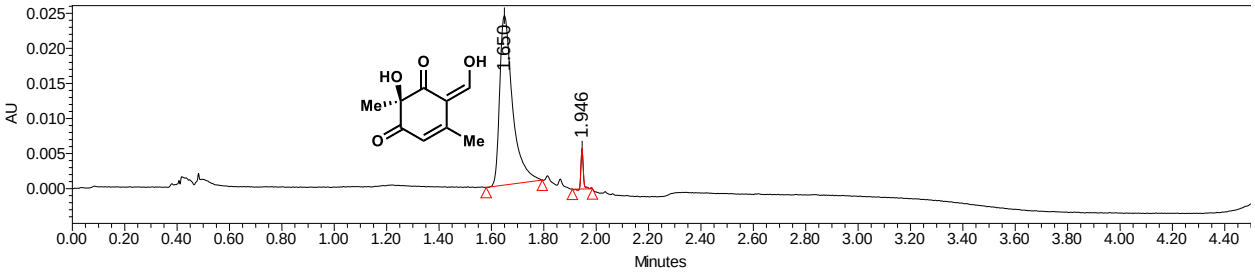


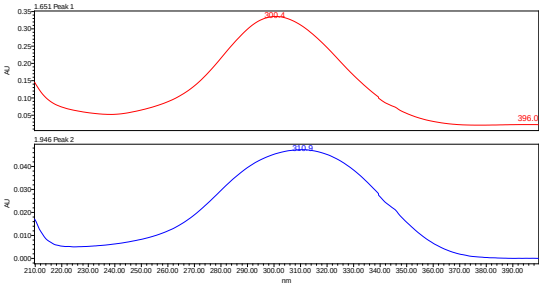

| | Retention Time | Area | % Area | Height |
|---|---|---|---|---|
| 1 | 1.650 | 82678 | 95.66 | 24152 |
| 2 | 1.946 | 3749 | 4.34 | 5727 |

## TropB only

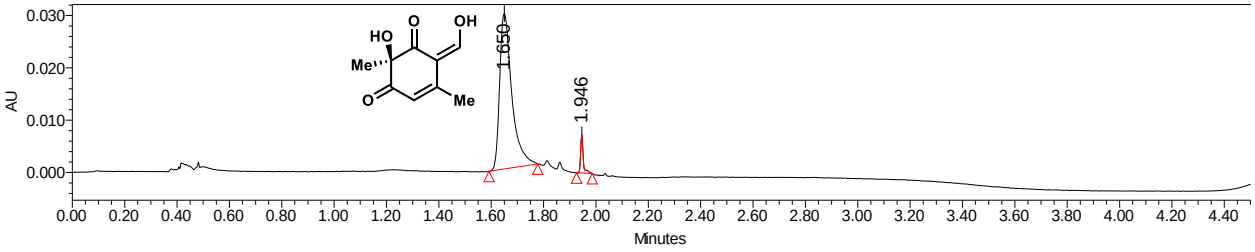


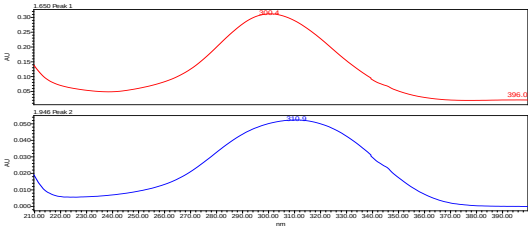

| | Retention Time | Area | % Area | Height |
|---|---|---|---|---|
| 1 | 1.650 | 96047 | 95.01 | 29701 |
| 2 | 1.946 | 5046 | 4.99 | 7337 |

**Figure 4.S24. Reaction of TropC R278K with TropB-generated dienone 4.10.** PDA traces of enzymatic reaction analyzed at 360 nm.

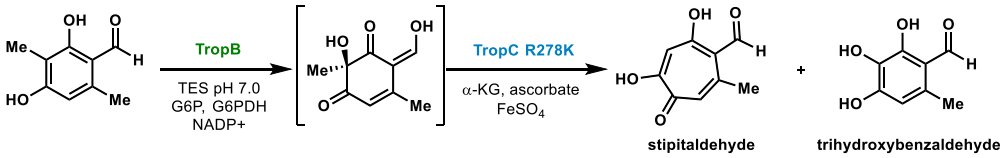


## With TropC

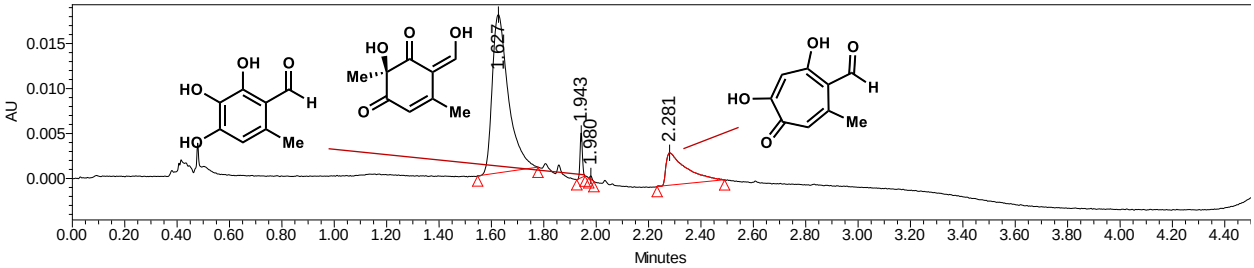


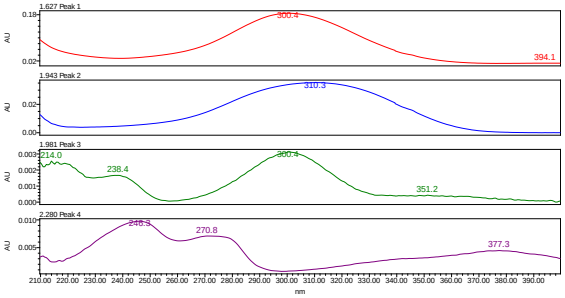


| | Retention Time | Area | % Area | Height |
|---|---|---|---|---|
| 1 | 1.627 | 75546 | 76.95 | 17601 |
| 2 | 1.943 | 3035 | 3.09 | 4982 |
| 3 | 1.980 | 207 | 0.21 | 372 |
| 4 | 2.281 | 19389 | 19.75 | 3622 |

## TropB only

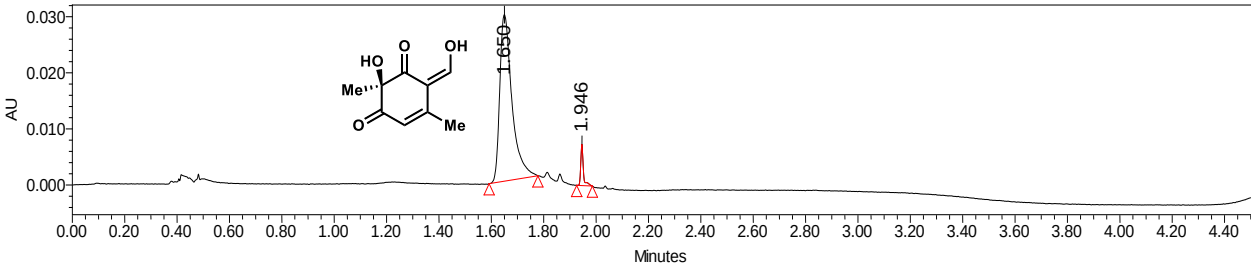


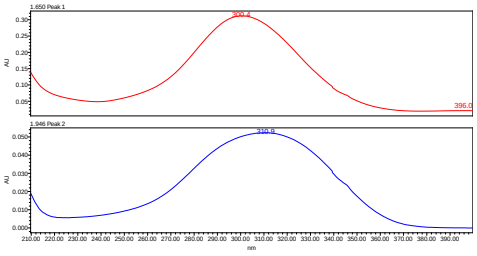


| | Retention Time | Area | % Area | Height |
|---|---|---|---|---|
| 1 | 1.650 | 96047 | 95.01 | 29701 |
| 2 | 1.946 | 5046 | 4.99 | 7337 |

**Figure 4.S25. Reaction of wild-type TropC with dienone 4.10. PDA traces of** enzymatic reaction analyzed at 300 nm.

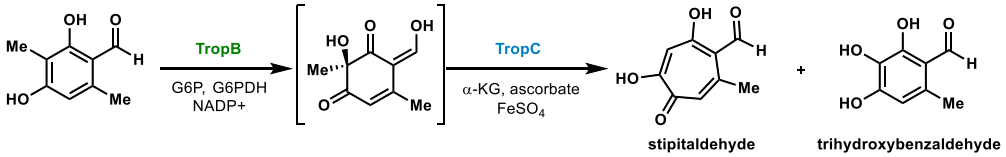


## With TropC

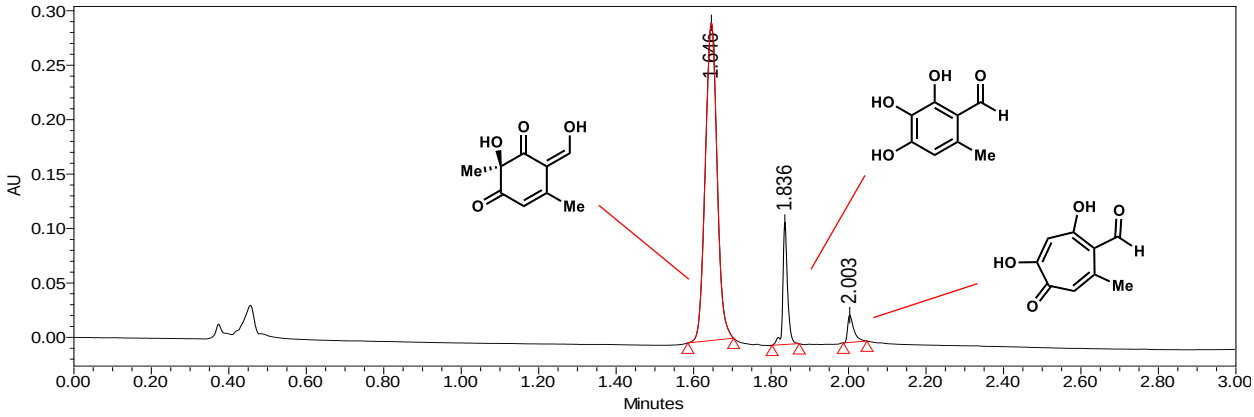


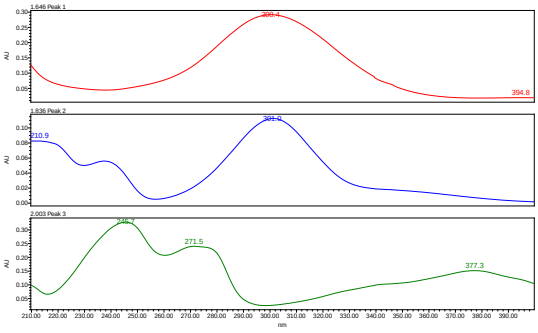

| | Retention Time | Area | % Area | Height |
|---|---|---|---|---|
| 1 | 1.646 | 620887 | 83.70 | 291746 |
| 2 | 1.836 | 93090 | 12.55 | 112386 |
| 3 | 2.003 | 27801 | 3.75 | 25219 |

**Figure 4.S26. Reaction of wild-type CitB with substrate 4.9.** PDA traces of enzymatic reaction analyzed at 300 nm.

## With CitB

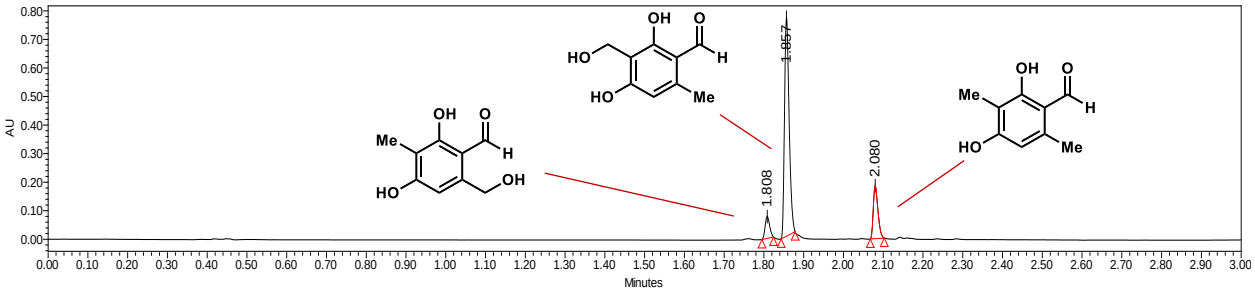


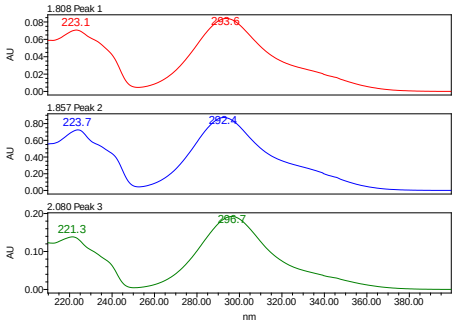


| | Retention Time | Area | % Area | Height |
|---|---|---|---|---|
| 1 | 1.808 | 60277 | 7.28 | 76765 |
| 2 | 1.857 | 617301 | 74.60 | 767275 |
| 3 | 2.080 | 149848 | 18.11 | 185817 |

## No enzyme control

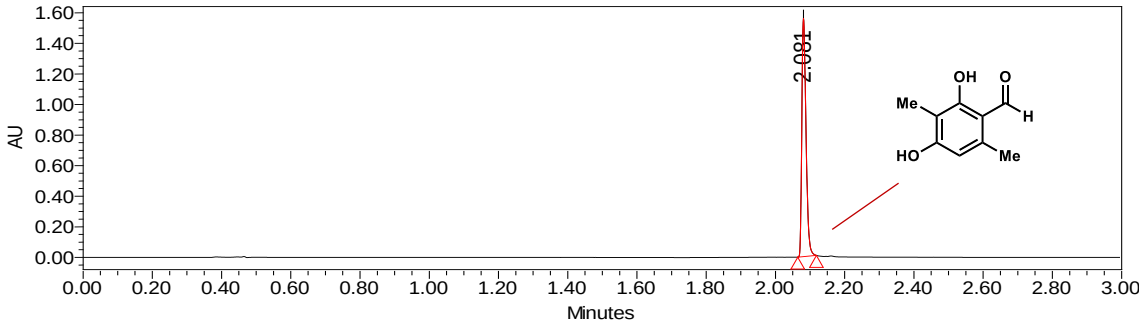


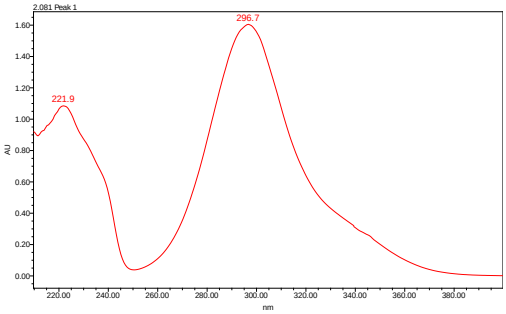


| | Retention Time | Area | % Area | Height |
|---|---|---|---|---|
| 1 | 2.081 | 1311812 | 100.00 | 1557555 |

**Figure 4.S27. Reaction of TropB with benzylic alcohol 4.25.** PDA traces of enzymatic reaction analyzed at 300 nm.

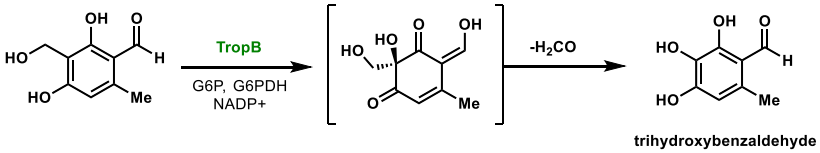


## With TropB

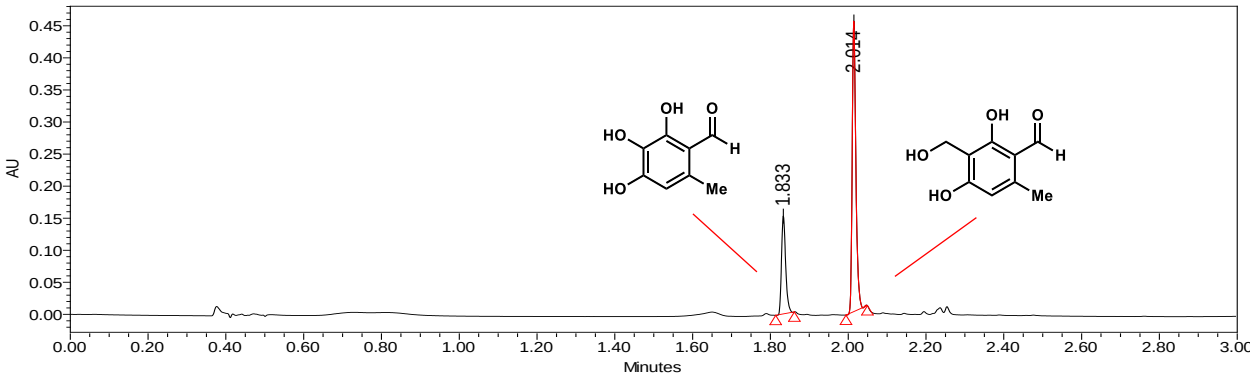


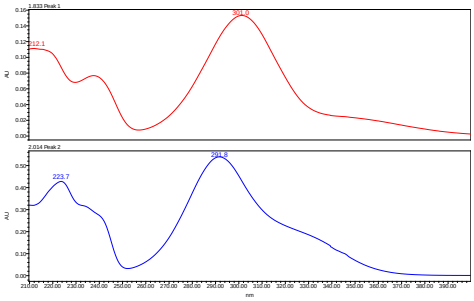

| | Retention Time | Area | % Area | Height |
|---|---|---|---|---|
| 1 | 1.833 | 112936 | 27.55 | 152592 |
| 2 | 2.014 | 296957 | 72.45 | 453413 |

3-hydroxyorcinaldehyde (**4.18**) product standard

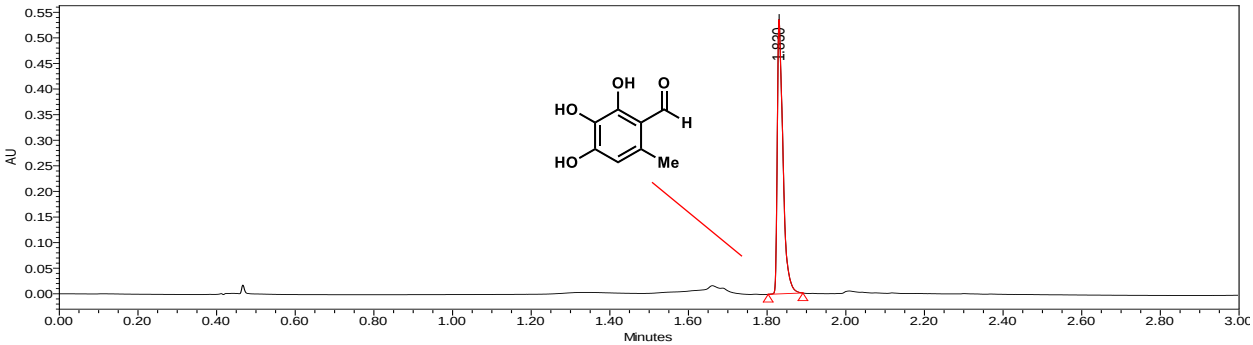


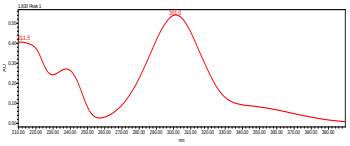

| | Retention Time | Area | % Area | Height |
|---|---|---|---|---|
| 1 | 1.830 | 538937 | 100.00 | 537068 |

**Figure 4.S28. Reaction of TropB and TropC with benzylic alcohol 4.25.** PDA traces of enzymatic reaction analyzed at 300 nm.

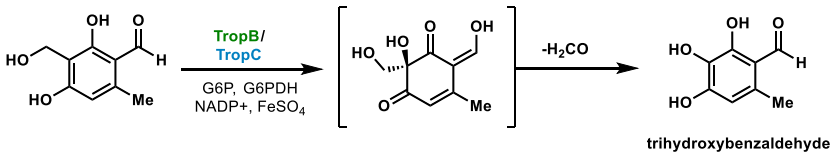


## With TropB and TropC

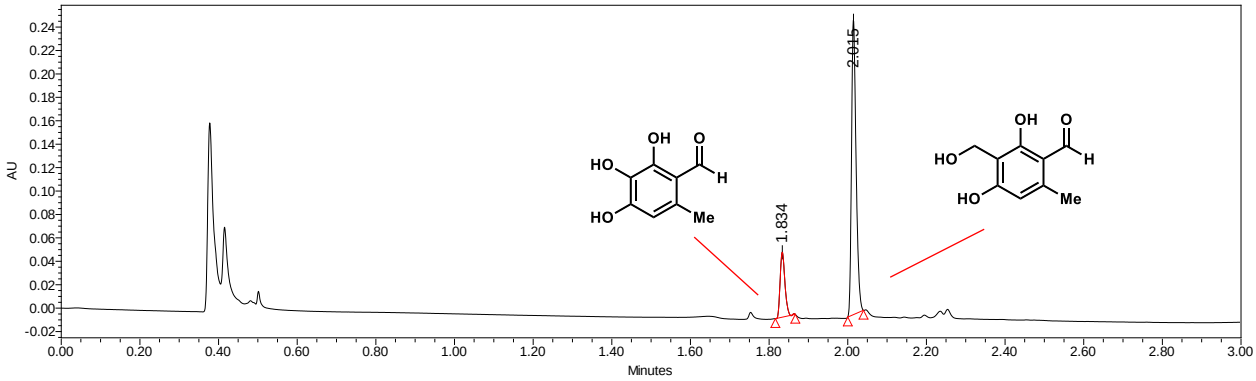


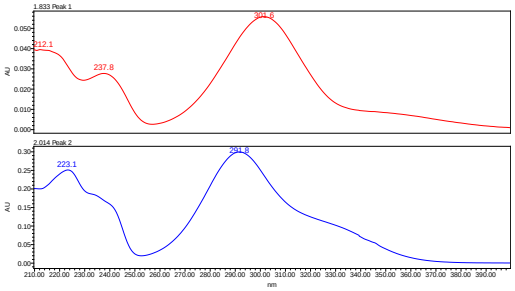

| | Retention Time | Area | % Area | Height |
|---|---|---|---|---|
| 1 | 1.834 | 47107 | 18.87 | 55552 |
| 2 | 2.015 | 202502 | 81.13 | 251750 |

3-hydroxyorcinaldehyde (**4.18**) product standard

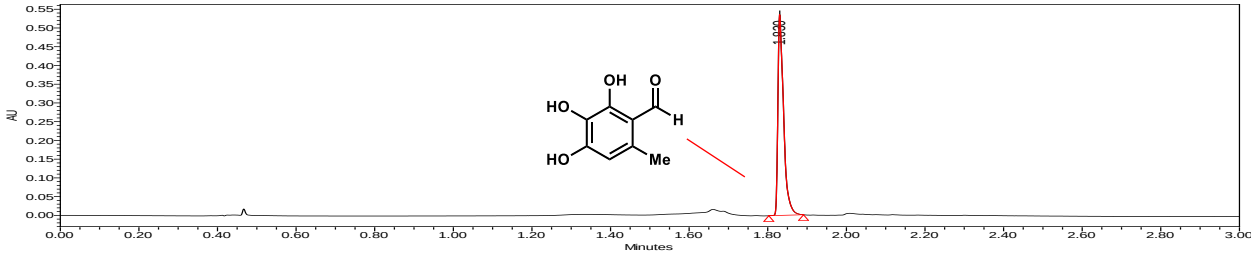


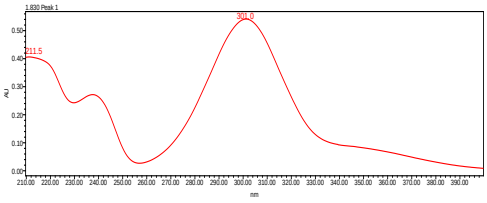

| | Retention Time | Area | % Area | Height |
|---|---|---|---|---|
| 1 | 1.830 | 538937 | 100.00 | 537068 |

**Part VII. NMR spectra of isolated products**

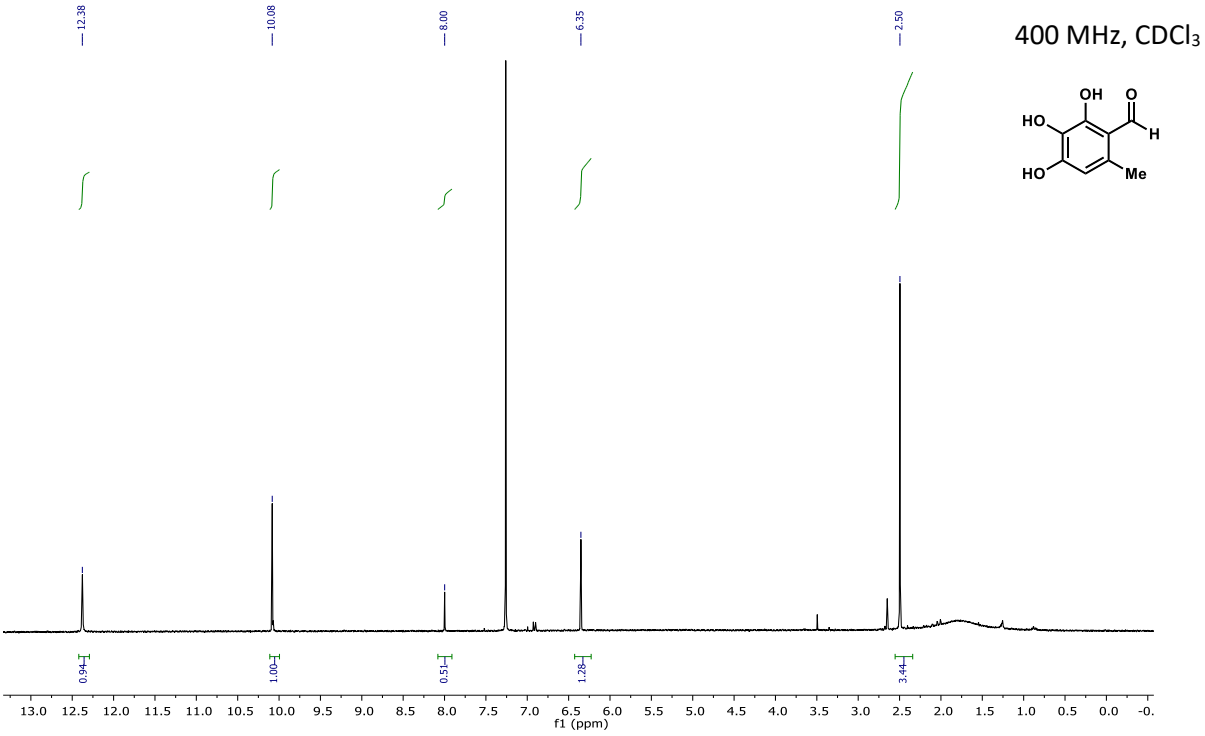

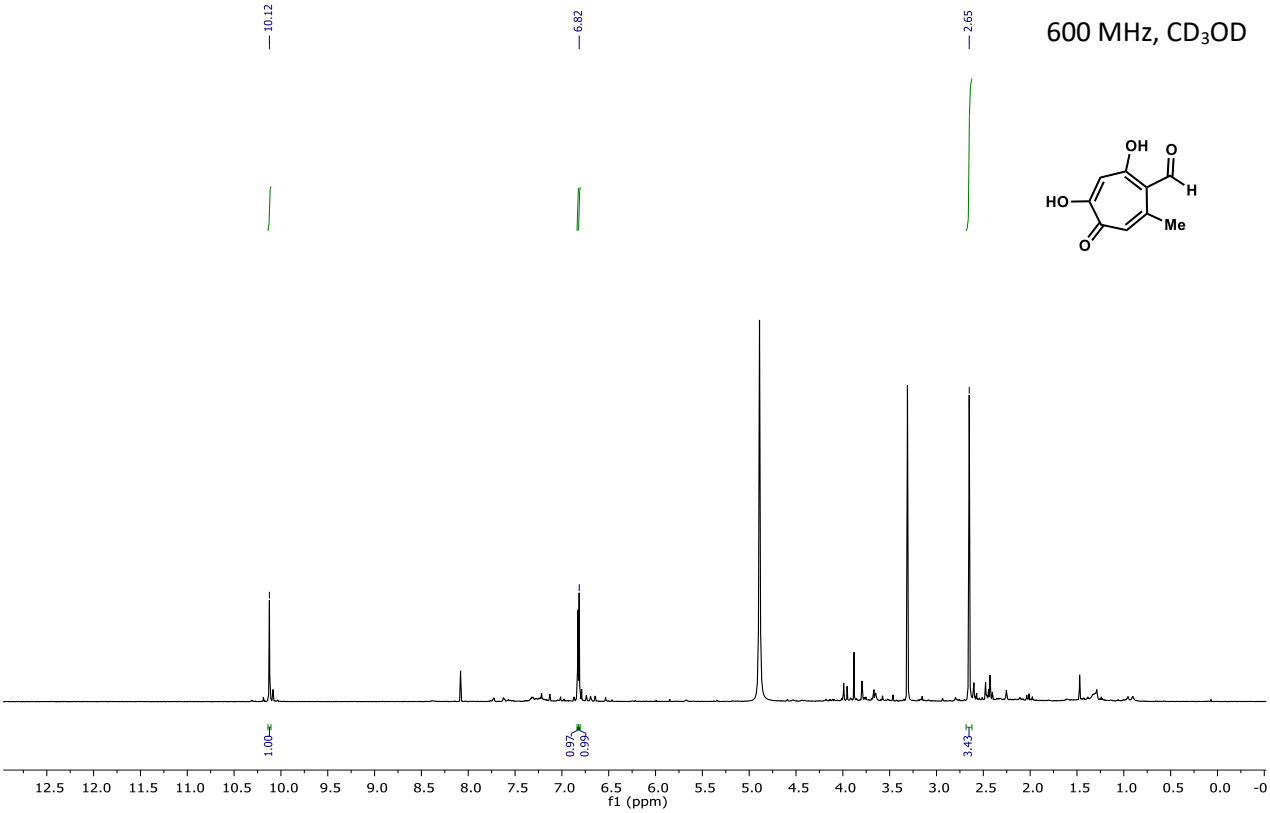
600 MHz, CD3OD
10.12
6.82
2.65
OH
O
H
HO
Me
O
1.00
0.97
0.99
3.43
12.5 12.0 11.5 11.0 10.5 10.0 9.5 9.0 8.5 8.0 7.5 7.0 6.5 6.0 5.5 5.0 4.5 4.0 3.5 3.0 2.5 2.0 1.5 1.0 0.5 0.0 -0
f1 (ppm)

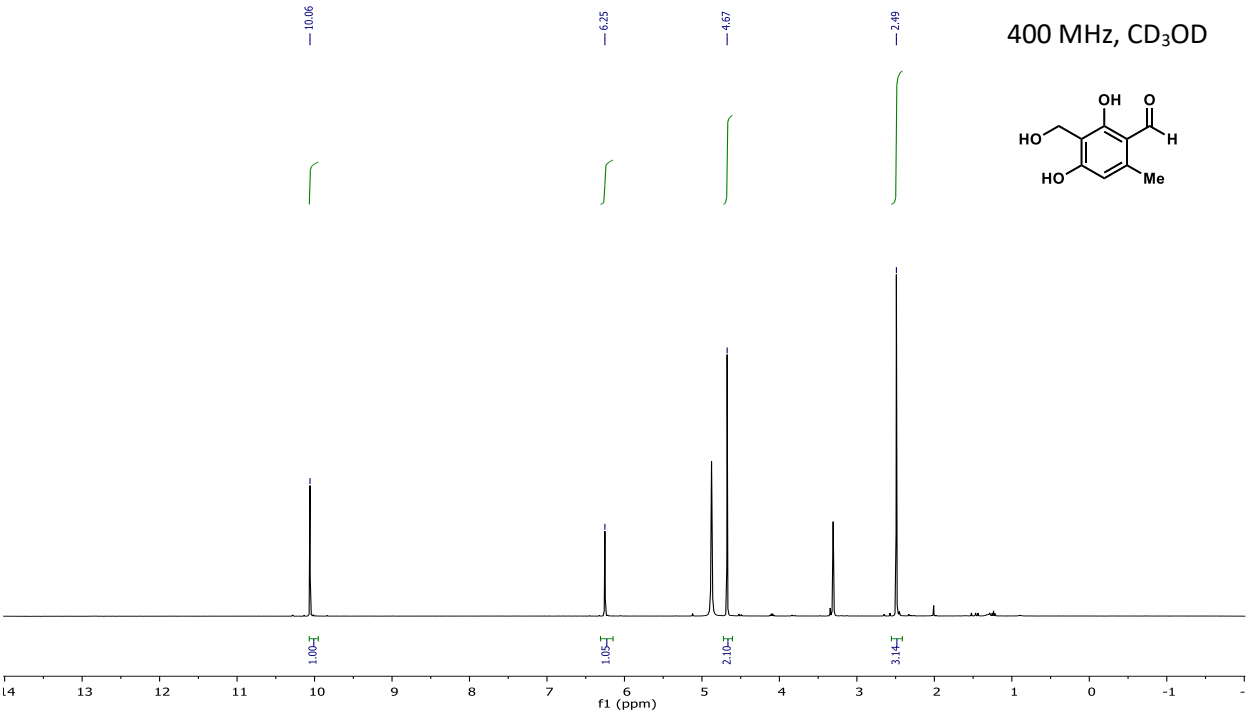
400 MHz, CD3OD
10.06
6.25
4.67
2.49
OH
O
H
HO
HO
Me
1.00
1.05
2.10
3.14
14 13 12 11 10 9 8 7 6 5 4 3 2 1 0 -1
f1 (ppm)

**Figure 4.S29. Previously reported rearomatization reactivity of *ortho*-dearomatized phenols.**[41]

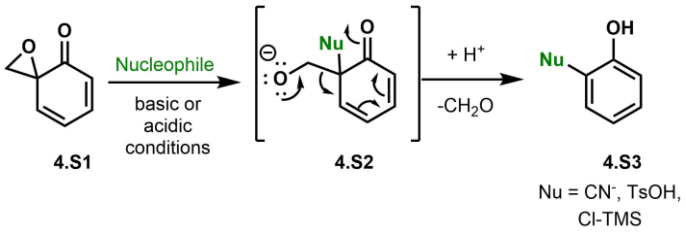


**Part VIII. X-ray crystallography**

**General considerations:** Our initial structure prediction analysis of TropC using the JPRED server suggested that the N-terminal region could be disordered, leading to potential challenges in crystal generation. In an effort to develop a TropC variant amenable to crystallization, we generated a construct containing a 7-residue N-terminal truncation (TropC-7N).[42] TropC-7N was purified to homogeneity and the N-terminal 6x His tag was removed by incubation with TEV protease (see Section II for details).

**Crystallization:** Crystals of TropC were grown using the sitting drop vapor diffusion method. Crystallization of the purified TropC was initially performed with commercially available screens from Rigaku and Molecular Dimension at 20°C and 4° C. Each drop consisted 1:2 mixture of protein solution (10-12 mg/ml in 50 mM Tris-HCl pH 7.4, 0.2 M NaCl and 1 mM TCEP) with reservoir solution. TropC crystals were observed after two weeks at 4˚C. TropC was crystallized in the condition of 0.2 M Magnesium Acetate, 20% PEG 8000, 0.01 M Yttrium (III) Chloride hexahydrate. Crystals were transferred to a cryo-protectant solution containing the corresponding conditions described above and 20% (v/v) glycerol before harvesting. The crystals were harvested and flash-frozen in liquid nitrogen prior to data collection.

**Data collection and processing:** Diffraction data were collected on LS-CAT 21-ID-D beamline at Advanced Photon Source (APS), Argonne National Laboratory using Eiger-9M detector. Data collection and processing statistics are summarized in Table 4.S2.

**Structure solution and refinement:** The structure of TropC was determined by molecular replacement method with MOLREP3 [43] in CCP4 suite, using the structure of T7H *Neurospora crassa* as a search model[44]. Model was built manually using the program Coot[45] and structure refinement was performed using refmac5[46-47] in CCP4 suite.[48] The structure was validated using MolProbity.[49] Open source program, PyMOL, was used for molecular visualization and generating figures.[50]

**Table 4.S2: Data collection and refinement parameters.**

| | TropC |
|---|---|
| **Data collection** | |
| Beamline | APS, LSCAT 21-IDD |
| Wavelength (Å) | 1.0332 |
| Temperature (K) | 100 |
| Resolution (Å) | 48.07-2.7 (2.873-2.7) |
| Space group | $P3_121$ |
| Cell dimensions (Å) | a = 111.0, b = 111.0, c = 89.9 |
| Cell dimensions (°) | α = β = 90, γ = 120 |
| Observed reflections | 100802 (13636) |
| Unique reflections | 17040 (2288) |
| $R_{merge}$ (%) | 0.070 (1.073) |
| $R_{pim}$ (%) | 0.034 (0.721) |
| <I/σ> | 14.4 (1.7) |
| CC(1/2) | 0.999 (0.766) |
| Multiplicity | 5.9 (6.0) |
| Completeness (%) | 95.4 (71.7) |
| Overall *B* (Å$^2$) (Wilson plot) | 64.9 |
| **Refinement** | |
| Resolution range | 48.07-2.7 |
| Number of reflections (work/test set) | 17015 (796) |
| $R_{work}/R_{free}$ (%) | 21.3/25.0 |
| No. of non-H atoms | |
| Protein | 2319 |
| Water | 5 |
| Ligand | 1 |
| B-factors (Å$^2$) | |
| Protein | 72.83 |
| Water | 69.4 |
| Ligand | 93.8 |
| Rmsd deviations | |
| Bond lengths (Å) | 0.005 |
| Bond angles (°) | 0.890 |
| Ramachandran plot | |
| Favored/allowed/outliers | 96.2/3.8/0 |
| MolProbity Score | 1.9 (99$^{th}$ percentile) |

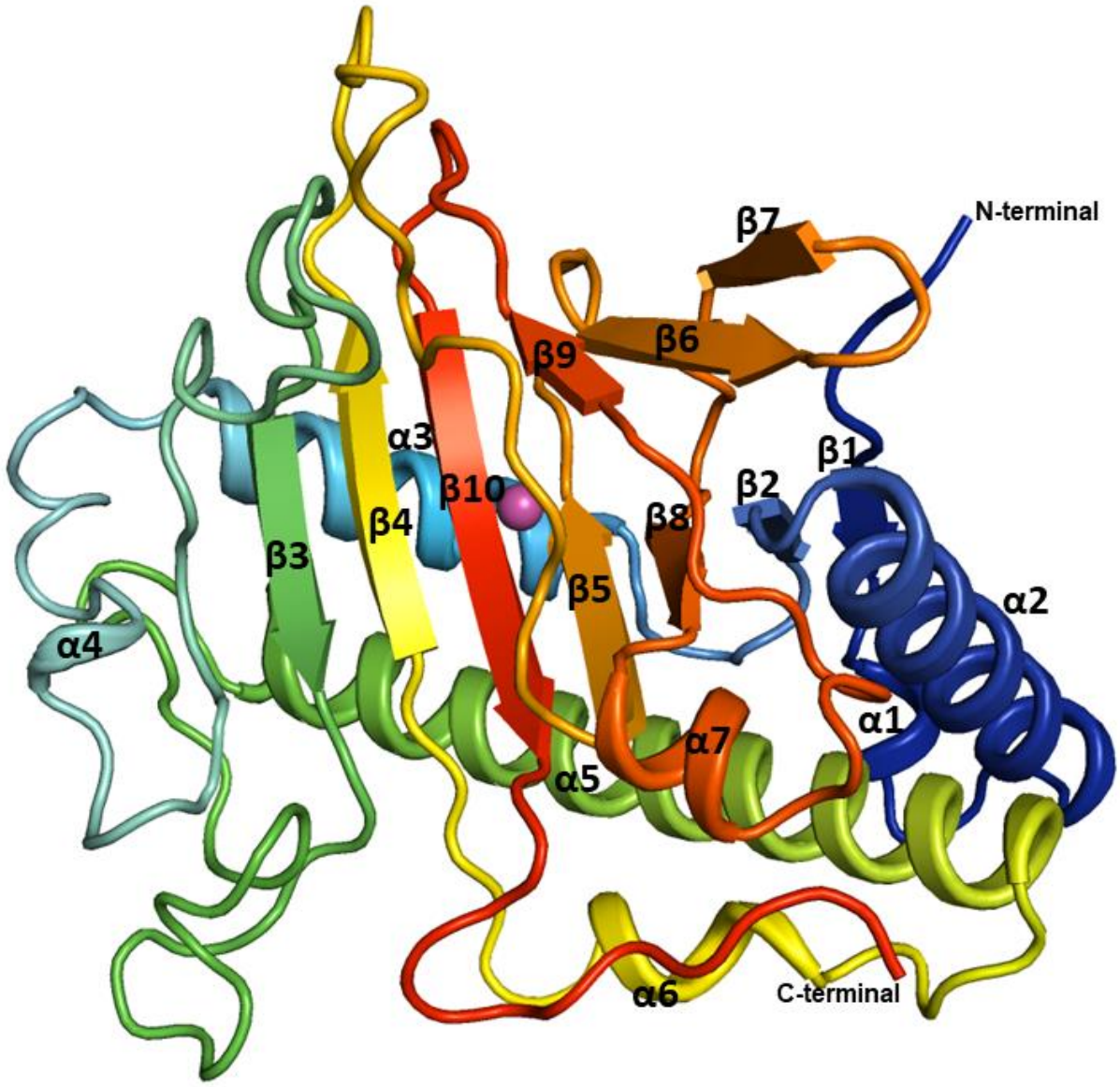


**Figure 4.S30. Structure of TropC from *T. stipitatus.***
Overall structure of TropC (PDB ID: 6XJJ) shown in ribbon representation colored in spectrum, which starts with blue (N-terminal) to red (C-terminal). Jelly-roll (or DSBH) motif at the center of the protein, which comprised of major (β1-5, β8 and β10) and minor (β6, β7 and β9) β-sheets. Fe(III) shown in purple sphere, located at the center of major and minor β-sheet, and in close proximity to β10. Helices (α1-7) are wrapped around the β-sheet. The enzymatic metal binding site is located in similar position as *PaI*PNS (6JYV) and T7H (5C3Q), which is positioned toward the C-terminal end of protein and in close proximity to β10.

| # No | Chain | Z-score | rmsd | %id | |
|---|---|---|---|---|---|
| **1** | 6jyv-A | 32.2 | 2.1 | 32 | PROBABLE IRON/ASCORBATE OXIDOREDUCTASE; |
| **2** | 5c3q-A | 31.8 | 2.1 | 29 | THYMINE DIOXYGENASE; |
| **3** | 3oox-A | 29.9 | 2.3 | 26 | PUTATIVE 2OG-FE(II) OXYGENASE FAMILY PROTEIN; |
| **4** | 1gp6-A | 29.5 | 2.2 | 25 | LEUCOANTHOCYANIDIN DIOXYGENASE; |
| **5** | 5v2z-A | 29.2 | 2.1 | 22 | 2-OXOGLUTARATE-DEPENDENT ETHYLENE/SUCCINATE-FORMI |
| **6** | 5o7y-A | 28.9 | 2.2 | 27 | THEBAINE 6-O-DEMETHYLASE; |
| **7** | 2vau-A | 28.8 | 2.3 | 22 | ISOPENICILLIN N SYNTHETASE; |
| **8** | 4xae-A | 27.9 | 2.4 | 31 | FERULOYL COA ORTHO-HYDROXYLASE 1; |
| **9** | 6tto-A | 27.4 | 2.1 | 24 | HYOSCYAMINE 6 BETA-HYDROXYLASE; |
| **10** | 3on7-B | 24.8 | 2.4 | 24 | OXIDOREDUCTASE, IRON/ASCORBATE FAMILY; |
| **11** | 5tcv-A | 24.5 | 2.3 | 25 | 1-AMINOCYCLOPROPANE-1-CARBOXYLATE OXIDASE 1; |
| **12** | 1unb-A | 23.3 | 2.6 | 20 | DEACETOXYCEPHALOSPORIN C SYNTHETASE; |
| **13** | 5udb-8 | 19.8 | 2.4 | 13 | DNA REPLICATION LICENSING FACTOR MCM2; |
| **14** | 6n1f-D | 14.4 | 3.2 | 11 | OXIDOREDUCTASE, 2OG-FE(II) OXYGENASE FAMILY; |
| **15** | 4kbz-A | 13.3 | 3.6 | 16 | EGL NINE HOMOLOG 1; |
| **16** | 4iw3-A | 13.2 | 2.9 | 16 | PUTATIVE UNCHARACTERIZED PROTEIN; |
| **17** | 5zm3-B | 12.8 | 3.1 | 13 | DIOXYGENASE ANDA; |
| **18** | 4nhy-A | 12.7 | 3.0 | 13 | 2-OXOGLUTARATE AND IRON-DEPENDENT OXYGENASE DOMAI |
| **19** | 6ec3-C | 12.4 | 3.2 | 11 | METHYLTRANSFERASE DOMAIN-CONTAINING PROTEIN; |
| **20** | 6iuq-B | 12.4 | 3.1 | 15 | PROLYL 4-HYDROXYLASE; |
| **21** | 4xbz-C | 12.3 | 2.8 | 12 | EVDO1; |
| **22** | 6nie-A | 12.3 | 3.3 | 8 | BESD, LYSINE HALOGENASE; |
| **23** | 5erl-D | 12.1 | 3.1 | 7 | SNON,SNON; |
| **24** | 5v1b-A | 12.1 | 3.6 | 12 | EGL NINE HOMOLOG 2; |
| **25** | 4nao-A | 12.1 | 3.7 | 13 | PUTATIVE OXYGENASE; |
| **26** | 3kt4-A | 12.0 | 3.3 | 7 | PKHD-TYPE HYDROXYLASE TPA1; |
| **27** | 5nci-B | 12.0 | 3.0 | 11 | LEUCINE HYDROXYLASE; |
| **28** | 4ie6-A | 12.0 | 3.6 | 10 | ALPHA-KETOGLUTARATE-DEPENDENT DIOXYGENASE FTO; |
| **29** | 5ybm-A | 11.9 | 3.4 | 11 | PRHA; |
| **30** | 5epa-A | 11.9 | 3.5 | 9 | SNOK; |

**Table 4.S3.** Top 30 structures similar to TropC from protein data bank (PDB) listed by DALI server[35]. Structure are ranked based on the Z-score value.

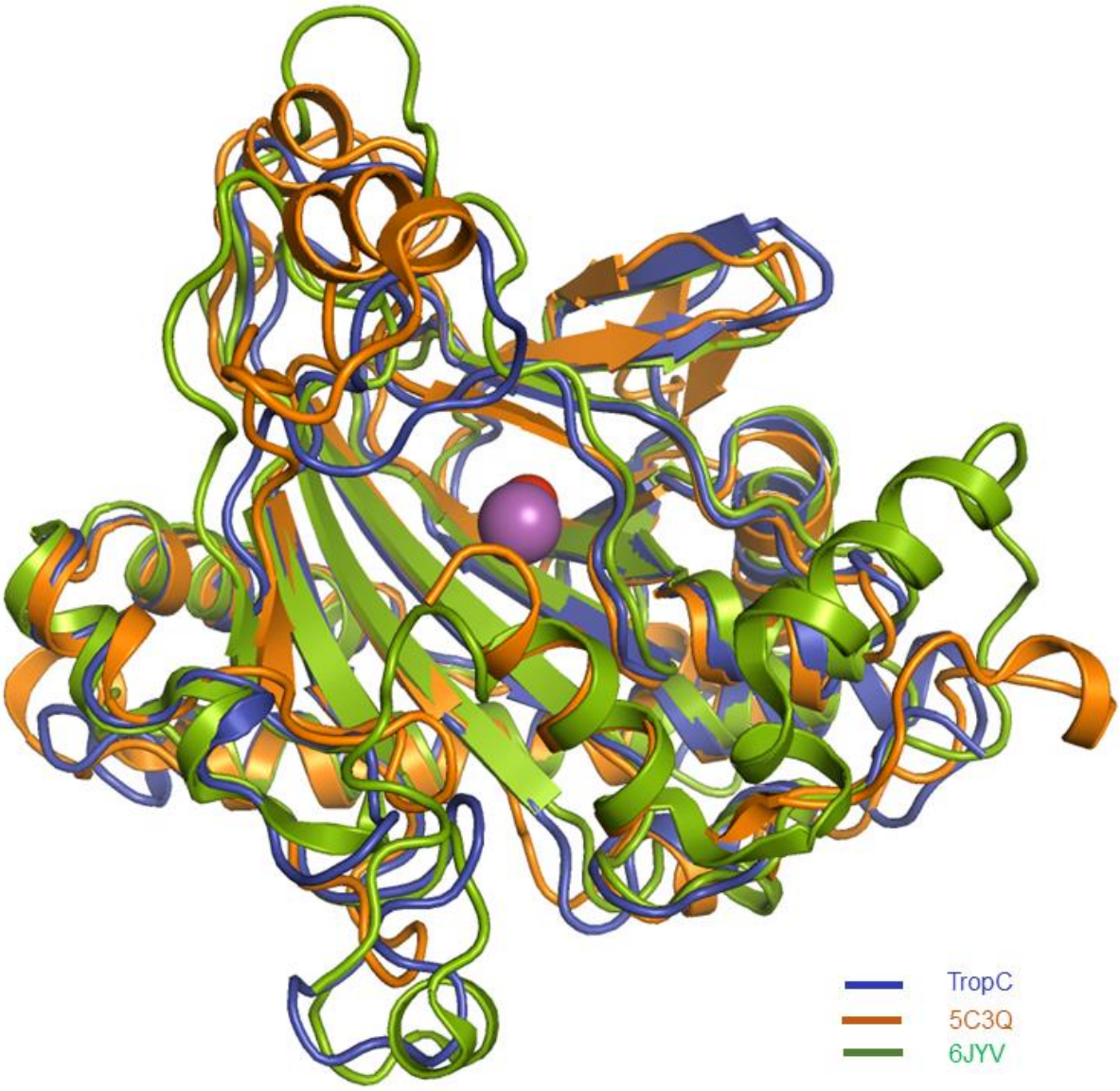


**Figure 4.S31. Superimposition of TropC (PDB ID: 6XJJ) with isopenicillin N synthase from *Pseudomonas aeruginosa* PAO1 (*PaI*PNS, PDB ID: 6JYV) and thymine-7-hydroxylase (T7H) of *Neurospora crassa* (PDB ID: 5C3Q).**

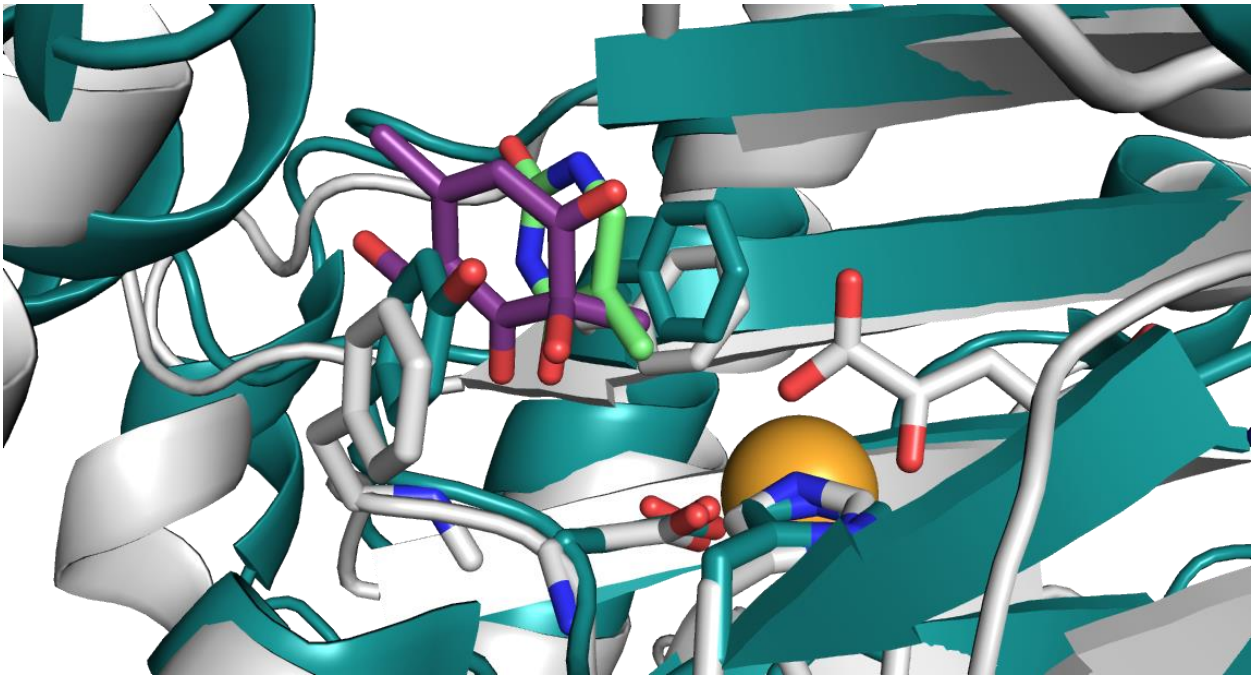

**Figure 4.S32. Superimposition of TropC (PDB ID: 6XJJ) and thymine-7-hydroxylase (T7H) of *Neurospora crassa* (PDB ID: 5C3Q).**
Close-up image of active site. TropC is pictured in grey with native substrate **4.10** in purple. T7H is pictured in teal with thymine shown in green.

**Part VIV. Quantum mechanical (QM) analysis of TropC-catalyzed reactions**

**General Computational Details:** All geometries and frequency computations were obtained using the unrestricted B3LYP density functional[51-52] and 6-311++G** basis set.[53-54] Reaction pathways were calculated using the single-ended growing string method.[55] Initial alignment of substrate and iron model was obtained using ZStruct.[56-58] All ground state geometries were confirmed to have no imaginary frequencies, and transition states were confirmed to have one imaginary frequency. Solvent corrections were performed using the SMD implicit solvent model (water)[59-61] and the cc-pVTZ basis set.[62-67] Reported energies are Gibbs free energies in solvent with gas-phase entropy and enthalpy corrections (at 298.15 K). Most simulations were performed using the Q-Chem 5.0 package,[68] except for the solvent computations, which were performed using ORCA 4.0.[69] A small non-heme iron model (Figure 4.S32) was used mimic the active site of TropC. Methylimidazoles represent histidine side chains, acetates represent aspartate side chains and succinate, respectively. A hydroxyl group was placed in a productive orientation for catalysis, and as a mimic of the Fe(III)-OH group after initial H-atom abstraction.

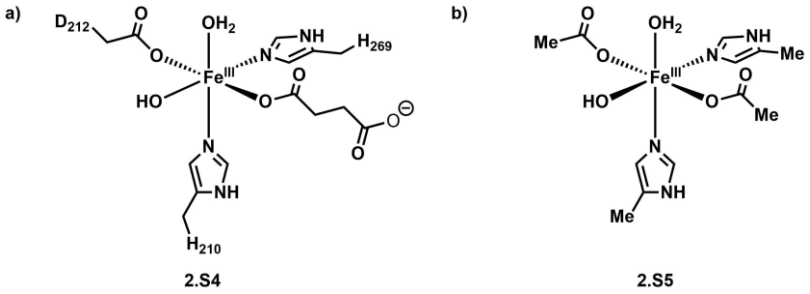


**Figure 4.S33**. **Active-site model before (a) and after (b) truncation of His210, Asp212, His269 and succinate.**

**Part X. XYZ Coordinates for QM calculations**

Integers preceding the coordinates represent the charge and multiplicity of the model, respectively.

Compound **4.14**

-1 2

| | | | |
|---|---|---|---|
| C | -1.36405068 | -1.04444925 | 0.16913242 |
| C | -1.45915056 | 0.31190738 | -0.26869486 |
| C | -0.28554711 | 0.95947356 | -0.85288205 |
| C | 1.09466613 | 0.30994795 | -0.49075439 |
| C | 1.01915666 | -1.23660759 | -0.40613088 |
| C | -0.19132751 | -1.78476718 | 0.09622804 |
| O | -0.30044119 | 1.98364475 | -1.52269526 |
| C | -2.66921645 | 1.09132468 | -0.24942917 |
| O | -3.78685400 | 0.76992397 | 0.17727125 |
| O | 2.09452996 | 0.67636495 | -1.41848883 |
| C | 1.41357514 | 0.83748332 | 0.87600449 |
| O | 2.02539566 | -1.87024130 | -0.75775811 |
| C | -2.59608233 | -1.75803877 | 0.67311221 |
| H | 0.85725578 | 0.50641152 | 1.74369756 |
| H | 2.04446893 | 1.71572266 | 0.93543639 |
| H | -2.52506060 | 2.10689144 | -0.66221531 |
| H | -3.39790032 | -1.73035359 | -0.06811200 |
| H | -3.00415839 | -1.25585346 | 1.55358611 |
| H | -2.36068665 | -2.79609046 | 0.92170180 |
| H | 2.61511614 | -0.14068631 | -1.51516834 |
| H | -0.20483860 | -2.84690128 | 0.31666894 |

**4.14**

Compound **4.16**

-1 2

| | | | |
|---|---|---|---|
| C | -1.32321465 | -1.03988654 | 0.21419164 |
| C | -1.39007402 | 0.32425418 | -0.17447546 |
| C | -0.18009975 | 1.04298777 | -0.60439486 |
| C | 1.26948593 | 0.17963835 | -0.46201451 |
| C | 1.05672415 | -1.31453846 | -0.41919394 |
| C | -0.16039692 | -1.80299589 | 0.12094035 |
| O | -0.14164956 | 2.08361048 | -1.28715414 |
| C | -2.60283559 | 1.09865564 | -0.21585736 |
| O | -3.75096181 | 0.74966098 | 0.09616481 |
| O | 2.27250203 | 0.55020730 | -1.33546093 |
| C | 1.07409494 | 0.99782463 | 0.70972805 |
| O | 1.97743103 | -2.01000848 | -0.90395541 |
| C | -2.57108589 | -1.75422595 | 0.68295646 |
| H | 0.65745715 | 0.57791273 | 1.61415998 |
| H | 1.55603390 | 1.96477056 | 0.73476049 |
| H | -2.43421348 | 2.13590494 | -0.56102868 |
| H | -3.34757052 | -1.73755859 | -0.08530076 |
| H | -3.01348004 | -1.25411600 | 1.54812585 |
| H | -2.33859154 | -2.79054105 | 0.94265854 |
| H | 2.58639562 | -0.30700825 | -1.68045282 |
| H | -0.21119599 | -2.87162435 | 0.30082671 |

**4.16**

Compound **4.19**

-1 2

| | | | |
|---|---|---|---|
| C | -2.51544722 | -1.71261253 | 0.73291417 |
| C | -1.31723648 | -0.93897085 | 0.20358618 |
| C | -0.19146631 | -1.71504774 | -0.01064276 |
| C | 1.09187639 | -1.37259732 | -0.56825818 |
| O | 1.86803001 | -2.22061600 | -1.11646024 |
| C | 1.59730649 | -0.03726647 | -0.45888863 |
| C | 0.96967314 | 1.05507017 | 0.30802773 |
| C | -0.43814432 | 1.43606988 | -0.21626141 |
| O | -0.56398938 | 2.58604909 | -0.65545511 |
| C | -1.51185653 | 0.46793074 | -0.08365824 |
| C | -2.82907289 | 1.04187117 | -0.26258200 |
| O | -3.93577462 | 0.48863803 | -0.22679102 |
| O | 2.80062695 | 0.16222538 | -1.02297890 |
| H | 0.86430425 | 0.74632632 | 1.35888882 |
| H | 1.58410863 | 1.95342826 | 0.25823812 |
| H | -2.78638526 | 2.12780156 | -0.45781491 |
| H | -3.30001380 | -1.79170083 | -0.02155678 |
| H | -2.97696943 | -1.19782104 | 1.57964654 |
| H | -2.20810635 | -2.71304784 | 1.04700828 |
| H | 3.00127970 | -0.73918939 | -1.38088968 |
| H | -0.29581195 | -2.78232256 | 0.16380103 |

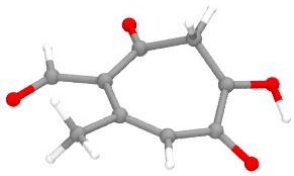

**4.19**

Compound **4.20**

-1 1

| | | | |
|---|---|---|---|
| C | -2.21373926 | -1.72739805 | 0.83750339 |
| C | -1.22169769 | -0.69199008 | 0.32730357 |
| C | 0.09972721 | -1.12083985 | 0.39560405 |
| C | 1.32780725 | -0.56850947 | -0.10206171 |
| O | 2.40551081 | -1.17106760 | -0.06260436 |
| C | 1.33538123 | 0.86758082 | -0.64930370 |
| O | 2.01827171 | 1.19075901 | -1.59684813 |
| C | 0.46764691 | 1.83574440 | 0.11149114 |
| C | -1.01396650 | 1.77850110 | -0.33269154 |
| O | -1.48195146 | 2.83216749 | -0.77381117 |
| C | -1.77185872 | 0.54880576 | -0.15689623 |
| C | -3.17865129 | 0.68808963 | -0.49225195 |
| O | -4.06912070 | -0.16814836 | -0.47660367 |
| H | 0.51511053 | 1.59164814 | 1.17939501 |
| H | 0.80738191 | 2.85482845 | -0.06459116 |
| H | -3.43231565 | 1.71294587 | -0.81091656 |
| H | -2.96065266 | -1.27759343 | 1.49402980 |
| H | -1.68738022 | -2.52110903 | 1.37150574 |
| H | -2.77855585 | -2.16339358 | 0.01093572 |
| H | 0.25961745 | -2.10733123 | 0.82185875 |

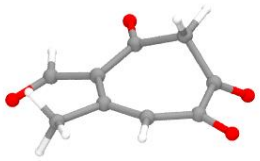

**4.20**

Compound **4.13**

-1 1

| | | | |
|---|---|---|---|
| C | -1.29438791 | -1.03884351 | 0.19797988 |
| C | -1.45664211 | 0.30204921 | -0.24074957 |
| C | -0.28614153 | 1.11253935 | -0.54693263 |
| C | 1.12812135 | 0.52401174 | -0.27055120 |
| C | 1.16750040 | -0.95953795 | 0.14290246 |
| C | -0.04552971 | -1.62914569 | 0.38223867 |
| O | -0.33134983 | 2.26635259 | -0.97033814 |
| C | -2.74007501 | 0.94336319 | -0.42549600 |
| O | -3.86374138 | 0.46624630 | -0.23605586 |
| C | 1.69247770 | 1.36284179 | 0.91047298 |
| O | 3.00885254 | 0.98292189 | 1.31003137 |
| O | 1.89184003 | 0.72827388 | -1.45239656 |
| O | 2.30165941 | -1.49085238 | 0.29768675 |
| C | -2.50146428 | -1.89908807 | 0.48386328 |
| O | 4.68512743 | -0.43512533 | -0.80821939 |
| H | 1.00220068 | 1.29934316 | 1.76333682 |
| H | 1.73893020 | 2.39772717 | 0.56975567 |
| H | -2.64888075 | 1.98784727 | -0.77129720 |
| H | -3.13791803 | -1.43995314 | 1.24338391 |
| H | -2.19082307 | -2.89303871 | 0.81419119 |
| H | -3.13510154 | -1.99021423 | -0.40153735 |

**4.13**

| | | | |
|---|---|---|---|
| H | 2.77711864 | 0.35508475 | -1.32492888 |
| H | 3.00227839 | 0.01382494 | 1.37952026 |
| H | 0.02123743 | -2.66303475 | 0.70398755 |
| H | 3.99032565 | -1.03282560 | -0.47279428 |
| H | 4.63979630 | 0.30785011 | -0.19237772 |

Compound **4.21**

-1 1

| | | | |
|---|---|---|---|
| C | 1.66584328 | 1.14862049 | 0.72194060 |
| C | 1.30004206 | 0.14491849 | -0.23662013 |
| O | 1.91202776 | 0.02791017 | -1.39888957 |
| C | 1.06282759 | -1.20094689 | 0.48678287 |
| O | 2.08057320 | -1.74624542 | 0.96672238 |
| C | -0.24340562 | -1.73919809 | 0.60470045 |
| C | -1.40296429 | -1.05636302 | 0.28978850 |
| C | -2.70139489 | -1.78923268 | 0.53789581 |
| C | -1.44637497 | 0.27329527 | -0.24429853 |
| C | -2.67461685 | 0.97038542 | -0.57672242 |
| O | -3.83632692 | 0.58286374 | -0.42797168 |
| C | -0.25281583 | 1.02406318 | -0.54527983 |
| O | -0.15790683 | 2.07435613 | -1.13734568 |
| O | 3.53385955 | 0.53363876 | 1.34904372 |
| O | 4.29287218 | 0.85926760 | -1.21462365 |
| H | 1.23776767 | 1.11346010 | 1.71723486 |
| H | 2.00458213 | 2.11284433 | 0.36258720 |
| H | -2.49386048 | 1.97564377 | -0.99804195 |
| H | -3.33236126 | -1.24856279 | 1.24668862 |
| H | -2.50131297 | -2.79311490 | 0.91897574 |

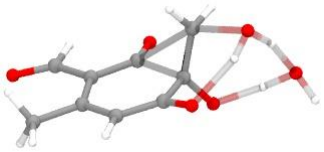

**4.21**

| | | | |
|---|---|---|---|
| H | -3.29167932 | -1.85644797 | -0.37816810 |
| H | 3.31535772 | 0.55625621 | -1.39838709 |
| H | 3.24256284 | -0.41126905 | 1.30428002 |
| H | -0.31373666 | -2.73089249 | 1.04052893 |
| H | 4.84302630 | 0.19105141 | -1.63226123 |
| H | 4.00578860 | 0.67669524 | 0.48571617 |

Compound **4.22**

-1 1

| | | | |
|---|---|---|---|
| C | -2.25401026 | -1.75617440 | 0.76590681 |
| C | -1.25372999 | -0.70106981 | 0.32139887 |
| C | 0.07508605 | -1.14386310 | 0.40799575 |
| C | 1.31639352 | -0.60605482 | -0.01985828 |
| O | 2.37512390 | -1.27049518 | -0.00694604 |
| C | 1.42542246 | 0.85503036 | -0.47758075 |
| O | 2.29103006 | 1.20339461 | -1.25394801 |
| C | 0.45891698 | 1.82017907 | 0.15002069 |
| C | -0.97693855 | 1.72907084 | -0.41104900 |
| O | -1.39320889 | 2.72609722 | -0.99955866 |
| C | -1.77906944 | 0.53762810 | -0.15282249 |
| C | -3.19794603 | 0.73707673 | -0.42589698 |
| O | -4.12109347 | -0.07354403 | -0.33774280 |
| O | 4.86330784 | -0.51778568 | -1.05924377 |
| O | 4.91999847 | -1.37214971 | 1.73885531 |
| H | 0.41619932 | 1.60820485 | 1.22522267 |
| H | 0.80375699 | 2.83749599 | -0.02474090 |
| H | -3.42095547 | 1.76749496 | -0.74948867 |
| H | -3.00532217 | -1.33874610 | 1.43741236 |

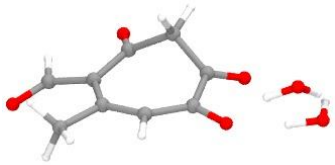

**4.22**

| | | | |
|---|---|---|---|
| H | -1.73823427 | -2.58255824 | 1.25743182 |
| H | -2.81469026 | -2.14238546 | -0.08845610 |
| H | 4.73744343 | 0.37266880 | -1.40237037 |
| H | 3.99137031 | -1.55121921 | 1.54049150 |
| H | 0.20102893 | -2.15734910 | 0.77681724 |
| H | 3.94644159 | -0.78425808 | -0.83687898 |
| H | 5.23217196 | -1.00761762 | 0.89490779 |

Compound **4.11**

0 1

| | | | |
|---|---|---|---|
| C | -0.85439202 | 1.68563917 | -0.36326391 |
| C | -1.71234651 | 0.57156895 | -0.12297394 |
| C | 1.48873710 | 0.78367638 | -0.12003378 |
| C | 1.27938417 | -0.65675756 | 0.20366492 |
| C | -0.01113898 | -1.26007927 | 0.32683275 |
| C | -1.29011572 | -0.77202637 | 0.19606475 |
| C | 0.56378187 | 1.75399660 | -0.35401837 |
| C | -3.14061480 | 0.83110182 | -0.21475631 |
| C | -2.37273202 | -1.81997771 | 0.42451121 |
| O | 2.77708068 | 1.09680858 | -0.17161068 |
| O | 2.32762589 | -1.30416952 | 0.36305958 |
| O | -1.38797411 | 2.86594568 | -0.64431437 |
| O | -3.65784830 | 1.92692051 | -0.47532417 |
| H | -3.03803062 | -1.54766948 | 1.24823117 |
| H | -1.91997812 | -2.77835817 | 0.67123625 |
| H | -2.99143547 | -1.96737555 | -0.46514929 |
| H | 0.95137246 | 2.74303070 | -0.57229337 |

**4.11**

| | | | |
|---|---|---|---|
| H | 3.23891283 | 0.24595211 | 0.02701084 |
| H | -3.81593197 | -0.01150886 | -0.03992552 |
| H | 0.08284370 | -2.31234044 | 0.57117286 |
| H | -2.39177514 | 2.76887516 | -0.64196393 |

Compound **4.13**

-1 1

| | | | |
|---|---|---|---|
| C | 1.32100899 | 0.26418288 | -0.37478702 |
| C | 1.27503132 | -1.26558389 | -0.26315958 |
| C | 0.03045125 | -1.79757631 | 0.20637017 |
| C | -1.14395862 | -1.07343043 | 0.23351158 |
| C | -1.23059529 | 0.28569895 | -0.23399977 |
| C | -0.03861443 | 0.90398429 | -0.74002563 |
| O | 2.27669274 | -1.95204738 | -0.49773944 |
| C | -2.38789320 | -1.77718379 | 0.71705182 |
| C | -2.44957813 | 1.05112473 | -0.32237119 |
| O | -3.58777062 | 0.72138462 | 0.02760597 |
| O | 0.03089452 | 1.94226218 | -1.42068726 |
| O | 2.28173262 | 0.70199434 | -1.32857826 |
| C | 1.69489141 | 0.84953305 | 1.03081984 |
| O | 2.85009581 | 0.29511280 | 1.62104940 |
| O | 4.68862162 | -0.48210547 | -0.51191699 |
| H | 0.87353172 | 0.68013974 | 1.73009939 |
| H | 1.80551853 | 1.93268382 | 0.87518461 |

**4.13**

| | | | |
|---|---|---|---|
| H | -2.28945230 | 2.05868538 | -0.74970151 |
| H | -2.83054447 | -1.24764455 | 1.56430175 |
| H | -2.15493678 | -2.80356802 | 1.01050947 |
| H | -3.16159704 | -1.78226632 | -0.05407308 |
| H | 1.83497112 | 1.46301019 | -1.74962220 |
| H | 3.56130334 | 0.20120437 | 0.96102703 |
| H | 0.02730673 | -2.84789842 | 0.47672019 |
| H | 4.04983114 | -1.22147756 | -0.51673861 |
| H | 4.21408402 | 0.14600479 | -1.07664368 |

Compound **4.23**

-1 1

| | | | |
|---|---|---|---|
| C | 1.31544095 | 0.27238757 | -0.44239450 |
| C | 1.26896676 | -1.19486812 | -0.25018860 |
| C | 0.06980728 | -1.78134729 | 0.14701800 |
| C | -1.13701692 | -1.07166703 | 0.19711175 |
| C | -1.22106789 | 0.27897950 | -0.21184467 |
| C | -0.02489527 | 0.91324595 | -0.73086785 |
| O | 2.34144262 | -1.92369798 | -0.35754406 |
| C | -2.35933824 | -1.81544666 | 0.66973084 |
| C | -2.44120786 | 1.05937986 | -0.23347677 |
| O | -3.56471301 | 0.70878914 | 0.13193907 |
| O | 0.00047277 | 1.98172078 | -1.36409411 |
| O | 2.25802968 | 0.68468323 | -1.41828891 |
| C | 1.80144293 | 0.93920762 | 1.04519690 |
| O | 2.96674894 | 0.48050515 | 1.49516454 |
| O | 4.42339843 | -0.57819943 | -0.16190066 |

**4.23**

| | | | |
|---|---|---|---|
| H | 0.95413742 | 0.75848951 | 1.73204013 |
| H | 1.79523876 | 2.00842273 | 0.74573894 |
| H | -2.28880013 | 2.08538671 | -0.61438480 |
| H | -2.79046559 | -1.33459338 | 1.55137398 |
| H | -2.10918695 | -2.85159129 | 0.90845732 |
| H | -3.14908486 | -1.79251208 | -0.08474810 |
| H | 1.84179221 | 1.48159255 | -1.79497589 |
| H | 3.87781263 | -0.02528555 | 0.60470743 |
| H | 0.09257052 | -2.83097338 | 0.41542866 |
| H | 3.25625638 | -1.37169427 | -0.37636340 |
| H | 4.40504843 | 0.02718918 | -0.91178226 |

Compound **4.24**

-1 1

| | | | |
|---|---|---|---|
| C | 1.16226593 | -0.04795429 | -0.98214112 |
| C | 1.18881948 | -1.33768179 | -0.49907100 |
| C | -0.00017014 | -1.88049954 | 0.04972638 |
| C | -1.16943847 | -1.14736563 | 0.13037308 |
| C | -1.20336571 | 0.20473908 | -0.33737424 |
| C | -0.01271755 | 0.78131956 | -0.91318224 |
| O | 2.29130145 | -2.14375757 | -0.53037436 |
| C | -2.39159886 | -1.80329367 | 0.73165138 |
| C | -2.37263483 | 1.05537297 | -0.28788378 |
| O | -3.49068253 | 0.78525442 | 0.16136253 |
| O | 0.12393779 | 1.96809539 | -1.37292856 |
| O | 2.23187594 | 0.57561537 | -1.59975804 |
| O | 4.48499912 | -0.31823596 | -0.31519501 |

**4.24**

| | | | |
|---|---|---|---|
| O | 3.01207510 | 0.80213915 | 2.05969664 |
| C | 1.93463272 | 1.20509940 | 1.67293292 |
| H | 1.00022317 | 0.94994854 | 2.20354846 |
| H | 1.83032420 | 1.86379817 | 0.79620664 |
| H | -2.18951108 | 2.05810626 | -0.71587995 |
| H | -2.75271039 | -1.25666992 | 1.60645557 |
| H | -2.15818767 | -2.83160957 | 1.02386019 |
| H | -3.22795064 | -1.81423397 | 0.02786833 |
| H | 1.81388514 | 1.45014988 | -1.81582363 |
| H | 4.31850864 | 0.02660594 | 0.57448182 |
| H | 0.04264983 | -2.89972257 | 0.41740736 |
| H | 3.11111898 | -1.61114950 | -0.55856107 |
| H | 3.89485639 | 0.21868083 | -0.87674231 |

Compound **4.18**

0 1

| | | | |
|---|---|---|---|
| C | 0.41330517 | 0.08871090 | -0.20328194 |
| C | -0.88184378 | -0.28298158 | 0.24161843 |
| C | 1.15856433 | -0.76712725 | -1.00694048 |
| C | 0.62833964 | -1.99918700 | -1.37605378 |
| C | -0.65056107 | -2.38070180 | -0.94358524 |
| C | -1.41335529 | -1.54630579 | -0.14458297 |
| O | 2.41159037 | -0.44488187 | -1.45791220 |
| O | 1.34079278 | -2.84275506 | -2.15762872 |
| O | 0.99437284 | 1.26314146 | 0.11336597 |
| C | -1.60659284 | 0.64809196 | 1.07647815 |
| O | -1.17070395 | 1.74970047 | 1.42930754 |

**4.18**

| | | | |
|---|---|---|---|
| H | -2.60995103 | 0.34626573 | 1.41425796 |
| C | -2.78777252 | -2.00001197 | 0.29432678 |
| H | -3.57178132 | -1.31586967 | -0.04271847 |
| H | -2.86519466 | -2.07884881 | 1.38271306 |
| H | -3.00598565 | -2.98315735 | -0.12373088 |
| H | 2.64348183 | 0.43161154 | -1.12287824 |
| H | 2.19054396 | -2.42968112 | -2.36537576 |
| H | -1.02444142 | -3.34884992 | -1.25423749 |
| H | 0.35489495 | 1.76110362 | 0.68487562 |

[$Fe^{III}$]

0 4

| | | | |
|---|---|---|---|
| C | 38.23926701 | 38.29629874 | 29.53710554 |
| N | 37.51798914 | 36.53354383 | 31.20562786 |
| H | 36.57979369 | 36.42065883 | 30.85451949 |
| C | 38.47794332 | 37.40109561 | 30.70591902 |
| C | 38.04802096 | 35.87599426 | 32.27156015 |
| H | 37.52185157 | 35.15020117 | 32.86958055 |
| N | 39.28494611 | 36.26706861 | 32.47751634 |
| C | 39.56590086 | 37.21519536 | 31.51655407 |
| H | 40.52482129 | 37.70584044 | 31.48585394 |
| C | 43.17144571 | 38.99031542 | 34.13308757 |
| C | 42.29929121 | 37.89270308 | 34.72239123 |
| O | 41.81177984 | 37.05054528 | 33.86259073 |
| O | 42.10233410 | 37.85427623 | 35.94139009 |
| C | 42.35063634 | 31.20755424 | 31.36745326 |
| N | 43.24710579 | 33.45069629 | 32.12753254 |
| H | 44.18388292 | 33.32551282 | 31.77660085 |

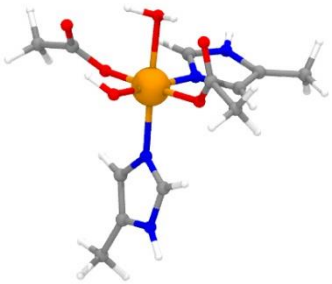

[$Fe^{III}$]

| | | | |
|---|---|---|---|
| C | 42.20717619 | 32.53510038 | 32.03066067 |
| C | 42.80204263 | 34.54207495 | 32.79466044 |
| H | 43.39294733 | 35.41270229 | 33.02047687 |
| N | 41.53826112 | 34.38048108 | 33.12648486 |
| C | 41.15541594 | 33.13769466 | 32.66220200 |
| H | 40.15958826 | 32.76864523 | 32.83712342 |
| Fe | 40.45422521 | 35.67867455 | 34.27965033 |
| O | 41.76393178 | 35.02188784 | 35.96638579 |
| H | 41.91088933 | 35.86532866 | 36.42605115 |
| H | 41.08838887 | 34.50407100 | 36.47718862 |
| O | 39.64345087 | 33.64057732 | 36.74668694 |
| C | 38.90092945 | 33.66328621 | 35.75878925 |
| O | 39.18269509 | 34.21179155 | 34.61874976 |
| C | 37.53237688 | 33.00691561 | 35.82810828 |
| O | 39.47350152 | 36.73538467 | 35.34864171 |
| H | 43.37302269 | 38.82858090 | 33.07435629 |
| H | 44.10751694 | 39.04958309 | 34.69209629 |
| H | 42.65822947 | 39.94753440 | 34.25938393 |
| H | 43.11736403 | 30.59335687 | 31.85068902 |
| H | 42.61405175 | 31.30528297 | 30.30919715 |
| H | 41.40657325 | 30.66468441 | 31.42637224 |
| H | 38.00518255 | 37.73104235 | 28.62875809 |
| H | 39.13480814 | 38.88665977 | 29.33901725 |
| H | 37.41555410 | 38.99416356 | 29.72014118 |
| H | 37.27644531 | 32.52731764 | 34.88140651 |
| H | 36.78976652 | 33.78715730 | 36.02249251 |
| H | 37.49881859 | 32.28424651 | 36.64273759 |

| | | | |
|---|---|---|---|
| H | 40.04210171 | 37.39867676 | 35.76639073 |

[$Fe^{II}$]

0 5

| | | | |
|---|---|---|---|
| C | 38.00896528 | 38.60216009 | 29.69941967 |
| N | 37.44311767 | 36.57497726 | 31.10723864 |
| H | 36.54072433 | 36.39738663 | 30.69423179 |
| C | 38.31091978 | 37.60279442 | 30.76403270 |
| C | 38.00814300 | 35.85188438 | 32.10860738 |
| H | 37.55700287 | 34.99686361 | 32.58628125 |
| N | 39.18365426 | 36.35258700 | 32.42217182 |
| C | 39.38424709 | 37.44098206 | 31.59759418 |
| H | 40.28446955 | 38.02884196 | 31.67266600 |
| C | 43.41914438 | 38.92014552 | 34.22782020 |
| C | 42.37756387 | 37.87552887 | 34.60258657 |
| O | 41.92761656 | 37.12994751 | 33.67064669 |
| O | 42.02355685 | 37.80990186 | 35.80655036 |
| C | 42.67677952 | 30.91175014 | 31.56208238 |
| N | 43.31056064 | 33.34787845 | 31.84365942 |
| H | 44.20186027 | 33.28922231 | 31.37617348 |
| C | 42.42062681 | 32.30082291 | 32.04018472 |
| C | 42.78370610 | 34.46959952 | 32.39942085 |
| H | 43.25848974 | 35.43774302 | 32.40695228 |
| N | 41.61239275 | 34.20336176 | 32.93598990 |
| C | 41.37437380 | 32.86052796 | 32.72218952 |
| H | 40.46981128 | 32.39741540 | 33.08122287 |
| Fe | 40.42007432 | 35.63146877 | 34.03791049 |

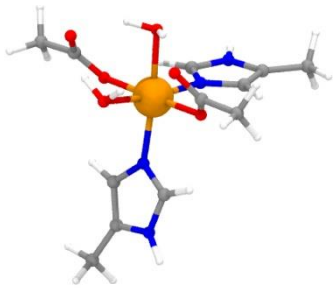

[$Fe^{II}$]

| | | | |
|---|---|---|---|
| O | 41.50236339 | 35.06648185 | 35.92094104 |
| H | 41.82624773 | 35.94452257 | 36.20268891 |
| H | 40.74049714 | 34.84705401 | 36.49473509 |
| O | 38.88011645 | 34.59535533 | 36.68499048 |
| C | 38.49125303 | 33.95855439 | 35.67381698 |
| O | 38.91179853 | 34.15450913 | 34.48556742 |
| C | 37.44625394 | 32.87164224 | 35.87981002 |
| O | 39.37128366 | 37.05835820 | 35.43679881 |
| H | 43.66423760 | 38.88583723 | 33.16633306 |
| H | 44.32129016 | 38.75931581 | 34.82349839 |
| H | 43.04003076 | 39.91218399 | 34.48621897 |
| H | 43.58396715 | 30.48771493 | 32.00529078 |
| H | 42.78229310 | 30.86608781 | 30.47287584 |
| H | 41.84086406 | 30.26930209 | 31.84161017 |
| H | 37.88323416 | 38.13085291 | 28.71888556 |
| H | 38.83105670 | 39.31483774 | 29.62206095 |
| H | 37.09824332 | 39.16945284 | 29.91861256 |
| H | 37.13523466 | 32.42476027 | 34.93556981 |
| H | 36.58154758 | 33.29282079 | 36.39810905 |
| H | 37.86155953 | 32.09724618 | 36.53044688 |
| H | 40.14321330 | 37.52446195 | 35.81591985 |
| H | 39.05735289 | 36.43225593 | 36.11794302 |

[$Fe^{II}_{W}$]

1 5

| | | | |
|---|---|---|---|
| C | 38.29039775 | 38.83670376 | 29.75970800 |
| N | 37.53658237 | 36.77152669 | 31.01303247 |
| H | 36.64900671 | 36.67456191 | 30.54167423 |
| C | 38.47470056 | 37.76259298 | 30.77755892 |
| C | 37.99765570 | 35.95779952 | 31.99438327 |
| H | 37.46624044 | 35.10388307 | 32.38327543 |
| N | 39.18400406 | 36.36718042 | 32.40646501 |
| C | 39.49047876 | 37.49087017 | 31.65574539 |
| H | 40.41310258 | 38.02923278 | 31.79963147 |
| O | 41.85072243 | 36.97229884 | 34.00977936 |
| C | 43.57033631 | 31.09423871 | 32.04199166 |
| N | 42.31206030 | 33.04076490 | 31.02418044 |
| H | 42.52637202 | 32.81918015 | 30.06272176 |
| C | 42.73306810 | 32.32422057 | 32.13438580 |
| C | 41.56117085 | 34.08597233 | 31.44022500 |
| H | 41.10549373 | 34.80007754 | 30.77370156 |
| N | 41.47280941 | 34.09040688 | 32.75946760 |
| C | 42.19988722 | 32.99525887 | 33.20039016 |
| H | 42.27404820 | 32.76830220 | 34.25038761 |
| Fe | 40.30225156 | 35.37404145 | 33.97139581 |
| O | 41.34696423 | 34.47121405 | 35.85400523 |
| H | 42.05698111 | 34.85023568 | 36.38219507 |
| H | 40.55814752 | 34.42433131 | 36.44137962 |
| O | 38.78087868 | 34.65033772 | 36.67645302 |
| C | 38.26068040 | 34.08817947 | 35.67774007 |

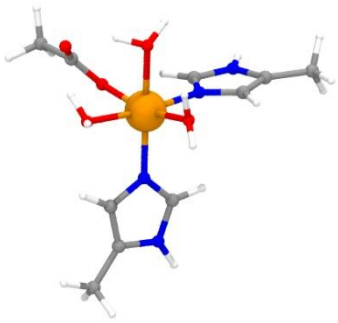

[$Fe^{II}_{W}$]

| | | | |
|---|---|---|---|
| O | 38.69486787 | 34.25298052 | 34.48107801 |
| C | 37.08552476 | 33.16530788 | 35.88259347 |
| O | 39.65143149 | 36.94327308 | 35.57106427 |
| H | 44.52848132 | 31.29140487 | 31.55179241 |
| H | 43.06194389 | 30.30230089 | 31.48388474 |
| H | 43.77916042 | 30.71432595 | 33.04216421 |
| H | 38.17329681 | 38.42358495 | 28.75336053 |
| H | 39.16047797 | 39.49362371 | 29.75134665 |
| H | 37.41096354 | 39.45129745 | 29.97460169 |
| H | 36.64628194 | 32.85713869 | 34.93562238 |
| H | 36.33978036 | 33.65398027 | 36.51211032 |
| H | 37.42898568 | 32.28031518 | 36.42529186 |
| H | 38.94075657 | 37.55949548 | 35.36168237 |
| H | 39.27579006 | 36.28775687 | 36.20999533 |
| H | 42.80309956 | 36.90259275 | 33.88383372 |
| H | 41.67882363 | 37.51081912 | 34.79463246 |

**Part XI. Molecular dynamics (MD) simulations**

**Model Construction:** To construct the model of TropC, we used the partial crystal structure described in this report and the Modeller software to model the C-terminal region for which no density was observed in X-ray crystallography experiments.[70] To develop a homology model for this region, we submitted the TropC amino acid sequence to the RCSB PDB[71] and JPred4 server for secondary structure prediction. These programs indicated that thebaine 6-O-demthylase crystal structure (PDB ID: 5O7Y, 27% sequence identity, Pymol superalign Cα-RMSD: 4.378) as the closest predicted related structure.[42, 72] Based on the structure prediction results, residues 307-323 of the C-terminal region were modeled as a helix.

To generate an initial substrate-bound structure for MD simulations, further analysis of the RCSB PDB structure revealed that non-heme iron enzyme thymine-7-hydroxylase (T7H) possesses structural similarity to the *apo* crystal structure of TropC (PDB ID: 5C3Q, 28% sequence identity, Pymol superalign Cα-RMSD: 3.139).[33] The deposited crystal structure of T7H was co-crystallized with substrate, nickel, and α-KG. In addition, similarities between the native substrates of TropC and T7H are evident. They are both small, cyclic substrates with a similar substitution pattern of a methyl group ortho to a hydroxyl group. To establish an initial substrate-bound structure for MD simulations, we overlaid the TropC coordinates with the T7H substrate, co-substrate and Fe coordinates. We then computationally replaced thymine with TropC native substrate **4.10** and converted the nickel atom to an iron atom to prepare our model for MD simulations. *Computations performed by Kevin Skinner*.

**System Preparation:** We submitted the TropC model coordinates to the CHARMM-gui for addition of all hydrogen atoms and protons, which were added according to their canonical protonation states.[73] These protonation states were determined based on the use of the Propka-3.1 software.[74-75] The tautomeric forms of histidine were assigned to maximize hydrogen bonds. To obtain an overall electrically-neutral charge model, 47 potassium and 42 chlorine atoms were added. A water box was used with periodic boundary conditions, and the particle mesh Ewald method was used to describe long-range electrostatic effects. Dimensions of the water box were established to fit the largest dimension of the protein plus 10 Å. All water molecules within 2.8 angstroms of heavy atoms were removed. The final model contained 53,819 atoms. Parameters for the substrate were obtained using CGenFF 4.0.[76-77] Parameters for iron were obtained from those described by Pang and coworkers.[78] A restrained active site was used (50 kcal/molÅ$^2$ force constant), in which the restraints were based off of crystal structure distances. Included in these restraints were a positional restraint on residue Phe213 to more closely resemble that of the complimentary residue in 5C3Q to maintain closure of the active site, and restraints based on H-bonds within the active site. A 5000 step molecular mechanics (MM) minimization was then was performed using the steepest decent algorithm using the CHARMM36 force field.[79]

*MD Simulations*

Simulations were performed with the OpenMM/CHARMM interface (version c42b1) using periodic boundary conditions, particle mesh Ewald for long range electrostatic interactions, and a Langevin thermostat (friction coefficient = 5).[80] A three-step MD protocol was used to obtain the pose described in the main text, which all used a 2 fs timestep. The first phase slowly heated the model from 10K to 298 K over 500 ps and included the restrained active site as well as harmonic restraints of 10.0 kcal mol/Å$^{-2}$ on all heavy atoms of the solute. The harmonic restraints

were then removed, and temperature was kept constant for an additional 500 ps. The MD simulations were performed for 11 ns, with the first ns used for equilibration.

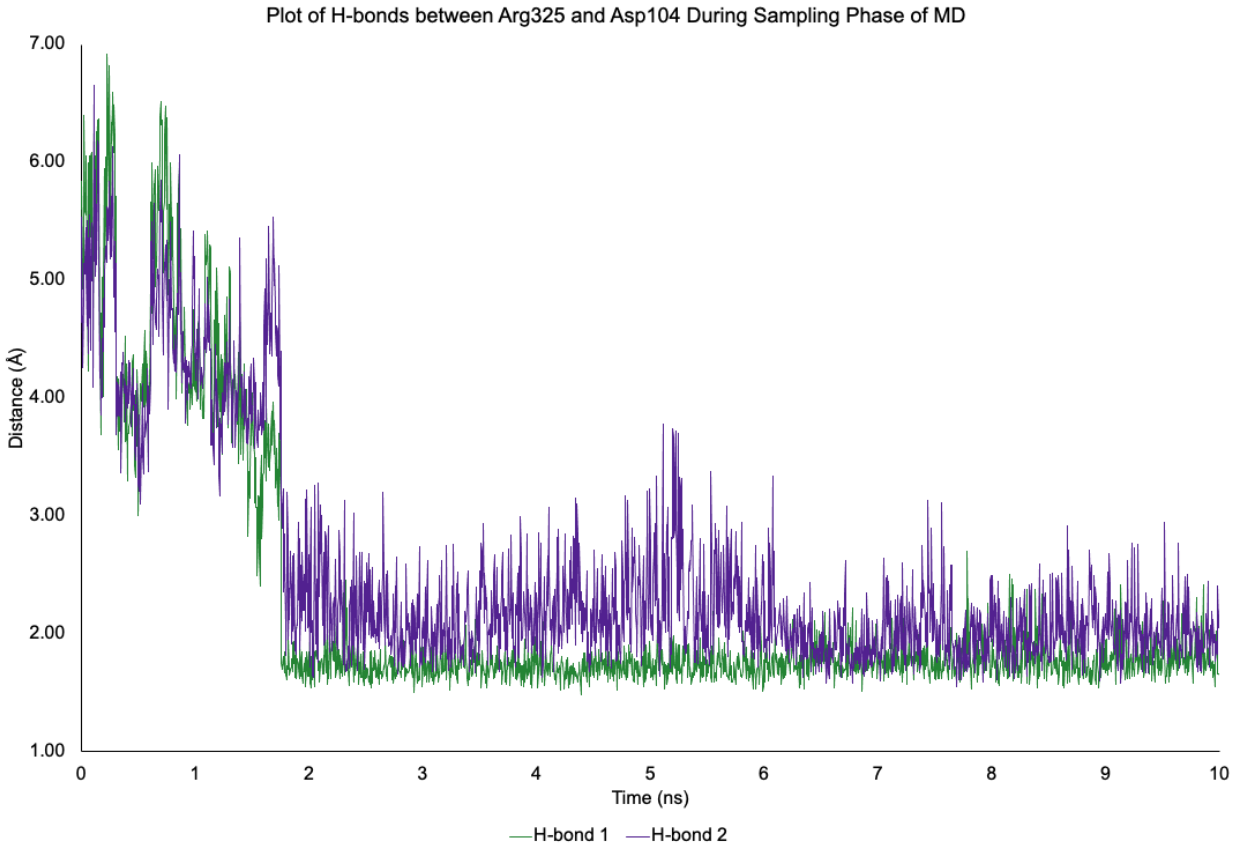


**Figure 4.S34. Tracking H-bond distance between Arg325 and Asp104 throughout the final 10 ns of sampling (MD).**
The first contact between substrate **4.10** begins, and remains, after ~1.75 ns.

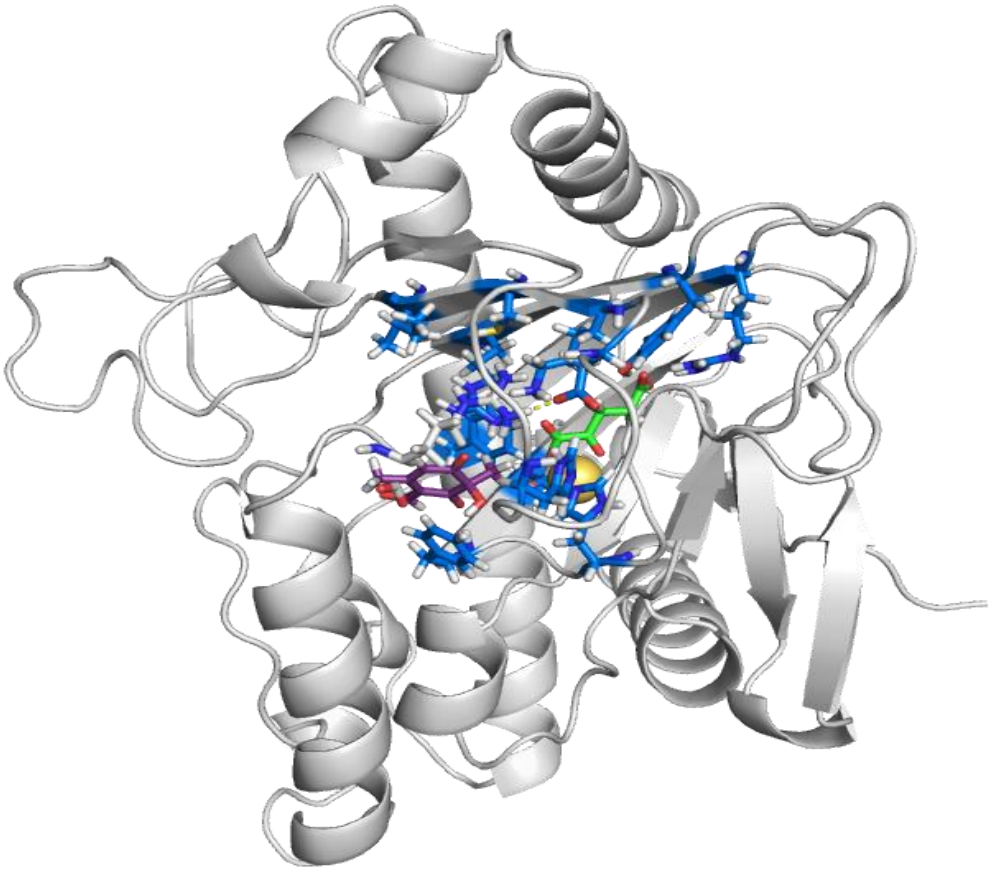

**Figure 4.S35. Full image of TropC with substrate bound from the final frame of MD simulation.**
Residues chosen for alanine screening mutagenesis are shown in blue, substrate **4.10** is shown in purple, cofactor α-ketoglutarate is shown in green and ferrous iron is shown in light brown.

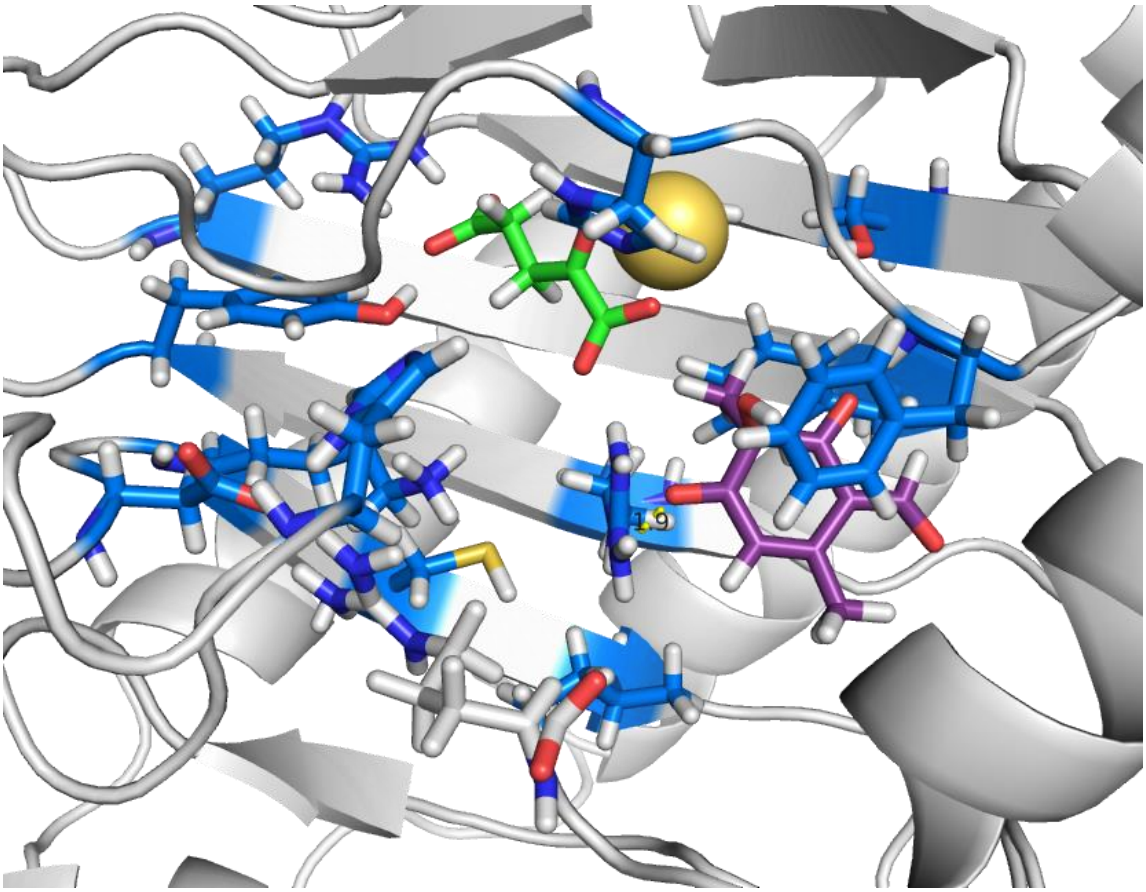


**Figure 4.S36. Close-up image of TropC active site with substrate bound from the final frame of MD simulation.**
The hydrogen bonding distance between R186 and substrate **4.10** is shown. Residues chosen for alanine screening mutagenesis are shown in blue, substrate **4.10** is shown in purple, cofactor α-ketoglutarate is shown in green and ferrous iron is shown in light brown.

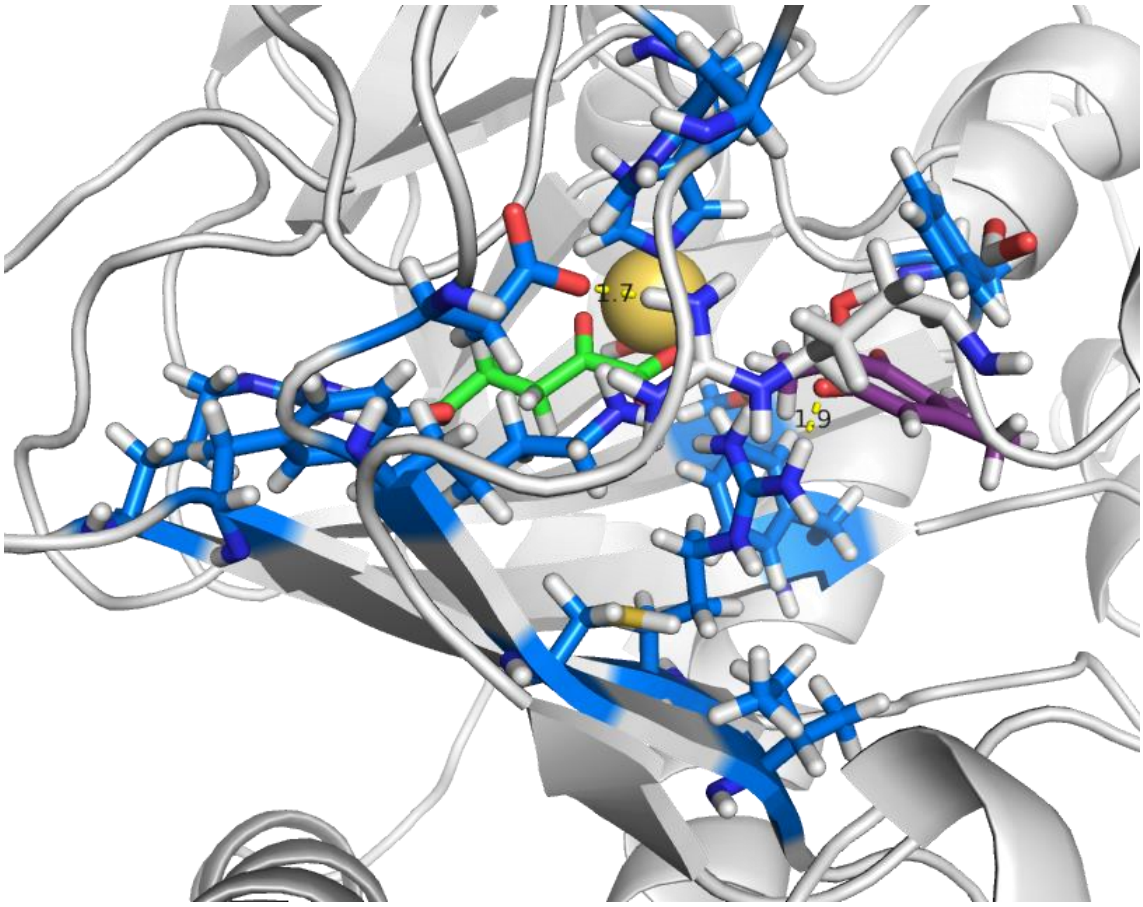


**Figure 4.S37. Close-up image of TropC active site with substrate bound from the final frame of MD simulation.**

The hydrogen bonding distance between D100 and R325 is shown. Residues chosen for alanine screening mutagenesis are shown in blue, substrate **4.10** is shown in purple, cofactor α-ketoglutarate is shown in green and ferrous iron is shown in light brown.

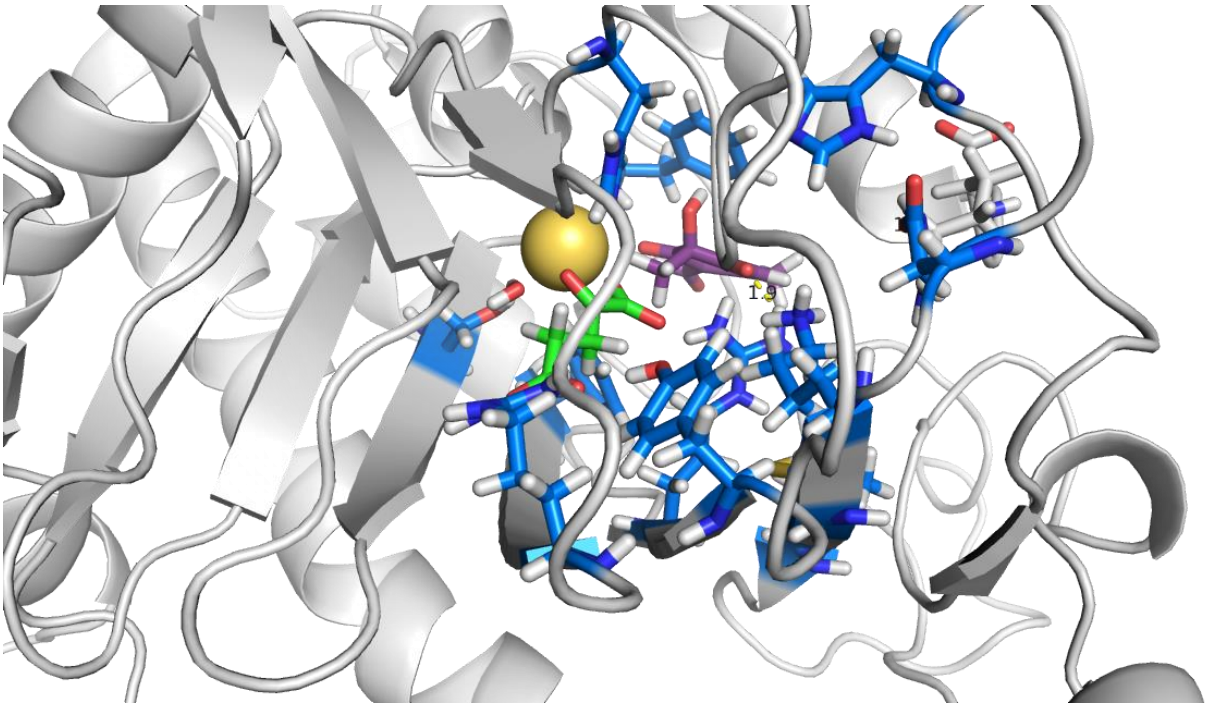

**Figure 4.S38. Close-up image of TropC active site with substrate bound from the final frame of MD simulation.**
Residues chosen for alanine screening mutagenesis are shown in blue, substrate **4.10** is shown in purple, cofactor α-ketoglutarate is shown in green and ferrous iron is shown in light brown.

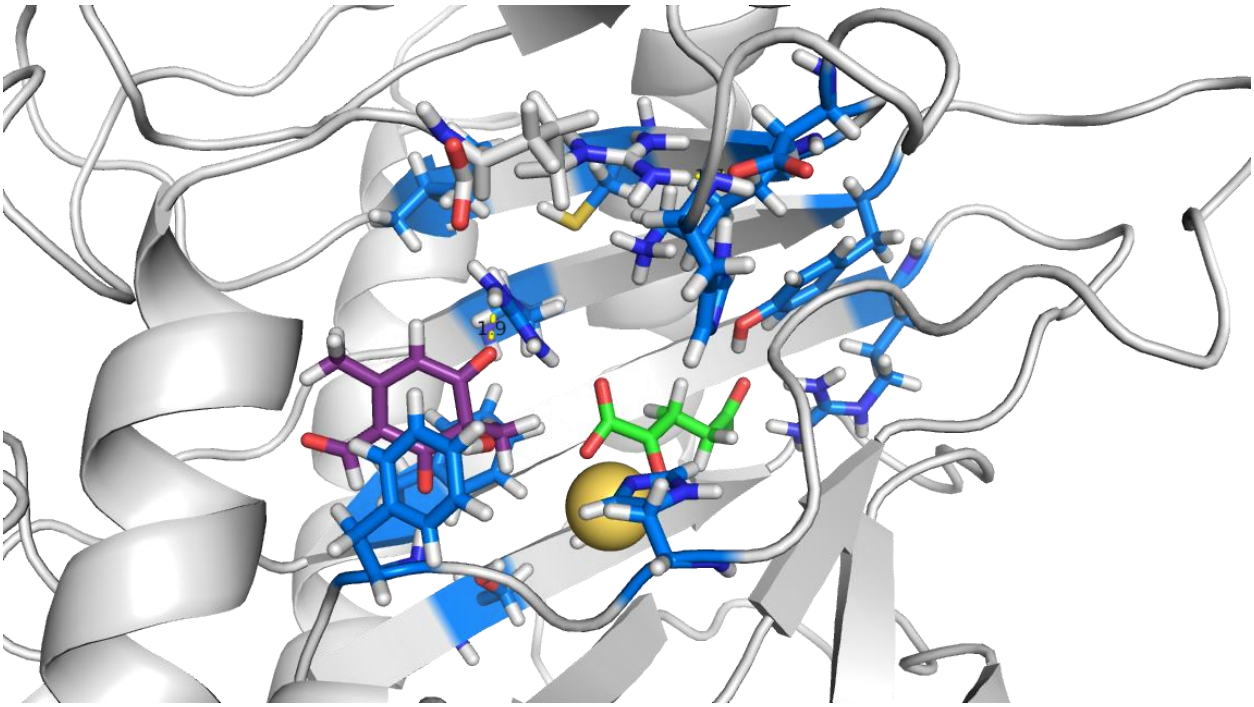

**Figure 4.S39. Close-up image of TropC active site with substrate bound from the final frame of MD simulation.**
Residues chosen for alanine screening mutagenesis are shown in blue, substrate **10** is shown in purple, cofactor α-ketoglutarate is shown in green and ferrous iron is shown in light brown.

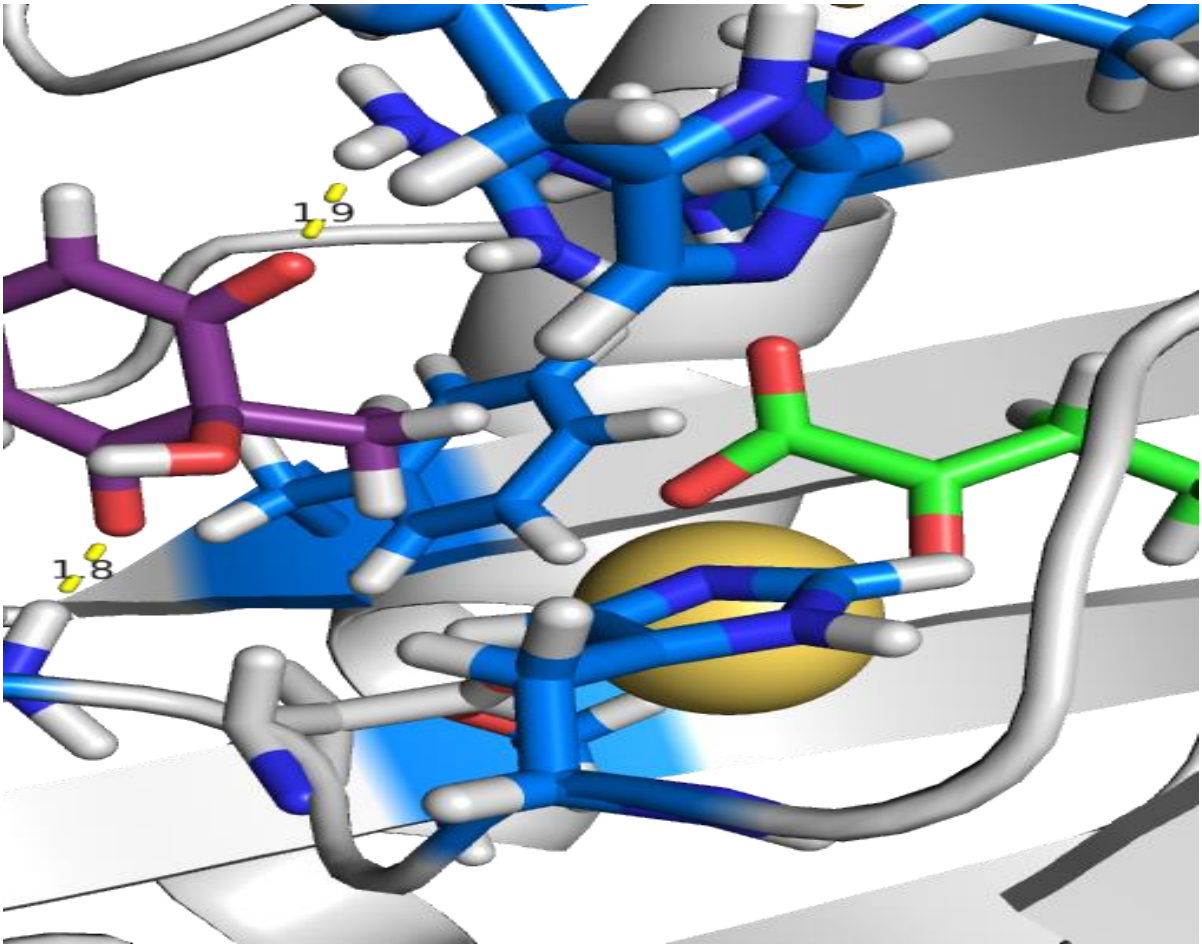


**Figure 4.S40. Observed 2-point binding between the amide backbone nitrogen of F213, substrate 4.10 and guanidinium nitrogen of R190 from the final frame of MD simulation.** Residues chosen for alanine screening mutagenesis are shown in blue, substrate **10** is shown in purple, cofactor α-ketoglutarate is shown in green and ferrous iron is shown in light brown.

## 4.9 References


(1) Walsh, C. T.; Moore, B. S., Enzymatic Cascade Reactions in Biosynthesis. *Angew. Chem. Intl. Ed.* **2019,** *58* (21), 6846-6879.

(2) Klas, K.; Tsukamoto, S.; Sherman, D. H.; Williams, R. M., Natural Diels–Alderases: Elusive and Irresistable. *J. Org. Chem.* **2015,** *80* (23), 11672-11685.

(3) Christianson, D. W., Structural and Chemical Biology of Terpenoid Cyclases. *Chem. Rev.* **2017,** *117* (17), 11570-11648.

(4) Herr, C. Q.; Hausinger, R. P., Amazing Diversity in Biochemical Roles of Fe(II)/2-Oxoglutarate Oxygenases. *Trends. Biochem. Sci.* **2018,** *43* (7), 517-532.

(5) Dowd, P.; Zhang, W., Free radical-mediated ring expansion and related annulations. *Chem. Rev.* **1993,** *93* (6), 2091-2115.

(6) Donald, J. R.; Unsworth, W. P., Ring-Expansion Reactions in the Synthesis of Macrocycles and Medium-Sized Rings. *Chem. Eur. J.* **2017,** *23* (37), 8780-8799.

(7) Bai, J.; Yan, L.; Liu, Y., Catalytic mechanism of the PrhA (V150L/A232S) double mutant involved in the fungal meroterpenoid biosynthetic pathway: a QM/MM study. *Phys. Chem. Chem. Phys.* **2019,** *21* (46), 25658-25668.

(8) Matsuda, Y.; Iwabuchi, T.; Fujimoto, T.; Awakawa, T.; Nakashima, Y.; Mori, T.; Zhang, H.; Hayashi, F.; Abe, I., Discovery of Key Dioxygenases that Diverged the Paraherquonin and Acetoxydehydroaustin Pathways in Penicillium brasilianum. *J. Am. Chem. Soc.* **2016,** *138* (38), 12671-12677.

(9) Nakashima, Y.; Mori, T.; Nakamura, H.; Awakawa, T.; Hoshino, S.; Senda, M.; Senda, T.; Abe, I., Structure function and engineering of multifunctional non-heme iron dependent oxygenases in fungal meroterpenoid biosynthesis. *Nat. Commun.* **2018,** *9* (1), 104.

(10) Nakamura, H.; Matsuda, Y.; Abe, I., Unique chemistry of non-heme iron enzymes in fungal biosynthetic pathways. *Nat. Prod. Rep.* **2018,** *35* (7), 633-645.

(11) Kovaleva, E. G.; Lipscomb, J. D., Versatility of biological non-heme Fe(II) centers in oxygen activation reactions. *Nat. Chem. Biol.* **2008,** *4* (3), 186-193.

(12) Timmins, A.; Visser, S. P. d., A Comparative Review on the Catalytic Mechanism of Nonheme Iron Hydroxylases and Halogenases. *Catalysts* **2018,** *8* (8), 314.

(13) Martinez, S.; Hausinger, R. P., Catalytic Mechanisms of Fe(II)- and 2-Oxoglutarate-dependent Oxygenases. *J. Biol. Chem.* **2015,** *290* (34), 20702-20711.

(14) Yan, L.; Liu, Y., Insights into the Mechanism and Enantioselectivity in the Biosynthesis of Ergot Alkaloid Cycloclavine Catalyzed by Aj_EasH from Aspergillus japonicus. *Inorg. Chem.* **2019,** *58* (20), 13771-13781.

(15) Jakubczyk, D.; Caputi, L.; Stevenson, C. E. M.; Lawson, D. M.; O'Connor, S. E., Structural characterization of EasH (Aspergillus japonicus) – an oxidase involved in cycloclavine biosynthesis. *Chem. Commun.* **2016,** *52* (99), 14306-14309.

(16) Tarhonskaya, H.; Szöllössi, A.; Leung, I. K. H.; Bush, J. T.; Henry, L.; Chowdhury, R.; Iqbal, A.; Claridge, T. D. W.; Schofield, C. J.; Flashman, E., Studies on Deacetoxycephalosporin C Synthase Support a Consensus Mechanism for 2-Oxoglutarate Dependent Oxygenases. *Biochemistry* **2014,** *53* (15), 2483-2493.

(17) Valegard, K.; Terwisscha van Scheltinga, A. C.; Dubus, A.; Ranghino, G.; Oster, L. M.; Hajdu, J.; Andersson, I., The structural basis of cephalosporin formation in a mononuclear ferrous enzyme. *Nat. Struct. Mol. Biol.* **2004,** *11* (1), 95-101.

(18) Jakubczyk, D.; Caputi, L.; Hatsch, A.; Nielsen, C. A.; Diefenbacher, M.; Klein, J.; Molt, A.; Schroder, H.; Cheng, J. Z.; Naesby, M.; O'Connor, S. E., Discovery and reconstitution of the cycloclavine biosynthetic pathway--enzymatic formation of a cyclopropyl group. *Angew. Chem. Int. Ed. Engl.* **2015,** *54* (17), 5117-51121.

(19) Cox, R., Oxidative rearrangements during fungal biosynthesis. *Nat. Prod. Rep.* **2014,** *31* (10), 1405-1424.

(20) Cox, R. J.; Al-Fahad, A., Chemical mechanisms involved during the biosynthesis of tropolones. *Curr. Opin. Chem. Biol.* **2013,** *17* (4), 532-536.

(21) Davison, J.; al Fahad, A.; Cai, M.; Song, Z.; Yehia, S. Y.; Lazarus, C. M.; Bailey, A. M.; Simpson, T. J.; Cox, R. J., Genetic, molecular, and biochemical basis of fungal tropolone biosynthesis. *Proc. Natl. Acad. Sci. U S A* **2012,** *109* (20), 7642-7647.

(22) Liu, N.; Song, W.; Schienebeck, C. M.; Zhang, M.; Tang, W., Synthesis of Naturally Occurring Tropones and Tropolones. *Tetrahedron* **2014,** *70* (49), 9281-9305.

(23) Reisman, S. E.; Nani, R. R.; Levin, S., Buchner and Beyond: Arene Cyclopropanation as Applied to Natural Product Total Synthesis. *Synlett* **2011,** *2011* (17), 2437-2442.

(24) Stevens, H. C.; Reich, D. A.; Brandt, D. R.; Fountain, K. R.; Gaughan, E. J., A New Tropolone Synthesis via Dichloroketene. *J. Am. Chem. Soc.* **1965,** *87* (22), 5257-5259.

(25) Barbier, M.; Barton, D. H. R.; Devys, M.; Topgi, R. S., A simple synthesis of tropones and related compounds. *Tetrahedron* **1987,** *43* (21), 5031-5038.

(26) Barbier, M.; Barton, D. H. R.; Devys, M.; Topgi, R. S., A simple synthesis of the tropone nucleus. *J. Chem. Soc. Chem. Commun.* **1984,** (12), 743-744.

(27) Abood, A.; Al-Fahad, A.; Scott, A.; Hosny, A. E.-D. M. S.; Hashem, A. M.; Fattah, A. M. A.; Race, P. R.; Simpson, T. J.; Cox, R. J., Kinetic characterisation of the FAD dependent monooxygenase TropB and investigation of its biotransformation potential. *RSC Adv.* **2015,** *5* (62), 49987-49995.

(28) Schor, R.; Schotte, C.; Wibberg, D.; Kalinowski, J.; Cox, R. J., Three previously unrecognised classes of biosynthetic enzymes revealed during the production of xenovulene A. *Nat. Commun.* **2018,** *9* (1), 1963.

(29) Zhai, Y.; Li, Y.; Zhang, J.; Zhang, Y.; Ren, F.; Zhang, X.; Liu, G.; Liu, X.; Che, Y., Identification of the gene cluster for bistropolone-humulene meroterpenoid biosynthesis in Phoma sp. *Fungal Genet. Biol.* **2019,** *129*, 7-15.

(30) Cho, K.-B.; Hirao, H.; Shaik, S.; Nam, W., To rebound or dissociate? This is the mechanistic question in C–H hydroxylation by heme and nonheme metal–oxo complexes. *Chem. Soc. Rev.* **2016,** *45* (5), 1197-1210.

(31) Timmins, A.; Fowler, N. J.; Warwicker, J.; Straganz, G. D.; de Visser, S. P., Does Substrate Positioning Affect the Selectivity and Reactivity in the Hectochlorin Biosynthesis Halogenase? *Front. Chem.* **2018,** *6*, 513.

(32) Borowski, T.; Wójcik, A.; Miłaczewska, A.; Georgiev, V.; Blomberg, M. R. A.; Siegbahn, P. E. M., The alkenyl migration mechanism catalyzed by extradiol dioxygenases: a hybrid DFT study. *J. Biol. Inorg. Chem.* **2012,** *17* (6), 881-890.

(33) Li, W.; Zhang, T.; Ding, J., Molecular basis for the substrate specificity and catalytic mechanism of thymine-7-hydroxylase in fungi. *Nucleic Acids Res.* **2015,** *43* (20), 10026-10038.

(34) Aik, W.; McDonough, M. A.; Thalhammer, A.; Chowdhury, R.; Schofield, C. J., Role of the jelly-roll fold in substrate binding by 2-oxoglutarate oxygenases. *Curr. Opin. Struct. Biol.* **2012,** *22* (6), 691-700.

(35) Holm, L.; Rosenstrom, P., Dali server: conservation mapping in 3D. *Nucleic Acids Res.* **2010,** *38*, W545-549.

(36) Zhang, H.; Che, S.; Wang, R.; Liu, R.; Zhang, Q.; Bartlam, M., Structural characterization of an isopenicillin N synthase family oxygenase from Pseudomonas aeruginosa PAO1. *Biochem. Biophys. Res. Commun.* **2019,** *514* (4), 1031-1036.

(37) Mitchell, A. J.; Dunham, N. P.; Bergman, J. A.; Wang, B.; Zhu, Q.; Chang, W. C.; Liu, X.; Boal, A. K., Structure-Guided Reprogramming of a Hydroxylase To Halogenate Its Small Molecule Substrate. *Biochemistry* **2017,** *56* (3), 441-444.

(38) Doyon, T. J.; Perkins, J. C.; Baker Dockrey, S. A.; Romero, E. O.; Skinner, K. C.; Zimmerman, P. M.; Narayan, A. R. H., Chemoenzymatic o-Quinone Methide Formation. *J. Am. Chem. Soc.* **2019,** *141* (51), 20269-20277.

(39) Baker Dockrey, S. A.; Lukowski, A. L.; Becker, M. R.; Narayan, A. R. H., Biocatalytic site- and enantioselective oxidative dearomatization of phenols. *Nat. Chem.* **2018,** *10* (2), 119-125.

(40) He, Y.; Cox, R. J., The molecular steps of citrinin biosynthesis in fungi. *Chem. Sci.* **2016,** *7* (3), 2119-2127.

(41) Cacioli, P.; Reiss, J., Reactions of 1-Oxaspiro[2.5]octa-5,7-dien-4-ones with nucleophiles. *Aust. J. Chem.* **1984,** *37* (12), 2525-2535.

(42) Drozdetskiy, A.; Cole, C.; Procter, J.; Barton, G. J., JPred4: a protein secondary structure prediction server. *Nucleic Acids Res.* **2015,** *43* (W1), W389-W394.

(43) Vagin, A.; Teplyakov, A., Molecular replacement with MOLREP. *Acta Crystallogr. D Biol. Crystallogr.* **2010,** *66* (Pt 1), 22-25.

(44) Li, W.; Zhang, T.; Ding, J., Molecular basis for the substrate specificity and catalytic mechanism of thymine-7-hydroxylase in fungi. *Nucleic Acids Res.* **2015,** *43* (20), 10026-10038.

(45) Emsley, P.; Cowtan, K., Coot: model-building tools for molecular graphics. *Acta Crystallogr. D Biol. Crystallogr.* **2004,** *60* (Pt 12 Pt 1), 2126-2132.

(46) Murshudov, G. N.; Vagin, A. A.; Dodson, E. J., Refinement of macromolecular structures by the maximum-likelihood method. *Acta Crystallogr. D Biol. Crystallogr.* **1997,** *53* (Pt 3), 240-255.

(47) Vagin, A. A.; Steiner, R. A.; Lebedev, A. A.; Potterton, L.; McNicholas, S.; Long, F.; Murshudov, G. N., REFMAC5 dictionary: organization of prior chemical knowledge and guidelines for its use. *Acta Crystallogr. D Biol. Crystallogr.* **2004,** *60* (Pt 12 Pt 1), 2184-2195.

(48) Winn, M. D.; Ballard, C. C.; Cowtan, K. D.; Dodson, E. J.; Emsley, P.; Evans, P. R.; Keegan, R. M.; Krissinel, E. B.; Leslie, A. G.; McCoy, A.; McNicholas, S. J.; Murshudov, G. N.; Pannu, N. S.; Potterton, E. A.; Powell, H. R.; Read, R. J.; Vagin, A.; Wilson, K. S., Overview of the CCP4 suite and current developments. *Acta Crystallogr. D Biol. Crystallogr.* **2011,** *67* (Pt 4), 235-242.

(49) Chen, V. B.; Arendall, W. B., 3rd; Headd, J. J.; Keedy, D. A.; Immormino, R. M.; Kapral, G. J.; Murray, L. W.; Richardson, J. S.; Richardson, D. C., MolProbity: all-atom structure validation for macromolecular crystallography. *Acta Crystallogr. D Biol. Crystallogr.* **2010,** *66* (Pt 1), 12-21.

(50) The PyMOL Molecular Graphics System, V., Schrödinger, LLC.

(51) Becke, A. D., Density-functional thermochemistry. III. The role of exact exchange. *J. Chem. Phys.* **1993,** *98* (7), 5648-5652.

(52) Lee, C.; Yang, W.; Parr, R. G., Development of the Colle-Salvetti correlation-energy formula into a functional of the electron density. *Phys. Rev. B* **1988,** *37* (2), 785-789.

(53) Krishnan, R.; Binkley, J. S.; Seeger, R.; Pople, J. A., Self-consistent molecular orbital methods. XX. A basis set for correlated wave functions. *J. Chem. Phys.* **1980,** *72* (1), 650-654.

(54) Clark, T.; Chandrasekhar, J.; Spitznagel, G. W.; Schleyer, P. V. R., Efficient diffuse function-augmented basis sets for anion calculations. III. The 3-21+G basis set for first-row elements, Li–F. *J. Comput. Chem.* **1983,** *4* (3), 294-301.

(55) Zimmerman, P. M., Single-ended transition state finding with the growing string method. *J. Comput. Chem.* **2015,** *36* (9), 601-611.

(56) Zimmerman, P. M., Automated discovery of chemically reasonable elementary reaction steps. *J. Comput. Chem.* **2013,** *34* (16), 1385-1392.

(57) Zimmerman, P. M., Navigating molecular space for reaction mechanisms: an efficient, automated procedure. *Molec. Simul.* **2015,** *41* (1-3), 43-54.

(58) Zimmerman, P., Reliable Transition State Searches Integrated with the Growing String Method. *J. Chem. Theor. Comput.* **2013,** *9* (7), 3043-3050.

(59) Marenich, A. V.; Cramer, C. J.; Truhlar, D. G., Universal Solvation Model Based on Solute Electron Density and on a Continuum Model of the Solvent Defined by the Bulk Dielectric Constant and Atomic Surface Tensions. *J. Phys. Chem. B* **2009,** *113* (18), 6378-6396.

(60) Marenich, A. V.; Olson, R. M.; Kelly, C. P.; Cramer, C. J.; Truhlar, D. G., Self-Consistent Reaction Field Model for Aqueous and Nonaqueous Solutions Based on Accurate Polarized Partial Charges. *J. Chem. Theor. Comput.* **2007,** *3* (6), 2011-2033.

(61) Marenich, A. V.; Cramer, C. J.; Truhlar, D. G., Generalized Born Solvation Model SM12. *J. Chem. Theor. Comput.* **2013,** *9* (1), 609-620.

(62) Jr., T. H. D., Gaussian basis sets for use in correlated molecular calculations. I. The atoms boron through neon and hydrogen. *J. Chem. Phys.* **1989,** *90* (2), 1007-1023.

(63) Wilson, A. K.; Woon, D. E.; Peterson, K. A.; Jr., T. H. D., Gaussian basis sets for use in correlated molecular calculations. IX. The atoms gallium through krypton. *J. Chem. Phys.* **1999,** *110* (16), 7667-7676.

(64) Woon, D. E.; Jr., T. H. D., Gaussian basis sets for use in correlated molecular calculations. IV. Calculation of static electrical response properties. *J. Chem. Phys.* **1994,** *100* (4), 2975-2988.

(65) Woon, D. E.; Jr., T. H. D., Gaussian basis sets for use in correlated molecular calculations. III. The atoms aluminum through argon. *J. Chem. Phys.* **1993,** *98* (2), 1358-1371.

(66) Kendall, R. A.; Jr., T. H. D.; Harrison, R. J., Electron affinities of the first-row atoms revisited. Systematic basis sets and wave functions. *J. Chem. Phys.* **1992,** *96* (9), 6796-6806.

(67) Balabanov, N. B.; Peterson, K. A., Systematically convergent basis sets for transition metals. I. All-electron correlation consistent basis sets for the 3d elements Sc–Zn. *J. Chem. Phys.* **2005,** *123* (6), 064107.

(68) Neese, F., The ORCA program system. *WIREs Comput. Molec. Sci.* **2012,** *2* (1), 73-78.

(69) Shao, Y.; Gan, Z.; Epifanovsky, E.; Gilbert, A. T. B.; Wormit, M.; Kussmann, J.; Lange, A. W.; Behn, A.; Deng, J.; Feng, X.; Ghosh, D.; Goldey, M.; Horn, P. R.; Jacobson, L. D.; Kaliman, I.; Khaliullin, R. Z.; Kuś, T.; Landau, A.; Liu, J.; Proynov, E. I.; Rhee, Y. M.; Richard, R. M.; Rohrdanz, M. A.; Steele, R. P.; Sundstrom, E. J.; Woodcock, H. L.; Zimmerman, P. M.; Zuev, D.; Albrecht, B.; Alguire, E.; Austin, B.; Beran, G. J. O.; Bernard, Y. A.; Berquist, E.; Brandhorst, K.; Bravaya, K. B.; Brown, S. T.; Casanova, D.; Chang, C.-M.; Chen, Y.; Chien, S. H.; Closser, K. D.; Crittenden, D. L.; Diedenhofen, M.; DiStasio, R. A.; Do, H.; Dutoi, A. D.; Edgar, R. G.; Fatehi, S.; Fusti-Molnar, L.; Ghysels, A.; Golubeva-Zadorozhnaya, A.; Gomes, J.; Hanson-Heine, M. W. D.; Harbach, P. H. P.; Hauser, A. W.; Hohenstein, E. G.; Holden, Z. C.; Jagau, T.-C.; Ji, H.; Kaduk, B.; Khistyaev, K.; Kim, J.; Kim, J.; King, R. A.; Klunzinger, P.; Kosenkov, D.; Kowalczyk, T.; Krauter, C. M.; Lao, K. U.; Laurent, A. D.; Lawler, K. V.; Levchenko, S. V.; Lin, C. Y.; Liu, F.; Livshits, E.; Lochan, R. C.; Luenser, A.; Manohar, P.; Manzer, S. F.; Mao, S.-P.; Mardirossian, N.; Marenich, A. V.; Maurer, S. A.; Mayhall, N. J.; Neuscamman, E.; Oana, C. M.; Olivares-Amaya, R.; O'Neill, D. P.; Parkhill, J. A.; Perrine, T. M.; Peverati, R.; Prociuk, A.; Rehn, D. R.; Rosta, E.; Russ, N. J.; Sharada, S. M.; Sharma, S.; Small, D. W.; Sodt, A.; Stein, T.; Stück, D.; Su, Y.-C.; Thom, A. J. W.; Tsuchimochi, T.; Vanovschi, V.; Vogt, L.; Vydrov, O.; Wang, T.; Watson, M. A.; Wenzel, J.; White, A.; Williams, C. F.; Yang, J.; Yeganeh, S.; Yost, S. R.; You, Z.-Q.; Zhang, I. Y.; Zhang, X.; Zhao, Y.; Brooks, B. R.; Chan, G. K. L.; Chipman, D. M.; Cramer, C. J.; Goddard, W. A.; Gordon, M. S.; Hehre, W. J.; Klamt, A.; Schaefer, H. F.; Schmidt, M. W.; Sherrill, C. D.; Truhlar, D. G.; Warshel, A.; Xu, X.; Aspuru-Guzik, A.; Baer, R.; Bell, A. T.; Besley, N. A.; Chai, J.-D.; Dreuw, A.; Dunietz, B. D.; Furlani, T. R.; Gwaltney, S. R.; Hsu, C.-P.; Jung, Y.; Kong, J.; Lambrecht, D. S.; Liang, W.; Ochsenfeld, C.; Rassolov, V. A.; Slipchenko, L. V.; Subotnik, J. E.; Van Voorhis, T.; Herbert, J. M.; Krylov, A. I.; Gill, P. M. W.; Head-Gordon, M., Advances in molecular quantum chemistry contained in the Q-Chem 4 program package. *Molec. Phys.* **2015,** *113* (2), 184-215.

(70) Martí-Renom, M. A.; Stuart, A. C.; Fiser, A.; Sánchez, R.; and, F. M.; Šali, A., Comparative Protein Structure Modeling of Genes and Genomes. *Annu. Rev. Biophys. Biomol. Struct.* **2000,** *29* (1), 291-325.

(71) Berman, H. M.; Westbrook, J.; Feng, Z.; Gilliland, G.; Bhat, T. N.; Weissig, H.; Shindyalov, I. N.; Bourne, P. E., The Protein Data Bank. *Nucleic Acids Res.* **2000,** *28* (1), 235-242.

(72) Kluza, A.; Niedzialkowska, E.; Kurpiewska, K.; Wojdyla, Z.; Quesne, M.; Kot, E.; Porebski, P. J.; Borowski, T., Crystal structure of thebaine 6-O-demethylase from the morphine biosynthesis pathway. *J. Struct. Biol.* **2018,** *202* (3), 229-235.

(73) Jo, S.; Kim, T.; Iyer, V. G.; Im, W., CHARMM-GUI: A web-based graphical user interface for CHARMM. *J. Comput. Chem.* **2008,** *29* (11), 1859-1865.

(74) Søndergaard, C. R.; Olsson, M. H. M.; Rostkowski, M.; Jensen, J. H., Improved Treatment of Ligands and Coupling Effects in Empirical Calculation and Rationalization of pKa Values. *J. Chem. Theor. Comput.* **2011,** *7* (7), 2284-2295.

(75) Olsson, M. H. M.; Søndergaard, C. R.; Rostkowski, M.; Jensen, J. H., PROPKA3: Consistent Treatment of Internal and Surface Residues in Empirical pKa Predictions. *J. Chem. Theor. Comput.* **2011,** *7* (2), 525-537.

(76) Vanommeslaeghe, K.; Hatcher, E.; Acharya, C.; Kundu, S.; Zhong, S.; Shim, J.; Darian, E.; Guvench, O.; Lopes, P.; Vorobyov, I.; Mackerell Jr., A. D., CHARMM general force field: A force field for drug-like molecules compatible with the CHARMM all-atom additive biological force fields. *J. Comput. Chem.* **2010,** *31* (4), 671-690.

(77) Yu, W.; He, X.; Vanommeslaeghe, K.; MacKerell Jr., A. D., Extension of the CHARMM general force field to sulfonyl-containing compounds and its utility in biomolecular simulations. *J. Comput. Chem.* **2012,** *33* (31), 2451-2468.

(78) Pang, X.; Han, K.; Cui, Q., A simple but effective modeling strategy for structural properties of non-heme Fe(II) sites in proteins: test of force field models and application to proteins in the AlkB family. *J. Comput. Chem.* **2013,** *34* (19), 1620-1635.

(79) Huang, J.; MacKerell Jr, A. D., CHARMM36 all-atom additive protein force field: Validation based on comparison to NMR data. *J. Comput. Chem.* **2013,** *34* (25), 2135-2145.

(80) Eastman, P.; Swails, J.; Chodera, J. D.; McGibbon, R. T.; Zhao, Y.; Beauchamp, K. A.; Wang, L.-P.; Simmonett, A. C.; Harrigan, M. P.; Stern, C. D.; Wiewiora, R. P.; Brooks, B. R.; Pande, V. S., OpenMM 7: Rapid development of high performance algorithms for molecular dynamics. *PLOS Comput. Biol.* **2017,** *13* (7), e1005659.

# Chapter 5: Conclusions and Future Directions

## 5.1 Conclusions

The elucidation of biosynthetic pathways in microorganisms and plants has enabled annotation of an immense number of enzymes, exposing the untapped synthetic potential of biocatalysts from secondary metabolism.[1-3] Yet, great effort is required to bridge the divide between biocatalyst discovery and the seamless integration of enzymes into the synthetic chemist's toolbox.[1-3] Our work actively engages with this challenge to establish and develop novel biocatalytic methods for complex molecule synthesis. We seek to harness the power of biocatalysis to improve upon current synthetic methods and to build complementary reaction platforms for challenging transformations. The search for candidate biocatalysts to fulfill this purpose led to non-heme iron (NHI) α-ketoglutarate-dependent (α-KG) dioxygenases, which remain largely underutilized as biocatalytic tools.[4] These enzymes are known to catalyze a wide variety of transformations in a highly selective manner.[5] In addition, scalable reaction platforms have been developed for NHI enzymes, owing to their simple reaction requirements of inexpensive α-KG and ferrous iron. This Chapter summarizes the results of the preceding three chapters describing the use of NHI enzymes in the chemoenzymatic synthesis of complex molecules and natural products.

Reactive intermediates, such as *ortho*-quinone methides (*o*-QMs), have been leveraged as building blocks in the synthesis of complex molecules.[6-9] The efficient and selective generation of reactive intermediates can be challenging. However, Nature has developed enzymatic methods to

directly access intermediates in the biosynthesis of secondary metabolites. Taking advantage of this catalyst-controlled selectivity, we leveraged NHI dioxygenases CitB and ClaD for site- and chemo-selective benzylic C–H hydroxylation of *o*-phenolic benzaldehydes.[10] The resulting benzylic alcohol products then underwent an elimination reaction under mild conditions, generating *o*-QM intermediates which were modified through 1,4-addition or [4+2] cycloaddition reactions in a modular, one-pot chemoenzymatic process. This reaction platform was applied to the synthesis of numerous complex molecules, the natural product (–)-xyloketal D, and the labelling of peptides. These transformations were performed on near-gram scale by using whole *E. coli* cells expressing the biocatalyst of interest. Chemoenzymatic generation of *o*-QMs provided several advantages over traditional synthetic methods in that the reactive intermediate could be generated in a single vessel with precise control over the site- and chemo-selectivity of the benzylic hydroxylation reaction.[10]

We have also utilized chemoenzymatic processes to access a variety of tropolones. Tropolones are a diverse class of natural products with a conserved seven-membered aromatic ring. NHI enzymes XenC and TropC were leveraged for the direct synthesis of diverse tropolones through a two-step enzymatic cascade. Synthesis of these tropolones was achieved on preparative scale, allowing isolation of these novel compounds. This cascade reaction was also applied to the racemic synthesis of 18-deoxyepolone B, a deoxy form of tropolone natural product epolone B. Furthermore, the hetero-Diels-Alderase XenE was shown to catalyze [4+2] reactions *in vitro* for the synthesis of 18-deoxyepolone B, demonstrating the potential to apply hetero-Diels-Alderases for synthetic purposes.

In addition to the chemoenzymatic synthesis of tropolones, we have explored the mechanism of ring expansion utilized by NHI enzyme TropC. Through structural characterization

of TropC, alanine-screening of the enzyme active site and computational analysis of potential reaction pathways, we have characterized the TropC ring expansion process as likely a radical rearrangement. This new mechanistic proposal is strongly supported by experimental and computational evidence as well as literature precedent for one-electron ring expansions in tropolone synthesis.

The studies described here have led directly to the development and characterization of biocatalysts as tools for complex molecule synthesis. Through these efforts, we have established and explored the synthetic utility of NHI enzymes and their ability to achieve selective and synthetically-challenging reactions. Furthermore, this work directly addresses the knowledge gap between enzyme discovery and chemoenzymatic synthesis, enabling integration of NHI biocatalysts into synthetic planning.

## 5.2 Future directions

*Structural characterization of NHI enzymes CitB and ClaD*

Through our development of a biocatalytic benzylic C–H hydroxylation platform, we characterized the substrate functionalities required for NHI enzymes CitB and ClaD to engage in productive catalysis. Although CitB and ClaD are homologs sharing 46% sequence identity, they are able to catalyze benzylic C–H hydroxylation on substrates with divergent functionalities, allowing them to serve as complementary biocatalysts. In an effort to identify and understand the biochemical foundation of these differences, we aim to perform structural characterization of these enzymes in collaboration with Prof. Markos Koutmos at the University of Michigan. We anticipate that a comparative structural analysis will enable elucidation of the amino acid residues responsible for substrate binding and subsequent catalysis, allowing rational design of more promiscuous

enzymes. Furthermore, the development of structural information on this subclass of α-KG-dependent hydroxylases will enable detailed characterization of the active site architectures which deliver site- and chemo-selective oxidation of phenolic substrates. This information is also crucial for efforts to characterize and classify homologs of CitB and ClaD, as no structural information is available for these functionally-related enzymes. We anticipate that these efforts, paired with bioinformatic analyses, will allow the identification of homologous biocatalysts possessing complementary substrate requirements, which we envision will broaden the synthetic utility of NHI enzyme-catalyzed benzylic oxidation.

*Characterization of XenE-catalyzed reaction product and application to chemoenzymatic synthesis*

We have developed a biochemical assay to demonstrate the activity of hetero-Diels-Alderase XenE in coupling an *ortho*-tropolinone methide (*o*-TM) with α-humulene through [4+2] reaction to generate tropolone meroterpenoids. Ongoing work aims to develop a preparative scale reaction for the isolation of XenE-generated Diels-Alder products and evaluation of the enantioselectivity of this reaction. We also aim to further characterize the XenE-catalyzed reaction by evaluating the coupling partners, such as other *o*-TM precursors and humulene derivatives, which could be productive substrates in this transformation. For this purpose, we will leverage the ability of NHI enzyme XenC to efficiently generate non-natural tropolones, screening these products as reactions partners in XenE-catalyzed reactions with α-humulene. In this way, we aim to efficiently and selectively generate a variety of tropolone meroterpenoids as potential bioactive compounds. In addition, we envision that the efficient and mild nature of a XenE-catalyzed Diels-Alder reaction will potentially enable direct bioassay screening of the reaction products, allowing

for high throughput, selective synthesis and screening of tropolone meroterpenoids. These efforts will seek to reduce existing barriers to synthetic access of tropolones, leading to detailed exploration of their biological activities and potentially the development of novel pharmaceuticals.

*Characterization of hetero-Diels-Alderase XenE*

In this work, substrates have been identified which are accepted by XenE as partners in the Diels-Alder rection. However, little is known about the enzyme active site architecture which permits the activity observed in these reactions. We aim to further investigate the biochemical characteristics of XenE through structural characterization using X-ray crystallography in collaboration with Attabey Rodríguez-Benítez (Prof. Alison Narayan and Prof. Janet Smith). Broadly, this analysis will provide architectural details on a previously uncharacterized class of enzymes which catalyze highly selective reactions in tropolone biosynthesis. In addition, we anticipate that substrate-bound structures will enable a detailed analysis of substrate binding poses which impart diastereoselectivity in the resulting reaction.

The chemoenzymatic approaches presented in this dissertation demonstrate the broad potential for biocatalysis to develop novel, streamlined synthetic routes to natural products and their analogs. The synthetic utility of these transformations is built upon the selective oxidation reactions performed by NHI dioxygenases. This work highlights the advantages offered by NHI biocatalysts in the selective synthesis of complex molecules, particularly when combined with chemical processes. One would anticipate that, as the number of known biosynthetic enzymes continues to increase, the incorporation of NHI dioxygenases in synthetic schemes will grow in a similar fashion.

## 5.3 References


(1) Bommarius, A. S., Biocatalysis: A Status Report. *Annu. Rev. Chem. Biomol. Engin.* **2015,** *6* (1), 319-345.

(2) Bornscheuer, U. T., The fourth wave of biocatalysis is approaching. *Philos. Trans. A Math. Phys. Eng. Sci.* **2018,** *376* (2110).

(3) Bornscheuer, U. T.; Huisman, G. W.; Kazlauskas, R. J.; Lutz, S.; Moore, J. C.; Robins, K., Engineering the third wave of biocatalysis. *Nature* **2012,** *485* (7397), 185-194.

(4) Zwick, C. R.; Renata, H., Harnessing the biocatalytic potential of iron- and α-ketoglutarate-dependent dioxygenases in natural product total synthesis. *Nat. Prod. Rep.* **2020**.

(5) Bugg, T. D. H.; Ramaswamy, S., Non-heme iron-dependent dioxygenases: unravelling catalytic mechanisms for complex enzymatic oxidations. *Curr. Opin. Chem. Biol.* **2008,** *12* (2), 134-140.

(6) Bai, W. J.; David, J. G.; Feng, Z. G.; Weaver, M. G.; Wu, K. L.; Pettus, T. R., The domestication of ortho-quinone methides. *Acc. Chem. Res.* **2014,** *47* (12), 3655-64.

(7) Singh, M. S.; Nagaraju, A.; Anand, N.; Chowdhury, S., ortho-Quinone methide (o-QM): a highly reactive, ephemeral and versatile intermediate in organic synthesis. *RSC Adv.* **2014,** *4* (99), 55924-55959.

(8) Willis, N. J.; Bray, C. D., ortho-Quinone Methides in Natural Product Synthesis. *Chem. Eur. J.* **2012,** *18* (30), 9160-9173.

(9) Bruins, J. J.; Albada, B.; van Delft, F., ortho-Quinones and Analogues Thereof: Highly Reactive Intermediates for Fast and Selective Biofunctionalization. *Chem.* **2018,** *24* (19), 4749-4756.

(10) Doyon, T. J.; Perkins, J. C.; Baker Dockrey, S. A.; Romero, E. O.; Skinner, K. C.; Zimmerman, P. M.; Narayan, A. R. H., Chemoenzymatic o-Quinone Methide Formation. *J. Am. Chem. Soc.* **2019,** *141* (51), 20269-20277.